Vol. 175, September 30, 1985
Complete in one issue

ISSN 0003-2670

ANALYTICA CHIMICA ACTA

International journal devoted to all branches of analytical chemistry

ELSEVIER

ANALYTICA CHIMICA ACTA

International journal devoted to all branches of analytical chemistry
Revue internationale consacrée à tous les domaines de la chimie analytique
Internationale Zeitschrift für alle Gebiete der analytischen Chemie

PUBLICATION SCHEDULE FOR 1985

	J	F	M	A	M	J	J	A	S	O	N	D
Analytica Chimica Acta	167	168	169	170/1 170/2	171	172	173	174	175	176	177	178

Scope. *Analytica Chimica Acta* publishes original papers, short communications, and reviews dealing with ever aspect of modern chemical analysis both fundamental and applied.

Submission of Papers. Manuscripts (three copies) should be submitted as designated below for rapid and efficier handling:

Papers from the Americas to: Professor Harry L. Pardue, Department of Chemistry, Purdue University, West Lafayett IN 47907, U.S.A.

Papers from all other countries to: Dr. A. M. G. Macdonald, Department of Chemistry, The University, P.O. Box 36 Birmingham B15 2TT, England. Papers dealing particularly with computer techniques to: Professor J. T. Cler Universität Bern, Pharmazeutisches Institut, Baltzerstrasse 5, CH-3012 Bern, Switzerland.

Submission of an article is understood to imply that the article is original and unpublished and is not being considere for publication elsewhere. Upon acceptance of an article by the journal, authors will be asked to transfer the copyrigl of the article to the publisher. This transfer will ensure the widest possible dissemination of information.

Information for Authors. Papers in English, French and German are published. There are no page charge Manuscripts should conform in layout and style to the papers published in this Volume. Authors should consu Vol. 170 for detailed information. Reprints of this information are available from the Editors or from: Elsevier Editori Services Ltd., Mayfield House, 256 Banbury Road, Oxford OX2 7DH (Great Britain).

Reprints. Fifty reprints will be supplied free of charge. Additional reprints (minimum 100) can be ordered. An orde form containing price quotations will be sent to the authors together with the proofs of their article.

Advertisements. Advertisement rates are available from the publisher.

Subscriptions. Subscriptions should be sent to: Elsevier Science Publishers B.V., Journals Department, P.O. Bo 211, 1000 AE Amsterdam, The Netherlands. Tel: 5803 911, Telex: 18582.

Publication. *Analytica Chimica Acta* appears in 12 volumes in 1985. The subscription for 1985 (Vols. 167–178) Dfl. 2400.00 plus Dfl. 264.00 (p.p.h.) (total approx. US $986.70). All earlier volumes (Vols. 1–166) except Vols. 2 and 28 are available at Dfl. 231.00 (US $85.56), plus Dfl. 15.00 (US $5.56) p.p.h., per volume.

Our p.p.h. (postage, packing and handling) charge includes surface delivery of all issues, except to subscribers in th U.S.A., Canada, Japan, Australia, New Zealand, P.R. China, India, Israel, South Africa, Malaysia, Singapore, Sout Korea, Taiwan, Pakistan, Hong Kong and Brazil who receive all issues by air delivery (S.A.L. — Surface Air Lifted) a no extra cost. For the rest of the world, airmail and S.A.L. charges are available upon request.

Claims for issues not received should be made within three months of publication of the issues. If not they cannot b honoured free of charge.

For further information, or a free sample copy of this or any other Elsevier Science Publishers journal, readers in th U.S.A. and Canada can contact the following address: Elsevier Science Publishing Co. Inc., Journal Informatio Center, 52 Vanderbilt Avenue, New York, NY 10017, U.S.A., Tel: (212) 916-1250.

ANALYTICA CHIMICA ACTA
VOL. 175 (1985)

ANALYTICA CHIMICA ACTA

International journal devoted to all branches of analytical chemistry

ELSEVIER Amsterdam–Oxford–New York–Tokyo

Anal. Chim. Acta, Vol. 175 (1985)

0003-2670/85/$03.3(

Analytica Chimica Acta, 175 (1985) 1—22
Elsevier Science Publishers B.V., Amsterdam — Printed in The Netherlands

Review

ELECTROANALYTICAL APPLICATIONS OF CARBON FIBRE ELECTRODES

T. E. EDMONDS

Department of Chemistry, Loughborough University of Technology, Loughborough, Leicestershire LE11 3TU (Great Britain)

(Received 15th March 1985)

SUMMARY

The analytical uses of carbon fibre electrodes cover such diverse areas as coulometry, potentiometry, anodic stripping voltammetry, potentiometric stripping voltammetry, spectroelectrochemistry and kinetic measurements. The electrodes have been employed in a variety of cell types and locations, including conventional two and three electrode cells, flowing streams and in-vivo. The electroanalytical applications and theory are discussed in this review, along with the structure and surface properties of carbon fibres. Specialist instrumentation is also described.

The radical increase in the use of solid electrodes in electroanalysis over the past decade is due to four major factors. First electroanalytical chemists have become increasingly interested in oxidation as a unit process in the determination of organic molecules. The limited anodic range of the dropping mercury electrode (DME) has largely precluded its use above ca. 0.0 V vs. SCE, although this may be extended to +0.3 V in suitable media. Accordingly solid electrodes with extended anodic ranges have attracted greater analytical interest. Secondly, the ability of electroanalytical techniques to yield in-situ information in complex chemical environments, can best be utilized with solid electrodes. Thirdly, detectors for liquid chromatography based on electroanalytical devices occupy a small but significant part of the detector market. These detectors are normally operated by personnel who are not necessarily electroanalytical chemists, thus the device must be simple and rugged, and this would indicate that solid electrodes are preferable. Finally, there is more interest in the use of surface-modified electrodes for electroanalytical applications; again solid electrodes are essential in this area of research.

Many materials have been used to make solid electrodes, including several forms of carbon. In electroanalytical applications glass-like carbon and carbon paste are most frequently encountered. A recent review [1] discussed the use of glass-like carbon as an electrode material. Recently, increasing interest has been shown in the use of carbon fibre as an electrode material. Initial

0003-2670/85/$03.30

studies [2—6] concentrated on the use of these fibres for coulometric titrations, as well as describing their response to pH. Latterly the voltammetric and chronoamperometric behaviour of these electrodes has attracted more interest [7, 8]. Much of this interest has come from clinical research where the small size of the electrode has encouraged its use for in-vivo studies. In the broader field of analytical chemistry the utility of these devices is becoming more apparent.

MANUFACTURE AND STRUCTURE OF CARBON FIBRES

Manufacture of carbon fibres

Carbon fibres of high modulus have been produced by the pyrolysis of polymer textiles since 1964 [9, 10]. Many fibres are made from atactic polyacrylonitrile (PAN) as a starting material. The PAN fibres, produced by wet spinning, are stretched and heated to 200°C. A ladder polymer is formed of linked hydrogenated naphthylpyridine rings. This process increases the thermal stability of the polymer by preventing easy formation of small volatile fragments, and by inhibiting melting. The fibres are heated to 220°C, when some of the CH_2 groups are oxidised to ketones. After this final oxidation an inert atmosphere is introduced into the heating chamber and the temperature is taken to 300—400°C. Further cross-linking takes place between adjacent polymer chains, as water, hydrogen cyanide and nitrogen are eliminated. At this point the fibre consists of ribbons of largely carbon atoms, arranged in aromatic ring structures. These ribbons begin to resemble the basal planes of true graphitic structures although the distance between them is much greater than in graphite, and the atoms in a plane are not ordered with respect to those in neighbouring planes. Once the evolution of gases has decreased, the fibres are heated to above 400°C. Further evolution takes place of inter-ladder hydrogen, hydrogen cyanide and nitrogen, until by 1000°C the fibre has lost about 50% of its weight. This process, known as carbonization, yields fibres that have a non-graphitic carbon structure, are of low modulus and high strength. Heating at 2000°C causes the degree of perfection to increase so that the fibre begins to look more like graphite. These fibres are most frequently encountered in structural materials and in analytical applications. Further heating to 2700°C and stretching of these fibres causes them to undergo plastic deformation, giving additional strength, elastic modulus and preferred orientation. Generally, carbonized fibres are not converted to the graphitized form by this heat treatment. Accordingly, the term graphitized fibres should not be used for this type of material. (Further details on IUPAC suggestions for the nomenclature of different carbon forms are available [11]). In North America, α-cellulose (rayon) or polyphenylene oxide are the preferred starting materials.

Useful summaries of these procedures may be found in books on engineering materials [12], and a monograph on carbon fibres has recently appeared [13].

Structure of carbon fibres

The most convincing model of carbon fibre structure was proposed by Fourdeaux et al. [14]. The primary unit is a ribbon-shaped graphitic layer in which no correlation exists between the general direction of the borders of the ribbon and the direction of the *a*-axis of the internal two-dimensional hexagonal structure of the ribbons. The ribbons are around 6 nm wide and several hundred nanometres long. Several of these ribbons run parallel to form a microfibril. The microfibrils have a preferred orientation parallel to the fibre axis. Voids are formed between the boundaries of microfibrils because of their wrinkled nature and imperfect packing. Typically the voids are 20—30 nm long and 1 or 2 nm wide. There is a higher probability for lateral ribbon boundaries to be in contact with the lateral boundaries of adjacent ribbons. This gives rise to short-range order in the packing of adjacent stacks of ribbons (microfibrils). The microfibrils are generally orientated in a tree-ring structure, within the carbon fibre, so that the axial surface is made up of numerous graphitic basal planes, with a few lateral edges, whereas the cross-section of the fibre consists of concentric rings of graphitic edges.

At a higher level of structure, Sharp and Burnay [15] have reported a characteristic internal defect in heat-treated fibres. The defects consist of large (5—10 μm) long cavities probably produced by the volatilization of inclusions that are seen in fibres heat-treated at lower temperatures. These cavities occur at approximately one per millimetre and may be joined to other cavities by narrow holes.

The overall picture of these fibres is of a distinctly anisotropic porous medium. The axial surface appears to be relatively non-porous, but substantial systems of internal pores may be reached via the cross-sectional surface. This may explain the observation that the fibres swell in use [16]. Unpublished work by Jennings, however, has shown no change in the average diameter of Grafil-XAS carbon fibres after the fibres had been soaked for about four months in distilled water.

Most analytical applications of carbon fibres have involved PAN-based fibres. An alternative fibre with a different structure has been described by Otani [17]; these PVC pitch-based fibres are made by heating and drawing PVC at 400°C in nitrogen. The fibres are then cooled and treated with oxygen at 70°C and air at 260°C. The oxidised fibres may then be carbonized or heat-treated under strain to yield a fibre in which the graphite planes are arranged radially within the fibre [18]. This fibre presents a predominantly graphite edge structure both axially and in the cross-section. In this respect, pitch-based fibres more closely resemble glass-like carbon than do their PAN-based counterparts. Several manufacturers of this type of fibre are listed in reference [19]. Faradaic electron transfer occurs predominantly at the edge orientation of graphite planes [20], hence pitch-based fibres may make better analytical electrodes than their PAN-based counterparts.

SURFACES OF CARBON FIBRES

Several reports indicate that electrochemical pretreatment of carbon fibre electrodes gives rise to radically different voltammetric responses. Thus, after electrochemical pretreatment, the oxidation peaks of ascorbic acid, dopamine and 3,4-dihydroxyphenylacetic acid (DOPAC) were not only better resolved, but were also increased in height by a factor of 10—100 [21—24]. In the case of ascorbic acid, the peak potential was shifted from +600 mV vs. Ag/AgCl to −80 mV vs. Ag/AgCl, which is very close to its reversible formal potential. Similarly, Edmonds and Ji [25] showed that copper(II) ions are reduced electrochemically with increasing ease after electrochemical pretreatment of the fibre. They also demonstrated that electrochemical pretreatment increased the number of ionizable surface groups as determined by pH-stat experiments. In all cases, the pretreated fibres were found to increase the pH of the solutions in which they were immersed. It is hard not to conclude from these effects and from the pH response of fibres [26] that the surfaces are populated by redox groups of some sort. Some of the commercially available carbon fibres are physicochemically pretreated by the manufacturers, e.g., Courtaulds Grafil-XAS. There is now considerable evidence that these redox groups may be identified with the oxide functions that develop on any carbon surface in contact with the air.

The literature on surface oxidation and surface functionalization of carbon is extensive [27—54]. In 1944, Steenberg [28] differentiated two types of surface oxides on charcoals. The H-carbons absorbed protons from solution, and were formed by outgassing at temperatures of 800—1000° C, followed by cooling under an inert atmosphere, and exposing to oxygen at room temperature. L-Carbons absorbed base and were produced by more vigorous oxidation. Although the L-carbons were thought to be populated by carboxyl, phenolic or enolic hydroxyl groups, the basic surface oxide was not well understood. Over a decade later, it was suggested [29] that the H-carbons might contain quinol groups. The electrochemical evidence accumulated so far suggests that high-temperature treatment of carbon creates carboxyl groups [30, 31], whereas anodic oxidation in dilute mineral acid solutions results in the formation of quinone and hydroquinone groups [32—34], and possibly carboxyl. The situation is not clear-cut, however, and many different ways of oxidising carbon surfaces have been proposed (e.g., chemical oxidation in solution [36], anodic oxidation in solution [32—34], oxidation by oxygen [30], plasma oxidation [37] and high-temperature treatment with oxygen or oxygen and water [31, 38—40]) and many different end-products have been suggested. It has, however, been established that the preferred locations for these functional groups are on the graphite plane edges [41—43], rather than on the basal graphite planes.

In recent years, x-ray photoelectron spectroscopy (x.p.s.) has been used to study carbon and graphite surfaces. Early work [45] tended to confirm the broad conclusion of other techniques that two types of chemisorbed oxygen

occur on prismatic surfaces of graphite. Later, Donnet and Ehrenberger [46] were able to demonstrate that the surface functional groups produced by oxidation depended on the nature of the oxidising process, and on the parent material. Thus carbonised PAN fibres treated with nitric acid exhibited predominantly carbonylic functions, whereas oxidation of heat-treated PAN-based fibres with permanganate in sulphuric acid gave rise to C—OH type spectra. Ishitani [47] demonstrated not only that oxidation caused a significant increase in the number of surface oxide groups, but also that these groups were predominantly hydroxyl. Studying both carbonized and heat-treated fibres, he observed that surface oxidation barely altered the COOH/C=O/C—OH ratio. Heating the fibres after oxidation caused a decrease in the surface oxide groups. Argon ion etching of fibre surfaces showed that oxidised fibres had a thicker layer of oxides on their surface than untreated fibres, and that this layer was thinner for heat-treated fibres than for carbonised fibres. Clearly, oxidation of a fibre not only increases the surface density of functional groups, but may also increase the density of these groups below the surface. Indeed, it has been demonstrated [48] that carbon fibres may be bulk-functionalized by anodic oxidation in 97% sulphuric acid, followed by reduction. This process results in a high concentration of defects in the carbon crystal lattice, not only on the fibre surface, but throughout the fibre. These defects may then be oxidised irreversibly to functional groups. Recent x.p.s. work by Proctor and Sherwood [49] demonstrated that anodic oxidation of fibres in 0.5 M sulphuric acid gives rise to increased surface oxide density, and that this increase is a function of the potential at which the oxidation is done. In addition, low potentials (+0.5 V vs. SCE) appeared to favour the formation of C=O groups, whereas high potentials (+3.0 V vs. SCE) favour C—O— either as hydroxyl or ester. Acid and ester group proportions remain fairly constant.

The detailed picture of the chemical groups on the carbon fibre surface is confused, although some major points seem fairly clear. There are probably many closely related oxygen-containing functional groups on the surfaces of carbon fibres but carbonyl, carboxyl, hydroxyl and ester groups predominate. Anodic oxidation increases the surface density of all these groups, but the degree and method of oxidation alter their relative proportions. Anodic oxidation in solution favours the formation of carbonyl groups and hydroxyl groups. Evidence from other carbon surfaces suggests that these functional groups may be assigned to aromatic structures such as quinone, hydroxyquinone and phenols. Aromatic and aliphatic carboxylates are also present. These functional groups may be formed in the bulk of the fibre as well as just on the surface; i.e., prolonged oxidation will increase not only the surface density of functional groups, but also the surface thickness.

The implications of these surface oxide species for carbon fibres are quite dramatic. As has already been mentioned, procedures for surface preparation that increase the number of surface groups cause the voltammetric response of the fibres to be significantly altered. This is not unexpected when it is

realised that the locations in which the highest functional group densities are to be found are those areas in which faradaic electron transfer is preferred. This observation of improved electron-transfer at oxy-carbon surfaces is not recent. Panzer and Elving [30] noted that on a pyrolytic graphite surface that was freshly cleaved, lower residual currents and peak currents were obtained for the hexacyanoferrate(II)/(III) couple, compared with surfaces that were prepared by grinding. In addition, the couple appeared less reversible on the freshly-cleaved surface. Presumably the process of grinding the surface produces more oxidised sites than occur on freshly cleaved material. The reasons for increasing current sensitivity with increasing density of surface functional groups are not well understood. Three possibilities have been suggested [44]: resonance tunnelling via acceptor sites formed on the surface electronic band gap; alteration of the double-layer characteristics, thus enhancing the formation of the transition state; and direct interaction of surface groups with reactants.

Another important consequence of the surface chemistry of carbon fibres is the ease with which these surfaces may be chemically modified. Two recent reviews [50, 55] have stressed the readiness with which specifically active compounds may be attached via covalent linkages to surface carbon/oxygen species. These modified electrodes may be prepared by standard methods of organic chemistry to contain for example, catalysts or inhibitors. Trimethylsilanization of bulk oxidised carbon fibres was examined by Theodoridou et al. [51]. Bulk functionalized fibres were shown to be better modified than their surface functionalized counterparts, presumably because of the limited number of edge sites that are available at which functionalization and then modification may take place.

PREPARATION OF CARBON FIBRE ELECTRODES

Clearly, for a material as fine and fragile as carbon fibre, a method of mounting the fibre must be used to produce reasonably rugged electrodes. There are several problems in handling carbon fibres, not the least being the safety aspect. The fibres are easily inhaled, and care should be taken to prevent this happening. The fibres also acquire a static charge, which can make placing or positioning them in capillaries particularly difficult. The static may best be discharged by using an ion-generating pistol of the type used for domestic HiFi systems. The fibres may well be coated in a sizing material that should be removed by washing in acetone. Finally, the fibres are very small and the use of a microscope and high-quality forceps for manipulations is recommended.

Most workers have chosen either to seal the carbon fibres into glass capillaries [8, 16, 24, 25, 56, 57] or to attach the fibre directly to a conducting wire with conducting paint or epoxy [58]. In situations where the fibre is to be operated as a disc rather than as a cylindrical electrode [8], the glass capillary method is preferable. This is also the method of choice when the

electrode is to be used for in-vivo monitoring of electroactive species. A detailed account of a method for the preparation of a batch of 50 or so microelectrodes is available [57]. Generally, the capillary is pulled to a controlled tip diameter by a vertical capillary puller, and the fibre is inserted or floated into the pulled capillary and then sealed with epoxy or non-conducting wax. Some workers pull the capillary with the fibre in-situ, to form a snug fit between the glass and the carbon. It should be borne in mind that this procedure must alter the surface oxides, because it involves heating the fibre to several hundred degrees centigrade in air. Electrical contact with the fibre is most easily made by back-filling the capillary with mercury. An experienced worker can make 7 out of 10 electrodes with similar electrical and electrochemical properties. Carbon fibres can also be incorporated into multielectrode arrays [59] and in some instances operated as bundles of fibres [3].

APPLICATIONS IN COULOMETRY AND POTENTIOMETRY

Coulometry

The very high active surface of carbon fibres (a 1-cm length of 10,000 8-μm filaments has a surface area of 25 cm^2) has been exploited by Jennings et al. for the coulometric generation of iodine [3]. These authors found that the carbon fibre gave essentially similar results to platinum anodes for the titration of sodium thiosulphate with coulometrically generated iodine, although the accuracy of the titration was poorer. In this case, the carbon fibres were operated as a tow, to provide an electrode with high surface area, high limiting currents and improved current efficiency. In a later paper, the authors used the fibres as individual microelectrodes for the coulometric titration of hydrochloric acid or hydrogenphthalate [2]. Visual observation of an indicator colour change was not feasible for the small volumes that were titrated (5 μl). This problem was overcome by using a second carbon fibre as a pH detector. The titration cell consisted of a block of polystyrene resin into which were cast the two carbon-fibre electrodes, a silver counter electrode and the Ag/AgCl reference electrode. The area in which the electrodes were sited formed a shallow depression in which 15 μl of background electrolyte and 5 μl of the acidic sample were located. Efficient mixing of generated titrant and sample solution was achieved by vibrating the cell. A relative standard deviation of 1.4% was obtained for 5 titrations of 5 μl of 0.01 M hydrochloric acid.

Although the initial ideas of these papers appear not to have been taken-up by other workers this work established two important features of carbon fibres. First, the electrode characteristics of this relatively inexpensive and widely available material are sufficiently reliable to make it viable for use as an electroanalytical electrode. Secondly, the small size of the electrodes has important consequences for micro-scale electroanalytical chemistry.

Potentiometry

The potentiometric response to pH of carbon fibres was noted by Jennings et al. [4—6, 26], while coulometric work was under way. The first paper in this series [3] noted that a carbon fibre, sealed into a Pyrex glass tube with epoxy resins, responded to pH in the range 1—13. A linear relationship of about 50 mV/pH at ca. 20° was obtained, and the potential was stable in a given buffer to 1 mV within a few minutes. However, over a period of weeks, larger variations in potential and slope were observed, implying that electrodes must be calibrated each day. The potential was unaffected by the presence or absence of dissolved oxygen, but was strongly affected by oxidants such as cerium(IV), and reductants such as arsenic(III). Later papers [5, 6] concentrated on applications of this carbon-fibre pH-responsive electrode to conventional titrations in aqueous and non-aqueous solvents. Thus, the electrodes were used for end-point detection in titrations of hydrochloric acid and orthophosphoric acid in aqueous solutions and for titrations of glycine in anhydrous acetic acid. The advantage of this pH indicator were considered to be its low impedance and suitability for micro-volume pH measurements.

A more detailed consideration of the pH response of a range of carbon fibres was undertaken later [26]. In this case, the authors examined fibres of varying type from a single manufacturer. Fibres treated at low, medium and high temperatures were used in pristine and surface-treated (air and chemical oxidation) forms. A fibre surface treated at low temperature was found to give the most promising results. The electrode slope was found to be 80% of the Nernstian value. The variation in potential response was such that a pH discrimination of about 0.2 pH could be made with a certainty of 95%. Disadvantages of pH measurement with these electrodes included their slow equilibrium times (5—10 min), marked influence of electrode preparation on response, and variation in equilibrium potential.

These temperature-treated carbon fibres resemble the type of parent material which yields carbonyl functions on solution oxidation [46]. In addition, mild anodic oxidation [32—34, 49] and air oxidation of heat-treated (800—1000°C) carbons or carbon fibres has been shown to favour the formation of quinone/quinhydrone groups. It is an attractive thought that the pH response of these carbon fibres may be due, in part, to the classic quinone/quinhydrone couple. There is an increase in the active surface area of a carbon fibre on oxidation, but this is thought to exert only a secondary effect on the response of the fibre to pH. Some unpublished work in this area [60] demonstrated that electrochemical pretreatment of carbon fibres radically improves the pH response. In some cases, unresponsive fibres could be made to respond with an approximately 90% Nernstian slope over the pH range 1—13. In other cases, the linear range extended only as far as pH 9, becoming sub-Nernstian at higher pH values. This behaviour tends to support the quinone/quinhydrone idea. When ligands such as Tris, or *ortho*phosphate were present in the calibrating buffers, the pH response of the fibres was

distorted, whereas buffers such as oxalate, citrate, EDTA and tartrate generally caused no adverse effects, and in some cases improved the pH response. These results emphasise that these electrodes can at the very least be considered as one of the element/element oxide class of pH responsive devices.

Chronopotentiometry

Although there are no analytical applications of this technique at carbon fibre electrodes, a recent paper [61] developed a theoretical treatment (see also [62]). For a reversible redox couple, the transition time τ can be expressed as a function of I_{ss}/I, where I is the applied current, and I_{ss} is the steady-state diffusion current given by $4nFCD$. (n, F, C and D have their usual meanings). If I_{ss}/I is small then the transition time constant ($I\tau^{1/2}/C$) depends linearly on I_{ss}/I. As I_{ss}/I tends to unity, τ increases rapidly, approaching an infinitely high value at unity. Beyond this point, the electrode potential approaches a steady-state value corresponding to I. Aoki et al. [61] gave an approximate equation for τ from which D may be evaluated. Equations were also given for the potential/time curve and the 1/4-wave potential.

APPLICATIONS IN VOLTAMMETRY

Theory

By far the greatest number of applications of carbon fibres in electroanalysis has involved voltammetric determinations. Voltammetry at such small electrodes shows some striking differences when compared with voltammetry at more conventional electrodes. In a recent discussion paper, Wightman [7] described some of these features. When carbon fibre electrodes are operated in a disc configuration, the electrode diameter is much smaller than the diffusion zone for the time scale of a typical experiment. This feature produces a number of interesting electrochemical consequences. The rate of electrolysis at these electrodes is so low, because of the small electrode area, that it does not exceed the rate at which fresh depolarizer diffuses to the electrode. In linear sweep voltammetry (l.s.v.) at slow scan rates, the electrode operates in an hemispherical (some would say spherical) diffusion field. Accordingly, at slow scan rates, the peak-shaped scans of l.s.v. are replaced by the S-shaped curves familiar in d.c. polarography. The limiting current of the plateau of this curve may be described by the steady-state term of the appropriate chronoamperometric equation (see later). At faster scan rates, diffusion is predominantly linear, and conventional l.s.v. responses are obtained. At slow scan rates, the reverse l.s.v. scan is directly superimposable on the forward scan. This effect is due to the relative sizes of the diffusion zone and the electrode. The latter is relatively large, and the electroreduced (or oxidised) species diffuse away from the electrode before further electrochemical steps can occur, i.e., there is no accumulation of electroreduced or oxidised species at the electrode. Correction for IR drop in solution is of decreased significance, even in aprotic media, because of the small currents that occur.

Apart from the small currents expected at these electrodes, other effects are produced by their small diameters. For example, double potential-step chronoamperometry may be used for real-time residual current correction, because the reverse potential step displays very little faradaic current [8]. For much the same reasons, parallel chemical reactions coupled to an electrochemical step have a decreased effect on the observed current. For a typical catalytic mechanism,

$$Ox + ne^- \rightarrow Red \overset{k}{\rightarrow} Ox$$

where Ox and Red represent, respectively, the oxidised and reduced forms of the electroactive species. Because of the diffusion of the reduced form away from the electrode the enhanced current will not be seen unless the rate constant k has a large value. A system of this type involving the ascorbic acid-enhanced current for dopamine oxidation, has been closely studied [64]. Not only are catalytic mechanisms less obvious at microelectrodes, but subsequent reactions such as occur in an ECE mechanism also are diminished in effect. Thus the electroreduction of copper(II) ions in chloride media, which yields two or more peaks at a conventional electrode, yields only one peak at a carbon fibre electrode [25].

At conventional electrodes, preceding chemical reactions which give rise to kinetically controlled currents, generally depress the current relative to that obtained in the absence of the reaction. Thus, the current for $Ox + ne^- \rightleftharpoons Red$ will be greater than for the reduction involving a prior chemical step $A \underset{k_2}{\overset{k_1}{\rightleftharpoons}} Ox + Y + ne^- \rightleftharpoons Red + Y$ where the kinetics limits the rate of arrival of Ox species at the electrode. (A is the chemical precursor of Ox, and Y represents the products of the chemical reaction leading to the formation of Ox; k_1 and k_2 are the rate constants for the forward and back reactions, respectively.) At microelectrodes it would be expected that this effect would be enhanced, so that kinetic currents would give rise to proportionally even lower currents. This is of particular relevance for the measurement of complexed species at carbon electrodes, where prior dissociation of the complex is a necessary precursor to the electron-transfer step.

Theoretical studies on this problem yielded some surprising results. The kinetic current I_k at a stationary hemispherical electrode for a reversible reduction preceded by a chemical reaction under chronoamperometric conditions, is given [63] by

$$I_k = (nFACD/2)\{[h/(1 + hr)] + [h^2 r/(1 + hr)] \exp(\bar{h}^2 Dt) \operatorname{erfc}[\bar{h}(Dt)^{1/2}]\} \quad (1)$$

where n, F, A, C and D have their usual meanings, erfc is the error function complement, r is the radius of the electrode, and

$$h = K[(k_1 + k_2/D)^{1/2} + (1/r)]; \bar{h} = h + (1/r); K = k_1/k_2$$

For the case for a metal complex MX, dissociating to give the electroactive metal ion M and the free ligand X,

$$MX \underset{k_2}{\overset{k_1}{\rightleftharpoons}} M + X$$

then $K = k_1/k_2 = 1/\text{stability constant}$. In the absence of the complex, the current I obtained at a hemispherical electrode for a reversible reduction of the metal species under chronoamperometric conditions is given by

$$I = (nFCDA/2)[1/(tD\pi)^{1/2} + (1/r)] \tag{2}$$

Thus, the ratio of kinetic current to reversible current, I_k/I, is given by

$$I_k/I = \{[h/(1 + hr)] + [h^2r/(1 + hr)] \exp(\bar{h}^2Dt) \operatorname{erfc}[\bar{h}^2(Dt)^{1/2}]\}/$$
$$[1/(tD\pi)^{1/2} + (1/r)] \tag{3}$$

In Fig. 1, the value of I_k/I is plotted against k_1/k_2 for a range of values. (In effect, the ratio of the kinetic current to the diffusion current is plotted against the reciprocal of the stability constant for a range of different labilities.) Two sets of curves are recorded: one for conventional electrodes, and the other for microelectrodes ($r = 4 \times 10^{-4}$ cm; $D = 1 \times 10^{-5}$ cm^2 s^{-1}; $t = 0.1$ s). In view of the inherent assumptions involved in the derivation of

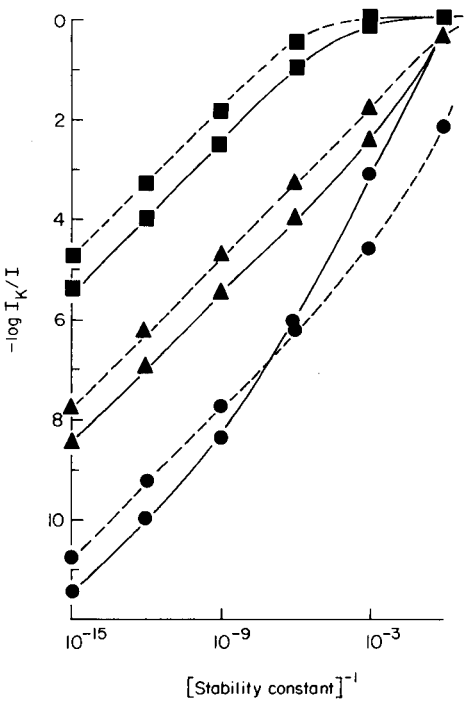

Fig. 1. Plot of kinetic current/diffusion current ratio against reciprocal of stability constant for three different labilities: (■) $k_1 = 10^6$; (▲) $k_1 = 10^0$; (●) $k_1 = 10^{-6}$. Broken lines are the curves for a conventional electrode, solid lines for a microelectrode. (See text for further details.)

Eqn. 2 from more complex expressions, the curves have been plotted only for K values upto 10°. Clearly, for the situation where $k_1 \ll 1$ and $k_2 \leqslant 1$, the microelectrode yields a kinetic current more nearly approaching the diffusion-controlled current than does the conventional electrode. Thus, under certain conditions, preceding chemical steps have a diminished effect on the observed current when microelectrodes are compared with conventional electrodes. This may be understood in terms of the relative sizes of the diffusion zones for the two types of electrode. The limited thickness of the diffusion zone that surrounds microelectrodes allows very little time for a diffusing species to dissociate; accordingly, kinetic currents are generally lower at the microelectrode. However Eqn. 1 takes into account the kinetics of the reverse reaction (the complexation of the metal by the ligand in this case). Where the kinetics of complexation (association) are fast (i.e., k_2 is large), the size of the diffusion zone is of little relevance in considering the possibility of dissociated metal ions recombining with the cloud of free ligand that surrounds the electrode. When the value of k_2 is low, then the size of the diffusion zone of free ligand species through which the metal ion must diffuse is of increasing importance. Once again, at microelectrodes this zone is relatively small; accordingly, more free metal ion (relatively) will reach the electrode than in the case of the conventional electrode.

The limited extent of the diffusion zone into the solution for a microelectrode isolates the electrode from bulk convection. This effect is crucial for in-vivo measurements, but also has interesting implications for carbon-fibre detectors in flowing systems such as flow injection analysis and liquid chromatography.

There are some problems in arriving at an equation to describe the chronoamperometric behaviour of a disc-shaped microelectrode. Dayton et al. [64] have shown that a reasonable approximation is made by considering the electrode as a hemisphere. Thus Eqn. 2 adequately describes the current that is obtained after a potential pulse to the diffusion-controlled portion of an electrochemical wave arising from a reversible reduction. Substituting typical values for D (1×10^{-5} cm^2 s^{-1}) and t (0.1 s) into Eqn. 2 indicates that for $t > 0.1$ s, the time-independent term predominates, and virtually steady-state currents are expected (and indeed obtained) within a relatively short time after pulse application. Similar derivations by Galus et al. [62], Swan [65] and Scharifker and Hills [66] have assumed a spherical diffusion zone around the electrode; nonetheless, their equations are directly comparable with Eqn. 2. The significance of these steady-state currents in l.s.v. is a function of the scanning speed. For voltage scan rates in excess of 100 mV s^{-1}, the I/E curve for the electrode resembles that of a conventional electrode. At slower scan rates, the I/E curve takes on a sigmoidal form as mentioned earlier. Steady-state currents can also be observed at conventional electrodes, but only by monitoring the current at each voltage increment for a considerable period, during which the steady-state contribution assumes significant proportions. Both Swan [65] and Scharifker and Hills [66] used microelectrodes

because of the increased rate of mass transfer arising from the steady-state term. This increase is in inverse proportion to the radius fo the electrode.

Conventional chronoamperometric equations where a potential step is made under conditions of charge-transfer control [67] or when a parallel chemical reaction is taking place [68] have been shown [64] adequately to describe the current/time behaviour of microelectrodes.

It is not always appropriate to use chronoamperometric equations for spherical or hemispherical diffusion zones to describe the currents at microelectrodes. Aoki et al. [69] have derived equations for l.s.v. under cylindrical diffusion conditions when the thickness of the diffusion layer becomes greater than the radius of the electrode. In the case of a reversible electrode reaction, it was shown to be impossible to obtain a steady-state voltammogram, even if the radius tended to zero. The authors derived an approximate expression for the peak current I_p:

$$I_p = a/nFCD = 0.466p + 0.335p \quad (4)$$

where a is the radius of the electrode, and p is given by $(nFa^2v/RTD)^{1/2}$ where v is the sweep rate. The symbols n, F, D, R and T have their usual meanings, and C is the concentration of the electroactive species. Values of p can be obtained from the expression

$$(I_p/nFC)(RT/nFav) = 0.446/p + 0.335p^{-1.85} \quad (5)$$

where all the parameters on the left-hand side of the equation can be obtained in a straightforward manner. An approximate expression for the peak potential for $\log p < -2$ was also given.

Applications to neurotransmitters

Many voltammetric applications of carbon fibres concern the in-vivo monitoring and in-vitro determination of neurotransmitters [21—24, 56—58, 70—87]. Several compounds are routinely monitored at these electrodes: ascorbic acid, dopamine, 3,4-dihydroxyphenylacetic acid (DOPAC), 3,4-dihydroxyphenylaniline (DOPA), 5-hydroxyindoleacetic acid (5HIAA) and uric acid. Indeed, such is the expertise in the in-vivo measurements that it is now possible to estimate the diffusion processes of these neurotransmitters in the mammalian brain [87]. Generally, workers have found it necessary to pretreat the electrodes electrochemically in order to resolve ascorbic acid and DOPAC. Even with pretreatment it is still difficult to resolve dopamine/DOPA/DOPAC, and 5-hydroxytryptamine/5HIAA. In some cases, the dopamine system may be manipulated by drugs in order to identify the peaks [22, 24]. Quantitative evaluation of concentration is not possible in these complex environments, although ionophoresis (ejection of a small controlled amount of a substance from a capillary orifice in the presence of an electrical field) may be used to provide some degree of quantitation. Armstrong-James et al. [70, 71] have used this technique in conjunction with fast-sweep cyclic voltammetry (f.s.c.v.) for measuring, in-vivo, the fate

of ejected dopamine, norepinephrine and enkephalins. Multi-barrel electrodes were used, incorporating a carbon fibre, reference and ionophoresis capillary.

Many papers are concerned primarily with neurochemical methods [74—83] and consequently have little to contribute on the electrochemical side, though of interest to the applications chemist. Others, however, contain some interesting comments on the electroanalytical chemistry [22, 24, 71—73]. Table 1 summarizes the principal features of the in-vitro electroanalytical determination of neurotransmitters presented in these references. Several waveforms were used, although those that yield peak signals, differential pulse voltammetry (dpv) and f.s.c.v., were preferred. In this respect, carbon fibres are like glass-like carbon. Mos et al. [84] considered the use of several waveforms at glass-like carbon for in-vitro and in-vivo determinations of dopamine, DOPAC, homovanillic acid and ascorbic acid. In terms of decreased poisoning of the electrode surface by oxidised analytes, normal pulse voltammetry (n.p.v.) and cyclic voltammetry were better than d.p.v. Generally, these glass-like electrodes could be operated for many hours before their response to the various electroactive species diminished significantly.

Other in-vitro studies of the oxidation of neurotransmitters at carbon fibre electrodes were reported by Ponchon et al. [72]. Half-wave potentials were recorded for dopamine, DOPA, norepinephrine, 5HIAA, homovanillic acid, methoxytyramine, normetanephrine, vanilmandelic acid and epinephrine, based on n.p.v. Detection limits around 10^{-6} M were obtained. When d.p.v. was used with electrochemically pretreated carbon fibres, linear response to dopamine was observed from 50×10^{-9} M to 0.5×10^{-6} M [23]. Stamford [86] reported some f.s.c.v. determinations of dopamine, DOPA, DOPAC, homovanillic acid and ascorbic acid at the 10^{-7}—10^{-5} M levels. An

TABLE 1

In-vitro determination of neurotransmitters

Waveform	Compounds resolved	Compounds unresolved	Ref.
Differential pulse voltammetry[a]	Ascorbic acid and DOPAC	DOPAC, dopamine and DOPA	22
Differential pulse voltammetry[a]	Ascorbic acid and DOPAC	DOPAC, dopamine and DOPA	24
Normal pulse voltammetry	Dopamine and homovanillic acid		72
Fast-sweep cyclic voltammetry	Ascorbic acid/dopamine and norepinephrine or enkephalins	Ascorbic acid and dopamine	71, 73

[a]Electrode subjected to electrochemical pretreatment.

attempt to extend the lifetime of microelectrode systems by the use of multifibre arrays has been described [85].

Undoubtedly, the small size of the carbon fibre electrode has been a major factor in its initial selection for in-vivo studies. The electrode can be inserted into selected regions of mammalian brain tissue, with great accuracy, and minimal disruption. However, aside from this physical aspect, electrochemical and surface characteristics of carbon fibre microelectrodes have proven advantageous. Thus at conventional electrodes, oxidation of dopamine in the presence of ascorbic acid results in an enhanced current caused by the following mechanism:

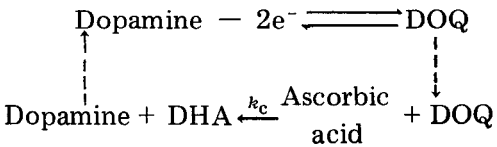

where DOQ and DHA represent the oxidised forms of dopamine and ascorbic acid, respectively. Typically, a large enhanced peak is seen for dopamine and no peak is recorded for ascorbic acid. Dayton et al. [64], using d.p.v. at carbon fibres, demonstrated that two peaks were obtained in a mixture of dopamine and ascorbic acid. One peak was associated with the oxidation of dopamine; the other arose from the oxidation of ascorbic acid. The dopamine peak showed little catalytic contribution from the ascorbic acid. Clearly, this greatly aids the interpretation of the composite peaks seen in in-vivo monitoring; these peaks often consist of signals for dopamine/DOPAC/DOPA in the presence of ascorbic acid. The remarkable changes in the voltammogram that can be brought about by electrochemical pretreatment of the carbon fibre have also been of great benefit in in-vivo analysis. These changes are a function of the carbon fibre material, for micro carbon-paste electrodes do not show such dramatic improvements. Finally, for such small electrodes, the measurement is effectively non-destructive, because so little of the electroactive material is consumed.

Apart from the oxidation of neurotransmitters and related species, various other voltammetric determinations have been reported. Thus Dayton et al. [8] investigated the electrochemical reduction of 4×10^{-4} M potassium hexacyanoferrate(III) in 1.0 M KCl, by d.p.v., cyclic voltammetry and chronoamperometry. These authors found that the differential current per unit area at the carbon fibre electrode was an order of magnitude higher than that obtained at a conventional electrode. To a certain extent, this enhanced current must arise from the greater contributions of the steady-state term in Eqn. 2, even at the relatively short delays (around 50 ms) between pulse application and current measurement for the PAR 174A polarographic analyser that was used in the experiment. The d.p.v. determination of copper(II) ions at carbon fibre electrodes has been reported [25]. Linear calibration from 1 to 50 mg l^{-1} was obtained with a relative standard deviation of 4—7% at 30 mg l^{-1}, depending on the fibre type. The fibres were

pretreated before each determination. A series of papers by Jannakoudakis and co-workers [88] covers the use of carbon fibre electrodes for oxidation of hydrazine and its methyl derivatives, reduction of dinitrobenzene, and reduction of nitrobenzene and *p*-benzoquinone in aqueous and aprotic media. Finally, two papers have appeared in the Russian literature, one describing a carbon fibre electrode for making determinations in micro volumes [89], the other being concerned with background current measurements at carbon fibres [90].

OTHER APPLICATIONS

Stripping voltammetry and potentiometric stripping analysis

Cushman et al. [58] studied the performance of low-modulus carbon fibre electrodes in the differential-pulse anodic stripping voltammetry of cadmium from mercury films. The mercury film was plated on during the deposition step. A linear response from 1 to 100 $\mu g\ l^{-1}$ cadmium was obtained, although peak splitting occurred at intermediate concentrations. The limit of detection was estimated at 0.04 μg. The conditioning potential (the potential at which the pristine electrode was held prior to electrodeposition) of −1.3 V vs. Ag/AgCl, was found to be the most critical factor in the reproducibility of the method. This conditioning potential has been reported for conventional electrodes [91], and is linked to the production of active sites on which mercury nucleation can occur. The method by which a carbon fibre electrode is prepared is known to influence the induction period for mercury nucleation on the surface [66]. Thus, the rate of nucleation depends on the surface preparation, and it is possible that this factor influences the mercury film formation, which in turn accounts for the lack of reproducibility for some conditioning potentials.

Three reports on potentiometric stripping analysis have appeared [92, 93]. Jennings and Morgan [92] point out that the signal that is measured in potentiometric stripping analysis is independent of electrode area. This feature was demonstrated for the determination of cadmium at the 1 $\mu g\ l^{-1}$ level in hydrochloric acid. Stirring during plating and stripping was unnecessary because of the enhanced mass transport that takes place at microelectrodes. Schulze and Frenzel [93] cited the low background currents obtained on carbon fibres, and their facility for use in microvolumes of sample solution as being advantageous for stripping analysis.

Voltammetry in flowing systems

The relatively small distance that the diffusion zone around a microelectrode extends into solution generally isolates the faradaic current from convection in solution. As a consequence of this, carbon fibre electrodes should make near-ideal detectors in flowing systems. The current at the electrode should be independent of flow rate, and thus much less susceptible to the pulsing that can arise in pumped streams. Such an amperometric

electrode, independent of flow rate, was described by Caudill et al. [59]. The electrode consisted of 100 carbon-fibre micro-disc electrodes, each of 5-μm radius; each disc was located at least 6 diameters away from its nearest neighbour, to ensure that each diffusion zone operated independently; the currents from the microelectrodes were summed. The authors were able to demonstrate that an improved signal-to-noise ratio was obtained (compared to a conventional glass-like carbon electrode) at positive potentials. At these potentials, the oxidation of buffer impurities gave rise to noisy baselines at glass-like carbon because of the strokes of the liquid chromatography pump; the microelectrode array was much less susceptible to this noise. However, the authors noted that the microelectrode array itself generated noise, that appeared to arise from flow irregularities. These irregularities were caused by microscopic flaws in the detector surface. An individual carbon-fibre electrode has been used as a detector for liquid chromatography [94]; the compounds detected were ascorbic acid, catechol and 4-methylcatechol.

Fundamental electrochemical studies

Several features of the electrochemistry at carbon fibre electrodes lend themselves to more fundamental studies. Principal amongst these is the enhanced mass-transfer rate arising from the significant steady-state component. Swan [65] investigated a wide range of microelectrodes purely from this point of view. Thus in the study of heterogeneous rate constants, methods requiring forced convective stirring or short-time measurements were supplemented by measurements at carbon fibre and other microelectrodes. It was shown that, for the determination of a heterogeneous rate constant, an upper limit of 0.1 cm s^{-1} at a 1-μm microelectrode was practicable. A similar point was made by Scharifker and Hills [66] in their paper describing the determination of the kinetics of the homogeneous redox reaction $Fe(CN)_6^{3-} + e^- \rightarrow Fe(CN)_6^{4-}$, and the heterogeneous electrochemical nucleation of metals by means of the $Hg_2^{+} + 2e^- \rightarrow 2\ Hg$ system. These authors asserted that "the results obtained with the redox reaction show that microelectrodes constitute a practical alternative to more complicated designs of electrodes with enhanced mass transfer, such as rotating disc electrodes or tubular electrodes".

Microelectrodes have been used for ultrafast voltammetry in conventional electrolytes [95]. The reduced double-layer capacitance and negligible *IR* drop observed at microelectrodes permitted the use of scan rates up to 20000 V s^{-1}, with minimal distortion of the *I/E* curves. In the same publication, the authors described voltammetry in resistive solutions such as acetonitrile with tetraalkylammonium perchlorate. A steady-state limiting current with minimal *IR* distortion was obtained for scan rates below 50 mV s^{-1}.

The number of electrons (n) involved in an electrode reaction has been evaluated by comparing the current vs. time transients obtained in chronoamperometry at micro and conventional electrodes [96]. The method was used for the determination of the number of electrons involved in the

electrode reaction of sulphur in dimethylsulphoxide. The authors pointed out that this method has distinct advantages over conventional coulometric determination of n values for systems where catalytic or disproportionation reactions take place after electron transfer.

Spectroelectrochemical studies at microelectrodes benefit from the relatively small currents obtained [16]. Lower demands are placed on the potentiostat, a low cell constant is obtained, less error from solution resistance occurs, and there is improved capability for making measurements involving fast reactions. The higher diffusional flux of reactants and the faster return to initial conditions render time-averaging more practicable because much higher duty cycles can be used. In addition, the diffusion zone around the electrode rapidly dilutes the products of the charge-transfer reaction and thus suppresses the second-order reactions of electrogenerated species.

Wightman [7] has pointed out that one of the original uses of microelectrodes was for the accurate determination of diffusion coefficients. Thus the potential of the electrode can be pulsed to a region in which the surface concentration of the species being studied is zero. The current is then measured over a period corresponding to the steady-state term of Eqn. 2. The decreased significance of convection on the current leads to a more accurate determination of the diffusion coefficient.

INSTRUMENTATION

The point has been made already that the lower capacitative charging currents and relatively better faradaic currents that are obtained at microelectrodes place less demand on potentiostats [16]. A full discussion of this in the context of the electronics of electrochemistry is outwith the scope of this review. However, it is pertinent to consider certain features of cell and instrument design arising from the electrochemical behaviour of microelectrodes. Intuitively, it might be said that the decreased value of the current I, should lead to a decreased value of IR, and so it should be possible to use a simple two-electrode cell geometry. Such a cell has been described [66]. For a two-electrode system, where the second electrode is much larger in area than the working electrode as in old-style polarographic systems, and is placed at an effectively infinite distance from the microelectrode, the total cell resistance R is given by $R = 1/(2\pi Kr)$, where K is the specific conductivity of the electrolyte. Thus the resistance increases as the radius of the microelectrode is made smaller, but the resistance per unit area of electroactive surface is low, and becomes lower with decreasing electrode radius. In fact, it has been calculated [66] that at microelectrodes the resistance per unit area is smaller than the uncompensated resistance between the Luggin capillary and the working electrode in conventional three-electrode cells. A large platinum foil or mercury pool was used as the second electrode. Millar [97] adopted the time-honoured method of employing a second electrode of the same material; in this case a carbon-fibre brush electrode was used.

The entire electrochemical set-up may be simplified to the point shown in Fig. 2. The input waveform is connected directly to the secondary electrode, and the resulting cell current is measured at the working electrode. The current follower, although a simple circuit, requires some careful thought. It must be positioned as close to the working electrode as possible to avoid picking up noise from extraneous sources. The operational amplifier should be a high-input impedance FET device with a low-input bias current (typically less than 0.1 pA) and a low voltage offset. The feedback resistor should not be carbon because this type can give rise to considerable noise in low-current applications: wirewound resistors are preferable, or best of all glass-encapsulated film resistors should be used.

A complete instrument design for pulse voltammetry at microelectrodes has been described by Ewing et al. [98]. This instrument provides for direct readout of the difference current obtained by subtracting the current measured during the back-step of double potential-step chronoamperometry, from the current measured during the forward step. This difference current has been shown [8] to be the faradaic signal corrected for the residual current. The instrument also gives a differential output. The duration between pulses, and the pulse width are easily alterable. These latter factors mean that the electrode may be held at a resting potential for a considerable part of the measurement cycle, thus minimizing the surface changes that might otherwise occur. Although the instrument has been designed to operate with a typical low-noise potentiostat, there seems to be no reason why it should not be used with a simple two-electrode system.

Other electrochemical applications

An area that is currently drawing interest is the application of carbon fibres for the electrowinning of trace toxic metals from effluents. Fleet and Das Gupta [99] were the first to explore this possibility when they constructed an electrochemical reactor with carbon fibre as the electrode material. Specific advantages to using this material were thought to be that it has a large surface area of 2.6×10^6 cm^2 g^{-1} for 8—10-μm diameter fibres, a hard vitreous surface, and a good working window from −1.4 to +1.2 V vs. SCE.

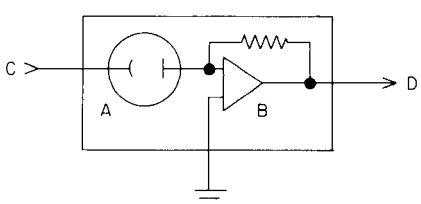

Fig. 2. Block diagram of minimal instrumentation for voltammetric studies at microelectrodes: (A) two-electrode cell; (B) current follower; (C) input for waveform generator; (D) output to recorder or other measuring device.

Conclusions

Initially, many of the practical applications of carbon fibre electrodes outstripped the theoretical understanding of their mode of action. Now, although there are well-developed theories to cover some areas of voltammetric, chronoamperometric and chronopotentiometric measurements, the performance of these electrodes is still poorly understood with respect to their surface conditions. The surface chemistry of carbon fibres, and its role in electrochemical reactions is an open field for research, as is the effect of bonding foreign molecules to these surface functional groups. The great diversity of carbon fibre types have by no means been exhaustively explored: valid intercomparisons have been made for very few fibres. Since the first analytical use of carbon fibre electrodes by Jennings in 1975 over 50 papers have been published in which these electrodes have played a prominent analytical role. These papers have originated from North America, Europe and Greece. This promising electrode material already plays a significant role in microelectroanalytical chemistry.

The author gratefully acknowledges the helpful comments and criticisms of Dr. V. K. Jennings (Lanchester Polytechnic).

REFERENCES

1 W. E. van der Linden and J. W. Dieker, Anal. Chim. Acta, 119 (1980) 1.
2 V. J. Jennings and T. D. Bailey, Anal. Chim. Acta, 84 (1976) 61.
3 V. J. Jennings, A. Dodson and R. J. Eastman, Anal. Chim. Acta, 76 (1975) 143.
4 V. J. Jennings and P. Pearson, Nature (London), 31 (1975) 256.
5 V. J. Jennings and P. Pearson, Anal. Chim. Acta, 82 (1976) 223.
6 V. J. Jennings, Analyst, 106 (1981) 1344.
7 R. M. Wightman, Anal. Chem., 53 (1981) 1125A.
8 M. A. Dayton, J. C. Brown, K. J. Stutts and R. M. Wightman, Anal. Chem., 52 (1980) 946.
9 R. Bacon and M. Tang, Carbon, 2 (1964) 221.
10 W. Watt, L. N. Phillips and W. Johnson, Brit. Pat. No. 1, 110, 791 (1964).
11 International Committee for the Characterization and Terminology of Carbon, Carbon, 20 (1982) 445.
12 B. Harris, in M. Langley (Ed.), Carbon Fibres in Engineering, McGraw-Hill, London, 1973, pp. 1—45.
13 J. B. Donnet and R. C. Bansal, in Carbon Fibres, International Fibre Science and Technology Series, M. Dekker, New York, 1984.
14 A. Fourdeaux, R. Perret and W. Ruland, in Carbon Fibres: Their Composites and Applications, Proceedings of the International Conference of the Plastics Institute, London, 1971.
15 J. V. Sharp and S. G. Burnay, in Carbon Fibres, Their Composites and Applications, Proceedings of the International Conference of the Plastics Institute, London, 1971.
16 R. S. Robinson and R. L. McCreery, Anal. Chem., 57 (1981) 997.
17 S. Otani, Carbon, 3 (1965) 31.
18 P. Kwizera, M. S. Dresselhaus, J. S. Perkins and C. R. Desper, in Extended Abstracts of 15th Carbon Conference, University of Pennsylvania, 1981, p. 102.
19 H. M. Hawthorn, in Carbon Fibres: Their Composites and Applications, Proceedings of the International Conference of the Plastics Institute, London, 1971.

20 R. M. Wightman, I. Strope, P. M. Plotsky and R. N. Adams, Nature (London), 262 (1976) 145.
21 M. Buda, F. Gonon, R. Cespuglio, M. Jouvet and J. F. Pujol, Hebd. Seances. Acad. Sci., 290 (1980) 431.
22 F. Gonon, M. Buda, R. Cespuglio, M. Jouvet and J. F. Pujol, Nature (London), 386 (1980) 902.
23 F. Gonon, C. M. Fombarlet, M. J. Buda and J. F. Pujol, Anal. Chem., 53 (1981) 1386.
24 M. P. Brazell and C. A. Marsden, Br. J. Pharmacol., 75 (1985) 539.
25 T. E. Edmonds and Guoliang Ji, Anal. Chim. Acta, 151 (1983) 99.
26 V. J. Jennings, in W. Franklyn Smyth (Ed.), Electroanalysis in Hygiene, Environmental, Clinical and Pharmacological Chemistry, Elsevier, Amsterdam, 1980, p. 199.
27 R. F. Strickland-Constable, Trans. Faraday Soc., 34 (1983) 1024.
28 B. Steenberg, Adsorption and Exchange of Ions on Activated Charcoal, Almqvist and Wishells, Uppsala, 1944.
29 V. A. Garten and D. E. Weiss, Aust. J. Chem., 8 (1955) 68.
30 R. E. Panzer and P. J. Elving, Electrochim. Acta, 20 (1975) 635.
31 J. P. Randin, in A. J. Bard (Ed.), Encyclopaedia of Electrochemistry of the Elements, Vol. 7, Dekker, New York, 1976, p. 22.
32 B. D. Epstein, E. Dalle-Molle and J. S. Mattson, Carbon, 9 (1971) 609.
33 K. F. Blurton, Electrochim. Acta, 18 (1973) 869.
34 K. Kinoshita and J. A. S. Bett, Carbon, 11 (1973) 403.
35 L. Horner and W. Brich, Justus Liebigs Ann. Chem., (1977) 1354.
36 H. P. Boehm, Adv. Catal., 16 (1966) 179.
37 A. M. Yacynych and T. Kuwana, Anal. Chem., 50 (1978) 640.
38 H. P. Boehm, E. Diehl, W. Heck and R. Sappok, Angew. Chem. Int. Ed. Engl., 3 (1964) 669.
39 B. F. Watkins, J. R. Behling, E. Kariv and L. L. Miller, J. Am. Chem. Soc., 97 (1975) 3549.
40 C. M. Ellioth and R. W. Murray, Anal. Chem., 48 (1976) 1247.
41 V. L. Snoeyink and W. J. Weber, Prog. Sur. Membr. Sci., 5 (1972) 63.
42 B. E. Firth, L. L. Miller, M. Milani, T. Rogers, J. Lennox and R. W. Murray, J. Am. Chem. Soc., 98 (1976) 8271.
43 G. G. Fedorov, Yu. A. Zarif'yants and V. F. Kisilev, Dokl. Akad. Nauk SSSR, 139 (1961) 1166.
44 H. Gunasingham and B. Fleet, Analyst, 107 (1982) 896.
45 J. M. Thomas, E. M. Evans, M. Barber and P. Swift, Trans. Faraday Soc., 67 (1971) 1875.
46 J. B. Donnet and P. Ehrenberger, Carbon, 15 (1977) 143.
47 A. Ishitani, Carbon, 19 (1981) 269.
48 E. Theodoridou, J. O. Besenhard and H. P. Fritz, J. Electroanal. Chem., 122 (1981) 67.
49 A. Proctor and P. M. A. Sherwood, Carbon, 21 (1983) 53.
50 R. D. Snell and A. G. Keenan, Chem. Soc. Rev., 8 (1979) 259.
51 E. Theodoridou, J. O. Besenhard and H. P. Fritz, J. Electroanal. Chem., 124 (1981) 87.
52 G. Picq, R. Reeves, P. Ribourg and P. Vennereau, J. Electroanal. Chem., 162 (1984) 225.
53 R. C. Engstrom and V. A. Strasser, Anal. Chem., 56 (1984) 136.
54 J. F. Rusling, Anal. Chem., 56 (1984) 578.
55 R. W. Murray, in A. J. Bard (Ed.), Electroanalytical Chemistry, Vol. 13, Dekker, New York, 1983.
56 M. Armstrong-James and J. Millar, J. Neurosci. Methods, 1 (1979) 279.
57 C. W. Anderson and M. R. Cushman, J. Neurosci. Methods, 4 (1981) 435.
58 M. R. Cushman, B. G. Bennett and C. W. Anderson, Anal. Chim. Acta, 130 (1981) 323.
59 W. L. Caudill, J. O. Howell and R. M. Wightman, Anal. Chem., 54 (1982) 2532.
60 S. Latif, M.Sc. Dissertation, Loughborough University of Technology, 1983.

61 K. Aoki, K. Akimoto, K. Tokuda, H. Matsuda and J. Osteryoung, J. Electroanal. Chem., 182 (1985) 281.
62 Z. Galus, J. O. Schenk and R. N. Adams, J. Electroanal. Chem., 135 (1982) 1.
63 E. Budevskii and G. Desimirov, Dokl. Akad. Nauk SSSR, 149 (1963) 120.
64 M. A. Dayton, A. G. Ewing and R. M. Wightman, Anal. Chem., 52 (1980) 2392.
65 D. N. Swan, Ph.D. Thesis, University of Southampton, 1980.
66 B. Sharifker and G. Hills, J. Electroanal. Chem., 130 (1981) 81.
67 I. Shain, K. J. Martin and J. W. Ross, J. Phys. Chem., 65 (1961) 259.
68 J. Delmastro and D. E. Smith, J. Phys. Chem., 71 (1967) 2138.
69 K. Aoki, K. Honda, K. Tokuda and H. Matsuda, J. Electroanal. Chem., 182 (1985) 267.
70 M. Armstrong-James, K. Fox, Z. L. Kruk and J. Millar, J. Neurosci. Methods, 4 (1981) 385.
71 M. Armstrong-James and K. Fox, J. Physiol. London, 335 (1982) 427.
72 J. L. Ponchon, R. Cespuglio, F. Gonon, M. Jouvet and J. F. Pujol, Anal. Chem., 51 (1979) 1483.
73 M. A. Dayton, A. G. Ewing and R. M. Wightman, Eur. J. Pharmacol., 75 (1981) 141.
74 M. P. Brazell and C. A. Marsden, Brain Res., 249 (1982) 167.
75 F. Gonon, M. Buda, R. Cespuglio, M. Jouvet and J. F. Pujol, Brain Res., 223 (1981) 69.
76 F. Gonon, F. Navarre and M. Buda, Anal. Chem., 56 (1984) 575.
77 R. N. Adams and C. A. Marsden, in L. Iverson, S. D. Iverson and S. N. Snyder (Eds.), Handbook of Psychopharmacology, Plenum Press, New York, 1982, pp. 1—74.
78 M. Armstrong-James, J. Millar and Z. Kruk, Nature (London), 288 (1980) 181.
79 M. Armstrong-James and J. Millar, J. Neurosci. Methods, 1 (1979) 279.
80 M. Armstrong-James and J. Millar, J. Neurosci. Methods, 2 (1980) 431.
81 K. Fox, M. Armstrong-James and J. Millar, J. Neurosci. Methods, 3 (1983) 37.
82 J. Millar, M. Armstrong-James and Z. Kruk, Brain Res., 205 (1981) 419.
83 Z. Kruk, M. Armstrong-James and J. Millar, Life Sci., 27 (1980) 2093.
84 J. Mos, P. J. Mostert, A. M. Van der Poel, W. Meelis and M. R. Kruk, paper presented at 1st British Meeting on Electrochemical Detection in Pharmacology and Neurochemistry, Nottingham, 1982.
85 C. Forni, J. Neurosci. Methods, 5 (1982) 167.
86 J. A. Stamford, paper presented at 1st British Meeting on Electrochemical Detection in Pharmacology and Neurochemistry, Nottingham, 1982.
87 M. A. Dayton, A. G. Ewing and R. M. Wightman, J. Electroanal. Chem., 146 (1983) 189.
88 P. D. Jannakoudakis, P. Karakinas and E. Theodoridou, Z. Phys. Chem., 129 (1982) 197, 130 (1982) 49, 131 (1982) 89.
89 G. G. Muhtyanu and I. I. Vataman, Izv. Akad. Nauk. Mold. SSR, Ser. Biol. Khim. Nauk., 3 (1982) 56.
90 A. N. Doronin and G. G. Muhtyanu, Zh. Anal. Khim., 39 (1984) 607.
91 T. E. Edmonds, Guogang Pu and T. S. West, Anal. Chim. Acta, 120 (1980) 41.
92 V. J. Jennings and J. E. Morgan, Anal. Proc., 20 (1983) 276; Analyst, 110 (1984) 121.
93 G. Schulze and W. Frenzel, Anal. Chim. Acta, 159 (1984) 95.
94 L. A. Knecht, E. J. Guthrie and J. W. Jorgenson, Anal. Chem., 56 (1984) 479.
95 J. O. Howell and R. M. Wightman, Anal. Chem., 56 (1984) 524.
96 A. S. Baranski, W. R. Fawcett and C. M. Gilbert, Anal. Chem., 57 (1985) 166.
97 J. Millar, paper presented at 1st British Meeting on Electrochemical Detection in Pharmacology and Neurochemistry, Nottingham, 1982.
98 A. G. Ewing, R. Withnell and R. M. Wightman, Rev. Sci. Instrum., 52 (1981) 454.
99 B. Fleet and S. Das Gupta, Nature (London), 263 (1976) 123.

Analytica Chimica Acta, 175 (1985) 23—35
Elsevier Science Publishers B.V., Amsterdam — Printed in The Netherlands

POLAROGRAPHIC DETECTION BY REVERSE-PULSE AMPEROMETRY IN CATION-EXCHANGE CHROMATOGRAPHY WITHOUT INTERFERENCE FROM DISSOLVED OXYGEN

TAISUNG HSI[a] and DENNIS C. JOHNSON*
Department of Chemistry, Iowa State University, Ames, IA 50011 (U.S.A.)
(Received 8th April 1985)

SUMMARY

Reverse-pulse amperometry (r.p.a.) at a static dropping mercury electrode (SDME) is applied for detection in high-performance cation-exchange chromatography for Cu^{2+}, Zn^{2+}, Ni^{2+}, Pb^{2+}, Cd^{2+} and Fe^{2+} using a tartrate eluent (pH 3.5—4.5). The technique of r.p.a. as applied eliminates the need for removal of dissolved oxygen because the anodic signals for oxidation of the reduction products are measured at a potential at which oxygen is not electroactive. Typical detection limits (S/N = 2) for a 100-μl sample are illustrated by the values 13 $\mu g\ l^{-1}$ Zn^{2+} (1.3 ng) and 64 $\mu g\ l^{-1}$ Cu^{2+} (6.4 ng). The detection limits are decreased by ca. 2 orders of magnitude by using preconcentration from a 10.0-ml sample on a cation-exchange fore-column.

The large activation overpotential for cathodic evolution of hydrogen at a dropping mercury electrode (DME) is advantageous in making possible the cathodic polarographic detection of numerous transition and heavy-metal cations in aqueous solutions. However, polarographic detection in liquid chromatography (l.c.) is impaired by the electroactivity of dissolved oxygen over ca. 70% of the available potential range, and the great difficulty of maintaining a suitably low level of oxygen in the chromatographic effluent. Numerous devices and procedures have been described for removal of dissolved oxygen from eluents and effluents [1], including enclosure of the entire l.c. system within a nitrogen atmosphere. Many of these techniques are reasonably effective but not without annoying inconveniences. The procedure of Bratin and Kissinger [2] is judged to be most efficient for l.c. if deaeration is necessary.

For the majority of cases (Co^{2+} is a known exception), the electroanalytical technique of reverse-pulse amperometry (r.p.a.) at a mercury electrode can be applied conveniently to avoid interference from dissolved oxygen even for air-saturated solutions [3]. The theory of reverse-pulse polarography (r.p.p.) has been described adequately for reversible and irreversible redox systems in

[a]Present address: Department of Chemistry, National Sun Yat-Sen University, Kaohsiung, Taiwan 800.

0003-2670/85/$03.30

conventional polarographic cells [4, 5]. In brief, detection of reducible metallic ions is achieved by use of a potential waveform which applies a large negative initial potential (E_i) during the majority of the drop lifetime, to achieve the transport-limited reduction of the analyte, followed by a positive step of the potential to a final value (E_f) near the anodic limit for mercury, at which the anodic analytical signal for oxidation of the cathodic product is measured without reaction of dissolved oxygen. Hence, cathodically active analytes are detected indirectly by way of an anodic reaction. Detection limits for r.p.p. are quite similar to those for normal pulse polarography (n.p.p.).

A quantitative theory of r.p.a. (i.e., r.p.p. at constant values of potential) at a DME or SDME in a fluid stream has not been developed exactly because of (i) the absence of an accurate description of the hydrodynamics at a partially shielded sphere in a stream, and (ii) the virtual impossibility at present of reproducing exactly the hydrodynamic conditions after dismantling and reassembling the detector system. However, a qualitative examination of the theory is worthwhile to note dramatic differences in the expected response depending on whether the cathodic product is dissolved in the mercury electrode or the electrolyte solution. The usual assumptions [5] are made: (i) equal values of diffusion coefficients (D) for reactant and product, (ii) the initial period of the potential waveform is much greater than the final (the "pulse") period, i.e., $t_i \gg t_p$, and (iii) the pulse period is very short, i.e., $t_p \to 0$. For the general reaction

$$\mathrm{ox} + ne^- \to \mathrm{red} \qquad (1)$$

the balance of fluxes at the electrode surface ($x = 0$) corresponding to the conclusion of the initial time period ($t = t_i$) can be expressed as

$$D(\mathrm{d}C_{ox}/\mathrm{d}x)_{x=0,t_i} = -D(\mathrm{d}C_{red}/\mathrm{d}x)_{x=0,t_i}$$

From the familiar Nernstian representation of the concentration gradient based on the distance (δ) equivalent to the thickness of the diffusion layer,

$$(\mathrm{d}C_{ox}/\mathrm{d}x)_{x=0,t_i} = [(C^b_{ox} - C^s_{ox})/\delta_{ox}]_{t_i}$$

and

$$(\mathrm{d}C_{red}/\mathrm{d}x)_{x=0,t_i} = [(C^b_{red} - C^s_{red})/\delta_{red}]_{t_i}$$

where the superscripts b and s represent the bulk ($x \to \infty$) and surface ($x = 0$) values of the designated concentrations, respectively. It is stipulated that $C^b_{red} = 0$, whether pertaining to an ionic product in the electrolyte solution or an amalgamated product in the mercury drop. Hence, for the transport-limited cathodic reaction (i.e., $C^s_{ox} = 0$),

$$C^s_{red,t_i} = (\delta_{red}/\delta_{ox})_{t_i} C^b_{ox} \qquad (2)$$

It should be noted that δ is taken as positive whether corresponding to the mercury or the aqueous phases. Detection of the limiting anodic signal at

the end of the pulse period (t_p) corresponds to the reverse of the reaction in Eqn. 1. Provided that $t_p \ll t_i$, so that $\delta_{red,t_p} \ll \delta_{red,t_i}$, Eqn. 2 is a good approximation for the effective "bulk" concentration of reduction products (red) at t_p and

$$C^b_{red,t_p} = (\delta_{red}/\delta_{ox})_{t_i} C^b_{ox} \quad (3)$$

The limiting current is, therefore,

$$i_{lim} = nFAD(\delta_{red,t_i}/\delta_{ox,t_i})(C^b_{ox}/\delta_{red,t_p}) \quad (4)$$

For the case in which red is dissolved in the mercury electrode,

$$\delta_{red,t_i}/\delta_{red,t_p} = (t_i/t_p)^{1/2} \quad (5)$$

and

$$i_{lim} = nFAD(t_i/t_p)^{1/2}(C^b_{ox}/\delta_{ox,t_i}) \quad (6)$$

The value of δ_{ox,t_i} is a function of the fluid flow rate (v_f), although this dependence is not known a priori. Hence, i_{lim} is expected to be a function of v_f when red is amalgamated.

For the case when red is ionic and dissolved in the diffusion layer,

$$\delta_{red,t_i} = \delta_{ox,t_i}$$

and

$$i_{lim} = nFAD(C^b_{ox}/\delta_{red,t_p}) \quad (7)$$

For very small t_p [4], $\delta_{red,t_p} = (\pi D t_p)^{1/2}$, and i_{lim} should be unaffected by variation of v_f. For the case in which the analyte ion is already in the reduced state, anodic detection is also predicted by Eqn. 7, which corresponds to n.p.p.

EXPERIMENTAL

Instrumentation

Current/potential (i/E) curves were obtained with the Model PAR 174A Polarographic Analyzer and PAR 303 static dropping mercury electrode (SDME mode, small drop size), from EG&G Princeton Applied Research, and an Omnigraphic 2000 X-Y recorder (Houston Instruments, Bellaire, TX). Flow-injection and chromatographic data were obtained with the PAR 174A and PAR 310 chromatographic detector and a SR-204 stripchart recorder (Heath-Schlumberger Instruments). Satisfactory performance of the Models 303 and 310 mercury electrodes required careful siliconization of the glass capillary, as discussed by Oehme [6], with freshly prepared solutions of 5% dichlorodimethylsilane in carbon tetrachloride (Aldrich Chemical Co.). Electrode potentials were measured with respect to a saturated silver chloride reference electrode (SSCE).

The flow-injection system was assembled from Altex valves, teflon tubing (0.8 mm i.d. × 1.5 mm o.d.), and tube-end fittings and couplers from Rainin

Instrument Co. (Woburn, MA). The capacity of the sample loop (V_s) of the pneumatically actuated sample-injection valve was found by acid-base titrations to be 100.0 μl. The pump was a Minipuls-2 peristaltic pump (Gilson Medical Electronics) with polyvinyl chloride pump tubing (0.76 mm i.d.). The pulse damper was of our own design consisting of an inverted glass T-tube (2 mm i.d.), containing an air bubble (ca. 0.5 ml) in the standpipe, followed by an adjustable needle valve for generating back-pressure. Typically, a back-pressure of ca. 1 atm above ambient (i.e., air bubble decreased by 50%) was sufficient to eliminate pulsations of the carrier stream.

The liquid chromatograph was assembled starting from a single-head Milton Roy minipump (0—6000 psi. 16—160 ml h^{-1}) from Laboratory Data Control (Riviera Beach, FL). The injection valve was a Valco 9080 (Laboratory Data Control) with a 100-μl sample loop. The cation-exchange separator column (4 mm i.d. × 50 mm) was packed with Durrum DC-4A sulfonated strong cation-exchange resin (9 ± 0.5 μm, 5 meq g^{-1}; Durrum Chemicals Corp., Palo Alto, CA) packed by an upflow slurry method [1]. For trace analysis of power-plant water, a glass preconcentrator column (2 mm i.d. × 50 mm) was used which was slurry-packed with Dowex 50W-X8 cation-exchange resin (44—60 μm; Dow Chemical Co., Midland, MI). The preconcentrator column was loaded by pumping 10.0 ml of sample at a rate of 1.0 ml min^{-1} with a Gilson peristaltic pump and was then inserted into the eluent stream by manual valve action. Interconnection of components was by teflon tubing (0.3 mm i.d.) using Omnifit gripper fittings which avoided need for flanging the tube ends. Eluents and samples were filtered through a Nylon-66 membrane filter (0.45 μm) from Rainin Instruments Co. (Emeryville, CA). Neither the chromatographic eluents nor the samples were deaerated.

Chemicals

All chemicals were analytical-reagent grade (Mallinckrodt, Fisher Scientific Co., or J. J. Baker Chemical Co.) and were used as received. Water was triply distilled with demineralization after the first distillation; the second distillation was from an alkaline solution of permanganate (0.01 M $KMnO_4$/0.1 M KOH), and the third distillation was from a slightly acidic solution (ca. 2 ml l^{-1} concentrated sulfuric acid). Water was stored in a quartz vessel under nitrogen. All solutions of Fe^{3+} in tartrate media were prepared and used under red light to prevent undesired photoreduction caused by u.v.-visible radiation.

Samples

Ground-water samples were acidified to pH 1.6 with concentrated hydrochloric acid (ca. 2 ml l^{-1}) and stored in polyethylene bottles. Just prior to analysis, each sample was filtered through a 0.45-μm membrane filter (Rainin), a 40.0-ml aliquot was transferred to a 50.0-ml volumetric flask, 4.0 ml of 10% sodium acetate and 1.0 ml of 5% (w/v) hydroxylammonium chloride was added to reduce Fe^{3+} to Fe^{2+}, and the mixture was diluted to volume. Samples of power-plant water were stored in polyethylene bottles which had been

rinsed several times with fresh portions of the sample. Samples were filtered prior to analysis and 10.0-ml aliquots were preconcentrated as described earlier. Samples of power-plant water were not treated with the reducing agent because of trace levels of Zn^{2+} and Fe^{2+} present in the sodium acetate; furthermore, additives in boiler water produce a reducing environment and Fe^{3+} is not expected to be present.

RESULTS AND DISCUSSION

Current/potential curves

Current/potential (i/E) curves illustrating the response of reverse-pulse polarography (r.p.p.) in air-saturated and oxygen-free solutions are shown for Cd^{2+} in Fig. 1; the experimental procedures were described previously [3]. The response for r.p.a. can be deduced immediately from these curves for r.p.p. because the amperometric technique corresponds quite simply to the case of constant values for the initial potential (E_i) and the pulse amplitude (ΔE), with detection occurring at $E_f = E_i + \Delta E$. Dissolved oxygen is not detected by direct faradaic reaction in r.p.p. or r.p.a. at $E_f > 0.0$ V vs. SSCE. Analytical interference by oxygen can result only if there is a significant rate for the oxidation of red by oxygen or the hydrogen peroxide produced in the first cathodic wave for oxygen ($0.0 > E_i > -1.1$ V). Oxidation by oxygen could be significant for ionic reduction products, e.g., Fe^{2+}; however, for $t_p = 0$, $C_{O_2,t_p} = 0$ within the short distance δ_{red,t_p}. Provided that full analytical resolution of a mixture is achieved by the chromatographic column, r.p.a. likely will be applied with $E_i \ll -1.1$ V and possible interference from hydrogen peroxide can be avoided completely.

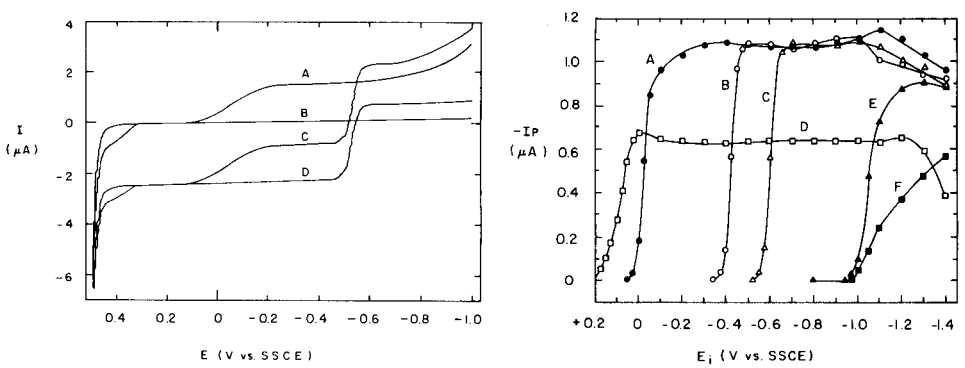

Fig. 1. Reverse-pulse polarograms in static solution. Conditions: PAR 303, (SDME, small); $E_i = -1.0$ V vs. SSCE, $\tau = 1$ s, $\phi = 5$ mV s^{-1}; 0.01 M HNO_3/0.10 M KNO_3. Curves: (A) air-saturated; (B) O_2-free; (C) 0.20 mM Cd^{2+}, air-saturated; (D) 0.20 mM Cd^{2+}, O_2-free. (Taken from ref. 3.)

Fig. 2. Hydrodynamic reverse-pulse polarograms (I_p/E_i) by flow-injection detection. Conditions: $E_f = +0.20$ V vs. SSCE, $\tau = 2$ s, air-saturated 0.10 M sodium hydrogentartrate at pH 4.5; $v_f = 0.61$ ml min^{-1}, $V_s = 190$ μl, $V_R = 330$ μl. Curves: (A) 0.10 mM Cu^{2+}; (B) 0.10 mM Pb^{2+}; (C) 0.10 mM Cd^{2+}; (D) 0.30 mM Fe^{3+}; (E) 0.10 mM Zn^{2+}; (F) 0.20 mM Ni^{2+}.

Hydrodynamic i/E curves were obtained by the flow-injection technique as plots of anodic peak current (I_p) for r.p.a. plotted as a function of E_i and are shown in Fig. 2. The electrolyte was 0.10 M sodium hydrogentartrate adjusted to pH 4.5 and detection was at $E_f = +0.20$ V. Metal ions were prepared with 0.10 M sodium hydrogentartrate at pH 4.5. The "dead volume" (i.e., retention volume) between injector and detector is V_R in the legend. The response for all cations except Ni^{2+} was approximately as expected for reversible reactions, i.e., $E_{1/2} \approx E^\circ$. The irreversibility of the nickel stripping reaction has been noted [7—9]. The i/E curves for Ni^{2+} by n.p.p. and r.p.p. are shown in Fig. 3. Although it is clear that a transport-limited cathodic wave is not obtained by n.p.p., an anodic current plateau is obtained for $E_f = 0.1 - 0.3$ V and $E_i < -1.2$ V by r.p.p. Frankly, an anodic plateau was not expected for Ni^{2+} because of the low solubility of nickel in mercury (4.8×10^{-5}% w/w) [9]. For insoluble products of reactions at E_i, e.g., Hg_2S(s), it was observed that a peaked response rather than a plateau is obtained for the stripping process in r.p.p. This occurs because the stripping process is not controlled by diffusion in the amalgam; and, for a fixed time prior to current sampling, the current goes to zero for $E_f \gg E_{1/2}$. Apparently in the case of Ni^{2+}, the solubility of Ni^0 in Hg is sufficient to yield an anodic plateau current and Ni^{2+} is easily detected by r.p.a.

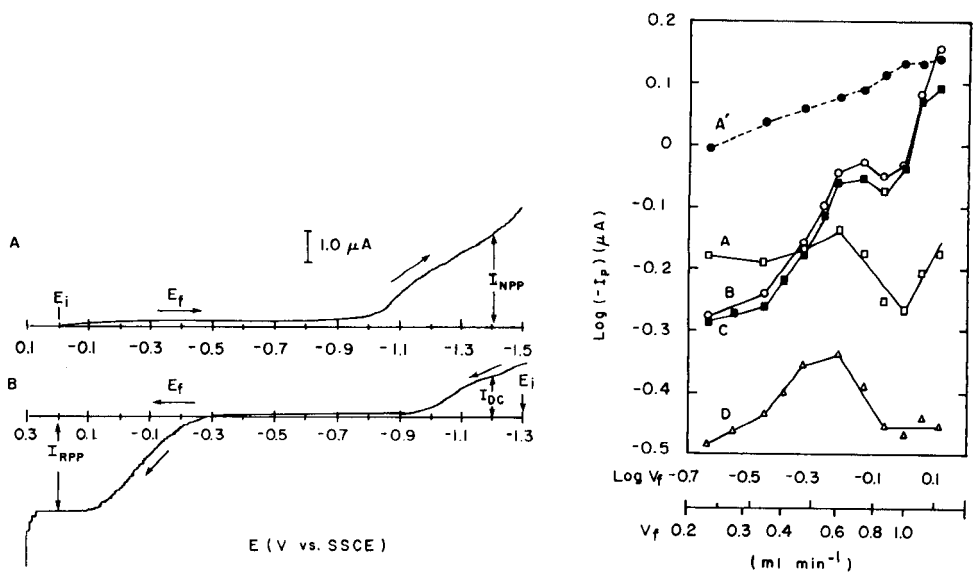

Fig. 3. Current/potential response for Ni^{2+} by n.p.p. and r.p.p. in static solution. Conditions: O_2-free 0.10 M sodium hydrogentartrate at pH 4.5, 1.0 mM Ni^{2+}; $\tau = 1$ s, $\phi = 10$ mV s^{-1}. Curves: (A) n.p.p., $E_i = 0.0$ V vs. SSCE; (B) r.p.p., $E_i = -1.3$ V vs. SSCE.

Fig. 4. Log ($-I_p$) vs. log v_f for r.p.a. at the SDME. (A—D) R.p.p. detection: $E_i = -1.30$ V, $E_f = +0.2$ V vs. SSCE, $\tau = 2$ s; air-saturated 0.10 M sodium hydrogentartrate at pH 4.5; $V_s = 190$ μl, $V_R = 330$ μl. (A') Photometric detection: 0.40 mM $(FeSCN)^{2+}$, peak signal in absorbance. Curves: (A) 0.40 mM Fe^{3+}; (B) 0.10 mM Cd^{2+}; (C) 0.10 mM Cu^{2+}; (D) 0.20 mM Ni^{2+}.

Variation of v_f

The dependence of I_p on v_f for r.p.a. applied to a flow-injection system is expected to be described empirically by

$$I_p = k v_f^{\alpha+\beta} C_{ox}^b \quad (8)$$

where k is a constant, C^b is the analytical concentration of the sample, and the fractional exponents α and β represent the separate contributions from the dependence of dispersion and detection, respectively [10]. The term α is a function of the flow-injection system and can be evaluated by photometric detection; β is characteristic of the hydrodynamic condition at the detector and can be determined from the slope of a plot of $\log I_p$ vs. $\log v_f$ with correction for the contribution of α. The plots of $\log I_p$ vs. $\log v_f$ for four metal ions are shown in Fig. 4. Included is the plot for photometric detection for injections of the Fe(III)/tartrate complex. For each metal detected by r.p.a. there is a significant drop in sensitivity in the approximate range $0.6 < v_f < 1.0$ ml min^{-1}. It is concluded that this corresponds to a region of hydrodynamic transition between two distinct patterns of convection around the electrode. Such a transition is to be expected for objects drastically interrupting the laminar flow of a stream [11]. The value of α in Eqn. 8 was found by photometric detection to be ca. 0.20. Because of the absence of a clearly monotonic relationship between I_p and v_f over a substantial range of v_f, no further effort was given to establish the value of β in Eqn. 8. A value of 0.6 ml min^{-1} was chosen for v_f for all further studies with flow injection and liquid chromatography to maximize sensitivity. For slightly higher values of v_f, unacceptable fluctuations occurred in I_p, probably because of instability in the convective pattern.

Variation of t_i

Sensitivity of r.p.a. is expected to increase with increasing t_i, according to Eqn. 6, for all metal ions having amalgamated reduction products. Plots of $\log I_p$ vs. $\log t_i$ are shown in Fig. 5 for the flow-injection system. For all cases except Fe^{3+}, the plots are linear with slopes of 0.73 ± 0.03. This value exceeds the value of 0.5 predicted in Eqn. 6, probably because of the failure of the approximation for linear diffusion which is inherent in Eqn. 6, i.e., $\delta = (\pi Dt)^{1/2}$, for diffusion of the metal ion to the slightly distorted and shielded spherical electrode. The slope for Fe^{3+} is 0.0 in agreement with Eqn. 7.

Applications of r.p.a. with long t_i in flow-injection and chromatographic systems can result in fewer data points than needed for accurate determination of the true peak shape. Perone and Jones [12] recommended a minimum of 10 points. In work described here, base-line widths of peaks virtually always exceeded 30 s, and the droptime ($\tau = t_i + t_p$) for the SDME was chosen to be 2.0 s.

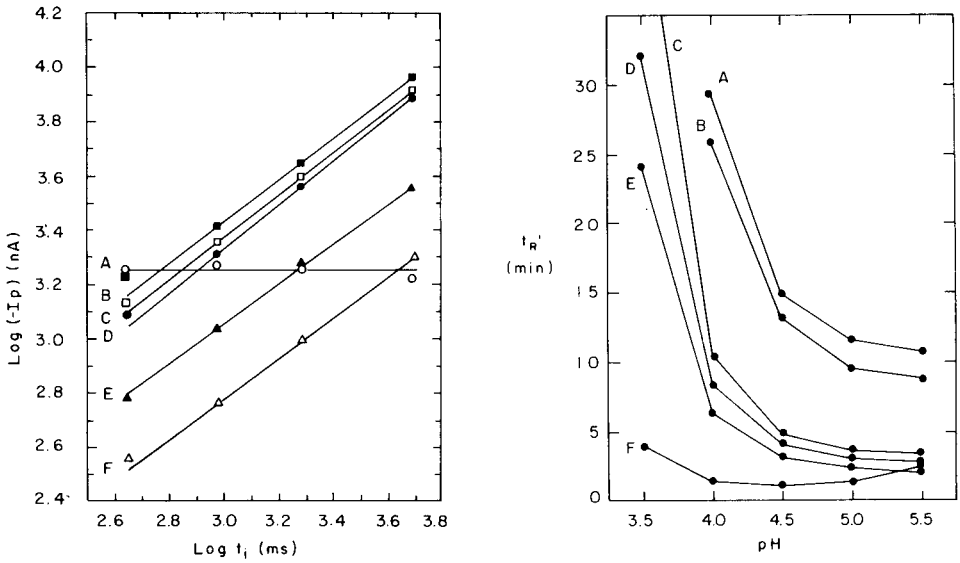

Fig. 5. Log I_p vs. log t_i for r.p.a. at the SMDE by flow-injection detection. Conditions: E_i = −1.25 V vs. SCE, E_f = +0.20 V vs. SSCE; air-saturated 0.10 M sodium hydrogentartrate at pH 4.5; v_f = 0.61 ml min^{-1}, V_s = 330 μl. Curves: (A) 1.0 mM Fe^{3+}; (B) 0.40 mM Cu^{2+}; (C) 0.40 mM Cd^{2+}; (D) 0.40 mM Zn^{2+}; (E) 1.0 mM Ni^{2+}; (F) 0.10 mM Cd^{2+}.

Fig. 6. Variation of adjusted retention time for tartrate eluent vs. pH. Conditions: E_i = −1.30 V, E_f = +0.20 V vs. SSCE; Durrum DC-4A cation exchange column (4 mm × 50 mm); 0.15 M sodium hydrogentartrate, v_f = 0.53 ml min^{-1}, V_s = 100 μl. Curves: (A) Fe^{2+}; (B) Cd^{2+}; (C) Pb^{2+}; (D) Ni^{2+}; (E) Zn^{2+}; (F) Cu^{2+}.

Chromatographic separations

Separations of divalent transition metal and heavy metal cations by cation-exchange chromatography are difficult using the conventional ionic eluents because of the similarity in values of the selectivity coefficients of the cations [13—15]. Resolution is improved substantially by use of suitable chelating eluent, e.g., tartrate [16—18], oxalate/citrate [19] and citrate/tartrate [20]. A tartrate eluent was chosen here because the $E_{1/2}$ for the Fe^{3+}/Fe^{2+} couple in tartrate media at pH 3.5—4.5 is accessible at a mercury electrode. Values of the adjusted retention time (t_R') are shown in Fig. 6 for the six cations using 0.15 M sodium hydrogentartrate as a function of pH. The peak for Fe^{3+} could not be resolved adequately from the "matrix peak" and data are given only for Fe^{2+}. Acceptable analysis time with 0.15 M sodium hydrogentartrate was obtained for pH > 4. However, significant broadening was observed for the Cu^{2+} peak at pH ⩾ 4.5. Fritz et al. [21] noted similar distortions for several cations at high pH. Rajan and Martel [22] and Bottari et al. [23, 24] concluded that formation of polynuclear Cu(II)/tartrate complexes is occurring for pH > 4; the peak broadening is probably the direct consequence of this fact.

Studies were made also of retention time as a function of the concentration of sodium hydrogentartrate at pH 4.0; typical chromatograms are shown in Fig. 7 for 0.25 M sodium hydrogentartrate. Chromatographic resolution of Zn^{2+} and Ni^{2+} was unsatisfactory for values of pH and sodium hydrogentartrate concentration for which run time was acceptable (ca. $\leqslant$10 min).

Retention times were decreased substantially by addition of Mg^{2+} to the eluent as shown in Fig. 8 for 0.10 M sodium hydrogentartrate at pH 4.5. The reversal of elution order for the Cd^{2+}/Fe^{2+} pair for 0.015 M Mg^{2+} should be noted. A typical chromatogram is shown in Fig. 7C for the optimum conditions. The total run time was ca. 10 min, and the resolution is considered satisfactory.

Applications

Linear calibration graphs (log I_p vs. log C^b) were obtained for all cations for the chromatographic separation in Fig. 7C; the average slope was 0.99 (std. dev. $\leqslant$0.02). Approximate limits of detection (LOD) for S/N = 2 are listed in Table 1. The lowest LOD (13 ng ml^{-1}) was for Zn^{2+}; and the poorest were for Fe^{2+} (100 ng ml^{-1}) and Ni^{2+} (120 ng ml^{-1}). The poor detectability of Fe^{2+} is expected because this ion is not accumulated (i.e., preconcentrated) in the mercury drop during the initial period (E_i) of the waveform.

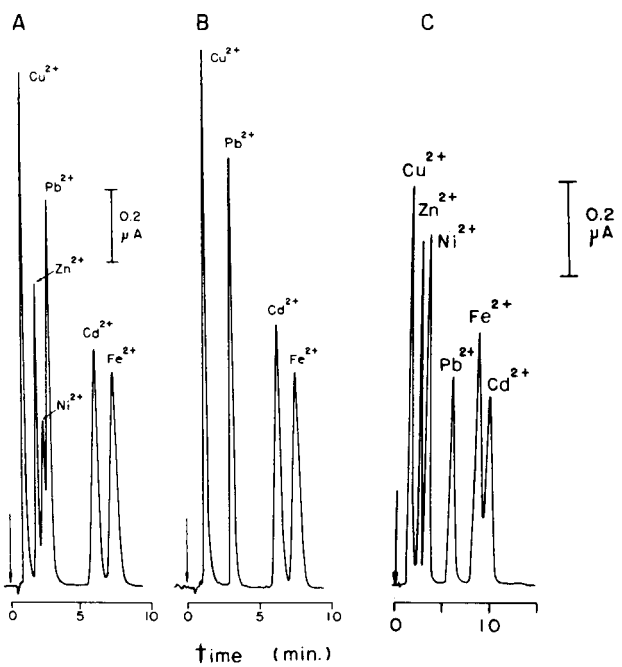

Fig. 7. Comparison of chromatographic separations. Conditions: v_f = 0.62 ml min^{-1}, V_s = 100 μl, E_f = +0.20 V vs. SSCE. Curves: (A) 0.25 M sodium hydrogentartrate at pH 4.0, E_i = −1.30 V; (B) 0.25 M sodium hydrogentartrate at pH 4.0, E_i = −0.80 V; (C) 0.10 M sodium hydrogentartrate + 0.060 M Mg^{2+} at pH 3.8, E_i = −1.30 V.

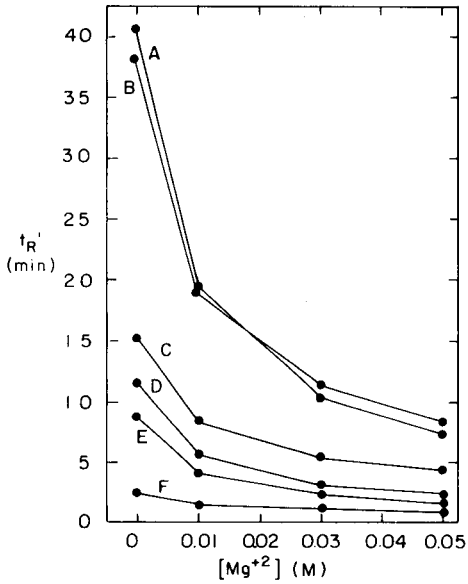

Fig. 8. Effect of Mg^{2+} on adjusted retention time. Conditions: identical to Fig. 7(C) except v_f = 0.62 ml min^{-1}, 0.10 M sodium hydrogentartrate + Mg^{2+} at pH 4.5. Curves: (A) Fe^{2+}; (B) Cd^{2+}; (C) Pb^{2+}; (D) Ni^{2+}; (E) Zn^{2+}; (F) Cu^{2+}.

Because Fe^{3+} was not resolved from the matrix peak, the Fe^{3+} in ground water was chemically reduced to Fe^{2+} by hydroxylammonium chloride in sodium acetate. Chromatograms are shown in Fig. 9 for the reagent blank and samples of ground water obtained near St. Joseph, MO (SJM) and on our university campus, Ames, IA (ISU). A small amount of Fe^{2+} detected in the reagent blank was traced to the reagent-grade sodium acetate. Only Fe^{2+} and Zn^{2+} were detected in the water samples; the Zn^{2+} level was substantially

TABLE 1

Limits of detection (S/N = 2)[a]

Metal ion	Detection limit		
	(ng/100 μl)	(ng ml^{-1})	(nmol ml^{-1})
Cu^{2+}	6.4	64	1.0
Zn^{2+}	1.3	13	0.20
Ni^{2+}	12	120	2.0
Pb^{2+}	8.3	83	0.40
Cd^{2+}	5.6	56	0.50
Fe^{2+}	10	100	1.8

[a]Conditions: v_f = 0.62 ml min^{-1}, V_s = 100 μl, E_i = −1.30 V, E_f = +0.20 V; 0.25 M sodium hydrogentartrate + 0.060 M Mg^{2+} at pH 3.8.

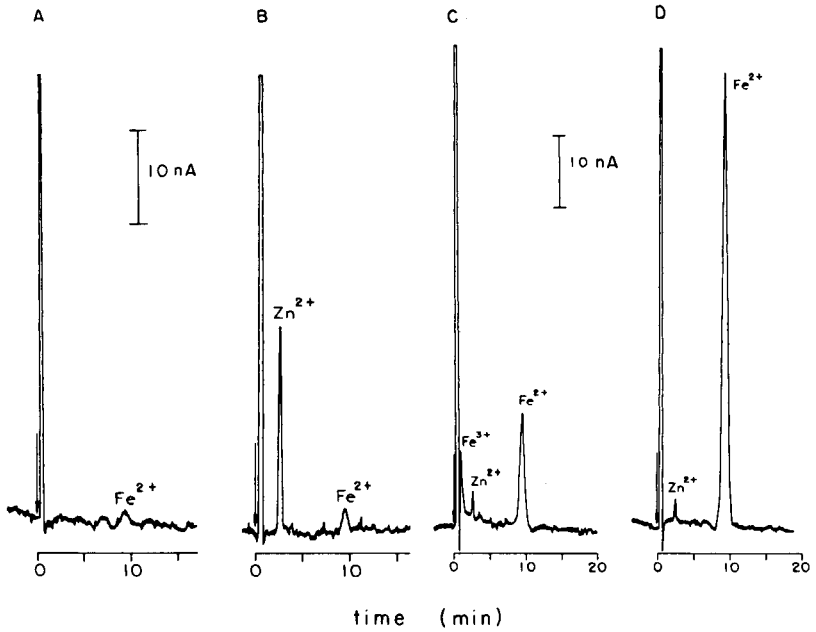

Fig. 9. Results from chromatographic analyses of ground water. Samples: (A) blank; (B) SJM; (C) ISU, without reducing buffer; (D) ISU, in reducing buffer.

larger for SJM, and Fe^{2+} was substantially higher for ISU. Linear calibration plots were obtained by the standard addition technique; and the results, corrected for the blank, were 22.3 ± 0.4 ng ml^{-1} Zn^{2+} and 4.46 ± 0.09 ng ml^{-1} Fe^{2+} for ISU, and 168 ± 4 ng ml^{-1} Zn^{2+} and 110 ± 10 ng ml^{-1} Fe^{2+} for SJM. As a confirmatory test, the 1,10-phenanthroline method yielded 4.60 ± 0.09 μg ml^{-1} Fe^{2+} for ISU and 110 ± 10 ng ml^{-1} Fe^{2+} for SJM.

An application of interest to us is for boiler waters. Typically, feedwaters for boiler-plant operations are demineralized, deaerated, and treated chemically to decrease corrosion rates in the boiler; e.g., sodium sulfite is added as an oxygen scavenger, cyclohexylamine as a surfactant and to neutralize the acidity from dissolved carbon dioxide, and disodium hydrogenphosphate is added to precipitate the scale-forming ions Ca^{2+} and Mg^{2+} [25, 26]. The dispersed solids are removed by a continuous "blow-down" process in which a small portion of the boiler water is drained. Primary ionic corrosion promoters include chloride and sulfate [27, 28] and these are target ions in analyses of blow-down waters and steam condensate by ion chromatography [29, 30]. Preconcentration is frequently used to enhance sensitivity. The presence of these ionic species is indicative of a potentially corrosive condition. Direct evidence of corrosion is, of course, the detection of the corrosion products, e.g., Fe^{2+}, Zn^{2+}, etc.

Preconcentration of metal ions from a 10.0-ml sample onto a high-capacity fore-column of Dowex 50W-X8 was successful in lowering the limits of

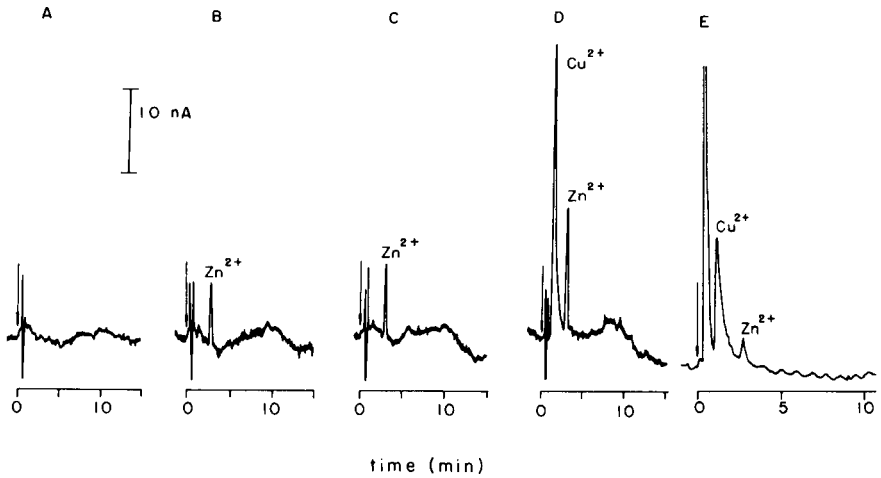

Fig. 10. Results from chromatographic analyses of boiler waters using preconcentration. Conditions: identical to Fig. 7(C) except 0.20 M sodium hydrogentartrate at pH 4.0; V_s = 10.0 ml except where noted. Samples: (A) triple-distilled water blank; (B) raw water; (C) turbine condensate; (D) boiler feedwater; (E) V_s = 0.50 ml blow-down water.

TABLE 2

Results for power-plant water[a]

Sample	Metal conc. found (ng ml^{-1})	
	Cu^{2+}	Zn^{2+}
Raw water	n.d.[b]	0.31
Turbine condensate	n.d.	0.35
Feedwater	13.3	0.63
Blow-down water	207	16.0

[a]Conditions are the same as for Fig. 10. [b]Not detectable.

detection in Table 1 by two orders of magnitude as compared to a 100-μl sample. The contribution of Zn^{2+} and Fe^{2+} impurity from the sodium acetate was much greater than the concentrations expected for boiler samples. Because the presence of the chemical oxygen scavengers in the boilers produce a reducing environment, all Fe^{3+} is expected to be reduced to Fe^{2+} and the chemical reduction step was eliminated. Typical chromatograms are shown in Fig. 10 and analytical results are shown in Table 2 for samples from the coal-fired power plant on this university campus. No Fe^{2+} was detected; the concentration of Cu^{2+} in the feedwater (13.3 μg l^{-1}) is well below the recommended maximum level.

Support of a portion of this work by Dionex Corporation (Sunnyvale, CA) is gratefully acknowledged.

REFERENCES

1 T. Hsi, Ph.D. dissertation, Iowa State University, Ames, IA, 1983.
2 K. Bratin and P. T. Kissinger, J. Liq. Chromatogr., 4, suppl. 2 (1982) 321.
3 P. Maitoza and D. C. Johnson, Anal. Chim. Acta, 118 (1980) 233.
4 K. B. Oldham and E. P. Parry, Anal. Chem., 42 (1970) 229.
5 J. Osteryoung and E. Kirowa-Eisner, Anal. Chem., 52 (1980) 62.
6 M. Oehme, Anal. Chim. Acta, 107 (1970) 67.
7 M. M. Nicholson, Anal. Chem., 32 (1960) 1058.
8 Kh. Z. Brainina, Stripping Voltammetry in Chemical Analysis, Wiley, New York, 1974, p. 32.
9 F. Vydra, K. Stulik and E. Julakova, Electrochemical Stripping Analysis, Halsted Press, New York, 1976, p. 59.
10 P. L. Meschi and D. C. Johnson, Anal. Chim. Acta, 124 (1981) 303.
11 K. W. Pratt, Jr. and D. C. Johnson, Electrochim. Acta, 27 (1982) 1013.
12 S. P. Perone and D. O. Jones, Digital Computers in Scientific Instrumentation: Applications to Chemistry, McGraw-Hill, New York, 1973, p. 246.
13 M. Marhol, Ion Exchangers in Analytical Chemistry: Their Properties and Use in Inorganic Chemistry, Elsevier Scientific, New York, 1982, Chap. 1 & 2.
14 F. R. Nordmeyer, L. D. Hansen, D. J. Eatough, D. K. Rollins and J. D. Lamb, Anal. Chem., 52 (1980) 852.
15 J. D. Lamb, L. D. Hansen, G. G. Patch and F. R. Nordmeyer, Anal. Chem., 53 (1981) 749.
16 Y. Takata and K. Fujita, J. Chromatogr., 108 (1975) 255.
17 J. E. Girard, Anal. Chem., 51 (1979) 836.
18 G. J. Sevenich and J. S. Fritz, Anal. Chem., 55 (1983) 12.
19 Transition Metal Analysis, Dionex Corp., Technical Note No. 10, Sunnyvale, CA, 1982.
20 R. W. Slingsby and J. M. Riviello, Liq. Chromatogr., 1 (1983) 354.
21 J. S. Fritz, D. T. Gjerde and C. Pohlandt, Ion Chromatography, Dr. Alfred Huethig, New York, 1982, Chap. 7.
22 K. S. Rajan and A. E. Martell, J. Inorg. Nucl. Chem., 29 (1967) 463.
23 E. Bottari and M. Vicedomini, J. Inorg. Nucl. Chem., 33 (1971) 1463.
24 E. Bottari, A. Liberti and A. Rufolo, Inorg. Chim. Acta, 3 (1969) 201.
25 J. W. McCoy, The Chemical Treatment of Boiler Water, Chemical Publishing Co., New York, 1981, Chap. 5.
26 D. M. Considine and G. D. Considine, Van Nostrand's Scientific Encyclopedia, 6th edn., Van Nostrand-Reinhold, New York, 1983, pp. 1156—9.
27 S. A. Borman, Anal. Chem., 52 (1980) 1409A.
28 D. F. Pensenstadler and M. A. Fulmer, Anal. Chem., 53 (1981) 859A.
29 T. S. Stevens, V. T. Turkelson and W. R. Albe, Anal. Chem., 49 (1977) 1176.
30 K. M. Roberts, D. T. Gjerde and J. S. Fritz, Anal. Chem., 53 (1981) 1691.

Analytica Chimica Acta, 175 (1985) 37—44
Elsevier Science Publishers B.V., Amsterdam — Printed in The Netherlands

VOLTAMMETRIC DETERMINATION OF TRACES OF SILVER IN SOME METALS AFTER DISSOLUTION OF THE SAMPLE IN MERCURY

STEFAN GŁODOWSKI and ZENON KUBLIK*
Department of Chemistry, University of Warsaw, Ul. Pasteura 1, 02093 Warsaw (Poland)
(Received 12th February 1985)

SUMMARY

The general possibility of analysing metals and alloys by dissolution of the sample in mercury and recording the anodic voltammogram is examined for the determination of silver in some metals. In order to obtain good separation of the silver peak from the anodic limit, acetonitrile is used in the supporting electrolyte. If the main component of the sample is more noble than mercury, analysis is simple and takes $\leqslant 20$ min. Significant amounts of base metals in samples must be removed from the amalgam prior to the anodic stripping; optimum conditions for the removal are given. The detection limits found for the determination of silver in gold and lead and in indium amalgam are 4×10^{-3}, 4×10^{-4} and 4×10^{-6} % respectively. Dissolution of the lead button in mercury seems to be a successful alternative to the cupellation procedure. Silver in mercury does not form intermetallic compounds with gold.

Dissolution of metals and alloys in mercury as an alternative to their dissolution in aqueous solution was proposed many years ago by Heyrovsky and Kalousek [1]. They suggested that an anodic polarogram recorded for the amalgam obtained would give quantitative information on the composition of the metallic sample and that, in some cases, such a procedure would be simpler than conventional methods based on dissolution of the sample in a suitable acid. However, until recently, such methods have not found analytical application, though amalgam polarography has been exploited successfully to determine the diffusion coefficients of many metals in mercury as well as in investigations of amalgams and intermetallic compounds. The proposal of Heyrovsky and Kalousek had one essential disadvantage, namely, it required handling relatively large volumes of amalgams. However, with the introduction of small stationary mercury electrodes, this disadvantage is no longer a problem. For example, it was shown recently that metallic contaminants of mercury are easily quantified from anodic voltammograms obtained after the sample of mercury to be analysed has been placed in the container of the hanging mercury drop electrode (HMDE) [2, 3]. Zebreva et al. [4] tried to determine the contaminants present in gallium after dissolving some gallium directly in the mercury drop.

0003-2670/85/$03.30

The aim of the present work was to establish whether or not the proposal of Heyrovsky and Kalousek [1] could be realized under voltammetric conditions at the HMDE. The problem is not simple. Reliable reports indicate that amalgams of many metals are unstable in contact with even traces of oxygen [2, 5—8]. Thus, during the dissolution of the metal in mercury, some of the dissolved metals may be lost. In this work, silver was chosen for study because it was known that silver amalgam is stable in the presence of oxygen [3]. Acetonitrile was chosen as the solvent because the silver dissolution peak is then well defined at mercury electrodes [3] whereas in aqueous solutions, the silver peak is completely masked by the mercury dissolution wave. In any scheme of analysis based on this amalgam formation, the procedures will depend on the kind of metal to be determined. Even significant amounts of noble metals should not interfere with the determination if they do not form intermetallic compounds with silver in mercury, whereas significant excesses of base metals must be removed from the amalgam prior to recording of the silver dissolution peak. Therefore, preliminary experiments were designed to find the optimum conditions for removal of significant amounts of base metals from the amalgam.

EXPERIMENTAL

Voltammetric curves were recorded with a Radelkis OH-105 polarograph and a three-electrode arrangement. A saturated calomel reference electrode was used; the counter electrode was a piece of platinum foil (ca. 2 cm^2). Two types of HMDE were used; one was of the type described by Kemula and Kublik [9] and the other was a mercury or amalgam drop suspended on the tip of a platinum contact fused into a glass capillary [10]. The small mercury or amalgam drops for suspension on the platinum were extruded from a microsyringe. The reproducibility of the volume of the drops was tested by weighing.

Electrolytic removal of the base metal from the amalgam was done either directly from the HMDE or from a larger amount of amalgam placed in a small cell with a bottom area of about 0.8 cm^2. In the latter case, the removal was done at constant current from a Radelkis OH-404/A potentiostat. The potential of the electrode during the removal was monitored with a digital voltammeter (Meratronic V-628). Solutions and amalgams were prepared as described earlier [3].

RESULTS

Preliminary experiments

The preliminary experiments had three aims: first, estimation of the complete dissolution of the metallic sample in mercury; second, evaluation of the utility of the HMDE with a platinum contact for the determination of silver; and third, optimization of conditions for the removal of base metals from the amalgam.

There is little information in the literature data on the kinetics of the dissolution of metals in mercury [11], but the rates of dissolution of lead [12] and silver [13] are transport-controlled. Under the present experimental conditions, it was found that the potential of a mixture of 34 g of mercury and 0.34 g of lead powder became constant after 10 min of stirring, i.e., complete dissolution of the lead sample did not take long. The rate of the dissolution of gold could not be monitored by measuring the potential of the amalgam formed; in this case, a weighed gold wire, held on a rod from the chuck of the stirrer, was immersed in the appropriate volume of mercury and the stirrer was rotated at 1000 rpm. The surface area of the gold wire in contact with mercury was ca. 12 mm^2. After different times, stirring was stopped, mercury was removed from the gold by heating and the gold wire was weighed again. Under these conditions, 10 min sufficed for dissolution of about 5 mg of gold, i.e., to prepare a gold amalgam with a gold concentration close to saturation. These experiments showed that the dissolution rate of gold in mercury is high; therefore in further experiments, gold amalgam was prepared by stirring the appropriate amounts of mercury and finely ground gold for 10 min at 1000 rpm.

Krasnova and Zebreva [14] showed that the HMDE with a platinum contact gives anodic stripping peaks of decreased height for zinc and cadmium because of the formation of intermetallic compounds between these metals and platinum. The present experiments showed that the dissolution peaks of silver from a drop of silver amalgam (5.5×10^{-5} and 1.7×10^{-2} mol dm^{-3}) suspended on the platinum contact were unchanged during 30 min of electrode aging. In addition, it was found that the heights of these peaks were consistent with the values predicted on the basis of the Nicholson and Shain equation [15].

As Fig. 1 shows, similar concentrations of base metals do not affect the silver peak. Stopping the voltage sweep for a period of time, as indicated for the cadmium peak, enabled about a 10-fold amount of base metal to be removed without essential change of the silver dissolution peak.

For removal of significant amounts of base metals from an amalgam, three procedures were examined for amalgams containing ca. 1 mol dm^{-3} lead and significantly smaller concentrations of silver. In procedure A, the amalgam was introduced into the container of the HMDE and lead was removed from the extruded drop of amalgam to the acetonitrile medium under potentiostatic control. Under these conditions the anodic voltammogram, recorded after 15 min of lead removal, exhibited a significant anodic current which severely affected the dissolution peak of silver. This effect is undoubtedly caused by diffusion of lead atoms from the highly concentrated amalgam present in the mercury thread to the hanging drop. A further disadvantage of the use of the HMDE filled with the concentrated amalgam is the significant adherence of such amalgams to the walls of the glass capillary. Such an effect leads, in turn, to decreased reproducibility of the results.

In procedure B, a drop of lead amalgam was suspended on the platinum contact and lead from the drop was electrolytically removed in the manner

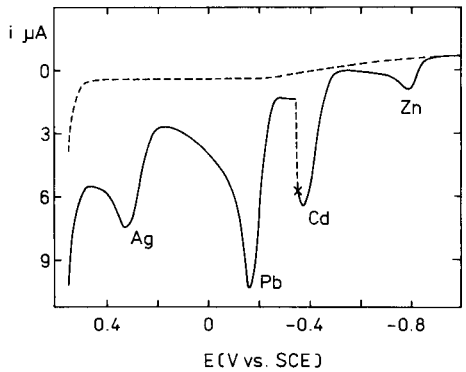

Fig. 1. Anodic voltammogram obtained for an amalgam containing 1.5×10^{-3} Ag, 7.6×10^{-4} Pb, 4.8×10^{-4} Cd and 9.8×10^{-5} mol dm^{-3} Zn. Solution: 0.1 mol dm^{-3} lithium perchlorate in acetonitrile medium. Voltage scan rate 1 V min^{-1}. Electrode surface area 0.038 cm^2. At the point marked X, the voltage scan was stopped for 30 s. (-----) Blank test.

described in procedure A. Under these conditions, the current flowing during the removal decayed much more quickly than in procedure B to the level observed for the pure mercury drop. This kind of removal of lead allowed silver to be determined when the concentration of silver was not too small. But when the silver concentrations were close to the detection level, the background currents were not smooth enough for realistic results to be obtained.

In procedure C, lead was removed from large amounts of amalgam (ca. 5 g) while both mercury and the aqueous phase were stirred strongly. Variations of the potential of the amalgam were monitored in parallel with the constant current (80 mA) passing through the cell. The time required for purification of ca. 5 g of lead amalgam containing ca. 1 mol dm^{-3} of lead was 30 min. The silver amalgam obtained in this procedure was introduced to the reservoir of the HMDE or a small drop of the amalgam was suspended on the platinum contact. Both procedures gave well defined curves even for very small concentrations of silver.

Determination of silver in metals more noble than silver

As an example of analysis of this type, the determination of small contents of silver in gold is presented. Gold dissolves easily in mercury; saturated gold amalgam contains at room temperature 0.12% (w/w) gold [16]. Silver can be determined in the presence of gold by the method proposed provided that these metals do not form stable intermetallic compounds in mercury. The literature lacks information on this subject, thus the influence of gold in the amalgam on the silver dissolution peak was examined. Anodic voltammograms were recorded for amalgams containing 1.66×10^{-2} mol dm^{-3} silver in the absence and presence of gold. The concentration of gold in the amalgam

was close to saturation. Both the shape and height of the peaks obtained under these conditions were not affected by the presence of gold, indicating that no intermetallic compounds were formed in mercury between silver and gold.

In further tests, a sample of accurately weighed gold (ca. 6 mg) was dissolved in 5 g of mercury to form an almost saturated amalgam. Figure 2 presents a comparison of the voltammetric curves obtained with the HMDE in acetonitrile medium for pure mercury, this gold amalgam, and a silver amalgam with known concentration of silver. It is evident that the silver peak at 0.32 V vs. SCE is quite well defined whether or not gold is present. The peaks are well separated from the dissolution current of mercury and their height is proportional to the concentration of silver in the amalgam [3]. The concentration of silver in gold amalgam was calculated by both absolute and comparative methods. For the former, the Nicholson and Shain equation [15] was used for evaluation of the silver concentration; the value of the diffusion coefficient of silver in mercury, necessary for calculations, was taken from previous work [3]. For the latter method, the height of the peak obtained for the gold amalgam was compared with peak heights obtained for silver amalgams with known concentration of silver. Both methods gave very close results. Typical results are given in Table 1. The detection limit and the standard deviations are not very low, but the method has the advantage

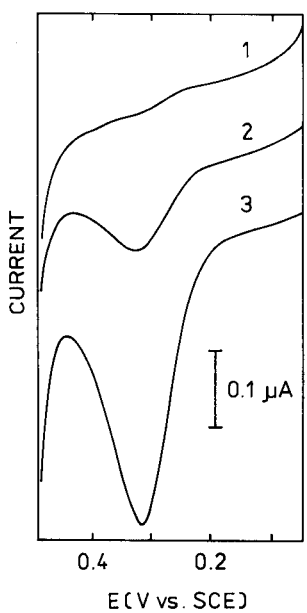

Fig. 2. Anodic voltammograms obtained in acetonitrile solutions containing 0.01 mol dm^{-3} lithium perchlorate: (1) blank test; (2) gold amalgam with 0.08 mol dm^{-3} gold (3N); (3) silver amalgam containing 1.2×10^{-4} mol dm^{-3} silver. Voltage scan rate 0.2 V min^{-1}. Electrode area 0.075 cm^2.

TABLE 1

Results of analyses of various materials

Matrix	Sample weight (g)	Conc. of major metal[a] (mol dm^{-3})	Silver content[b] (wt.%)	N	SD (wt.%)	RSD (%)	DL (wt.%)
Gold (3N)	0.006	0.08	0.028	10	2.3×10^{-3}	8.3	4×10^{-3}
Gold (4N)	0.006	0.08	0.006	6	7.9×10^{-4}	13.2	4×10^{-3}
Lead (TG)	0.05	0.65	6.3×10^{-3}	7	5.1×10^{-4}	8.2	4×10^{-4}
Lead (AR)	0.05	0.65	—[c]	3	—	—	4×10^{-4}
Lead, button A	0.05	0.65	5.2×10^{-2}	10	2.2×10^{-3}	4.3	4×10^{-4}
Lead, button B	0.05	0.65	2.8×10^{-1}	7	7.0×10^{-3}	2.5	4×10^{-4}
Indium amalgam	5.0	3.5	7.1×10^{-5}	10	5.1×10^{-6}	7.2	4×10^{-6}

[a]In mercury. [b]Mean of N determinations with standard deviation (SD), relative standard deviation (RSD) and detection limit (DL). [c]Below the detection limit.

of being fast. This advantage is markedly greater if the sample to be analysed is in the form of amalgam, i.e., in plants exploiting the amalgamation process for recovery of gold and silver from ores.

Determination of silver in indium amalgam

Indium is often purified by the electrolytic amalgam method [17, 18]. During the process, the contaminants accumulate in the amalgam and accurate knowledge of the extent of contamination of the amalgam is an essential factor in obtaining the pure product. The indium amalgam analysed in this work contained about 3.5 mol dm^{-3} indium and smaller concentrations of zinc, lead and copper. Metals more basic than mercury were removed from the amalgam by procedure C (see above). The anodic voltammograms obtained in acetonitrile medium by using the HMDE suspended on the platinum contact were well defined and exhibited a marked peak of silver. The height of the peak was unchanged in experiments run during one month, which means that the silver amalgam is stable in time.

The results of analyses of an indium amalgam are presented in Table 1. The detection limit attained in this case is significantly lower than that obtained for silver in gold samples. Each analysis takes no longer than 45 min, the time-consuming step being the removal of indium from the amalgam.

Determination of silver in lead

Lead is readily soluble in mercury [16]; saturated lead amalgam contains 0.96 mol of lead per dm^3 of amalgam at 25°C. Lead is often contaminated

by traces of silver. Higher concentrations of silver are present in the lead buttons prepared for the fire-assay preconcentration of traces of noble metals from ores [19].

In this work, samples of analytical-reagent (AR) lead, technical-grade (TG) lead and lead buttons were analysed for silver. Accurately weighed samples of lead (ca. 50 mg) were dissolved in pure mercury (ca. 5 g) giving almost saturated lead amalgams which were analysed in a manner similar to that described for indium amalgam. The dissolution peak of silver obtained after removal of lead was well defined. The results of these analyses are given in Table 1.

DISCUSSION

The results described above show that the method of analysing metals and alloys suggested by Heyrovsky and Kalousek [1] can be applied successfully for the determination of traces of silver in some metals and amalgams. Though the detection limits found for silver in gold and lead are not very low, they are adequate for determining silver in some sorts of gold, in crude lead and in the lead buttons obtained in the crucible or scorification fusion of silver ores. The dissolution of lead buttons in mercury followed by electrolytic removal of lead from the amalgam could be a successful alternative to the cupellation step in routine fire-assay methods. During cupellation, some silver is lost [19], whereas during dissolution of lead button in mercury there are no losses of silver. The detection limit found for the determination of silver directly in amalgams is much lower. The method proposed could be useful in hydrometallurgical plants and in plants exploiting the amalgamation process for the recovery of silver from ores. Unfortunately, the method cannot be exploited for the analysis of metals poorly soluble in mercury, e.g., copper, which is often contaminated by traces of silver.

Comparison of the method proposed here with conventional methods based on dissolution of the metal sample in aqueous solution followed by electrolytic determination of silver on the surface of the platinum [20—22] or carbon [22—25] electrodes shows that the methods are to some extent complementary. A serious disadvantage of the conventional methods is the poor shape of the reduction or oxidation peaks at the solid electrodes. Because of this, some authors prefer to preconcentrate silver electrolytically, but to determine it by non-electrolytic methods [26, 27]. The main advantage of the proposed method is the possibility of determining silver in the presence of significant amounts of gold; for such samples, the conventional method requires prior separations. In contrast, the proposed method requires prior separations for base matrices, whereas the conventional method can be used directly [24].

The results obtained by methods based on dissolution of the sample in mercury can be affected by the formation of intermetallic compounds in the mercury phase. However, in this work no evidence was obtained that

silver in mercury forms intermetallic compounds with the other metals studied. This work was supported by Project MR-I-32.

REFERENCES

1 J. Heyrovsky and M. Kalousek, Collect. Czech. Chem. Commun., 11 (1939) 464.
2 S. Głodowski and Z. Kublik, Anal. Chim. Acta, 149 (1983) 137.
3 S. Głodowski and Z. Kublik, Anal. Chim. Acta, 156 (1984) 61.
4 A. J. Zebreva, S. A. Levitskaya and S. H. Aldamzharova, Mikrochim. Acta (Wien), II (1981) 361.
5 F. Chao and M. Costa, Bull. Soc. Chim. Fr., 54 (1968) 548.
6 M. Pelletier, J. Buffle and D. Monnier, Chimia, 25 (1971) 61.
7 J. Buffle, M. Pelletier and D. Monnier, J. Electroanal. Chem., 43 (1979) 185.
8 V. I. Kravcov, L. Ja. Smirnova and O. V. Jemelyanova, Elektrokhimiya, 18 (1982) 500.
9 W. Kemula and Z. Kublik, Anal. Chim. Acta, 18 (1958) 104.
10 R. D. DeMars and I. Shain, J. Am. Chem. Soc., 81 (1959) 2654.
11 Z. Galus, CRC Crit. Rev. Anal. Chem., 4 (1975) 396.
12 J. A. R. Bennett and J. B. Lewis, J. Chim. Phys., 55 (1958) 83.
13 F. W. Hinzner and D. A. Stevenson, J. Phys. Chem., 67 (1963) 2424.
14 I. E. Krasnova and A. J. Zebreva, Zh. Anal. Khim., 23 (1968) 1039.
15 R. S. Nicholson and I. Shain, Anal. Chem., 36 (1964) 706.
16 M. T. Kozlowski, A. J. Zebreva and V. P. Gladyshev, Amalgamy i ikh Primenenye, Alma-Ata, 1971.
17 D. Effer, J. Electrochem. Soc., 108 (1961) 357.
18 P. P. Pugatchewich, Rabota so Trutyu, Izd. Khimiya, Moskva, 1972.
19 N. H. Purman (Ed.), Standard Methods of Chemical Analysis, 6th edn., Vol. 1, D. Van Nostrand, Princeton, NJ, 1962.
20 Ch. Z. Brainina, T. A. Rygaylo and W. B. Belavskaya, Zavod. Lab., 29 (1963) 393.
21 Ju. Lyalikov and L. G. Madan, Zavod. Lab., 34 (1968) 8.
22 E. Lachowicz, J. Gawełand Z. Trybuła, Chem. Anal., 28 (1983) 677.
23 E. Temmerman and F. Verbeek, Anal. Chim. Acta, 58 (1972) 263.
24 H. Monien, H. Specker and K. Zinke, Z. Anal. Chem., 225 (1967) 342.
25 S. Rubel, E. Stryjewska and J. Golimowski, Chem. Anal., 24 (1979) 247.
26 W. Lund, Y. Thomassen and P. Doevle, Anal. Chim. Acta, 93 (1977) 53.
27 Z. Boguszewska, M. Krzyzanowska and Z. Skorko-Trybuła, Chem. Anal., 29 (1984) 147.

Analytica Chimica Acta, 175 (1985) 45—53
Elsevier Science Publishers B.V., Amsterdam — Printed in The Netherlands

ANODIC STRIPPING VOLTAMMETRY WITH FLOW INJECTION ANALYSIS

CAROLYN WECHTER, NEAL SLESZYNSKI, JOHN J. O'DEA
and JANET OSTERYOUNG*

Department of Chemistry, State University of New York at Buffalo, Buffalo, NY 14214 (U.S.A.)

(Received 8th April 1985)

SUMMARY

A flow cell with a wall-jet electrode design is used for anodic stripping voltammetry of lead at concentrations of about 10^{-7} mol dm^{-3}. Maximum peak heights are obtained for narrow nozzle diameters and short nozzle-to-electrode distances. Linear calibration plots are obtained for almost four decades of change in concentration and can be extended by judicious choice of sample volume. Increasing sample throughput rates by increasing the solution flow rate decreases the analytical signal. Square wave voltammetry provides shorter analysis times and better sensitivity than differential pulse voltammetry.

The increasing release of lead and other heavy metals into the environment has increased the necessity for the quantification of heavy metals [1]. Anodic stripping voltammetry (a.s.v.) has long been recognized as a useful technique for the determination of trace metals, especially in environmental samples [2—7]. Use of a preconcentration period, during which the metals are reduced into a mercury electrode, allows detection at the sub-μg l^{-1} level in some cases. A variety of waveforms, including staircase, differential pulse and square wave, has been used during the anodic scan to oxidize the metal out of the electrode. This mercury electrode is commonly a hanging mercury drop electrode (HMDE), or a mercury film plated onto a solid electrode. For many metals and matrices, a.s.v. is the method of choice. The sensitivity of a.s.v. is usually limited by the amount of time necessary to plate the metal into the mercury film.

Flow injection analysis (f.i.a.) has steadily been gaining popularity since its inception in the 1970's as a rapid, precise, and versatile technique for sample presentation [8]. Many detection techniques have been used including potentiometry, photometry, refractometry, and conductimetry [7—10]. Stripping voltammetry has also been combined with f.i.a. for a variety of metals [7, 8]. Total analysis time can be greatly reduced by presenting the sample to the electrode using f.i.a., and reproducibility of experimental conditions should be greatly enhanced over those routinely obtainable in normal a.s.v.

0003-2670/85/$03.30

The term wall jet was first introduced by Glauert [11]. This describes an arrangement in which the solution is introduced as an impinging jet perpendicular to the electrode surface. The wall jet electrode has been numerically defined [12], with the electrode radius much larger than the solution inlet. The use of a wall jet electrode in a flow cell should increase sensitivity, because the narrow inlet maintains high linear flow rates. The recently published work of Elbicki et al. [13] suggests that the mere geometric relationship of the solution impinging normally to the electrode surface will not result in classic wall jet behavior. Under the conditions used in these experiments, unless the electrode surface is $\geqslant 2.3$ inlet diameters away from the inlet, less than 100% of the electrode exhibits wall jet behavior. For a flow cell of typical dimensions, an electrode of a wall jet design actually behaves as a thin-layer electrode. Work has been done on deriving equations for the steady-state current at an amperometric detector [14]. During voltammetric experiments when a steady state is not achieved, these equations should be integrated and the peak area, not the peak height, compared to these integrated equations [13].

This paper describes an investigation of the use of an electrochemical cell of the wall jet design for the determination of lead at a mercury film. Two waveforms have been examined, square wave and differential pulse (Fig. 1), and their sensitivities and sample throughput rates are compared. Experimental variables are investigated to optimize the signal obtained. The a.s.v./f.i.a. combination could be automated, making it an attractive technique for con-

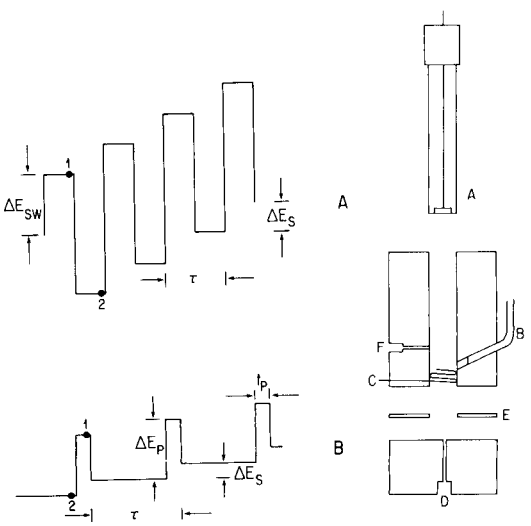

Fig. 1. Waveforms used. $i = i_1 - i_2$. Typical values: ΔE_s = 2—10 mV. (A) Square wave, τ = 0.001—0.1 s, $\Delta E_{sw} = 50/n$ mV. (B) Differential pulse, τ = 0.3—2 s, $\Delta E_p = 2\Delta E_{sw}$.

Fig. 2. Diagram of plexiglas flow cell: (A) glassy carbon working electrode; (B) SCE; (C) Pt wire counter electrode; (D) solution inlet; (E) 0.127-mm teflon spacers; (F) solution outlet.

tinuous analysis, especially for monitoring environmental samples. The entire system could also be mobilized for use with remote or unattended determination of heavy metals. Other techniques commonly used for determination of lead are not noted for their mobility, especially atomic absorption and inductively-coupled plasma emission spectrometry.

EXPERIMENTAL

Solutions

The carrier solution, 1.0 M in acetic acid and 1.0 M in sodium acetate (pH 4.7), was prepared from anhydrous acetic acid, reagent-grade sodium carbonate (Baker, lot analysis 2 ppm heavy metals) and deionized water (Millipore). All lead standards were obtained by dilution of 0.1 M lead nitrate (Fischer) in this buffer. The iron(II) solutions were prepared from potassium hexacyanoferrate(II) (Mallinckrodt), and mercury plating solutions for the film electrode from mercury(II) nitrate (Mallinckrodt) and acetate buffer. Heavy metals were removed from the carrier solution by bulk electrolysis at a mercury pool, by using a reagent cleaning system from Environmental Sciences Associates (Model 2014P) as the solvent reservoir. A maximum of 4 l of stirred solution could be continuously electrolyzed under argon at an applied potential of −1.2 V vs. Ag/AgCl.

Instrumentation

An EC-220 stripping voltammeter (IBM) and an Omnigraphic 2000 X-Y recorder (Houston Instruments) were used to record differential pulse voltammograms. Square wave and differential pulse voltammograms were obtained with an EG&G PARC 384B polarographic analyzer. This software-controlled instrument was interfaced with a DEC PDP 8/f computer for digital data acquisition and analysis. A 15-point sliding symmetrical array was used for run-time smoothing of the data. This is an integral feature of the 384B software package. The reciprocating pump was an IBM prototype h.p.l.c. pump with a rotating head controlling three pistons. The air hammer used to deaden pulsations was an empty l.c. column located immediately downstream from the pump. A shunt valve was used to prevent the air hammer, pressurized and partially filled, from draining once the pump was shut off.

The carrier acetate buffer and all the lead samples were purged with purified argon to remove oxygen. Three polypropylene bottles were placed into a plexiglas tank with a tight fitting cover and submerged up to their necks in deionized water to decrease the amount of gas and oxygen present in the sample environment. The lead solutions were deoxygenated in these bottles and samples were removed with a syringe fitted with narrow diameter tubing which was fed into the sample bottle through a small opening in the cover of the plexiglas container. The purged buffer was pumped from the glass solvent reservoir through the stainless steel pump and to an injection port

(polyethylene) where it either passed directly to the electrochemical cell or continued through the sample loop and then to the cell. Loop volumes ranging from 0.1 to 5.0 ml were available.

The plexiglas flow cell (Fig. 2) was 8 cm high and 5 cm in diameter. The working volume could be adjusted by inserting teflon spacers (E), 0.127 mm thick, between the bottom and middle segments of the cell, yielding volumes that varied between 16 and 64 μl. The working electrode (A) was a glassy carbon disc electrode, 0.4 cm radius, sealed in a teflon sheath (Pine Instruments). Prior to plating a mercury film on this electrode, its surface was polished with 0.05-μm alumina. A threaded saturated calomel electrode (SCE) with a vycor frit (B) and a platinum wire counter electrode (C) were installed in the flow cell downstream of the working electrode. All potentials are reported vs. this SCE. Two solution inlets (D), 0.03 cm and 0.15 cm, were available.

Procedures

The thin mercury film was plated in situ by injecting 0.5 ml of 0.02 M mercury(II) into the system with a solution flow rate of 0.5 ml min^{-1}, and the mercury film was deposited at —0.9 V. A film thickness of 100 nm was estimated by comparison of the mercury stripping curves to those from films plated on a rotating electrode (plating charge 0.06 coulombs, 100 nm thick). Films prepared in this manner were stable for a day.

The potential applied to the working electrode during the course of an experiment is described in Fig. 3. The mercury-covered electrode was held at 0.0 V as the pump was turned on and the sample loop filled. Then the potential was stepped to —0.9 V and the lead sample was injected into the flow system. The lead sample volume (typically 1.0 ml) was followed by four times its volume of acetate buffer during this reductive preconcentration

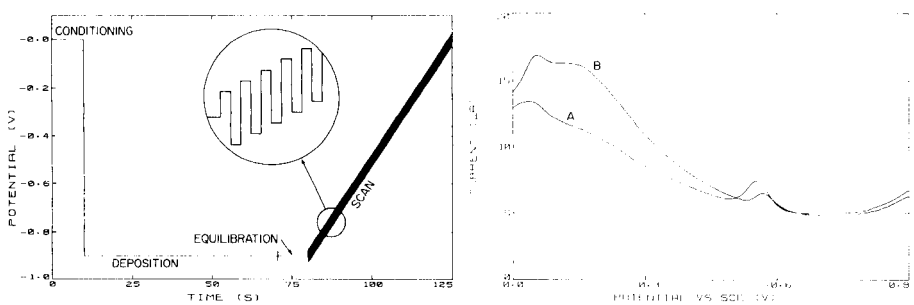

Fig. 3. Applied potential of working electrode as a function of time: mercury electrode conditioned at 0.0 V, sample deposition at —0.90 V; quiescent equilibration at —0.90 V; potential scanned to 0.0 V via square wave (shown here) or differential pulse voltammetry.

Fig. 4. Typical background square-wave voltammograms: (A) quiescent stripping solution; (B) stripping into solution flowing at 5 ml min^{-1}. Plating time 60 s, plating solution flow rate 5 ml min^{-1}, square wave frequency 10 Hz, ΔE_s = 2 mV, ΔE_{sw} = 24 mV.

period to ensure the complete passage of the sample past the electrode surface as well as to provide clean buffer for the stripping step. Then the pump was turned off and the shunt valve closed. Thus a quiescent solution was obtained in the flow cell. After allowing 10 s for the equilibration of the mercury film electrode, the potential was scanned to 0.0 V by differential pulse or square wave voltammetry. The cycle was then repeated. Background voltammograms were obtained under the same conditions used for the lead samples.

RESULTS AND DISCUSSION

The ability to record stripping curves under flowing conditions simplifies the experimental procedure. A study was made to determine the effect of solution flow on the stripping peak height as well as on the background noise levels. As shown in Fig. 4, the background curve obtained by stripping into a flowing solution (B) has a decreased signal compared to the curve for a quiescent solution (A). This is attributed to the voltammetric waveforms used. When differential pulse voltammetry is used, in the region of the reduction potential of the metal couple, the metal is stripped out of the film on the anodic step, and replated into the mercury film on the cathodic step. If under flowing conditions, as the Prandtl layer decreases, the metal ion is removed from the vicinity of the electrode before it is replated, the signal is decreased. For square wave voltammetry, the metal ion is produced in the forward anodic pulse, and replated during the reverse pulse. The net signal, which is found by subtracting the reverse current from the forward current, is decreased as the metal ion is swept away. For both techniques, the shape of the stripping curve is altered, and the slope of the curve in the anodic region is increased. Consideration of both signal and noise effects resulted in performing all further experiments under quiescent conditions. The optimum step height was 2 mV. Peak broadening was observed for larger increments, possibly owing to the data smoothing routines of the 384B.

For a given flow rate ($cm^3\ s^{-1}$), decreasing the nozzle diameter increases the linear velocity ($cm\ s^{-1}$) of the solution impinging on the electrode surface. As the convective mass transport to the surface is increased, more of the lead sample should be plated during the preconcentration period. Experimentally, it was observed that stripping currents decreased as the nozzle diameter increased, and an inlet diameter of 0.3 mm was used.

The use of higher solution flow rates could decrease the sample analysis time, but will also affect the sensitivity of the technique. The amperometric peak area, Q, depends on the solution flow rate, U, as described by Elbicki et al. [13].

$$Q = knFP^{2/3}U^{-2/3}M \quad (1)$$

where k is a numerical constant, P a parameter that includes the diffusion coefficient, kinematic viscosity of the solution and cell dimensions, M the

amount of electroactive material injected, and n and F have the usual electrochemical meaning. This equation applies when the solution flow is concurrent with electrochemical detection. To test its applicability for this flow cell, an amperometric experiment was done. A 2.0 mM hexacyanoferrate(II) solution was injected into the system and the response was examined for the glassy carbon electrode at a potential of +0.7 V. The current was recorded as a function of time for various flow rates. These curves were integrated, and a plot of log charge vs. log flow rate (U) produced a slope of −0.679, in agreement with Eqn. 1. The percent of iron oxidized ranged from 8.3% at 0.47 cm^3 min^{-1} to 1.06% at 8.3 cm^3 min^{-1}. As discussed earlier, stripping peak heights should be used for comparison with amperometric detection theory. A plot of log i vs. log U had an experimental slope of −0.66 ± 0.02, in agreement with a theoretical value of −0.67. As the volume flow increases, the Prandtl layer becomes thinner, but the residence time of the sample within the effective volume is decreased. The increase in sample throughput with higher flow rates must be balanced against the loss in sensitivity. The concentration factor is V_sF/V_{Hg}, where V_s and V_{Hg} are the volume of sample and mercury film, respectively, and F is the coulometric efficiency. If V_s = 0.5 ml and F = 0.05 (intermediate flow rate), this factor is 10^4, which should provide adequate sensitivity to determine lead in the 10 pM range.

Although not included as a parameter in equations describing the current for a wall jet electrode, the distance between the inlet nozzle and the electrode surface affects the mass transport to the electrode surface, and thus the current. This effect has been investigated by other workers [14, 15]. Gunasingham and Fleet [14] found that the current decreases with increasing distance, reaches a minimum, and then increases to a limiting value. This agrees with the work of Glauert [11], with the current initially decreasing as the radial velocity gradient increases. Figure 5 shows the currents obtained

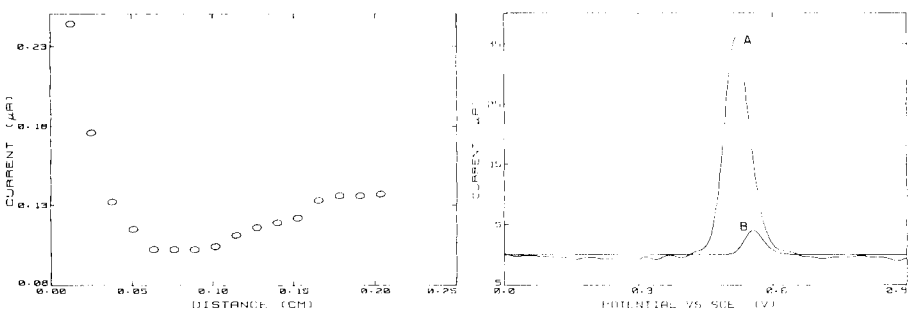

Fig. 5. Peak current as a function of the distance between the inlet nozzle and electrode surface. 5.0 ml of 2.0 × 10^{-3} M $Fe(CN)_6^{-4}$ injected; glassy carbon electrode at +0.70 V, solution flow rate 4.4 ml min^{-1}.

Fig. 6. Square wave (A) and differential pulse (B) voltammograms after background subtraction. Lead(II) concentration 5.0 × 10^{-7} M, sample volume 1.0 ml, solution flow rate 5 ml min^{-1}. (A) Square wave: f = 120 Hz, ΔE_{sw} = 24 mV, ΔE_s = 2 mV. (B) Differential pulse: τ = 0.3 s, t_p = 50 ms, ΔE_p = 24 mV, ΔE_s = 2 mV.

as a function of the spacing between the inlet and electrode surface for a 2.0 mM hexacyanoferrate(II) solution. A discrete volume (5.0 ml) was injected into the cell with an applied potential of +0.70 V. Integrating the current/time curves and plotting the charge as a function of distance produces a similar curve. Thus performance for this cell is optimized with the use of a single 0.127-mm spacer. Then the ratio of nozzle diameter to the distance between nozzle and electrode is less than 2.3, and the behavior is that of a thin-layer cell.

According to Eqn. 1, the analytical signal depends on the amount of material injected into the system. This amount can be altered by changing either the sample concentration, sample volume or both. Thus a calibration curve could be obtained with a combination of several standard solutions and loop sizes, as represented in Table 1. This allows expansion of the linear concentration range of the technique without requiring sample dilution or concentration. A linear plot is obtained for nearly four orders of magnitude, up to 10^{-4} M. Relative standard deviations ranged from 0.5% for 50 μM lead(II) up to 10% for 0.5 μM lead(II) (n = 7). The difficulties associated with working with a species as ubiquitous as lead include preparing and maintaining standard solutions at low concentrations. Once cleaned, a closed system remains clean and ameliorates this problem. It should be pointed out, however, that the lower limits in this work were determined not by sensitivity but by trace contamination arising from the general laboratory conditions.

The square wave and differential pulse voltammograms shown in Fig. 6, obtained under typical but not necessarily optimum conditions, indicate the superiority of square wave stripping in two ways. The square wave peak current is approximately nine times greater than that for differential pulse. This larger signal should yield lower detection limits. The effective scan rates of the two techniques are 200 mV s^{-1} and 6.7 mV s^{-1}, respectively. Thus, the 900 mV scanned required 4.5 s with the square wave waveform, but 2 min 14 s with differential pulse voltammetry. Therefore, because of both its

TABLE 1

Data for calibration curve prepared from three standard sample concentrations and three sample-loop volumes[a]

Concentration (mol dm^{-3})	Volume (cm^3)	Peak height (μA)
1.0×10^{-7}	1.0	0.363
3.0×10^{-7}	0.50	0.640
	1.0	1.72
	5.0	7.66
5.0×10^{-7}	0.50	1.02
	1.0	1.79
	5.0	11.87

[a]Conditions: solution flow rate 4.7 ml min^{-1}, square wave frequency 10 Hz, ΔE_p = 24 mV, ΔE_s = 2 mV.

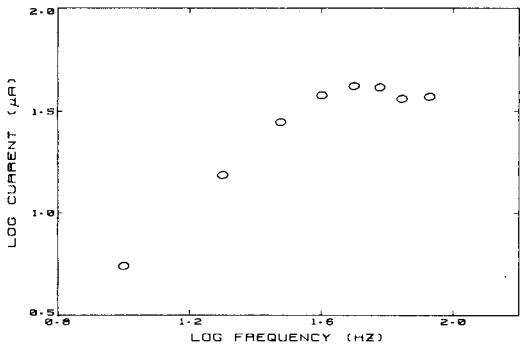

Fig. 7. Dependence of current on square-wave frequency. 1.0 ml sample of 5.0×10^{-7} M Pb(II), plating solution flow rate 5 ml min^{-1}, ΔE_{sw} = 24 mV, ΔE_s = 2 mV, backgrounds subtracted.

shorter sample analysis time and greater sensitivity, square wave voltammetry is the preferred technique for these experiments.

The theoretical slope of a log current vs. log square-wave frequency for the case of semi-infinite linear diffusion is 0.5. Experimentally, under the present conditions at the mercury film electrode, this plot is linear at low frequencies, and reaches a maximum at higher frequencies (Fig. 7). Furthermore, the slope at low frequencies is much greater than 0.5. A seven-fold increase in peak height was obtained by increasing the frequency from 10 Hz to 40 Hz. By analogy with results for staircase voltammetry, the linear range lies in the thin-film region, in which the response is determined by restricted diffusion in the film [16]. At higher frequencies it may be that the usual model for voltammetry at mercury films does not apply for the square waveform. More detailed investigations of the parametric response for the square waveform are presently under way [17].

It is concluded that in the configuration of Fig. 2, this cell gives optimum performance with small nozzle diameters (0.3 mm) and narrow spacing (0.127 mm) between nozzle and electrode. The best stripping technique is square wave voltammetry with parameters ΔE_{sw} = 24 mV (for n = 2), ΔE_s = 2 mV, and moderate frequencies (ca. 40 Hz). The value of ΔE_s depends on the choice of instrument, while the choice of frequency may depend on film thickness. Differential pulse voltammetry also works well as a stripping technique in this configuration. Using f.i.a. to present the sample in the plating step provides a clean system capable of good concentration factors with short plating times.

The authors thank Mary Schreiner for helpful discussions, and John Muerle for donation of the PDP 8/f computer and accessories. This work was supported in part by the National Science Foundation under Grant No. CHE 8305748.

REFERENCES

1 D. M. Settle and C. C. Patterson, Science, 207 (1980) 1167.
2 T. R. Copeland and R. K. Skogerboe, Anal. Chem., 46 (1974) 1257A.
3 T. M. Florence, J. Electroanal. Chem., 27 (1970) 273.
4 S. H. Lieberman and A. Zirino, Anal. Chem., 46 (1974) 20.
5 B. Lazar and S. Ben-Yaakov, J. Electroanal. Chem., 108 (1980) 143.
6 M. Wojciechowski, W. Go and J. Osteryoung, Anal. Chem., 57 (1985) 155.
7 J. Wang, H. D. Dewald and B. Greene, Anal. Chim. Acta, 146 (1983) 45.
8 J. Růžička and E. H. Hansen, Flow Injection Analysis, Wiley, New York, 1981.
9 D. Betteridge, Anal. Chem., 50 (1978) 832A.
10 J. Růžička and E. H. Hansen, Anal. Chim. Acta, 99 (1978) 37.
11 M. B. Glauert, J. Fluid Mech., 1 (1956) 625.
12 D.-T. Chin and C.-H. Tsang, J. Electrochem. Soc., 125 (1978) 1461.
13 J. M. Elbicki, D. M. Morgan and S. G. Weber, Anal. Chem., 56 (1984) 978.
14 H. Gunasingham and B. Fleet, Anal. Chem., 55 (1983) 1409.
15 J. Yamada and H. Matsuda, J. Electroanal. Chem., 44 (1973) 189.
16 J. Christie and R. A. Osteryoung, Anal. Chem., 48 (1976) 869.
17 P. Sekhar, J. O'Dea and J. Osteryoung, unpublished work.

Analytica Chimica Acta, 175 (1985) 55—67
Elsevier Science Publishers B.V., Amsterdam — Printed in The Netherlands

TENSAMMETRY WITH ACCUMULATION ON THE HANGING MERCURY DROP ELECTRODE
Part 3. The Behaviour of Triton X-100 in Mixtures with PEG-9000

ZENON ŁUKASZEWSKI*, HANNA BATYCKA and WŁODZIMIERZ ZEMBRZUSKI
Institute of General Chemistry, Technical University of Poznań, 60-965 Poznań (Poland)
(Received 16th November 1984)

SUMMARY

The behaviour of Triton X-100, which can be present in monomeric or associated form, and its mixtures with PEG-9000, which does not undergo association, is described. The tensammetric curve of Triton X-100 alone shows one or two peaks at negative potentials, depending on the concentration of Triton X-100, i.e., on the presence of associated forms. For <2 mg l^{-1}, there is one broad peak, related to monomers of Triton X-100. The calibration plot for this peak is sigmoidal but its rising section (0.05—0.20 mg l^{-1}) is approximately linear. The calibration curve of the second, much narrower, peak related to associated forms of Triton X-100, grows parabolically with increasing concentration of Triton X-100. The behaviour of a mixture of PEG-9000 with a larger amount of Triton X-100 is similar to the behaviour of a model mixture of components with sufficiently different properties (e.g., PEG 1500/PEG 9000). The peak for PEG-9000, the stronger surfactant, is relatively less affected by a large amount of Triton X-100. Even this effect can be decreased by using a suitable preconcentration potential (—1.45 V vs. SCE) so that PEG-9000 can be determined in the presence of a 1000-fold amount of Triton X-100. Both peaks of Triton X-100 are greatly decreased by the presence of PEG-9000 and the broad peak can be completely suppressed. Triton X-100 cannot be determined accurately in the presence of unknown amounts of PEG-9000.

The accumulation of surfactants on the hanging mercury drop electrode (HMDE) prior to the measurement stage, together with the differentiating action of the preconcentration potential, increases the analytical possibilities of tensammetry in comparison with its classical variant based on the DME. These new possibilities can be important for the analysis of surfactant mixtures, which has been illustrated for the example of a mixture of poly(ethylene glycols) having different molecular weights [1]. However, this example concerns an exceptional case of a mixture of surfactants that does not undergo association, and thus is rather a strictly intermediate model than one having practical significance. Usually, surfactants undergo association, in stages after exceeding a certain concentration. Each variety of a surfactant (i.e., in terms of different degrees of association) behaves as an individual surfactant in adsorption processes. Hence, a surfactant which undergoes association behaves as a surfactant mixture after exceeding a certain concentra-

0003-2670/85/$03.30

tion. This complicates the tensammetric curve and so the possibilities for analysis. Of course, the presence of another surfactant in the system, given the possibilities of mutual interferences between surfactants and their competition in the adsorption process, further complicates the interpretation of tensammetric data for such systems. That is why it is necessary to investigate the behaviour of surfactants undergoing association and their mixtures under conditions of tensammetry with accumulation on HMDE.

The purpose of this investigation was first to establish the behaviour of Triton X-100 as an example of a surfactant which undergoes association even when present alone in solution, as well as its behaviour in a mixture with a stronger nonionic surfactant which does not undergo association, and then to estimate the possibility of using tensammetry with accumulation on the HMDE to determine the components of such mixtures. Triton X-100 is a polydispersed polyoxyethyleneoctylphenol monoether having an average of 9.5 oxyethylene units. Polyoxyethylenealkylphenol monoethers are very widely used surfactants but their biodegradation is not satisfactory. That is why methods are needed for the determination of trace concentrations of these surfactants. In addition to a study of the behaviour of Triton X-100 present alone in solution, the behaviour of Triton X-100 in a mixture having a stronger surfactant was also examined. A poly(ethylene glycol) having a molecular weight (m.w.) of 9000 was chosen. The behaviour of PEG-9000 was very well known from the earlier papers [1, 2], and did not create any additional complications of the system from its own association. The behaviour of polyoxyethylenealkylphenol monoethers, including Triton X-100, under conditions of classical tensammetry has been described in numerous papers, and was critically reviewed by Jehring in his monograph [3]. The critical micelle concentration of Triton X-100 is 0.016% [4] or 0.0053% [5], depending on the conditions of its determination.

EXPERIMENTAL

An OH-105 polarograph (Radelkis) was used with a voltage scan rate of 400 mV min^{-1}. The applied amplitude of the alternating voltage was 2 mV. Controlled-temperature Kemula electrode equipment (Radiometer) was used with an additional mercury pool auxiliary electrode. The potential was checked with a digital voltmeter (N-517; Mera-Tronic, Poland). All potentials cited in this paper are against the saturated calomel electrode.

Triton X-100 (Merck) and poly(ethylene glycol) of m.w. (nominal mean) 9000 (Fluka) were used without additional purification.

The sodium sulphate used for preparation of the supporting electrolyte was purified by double crystallization and ignition at 600°C. All solutions were prepared in water thrice-distilled from quartz. Only freshly distilled water was used. Only glass and quartz vessels were used. The supporting electrolyte in all studies was aqueous 0.5 M sodium sulphate.

RESULTS AND DISCUSSION

The behaviour of Triton X-100

Preconcentration of Triton X-100 on the HMDE causes the appearance of one or two negative peaks on the tensammetric curves, depending on the concentration of Triton X-100; this is similar to the case of classical tensammetry. Some examples of these peaks are shown in Fig. 1. The less negative peak at about −1.6 V vs. SCE appears independently of the concentration of Triton X-100. This peak is wide and sometimes bulges on its decreasing section, indicating that it may be composed of two closely adjacent peaks. The more negative of the two peaks of Triton X-100 (at about −1.8 V) is very narrow and appears for concentrations of Triton X-100 exceeding 1–2 mg l^{-1}. It is possible to assume, as with classical tensammetry [3], that a broad peak corresponds to adsorption of the Triton X-100 monomer and the narrow peak to associated forms of Triton X-100.

The influence of the preconcentration potential on the heights of both negative tensammetric peaks of Triton X-100 was investigated over a wide range of potentials, and for surfactant concentrations from 0.05 to 50 mg l^{-1}. The most characteristic dependences, which display the behaviour of both negative peaks of Triton X-100, are shown in Fig. 2. A similar dependence for a longer preconcentration time is shown by curves (a) and (b) in Fig.3. For concentrations of Triton X-100 less than 2 mg l^{-1} only the one broad peak appears on the tensammetric curves. The dependence of this peak height on

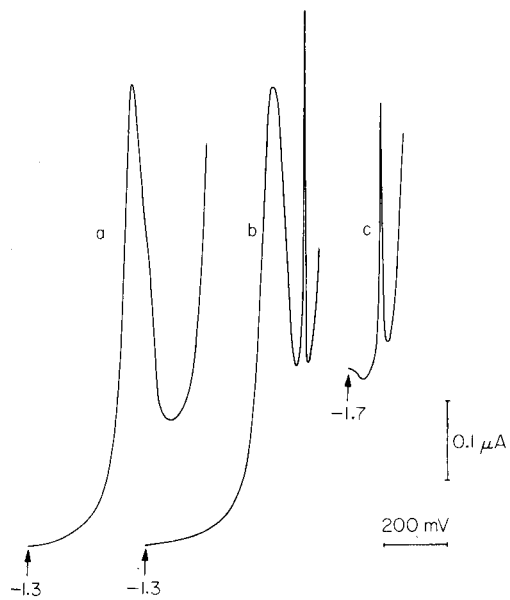

Fig. 1. A.c. polarograms of Triton X-100. Concentration of Triton X-100: (a) 1.0, (b, c) 10 mg l^{-1}. Preconcentration potential: (a, b) −1.30 V, (c) −1.70 V vs. SCE. Preconcentration time 5 min.

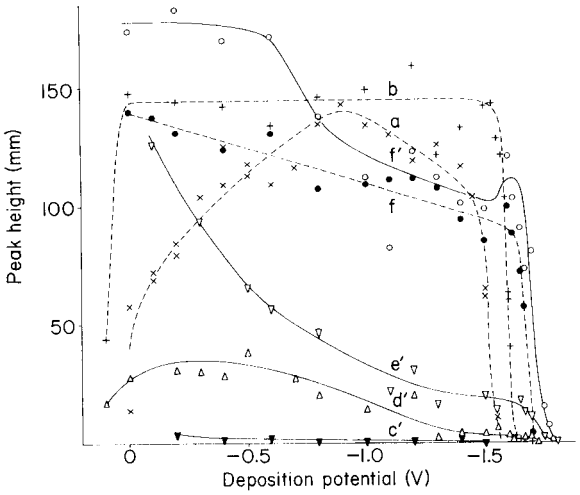

Fig. 2. The dependences of the heights of both tensammetric peaks of Triton X-100 on the preconcentration potential: (---) the broad peak; (—) the narrow peak. Concentration of Triton X-100: (a) 0.5, (b) 1.0, (c') 2.0, (d') 5.0, (e') 7.0, (f) and (f') 10 mg l^{-1}. Preconcentration time 5 min; 100 mm = 0.40 μA.

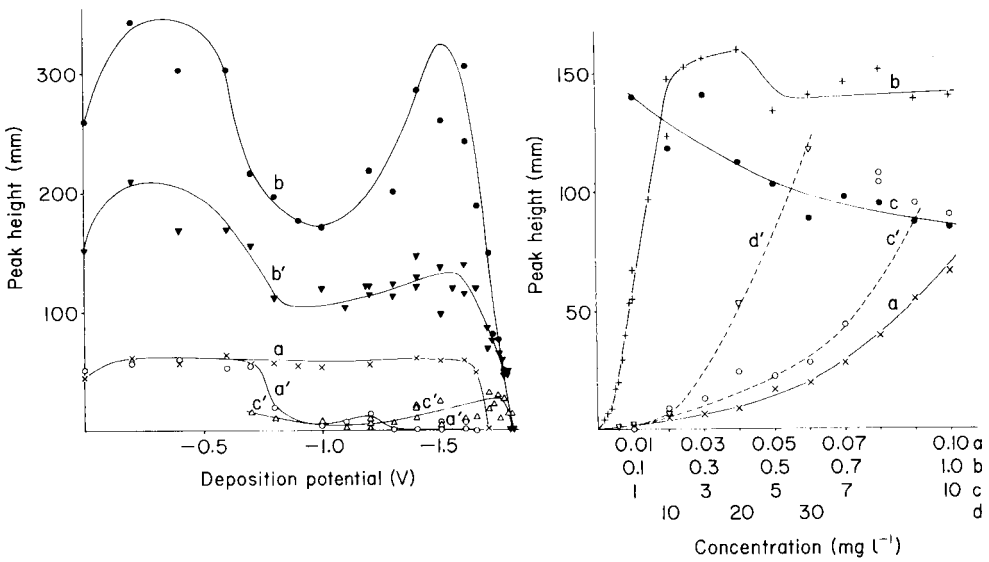

Fig. 3. The dependences of the heights of tensammetric peaks on preconcentration potential for 10 mg l^{-1} Triton X-100: (a, b) alone in solution; (a', b', c') in a mixture of 10 mg l^{-1} PEG-9000. Preconcentration time 10 min; 100 mm = 0.80 μA. See text for further explanation.

Fig. 4. The dependences of the heights of the tensammetric peaks of Triton X-100 on its concentration: (—) the broad peak; (---) the narrow peak. Curves: (a) 0.01—0.10 mg l^{-1}; (b) 0.1—1.0 mg l^{-1}; (c, c') 1—10 mg l^{-1}; (d) 10—30 mg l^{-1}. Preconcentration potential —1.00 V vs. SCE; preconcentration time 5 min; 100 mm = 0.40 μA.

the preconcentration potential varies greatly with the concentration of Triton X-100. For most preconcentration potentials, increase in the Triton X-100 concentration is the primary cause of the changing height of the broad peak (curves a, b, f, Fig. 2). The decrease of the broad peak is accompanied by the appearance of the second, narrow peak. This effect may be caused by the competitive adsorption of associates of Triton X-100 with respect to the monomer. The dependences of the height of the broad peak on the preconcentration potential and on the concentration of Triton X-100 are obviously very complicated (Fig. 2). This is in part due to a shift of the surfactant desorption potential as the surfactant concentration increases; for example, the desorption peak potential changes from −1.584 V at 0.5 mg l^{-1} to −1.719 V vs. SCE at 10 mg l^{-1}.

The narrow peak of Triton X-100 (Fig. 1, curve b) first appears at a concentration of 2 mg l^{-1} after 5 min of preconcentration. However, there are indications of this peak even at lower concentrations, particularly for long preconcentration times. The dependences of the height of this narrow peak on the preconcentration potential for different concentrations of Triton X-100 are displayed in Fig. 2 (curves c′, d′, e′ and f′) and, for a 10-min preconcentration time, also in Fig. 3 (curve b). Figure 2 shows a disproportionately sharp increase of this peak height with increasing surfactant concentration. There is also a considerable rise of the corresponding curves in Fig. 2 as the preconcentration potential is shifted towards 0 V. Somewhat different is the corresponding dependence in Fig. 3 (curve b), because of the longer preconcentration time (10 min). Two maxima are visible, separated by a minimum at a preconcentration potential of about −1.0 V vs. SCE. All these results testify to the easier adsorption of associates (which is probably responsible for the appearance of the narrow peak) in the range of preconcentration potentials from 0 to −0.6 V, and also, for higher concentrations of Triton X-100 and longer preconcentration times, in the range from about −1.4 to −1.6 V vs. SCE. Worse conditions for preconcentration of associates in the intervening potential range seem to be connected with preferred adsorption of Triton X-100 monomer (the broad peak) in this range (Fig. 2, curve a). The other curves in Fig. 3 are discussed in detail later in this paper.

Given a sufficiently high concentration of Triton X-100, its associates adsorb over a wider potential range than the monomers (cf. curves f and f′ in Fig. 2). Between curves (f) and (f′) there is a narrow potential range in which the preconcentration of only associates of Triton X-100 is possible. The separate narrow peak obtained under these conditions is clear from Fig. 1(c).

The dependences of the heights of both peaks of Triton X-100 on the concentration were investigated for the range 0.01—30 mg l^{-1}; a 5-min preconcentration at −1.00 V vs. SCE was used in all cases. The results are shown in Fig. 4. The calibration curve relevant to the broad peak has an approximately linear section between 0.2 and 0.4 mg l^{-1} Triton X-100 (curve b). However, the start of this curve is almost parabolic; this is shown more

clearly by curve (a) which pertains to a lower range of Triton X-100 concentration. At concentrations exceeding 0.4 mg l^{-1} the peak height decreases with increasing Triton X-100 concentrations (see curve c); in parallel, the narrow peak appears and increases. In the concentration range examined, the height of the narrow peak increases parabolically, beginning from 1 mg l^{-1} (curves c′ and d′). The results for 1—30 mg l^{-1} show an approximately linear dependence if the square root of the peak height is plotted against the concentration of Triton X-100. Solutions more concentrated than 30 mg l^{-1} were difficult to test because of strong foaming during the initial deaeration of the solution. This range of concentrations is typical for classical tensammetry.

Apart from the preconcentration potential and surfactant concentration, the preconcentration time is also important. The dependence of the height of the broad peak on the preconcentration time was investigated over the range 0.5—21 min; a preconcentration potential of —0.50 V vs. SCE was used with two concentrations (0.05 and 0.20 mg l^{-1}) of Triton X-100. The results are shown in Fig. 5. When only monomers of Triton X-100 exist in the solution (i.e., for the special case of 0.05 mg l^{-1}), the dependence of the peak height on preconcentration time is similar to those of peak height vs. concentration of Triton X-100 (cf. curve a in Fig. 5 and curve b in Fig. 4). In its rising section this dependence is approximately linear. The formation of the plateau corresponds to attainment of an equilibrium between the elec-

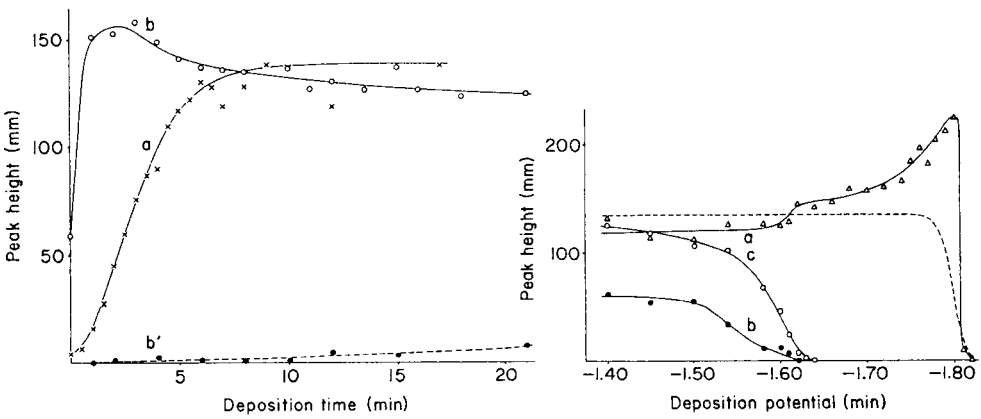

Fig. 5. The dependence of the height of the broad tensammetric peak on preconcentration time at different concentrations of Triton X-100 (solid lines): (a) 0.05; (b) 0.20 mg l^{-1}. (---) The initial stage of formation of the narrow peak of Triton X-100 (0.2 mg l^{-1}) at increasing preconcentration time. Preconcentration potential —0.50 V vs. SCE; 100 mm = 0.40 μA.

Fig. 6. The dependences of the heights of both tensammetric peaks of a mixture of 0.05 mg l^{-1} PEG-9000 and 1.0 mg l^{-1} Triton X-100 on preconcentration potential: (a) narrow peak; (b) broad peak. (c) The relationship for the broad peak of 1.0 mg l^{-1} Triton X-100 alone. (---) The dependence for 0.05 mg l^{-1} PEG-9000 [1]. Preconcentration time 10 min; 100 mm = 0.40 μA.

trode surface and the solution (i.e., accumulation of the surfactant stops). It is interesting to note that after increasing preconcentration times, the narrow peak corresponding to the associates is not significant. With the higher concentration of Triton X-100 (0.2 mg l^{-1}), there is an equilibrium between the electrode surface and the solution for all the preconcentration times tested. The very small concentration of associates in solution means that the narrow peak does not appear for short preconcentration times but later there is partial displacement of the monomers from the mercury surface by associates; the mutual influence of the two varieties of Triton X-100 appears as a reduction in the broad peak (curve b) and an increase in the narrow peak (curve b').

For analytical purposes, both peaks can be used. Based on the height of the broad peak, it is possible to determine Triton X-100 in the range 0.05—0.20 mg l^{-1} (Fig. 4, curve b). The linear range of the calibration curve can be shifted by increasing or decreasing the preconcentration time.

The appearance of the narrow peak on the tensammetric curve is a signal that the level of concentration of Triton X-100 necessary for formation of associates has been exceeded. It is difficult to judge the degree of association, but undoubtedly it is much smaller than that of micelles, because the narrow peak appears even for Triton X-100 concentrations two orders of magnitude less than the critical micelle concentration (c.m.c.). The narrow peak may also be used to determine Triton X-100 in the range 1—30 mg l^{-1}, by using the appropriate calibration curve.

The behaviour of a mixture of Triton X-100 and PEG-9000

Because Triton X-100 at concentrations <2 mg l^{-1} is monomeric in solution, but monomeric and associated at higher concentrations, the behaviour of mixtures of Triton X-100 and PEG-9000 greatly depends on the concentration of Triton X-100. A mixture with <2 mg l^{-1} Triton X-100 should behave like a typical two-component mixture, whereas a mixture with >2 mg l^{-1} Triton X-100 should behave as a three-component mixture.

The behaviour of two mixtures was investigated: (1) a mixture of PEG-9000 and 1 mg l^{-1} Triton X-100, and (2) a mixture of PEG-9000 and 10 mg l^{-1} Triton X-100. First, the influence of the preconcentration potential on the behaviour of the tensammetric curves of a mixture of 0.05 mg l^{-1} PEG-9000 and 1 mg l^{-1} Triton X-100 was studied; the preconcentration time was 10 min at a potential in the range from 0 to -1.85 V vs. SCE. When the preconcentration potential was more positive than -1.61 V, two peaks appeared on the tensammetric curves; the first peak, at less negative potential, was wide and corresponded to monomeric Triton X-100; the second was narrow, corresponding to PEG-9000. When the preconcentration potential was more negative than -1.61 V, only one narrow peak appeared, corresponding to PEG-9000. The dependence of the heights of both peaks on the preconcentration potential for the range from -1.40 to -1.82 V vs. SCE is shown in Fig. 6 (curves a and b). In this interesting range of preconcentration poten-

tials, more measuring points were obtained. For comparison, Fig. 6 includes the corresponding curves for 0.05 mg l^{-1} PEG-9000 and for 1 mg l^{-1} Triton X-100. The dependences for the mixture in the potential range from −0.20 to −1.40 V were the same as the plateaux shown by curves (a) and (b) in Fig. 6.

The broad peak of the mixture reacts to changes of preconcentration potential just like Triton X-100 alone (curves b and c, Fig. 6), but the peak for the mixture is significantly smaller than that for Triton X-100 alone. In the range of adsorption of monomeric Triton X-100, i.e., at preconcentration potentials more positive than −1.62 V, the height of the narrow peak of the mixture, which corresponds to PEG-9000, is a little less than that of PEG-9000 alone. Accumulation outside the adsorption range of Triton X-100 (i.e., within the range from −1.62 to −1.80 V) causes an increase in the narrow peak (curve a and dashed line). This means that monomeric Triton X-100 slightly decreases the PEG-9000 peak when Triton X-100 is adsorbed, but increases the peak when it is apparently not adsorbed, even though in the latter case only the PEG-9000 peak appears. Such surprising behaviour of a surfactant mixture is typical for mixtures of components having sufficiently different adsorption properties, and has been described previously for a mixture of PEG-9000 with an excess of PEG-1500 [2], and for a mixture of Rokanol RZ-12 with an excess of Triton X-100 [6].

The above results show the strong inhibiting influence of a comparatively small concentration of PEG-9000 on the peak of monomeric Triton X-100; this effect makes it impossible to determine Triton X-100 in the presence of an unknown concentration of PEG-9000. It is possible to obtain only the PEG-9000 peak from the mixed solution, by preconcentrating at <-1.63 V vs. SCE, but the peaks obtained will then be higher than those of PEG-9000 alone; this is obvious from Fig. 6. Accumulation at a potential more positive than −1.63 V seems more profitable; although two peaks will appear, the height of that corresponding to PEG-9000 (the narrow peak) will be similar to the value when PEG-9000 is alone in solution.

In order to examine the above possibilities, calibration curves for PEG-9000 in the concentration range 0.01—0.10 mg l^{-1} were obtained in the presence of 1 mg l^{-1} Triton X-1000. Preconcentration was done for 10 min at different potentials within the range from −1.20 to −1.76 V vs. SCE. In all the cases examined, the plots were linear as outlined in Table 1, which also gives the results for PEG-9000 alone. A similar value of the slopes for the mixture examined and for PEG-9000 alone can be obtained for preconcentration at a potential of about −1.45 V vs. SCE.

The inhibiting influence of PEG-9000 on the peak of monomeric Triton X-100 was examined in greater detail. The solutions tested had a constant concentration of Triton X-100 (1 mg l^{-1}), but the concentration of PEG-9000 varied in the range 0.01—0.10 mg l^{-1}. Different preconcentration potentials in the range from −1.20 to −1.50 V vs. SCE were applied. The results (Fig. 7) showed a decrease in the broad peak of Triton X-100, which was a

TABLE 1

The main characteristics of calibration graphs for PEG-9000 in the presence of an excess of Triton X-100 (1 mg l^{-1}) obtained after preconcentration at different potentials

Preconcentration potential (V vs. SCE)	Slope[a] (mm/0.1 mg l^{-1})	Intercept (mm)	Correlation coefficient
−1.20	200.9	−0.5	0.997
−1.30	212.8	−9.9	0.995
−1.35	246.4	−1.7	0.996
−1.40	250.9	+0.03	0.990
−1.45	254.7	−5.5	0.995
−1.50	271.4	−6.8	0.992
−1.64	283.2	+18.7	0.996
−1.70	327.5	+4.7	0.998
−1.76	382.4	+4.9	0.987
PEG-9000 alone			
−1.76	260.4	+0.67	0.999

[a]100 mm = 0.40 μA.

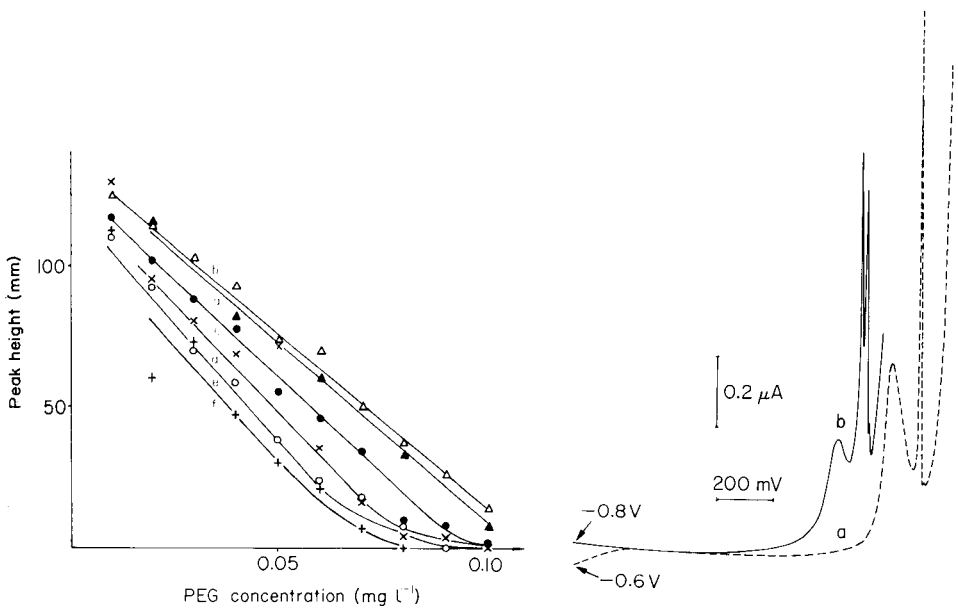

Fig. 7. The dependence of the height of the broad peak of Triton X-100 (1.0 mg l^{-1}) on concentration of PEG-9000, at different preconcentration potentials: (a) −1.20, (b) −1.30, (c) −1.35, (d) −1.40, (e) 1.45 and (f) −1.50 V vs. SCE. Preconcentration time 10 min; 100 mm = 0.04 μA.

Fig. 8. A.c. polarograms of a mixture of 0.10 mg l^{-1} PEG-9000 and 10 mg l^{-1} Triton X-100, obtained at different preconcentration potentials: (a) −0.60 V; (b) −0.80 V vs. SCE. Preconcentration time 10 min.

linear function of the PEG-9000 concentration; this is clearly seen for preconcentration potentials of −1.30 and −1.35 V. The addition of enough PEG-9000 leads to complete disappearance of the broad peak. This happens because PEG-9000, being a stronger surfactant, displaces monomeric Triton X-100 from the mercury surface.

Mixtures having >2 mg l^{-1} Triton X-100 behave in a more complicated way and should be considered as three-component mixtures. In order to examine such mixtures, the influence of the preconcentration potential (for 10 min) on the tensammetric curves was tested for a mixture of 0.1 mg l^{-1} PEG-9000 and 10 mg l^{-1} Triton X-100. The tensammetric curves obtained after preconcentration at potentials in the range from 0 to −0.7 V vs. SCE showed two peaks, similar to those of Triton X-100 alone (curve a, Fig. 8). It seems probable that these two peaks correspond to the usual monomer and associated forms of Triton X-100. Measurements after preconcentration at potentials from −0.8 to −1.8 V vs. SCE provided different tensammetric curves, having four peaks (e.g., curve b, Fig. 8). The third of these peaks (from the left) corresponds to PEG-9000 and the others probably correspond to different varieties of Triton X-100. The dependences of the peak height on the preconcentration potential for these three Triton X-100 peaks are shown in Fig. 3 (curves a′, b′ and c′) and the dependence for the third peak, corresponding to PEG-9000, is shown in Fig. 9 (curve b). For comparison, Fig. 3 includes the corresponding curves for 10 mg l^{-1} Triton X-100 alone (curve a for the broad peak and curve b for the narrow peak), and Fig. 9 includes the curve (a) for 0.1 mg l^{-1} PEG-9000 alone. The influence on the tensammetric curves of the concentration of PEG-9000 (0.01—0.12 mg l^{-1}) in a mixture with 10 mg l^{-1} Triton X-100 was also studied. The two preconcentration potentials tested, −1.20 and −1.76 V vs. SCE, were selected on the basis of Fig. 3. The results obtained with a preconcentration potential of −1.20 V are shown in Fig. 10.

The least negative (broad) peak in Fig. 8 (curves a and b) is connected with monomeric Triton X-100. The presence of 0.1 mg l^{-1} PEG-9000 in solution does not affect the height of this peak if the preconcentration potential is between 0 and −0.7 V (cf. curves a and a′, Fig. 3). However, at the other preconcentration potentials tested, PEG-9000 affects this peak considerably and can cause its disappearance. The influence of the PEG-9000 concentration on the damping of the broad peak of Triton X-100 at a preconcentration potential of −1.20 V vs. SCE, is shown in Fig. 10 (curve a). This influence is similar to that of the mixture containing less Triton X-100 (Fig. 7), and the reason for such behaviour is the same.

In the mixture examined, the second peak of Triton X-100 appears at −1.80 V vs. SCE (second peak from the left on both curves in Fig. 8); 0.1 mg l^{-1} PEG-9000 decreases this peak over the whole range of potentials examined (Fig. 3). However, the inhibition of this peak by increasing concentrations of PEG-9000 is extremely irregular when a preconcentration potential of −1.20 V is used ("curve" b, Fig. 10). This is probably due to

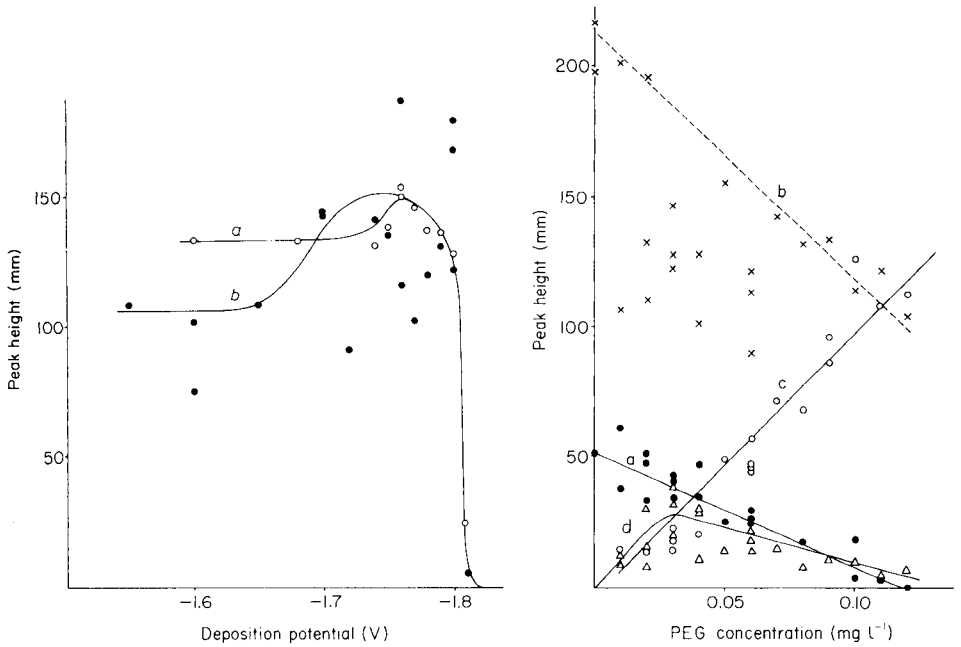

Fig. 9. The dependences on preconcentration potential of the heights of tensammetric peaks for 0.10 mg l^{-1} PEG-9000: (a) alone; (b) in a mixture with 10 mg l^{-1} Triton X-100. Preconcentration time 10 min; 100 mm = 0.80 μA.

Fig. 10. The dependences of the heights of the different peaks on the concentration of PEG-9000: (a) the broad peak, (b) the narrow peak, (c) the peak for PEG-9000, (d) the small peak for Triton X-100 (10 mg l^{-1}). Preconcentration potential −1.20 V vs. SCE; preconcentration time 10 min; 100 mm = 0.80 μA.

competing effects of PEG-9000 and associates of Triton X-100 with respect to adsorption processes and to the non-additivity of currents of closely located peaks caused by baseline problems.

The very small peak of Triton X-100 (the fourth in Fig. 8, curve b), probably is caused by the mutual effects of PEG-9000 and Triton X-100. This peak is situated at −1.83 V vs. SCE and appears only when Triton X-100 is present with other surfactants. The changes of this peak height with preconcentration potential are shown in curve (c′) of Fig. 3 and the changes with increasing concentration of PEG-9000 are shown in Fig. 10 (curve d). A similar peak appears in tensammetric curves of Triton X-100 in the presence of sodium alkylbenzenesulphonate [6]. The appearance of this small peak is probably connected with the polydispersed nature of Triton X-100. The behaviour of Triton X-100 is generally the average behaviour of a multicomponent mixture with different numbers of oxyethylene units. The presence of another surfactant (e.g., PEG-9000) may influence certain components of Triton X-100 in such a way as to produce the small peak.

In contrast to the behaviour of the Triton X-100 peaks in these mixtures, the peak of PEG-9000 usually changes only slightly even when Triton X-100 is in great excess. Only for preconcentration potentials from 0 to −0.7 V vs. SCE is there no peak from PEG-9000 when 10 mg l^{-1} Triton X-100 is present. For preconcentration potentials from −0.8 to −1.65 V vs. SCE, the peak height for PEG-9000 is about 20% lower than that obtained in absence of Triton X-100. This lowering (Fig. 9) is again probably caused by competing adsorption of PEG-9000 and Triton X-100. For preconcentration potentials from −1.70 to −1.81 V vs. SCE, the peak heights for PEG-9000 are similar whether or not Triton X-100 is present (Fig. 9), though the data for the mixture are extremely scattered. Although the tensammetric curves of the mixture containing 10 mg l^{-1} Triton X-100 are very complicated, the calibration plot for PEG-9000 in such a mixture is reasonably linear (curve c, Fig. 10). The straight lines obtained at preconcentration potentials of −1.20 and −1.76 V are characterized by slopes of 211 and 301 mm/0.1 mg l^{-1} PEG-9000 with intercepts of −6.5 and + 4.6 mm and correlation coefficients (r) of 0.963 and 0.980, respectively. Comparison of these slopes with those in Table 1 indicates that the slopes obtained for a preconcentration potential of −1.20 V are similar for mixtures having 1 and 10 mg l^{-1} Triton X-100; however, they are about 20% lower than the slopes for PEG-9000 alone. When the preconcentration potential is −1.76 V, both slopes for the mixtures are higher than the slope for PEG-9000 alone. The optimal value for the preconcentration potential is −1.45 V, which was chosen earlier in this paper for the mixture containing 1 mg l^{-1} Triton X-100. This choice minimizes the difference in results between a mixture containing a variable concentration of Triton X-100 and PEG-9000 alone.

From the analytical point of view, this investigation leads to the conclusion that PEG-9000, as a much stronger surfactant than either the monomeric or associated form of Triton X-100, greatly affects the behaviour of both forms of Triton X-100, even when Triton X-100 is present in great excess. Therefore the routine determination of Triton X-100 in the presence of PEG-9000 is impossible. Fortunately, such a mixture is rather artificial. Usually, poly(ethylene glycols) with m.w. < 1000 occur together with oxyethylated alkylphenols; these are much weaker surfactants than Triton X-100 or PEG-9000. The influence of an excess of Triton X-100 on the behaviour of PEG-9000 is rather small so that PEG-9000 can still be determined. Such behaviour is in agreement with that foreseen by Breyer and Bauer [7].

This research was supported by the Committee of Analytical Chemistry of the Polish Academy of Sciences.

REFERENCES

1 H. Batycka and Z. Łukaszewski, Anal. Chim. Acta, 162 (1984) 207.
2 H. Batycka and Z. Łukaszewski, Anal. Chim. Acta, 162 (1984) 215.

3 H. Jehring, Elektrosorptionsanalyse mit der Wechselstrom-Polarographie, Akademie-Verlag, Berlin, 1974.
4 N. Schönfeld, Grenzflächenaktive Äthylenoxid-Addukte, Wissenschaftliche Verlagsgesell-Schaft MBH, Stuttgart, 1976.
5 D. Vollhardt, Tenside Deterg., 12 (1975) 255.
6 M. K. Pawlak and Z. Łukaszewski, Chem. Anal. (Warsaw), 30 (1985) 377.
7 B. Breyer and H. H. Bauer, Alternating Current Polarography and Tensammetry, Interscience, New York, 1963.

Analytica Chimica Acta, 175 (1985) 69—77
Elsevier Science Publishers B.V., Amsterdam — Printed in The Netherlands

ELECTROCHEMICAL CHARACTERIZATION AND DETERMINATION OF *N*-ACETYLPENICILLAMINE THIONITRITE

ESTHER SANS TAKEUCHI and JANET OSTERYOUNG*

Department of Chemistry, State University of New York at Buffalo, Buffalo, NY 14214 (U.S.A.)

HO-LEUNG FUNG

Department of Pharmaceutics, State University of New York at Buffalo, Buffalo, NY 14214 (U.S.A.)

(Received 8th April 1985)

SUMMARY

Square-wave voltammetry and cyclic voltammetry are used to investigate the electrochemistry of *N*-acetylpenicillamine thionitrite. Thionitrites have been proposed as intracellular intermediates in organic nitrate-induced mammalian vasodilatation. Although these intermediates have been demonstrated indirectly, no sensitive direct determinations have been developed. The electrochemical behavior of this thionitrite at mercury and vitreous carbon electrodes in buffered aqueous media is here described. At mercury, below pH 6.0 one reversible anodic wave and one irreversible cathodic wave are seen. On solid electrodes, only the irreversible wave is present. A determination for thionitrite based on the irreversible cathodic wave is presented. When square-wave voltammetry is used, the current response is linear with concentration in the range of 1—200 $\mu g\ l^{-1}$ (40 μM—1.5 mM). *N*-Acetylpenicillamine does not interfere.

Thionitrites, RSNO, are the subject of current pharmacological research. Compounds which contain this functional group show vascular dilating properties in animals and have been implicated as intermediates for the therapeutic action of organic nitrates, an important class of cardiovascular drugs [1]. Because of the instability of thionitrites, procedures for determining thionitrites have utilized only direct spectrophotometry in the ultraviolet or visible region [1, 2]. These methods are not specific for the thionitrite functional group, and because of the low absorptivities (ϵ = ca. 700 $l\ mol^{-1}\ cm^{-1}$ [2]), they are not very sensitive.

N-Acetylpenicillamine thionitrate (I) has been prepared previously and its crystal structure has been reported [3]. There is hydrogen bonding between the carboxyl and amide groups in the solid, but the structural features do not explain the unusual stability of this thionitrite compound. The thionitrite is readily reduced by tetrahydroborate to give the disulfide. Light presumably promotes the homolytic reaction

0003-2670/85/$03.30

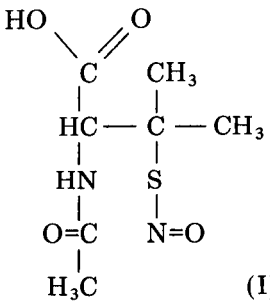

(I)

$$R{-}S{-}N{=}O \rightarrow R{-}S^{\bullet} + {}^{\bullet}NO \quad (1)$$

which is then followed by reaction with RSNO

$$R{-}S^{\bullet} + R{-}S{-}N{=}O \rightarrow RSSR + NO \quad (2)$$

The redox chemistry of this compound at mercury and carbon electrodes is reported below. This seems to be the first electrochemical investigation of the thionitrite functionality. In addition, the cathodic reaction is used as the basis for a more sensitive and selective technique for the determination of *N*-acetylpenicillamine thionitrite (I).

EXPERIMENTAL

Materials

N-Acetylpenicillamine thionitrite was prepared from *N*-acetylpenicillamine (Aldrich Chemical Co.) by the method of Field et al. [3]. Ultraviolet spectra were recorded in acetonitrile and in 1:1 acetonitrile/water. An absorbance maximum at 595 nm was found in both cases, which agrees well with previously reported spectra [3]. Fresh solutions of I were prepared daily and kept in the dark. Decomposition during a single day was not a problem. Acetonitrile (Burdick and Jackson, UV), ethanol (U.S. Industrial Chemicals) and salts for preparation of buffer solutions were used as received. Water was purified by passing distilled water through a Millipore Milli-Q purification system.

Methods

Voltammetric experiments were done in a standard 3-electrode cell with a platinum wire auxiliary electrode and a saturated calomel reference electrode. All potentials were measured and are reported with respect to this electrode. Solutions were deaerated with purified argon. Cyclic voltammetry was done with an IBM EC/225 voltammetric analyzer. Experiments involving square-wave voltammetry were done with a voltammetric instrument based on a Digital Equipment Corp. PDP 8/e minicomputer and a homemade interface [4].

Working electrodes were an EG&G PARC static mercury drop electrode (SMDE) Model 303 with a small drop size of area 0.0120 cm^2 or a commer-

cial, glass-shrouded vitreous carbon electrode with area 0.283 cm^2. The carbon electrode was polished prior to use with 1.0-μm alumina on a nylon polishing cloth by using a Buehler Minimet polisher equipped with a specially designed electrode holder [5].

Bulk electrolysis was done by using a working electrode of reticulated vitreous carbon (Normar Industries, Anaheim, CA; Normar Industries is no longer supplying RVC; it can be obtained now from Electrosynthesis Corporation, East Amherst, NY). In addition to platinum auxiliary and saturated calomel electrodes, a vitreous carbon disk electrode was placed in the cell to monitor voltammetrically the progress of the reaction. Potential control was maintained with an EG&G PARC Model 174 polarographic analyzer.

RESULTS AND DISCUSSION

Cyclic voltammetry at a static mercury drop electrode

N-Acetylpenicillamine thionitrite (I) in aqueous solutions of pH 6—7 shows a reversible wave on mercury with separation of the cathodic and anodic peak potentials equal to 60 ± 5 mV (Fig. 1). The open-circuit potential at pH 6.0 is —0.27 V; the cathodic wave does not appear unless the potential has been made more positive than this value. Over the range of scan rates $0.005 \leqslant v \leqslant 0.100$ V s^{-1}, diffusion control is demonstrated by $\partial \log i_p / \partial \log (v^{1/2}) = 0.97$. Calculation of n from the Randles—Sevcik equation [6], using $D_0 = 7.8 \times 10^{-6}$ cm^2 s^{-1} reported for penicillamine [7], yielded $n = 0.98$, suggesting that this electrochemical process is a one-electron oxidation.

The voltammetry of compound I at mercury depends on pH. The potential at half-peak height, $E_{p/2}$, of the reversible wave shifts to more negative values with increasing pH. A plot of $E_{p/2}$ vs. pH (over the pH range 1—7) yields a straight line with a slope of 57 mV/pH unit. This is consistent with a one-proton, one-electron transfer. Above pH 7.0 the wave becomes more irreversible. At scan rates of $0.020 \leqslant v \leqslant 0.100$ V s^{-1} the cathodic peak current exceeds the anodic peak current, and the peak separation is greater than 0.070 V. Below pH 5.0, an adsorption prewave is present.

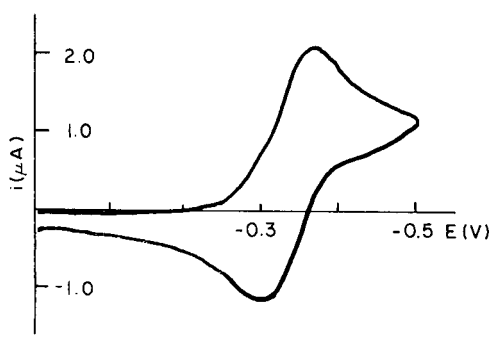

Fig. 1. Cyclic voltammogram of 1 mM *N*-acetylpenicillamine thionitrite at the SMDE in 0.1 M KH_2PO_4, pH 6.0; v = 50 mV s^{-1}.

On mercury, the voltammetric behavior of compound I is similar to that of *N*-acetylpenicillamine (II), and of the parent compound, penicillamine, in

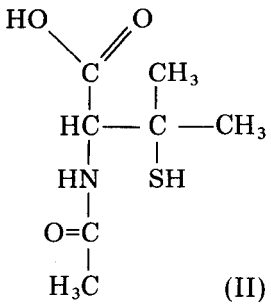

(II)

the potential range of the reversible wave. Voltammograms have the same $E_{p/2}$ values and display the same pH dependence. An adsorption prewave similar to that of the thionitrite (I) has also been reported in the polarography of penicillamine [7]. The electrode reaction of penicillamine on mercury has been reported [7] to be

$$RSH + Hg \rightleftharpoons RSHg + H^+ + e^- \quad (3)$$

The anodic oxidation of mercaptans on mercury anodes to form mercury mercaptides is a well-known general reaction [8]. It is reasonable to suggest, therefore, considering reactions 1 and 3, that the overall reaction responsible for the reversible wave of Fig. 1 is

$$RSNO + Hg + H_2O \rightarrow RSHg + HONO + H^+ + e^- \quad (4)$$

The organic mercaptide product in reaction 4 is that which would result from anodic oxidation of mercury in the presence of compound II. Furthermore, the thionitrite I is prepared by the reaction of compound II with nitrous acid. It is extremely difficult to ensure that preparations of compound I contain no HONO. In fact, in solution the reaction

$$RSNO + H_2O \rightleftharpoons RSH + HONO \quad (5)$$

(I) (II)

may be an equilibrium. Therefore, further elucidation of the reversible anodic reaction was not attempted.

In acidic media, an irreversible cathodic wave is seen at a potential about 800 mV negative of the reversible wave (Fig. 2a). In view of reaction 5, it is possible that the irreversible wave is due to residual nitrous acid [9]. Addition of excess of ammonium sulfamate, which is known to react quantitatively with nitrous acid [10], did not eliminate the irreversible reduction wave (Fig. 2b). When mercury(II) nitrate was added, however, the irreversible wave was eliminated while the reversible wave remained. It has been previously demonstrated [10] that mercury(II) salts react with thionitrite functionalities to form mercury(II) complexes:

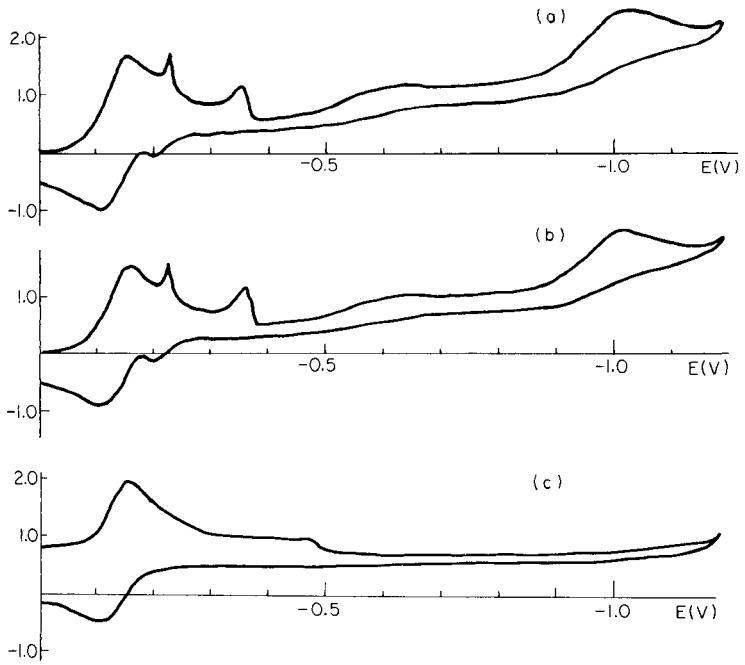

Fig. 2. (a) Cyclic voltammograms. (a) 1 mM *N*-acetylpenicillamine thionitrite at the SMDE in 0.1 M potassium hydrogenphthalate, pH 3.0; v = 50 mV s^{-1}. (b) After adding 10-fold excess of ammonium sulfamate. (c) After adding 2 equivalents of mercury(II) nitrate.

$$RSNO + Hg^{2+} + H_2O \rightarrow RSHg^{+} + HONO + H^{+} \quad (6)$$

Thus, the irreversible wave is consistent with a reduction of the thionitrite moiety of *N*-acetylpenicillamine thionitrite.

Electrochemistry with carbon electrodes

Because of the reactivity of the thionitrite functionality with mercury salts and the electrochemical reactivity of penicillamine on mercury [9, 11—14], carbon electrodes were explored as materials for thionitrite reduction. In acidic buffer, for a carbon electrode, only the irreversible reduction wave is present, whereas the parent penicillamine compound II is not electroactive. The thionitrite reduction wave of compound I depends on the surface pretreatment of the carbon electrode. If the carbon surface is polished with 1-μm alumina prior to use, the wave appears as in Fig. 3(a). Further polishing on a clean wet nylon cloth yields the more irreversible voltammogram shown in Fig. 3(b). Ultrasonic cleaning of the electrode prior to use yields the voltammogram shown in Fig. 3(c). These results resemble the observations of Kuwana and co-workers [15, 16] on the role of alumina in electrochemistry at carbon electrodes. Carbon paste electrodes were also used to observe the

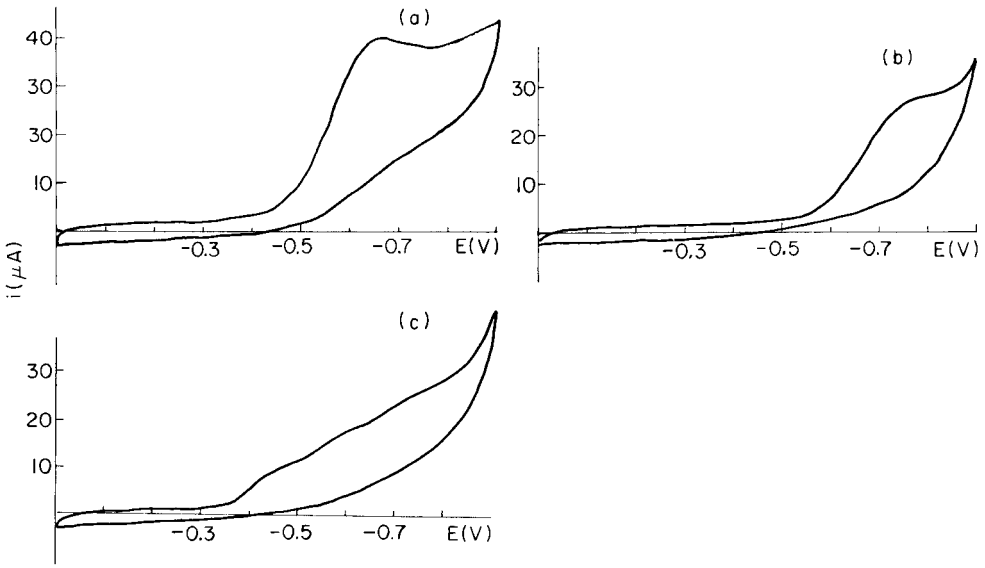

Fig. 3. Cyclic voltammogram of 1 mM *N*-acetylpenicillamine thionitrite on vitreous carbon in a 0.1 M HCl/KCl buffer at pH 2.0 (v = 50 mV s^{-1}). Electrode treatment: (a) polished with 1-μm alumina; (b) after further polishing on a wet cloth; (c) as (a) after sonifying the electrode in distilled water.

thionitrite reduction. However, the wave was 120 mV more negative than on glassy carbon and gave a smaller peak current.

The solution pH affects the thionitrite reduction at carbon. The peak current increases as the pH is decreased; maximum values of peak current are obtained at pH 2.0 (Fig. 4). Above pH 7.0 the reduction wave is no longer visible. The potential of the reduction wave also seems to shift to more negative values with increasing pH. The neutralization point of 0.05 M aqueous *N*-acetylpenicillamine thionitrite was determined by titration with 0.1 M sodium hydroxide; the pH at the end-point was found to be 6.8. The pK_a (evaluated as the pH at the half-equivalence point) was 3.3.

The number of electrons involved in the thionitrite reduction on carbon was established in two ways. The first method used was an exhaustive electrolysis of a 1 mM solution of *N*-acetylpenicillamine thionitrite in 0.1 M HCl/KCl buffer at pH 2.0 with a block of reticulated vitreous carbon (RVC) as the working electrode. A current/time curve was recorded during the electrolysis, which was monitored by both cyclic voltammetry on a glassy carbon disk in the cell and by the return of the electrolysis current to background values. Integration of the current/time trace yielded the value of n = 0.90.

The value of n was also estimated from cyclic voltammetry. The change in E_p with scan rate was measured over the range of 0.010—0.200 V s^{-1} ($\partial E_p/\partial \log v$ = —0.056 V). From this value, αn_a = 0.53. This value was then used

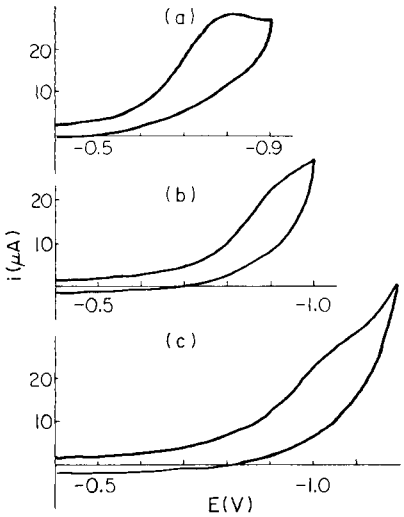

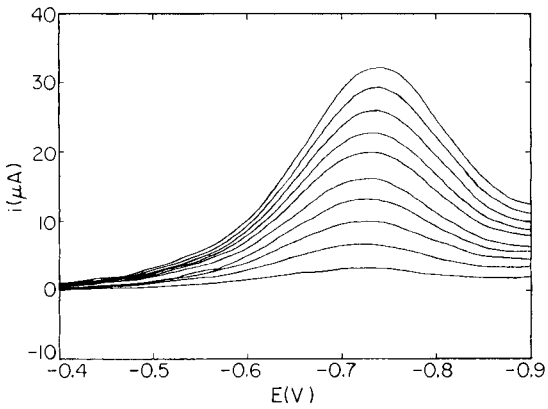

Fig. 4. Cyclic voltammogram of 0.5 mM *N*-acetylpenicillamine thionitrite on a vitreous carbon electrode (v = 50 mV s^{-1}): (a) 0.1 M HCl/KCl, pH 2.0; (b) 0.1 M potassium hydrogenphthalate, pH 4.0; (c) 0.1 M KH_2PO_4, pH 6.0.

Fig. 5. Square-wave voltammetry of *N*-acetylpenicillamine thionitrite from 0.1 mM to 1 mM in steps of 0.1 mM, in 0.1 M HCl/KCl, pH 2.0. Step height 5 mV, amplitude 25 mV, frequency 10 Hz.

with values of peak current to obtain n by using the expression for a totally irreversible reaction [6]. Again, the value of $D_0 = 7.8 \times 10^{-6}$ cm^2 s^{-1} reported for penicillamine was used [7]. This method gave n = 0.86.

Bulk electrolysis on RVC was also used to investigate the reduction products. After exhaustive reduction at —0.75 V vs. SCE in 0.1 M HCl/KCl at pH 2.0, the solution was examined by u.v. spectroscopy and normal-pulse voltammetry. Spectra of the solution after electrolysis showed maxima at 206 and 261 nm. Ultraviolet spectra were then recorded for samples of *N*-acetylpenicillamine thionitrite (I), *N*-acetylpenicillamine (II) and *N*-acetylpenicillamine disulfide in the same buffer solution. The thionitrite showed a maximum at 595 nm which was no longer present in the spectrum after electrolysis. The disulfide had a maximum at 216 nm, whereas *N*-acetylpenicillamine had maxima at 206 and 261 nm. Thus, the spectrum of the electrolysis product matched that of *N*-acetylpenicillamine.

Normal pulse polarography was applied to the solution after electrolysis. An anodic wave with $E_{1/2}$ = —0.18 V was found. A similar anodic wave was present in solutions of *N*-acetylpenicillamine. Solutions of *N*-acetylpenicillamine disulfide showed an additional cathodic wave at —1.08 V which was not present in the polarography of the other solutions. Thus, the spectral and polarographic data point to the production of *N*-acetylpenicillamine in the reduction of the thionitrite (I). These data do not prove, but suggest, that the cathodic reduction at ca. —0.8 V is due to the reactions

$$RSNO + H^+ \rightleftharpoons (RSNO)H^+; (RSNO)H^+ + e^- \rightleftharpoons RSH + NO$$

(I)

Quantitative method for the thionitrite(I)

Square-wave voltammetry [17] was used to develop a method for the determination of *N*-acetylpenicillamine thionitrite. Even at solid electrodes, this technique is superior to linear-scan voltammetry both in sensitivity and in rejection of background currents [17]. The measurements were done on freshly polished carbon electrodes in pH 2.0 or 3.0 buffer solutions to maximize the peak height of the reduction wave. The experiments were conducted by using a step height of 5 mV, an amplitude of 25 mV and frequencies of 10, 30 or 200 Hz. Three voltammograms were recorded and averaged for each concentration. Concentrations were increased by adding aliquots of freshly prepared 0.01 M stock solutions to the cell. After each addition, the solutions were stirred and deaerated for 4 min.

A typical result is shown in Fig. 5. The resulting calibration curve from the values of peak current has a sensitivity (slope) of 32.3 μA mM^{-1} with an intercept 0.300 μA and correlation coefficient 0.997. Figure 6 shows an example of the upper limit of linear response of current to concentration. At pH 2.0 and 30 Hz, the upper useful concentration limit is about 1.5 mM. This upper range is similar at pH 3.0 for a frequency of 10 Hz. Figure 7 shows the current response in the concentration range 10^{-5}—10^{-4} M at pH 3.0 and 10 Hz. The calibration graph for these data has a slope of 21.3 μA mM^{-1}, intercept 0.333 μA and correlation coefficient 0.9995.

The detection limit, *d.l.*, for square-wave voltammetry can be estimated from $d.l. = 3\ s/m$, where s is the standard deviation of a least-squares line

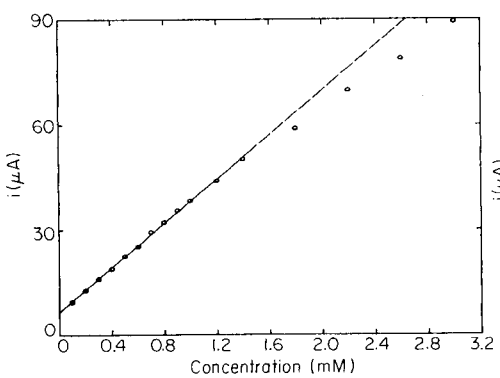

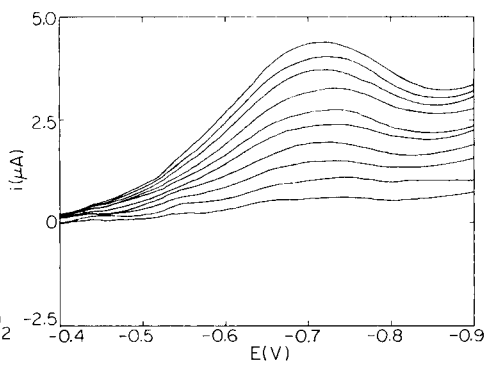

Fig. 6. Square-wave peak current vs. concentration for *N*-acetylpenicillamine thionitrite on a vitreous carbon electrode at 30 Hz in 0.1 M HCl/KCl buffer, pH 2.0.

Fig. 7. Square-wave voltammetry of *N*-acetylpenicillamine thionitrite from 0.01 to 0.2 mM in steps of 0.01 mM in 0.1 M potassium hydrogenphthalate, pH 3.0. Step height 5 mV, amplitude 25 mV, frequency 10 Hz.

fitted to the background in the potential range of interest and m is the slope of the calibration plot [18]. According to this method, at pH 2.0 and 10 Hz, the detection limit is 40 μM. At 30 Hz, the limit is 50 μM and at 200 Hz the limit is 280 μM. At pH 3.0 and 10 Hz, the limit is 60 μM. The lowest detection limit was obtained at pH 2.0 at a frequency of 10 Hz. The analytical signal increases as the square root of frequency, but at higher frequencies the background noise increases more rapidly with frequency than does the signal. However, the detection limit of 40 μm is more than 100-fold below that previously reported for a spectral method [3]. The voltammetry was examined in the presence and absence of *N*-acetylpenicillamine with no effect on the detection limits.

Thus, square-wave voltammetry can be used to determine the concentration of *N*-acetylpenicillamine thionitrite and distinguish it from *N*-acetylpenicillamine in acidic media on a carbon electrode. The useful range is 40 μM to 1.5 mM over which current response is linear with concentration with correlation coefficients of at least 0.999. The electrochemical method has better sensitivity than spectral methods and allows selective determination in the presence of *N*-acetylpenicillamine.

This work was supported in part by NSF grant CHE 8305748 and by NIH grant GM20852.

REFERENCES

1 L. J. Ignarro, H. Lippton, J. D. Edwards, W. H. Baricos, A. L. Hyman, P. J. Kadowitz and C. A. Gruetter, J. Pharmacol. Exp. Ther., 218 (1981) 739.
2 S. Oae, Y. H. Kim, D. Fukushima and K. Shinhama, J. Chem. Soc., Perkin Trans. 1: (1978) 913.
3 L. Field, R. V. Dilts, R. Ravichandran, P. G. Lenhert and G. E. Carnahan, J. Chem. Soc. Chem. Comm., (1978) 249.
4 T. R. Brumleve, J. J. O'Dea, R. A. Osteryoung and J. G. Osteryoung, Anal. Chem., 53 (1981) 702.
5 M. Shreiner, J. J. O'Dea, N. Sleszynski and J. G. Osteryoung, Anal. Chem., 56 (1984) 116.
6 A. J. Bard and L. R. Faulkner, Electrochemical Methods, Wiley, New York, 1980.
7 M. Jemal and A. M. Knevel, J. Electroanal. Chem., 95 (1979) 201.
8 A. P. Tomilov, S. G. Mairanovskii, M. Ya. Fioshin and V. A. Smirnov, Electrochemistry of Organic Compounds, Halsted Press, New York, 1972, p. 470.
9 D. T. Sawyer and J. L. Roberts, Jr., Experimental Electrochemistry for Electrochemists, Wiley, New York, 1974.
10 B. Saville, Analyst, 83 (1958) 670.
11 U. Forsman, J. Electroanal. Chem., 111 (1980) 325.
12 R. Saetre and D. L. Rabenstein, Anal. Chem., 50 (1978) 276.
13 T. M. Florence, J. Electroanal. Chem., 97 (1979) 219.
14 J. J. Vallon and A. Badinand, Anal. Chim. Acta, 42 (1968) 445.
15 J. Zak and T. Kuwana, J. Am. Chem. Soc., 104 (1982) 5514.
16 S. Dong and T. Kuwana, J. Electrochem. Soc., 131 (1984) 813.
17 J. Osteryoung and R. A. Osteryoung, Anal. Chem., 57 (1985) 101A.
18 J. A. Turner, J. H. Christie, M. Vukovic and R. A. Osteryoung, Anal. Chem., 49 (1977) 1904.

Analytica Chimica Acta, 175 (1985) 79—88
Elsevier Science Publishers B.V., Amsterdam — Printed in The Netherlands

DETERMINATION OF NICKEL AND COBALT IN NATURAL WATERS AND BIOLOGICAL MATERIAL BY REDUCTIVE CHRONOPOTENTIOMETRIC STRIPPING ANALYSIS IN A FLOW SYSTEM WITHOUT SAMPLE DEOXYGENATION

H. ESKILSSON and C. HARALDSSON

Department of Analytical and Marine Chemistry, Chalmers University and University of Göteborg, S-412 96 Göteborg (Sweden)

D. JAGNER*

Department of Technical Analytical Chemistry, Chemical Center, University of Lund, P.O. Box 124, S-221 00 Lund (Sweden)

(Received 18th March 1985)

SUMMARY

The instrumental set-up consists of a thin-layer cell with a glassy carbon working electrode and an inlet valve by means of which six different solutions can be sucked through the cell. The system is controlled by a microprocessor and suction is provided by means of a peristaltic pump. In the first step of the analytical cycle, a mercury film is plated onto the glassy carbon electrode and then the sample solution is allowed into the cell and nickel(II) and cobalt(II) are potentiostatically adsorbed onto the mercury film as their dimethylglyoxime complexes. Nickel(II) and cobalt(II) are then reduced in a medium of 5 M calcium chloride by means of constant current and simultaneously the microprocessor records the potential vs. time behaviour of the working electrode. Finally the mercury film is removed by mild oxidation in an iodine/iodide solution and the glassy carbon surface is cleaned with ethanol and sodium hydroxide prior to the next analytical cycle. The cobalt(II) and nickel(II) concentrations are evaluated by means of a standard addition procedure. The technique was applied to drinking, estuarine and sea water samples. The detection limits on the one sigma level after one minute of potentiostatic adsorption were 9 and 11 ng l^{-1} for nickel(II) and cobalt(II), respectively. Nickel(II) and cobalt(II) were determined in reference samples of bovine liver and sea-water sediments after acid digestion. In order to obtain correct cobalt values, it was necessary to reduce cobalt(III) species formed during the acid digestion with sodium tetrahydroborate.

The determination of trace concentrations of nickel and cobalt by using electroanalytical stripping techniques has been described by Pilar et al. [1]. Their method is based on the potentiostatic adsorption of the dimethylglyoxime complexes [2, 3] on a mercury drop electrode and the subsequent generation of the analytical signals by means of reductive differential pulse stripping voltammetry. The method is highly sensitive and under optimum conditions nickel concentrations down to 1 ng l^{-1} can be detected. It is, however, a batch procedure and, furthermore, it is necessary to deoxygenate the samples prior to adsorption, thus it is not an easily automated technique.

0003-2670/85/$03.30

Consequently, it was considered interesting to exploit the results of Pilar et al. [1] in a study of automated electroanalytical techniques based on the flow potentiometric stripping technique [4—6]. In order to do so, the method of Pilar et al. [1] would, however, have to be modified extensively. Normally, flow potentiometric stripping analysis is based on the potentiostatic reduction and simultaneous amalgamation of the trace metal analytes on a freshly prepared mercury film electrode and the subsequent chemical re-oxidation of these elements in a suitable matrix. During oxidation, the potential of the working electrode is monitored at constant time intervals and the time needed for the re-oxidation of an element provides the analytical signal. In order to apply these principles to the earlier results [1], it is necessary to investigate the possibility of adsorbing the dimethylglyoxime complexes on a freshly prepared mercury film electrode and also to investigate reagents capable of chemical reduction of these complexes. After the commencement of this work, Meyer and Neeb [7] reported on the successful adsorption of the nickel and cobalt dimethylglyoxime complexes on a mercury film electrode. Preliminary investigations showed that chemical reduction of nickel(II) and cobalt(II) in these complexes was feasible by using strong reductants such as sodium tetrahydroborate. Solutions of such reagents are, however, not stable on storage and thus not suitable in routine analysis. For this reason the idea of chemical reduction was abandoned early in the investigation.

An alternative way of obtaining a constant reduction rate is by means of a constant reducing current. In this approach, the potential vs. time behaviour can be monitored and evaluated in the same way as in normal potentiometric stripping analysis [8]. In the flow system the reducing current will, however, not only reduce adsorbed nickel(II) and cobalt(II) in their dimethylglyoxime complexes but also reduce all oxidants (e.g., dissolved oxygen) present in the stripping medium. Consequently, the stripping medium must be deoxygenated prior to analysis. Traditionally, this is achieved by inert gas bubbling. In an automated flow system it is, however, almost impossible to prevent oxygen from diffusing through the teflon tubings. An alternative way of obtaining virtually oxygen-free stripping solutions is by means of concentrated electrolytes, e.g., 5 M calcium chloride or nitrate. Such solutions have been used previously in order to reduce the oxidation rate in normal flow potentiometric stripping analysis [5] and it has been found that they are stable for several weeks even if they are exposed to air humidity.

This paper describes the automated determination of trace concentrations of nickel(II) and cobalt(II) in aqueous solutions. Special attention is focused on the complications in the determination of cobalt in biological material after oxidative acid treatment because of the difficulties in the formation of the cobalt(II) dimethylglyoxime complex.

EXPERIMENTAL

Electrochemical flow cell and flow system

The thin-layer flow cell is shown in detail in Fig. 1. It consists of a glassy carbon electrode (2 mm diameter) pressure-fitted into a teflon cylinder. A 0.1-mm teflon spacer separates the working electrode from the reference and counter electrode compartment. The flow channel in the teflon spacer is 2×6 mm^2. The reference electrode is a Radiometer K4040 calomel electrode and the counter electrode a 20-mm platinum wire (0.5 mm diameter). A 3-mm zirconium dioxide cylinder (2 mm diameter) separates the counter electrode department from the solutions in the flow channel (Fig. 1). The resistance in the zirconium cylinder when the counter electrode department is filled with 1 M KCl is less than 50 Ω.

The flow system shown in Fig. 2 consists of a Gilson Minipuls-2 peristaltic pump by means of which six different solutions can be sucked into the flow cell through an Altex 401 rotated valve [4—6]. All connections were made with 1-mm i.d. teflon tubings and the flow rate could be varied between 0.024 and 2.4 ml min^{-1}.

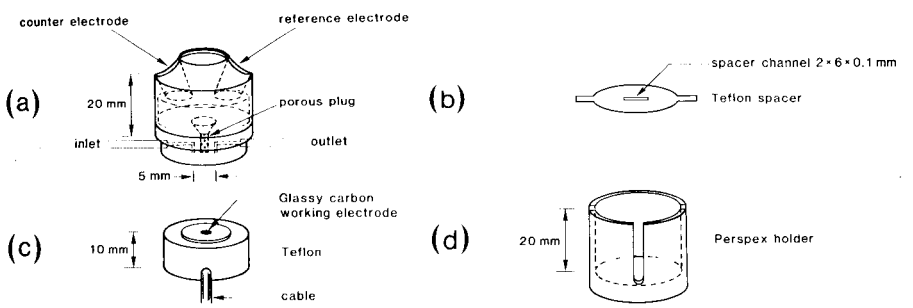

Fig. 1. Electrochemical flow cell: (a) perspex counter and reference electrode compartment; (b) teflon spacer; (c) pressure-fitted glassy carbon electrode; (d) perspex holder for teflon spacer and glassy carbon electrode. The cell is held together by a clamp.

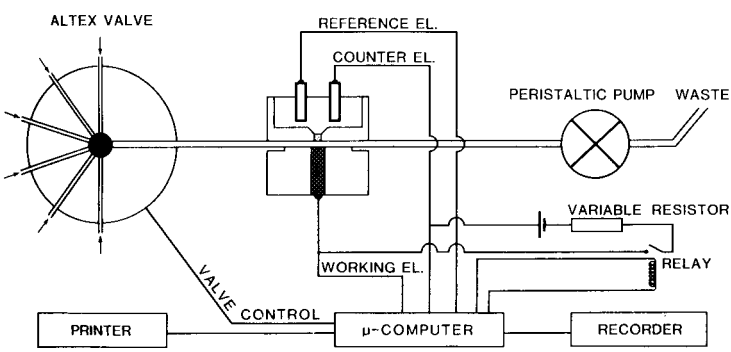

Fig. 2. Flow system.

Instrumentation

The measurement system consists of a Radiometer ISS-820 ion scanning system and a purpose-built microcomputer system which has been described in detail elsewhere [8]. After formation of the mercury film and adsorption of the dimethylglyoxime complexes, the potentiostatic circuitry is disconnected and the reducing current through the working and counter electrodes is connected simultaneously (cf. Fig. 2). A constant reducing current is provided by means of a 4.5-V battery and a variable (1—10 MΩ) load resistance (Fig. 2). During reduction of nickel(II) and cobalt(II) in their dimethylglyoxime complexes, the working electrode potential is sampled at a real time rate of 30 kHz. The potential readings are divided into channels with a width of 2.5 mV. In this way, the potential range scanned, typically —0.5 to —1.2 V vs. SCE, is subdivided into potential regions of 2.5 mV. During potential sampling, the number of potential readings (referred to below as counts) falling in each 2.5-mV potential region are summed. Each count thus corresponds to 33 μs. The stripping time (number of counts) for an element is evaluated as the number of counts between two preprogrammed potential boundaries. The boundaries used were adjusted slightly from day to day but were normally —0.865 to —1.005 V vs. SCE for nickel and —1.005 to —1.105 for cobalt.

Reagents

Stock standard solutions of mercury(II), nickel(II) and cobalt(II) all 1 g l^{-1} in 0.2 M nitric acid, were prepared from Titrisol ampoules (Merck) and standards of lower concentrations were obtained by appropriate dilution with doubly distilled water. Analytical-grade reagents and solvents were used unless otherwise noted. Nearly saturated calcium chloride solution (5 M) was prepared from calcium chloride dihydrate (Merck) dissolved in doubly distilled water. The dimethylglyoxime stock solution was 0.1 M in 95% ethanol. The 3 M ammonia buffer of pH 9.2 was made from equal volumes of 7.5 M isothermally distilled ammonia and 6.5 M sub-boiled hydrochloric acid, by suitable dilution with doubly distilled water. The 1 M acetate buffer was prepared from sodium acetate and acetic acid. The sodium tetrahydroborate solution was 0.25 M in 0.1 M sodium hydroxide.

Reference sea-water sample NASS-1 was obtained from the National Research Council, Canada [9]. Reference sediment samples, MESS-1 and BCSS-1, were obtained from the same source. The bovine liver sample was obtained from the National Bureau of Standards, U.S.A.

Procedures

Wet digestion of sediment and biological material. The sample (1 g) is weighed into a 100-ml Pyrex flask. After addition of 5 ml of concentrated sulphuric acid and 15 ml of concentrated nitric acid the mixture is heated to boiling for 2 h. Subsequently, 5 ml of 35% hydrogen peroxide is added slowly in portions and boiling is continued for 15 min. The solution is finally

diluted to 100 ml with doubly distilled water. Blank samples are obtained by using the same digestion procedure with doubly distilled water instead of the sample.

Electroanalytical procedure for natural waters. To 100 ml of sample, 2.5 ml of the pH 9.2 ammonia buffer and 1 ml of the dimethylglyoxime solution are added. The operational sequence consists of five different procedures, namely, formation of a fresh mercury film, potentiostatic adsorption of the dimethylglyoxime complexes onto the mercury film surface, constant-current reduction of the metal ions in their dimethylglyoxime complexes and simultaneous real-time recording of the mercury electrode potential, removal of the mercury film by chemical oxidation of mercury in a strongly complexing medium, and finally cleaning of the glassy carbon surface in one or two different solutions prior to the formation of a new mercury film in the next cycle. Each of these procedures is done in a different solution. The compositions of these solutions in the determination of nickel and cobalt in natural waters are shown in Table 1. Also shown in the table are the potentials applied to the working electrode and the times that the different solutions are in the flow cell. The metal concentrations are evaluated by two or three standard additions of appropriate magnitude. The operational sequence in Table 1 was used for the determination of both nickel(II) and cobalt(II) in natural waters. Normally the concentration of cobalt(II) in the samples was below the detection limit of the method. Slightly improved sensitivity for cobalt(II) could be obtained by using the pH 5.2 buffer as described below.

TABLE 1

Electroanalytical cycle for the determination of nickel and cobalt in natural waters and acid digests of biological material. For the determination of cobalt in great excess of nickel, a potentiostatic adsorption potential of −0.75 V vs. SCE is used

Solution[a]	Duration (s)	Potential (V vs SCE)	Current (μA)	Remarks
0.001 M Hg(II) 0.2 M HCl	20	−0.5	—	Plating of Hg on film
Sample pH 5.2 or 9.4, 0.001 M dimethylglyoxime	5—180	−0.5	—	Adsorption of Ni(II) and Co(II) complexes
5 M $CaCl_2$	20	−0.5	—	Rinsing
5 M $CaCl_2$	0.5—5	—	1	Reduction of Ni(II) and Co(II); potential vs. time recorded
0.005 M I_2 in 1 M KI	30	—	—	Hg film removed
50% Ethanol	10	—	—	Rinsing glassy carbon surface
1 M NaOH	Until next cycle	—	—	Rinsing glassy carbon surface

[a] All solutions were pumped at a flow rate of 2.4 ml min^{-1}.

Electroanalytical procedure for the determination of nickel in sediment and biological material. An aliquot (0.5—5 ml) of the diluted acid digest is transferred to a polyethylene bottle and diluted to 80 ml with doubly distilled water. After that, 2.5 ml of the pH 9.2 ammonia buffer and 1 ml of the dimethylglyoxime solution are added and the volume is adjusted to 100 ml. The magnitude of the acid digest aliquot should be chosen so that the analytical signals are within the linear range of the calibration curve as discussed below. The nickel concentration is evaluated by means of two or three standard additions using the sequence in Table 1.

Electroanalytical procedure for the determination of cobalt in sediment and biological material. To an aliquot (0.5—5 ml) of the diluted acid digest, 2 ml of the sodium tetrahydroborate solution is added and the mixture is diluted to 80 ml with doubly distilled water. After that, 5 ml of the pH 5.2 buffer and 1 ml of the dimethylglyoxime solution are added and the volume is adjusted to 100 ml. Cobalt(II) is evaluated by two or three standard additions by using the analytical sequence of Table 1 with an adsorption potential of —0.75 V vs. SCE.

RESULTS

General features of the stripping curve

Figure 3 shows the stripping curve obtained from a water sample containing 1 $\mu g\ l^{-1}$ each of cobalt(II) and nickel(II) analyzed according to the sequence of Table 1 with a potentiostatic adsorption time of 65 s at a potential of —0.50 V vs. SCE. In Fig. 3(a) the primary stripping curve (i.e. potential vs. time) is shown; this stripping curve was recorded by a normal strip-chart recorder without the aid of the computer. Figure 3(b) shows the

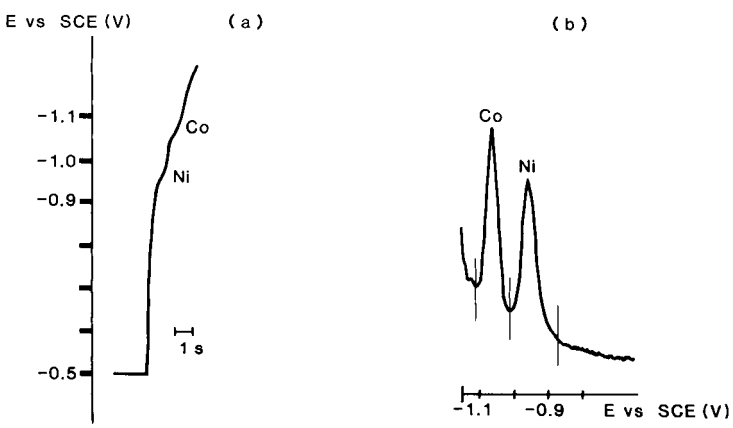

Fig. 3. Stripping signals obtained after 65 s of potentiostatic adsorption at —0.5 V vs SCE in a sample containing 1.0 $\mu g\ l^{-1}$ each of nickel(II) and cobalt(II). (a) Potential vs time recorded by a strip-chart recorder; (b) $dt(dE)^{-1}$ vs. potential output by the micro computer.

computer display $dt(dE)^{-1}$ of the same stripping curve. As can be seen from Fig. 3, well defined stripping signals are obtained both for nickel and cobalt, the stripping potential in the 5 M calcium chloride medium being −0.95 and −1.05 V vs. SCE, respectively.

Optimum sample pH

The dependence of the signal on the sample pH was investigated by processing a sample containing 2 μg l^{-1} each of cobalt(II) and nickel(II), according to the sequence in Table 1, the potentiostatic adsorption time being 65 s and the potential −0.50 V vs. SCE. The sample pH was varied between 4.2 and 10.2 by means of the acetate and ammonia buffers. From the results shown in Fig. 4 it can be concluded that the sample pH is not a critical parameter; both nickel(II) and cobalt(II) can be determined in the pH range 5—10. For cobalt(II), the highest sensitivity is obtained at approx. pH 5.3.

Linear range, sensitivity and detection limit

As in all electrochemical surface adsorption techniques, the relation between the signal and the analyte concentration is linear only at low surface coverage. The surface coverage is proportional to the sample concentration of metal dimethylglyoxime complexes and the time of potentiostatic adsorption. This is illustrated in Fig. 5 where a sample containing 2 μg l^{-1} each of nickel and cobalt as their dimethylglyoxime complexes was analysed according to the sequence in Table 1, the potentiostatic adsorption time being varied between 5 and 160 s. It can be seen that there is a linear relationship between stripping signal and potentiostatic deposition time in the region 0—50 s. By varying the sample concentration of nickel(II) and

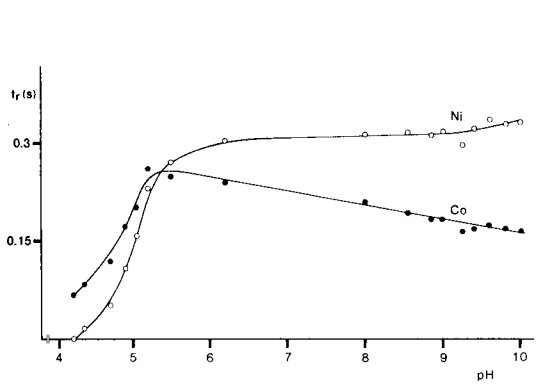

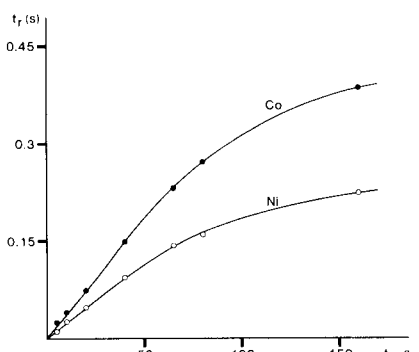

Fig. 4. The dependence on sample pH of the analytical signals: (○) nickel(II); (●) cobalt(II).

Fig. 5. The dependence of the stripping time (t_r) on the potentiostatic adsorption time (t_a) in a sample containing 2 μg l^{-1} each of nickel(II) (○) and cobalt(II) (●). Potentiostatic adsorption at −0.50 V vs. SCE for 65 s.

cobalt(II) and by varying the potentiostatic deposition time, it was concluded that with the present cell design and flow rate there is a linear relationship between the stripping signal and the sample concentration of nickel(II) and cobalt(II) as long as ([Ni(II)] + [Co(II)]) × potentiostatic deposition time is less than 150 $\mu g\ l^{-1}$ s, equivalent to 2.5 μM s, the atomic weights of nickel and cobalt being very close to each other. A consequence of this is that it is difficult to determine one element in the presence of a great excess of the other. For the determination of cobalt(II) in the presence of nickel(II), the problem can be partly overcome by using a potentiostatic adsorption potential of −0.75 V vs. SCE. At this potential the nickel(II) dimethylglyoxime complex is reduced immediately (cf. Fig. 3) and competitive adsorption from this complex can be avoided.

The sensitivity of the technique can be estimated from Figs. 3 and 5. If the sample contains organic substances capable of competitive adsorption on the mercury film surface, the sensitivity will decrease. Even so, there will be a linear relationship between the sample concentration of metal dimethylglyoxime complex and the stripping signal provided that the same time of potentiostatic adsorption is used in the sample and after standard addition. High concentrations of organic substances will make the determination of cobalt(II) and nickel(II) impossible. The same is true if the adsorbed matter is electroactive and can be reduced in a potential region where it overlaps the nickel and cobalt reduction.

In order to estimate the detection limit a water sample containing 0.1 $\mu g\ l^{-1}$ nickel(II) and 0.2 $\mu g\ l^{-1}$ cobalt(II) was analyzed ten times according to the cycle in Table 1, the adsorption potential being −0.5 V vs. SCE and the adsorption time 70 s. The average number of counts was 815 for nickel and 1650 for cobalt, the standard deviations being 70 and 85, respectively. This indicates detection limits on the one sigma level of 8.6 $ng\ l^{-1}$ for nickel(II) and 10.5 $ng\ l^{-1}$ for cobalt(II) at an adsorption time of 70 s.

Determination of nickel and cobalt in natural waters

Nickel(II) and cobalt(II) were determined in tap water, estuarine water and sea water and the results are summarized in Table 2. In all samples, the cobalt(II) concentration was below the detection limit of the technique. The results obtained for nickel(II) were compared with the results obtained by a combined liquid-liquid extraction/graphite-furnace atomic absorption (a.a.s.) technique [10]. As can be seen from Table 2, there is good agreement between the results obtained with the present technique and by a.a.s. and also with the certified value of the standard sea-water sample. All sea-water samples in Table 2 were filtered prior to use. It was not possible to use the present technique for the determination of nickel in unfiltered estuarine water because of competitive adsorption of organic matter.

Determination of nickel and cobalt in sediment and organic material

Nickel could be determined in the acid digests without any complications. In Table 3 the results obtained for nickel with the present technique are

TABLE 2

Results obtained in the determination of nickel in natural waters. All saline samples were filtered prior to treatment

Sample	Nickel concentration ($\mu g\ l^{-1}$)		
	Present technique	A.a.s	Certified value
Tap water	0.4	0.3	—
Reference sea water NASS-1	0.26	—	0.257 ± 0.027
Göta River estuary			
salinity 6.5°/₀₀	0.74	0.71	—
salinity 18°/₀₀	0.58	0.62	—
Skagerak			
depth 20 m	0.23	0.31	—
depth 150 m	0.21	0.19	—
depth 440 m	0.19	0.19	—

TABLE 3

Results obtained in the determination of nickel and cobalt in acid digests of sediment and biological material. In the determination of cobalt, all samples were treated with sodium tetrahydroborate as indicated in the procedures

Element	Sample	Element concentration ($mg\ kg^{-1}$)		
		Present technique	Certified value	A.a.s
Ni	Sediment MESS-1	25.2	29.5 ± 2.7	—
Ni	Sediment BCSS-1	56.9	55 ± 3.6	—
Ni	Bovine liver	1.3	—	1.4
Co	Sediment MESS-1	10.3	10.8 ± 1.9	—
Co	Sediment BCSS-1	12.9	11.4 ± 2.1	—
Co	Bovine liver	0.22	—	0.3

compared with the certified values of the two reference sediment samples and the results from a.a.s for the bovine liver sample. Attempts to determine cobalt in the acid digests without prior treatment with reducing agents yielded far too low values in the standard addition procedure. This was attributed to the presence of cobalt(III) species in the acid digest. During the oxidative treatment of biological material, cobalt(II) is most likely oxidized to cobalt(III). The reduction of cobalt(III) in the acid digests seems to be slow. This suggestion is supported by the fact that correct cobalt values were obtained if the acid digest was treated with sodium tetrahydroborate before addition of dimethylglyoxime. Moreover, correct cobalt values were obtained if the acid digest was allowed to stand for more than a month.

Further evidence was provided by making the cobalt(II) standard additions before the oxidative acid treatment. This procedure yielded correct cobalt values without any treatment with sodium tetrahydroborate (cf. Table 3). The sensitivity was, however, considerably reduced compared with that obtained for the reduced digests. Table 3 summarizes the results obtained for cobalt in the sediment and bovine liver samples after treatment with sodium tetrahydroborate.

DISCUSSION

The results show that it is possible to determine nickel and cobalt in a flow system by using a freshly prepared mercury film on a glassy carbon substrate as the working electrode. The advantage of this approach compared with the batch technique is the possibility for automation and the shorter total time of analysis because the sample deoxygenation step can be omitted. A typical time for an analytical cycle is 2 min.

A major disadvantage of both the flow and batch techniques is the limited range of linearity. For this reason, the use of such techniques is limited to the determination of nickel and cobalt in the $\mu g\ l^{-1}$ and sub-$\mu g\ l^{-1}$ range, e.g., in tap water and sea water. In a more computerized version of the flow system than that used in this investigation, it would be possible to check automatically whether or not the signals obtained from the sample and sample plus standard additions are within the linear range. If not, the samples could then be rerun with a shorter potentiostatic adsorption time.

Another disadvantage of both the flow and batch approaches is competitive adsorption of organic matter present in the sample. This is of no importance in the determination of the elements in biological material because all organic matter is destroyed in the oxidative acid treatment. It does, however, make the determination of nickel(II) and cobalt(II) in coastal waters and certain lake waters very difficult. Pilar et al. [1] have shown that this problem can be solved by means of ultraviolet treatment of the sample. No doubt, this is also applicable to the flow approach.

REFERENCES

1 B. Pilar, P. Valenta and H. W. Nürnberg, Fresenius Z. Anal. Chem., 307 (1981) 337.
2 P. Nangniot, J. Electroanal. Chem. Interfacial Electrochem., 14 (1967) 197.
3 E. N. Vinogradova and G. V. Prokhorova, Zh. Anal. Khim., 23 (1968) 1666.
4 L. Anderson, D. Jagner and M. Josefson, Anal. Chem., 54 (1982) 1371.
5 H. Eskilsson and D. R. Turner, Anal. Chim. Acta, 161 (1984) 293.
6 D. Jagner, Trends Anal. Chem., 2 (1983) 53.
7 A. Meyer and R. Neeb, Fresenius Z. Anal. Chem., 315 (1983) 118.
8 A. Granéli, D. Jagner and M. Josefson, Anal. Chem., 52 (1980) 2220.
9 S. S. Berman, R. E. Sturgeon, J. A. H. Desaulniers and A. P. Mykytiuk, Mar. Pollut. Bull., 14 (1983) 69.
10 L.-G. Danielsson, B. Magnusson, S. Westerlund and K. Zhang, Anal. Chim. Acta, 144 (1982) 183.

Analytica Chimica Acta, 175 (1985) 89—97
Elsevier Science Publishers B.V., Amsterdam — Printed in The Netherlands

AMPEROMETRIC DETERMINATION OF GLUCOSE WITH A FERROCENE-MEDIATED GLUCOSE OXIDASE/POLYACRYLAMIDE GEL ELECTRODE

MARK A. LANGE and JAMES Q. CHAMBERS*
Department of Chemistry, University of Tennessee, Knoxville, TN 37996-1600 (U.S.A.)
(Received 11th April 1985)

SUMMARY

Enzyme electrodes were constructed by immobilization of glucose oxidase and ferrocene into cross-linked polyacrylamide gels. Electrogenerated ferrocinium ion acts as a direct electron mediator between glucose oxidase and a reticulated vitreous carbon (RVC)/graphite support bed. The electrode is easily constructed, gives a current response proportional to glucose concentrations up to 30 mM, and has good chemical stability in water and air.

Most methods for determining glucose levels using immobilized glucose oxidase are based on the following reaction:

$$\text{D-Glucose} + O_2 \xrightarrow[\text{oxidase}]{\text{glucose}} \text{gluconolactone} + H_2O_2 \qquad (1)$$

The enzyme electrode of Updike and Hicks [1], for example, measures the decrease in oxygen pressure through a polyacrylamide gel containing glucose oxidase that is coated on an amperometric oxygen electrode. These electrodes typically give a linear relation between the rate of oxygen depletion and glucose concentration over the range 0—75 mg/100 ml. Amperometric determination of hydrogen peroxide produced in the above reaction can also be used to follow the glucose concentration. The concepts and methodology involved in the construction and use of these "enzyme electrodes" have been discussed by Sittampalam and Wilson [2].

In another approach, oxygen in Eqn. 1 is replaced with an electron acceptor which can be generated at an electrode surface. If the enzyme is immobilized at the electrode/solution interface, the resulting electrode is in principle an electrocatalytic sensor for the substrate. This approach was used by Cass et al. [3] who devised an electrode for the detection of glucose in which the oxidase was covalently attached to an oxidized graphite surface and in which a substituted ferrocene/ferricinium couple trapped within a membrane at the electrode surface was used as a mediator. This electrode successfully catalyzed the direct electrochemical oxidation of D-glucose in the absence of oxygen.

0003-2670/85/$03.30

Many methods of immobilizing enzymes have been developed and recently reviewed [4, 5]. One of the most versatile methods is entrapment in cross-linked polyacrylamide gels. The hydrophilic environment within the hydrogen-bonded structure of these gels is conducive to maintaining the enzymatic activity of the entrapped enzymes. Several enzymes have been immobilized in this manner [6].

This paper describes the fabrication and evaluation of a glucose oxidase electrode in which the enzyme and the ferrocene couple are trapped within a polyacrylamide gel. This electrode design has the potential advantage that greater than monolayer loadings of enzyme can be used. Furthermore, the electrode does not employ a membrane per se, which should promote greater access of substrate to the immobilized catalytic sites.

EXPERIMENTAL

Reagents and apparatus

Glucose oxidase (E.C. No. 1.1.3.4 from *Aspergillus niger*; Sigma) had an activity of 192000 units g^{-1} of solid [7]. D-Glucose was obtained from Mallinckrodt, and ferrocene and its derivatives from ROC/RIC. Argon-saturated Sorensen phosphate buffer solutions (0.0667 M) were used.

Voltammetry was done on a BAS-100 Electrochemical Analyzer and recorded with a Bausch and Lomb digital plotter (Model No. DMP-40). All potentials are referred to the saturated calomel reference electrode used.

Electrode construction

Acrylamide was photopolymerized using riboflavin as the photosensitizer and a 500-W tungsten lamp as the light source in a manner similar to that described by Oster [8]. Additon of 0.14% (w/w) *N,N*-methylene-bis-acrylamide (*N,N*-MBA) produces a gel of workable viscosity after 15 min of exposure to light. If more *N,N*-MBA is added, the gel becomes too stiff for mixing with other components. If less *N,N*-MBA is used, the addition of a gelling agent, 3-(dimethylamino)propionitrile, is recommended. If no cross-linking agent is added, 45 min of exposure to the light produces a gel of equivalent viscosity. After the gel has formed, it is mixed with powdered graphite (Union Carbide Corp., Grade 38), glucose oxidase, and ferrocene and then packed into a strip of RVC with contact being made with an alligator clip. Typically, electrode geometrical areas of ca. 1 cm^2 were exposed to solution in the experiments reported below. Rotating electrodes were constructed from a brass rod machined to mate with the shaft of a Pine Rotator (Pine Instrument Co.). A teflon sleeve that screwed onto the brass rod held a piece of RVC in place in a shallow well. The well was packed with the gel/graphite composite to define a surface area of ca. 0.28 cm^2.

RESULTS AND DISCUSSION

Voltammetry

Figure 1 shows the idealized reaction scheme on which the electrode design is based. The polyacrylamide gel containing the enzyme and the mediator is viewed as being in contact with the graphite surface. The RVC bed supports the polyacrylamide gel/graphite powder composite, makes contact with the graphite particles, and acts as a collector electrode for the catalytic current. The electrical resistance of the resulting electrode assembly is that of a typical carbon paste electrode, i.e., less than 25 Ω.

Initial experiments were done with poly(vinylferrocene), PVF, as the mediator in order to eliminate the possible loss of low-molecular-weight mediators from the electrode. As shown by Geno et al. [9], polymers can readily be incorporated into the matrix of a carbon paste to give a polymer-modified electrode that can support large current densities. However, while electrodes made from PVF and polyacrylamide were electroactive, they were not electrocatalytic when glucose oxidase was incorporated in the electrode composite. Attempts to construct a catalytically active electrode by polymerization of vinylferrocene in the presence of glucose oxidase were also unsuccessful. Accordingly, the use of monomeric ferrocene couples that might have the mobility necessary to shuttle electrons between the catalytic sites and the graphite surface was investigated.

Figure 2A shows a cyclic voltammogram obtained in a blank solution when ferrocene is added to the polyacrylamide/glucose oxidase/graphite composite. The salient feature of this voltammogram is that the ferrocene/ferrocinium wave remains constant over many cycles indicating that neither the ferricinium ion nor ferrocene leach out of the electrode to an appreciable extent when the potential is cycled through the ferrocene wave. It is interesting that similar behavior was noted for ferrocene by Kuwana and French [10] in the original experiments on the loading of Nujol carbon paste films with electroactive species. The capability of loading carbon paste with electroactive species and performing voltammetry on the species in the paste when the electrodes are immersed in blank solutions has been known for some time [10—12]. In the case of the polyacrylamide/ferrocene/graphite

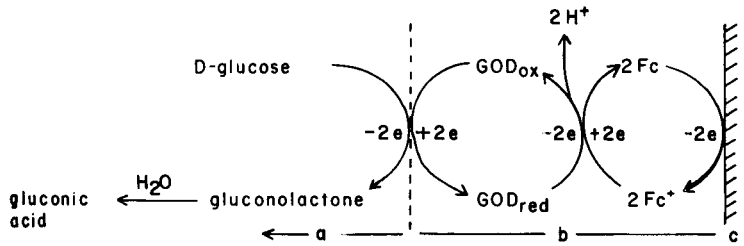

Fig. 1. Electrocatalysis scheme: (a) buffered glucose solution; (b) polyacrylamide network; (c) RVC support bed.

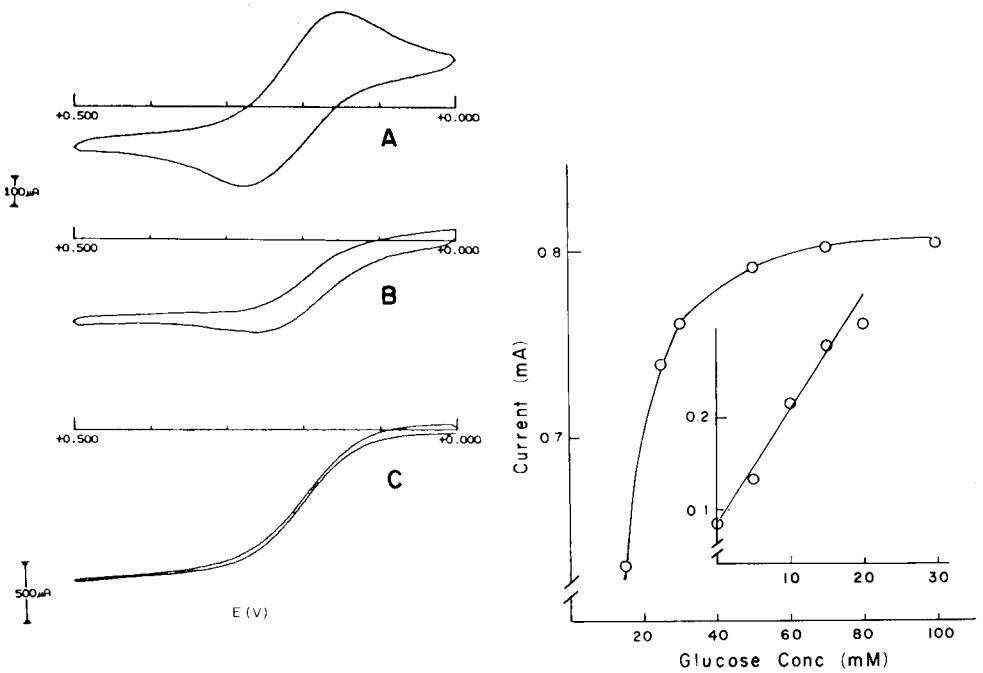

Fig. 2. Cyclic voltammograms of a glucose oxidase/polyacrylamide modified electrode in contact with pH 7 phosphate buffer (sweep rate, 20 mV s^{-1}; geometrical electrode area, 2 cm^2; reference electrode, SCE.) (A) Background showing ferrocene couple (100 μA/div.). (B) Same electrode in 200 mM mannose pH 7 solution (100 μA/div.). (C) Same electrode in 100 mM D-glucose pH 7 solution (500 μA/div.).

Fig. 3. Variation of limiting current at 0.45 V vs. SCS with glucose concentration (sweep rate, 20 mV s^{-1}). Insert shows linearity in the 0—15 mM glucose region on a separate electrode.

electrode both halves of the ferrocene/ferrocinium couple are stabilized by the polyacrylamide environment at relatively high concentrations. The wave shape of the voltammogram in Fig. 2A indicates that semi-infinite diffusion of ferrocene species within the polyacrylamide/graphite composite controls the current at potentials outside the peak potential separation.

When the electrode of Fig. 2A is transferred to a solution containing 100 mM D-glucose, the ferrocene voltammetric wave shape changes to that characteristic of a catalytic electrode process as shown in Fig. 2C. In this voltammogram, the diffusional tail on the anodic current is no longer present, indicating that the current is controlled by the rate of neutral ferrocene regeneration at the electrode/solution interface and not by the mass transport of ferrocene. The limiting current in the region of 0.4—0.5 V has increased by ca. five-fold and the ferricinium reduction wave on the reverse potential sweep is significantly attenuated in Fig. 2C.

Appropriate control experiments demonstrated that both the ferrocene mediator and enzyme were required to obtain catalytic activity. Neither

glucose nor glucose oxidase exhibited electroactivity in the potential range of the ferrocene wave. Ferrocene-doped polyacrylamide/graphite electrodes were not electrocatalytic for the oxidation of D-glucose when glucose oxidase was omitted from the gel formation. The electrodes were also somewhat electrocatalytic for the oxidation of D-mannose, an epimer of D-glucose, in qualitative accord with the known selectivity of glucose oxidase for these substrates [13]. This is demonstrated by the cyclic voltammogram of Fig. 2B showing the electrode response in 200 mM mannose.

A calibration curve (Fig. 3) constructed by measuring the limiting current at +0.450 V vs. SCE, was linear in the range 0—15 mM glucose. At higher concentrations, in agreement with previous results [3], the electrode became unresponsive to additional amounts of substrate. Under these conditions, the catalytic sites of the enzyme are presumably saturated with substrate.

Electrode stability

The electrocatalytic activity of the polyacrylamide/graphite/glucose oxidase/ferrocene composite is remarkably stable chemically. The electrodes can be used repeatedly and show excellent physical and chemical stability when stored in air. Only a 3% decrease in the limiting current (in a 50 mM glucose solution) was observed for an electrode stored at 0°C in air for 120 h. After 360 h, a 9% decrease was observed. Interestingly, after storage, these electrodes usually required 5—10 potential cycles before exhibiting full electrocatalytic activity. This is shown in Fig. 4 where the first 10 positive-going potential sweeps on an enzyme electrode that had been stored at 0°C for 360 h are shown. On successive sweeps, the limiting current increases and approaches a constant value. This "break-in" phenomenon is probably due to hydration of the polyacrylamide gel which would increase access of

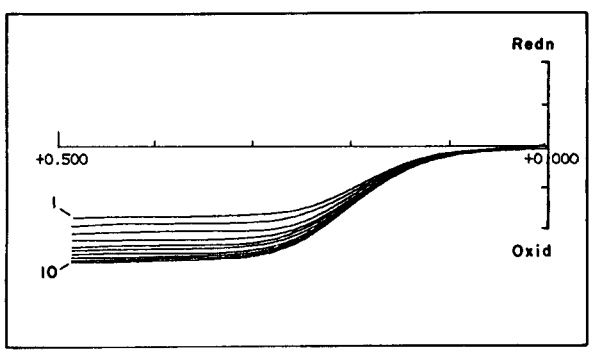

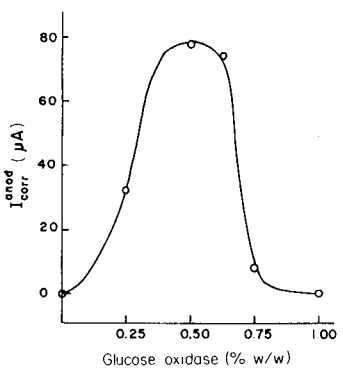

Fig. 4. Typical "catalytic break-in" after electrode has been stored in air. Scans 1—10 are shown. Conditions: 50 mM glucose; sweep rate, 20 mV s^{-1}.

Fig. 5. Plot of I_{corr}^{anod} vs. % (w/w) glucose oxidase in pH 7, 50 mM glucose solution.

the substrate and mediator to the catalytic sites in the electrode composite. Similar solvent swelling "break-in" phenomena have been observed for electroactive polymer films on electrode surfaces. At room temperature, the electrocatalytic activity of the electrodes decreases more rapidly. An identical electrode to the above showed a 51% decrease in the limiting current after 120 h at room temperature.

Unfortunately, the physical stability of the polyacrylamide/graphite composite in aqueous solutions is a serious drawback to the development of useful sensors based on this approach. In order to achieve full electrocatalytic activity, the gel should be completely swollen with solvent so that the substrate can encounter the catalytic sites. The polyacrylamide gels are hydrophilic and readily swell in water, but this lessens the tendency of the polyacrylamide/graphite to stick together and maintain electrical contact with the RVC bed. Electrodes that are left in contact with water and cycled through the ferrocene/ferrocinium wave fall apart after about 4 hours. This inability to maintain physical integrity was pH-dependent and limited the useable range to pH 7—9.

Several possibilities for improving the physical stability of these electrodes are under investigation. These include selectively cross-linking a thin "surface layer" by using the method of Oster [8] and the incorporation of gelling agents into the electrode formulation.

Optimization of electrode composition

A complete study for the optimization of the electrode response was not done. However, the effect of variation of the percent enzyme was studied for the composition 16% ferrocene, 25% graphite, and 59.5 ± 0.5% polyacrylamide. Each electrode was cycled in 50 mM glucose, pH 7 solution until maximum catalytic current was obtained. The resulting plot of I_{corr}^{anod} = $I(0.45\ V) - I(Fc^{0/+})$ vs. % (w/w) glucose oxidase shows a pronounced maximum (Fig. 5). This "corrected limiting current" is calculated by subtracting the diffusion current for the ferrocene oxidation from the current arising from the electrocatalyzed oxidation of glucose. This suggests that there is an optimum ratio of enzyme to mediator. The decrease at 0.75% glucose oxidase may be related either to disruption of the charge-transport process though the film or attenuation of charge transfer to the enzyme—substrate complex.

Electrode kinetics

Two factors limited the study of the kinetics of the ferricinium ion oxidation of glucose. First, while the theory of electrocatalysis of electrochemical reactions of redox polymer films has been treated in elegant fashion, principally by Andrieux, Saveant and coworkers [14—16], most published working treatments involve simple electron transfer cross-reactions. The scheme of Fig. 1 involves additional steps of complexity in these treatments. More frustratingly, it proved impossible to study the electrocatalysis by using hydro-

dynamic voltammetric methods and rotating disks constructed with the enzyme/polyacrylamide/graphite composite, because even moderate rotation rates caused the electrodes to lose electrocatalytic activity. This behavior is illustrated by Fig. 6 which shows the effect of electrode rotation on the limiting current. As the rate of rotation is increased, a point is reached at which the limiting current decreases. At this point, if the electrode rotation is arrested and a cyclic voltammogram obtained, electrocatalysis is not observed, only the quasi-reversible ferrocene couple is seen in the voltammograms. The electrodes can also be deactivated by rotation at open circuit. Presumably this behavior is a result of loss of enzyme from the interface region of the rather loose polyacrylamide network.

At zero rotation rate and high glucose concentration, the sweep rate dependence of the peak current ratio, i_p^{cath}/i_p^{anod}, was in accord with theory for a pseudo-first-order follow-up reaction [17]. At 50 mM glucose, the measured value of the apparent rate constant (k_f^{app}) was 1.2 ± 0.2 s^{-1}. The value of k_f^{app} decreased significantly as the glucose concentration decreased (Fig. 7).

Measurement of D-glucose in plasma

The ability of these electrodes to determine glucose levels in human plasma was examined (Table 1). Plasma samples (2—3 ml) were diluted with either distilled water or buffer to 5—6 ml and analyzed for glucose by standard addition of a 0.28 M glucose solution. Linear responses were obtained for successive additions of the standard solution, so that the

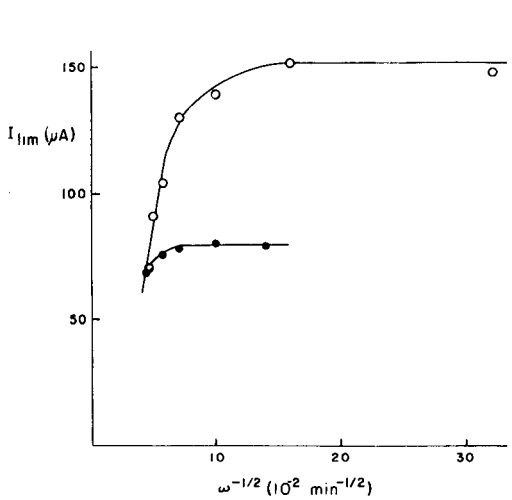

Fig. 6. Rotating disk limiting current vs. $\omega^{-1/2}$: (○) obtained with a freshly prepared electrode; (●) electrode rotated at 300 rpm for 30 min before experiment.

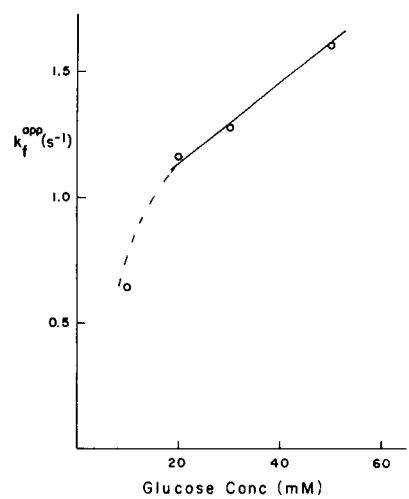

Fig. 7. Plot of pseudo first-order rate constant vs. substrate concentration.

TABLE 1

Comparison of enzyme electrode and clinical analysis of glucose levels in human serum

Sample no.[a]	Glucose concentration (mg ml^{-1})		Absolute error (mg)
	Kodak Ektachem[b]	Enzyme electrode	
1	0.85	1.2	+0.7
2	1.40	1.8	+0.8
3	1.80	3.25	−2.9
4	1.95	3.9	+3.9
5	2.90	2.0	−1.8
6	2.70	2.1	−1.9
Control	1.80	2.0	+0.2

[a]Volume taken, 2.0 ml, except for sample 6 (3.0 ml). [b]Precision, ±2.1% in dynamic range.

conventional standard additions method was applicable. The results were then compared to the clinical results obtained using a Kodak Ektachem 400 Analyzer, which has a reported precision of ±2.0%. The results in Table 1 indicate that the glucose levels in these plasma samples are just below the concentration level that can be detected with these electrodes at a reasonable accuracy or precision. Attempts were made to improve the precision by averaging repeated scans and subtraction of background currents obtained at electrodes without added enzyme. However, these efforts were not successful.

It is likely that the relatively high viscosity of the plasma samples, compared to aqueous glucose solutions, decreases the mass transport of glucose into the polyacrylamide gel. This would decrease the current response to glucose for a given electrode composition and would affect the precision of the measurement. Analysis of a control glucose sample at the concentration level of glucose in blood plasma indicated somewhat better precision than was obtained for the plasma samples (11% vs. ca. 50% error).

Conclusion

The principle of using polyacrylamide gels for the construction of electrocatalytic enzyme electrodes for the direct mediation of an enzyme catalyzed reaction has been demonstrated. Substrate-selective electrodes can be fabricated in the manner described by using an enzyme that can be immobilized in a polyacrylamide matrix and a suitable electron mediator. The glucose electrodes described have response characteristics roughly equivalent to those of CASS et al. [3]. However, while the chemical stability of the electrodes was excellent when stored in air, their physical stability in aqueous solutions represents a drawback to their analytical utility.

This research was supported by grants from the National Science Foundation (CHE-8219110) and Martin Marietta Corporation. Plasma samples were supplied by The University of Tennessee Memorial Hospital and Research Center.

REFERENCES

1 S. J. Updike and G. P. Hicks, Nature, 214 (1967) 986.
2 G. Sittampalam and G. S. Wilson, J. Chem. Educ., 59 (1982) 70.
3 A. E. G. Cass, G. Davis, G. D. Francis, H. A. O. Hill, W. J. Aston, I. J. Higins, E. V. Plotkin, L. D. L. Scott and A. P. F. Turner, Anal. Chem., 56 (1984) 667.
4 A. S. Attiyat and G. D. Christian, Am. Biotech. Lab., 2 (1984) 8.
5 V. Razumas, J. J. Jasaitis and J. J. Kulys, Bioelectrochem. Energetics, 12 (1984) 297.
6 M. D. Trevan, Immobilized Enzymes, Wiley, Chichester, 1980.
7 Worthington Enzymes Manual, Worthington Biochem. Corp., 1972, p. 19.
8 G. Oster, Nature, 173 (1954) 300.
9 P. W. Geno, K. Ravichandan and R. P. Baldwin, J. Electroanal. Chem., 183 (1985) 155.
10 T. Kuwana and W. G. French, Anal. Chem., 36 (1964) 241.
11 D. G. Davis and M. E. Everhart, Anal. Chem., 36 (1964) 38.
12 C. A. H. Chambers and J. K. Lee, J. Electroanal. Chem., 14 (1967) 309.
13 M. Dixon and E. C. Webb, Enzymes, Longman, London, 3rd edn., 1979, p. 243.
14 C. P. Andrieux and J. M. Saveant, J. Electroanal. Chem., 134 (1982) 163; 142 (1984) 1.
15 C. P. Andrieux, J. M. Dumas-Bouchiat and J. M. Saveant, J. Electroanal. Chem., 131 (1982) 1; 169 (1984) 9.
16 C. Anson, J. M. Saveant and K. Shigehara, J. Phys. Chem., 87 (1983) 214.
17 R. S. Nicholson and I. Shain, Anal. Chem., 36 (1964) 706.

Analytica Chimica Acta, 175 (1985) 99—105
Elsevier Science Publishers B.V., Amsterdam — Printed in The Netherlands

THE OSCILLATION FREQUENCY OF A QUARTZ RESONATOR IN CONTACT WITH A LIQUID

K. KEIJI KANAZAWA* and JOSEPH G. GORDON II
IBM Research Laboratory, K33-281, 5600 Cottle Road, San Jose, CA 95193 (U.S.A.)
(Received 22 June 1984)

SUMMARY

A simple relationship is derived which expresses the change in oscillation frequency of a quartz crystal in contact with a fluid in terms of material parameters of the fluid and the quartz. The relationship is $\Delta f = -f_0^{3/2}(\eta_L \rho_L / \pi \mu_Q \rho_Q)^{1/2}$, where f_0 is the oscillation frequency of the free (dry) crystal, η_L and ρ_L are the absolute viscosity and density of the liquid, respectively, and μ_Q and ρ_Q are the elastic modulus and density of the quartz. This relation is obtained from a simple physical model which couples the shear wave in the quartz to a damped shear wave in the fluid. Quantitative comparisons with two test cases, aqueous solutions of glucose and ethanol at various concentrations, demonstrate the accuracy of this model.

Several reports have appeared in which a quartz resonator is operated with one face in contact with a liquid. Konash and Bastiaans [1] studied the behavior of the quartz crystal in a flow cell simulating a liquid chromatographic detector. They observed changes in the resonance frequency of the crystal when different liquids passed through the cell, and attributed these changes either to density differences or to surface adsorption. Nomura and Minemura [2], also using a flow cell, ascribed the frequency changes observed to a combination of density and bulk conductivity. Bruckenstein and Shay [3] focused on the frequency changes resulting from metal deposition and from oxide formation, and showed that the mass sensitivity to thin films is the same in the fluid as in vacuum.

These studies demonstrated that a quartz crystal can oscillate in contact with a liquid. In addition, they show that the liquid causes a significant shift in the resonance frequency. Although Nomura and Minemura [2] obtained a relationship between the observed frequency shift and the fluid density and conductivity, it was an empirical, four-parameter fit to experimental data and was not based on a physical model. The present analysis is based on the coupling of the crystal motion to a shear wave in the fluid, because common AT-cut crystal oscillates in a shear mode. A quantitative description of the velocity distribution in the fluid is obtained which permits one to understand in a simple physical way how the viscosity and density of the fluid affect the oscillation. This analysis leads to a simple expression for the frequency shift.

0003-2670/85/$03.30

THEORY

The coupling of shear waves between a piezoelectric crystal and a liquid received attention as long ago as 1949 [4], where quartz receiver/transmitter pairs were used to study the shear viscosity and shear elasticity of polymeric liquids. However, studies of the effects of liquids on quartz crystal resonators did not appear until recently. Glassford [5] analyzed the decrease in mass sensitivity with increasing thickness of viscous overlayer by using a Rayleigh perturbation approach, which relates the change in frequency of a dissipation-free oscillating system to the ratio of peak potential energy to kinetic energy in the system. He showed that, in the thin film limit, the mass sensitivity is equal to that in vacuum and decreases monotonically with increasing film thickness. As Glassford stated, the Rayleigh technique is valid only in the loss-free limit and is probably not applicable to thick liquid films in which damping is appreciable. Mecea and Bucur [6] used an approach that they termed the energy transfer method. Their final result is valid only for very thin films. Crane and Fischer [7] treated the losses by invoking a transmission line analog. Unfortunately, with this electrical analog, it is difficult to visualize the physical behavior of the overlayer.

The case of a quartz resonator in which one face is in contact with a viscous liquid of infinite extent is discussed here. The method used treats the resonance phenomenon as arising from the matching of the shear waves in the quartz and in the overlayer to specific boundary conditions. The shear waves in the quartz and liquid are obtained from the differential equations which describe the bulk response to shear stresses. The resonance condition obtains directly from this shear wave analysis, without invoking Rayleigh perturbation, energy equivalences or transmission line analogs, and the direct physical description of the behavior is preserved.

The coordinate system is defined such that the shear stresses lie along the x direction in the x-y plane as shown in Fig. 1. If the shear stress is written as F_x/A, the resulting stress/strain relation in the quartz is given by

$$F_x(z, t)/A = \mu \, \partial u_x(z, t)/\partial z \tag{1}$$

where μ is the shear modulus of the quartz crystal and u_x is the elastic displacement along x. The net force acting on a slab of thickness dz gives rise to an acceleration of the slab, which, for a region of area A, is given by

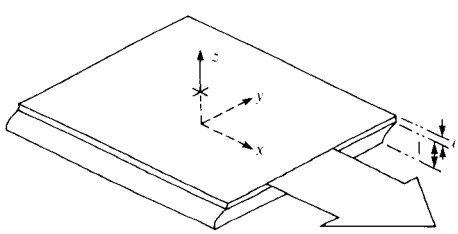

Fig. 1. The coordinate system used in the analysis.

$$[\partial F_x(z, t)/\partial z]\,dz = \rho A\,dz\,\partial^2 u_x(z, t)/\partial t^2 \tag{2}$$

where ρ is the density of the quartz. These two relations can be combined to yield a partial differential equation describing the behavior of $u_x(z, t)$:

$$\partial^2 u_x(z, t)/\partial z^2 = (\rho/\mu)\partial^2 u_x(z, t)/\partial t^2 \tag{3}$$

This is the Helmholtz wave equation having as a general steady-state solution

$$u_x(z, t) = \tilde{U}_+ \exp[-j(kz - \omega t)] + \tilde{U}_- \exp[j(kz + \omega t)] \tag{4}$$

where k is the propagation constant given by

$$k = \omega(\rho/\mu)^{1/2}. \tag{5}$$

This solution describes shear waves travelling in the $+z$ direction with amplitude $|\tilde{U}_+|$ and the $-z$ direction with amplitude $|\tilde{U}_-|$.

The lower boundary of the crystal is taken to be $z = 0$. There, the surface is unconstrained, i.e., $F_x(0, t) = 0$. Then from Eqn. 1, $|\partial u_x(z, t)/\partial z|_{z=0} = 0$. This implies that $\tilde{U}_+ = \tilde{U}_-$. Moreover, if the phase of the oscillation at this lower boundary is defined as zero, then $\tilde{U}_+ = \tilde{U}_- = U_0$, a real quantity. The strain behavior in Eqn. 4 then becomes

$$u_x(z, t) = 2U_0 \cos(kz) \exp(j\omega t) \tag{6}$$

In the simplest case, the free resonator, the upper surface at $z = l$ is also unconstrained so that $|\partial u_x(z, t)/\partial z|_{z=0} = 0$. From Eqn. 6, this condition requires that $kl = n\pi$. For the fundamental mode of oscillation, $n = 1$, the resonance condition can be obtained using Eqn. 5:

$$\omega_0 = (\mu/\rho)^{1/2}(\pi/l) \tag{7}$$

In frequency units, Eqn. 7 can be written $f_0 = \frac{1}{2}(\mu/\rho)^{1/2}(1/l)$. The coefficient $\frac{1}{2}(\mu/\rho)^{1/2}$ is called the "frequency factor" and has the value 1.668×10^5 Hz-cm for AT-cut quartz [8]. Given 2.648 gm cm^{-3} as the density of quartz, the shear modulus can be calculated to be $\mu = 2.947 \times 10^{11}$ dyne-cm^{-2}. From Eqn. 6, the shear wave velocity is then $\omega/k = (\mu/\rho)^{1/2} = 3.336 \times 10^5$ cm s^{-1}.

In the case of present interest, the upper surface is not unconstrained, but rather is connected with a liquid. The stress relation for the fluid is described by

$$F_x(z, t)/A = \eta_L \partial v_x(z, t)/\partial z \tag{8}$$

where η_L is the absolute viscosity, and v_x the fluid velocity in the x direction. For a slab of thickness dz, the net force on the slab again gives rise to an acceleration as described by

$$\partial F_x(z, t)/\partial z = \rho_L A\,\partial v_x(z, t)/\partial t \tag{9}$$

where ρ_L is the fluid density. Relations 8 and 9 can be combined to yield the differential equation for the fluid velocity,

$$\partial^2 v_x(z, t)/\partial z^2 = (\rho_L/\eta_L)\,\partial v_x(z, t)/\partial t \tag{10}$$

This has the form of the diffusion equation and is identical to Glassford's Eqn. 4. To match the solutions of this equation to the quartz motion, those periodic solutions which have the same period as the quartz oscillations are chosen. Moreover, it is assumed that the fundamental frequency is the largest component in the Fourier spectrum and only that solution is retained. This is the same approximation as used in all previous work and, from the accuracy of the resulting solution, is very good. The solution to Eqn. 10 having a fundamental frequency ω can then be written

$$v_x(z, t) = \tilde{V}_+\{\exp[-(j\omega\rho_L/\eta_L)^{1/2}(z-l)]\}\exp(j\omega t) + \tilde{V}_-\{\exp[(j\omega\rho_L/\eta_L)^{1/2}(z-l)]\}\exp(j\omega t) \quad (11)$$

Because $v_x(z, t)$ must remain finite as $z \to \infty$, then $\tilde{V}_- = 0$. It is now assumed that the first layer of fluid is rigidly bound to the quartz surface. Then at $z = l$, the amplitude of v_x must match the amplitude of the velocity of the quartz plate. Thus $\tilde{V}_+ = \tilde{V}_0$, and the explicit expression for v_x can be written

$$v_x(z, t) = \tilde{V}_0 \exp[-k_L(z-l)]\exp\{-j[k_L(z-l) - \omega t]\} \quad (12)$$

where $k_L = (\omega\rho_L/2\eta_L)^{1/2}$. This solution describes a shear wave travelling in the $+z$ direction, with extremely heavy damping. The reciprocal of the propagation constant is the characteristic decay length, δ, of the envelope function. For a fluid like water, δ is 2500 Å and the velocity profile is shown in Fig. 2. The profile is shown at three different times, corresponding to peak surface velocity, intermediate surface velocity and zero surface velocity.

The constant $\tilde{V}_0$ is the velocity of the quartz surface at $z = l$ and is evaluated from the time derivative of Eqn. 6. Specifically

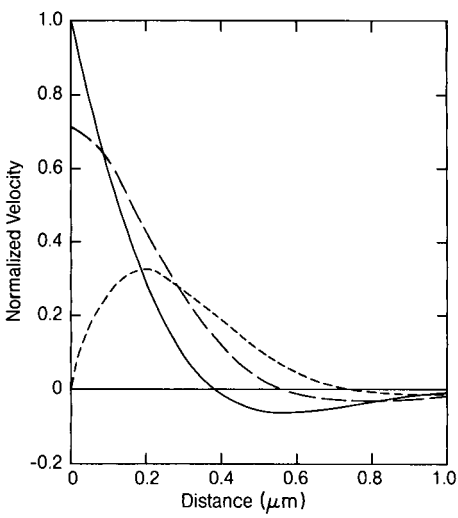

Fig. 2. Shear velocity profiles in the fluid at three different times: (- - -) peak surface velocity; (— — —) intermediate surface velocity; (——) zero surface velocity.

$\partial u_x(z, t)/\partial t = j\omega 2U_0 \cos(kl) \exp(j\omega t)$

so that

$$\tilde{V}_0 = j\omega 2U_0 \cos(kl). \tag{13}$$

The solution in Eqn. 11 then is written

$$v_x(z, t) = j\omega 2U_0 \cos(kl) \exp[-k_L(z-l)] \exp\{-j[k_L(z-l) - \omega t]\} \tag{14}$$

Within this approximation, the in-phase component of the shear stress on the liquid side of the interface must be equal and opposite to the shear stress on the quartz side, as required by Newton's law. Using Eqns. 1 and 8, one is led to the resonance condition

$$\tan \omega(\rho/\mu)^{1/2} l = -(\omega \rho_L \eta_L / 2\rho\mu)^{1/2} \tag{15}$$

Writing the angular frequency ω as $\omega = \omega_0 + \Delta\omega$, where ω_0 is the resonant frequency of the unloaded crystal, and recognizing, from Eqn. 7, that $(\rho/\mu)^{1/2} l = \pi/\omega_0$, Eqn. 15 can be transformed to

$$\tan(\Delta\omega/\omega_0)\pi = -(\omega_0 + \Delta\omega)^{1/2}(\rho_L \eta_L / 2\rho\mu)^{1/2} \tag{16}$$

For common liquids, $\Delta\omega/\omega_0$ is a very small quantity and the resonance condition in Eqn. 16 can be approximated by

$$\Delta\omega = -(\omega_0^{3/2}/\pi)(\rho_L \eta_L / 2\rho\mu)^{1/2}$$

or in terms of frequency

$$\Delta f = -f_0^{3/2}(\rho_L \eta_L / \pi\rho\mu)^{1/2} \tag{17}$$

EXPERIMENTAL

Relation 17 was tested for aqueous solutions containing various amounts of glucose or ethanol. A flow cell similar to that described by Nomura and Minemura [2] was constructed in which the crystal formed one end face of the cylindrical cell. The oscillation frequency is quite sensitive to stresses caused by mounting and to changes in the hydrostatic pressure of the fluid. Consequently, like Nomura and Minemura, we report the frequency change relative to pure water rather than to vacuum. Glucose solutions were used to mimic the earlier experiment with sucrose [2], because no problems were reported with adsorption. A preliminary publication [8] reported quantitative agreement between Eqn. 17 and the observed frequency shifts for glucose solutions and for the earlier data on sucrose solutions. The present results on glucose are reproduced in Fig. 3. Because Nomura and Minemura used a 9-MHz crystal and a 5-MHz crystal was used here, the quantitative agreement of Eqn. 17 with both sets of data establishes the correctness of the dependence on f_0. Note that there are no adjustable parameters in this analysis. The fundamental frequency, f_0, is that for an unmounted crystal suspended in air and ρ_L and η_L were taken directly from the CRC Handbook [9].

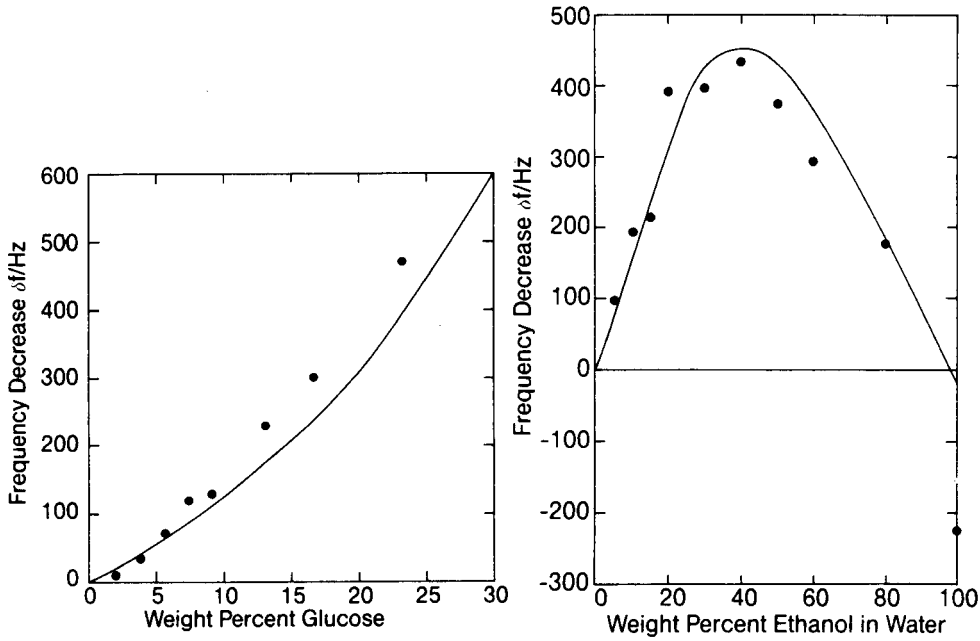

Fig. 3. Change in resonance frequency, relative to water, vs. the concentration of glucose in water: (——) calculated from Eqn. 17; (•) experimental points.

Fig. 4. Change in resonance frequency, relative to pure water, vs. the weight fraction of ethanol in water/ethanol mixture: (——) calculated from Eqn. 17; (•) experimental points.

Water/ethanol solutions are an even more stringent test of Eqn. 17. It is expected that the resonance frequency should first decrease as the fraction of ethanol increases, reaching a minimum near 40% ethanol and then increasing to a value greater than that for pure water at 100% ethanol. The density change over this range is only about 25%, varying from 0.9982 to 0.7893, whereas the viscosity has a more complex behavior, increasing from 1.002 cp to a maximum value of 2.852 and then decreasing again. The results are plotted in Fig. 4. The prediction of Eqn. 17 is the solid curve. Though there is a significant scatter in the data and the points at high ethanol fractions all lie under the predicted curve, the agreement is remarkable, especially in view of the fact that there are no adjustable parameters, and provides excellent support for relation 17.

DISCUSSION

An expression which accurately describes the frequency change induced by immersing one face of a quartz resonator in a liquid has been derived. The significant result is that the frequency shift produced by the liquid is a function of the viscosity as well as the density of the liquid.

The theory is based on a simple physical model which treats the quartz as a lossless elastic solid and the liquid as a purely viscous fluid. The frequency shift arises from coupling the oscillation of the crystal, a standing shear wave, with a damped propagating shear wave in the liquid.

This simple shear wave model also provides a simple physical explanation for why the viscosity is important. For small mass changes, the oscillation frequency of the resonator will decrease linearly with increasing mass. Now, the crystal does not drive the entire bulk of the liquid because the transverse displacement dies off exponentially in the liquid with characteristic decay length δ (see Fig. 2 and Eqn. 13). This is the effective thickness of the liquid treated as a rigid sheet, so the added mass is $\delta \rho_L$. The decay length, δ, varies with $(\eta_L)^{1/2}$; so, as the viscosity increases so does the effective thickness and hence the total mass, $\delta\rho_L = (2\rho_L\eta_L/\omega)^{1/2}$, which has exactly the same dependence on viscosity and density as Eqn. 17. Thus this simple picture leads to the correct form of the frequency dependence.

While there may be other, less important, contributions which are not included here, the results shown in Figs. 3 and 4 are a convincing test of the essential correctness of this model.

REFERENCES

1 P. L. Konash and G. J. Bastiaans, Anal. Chem., 52 (1980) 1929.
2 T. Nomura and A. Minemura, Nippon Kagaku Kaishi, 1980 (1980) 1261.
3 S. Bruckenstein and M. Shay, Abstracts, Pittsburgh Conference and Exposition, Atlantic City, NJ, March 1983.
4 W. P. Mason, W. O. Baker, H. J. McSkimin and J. H. Heiss, Phys. Rev., 75 (1949) 936.
5 A. P. M. Glassford, J. Vac. Sci. Technol., 15 (1978) 1836.
6 V. Mecea and R. V. Bucur, Thin Solid Films, 60 (1979) 73.
7 R. A. Crane and G. Fischer, J. Phys. D, 12 (1979) 2019.
8 K. K. Kanazawa and J. G. Gordon II, Anal. Chem., 57 (1985) in press.
9 R. C. Weast (Ed.), Handbook of Chemistry and Physics, 63rd edn., CRC Press, Boca Raton, FL, 1982–1983.

Analytica Chimica Acta, 175 (1985) 107—116
Elsevier Science Publishers B.V., Amsterdam — Printed in The.Netherlands

BEHAVIOUR OF PIEZOELECTRIC QUARTZ CRYSTALS IN SOLUTIONS WITH APPLICATION TO THE DETERMINATION OF IODIDE

T. NOMURA* and M. WATANABE

Department of Chemistry, Faculty of Science, Shinshu University, Asahi, Matsumoto 390 (Japan)

T. S. WEST

The Macaulay Institute for Soil Research, Craigiebuckler, Aberdeen, AB9 2QJ (Great Britain)

(Received 5th March 1985)

SUMMARY

The frequency of oscillation of a piezoelectric quartz crystal immersed in solution changes with the temperature of the solution and with the ambient temperature of the oscillator, especially where the latter is transistorized. The frequency is also affected by the specific gravity, viscosity and specific conductivity of the solution. When all the properties are maintained constant, iodide present in the solution electrodeposits on the silver electrodes of a crystal to produce a reproducible change in frequency which allows iodide to be determined in the range 0.5—7 μM. Thiosulphate, cyanide, sulphide, Fe(III), Hg(II) and Ag interfere, but procedures for preventing their interference are given.

Piezoelectric quartz crystals have been used mainly for the determination of atmospheric substances [1] because it is generally believed that the crystal oscillates only in the dry state. Such crystals are usually coated with a substrate that reacts with the analyte in the atmosphere and the frequency change resulting from the increased mass is measured. The frequency changes are usually markedly affected by atmospheric moisture. Substances in solution have been determined from the frequency difference for the dry crystal before and after exposure to dissolved analytes [2]. The precision of such methods was poor.

It has been found that a crystal in contact with a liquid on only one side is able to oscillate and that its frequency changes with the specific gravity and the specific conductivity of the solution [3]. When these properties are maintained constant by means of a concentrated pH buffer solution, cyanide and metal ions in the solution react with the electrode on the crystal, and can be determined by the frequency shifts resulting from the changes in mass [4]. A crystal connected to a modified oscillator was also found to oscillate when the whole crystal was immersed [5]. The frequency change was affected by the specific gravity and viscosity and was also proportional to the specific

0003-2670/85/$03.30

conductivity [6]. Reactive substances in the solution could again be determined when the other properties of the solution were maintained constant with a buffer, as mentioned above. With the circuitry used, a potential difference of ca. 1.5 V was imposed on the electrodes. Several metal ions consequently electrodeposited on the electrodes [6], and some could be determined selectively by using masking reagents to prevent the electrodeposition of other metal ions [7]. It was also found that the frequency shifts of the totally immersed crystal caused by changes in temperature of the solution were much larger than those of a crystal in contact with the solution on one side only.

In this paper, the dependence of the crystal frequency on the temperature of the solution in which the crystal is immersed, the ambient temperature of the oscillator, and the specific gravity, specific conductivity and viscosity of the solution was investigated with transistorized [5] and integrated circuits (i.c.) [8]. Subsequently, the determination of iodide with a silver-plated crystal was investigated.

EXPERIMENTAL

Apparatus and chemicals

The apparatus used was as described previously [7]. The solutions were thermostatted (20 ± 0.05°C) and the vessels containing water, sample and reagent blank solutions and the oscillators were held at 25 ± 0.5°C in a thermostatted air bath. The AT-cut, 9-MHz piezoelectric quartz crystal had platinum-plated gold electrodes, and was directly connected to a transistorized oscillator [5] supplied with 6 V or a normal i.c. oscillator (normal TTL) [8] or a low-power shot key oscillator (LS-TTL) [9] (Fig. 1) supplied with 4.5 V. Iodide was determined by means of a crystal having silver electrodes [10] connected to the normal TTL oscillator. The specific conductivity, specific gravity and viscosity of the solutions were measured with

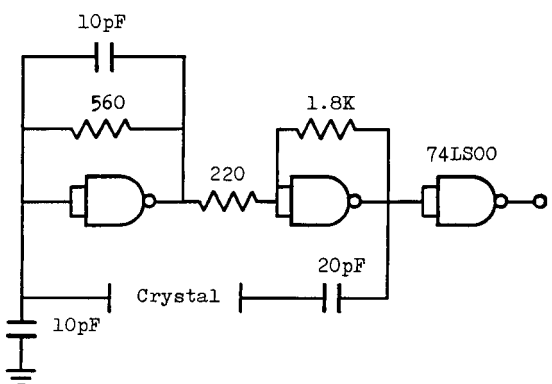

Fig. 1. Oscillator circuit (LS-TTL) [9] (units are ohms unless otherwise stated).

a Universal Bridge Model 4255A (Yokogawa-Hewlett Packard Co.), pycnometer (volume 25 cm^3) and Ostwald viscometer, respectively.

The solutions were prepared from analytical-grade reagents (Wako Pure Chemicals). The iodide stock solution (0.1 M) was prepared by dissolving potassium iodide in water, and standardized by the Volhard method. Redistilled water was used throughout.

Procedures

Dependence of frequency change on the specific conductivity, specific gravity and viscosity. Transfer the salt solutions and water to their respective containers and pass the water through the cell at 6.9 ml min^{-1}. When the crystal frequency has become constant (F_1), pass the salt solution until the frequency is constant (F_2). Calculate the frequency change, $\Delta F = F_1 - F_2$, and pass water through the cell for the next measurement.

Determination of iodide (0.5—7 μM). Transfer the sample or standard solution containing 1 mM acetate buffer (pH 4.1) and the reagent blank solution to their containers. Pass the reagent blank solution through the cell at 11.2 ml min^{-1}. When the crystal frequency has become constant (F_1), pass the sample or standard solution for exactly 5 min, and then the reagent blank solution again until the frequency is constant (F_2). The frequency change, $\Delta F = F_1 - F_2$, is proportional to the concentration of iodide, and a calibration graph can be constructed on this basis. To remove the iodide deposited on the electrode, pass 0.01 M ammoniacal buffer solution (pH 9.4) containing 2 mM sodium thiosulphate through the cell with a contact time of 30 s per 50 Hz of frequency change (ΔF) due to deposited iodide, and then pass the reagent blank solution for the next experiment. When the frequency change becomes noisy, replate the crystal with silver as described previously [10]. At least 30 determinations could be done before replating.

Removal of interferences. Transfer the sample solution to a 100-ml dark-glass Erlenmeyer flask, add 4 ml of 0.1 M sodium acetate, 4 ml of 0.1 M sodium sulphide and ca. 40 mg of zinc powder, and dilute to ca. 20 ml with water. Heat at just below boiling for 15 min and filter. Heat again for 20 min after adding 2 ml of 3% hydrogen peroxide, decompose the hydrogen peroxide with the addition of a small amount of manganese dioxide powder, and cool to room temperature. Transfer the solution to a 200-ml volumetric flask, add 16 ml of 0.1 M acetic acid, dilute to the mark with water and follow the recommended procedure.

RESULTS AND DISCUSSION

Dependence of the crystal frequency on temperature

The frequency of the crystal immersed in water changed with temperature to an extent that depended on the oscillator used to drive the crystal. The oscillators were operated in an air bath thermostatted at 20 ± 0.5°C, and the water temperature was varied in the range 15—30°C by means of a

thermostatted water bath and circulator. All measurements were made with the same crystal. As shown in Fig. 2, the frequency of the crystal increased with increasing solution temperature, but a smaller change was obtained with the normal TTL oscillator. The frequency of an AT-cut crystal is much less dependent on the ambient temperature when it is situated in a gaseous environment [11]. It was supposed that the observed frequency shifts in solution were caused by changes in the specific gravity and viscosity of the water caused by temperature changes. However, when the water temperature was maintained at 20 or 25 ± 0.05°C and the temperature of the air bath was increased, the frequency of the crystal immersed in water behaved differently, as shown in Fig. 3. The transistorized oscillator in particular gave a pronounced decrease in frequency with rise of temperature. The frequency changed by 1 kHz between 20 and 27°C in the air bath. These observations indicate that the temperature of the test solution should be maintained constant, as should the temperature where the transistorized oscillator is used.

Behaviour of the crystal immersed in aqueous solution

The frequency of a crystal connected to the transistorized oscillator and immersed in an aqueous solution is proportional to the specific conductivity and the specific gravity of the solution [6]. The crystal had a potential

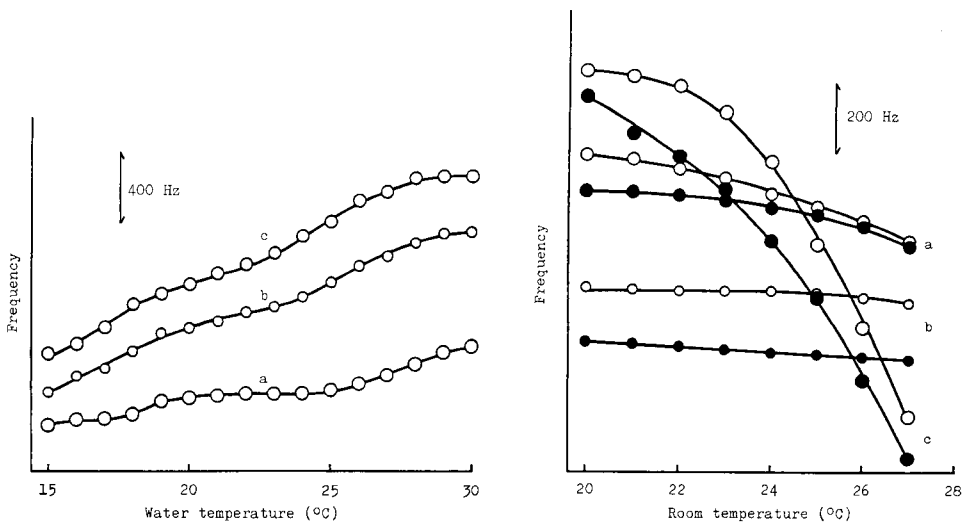

Fig. 2. Frequency shifts of crystals connected to: (a) normal TTL; (b) LS-TTL; (c) transistorized oscillators immersed in water of various temperatures. (Flow rate of water was 6.9 ml min^{-1}.)

Fig. 3. Frequency shifts of crystals immersed in water at: (•) 20°C; (○) 25°C, connected to various oscillators (a—c as in Fig. 2) at various temperatures. (Flow rate of water as in Fig.2.)

difference of 0.43 V between the electrodes as shown by measurement with a National VP-551A oscilloscope, thus several metals could be electrodeposited on one electrode [6]. With the i.c. oscillators, however, there was only 0.1 V between the electrodes and only a few metals could be electrodeposited [7]. The frequency changes of a crystal connected to an i.c. oscillator on immersion in aqueous solutions having various specific conductivities, compared to pure water, are shown in Fig. 4. The frequency with both oscillators depended on the specific conductivity of the solution when dilute solutions were used. When the LS-TTL oscillator was used, the minimum frequency was obtained in solutions having a specific conductivity of ca. 0.4 mS cm^{-1}; there was no frequency change with 1 mS cm^{-1} (6 mM sodium chloride or 0.2 M acetic acid). When a normal TTL oscillator was used, the frequency decreased sharply with increasing specific conductivity.

The frequency change of a crystal connected to the LS-TTL oscillator and immersed in sucrose or glycerine solutions of various concentrations (i.e., non-electrolyte solutions) is shown in Table 1. As with the normal TTL oscillator [8], the frequency change increased with increasing concentration as described by $\Delta F = -aD - bN + c$, where ΔF is in Hz and the specific gravity and the relative viscosity against water are D and N, respectively; a, b and c are constants for the various solutes. This equation could be applied to methanol, ethanol, methanol/water or ethanol/water mixtures but with poor agreement because commercial chemicals were used without further purification. The reason for different constants among the solutes is that the frequency is modified by factors other than the specific conductivity, specific gravity and viscosity. To measure the change in mass of the electrode unequivocally as a frequency change of the crystal, the specific conductivity, specific gravity and viscosity of the solution should be maintained constant, e.g., by using a pH buffer solution.

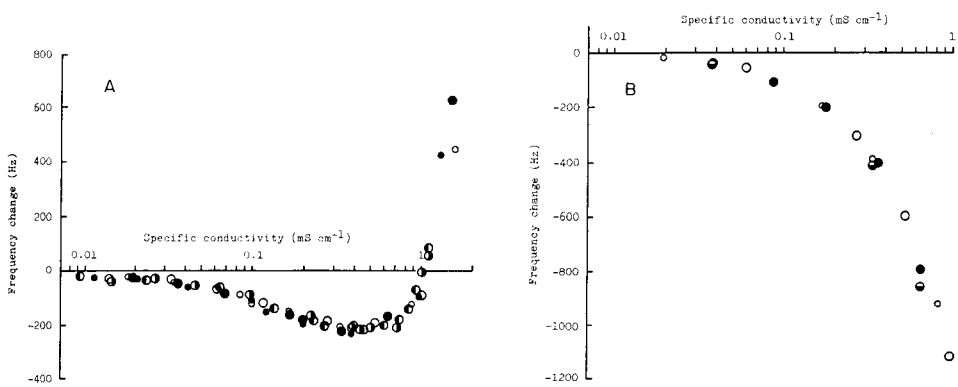

Fig. 4. Dependence of frequency change on the specific conductivity for different solutions: (○) NaCl; (●) KCl; (●) Na_2SO_4; (○) $AlCl_3$; (◐) CH_3COOH; (◑) NH_3; (◒) $Na_2S_2O_3$. Oscillator: (A) LS-TTL; (B) normal TTL. (Flow rate 6.9 ml min^{-1}, 20 ± 0.05°C.)

TABLE 1

Effects of sucrose and glycerine concentration on the frequency of oscillation

Concentration (% w/w)	Specific gravity	Relative viscosity	Frequency change (Hz)	Concentration (% w/w)	Specific gravity	Relative viscosity	Frequency change (Hz)
Sucrose				*Glycerine*			
0.4	1.00371	1.00644	−27	2	1.00561	1.04385	−204
0.6	1.00475	1.01114	−50	4	1.01032	1.10199	−392
0.8	1.00551	1.01437	−74	6	1.01493	1.16117	−554
1.0	1.00619	1.02278	−95	8	1.01964	1.23050	−726
2.0	1.01003	1.04926	−203	10	1.02401	1.29112	−900
3.0	1.01400	1.09625	−278	12	1.02894	1.37284	−1133
4.0	1.01800	1.09625	−408	14	1.03382	1.45934	−1274
				16	1.03847	1.53520	−1436

Determination of iodide

Selection of buffer solution. By reacting with the silver electrode of the oscillating crystal, iodide and sulphide produced a frequency decrease and cyanide and thiosulphate an increase in 0.01 M ammoniacal (pH 9.4) and acetate (pH 4.6) buffer solutions at a flow rate of 6.9 ml min^{-1}. The frequency changes were greatest for iodide in an acetate buffer and for cyanide in an ammoniacal buffer. The silver electrodes gradually dissolved in ammoniacal solution as a soluble ammine, resulting in a steady frequency increase. Thus, to determine iodide, a 1 mM acetate buffer was used because it had sufficient buffering capacity, and a large volume of acetate was not required.

Dissolution of silver iodide deposited on the electrode. The frequency changes caused by incremental depositions of iodide gradually decreased because the deposition sites on the silver electrode surface became saturated. To avoid this problem, the deposited iodide was removed from the surface of the electrode at the end of an experiment. Cyanide or thiosulphate solution dissolved the silver iodide deposited on the electrode. The former was the more efficient and the electrodes maintained good reproducibility for subsequent determinations of iodide. Nevertheless, the poisonous nature of cyanide is a disadvantage. Thus thiosulphate was used to remove the iodide deposited. However, the excess of thiosulphate also dissolved the silver electrodes, resulting in poor reproducibility.

The iodide determination was also examined by using a normal TTL oscillator, which produced less noise than a LS-TTL. The frequency of the crystal connected to the former, as shown in Fig. 4, was sharply decreased at specific conductivities of >0.4 mS cm^{-1} in comparison to the latter. Also the frequency change on dissolution of silver iodide with high concentrations of thiosulphate could not be recorded. The behaviour of the silver iodide deposited on the electrode was investigated, therefore, with the LS-TTL oscillator and a dilute thiosulphate solution without ammoniacal buffer.

The frequency of oscillation of a crystal with silver electrodes gradually increased at a rate of 18 Hz min^{-1} with 0.01 M ammoniacal buffer solution (pH 9.4) because of slow dissolution of the silver. When the thiosulphate solution was passed through the cell containing the silver iodide-coated electrode, the frequency immediately decreased because of the conductivity effect of the thiosulphate, and then rapidly increased as the silver iodide deposit was removed; finally, there was a slow progressive increase caused by slow dissolution of the silver electrode (Fig.5). The length of the steep rising slope was proportional to the amount of the silver iodide, calculated from the deposited iodide, and the same slope lengths were recorded with repeated experiments. The subsequent slower increases agreed exactly with those observed when no iodide had been deposited on the silver electrodes.

Similar experiments were done with the normal TTL oscillator, and thiosulphate of various concentrations in 0.01 M ammoniacal buffer solution (pH 9.43) at a flow rate of 11.2 ml min^{-1}. The frequency of the crystal was measured every min, followed by flushing with water in order to measure

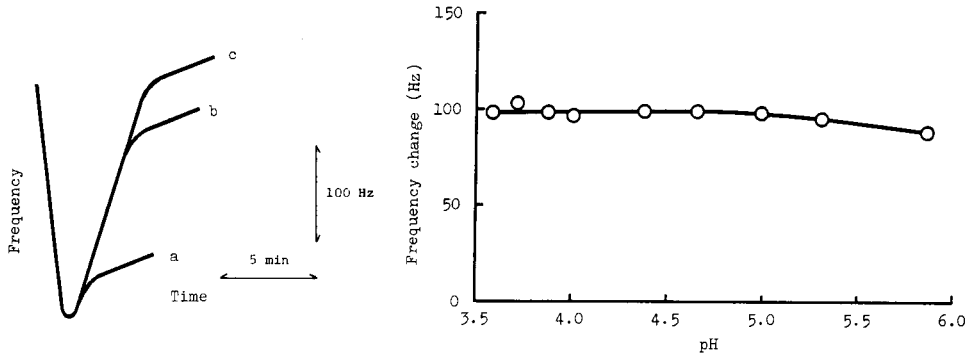

Fig. 5. Frequency changes of a silver-plated crystal on which various amounts of iodide, corresponding to: (a) 0; (b) 72; (c) 102 Hz frequency changes had been deposited when thiosulphate (2.5 mM) was passed over the crystal at 6.9 ml min^{-1}.

Fig. 6. Dependence of frequency change on pH for 5 μM iodide in 1 mM acetate buffer. (Flow rate 11.2 ml min^{-1}, reaction time 5 min.)

the frequency in water, until the rate of frequency change was the same as that of the baseline value for the dissolution of the silver electrodes. The results agreed exactly with those for the LS-TTL oscillator. They showed that thiosulphate concentrations in the range 0.5—2.5 mM gave two frequency change slopes caused by the dissolution of the silver iodide and the silver electrodes, that silver iodide was dissolved first and then the silver electrodes dissolved, and that higher concentrations of thiosulphate caused faster dissolution. A slower flow rate of thiosulphate solution (9.1 ml min^{-1}) gave similar results, but took longer to dissolve the deposited silver iodide. Dissolution of the iodide by using acetate buffer (pH 4.1) and phosphate buffer (pH 6.7) was unsuitable because of slow dissolution. From these results it was decided that deposited iodide should be dissolved by passing 2 mM thiosulphate in 0.01 M ammoniacal buffer (pH 9.43) over the crystal at a rate corresponding to 30 s per 50-Hz frequency change.

Dependence of frequency change on pH. The effect of pH on the frequency change was investigated by using 1 mM acetate buffer solution because the deposition of iodide above or below pH 3.5—6.0 was slow, especially in alkaline solution (pH 9.4). A higher concentration of buffer solution (0.01 M) gave the same results. At pH 3.6—4.7, as shown in Fig. 6, large frequency changes were observed. The frequency change decreased with increasing pH above pH 4.7. This decrease in rate was more pronounced at the slower flow rate (6.9 ml min^{-1}).

Effect of the flow rate and reaction time. It was supposed that a faster flow rate would give a larger frequency change because of the stirring effect it would produce. However, as is shown in Fig. 7, this was not found in practice. On the other hand, the frequency change was directly proportional to the reaction time (i.e., the period of the time required to pass the iodide solution

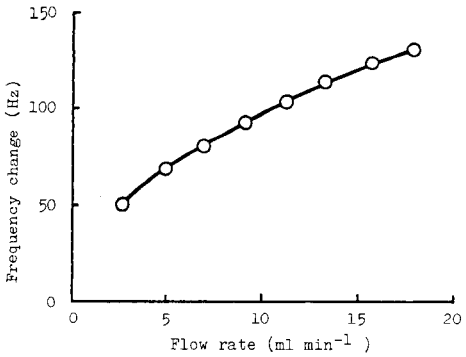

Fig. 7. Dependence of frequency change on flow rate for 5 μM iodide in 1 mM acetate buffer (pH 4.1). (Conditions as in Fig. 6.)

through the cell at 11.2 ml min^{-1}) over the range 90 s—10 min. Thus a longer time could be used for lower concentrations of iodide; 5 min was used in the present procedure.

Calibration and reproducibility. The calibration graph of frequency change (ΔF) against iodide concentration [I^-] was linear over the range 0.5—7 μM, and is described by [I^-] = (ΔF/20.0) $\times$ 10^{-6} M, where ΔF is measured in Hz. The standard deviation was 4.02 Hz (4.0%) for 6 determinations of 5 μM iodide. The system should be recalibrated when the quartz crystal has been replated with silver.

Effect of other ions. The effects of other ions on the determination of 5 μM iodide were investigated; changes in frequency of more than $\pm$5% were considered to constitute an interference. The tolerance limits for these ions are shown in Table 2. The interferences of silver and mercury(II) arose from the formation of iodide precipitates in solution, thus resulting in low recoveries. Iron(III) gave a high recovery because of the adsorption of the hydrated oxide on the electrodes. Cyanide, thiosulphate and sulphide interfered by causing low recoveries. Both cyanide and thiosulphate dissolved the electrodes to form soluble silver complexes. These interferences (100-fold

TABLE 2

Tolerance limits for ions in the determination of 5 μM iodide

Tolerance limit Ion: iodide mole ratio	Ions
100	Bromide, carbonate, chloride, phosphate, sulphate, thiocyanate, aluminium, ammonium, cadmium, cobalt (II), copper (II), lead, nickel, zinc
1	Thiosulphate
<1	Cyanide, sulphide, iron (III), mercury(II), silver

amounts) except for thiosulphate (maximum 50-fold) could be eliminated by the method given above, in which the anions were oxidized with hydrogen peroxide, silver and iron(III) were precipitated as sulphide and hydrated oxide, respectively, and mercury(II) was amalgamated by adding zinc powder.

The authors record their thanks for financial assistance from the Education Ministry of Japan in support of this work.

REFERENCES

1 J. F. Alder and J. J. McCallum, Analyst, 108 (1983) 1169.
2 J. P. Mieure and J. L. Jones, Talanta, 16 (1969) 149.
3 T. Nomura and A. Minemura, Nippon Kagaku Kaishi, 1980 (1980) 1621.
4 See, e.g., T. Nomura and M. Iijima, Anal. Chim. Acta, 131 (1981) 97.
5 T. Nomura and M. Okuhara, Anal. Chim. Acta, 142 (1982) 281.
6 T. Nomura and M. Maruyama, Anal. Chim. Acta, 147 (1983) 365.
7 T. Nomura and K. Tsuge, Anal. Chim. Acta, 169 (1985) 257.
8 T. Nomura and T. Nagamune, Anal. Chim. Acta, 155 (1983) 231.
9 S. Nakajima, Transistor Gijutsu, 19 (1982) 348.
10 T. Nomura and T. Mimatsu, Anal. Chim. Acta, 143 (1982) 237.
11 G. Sauerbrey, Z. Phys., 155 (1959) 206.

Analytica Chimica Acta, 175 (1985) 117—126
Elsevier Science Publishers B.V., Amsterdam — Printed in The Netherlands

EVALUATION OF THE ZIRCONIA pH SENSOR AT 95°C

TRUMAN S. LIGHT* and KENNETH S. FLETCHER
Corporate Research Center, The Foxboro Company, Foxboro, MA 02035 (U.S.A.)
(Received 19th April 1985)

SUMMARY

An yttria-stabilized zirconia electrode for measuring pH at elevated temperature and pressure has been described by Niedrach, who verified its response at 95°C in comparison with glass pH electrodes. The present paper reports studies at 95°C on zirconia tubes available from three different commercial sources. This study, conducted with conventional aqueous internal filling solution and conventional internal and external reference electrodes, was designed to obtain fundamental pH electrode parameters of slope, resistance, asymmetry potential, and time of response in standard buffers and known strength acids and bases. A coulometric experiment is reported to aid in assessing the efficiency of the zirconia electrode. Uncertain performance found in this evaluation may be attributed to chemical, physical, and surface problems in the commercially available zirconia tubes or to less than ideal pH response for zirconia membranes.

One of the most important chemical qualities of water is its pH. The measurement of pH at temperatures above 125°C has long been difficult and impractical. Increased need for this measurement has come about from diverse sources such as high-temperature measurements on geothermal wells in the presence of high brine content and hydrogen sulfide, in high pressure water systems such as those found in the power industry with both nuclear and conventionally fired fuel sources, and in industries using chemical processes at elevated temperature such as the alkaline digestion of wood pulp in paper production.

An yttria-stabilized zirconia electrode for measuring pH at elevated temperature and pressure has been described by Niedrach [1—3] and by Niedrach and Stoddard [4, 5]. Macdonald and co-workers [6—8] have confirmed this sensor but reported difficulties which were attributed to the high-temperature zones in which the internal and reference electrodes were situated. Tsuruta and Macdonald [6, 7] described somewhat different construction, using matched measuring and reference electrodes each of which has its internal silver/silver chloride reference electrode at ambient temperature, and therefore has thermal liquid junctions. Hettiarachchi and Macdonald [8], in a preliminary report, used a solid mercury-calomel fill for the internal reference and also a reference hydrogen electrode against a pressure-balanced silver/silver chloride reference electrode for pH measurements at 175—275°C.

0003-2670/85/$03.30

They thought that the hydrogen reference electrode eliminated the errors of using calculated pH values at elevated temperatures. Their preliminary report attributed the lack of precision in earlier studies to the uncertainty in the calculated pH values of the buffer solution used for calibration at elevated temperatures.

A study of the stabilized zirconia pH sensor over the temperature range 100—300°C was reported by Danielson and Koski [9]. They used silver/silver chloride and hydrogen reference electrodes and four different types of solid internal electrodes, namely silver coating, silver powder, graphite powder and Cu/Cu_2O powder mixture. They reported 81—100% Nernstian response for three sensors at 100°C and 100% Nernstian response at higher temperatures and discovered that the internal half cell was poised by oxygen. Activation energy measurements implied the same mobile oxide ion process for solution pH and gaseous oxygen sensors.

At temperatures above 100°C, the reference electrode becomes a problem not only because of the instability of the typical silver/silver chloride or mercury/calomel electrode potential at this temperature, but also because of the contamination of the internal fill solution if the back pressure becomes greater than the internal pressure. Danielson [10] has addressed this problem and reported a "refreshed" (i.e., flowing) reference electrode, using a liquid chromatographic high-pressure pump and an internal potential element of silver/silver chloride at ambient temperature containing a liquid junction thermal potential.

Earlier investigations in this laboratory were done with three different commercial sources of zirconia/yttria electrodes. Solid internal electrodes evaluated included Pt/Hg, Pt/Hg/HgO, and Cu/CuO which have been reported at various times by Niedrach [1—5]. Liquid internal electrodes included $Ag/AgCl/Cl^-$, pH buffers, and Pt/redox solution combinations. Temperatures studied ranged from 95 to 200°C. Solutions studied included varying concentrations of strong acids and bases and National Bureau of Standards buffers. Reference electrodes were patterned after several models suggested by Danielson [10]. These studies showed a lack of reproducibility, poor Nernstian response, and difficulty with stability of the reference electrode over the time duration needed to run elevated temperature/pressure experiments. Doubts were raised as to the proper physical and surface composition of the zirconia electrodes as well as to the more inherent question concerning the suitability of zirconia/yttria as a pH electrode in the temperature range 100—300°C.

In the present study, a set of experiments was devised for evaluation of zirconia pH sensors by comparison with fundamental properties of glass pH electrodes [11]. A somewhat similar study has been reported by Niedrach [2]. He used zirconia tubes from non-commercial sources which were custom-fabricated and filled with mercury internal contacts. Employing calculated pH values, he reported a linear response for the zirconia electrodes and non-linear response for the glass electrodes attributed to the alkaline

error of the glass electrodes. He also reported more erratic behavior with glass electrodes than with the zirconia electrodes and that some of the specially prepared zirconia tubes were more sluggish than others. In the study reported here, at 95° C, high-purity zirconia tubes available from three different commercial sources are used, internally filled with a standard pH buffer solution and a known added chloride content. A low-alkali-error glass electrode known to behave ideally over a wide range of pH was used for comparison. For one experiment, a symmetric electrochemical cell construction was used so that the internal and external reference electrodes were identical in composition and maintained at 25° C. In other experiments, standard buffers, acid-base titration, and standard acids and bases were used. A coulometric experiment was also done to assess electrode efficiency. The intent of this study was to eliminate many of the variables that might have contributed to the uncertainty of earlier results and to permit an assessment of the validity and practicality of zirconia membranes for potentiometric pH measurement.

EXPERIMENTAL

Yttria-stabilized zirconia tubes, 150-mm length and 6.4-mm outside diameter, were obtained from three sources: (a) Zircoa-Corning (Solon, Ohio), 8% by weight yttria (composition 1372), density 5.8 g cm^{-3}, color yellow; (b) McDanel Refractory Co. (Beaver Falls, Pennsylvania), 12% by weight yttria, density 5.6 g cm^{-3}, purity 99.6%, color white; (c) Viking Chemicals (Follenslev, Denmark), 12.9% by weight yttria, density 5.9 g cm^{-3}, purity 99.99%, color white.

The symmetrical electrochemical cell is shown in Fig. 1 and was constructed from zirconia tubes, the tip from a ceramic junction reference

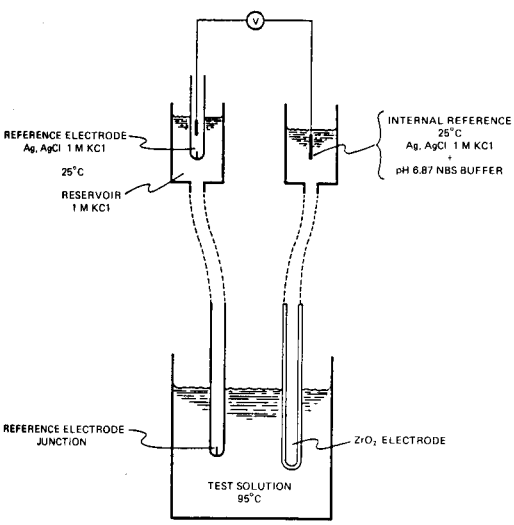

Fig. 1. Electrochemical test cell used for evaluating zirconia pH electrodes at 95° C.

electrode, and a silver/silver chloride/1 M potassium chloride (Foxboro Q0105AW) reference electrode. A low-alkaline-error, high-temperature (110°C) Foxboro Q0104AN glass electrode was used. The zirconia tube was filled with National Bureau of Standards (NBS) buffer, pH 6.89 at 95°C [12] which had been made 1 M in potassium chloride. A silver/silver chloride electrode was the internal reference element. Both the internal and reference silver chloride electrodes were at ambient (25°C) temperature and connected to the 95°C zone by flexible tubing as shown in Fig. 1. Voltages were measured with an Orion Model 901 pH-millivolt meter with dual high-impedance input.

For the coulometric experiment, a Princeton Applied Research, Model 173 potentiostat/galvanostat was used.

NBS buffers were used as indicated in Table 1. Directions for preparation and standard pH values for these buffers over the range 0—95°C are given by Bates [12]. All chemicals used were reagent grade.

RESULTS AND DISCUSSION

The silver/silver chloride reference electrodes for both the internal and reference electrodes were maintained at ambient (25°C) temperature and the internal solution of the zirconia electrode was the NBS pH 6.89 (95°C) phosphate buffer made 1.00 M in potassium chloride [12]. The thermal junction cell used in this study is somewhat similar to that of Tsuruta and Macdonald [6] and a theoretical discussion has been given by deBethune et al. [13]. The cell is shown in Fig. 1 and is depicted as follows:

Ag/AgCl	1 M KCl	1 M KCl	Test soln.	ZrO_2	1 M KCl +	Ag/AgCl	(A)
1 M KCl				membrane	pH 6.89 NBS	1 M KCl + pH 6.87 NBS	
25°C	25°C	95°C	95°C	95°C	95°C	25°C	

TABLE 1

Zirconia electrodes in standard buffers at 95°C

Electrode	E.m.f. (mV)				Nernst slope (%)
	Buffer pH 4.227	Buffer[a] pH 6.886	Buffer pH 8.833	Difference[b]	
Glass	+169.6	−18.9	−165.4	335.0	(100.0)
Corning-Zircoa	+168.4	+48.8	−62.4	230.8	69
McDanel-1	+173.3	+44.5	−76.6	249.9	75
McDanel-2	+162.4	+24.8	−93.5	255.9	76
Viking	+162.6	+39.1	−76.6	239.2	71

[a] 1 M KCl added; this column is also the asymmetry potential for the zirconia electrodes.
[b] E.m.f. difference between buffers of pH 4.227 and 8.833.

The object of these experiments was to measure the several zirconia electrodes and compare them with the glass electrode in a variety of known pH solutions at 95° C. Niedrach [2] reported comparison of the zirconia sensors with mercury internal contacts, with glass electrodes at 95° C, and Tsuruta and Macdonald [6], conducting their study over the temperature range 100—275° C, reported using liquid internal filling solutions with the reference zones at 25° C. One of the interesting experiments in the present study was to immerse the zirconia electrode in the same solution as its internal filling solution. This eliminated consideration of problems that might be caused by solid- or mercury- internal contacts. The "symmetrical" cell thus formed, with a theoretical e.m.f. of 0 mV, furnished a means of determining the asymmetry potential of the zirconia electrode.

The results of these experiments are given in Tables 1—4. Table 1 shows data obtained from measurement in three different NBS buffer solutions of known pH at 95° C. In the pH 6.886 buffer the electrochemical cell is symmetrical and the ideal theoretical e.m.f. of such a cell is 0 mV. The four zirconia electrodes listed in Table 1 show e.m.f. values, and therefore asymmetry potentials ranging from +25 to +50 mV. The glass electrode, showing −18.9 mV, was not part of the symmetrical cell concept. Its sealed internal solution and reference electrode are designed to give 0 mV when measured in a pH 7.00 buffer at 25° C vs. a silver/silver chloride, 4 M potassium chloride reference electrode. Performance of a commercial glass electrode would typically show a few tenths of a millivolt asymmetry potential. If this number were as large as 5 mV, the pH-sensitive glass membrane would be judged to be strained and the electrodes not acceptable. Interpretation of the +25 to +50 mV asymmetry potential in the zirconia electrodes is speculative. No mechanism has been established for the zirconia electrode operation and no reference values have been reported for asymmetry potentials. The large asymmetry potential might suggest that the interior and exterior surfaces of the zirconia electrode are dissimilar. A detailed chemical and physical study

TABLE 2

Acid—base response of ZrO_2 electrodes at 95° C[a]

Electrode	E.m.f. (mV)				Nernst slope (%)
	Acid	Base	Difference	Resistance (MΩ)	
Glass	+238.8	−254.4	493.2	3.3	(100)
Corning-Zircoa	+196.3	−212.3	408.7	326	83
McDanel-1	+212.4	−198.8	411.2	339	83
McDanel-2	+195.9	−198.5	394.4	302	80
Viking	+208.6	−185.5	394.1	242	80

[a]3.0 ml of 1.0 M sodium hydroxide added to 150 ml of 0.0005 M sulfuric acid.

TABLE 3

Response of ZrO_2 electrodes in alkaline solutions at 95° C

Electrode	E.m.f. (mV)			Nernst slope[a] (%)
	1.0 M NaOH	0.10 M NaOH	Difference	
Glass	−361.4	−300.4	97.5[b]	(100)
Corning-Zircoa	−312.5	−234.8	77.7	80
McDanel-1	−352.6	−264.4	88.2	90
McDanel-2	−354.8	−280.8	74.0	76
Viking	−301.7	−229.5	72.2	74

[a]Nernst slopes corrected for estimated sodium-ion error in glass electrode. [b]Corrected by 36.5 mV for estimated sodium-ion error corresponding to 0.5 pH between 0.1 M and 1.0 M NaOH at 95° C.

TABLE 4

Response of ZrO_2 electrodes in acid solutions at 95° C

Electrode	E.m.f. (mV)			Nernst slope (%)
	0.005 M H_2SO_4	0.0005 M H_2SO_4	Difference	
Glass	+312.4	+249.2	63.2	(100)
Corning-Zircoa	+267.8	+198.2	69.6	110
McDanel-1	+283.8	+209.8	74.0	117
McDanel-2	+282.8	+208.5	74.3	118
Viking	+249.3	+192.2	57.1	90

of these surfaces would be of interest, but this was not done in the present study.

Table 1 also shows the Nernst slope of the zirconia electrodes calculated from NBS buffers with reference to the glass electrode [11, 12]. Over the range pH 4.23—8.83, which is a pH shift of 4.60, the glass electrode changed 335.0 mV at 95° C; the Nernst coefficient is 73.046 mV/pH at this temperature giving a theoretical Nernst shift of 336.0 mV and an actual Nernst slope of 99.7% for the glass electrode. When compared to the glass electrode, the four zirconia electrodes showed Nernst slopes from 69 to 76% in the NBS buffers of Table 1.

The results of a one step acid-base reaction at 95° C are shown in Table 2. The experiment consisted of adding 3.0 ml of 1.0 M sodium hydroxide to 150 ml of 0.0005 M sulfuric acid giving a pH change from 3.28 to 10.03, according to the glass electrode. The Nernst slope of the four zirconia electrodes varied from 80 to 83% when compared to the glass electrode. Because the glass electrode has a sodium-ion error that increases with alkalinity and

temperature, the experimentally observed Nernst slope probably is expected to be less than shown in Table 2. The resistance of the electrodes was also calculated from data in Table 2 and is about 3 MΩ for the glass electrode and 300 MΩ for the zirconia electrodes at 95° C. These values can be compared with 25° C values of approximately 300 MΩ for the glass electrode and 3000—6000 MΩ for the zirconia electrodes.

Data for zirconia electrodes measured in two different concentrations of sodium hydroxide at 95° C are shown in Table 3. Values for the Nernst slope would range up to 145% if the zirconia electrodes were compared with the glass electrode. However, it is well known that the corrections for the sodium-ion error of the glass electrode in strong, hot sodium hydroxide solutions are very large and not very stable. In order to calculate the Nernst slope of Table 3, the assumption was made that the differential error of 0.5 pH, equivalent to 36.5 mV at 95° C, existed between the 1.0 M and 0.1 M sodium hydroxide solutions. The Nernst slopes of the four zirconia electrodes under test then average 80% and were quite similar to the values reported in Tables 1 and 2.

The same zirconia and glass electrodes were compared in sulfuric acid solutions at 95° C as shown in Table 4. Nernst slopes ranging from 90 to 118% were found. The glass electrode is believed to have no error in acid solutions, although correction for liquid junction potential would be uncertain. The erratic Nernst slope found from these four zirconia electrodes in sulfuric acid solutions is not explainable at this point. However, it should be noticed that Tsuruta and Macdonald [6] discussed the possibility of existence of an "acid error" with their zirconia pH electrodes.

In all of the solutions tested, the time of response of the zirconia and glass electrodes was less than 30 s for a step change (to within one mV of the equilibrium potential) from acid to alkaline solutions. The reproducibility for the same electrodes in the same solution over a period of one week was somewhat variable. The differences with the zirconia electrode ranged from 10 to 30 mV in this period while the glass electrode differences ranged from a few tenths to 5 mV.

The charge carrier in stabilized zirconia is well known to be the oxide ion, O^{2-}, and this property has been successfully exploited for coulometric titrations with generated oxygen in molten salts [14]. Here, platinum electrodes deposited on opposing sides of zirconia cells operate reversibly for the O_2/O^{2-} system at the high temperatures used. It was of interest, therefore, to test the transport mechanism of zirconia under the conditions of this work, namely relatively low temperature compared with the molten salt work and in aqueous solvent systems. Further, because successful potentiometric response implies rapidly reversible interfacial exchange reactions, it is to be expected that pumping charge through zirconia membranes in contact with aqueous systems would result in generation of hydroxide ion. Absence of metallic electrodes in direct contact with the zirconia membrane would avoid redox processes involving oxygen gas. An analogous experiment was

accomplished with 100% current efficiency for generation of fluoride ion through lanthanum trifluoride membranes as reported by Durst and Ross [15]. Because of the relatively high resistance of our cells, only moderate currents of 5—100 μA could be used. The experimental arrangement is shown in Fig. 2 where hydroxide ion was electrolytically pumped from the external potassium hydroxide solution into the internal electrode compartment containing 0.1 M KCl. The hydroxide ion pumped into this compartment was determined by titration with standardized acid. The results of three coulometric experiments on two kinds of zirconia electrodes are given in Table 5 and show an average current efficiency of only 34.2%. This places doubt on utilizing the mobility of oxide ions as the mechanism of the zirconia pH response.

Table 6 summarizes some general conclusions from this study of zirconia pH electrodes at 95°C, and makes a comparison to typical commercially available glass electrodes. The Nernst slopes varied from 75 to 145% with the suspicion that the values above 100% obtained in alkaline solution were not valid because of the inherent sodium-ion error of the glass electrode. In standard buffers, the Nernst slope was in the 70—80% range. Tsuruta and Macdonald [6] had observed an "acid error". Glass electrodes, when evaluated with care, are found to have slopes of 100 ± 0.5% [11].

The resistance of zirconia electrodes ranged around 300 MΩ at 95°C. Although greater than glass electrodes at the same temperature, this resistance is comparable to that of glass electrodes at room temperature and therefore

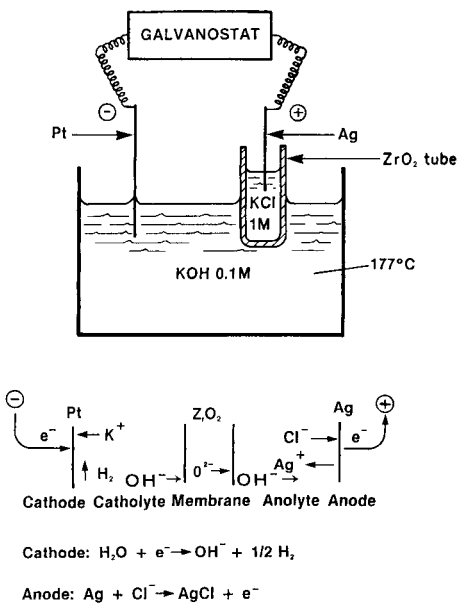

Fig. 2. Coulometric experiment for "pumping" hydroxide ion into the internal compartment of a zirconia pH sensor.

TABLE 5

Coulometric generation of hydroxide ion with ZrO_2 electrode at 177° C

Electrode	Current (μA)	Time (h)	Titrated volume of 0.001 M HCl	Efficiency (%)
Zircoa	100	24.5	35.70	39.1
Viking	75	17.5	14.25	29.1
Viking	71.6	18.0	16.55	34.4
			Av.	34.2

TABLE 6

Comparison of ZrO_2 electrodes with glass electrodes at 95° C

	ZrO_2	Glass
Nernst slope (%)	75—120	100.0 ± 0.5
Resistance (MΩ)	300	0.5—5
Asymmetry potential (mV)	25—50	<5
Time of response (s)	<30	<30
Reproducibility (mV)	10—30	1—5

well within the measurement capability of the modern pH meter. The asymmetry potential of the zirconia electrodes ranges from 25 to 50 mV and appears large compared to glass electrodes. This may be attributed to differences between the inner and outer surfaces of the zirconia, a "strain" existing between these two surfaces or some other unknown physical or chemical property of the zirconia.

The rapid 30-s time of response of the zirconia electrode appears to be equivalent to that of the glass electrode.

The zirconia electrodes used were remarkably inert in hot acidic and alkaline solutions. No evidence of attack or diffusion through the zirconia surfaces was evident even in experiments ranging over 200° C with corresponding pressure.

Other workers, performing a similar evaluation of zirconia electrodes, but using different cell construction and specially formulated zirconia electrodes, obtained apparently better results than those reported in the present paper. The quantitative results reported here with a variety of commercially available and high-purity zirconia tubes and with proven electrochemical cell construction would indicate that caution is necessary in accepting zirconia electrodes as equivalent in accuracy and reliability to glass electrodes.

The experimental assistance of W. Vallett is gratefully acknowledged. This paper was presented at the International Chemical Congress of Pacific Basin Societies, Honolulu, Hawaii, December 1984.

REFERENCES

1 L. W. Niedrach, Science, 207 (1980) 1200; J. Electrochem. Soc., 127 (1980) 2122; 129 (1982) 1445.
2 L. W. Niedrach, Anal. Chem., 55 (1983) 2426.
3 L. W. Niedrach, U.S. Patent 4,264,424, May 1981.
4 L. W. Niedrach and W. H. Stoddard, J. Electrochem. Soc., 131 (1984) 1017.
5 L. W. Niedrach and W. H. Stoddard, Paper presented at the 85th Annual Meeting of the American Ceramic Society, Chicago, IL, April 1983; Final Report-Task III and Year-End Summary, Pacific Northwest Laboratory, Battelle Memorial Institute (Division of Geothermal Energy, Report No. PNL 4651, February 1983); Final Report-Task I, Pacific Northwest Laboratory, Battelle Memorial Institute (Division of Geothermal Energy, Report No. PNL 3857 UC-66, March 1981).
6 T. Tsuruta and D. D. Macdonald, J. Electrochem. Soc., 129 (1982) 1221.
7 D. D. Macdonald, U.S. Patent 4,406,766, September 27, 1983.
8 S. Hettiarachchi and D. D. Macdonald, J. Electrochem. Soc., 131 (1984) 2206.
9 M. J. Danielson and O. H. Koski, J. Electrochem. Soc., (1985) 296.
10 M. J. Danielson, Corrosion, 35 (1979) 200; 39 (1983) 202.
11 T. S. Light and K. S. Fletcher, Anal. Chem., 39 (1967) 70.
12 R. G. Bates, Determination of pH, Theory and Practice, 2nd edn., Wiley, New York, 1973, p. 73.
13 A. J. deBethune, T. S. Light and N. Swendeman, J. Electrochem. Soc., 106 (1959) 616.
14 J. Fouletier, Sensors and Actuators, 3 (1982/83) 295.
15 R. A. Durst and J. W. Ross, Anal. Chem., (1968) 1343.

Analytica Chimica Acta, 175 (1985) 127—134
Elsevier Science Publishers B.V., Amsterdam — Printed in The Netherlands

DETERMINATION OF BORON AT LOW ABUNDANCE LEVELS IN GEOLOGICAL MATERIALS WITH A TETRAFLUOROBORATE-SELECTIVE ELECTRODE

FRIEDRICH KLUGER and CHRISTIAN KOEBERL*

Institute for Analytical Chemistry, University of Vienna, P.O. Box 73 A-1094 Vienna (Austria)

(Received 17th July 1984)

SUMMARY

A modified procedure based on the tetrafluoroborate-selective electrode is presented for the determination of low amounts of boron in geological materials. The main modifications are the use of hexamethylenetetramine as the buffer solution and a reduction of the temperature during measurement to 1—2°C to prevent hydrolysis; the latter precludes application of the usual method to solutions with low boron levels at very high total ionic strength. Satisfactory results can be obtained in the 10—200 $\mu g\ g^{-1}$ range (by using up to 250 mg of sample) without much sample handling. The method was tested for the analysis of terrestrial rhyolites (from Lipari/Italy, and Iceland) and tektites (thailandite, and Muong Nong-type tektites).

Data available for boron in geological materials are relatively sparse, largely because precise, fast determinations of boron in such materials pose many problems, particularly in the sample preparation step. Contamination or loss of boron is one of the main problems. A classical method for the determination of boron in rocks and minerals was used by Harder [1, 2], to assess the importance of boron in the geochemical cycle. For this purpose, Harder carefully analyzed a large collection of different rocks. He used emission spectrography based on the boron lines at 249.68 and 249.78 nm, which were examined photographically.

More recently, neutron activation analysis has been applied. Furst et al. [3] and Weller et al. [4] used the $^{10}B\ (n, \alpha)\ ^{7}Li$ reaction with subsequent particle track counting. Weller et al. [4] also developed a rather tedious and complicated method based on the reaction $^{11}B\ (d, p)\ ^{12}B$ which involved sample bombardment with a deuteron beam and measurement of the β-decay of boron-12. Another activation method involving β-counting of 20.4-ms boron-12 takes advantage of rapid instrumental neutron activation analysis for geological samples [5]; the sample is irradiated in the reactor core and transferred to the measuring chamber by means of a very fast pneumatic transportation system (10—15 ms transfer time). Another non-destructive technique which yields good results for boron, but also requires expensive instrumentation is the prompt-gamma neutron activation technique [6—10].

0003-2670/85/$03.30

Various methods require destruction of the samples; spectrophotometry [11—14], ion chromatography [15], and flame emission [16] or absorption [17] spectrometry have been applied. These methods are far from ideal. The most promising technique seems to be inductively-coupled plasma atomic emission spectrometry, which provides very good sensitivity [18, 19], but sample preparation requires great care to avoid loss of boron or contamination.

The potentiometric determination of boron with a tetrafluoroborate-selective electrode was first reported by Carlson and Paul [20]. Most applications of this rapid, simple method have dealt with the determination of relatively high amounts of boron, e.g., in borosilicate glasses [21], silicon [22], or aluminium oxide/boron carbide matrices [23]. Very often, these procedures are restricted to high amounts of boron in the samples; the sensitivity of the electrode in these matrices is not good enough for trace measurements. Some of the problems that limit the usage of this method for low concentrations have been discussed [22, 24]. The approach described here avoids most of these problems and leads to a considerable improvement in the limit of detection of the method.

EXPERIMENTAL

Equipment and reagents

An Orion model 93-05 tetrafluoroborate-selective electrode and a double-junction reference electrode (Orion model 92-02) with a 0.06 M ammonium sulfate bridge were used. Potentials were recorded on an Orion 701A mV/pH meter. Polypropylene pipets and volumetric flasks were used throughout; reagent solutions were stored in polyethylene bottles. For potential measurements, solutions were stirred magnetically with a teflon-coated bar in a 50-ml polyethylene cup.

Deionized water was used throughout. Chemicals were of analytical-reagent grade.

Stock solutions (10^{-4} M, 2×10^{-3} M, and 0.04 M tetrafluoroborate, containing 0.6 M hydrofluoric acid in excess) were prepared by mixing boric acid and hydrofluoric acid (22 M) in appropriate amounts and diluting with water. A solution of hexamethylenetetramine, saturated at room temperature (20°C), was used for sample solutions containing $>2 \times 10^{-4}$ M tetrafluoroborate. For solutions containing $<2 \times 10^{-4}$ M tetrafluoroborate, the solution of hexamethylenetetramine was saturated at 4°C.

Preliminary studies

Hydrofluoric acid is useful both for the dissolution of silicates and for conversion of boron to tetrafluoroborate without introduction of other anions. It has been noted [13] that hexafluorosilicate does not seem to interfere. It is shown below that excess of fluoride does not affect the procedure recommended here.

Hexamethylenetetramine was found to be superior to all other buffer solutions proposed to date, and was also suitable for neutralizing the excess of hydrofluoric acid. Another advantage is that hexafluorosilicate is hydrolyzed. Hexamethylenetetramine provides a buffering effect and serves to adjust the ionic strength of the final solutions. At low concentrations of tetrafluoroborate, the hydrolytic reaction

$$BF_4^- + H_2O \rightleftharpoons BF_3OH^- + HF \quad (1)$$

causes irreproducible measurements under the usual conditions. The hydrogen ion concentration affects the dissociation of hydrofluoric acid, and thus the hydrolysis constant: $K' = [BF_3OH^-]c_{HF}/[BF_4^-]$. If only one hydrolysis step (Eqn. 1) is considered, the hydrolysis constant can be written to incorporate the effect of pH:

$$K = \{[BF_3OH^-][H^+]c_{HF}/([H^+] + K_{HF})\}/[BF_4^-] \quad (2)$$

where c_{HF} is the total concentration of hydrofluoric acid produced by hydrolysis, and K_{HF} is the acidity constant for hydrofluoric acid.

If the concentration of tetrafluoroborate exceeds 2×10^{-4} M, no hydrolytic reaction occurs during 15 min at room temperature [22]. Furthermore, solutions of tetrafluoroborates in pure water are stable at even lower concentrations. However, the picture changes completely when the solutions are of high ionic strength. It was found here that at low tetrafluoroborate concentrations and high ionic strength of the sample solutions, hydrolysis prevents measurements under the standard conditions recommended in the literature (e.g., Lanza and Buldini [22]). Some tests showed that cooling the solutions during the measurement (and also during the preparation of the solutions) effectively prevents hydrolysis of tetrafluoroborate in hexamethylenetetramine solutions. A temperature of 1—2°C yields the best results without excessive retardation of the electrode response time. With these two main improvements the linear behaviour of the electrode in such solutions can be extended by about two orders of magnitude to lower concentrations.

The influence of cations on the dissociation behaviour of tetrafluoroborate was checked by spiking synthetic glass sample solutions with borate. Alkali metal, alkaline earth and rare-earth elements, as well as Mn, Al, Fe, Ti, Zr, and Pb, had no effect on the complete recovery of the spiked amounts (up to 10% B_2O_3 by weight).

Tourmaline and some calcium borosilicates like danburite and homilite are decomposed quantitatively with hydrofluoric acid only at elevated temperatures and pressures. In the present work, results are presented for samples treated with hydrofluoric acid at room temperature (see below), a preparation technique that is restricted to natural and synthetic glasses. However, some preliminary experiments showed that the proposed method can also be applied to a wide range of other rocks and minerals after pyrohydrolytic separation. This sometimes yields even better results than the decomposition in closed systems [25].

Procedure

Place an accurately weighed powdered sample (up to 250 mg) in a 25-ml volumetric flask, suspend the powder in 1 ml of water, add 3 ml of 22 M hydrofluoric acid and stopper the flask. After 10 min, shake gently and allow to stand overnight. Prepare two flasks as blanks, using water and hydrofluoric acid only.

When concentrations less than 200 $\mu g\ g^{-1}$ boron are expected, as is the case for most natural glasses and sedimentary rocks, use precooled (ca. 4°C) solutions and an ice bath for the following procedures. Place the volumetric flask in the thermostatted (ice) bath, add 20 ml of the appropriate hexamethylenetetramine solution (see above) and adjust the volume to 25 ml with water. Shake and transfer the content of the flask to a polyethylene cup.

For potential measurements, the following procedure is recommended. Mix 10 ml of hexamethylenetetramine solution at room temperature with 10 ml of water, add 3 ml of 22 M hydrofluoric acid and 1 ml of 2×10^{-3} M tetrafluoroborate stock solution. Stir in the thermostatted bath (adding ice if necessary) and allow the electrodes to equilibrate to the temperature for about 1 h. Then prepare one of the blanks, insert the electrodes in this solution, and wait for the potential to stabilize (usually 30 min). For construction of the calibration curve, add successively 50, 50, 100, 250, and 500 μl of 10^{-4} M stock solution, followed by 50, 100, 250 and 500 μl 2×10^{-3} M stock solution. Next insert the electrodes in the second blank (without any spiking) and wait again for a stable reading. Exchange the blank, which is set aside in an ice bath, for a sample solution (prepared depending on the concentration; at low concentrations the solution is stored at 4°C) and read the potential after 5 min. Before inserting another sample solution, allow the electrode reading to equilibrate in the second blank. With large amounts of sample, it was sometimes necessary to do standard additions, and in cases of nonlinear behaviour the resulting second-order curve had to be evaluated.

Samples with boron concentrations of more than 200 $\mu g\ g^{-1}$ (in the sample) are treated at room temperature, and only one blank solution is necessary for construction of the calibration graph. Prepare this solution by adding 10 ml of water to 10 ml of the saturated hexamethylenetetramine solution and adjusting the volume with water. The calibration graph is prepared and measurements are made as described above.

The results were found to be reproducible to better than 10% (relative standard deviation) for samples with 10—100 $\mu g\ g^{-1}$ boron and better than 5% for materials containing more than 100 $\mu g\ g^{-1}$ boron. Measurements had to be made away from direct sunlight and with the ambient temperature kept stable within ±1°C.

RESULTS AND DISCUSSION

Volcanic glasses

Three obsidian samples and two samples of pumice were available from Lipari (Italy). They and two obsidian samples from Iceland were analyzed. The results are presented in Table 1. Notes on the petrology, geology and main- and minor/trace element chemistry of these samples have been published [26, 27].

With the exception of the vesicular obsidian, which is discussed below, the mean boron content of the rhyolitic samples from Lipari was 210 ± 21 $\mu g\ g^{-1}$, in close agreement with the value of 193 $\mu g\ g^{-1}$ given by Taddeucci [28] for an obsidian sample from Lipari (unfortunately, the source of the sample was not described). Harder [1] gave 143 $\mu g\ g^{-1}$ boron for an obsidian sample from Lipari, which was also from an unspecified location. For the "Rouche Rosse" obsidian, Harder [1] gave 60 $\mu g\ g^{-1}$, but again direct comparison is impossible, because the present samples were from the "Forgia Vecchia", whereas the pumice samples were collected from "Capo Bianco" and "Acquacalda", respectively. The higher boron content of the vesicular obsidian Li-36A compared to samples Li-36 and Li-36B, seems to indicate trapped volcanic gases. As these gases can contain hydrogen fluoride and boron compounds, an enrichment of boron should be accompanied by a similar enrichment in fluorine, and this is exactly what was found earlier [26]. The thermal outgassing during the evolution of the pumices did not reduce the concentrations of fluorine or boron noticeably.

Data for the Icelandic samples are rare. Harder [1] tabulated a liparite-obsidian sample from Öraefajökull (ca. 7 $\mu g\ g^{-1}$ boron) and one obsidian from Hrafntinuh-Ryggur (ca. 6 $\mu g\ g^{-1}$ boron). Because the acidic rocks of Iceland are formed by local partial remelting of less siliceous precursors (Tholeiites and basalts [29]) and partial or complete remelting of xenoliths [30], samples from different locations are not comparable. It would have been interesting to find out whether or not other granitophilic elements

TABLE 1

Boron contents found for pumice and obsidian samples from Lipari (Italy)[a] and Landmannalaugar (Iceland)[b]

Sample	Boron content ($\mu g\ g^{-1}$)	Sample	Boron content ($\mu g\ g^{-1}$)
Li-24 (pumice)	218	Li-36B (black obsidian)	234
Li-33 (pumice)	203	Obsidian 4 (black)[b]	14
Li-36 (red obsidian)	185	Obsidian 5 (black)[b]	12
Li-36A (red obsidian)[c]	297		

[a]For detailed descriptions of these samples, see Kiesl et al. [26]. [b]For detailed descriptions of these samples, see Klein et al. [27]. [c]With 35% (by volume) irregular vesicles.

correlate with the present result of a doubled boron content or not, but no chemical analysis was reported by Harder [1].

Tektites

There has been much controversy about the origin of tektites [31]; any new data could be useful. A very interesting subgroup are the Muong Nong-type tektites, which belong to the Australasian tektite stream field and are different from normal (splash-form) tektites in respect of their petrology and chemistry. The enrichment in volatile elements is significant [32, 33]. The samples analyzed in the course of this work were also included in a multi-element evaluation program, designed to cover about 50 volatile and non-volatile elements [33—36].

The results for 19 Muong Nong-type tektites and for one thailandite (also from the Australasian strewn field, but a splash-form tektite) are given in Table 2. A full discussion will be published elsewhere; what follows is only a brief discussion of these results. Analysis of 41 samples from the Australasian strewn field (splash-form tektites) [37] yielded an average of 27.2 ± 10.5 $\mu g\ g^{-1}$ boron. The present data for the Muong Nong tektite samples from the Australasian strewn field gave an average of 47.7 ± 17.7 $\mu g\ g^{-1}$ boron. The only trace element data sets for Muong Nong tektites that are available for comparison are seven analyses reported by Chapman and Scheiber [38]. They were among the first to note the enrichment of some elements, including boron, therefore they designated this group as HCu,B-indochinites (high copper-boron). Their analyses yielded an average of 55.3 ± 14.9 $\mu g\ g^{-1}$ boron. The present data clearly support the results of Chapman and Scheiber [38].

Taylor and Kaye [37] and Chapman and Scheiber [38] have discussed the finding that usually there is no loss of boron in the impact production pro-

TABLE 2

Boron contents found for 19 Muong Nong tektite samples (MN8301—MN8319) and a thailandite sample (T8203)

Sample no.	Boron content[a] ($\mu g\ g^{-1}$)	Sample no.	Boron content[a] ($\mu g\ g^{-1}$)	Sample no.	Boron content[a] ($\mu g\ g^{-1}$)
MN8301	44.3[b]	MN8308	30.8	MN8315	65.5
MN8302	30.8	MN8309	50.6	MN8316	41.2
MN8303	30.5	MN8310	77.5	MN8317	48.3
MN8304	31.7	MN8311	88.2	MN8318	48.8
MN8305	31.2	MN8312	60.9	MN8319	37.0
MN8306	40.4	MN8313	71.0	T8203	<12[c]
MN8307	27.6	MN8314	51.7		

[a]Averages of at least two determinations. [b]A value of 41.2 $\mu g\ g^{-1}$ was found by inductively-coupled plasma spectrometry (Perkin-Elmer ICP-6000). [c]This value is not definitive because only 100 mg of sample was available. The result from i.c.p. spectrometry was 11.9 $\mu g\ g^{-1}$.

cess. This was inferred from Henbury crater materials, where the underlying rocks showed about the same boron abundances as the impact glasses. It has been noted, however, that there may be some process (like fractional vaporization in a near vacuum) which leads to a loss of boron. Such a mechanism must be sought to explain the differences between the volatile-rich Muong Nong tektites and the rest of the Australasian tektites. It is clear, however, that the boron abundances observed in tektites are not consistent with those in igneous rocks; Harder [1] gave an average of 10 $\mu g\ g^{-1}$ boron for igneous rocks and 85 $\mu g\ g^{-1}$ boron for sedimentary rocks [2]. As there is no known process for the enrichment of boron during tektite production, there seems to be no way to make tektites out of igneous rocks.

Conclusions

It is possible to extend the accessible concentration range to lower abundances of boron in geological materials by almost two orders of magnitude by using a modified technique with the tetrafluoroborate-selective electrode. The powdered samples were treated with hydrofluoric acid only (thus minimizing any contamination or loss during sample preparation), thus the resulting solutions were of very high ionic strength. Previously described procedures for measurement failed to give reproducible results for such solutions, mainly because of insufficient buffering and hydrolytic reactions. The introduction of a special buffer solution (hexamethylenetetramine) and temperature reduction to about 1—2°C effectively prevents hydrolysis and therefore allow measurements at tetrafluoroborate concentrations at the 10^{-5} M level in solutions of high ionic strength. Two different geochemical problems (the analysis of terrestrial natural glasses: obsidians and tektites) are used to demonstrate that precise and fast results are obtainable in the 10—200 $\mu g\ g^{-1}$ region.

We thank W. Kiesl for comments on the manuscript.

REFERENCES

1 H. Harder, Nachr. Akad. Wiss. Göttingen, Math. Phys. Kl., 5 (1959) 67.
2 H. Harder, Nachr. Akad. Wiss. Göttingen, Math. Phys. Kl., 5 (1959) 123.
3 M. Furst, H. A. Lowenstam and D. S. Burnett, Geochim. Cosmochim. Acta, 40 (1976) 1381.
4 M. R. Weller, M. Furst, T. A. Tombrello and D. S. Burnett, Geochim. Cosmochim. Acta, 42 (1978) 999.
5 C. Koeberl and F. Grass, Meteoritics, 18 (1983) 325.
6 E. S. Gladney, E. T. Jurney and D. B. Curtis, Anal. Chem., 48 (1976) 2139.
7 D. B. Curtis, E. S. Gladney and E. T. Jurney, Geochim. Cosmochim. Acta, 44 (1980) 1945.
8 M. D. Higgins, Geostandards Newsl., 8 (1984) 31.
9 M. D. Higgins and D. M. Shaw, Nature, 308 (1984) 172.
10 M. D. Higgins, M. G. Truscott, D. M. Shaw, M. Bergeron, G. H. Buffet, J. R. D. Copley and W. V. Prestwick, Proc. Int. Symp. on Use and Development of Low and Medium Flux Research Reactors, 1984, preprint.
11 J. W. Mair and H. G. Day, Anal. Chem., 44 (1972) 2015.

12 M. R. Hayes and J. Metcalf, Analyst, 87 (1962) 956.
13 P. Lanza and P. L. Buldini, Anal. Chim. Acta, 70 (1974) 341.
14 H. K. L. Gupta and D. F. Boltz, Anal. Lett., 4 (1971) 161.
15 C. J. Hill and R. P. Lash, Anal. Chem., 52 (1980) 24.
16 E. J. Agazzi, Anal. Chem., 39 (1967) 233.
17 W. W. Harrison and N. J. Prakash, Anal. Chim. Acta, 49 (1970) 151.
18 B. Welz, Chemie-Technik, 4 (1980) 161.
19 J. W. Owens, E. S. Gladney and D. Knaf, Anal. Chim. Acta, 135 (1982) 169.
20 R. M. Carlson and J. L. Paul, Anal. Chem., 40 (1968) 1292.
21 R. L. Kochen, Anal. Chim. Acta, 75 (1974) 451.
22 P. Lanza and P. L. Buldini, Anal. Chim. Acta, 75 (1975) 149.
23 H. E. Wilde, Anal. Chem., 45 (1973) 1526.
24 J. Gulens and P. K. Leeson, Anal. Chem., 52 (1980) 2235.
25 H. Uchida, T. Uchida and C. Iida, Anal. Chim. Acta, 116 (1980) 433.
26 W. Kiesl, F. Kluger, H. H. Weinke, H. Scholl and P. Klein, Chem. Erde, 37 (1978) 40.
27 P. Klein, F. Kluger and H. Wieseneder, Tschermaks Mineral. Petrogr. Mitt., 26 (1979) 1.
28 A. Taddeucci, Period. Mineral., 33 (1964) 73.
29 R. K. O'Nions and K. Grönveld, Earth Plan. Sci. Lett., 19 (1973) 397.
30 U. Sigurdsson, Geol. Mag., 105 (1968) 440.
31 J. A. O'Keefe, Tektites and their Origin, Elsevier, Amsterdam, 1976.
32 O. Müller and W. Gentner, Meteoritics, 8 (1973) 414.
33 C. Koeberl, F. Kluger, W. Kiesl and H. H. Weinke, Lunar Plan. Sci., 15 (1984) 445.
34 C. Koeberl, R. Berner and F. Kluger, Lunar Plan. Sci., 15 (1984) 441.
35 C. Koeberl, F. Kluger, R. Berner and W. Kiesl, Lunar Plan. Sci., 15 (1984) 443.
36 C. Koeberl, F. Kluger and W. Kiesl, Proc. Lunar Plan. Sci. Conf. 15 (J. Geophys. Res. Suppl., 89 (1984) C351).
37 S. R. Taylor and M. Kaye, Geochim. Cosmochim. Acta, 33 (1969) 1083.
38 D. R. Chapman and L. C. Scheiber, J. Geophys. Res., 74 (1969) 6737.

Analytica Chimica Acta, 175 (1985) 135—145
Elsevier Science Publishers B.V., Amsterdam — Printed in The Netherlands

FLOW CHARACTERISTICS IN A SEGMENTED CLOSED-TUBE DESIGN FOR ION-MOBILITY SPECTROMETRY

G. A. EICEMAN, C. S. LEASURE and V. J. VANDIVER

Department of Chemistry, New Mexico State University, Las Cruces, NM 88003 (U.S.A.)

G. RICO

Department of Electrical Engineering, New Mexico State University, Las Cruces, NM 88003 (U.S.A.)

(Received 19th December 1984)

SUMMARY

Closed-tube design with unidirectional flow of drift gas in ion-mobility spectrometry (i.m.s.) was found to provide residence times for analyte from 10 s to 10 min based on drift gas flow rate. The volume of drift gas necessary to restore reactant ions completely to the original intensity, after addition of excess (>900 mg l^{-1}) of analyte to the ion source, was three times the inner volume of the tube, regardless of flow rate. Contamination of the i.m.s. tube from analyte in the external atmosphere occurred readily in the open-tube design and in the closed-tube design with or without a slight vacuum attached to the tube. Rates of migration of analyte from outside to inside the tube were similar in all designs and the present closed-tube design was largely non-resistant to external contamination. Product-ion intensities for aromatic and polynuclear aromatic hydrocarbons were independent of drift flow rate from 100 to 800 ml min^{-1} in the closed-tube design with no formation of artifacts. Plots of ion intensity vs. concentration of *o*-xylene were linear in two ranges, 0.05—0.08 $\mu g\ l^{-1}$ and 0.1—2 $\mu g\ l^{-1}$, with slopes of 1.2×10^{-9} A l μg^{-1} in the first range and 1.0×10^{-11} A l μg^{-1} in the second range. No changes in mobility of aromatic product-ion peaks were seen with increases in concentration when the analyte was added to the drift gas rather than near the reaction region in unidirectional flow.

Ion-mobility spectrometry (i.m.s.) is a technique for separation and detection of organic compounds as gaseous ions at atmospheric pressure [1]. Reactant ions are formed through β-emission into air or nitrogen and the analyte is converted to product ions through ion-molecule reactions with reactant ions. Product ions are separated in a voltage gradient and against an inert drift gas with flow which is in the opposite direction to product ions. Because processes involved in the operation of i.m.s. are based on separation and formation of product ions through gentle ionization with limited fragmentation, i.m.s. was originally referred to as plasma chromatography [2]. Development of i.m.s. for use as a chemical sensor of toxic organic compounds in atmospheric samples has been attractive because of its features of ultra-high sensitivity, convenient operation at atmospheric pressure and relative simplicity. Moreover, ion-mobility spectrometry is sensitive to com-

0003-2670/85/$03.30

pounds with various functional groups and limits of detection can be as low as 0.1 $\mu g\,l^{-1}$ without sample pretreatment or pre-enrichment [3—6]. A partial listing of compounds detected by using i.m.s. includes drugs [7], explosives [8], plastics [9], pesticides [10], environmental pollutants [11], biomedical compounds [12], and volatile inorganic compounds [13]. Also, i.m.s. has been used as a preseparator for mass spectrometry (m.s.) in i.m.s./m.s. instrumentation [14] and has been used successfully as a tunable gas chromatography (g.c.) detector with high-resolution capillary columns [15]. Recently, attention has been directed toward development of alternative ionization sources [16—18] and selective chemical reactions in the ion source for additional selectivity [19].

Notwithstanding over 100 publications on the response, sensitivity and performance of i.m.s. during the 1970s, physical designs of drift tubes have not been greatly altered since inception of i.m.s. However, since 1980, tube construction has been modified, with a variable-parameter plasma chromatograph [16], a closed-tube i.m.s. design [20], and a continuous-tube design [21]. Similarities exist amongst all these tubes inasmuch as ion source, reaction region, drift region and detector plate were used in every design. In the commercially designed i.m.s., drift rings were separated by insulating beads, retained by using compression, and placed in a large cylindrical housing with estimated volume of 2 l. In the Karasek design, rings were positioned and supported in a slotted ceramic rail and external volume was near 2.5 l. Two major disadvantages generally associated with i.m.s. have been limited resolution of mixtures [22] and unreliable response caused by overloading the ion source [23]. This last feature has been associated with longevity of analyte in the instrument, leading sometimes to severe memory effects and even failure because of the high sensitivity of i.m.s. In a major change in i.m.s. design in 1980, Baim and Hill [20] built and operated a closed-tube i.m.s. as a tunable g.c. detector. In this system, residence times of product ions in the source were reported to be as low as 1 ms and problems of contamination associated with open-tube designs were reduced. While this design had promise to reduce the second problem cited above, emphasis was placed on its use as a fast g.c. detector with less attention given to the characteristics of closed-tube designs as chemical sensors or for separations. The aim of the present study was to evaluate properties and effects of flow in a closed-tube design with attention toward possible use in chemically hostile environments, particularly where external contaminants are at high concentrations.

EXPERIMENTAL

Instrumentation

The closed-tube i.m.s. shown in Fig. 1 was constructed here by using stainless steel drift rings and Macor (Corning Glass Co.) insulators. The dimensions of the rings were 3-cm inner diameter, 7-cm outer diameter and 0.5 cm width; the inner diameter of the reaction ring was 1 cm. The activity of the

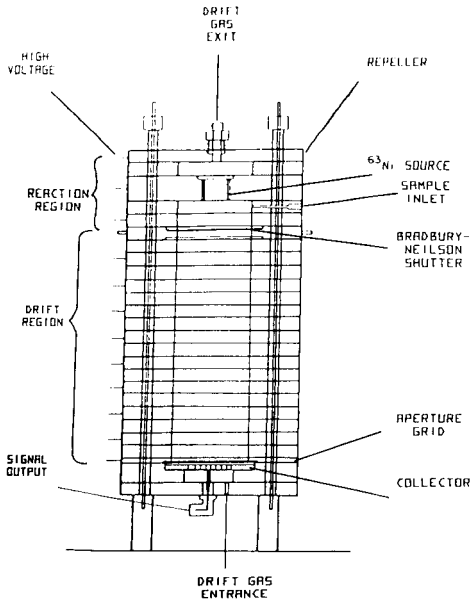

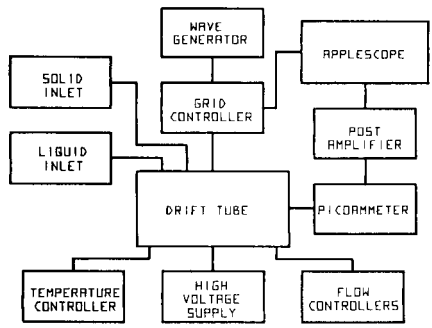

Fig. 1. Closed-tube design for the ion-mobility spectrometer.

Fig. 2. Block diagram for components in the ion-mobility spectrometer.

β-source was 11.7 mCi of nickel-63 (New England Nuclear, Boston, MA) electroplated on nickel foil which was placed on the inside of a Pyrex glass sleeve and fitted into the reactor ring. An aperture grid was placed 2 mm from the detector and was fabricated from 80-mesh stainless steel spot welded to a drift ring. A shield ring with BNC connector was used to shield the detector electrically from external noise. Contact between the BNC and detector plate was through a copper wire spring. Nitrogen (99.5% purity) was passed through 13X molecular sieves (Alltech, Deerfield, IL) and was used for both drift and carrier gases. The i.m.s. was placed in the oven (22 cm × 23 cm × 25 cm) of a Hewlett-Packard model 5721 gas chromatograph. No modifications were made to the oven, except for placing power, signal and gas flow lines through the oven wall into the i.m.s.

Signals were amplified by a Keithley Model 427 picoammeter with additional variable amplification of 10^3 using a high-speed operational amplifier. Signals were processed through digital signal averaging using an Apple IIe modified with Applescope (RC Electronics, Santa Barbara, CA). Applescope is a commercially available package of hardware and software for collection and averaging of repetitive signals [24]. Generally, 500 scans were acquired per spectrum. The Apple IIe was also equipped with dual disk drives and an Epson model FX100 printer. The high-voltage supply was a Gamma High Voltage model RR 10-6R (Mount Vernon, NY). Gas flows were controlled by using Nupro fine metering valves. The inlet design was based on contin-

uous leak into the i.m.s. of vapors from the headspace of pure solid or of pure liquid analyte. A schematic diagram of the total system used in these studies is shown in Fig. 2.

Procedures

Residence time study. Large amounts of analyte were delivered rapidly from a micro-liter syringe through the repeller to the ion source of the i.m.s. tube, with no drift gas flow. Then, drift gas flow was started and spectra were collected every 30 s for 10 min. Because 0.1—0.5 mg of analyte was introduced into the system with total internal volume of 85 ml, initial concentrations were roughly between 1.2 and 5.9 mg l^{-1}. Compounds studied were benzene, toluene, *o*-xylene, and chlorobenzene, which were chosen for defined and regular decreases in vapor pressures. Drift gas flows of 20, 50, 75 and 100 ml min^{-1} were used in unidirectional flow fashion. Other conditions were: amplification, 1.0×10^{11} V A^{-1}; voltage on the tube from repeller to detector (at ground), 2500 V; tube length, 8.0 cm; and temperature, 210°C.

External contamination study. To assess external contamination in the closed-tube and open-tube designs, vapors of *o*-xylene were leaked into the oven chamber which was external to the i.m.s. tube. Spectra were acquired at intervals from 0 to 20 min. The tube was used in three physical configurations including the closed tube with unidirectional flow with drift gas at 300 ml min^{-1}, the open-tube design with each Macor ring replaced by three 5-mm thick glass spacers and with drift gas flow at 800 ml min^{-1} and carrier gas flow at 17 ml min^{-1} (the maximum flow on the inlet used here), and a closed-tube design with a vacuum pump attached to the repeller ring and drift gas lines opened to the ambient atmosphere. The amplification (V A^{-1}) in these studies was 1.0×10^{11} in the first and 5×10^{11} in the latter two. The oven temperature was kept at 210°C and the voltage applied to the tubes was 3000 V. The drift length of the closed tube was 9.0 cm and the drift length of the open tube was 9.0 cm. The flow of *o*-xylene continuously into the oven was estimated at 37.6 mg min^{-1} and the external (oven) volume was estimated as 1.5 l. Because clearance of analyte from the oven was believed to be low, the concentration of analyte was estimated from 20 mg l^{-1} in the first minute to over 400 mg l^{-1} at the finish.

Effects on ion intensity from gas flows. In the closed-tube design, the relative intensity of the three reactant ions was influenced by drift gas flow rate. Effects on intensity from the drift gas flow rate were then characterized for reactant ions and for product ions with aromatic compounds including benzene, toluene, naphthalene, and anthracene. The sample was introduced continuously as vapor from headspace over the pure compounds. The amount of compound added was between 0.11 and 0.31 mg min^{-1} and was controlled through the flow of nitrogen into the headspace of the vial at 25°C. Flow rates were stepped at 100 ml min^{-1} intervals from 100 to 800 ml min^{-1}. The concentrations of analyte in the i.m.s. at extremes of flow were estimated as 200 to 1600 mg l^{-1}. Amplification was different with each compound and

was in the range of 1.2×10^{11} to 2.0×10^{11} V A^{-1}. The voltage on the tube was 3000 V and the tube temperature was 210°C.

Analyte-doped drift gas. In contrast to past operation with all i.m.s. tubes, analyte was added here not near the reactor ring but rather through the collector as part of the drift gas. The analyte was introduced into the drift gas by sweeping vapor from the headspace of samples through a fused-silica capillary tube into a 2.5-mm Swagelok T-union which was coupled to the drift gas. Drift gas was added to the i.m.s. tube at the detector end of the tube with unidirectional flow at 300 ml min^{-1} toward the reactor ring as shown in Fig. 1. Analyte was metered into the carrier gas at a range of concentrations from just detectable to severely overloaded and spectra were collected at each concentration. Three compounds used here were *o*-xylene, naphthalene and pyrene, and limits of detection were calculated for this alternative flow scheme. Conditions of operation were: temperature, 210°C; tube voltage, 3000 V; drift length, 9.0 cm; and amplification, 1.0×10^{11} to 1.0×10^{12} V A^{-1}.

RESULTS AND DISCUSSION

The tube shown in Fig. 1 was based on an approach developed by Baim and Hill [20]. It was chosen here for simplicity, physical integrity, low memory effects and possible resistance to contamination external to the tube. Only two minor modifications were made in the original design: (1) fabrication of both insulator and drift rings with the same geometry and dimensions and (2) assembly of the tube with three internal support rods for compression and alignment of rings. These changes were not expected to influence the performance of the i.m.s. and were made for convenience of fabrication and assembly. Major advantages obtained with a closed-tube unidirectional flow design were the limited residence time for analyte and the brief time necessary for recovery after severe overloading of the tube. In Fig. 3, plots are shown for intensities of product ions and reactant ions vs. time as a function of drift flow after initial plug injection of 0.1—0.5 mg (900—4000 mg l^{-1}) of analyte at a location adjacent to the reactor ring (Fig. 1). The presence of analyte in the i.m.s. was measured by using the peak heights of product and reactant ions. With increasing time at every drift gas flow rate, this extreme concentration of analyte was reduced in a relatively short time of 2—10 min. As expected, with larger drift flow rates (curves A and B), the analyte was removed more quickly than at lower drift flows (curves C and D). No major trends in residence time as a function of molecular weight or vapor pressure were observed for these analytes. Because the internal volume of the closed-tube i.m.s. was 85 ml, the number of tube volumes necessary to restore the reactant ions to the original intensity was evaluated from the curves in Fig. 3. The number of tube volumes necessary completely to restore the i.m.s. to original operation for each drift gas flow was 2.7 at 100 ml min^{-1}, 3.1 at 75 ml min^{-1}, 3.2 at 50 ml min^{-1}, and 2.6 at

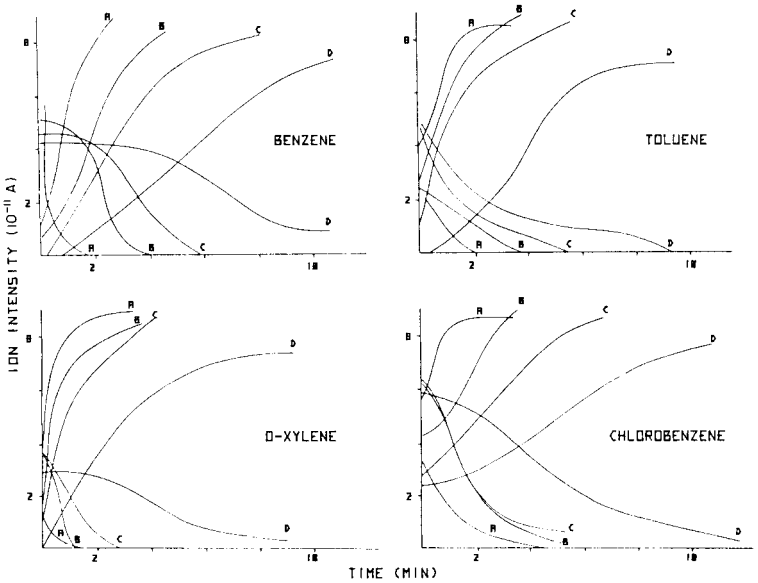

Fig. 3. Plots of ion intensity for reactant ions (positive slopes) and product ion (negative slopes) after introduction of analyte into the reaction region. Drift gas flow rate (ml min^{-1}): (A) 100; (B) 75; (C) 50; (D) 25.

20 ml min^{-1}, as averages for all compounds. When the drift gas flow rates were near the commonly used values of 200—300 ml min^{-1}, times of only 10—30 s were necessary for complete restoration. These times were near but slightly larger than those reported by Baim and Hill [20], but the concentrations here were also 10^3—10^5 greater than those used by Baim and Hill. Such results compared favorably with open-tube designs in which analyte at $\mu g\ l^{-1}$ concentration levels could be detected 100 min after initial injection [25]. Differences in tube volumes necessary to clear the analyte were considered insignificant and no spurious flow behavior was observed. In all further studies, drift flows were set to 300 ml min^{-1}. Clearance of analyte was detected in all the above studies not only in reduction of product-ion intensities for the analyte but also in restoration of the reactant-ion intensity which varied inversely with product-ion intensity as shown in Fig. 3. Thus, even under conditions of severe concentration overloading, the closed-tube design exhibited relatively slight memory effects. There was no evidence in peak shape or mobilities for chemical decomposition of residual analyte with residence times of 2—10 min.

In Fig. 4, intensities of product ions were plotted vs. time after the initial introduction of *o*-xylene into the external oven volume. Three configurations of the i.m.s. tube were used to evaluate the tube contamination from diffusion of contaminants from the external volume into the ion source or drift

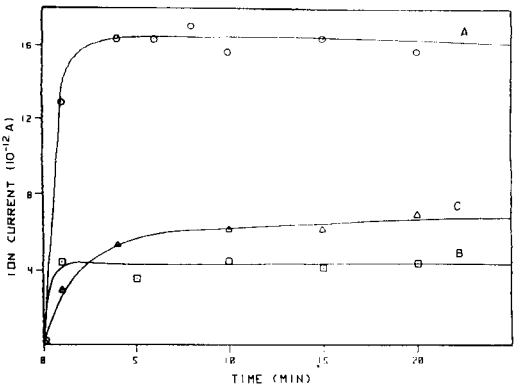

Fig. 4. Plot of product-ion current for *o*-xylene vs. time after initial release of analyte into the atmosphere external to the i.m.s. tube in three configurations: (A) open-tube with drift flow; (B) closed-tube with vacuum; (C) closed-tube with drift flow.

region. As shown in curve A (Fig. 4), *o*-xylene (shown in product ion intensity) diffused rapidly into the open-tube design and saturation was reached within 2 min. While a flow diagram for open-tube i.m.s. has been proposed [25], back-diffusion of unionized analyte from the external volume into the tube was not included in the model and has not been demonstrated previously. In curve B, application of a slight vacuum to the closed-tube design led to transport with saturation within 1 min. Ion currents in curve B were low because peak heights were used and the peaks for product ions were broad. With a slight vacuum, molecules diffused readily into the tube despite the closed-tube design, which should lead otherwise to restoration in back-diffusion. When the vacuum was removed and the closed-tube design was operated with unidirectional flow of drift gas at 300 ml min^{-1}, rapid diffusion of analyte from oven to i.m.s. tube was not expected. However, as shown in curve C, saturation occurred from diffusion through the insulator and drift rings within 5 min. While this diffusion (with slight positive pressure from drift gas flows) was slower than when the system was operated with a vacuum, the practical consequences were the same.

Thus, while residence times for the analyte in the flow region were short, the segmented closed-tube design was not effective in significantly reducing external contamination. In further development of closed-tube designs, gas-tight seals should be incorporated into the assembly of rings in order to eliminate such contamination. Moreover, in closed-tube designs, effluent should be vented externally to the tube housing or oven. A hermetically sealed tube should be developed, particularly when i.m.s. is to be used in chemically hostile environments. Spectra from this study are shown in Fig. 5 for reactant ions, product ions and reactant ions when *o*-xylene was introduced into the oven chamber and the product ions of *o*-xylene were introduced near the reactor ring. As seen in these spectra, performance of the total instrumentation was good with a peak width at half height for *o*-xylene of 0.3 ms.

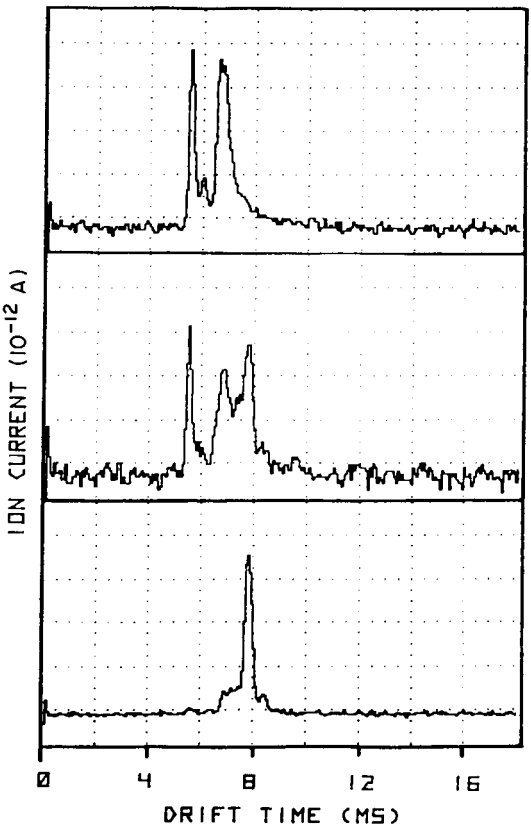

Fig. 5. Ion-mobility spectra for (A) reactant ions and (B) *o*-xylene (K_o = 2.03 cm^2 V^{-1} s^{-1}) in external atmospheres with closed-tube i.m.s.; (C) *o*-xylene with normal unidirectional flow of drift gas.

With the closed-tube design, increases in drift gas flow rate yielded changes in reactant-ion intensities. While the water of hydration in reactant ions may change as a function of partial pressures for water [26], the probability and extent of changes in reactant-ion composition were unknown and have never been reported for open-tube designs. More serious are possible changes in product-ion identities through changes in drift gas flow rates. Four aromatic and polynuclear aromatic compounds were selected for characterization at drift flows from extremes of high and low flow in attempts to detect any changes in product-ion identity. In Fig. 6, intensities for product ions are shown for benzene, toluene, naphthalene and anthracene at flows from 100 to 800 ml min^{-1} in the closed-tube design. No changes in mobility for product ions were seen in this range of flow, and peak broadening for the same product ions was not detected. However, the relative ion intensity was changed with different drift gas flow rates as shown in Fig. 6. Although the reduced mobilities were similar to literature values, ions were not identified by mass

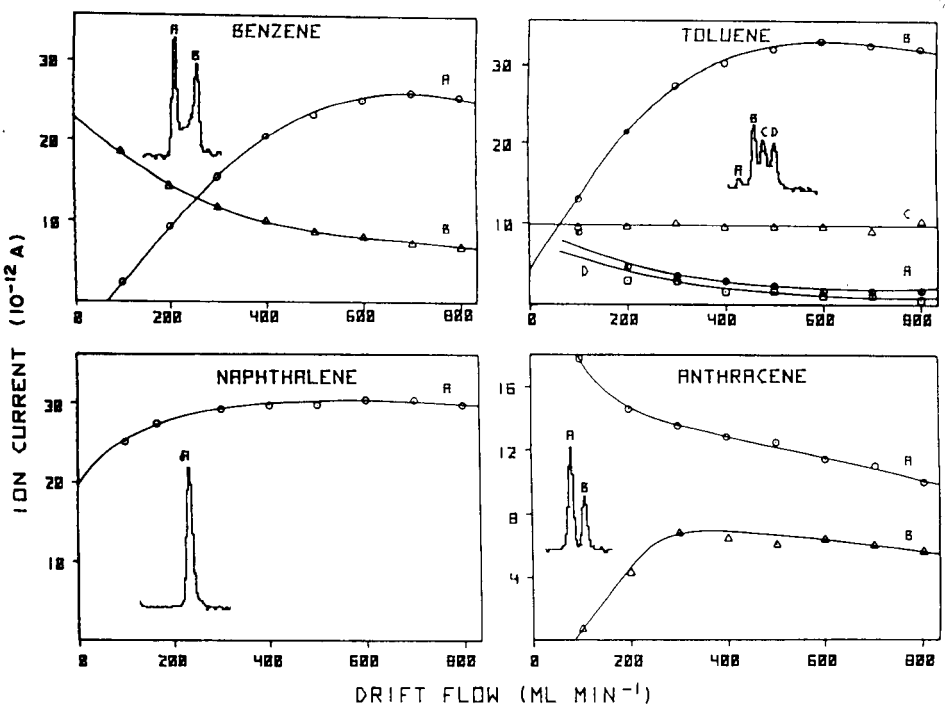

Fig. 6. Product-ion intensity drift gas flow for benzene, toluene, naphthalene and anthracene. Reduced mobilities (K_0 = cm^2 V^{-1} s^{-1}) were as follows: for benzene, (A) 2.52, (B) 2.05; for toluene, (A) 2.37, (B) 2.16, (C) 2.04, (D) 1.93; for naphthalene, (A) 1.89; for anthracene, (A) 1.65, (B) 1.56.

and possible mechanisms for this flow-related behavior would be entirely speculative.

An advantage of operation with unidirectional flow with closed-tube designs is the possibility for further simplification of flow connections. For example, introduction of sample with the drift gas near the detector plate could lead to elimination of inlet ring near the center of the tube. However, possible ion/molecule reactions in the drift region would be expected to interfere with formation of multiple-product ion peaks or broadened peaks. In Fig. 7, plots are shown for three aromatic and PAH compounds as product-ion current vs. concentration of the analyte in vapor introduced into the drift gas at the detector. All spectra at any concentration used here were normal and no evidence for changes in ion identity was found, as shown by spectra for *o*-xylene at several concentrations (Fig. 8). A pseudomolecular ion is shown at 0.05 μg l^{-1} in Fig. 8A and was unchanged up to 2 μg l^{-1} (Fig. 8D). Peak width at half height was 0.3 ms and was identical to the characteristics shown in Fig. 5. These results are consistent with those for all other aromatic compounds tested and offer support for alternative operation of i.m.s. in this new design. However, the presence of reactive moieties such

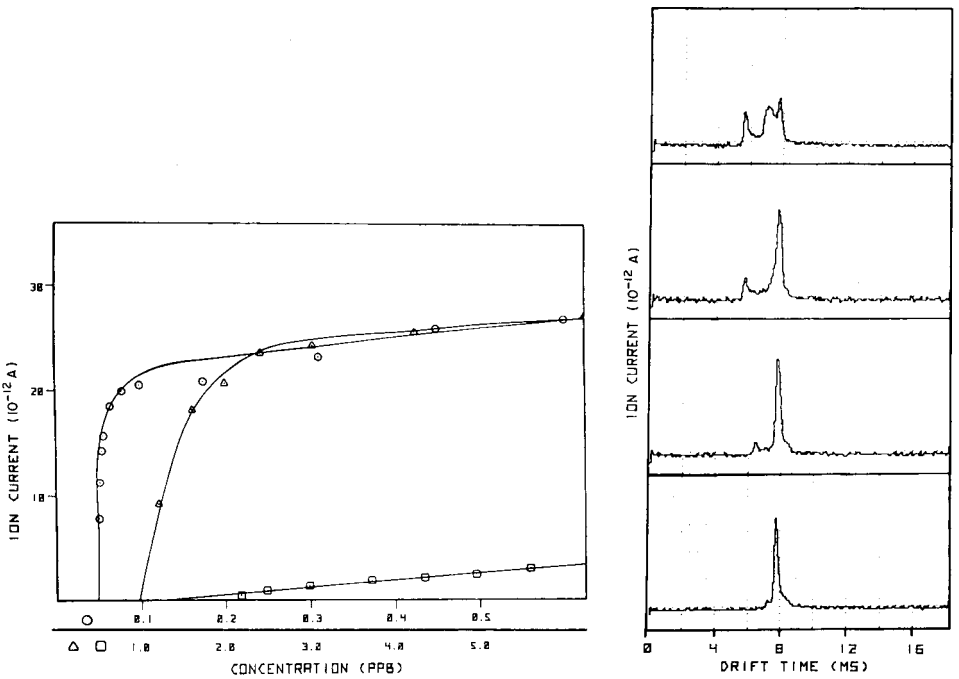

Fig. 7. Ion current for product ions vs. gaseous concentrations in drift gas in closed-tube i.m.s.: (A) *o*-xylene; (B) naphthalene; (C) pyrene.

Fig. 8. Spectra for *o*-xylene (K_0 = 2.03 $cm^2\ V^{-1}\ s^{-1}$) at different concentrations in the drift gas flow: (A) 0.05, (B) 0.20, (C) 0.45, (D) 2.0 $\mu g\ l^{-1}$.

as amines and carboxylic acids may preclude this flow design. Calibration plots for pure compounds were linear at low concentrations in the range 0.05—0.15 $\mu g\ l^{-1}$ for *o*-xylene and 1—1.5 $\mu g\ l^{-1}$ for naphthalene after which the intensity of available reactant ions was zero. At concentrations of 0.1—1.5 $\mu g\ l^{-1}$ for *o*-xylene and 2—5 $\mu g\ l^{-1}$ for naphthalene the plots were again linear. Slopes for *o*-xylene were 1.2×10^{-9} A l μg^{-1} for 0.05—0.08 $\mu g\ l^{-1}$ and 1.1×10^{-11} A l μg^{-1} for 0.1—2 $\mu g\ l^{-1}$. Slopes for naphthalene were 3.6×10^{-11} A^{-1} for 1.0—1.5 $\mu g\ l^{-1}$ and 1.0×10^{-12} A l μg^{-1} for 2—5 $\mu g\ l^{-1}$. At a concentration of 2 $\mu g\ l^{-1}$ (the maximum concentration possible for *o*-xylene with the inlet system used here), a decrease of <10% in product-ion intensity was seen. Causes for the break in the calibration plot are unknown but are evidence for a dual mechanism in ion formation. Results for pyrene were similar in that a linear plot with slope 1.7×10^{-12} A l μg^{-1} was obtained between 1 and 6 $\mu g\ l^{-1}$. However, a second linear region was not detected and no explanation for this behavior is available at present.

All parts of the ion mobility spectrometer were machined by J. Tobin who also participated in evaluation of designs. This work was supported through

grant No. DE-AS04-83ER60184 from the Department of Energy (project director, Dr. Gerald Goldstein).

REFERENCES

1 M. J. Cohen and F. W. Karasek, J. Chromatogr. Sci., 8 (1970) 330.
2 F. W. Karasek, Res. Dev., 21 (1970) 34.
3 F. W. Karasek and D. W. Denney, Anal. Chem., 46 (1974) 1312.
4 F. W. Karasek and O. S. Tatone, Anal. Chem., 44 (1972) 1758.
5 S. A. Benezra, J. Chromatogr. Sci., 14 (1976) 122.
6 F. W. Karasek, S. H. Kim and S. Rokushika, Anal. Chem., 50 (1978) 2013.
7 F. W. Karasek, D. W. Karasek and S. H. Kim, J. Chromatogr., 105 (1975) 345.
8 F. W. Karasek and D. W. Denney, J. Chromatogr., 92 (1974) 141.
9 T. W. Carr, Thin Solid Films, 45 (1977) 115.
10 H. A. Moye, J. Chromatogr. Sci., 13 (1975) 285.
11 F. W. Karasek, Anal. Chem., 43 (1971) 1982.
12 F. W. Karasek, H. H. Hill and S. H. Kim, J. Chromatogr., 117 (1976) 327.
13 W. M. Watson and C. F. Kohler, Environ. Sci. Technol., 13 (1979) 1243.
14 F. W. Karasek, M. J. Cohen and D. L. Carroll, J. Chromatogr. Sci., 9 (1971) 390.
15 M. A. Baim, F. J. Schuetze and H. H. Hill, Am. Lab., 14 (1982) 59.
16 F. W. Karasek and S. H. Kim, Study of Technology Relating to Plasma Chromatography Sensing Tubes, Final Report, DREV 85077-00227, 12/23 (1980) 32.
17 M. A. Baim and H. H. Hill, Anal. Chem., 55 (1983) 1761.
18 D. M. Lubman and M. N. Kronick, Anal. Chem., 54 (1982) 1546.
19 C. J. Proctor and J. F. J. Todd, Anal. Chem., 56 (1984) 1794.
20 M. A. Baim and H. H. Hill, Anal. Chem., 54 (1982) 38.
21 J. P. Carrico, D. W. Sickenberger, G. E. Spangler and K. N. Vora, J. Phys. E.: 16 (1983) 1058.
22 M. M. Metro and R. A. Keller, Sep. Sci., 9 (1974) 521; J. Chromatogr. Sci., 11 (1973) 520.
23 R. A. Keller, Am. Lab., 7 (1975) 35.
24 G. Rico, G. A. Eiceman, C. D. Leasure and V. J. Vandiver, Anal. Instrum., 13 (1984) 289.
25 F. W. Karasek, Int. J. Environ. Anal. Chem., 2 (1972) 157.
26 G. E. Spangler and C. I. Collins, Anal. Chem., 47 (1975) 393.
27 S. H. Kim, K. R. Betty and F. W. Karasek, Anal. Chem., 50 (1978) 2006.

Analytica Chimica Acta, 175 (1985) 147—151
Elsevier Science Publishers B.V., Amsterdam — Printed in The Netherlands

SPECIATION OF CHROMIUM IN SEA WATER

F. AHERN, J. M. ECKERT* and N. C. PAYNE

Department of Inorganic Chemistry, University of Sydney, Sydney, N.S.W. 2006 (Australia)

K. L. WILLIAMS

Department of Geology and Geophysics, University of Sydney, Sydney, N.S.W. 2006 (Australia)

(Received 11th April 1985)

SUMMARY

Dissolved chromium(III) and (VI) are coprecipitated separately from sea water, and chromium in the precipitates and particulate matter is determined by thin-film x-ray fluorescence spectrometry. In combination with an ultraviolet irradiation procedure which releases bound metals, the method provides information about the speciation of chromium in near-shore surface sea water. The ratios of labile Cr(III)/(III+VI) generally lie in a narrow range (0.4—0.5) as do the sums of labile Cr(III) and (VI) concentrations (0.3—0.6 $\mu g\ l^{-1}$). Bound chromium is variable (0—3 $\mu g\ l^{-1}$) and constitutes from 0 to 90% of total dissolved chromium. Acidification of the samples in the traditional manner for trace metal determination is shown to alter the proportion of Cr(III) to Cr(VI).

Since the mid-1960s, there have been numerous attempts to determine the distribution of dissolved chromium in natural waters between the two common oxidation states of chromium, Cr(III) and Cr(VI) [1]. Interest in this matter stems from the fact that these two oxidation states have quite different geochemical and biological properties. Only recently, however, have studies of Cr(III) and Cr(VI) in natural waters been reported which also include values for total dissolved chromium measured after sample digestion [2, 3]. These studies indicate that a substantial fraction of the total dissolved chromium is bound, presumably to dissolved organic matter, and it has been suggested that the failure to consider organic chromium species is at least one reason for the inconsistencies in earlier research [3]. The problem is a common one in trace element speciation. There are at present no analytical techniques with sufficient sensitivity and selectivity to permit the direct determination of the individual species. Preliminary separation steps such as liquid-liquid extraction, coprecipitation, ion exchange or electrodeposition are necessary and these could, by taking species out of the system, displace equilibria and so alter the concentrations that the method is intended to measure.

In question is the extent to which organic chromium species contribute to the apparent levels of Cr(III) and (VI) as measured by the various methods.

0003-2670/85/$03.30

Nakayama et al. [3, 4], the first to address this question, provided evidence, in the form of studies with model organic ligands and synthesized chromium complexes, that organic chromium did not contribute in their method. They therefore called the labile (i.e., responsive) fractions "inorganic" Cr(III) and (VI) and the bound fraction "organic" chromium. These labels, however, are a gamble because so little is known about the nature of the organic ligands which actually bind chromium in natural waters. Model complex studies by Osaki et al. suggest that such labels may indeed be an over-simplification [5].

In a previous paper [6], it was reported that dissolved Cr(III) and (VI) can be separately coprecipitated at $\mu g\ l^{-1}$ levels and chromium in the precipitates can be determined by thin-film x-ray fluorescence (x.r.f.) spectrometry. Chromium(III) is preconcentrated in the well-known reaction with hydrated iron(III) oxide and Cr(VI) with tris(pyrrolidinedithiocarbamato)-cobalt(III). The preference of the cobalt complex for Cr(VI) was also reported, independently, by Fujiwara et al. [7].

The x.r.f. method has now been used, with an ultraviolet irradiation procedure which releases bound metals, to obtain information about the speciation of chromium in near-shore surface sea water. The results are presented and the effect of organic chromium species on the method is discussed.

EXPERIMENTAL

Apparatus, reagents and separation procedures

The x.r.f. spectrometer, filtration equipment and reagents were described previously [6]. The procedures for the coprecipitations of Cr(III) and (VI) and for the separation of the precipitates on 0.4-μm pore-size membrane filters were also as described, with one change. Chromium(III) was coprecipitated in the original work from 100-ml sea-water aliquots and Cr(VI) from the resulting filtrates. In the present study, the two forms were preconcentrated from different 100-ml aliquots, a procedure which is simpler and reduces the risk of contamination in the separation of Cr(VI).

General procedures

Sample collection and treatment. Surface sea-water samples were collected in polyethylene bottles from Palm Beach and Avalon Beach on the Warringah Peninsula, north of Sydney, N.S.W. The samples were filtered within 4 h of collection and the membrane filters were retained for the determination of particulate chromium. Quadruplicate 100-ml aliquots of the filtrate were treated immediately and without acidification to coprecipitate dissolved Cr(III) and further quadruplicate 100-ml aliquots to coprecipitate Cr(VI).

The rest of the filtrate was acidified in the traditional manner for trace metal determinations, with 5 ml of nitric acid (Merck, Suprapur) added to each litre of filtrate. A portion was treated within 24 h to release bound metals and the remainder was allowed to stand for at least 24 h, for use in

a study of the effect of acidification on the distribution of dissolved chromium between the two oxidation states. Chromium(III) and (VI) were separated from both portions as before.

Release of bound metals. Acidified filtrate was irradiated with a 35-W U-tube immersion lamp for 6 h after addition of hydrogen peroxide (0.5 ml of 30% solution per litre of filtrate) [8]. The excess of peroxide was removed by gently boiling the digested sample for at least 3 h and the pH was raised to about 7 with sodium hydroxide (Merck, Suprapur) before analysis for dissolved Cr(III) and (VI). Total dissolved chromium was obtained by adding the values found for the concentrations of Cr(III) and (VI) in the digested filtrate; bound chromium was calculated by subtracting from the total the sum of the labile Cr(III) and (VI) levels in the unacidified filtrate.

X.r.f. spectrometry. The loaded filters were mounted with the sample side towards the x-ray beam and teflon sleeves, 2 mm thick, were fitted inside the sample holders to reduce background scattered from the holders. The following working conditions were used: gold anode tube operated at 60 kV and 45 mA, fine collimator, LiF_{200} crystal, 2θ values of 69.34° (for peak) and 68.44° and 70.24° (for background), automatic pulse-height selection, flow and scintillation detectors in tandem, and counting times of 100 s and 40 s for peak and background, respectively. These conditions yielded linear net Cr K_α intensities of 12—14 cps per $\mu g\ l^{-1}$ chromium for water samples containing 0—3 $\mu g\ l^{-1}$ chromium.

RESULTS AND DISCUSSION

The results for the unacidified sea waters are given in Table 1. In all but one of the samples, the labile Cr(III)/(III + VI) ratios were found to lie in the range 0.4—0.5. The Cr(VI) oxidation state was favoured, but only marginally, in these near-shore surface samples. A ratio of 0.69 was observed for the remaining sample, which was collected in January 1985 during a period of industrial action at Sydney Metropolitan sewage treatment plants. Although the nearest major outfall is 15 km from the point of sample collection, the high Cr(III) content of this sample is almost certainly due to abnormal pollution.

Ths sums of the labile Cr(III) and (VI) concentrations also fell in a narrow range (0.3—0.6 $\mu g\ l^{-1}$) but bound chromium proved to be highly variable, ranging from 0 to 3 $\mu g\ l^{-1}$ and constituting from 0 to 90% of the total dissolved chromium. This large variation was not reflected in either the Cr(III)/(III + VI) ratios or the sums of the labile Cr(III) and (VI) concentrations. Organic chromium species, if they contribute to the labile fractions, must do so to roughly the same extent whether the bound organic chromium concentration is negligible or very large. More likely, the labile fractions measured in these samples are essentially "inorganic".

Many authors in this field have used the term "total chromium" when referring to the sum of labile Cr(III) and (VI). In fact, there appear to be

TABLE 1

Chromium in unacidified surface sea water

Collected	Salinity (‰)	Chromium content ($\mu g\ l^{-1}$)					Cr(III)/(III + VI) ratio
		Particulate[c]	Dissolved				
			Labile Cr(III)[c]	Labile Cr(VI)[c]	Total[c]	Bound[d]	
Jan., 1983[a]	37.5	0.08	0.22	0.27	2.3	1.8	0.45
Jan., 1984[a]	33.8	0.06	0.25	0.31	0.6	0	0.45
Feb., 1984[b]	34.8	0.04	0.10	0.16	3.4	3.1	0.38
May, 1984[b]	35.5	0.23	0.29	0.27	0.6	0	0.52
Dec., 1984[b]	35.7	0.06	0.15	0.24	0.4	0	0.38
Jan., 1985[b]	36 3	0.10	0.43	0.19	1.8	1.2	0.69

[a]Surface waters from Palm Beach. [b]Surface waters from Avalon Beach. [c]Mean of 4 determinations; relative standard deviations 10—15%. [d]Bound Cr is the total dissolved Cr minus the labile Cr(III + VI) in the unacidified filtrate.

TABLE 2

Effect of acidification[a]

Collected	Labile Cr(III)[b] ($\mu g\ l^{-1}$)	Labile Cr(VI)[b] ($\mu g\ l^{-1}$)	Cr(III)/(III + VI) ratio
Jan., 1983	0.46	0.18	0.72
Jan., 1984	0.27	0.21	0.56
Feb., 1984	0.41	0.17	0.71
May, 1984	0.25	0.23	0.52
Dec., 1984	0.32	0.20	0.62
Jan., 1985	0.50	0.25	0.67

[a]Samples allowed to stand for at least 24 h after addition of nitric acid (5 ml l^{-1} of filtrate). [b]Mean of 4 determinations; relative standard deviation 10—15%.

only two previous papers on chromium speciation in natural waters which contain data for total dissolved chromium, measured after sample digestion, together with data for Cr(III) and (VI). Batley and Matousek [2] obtained Cr(III)/(III + VI) ratios of 0.4 and 0.25 for two sea-water samples; and Nakayama et al. [3] reported a mean ratio of 0.4 for 14 samples taken from various depths in the Japan Sea and 0.3 for 16 samples from the Pacific Ocean. Neither group observed bound chromium levels in excess of 0.35 $\mu g\ l^{-1}$

Table 2 shows the results obtained for labile Cr(III) and (VI) after sample acidification. The Cr(III)/(III + VI) ratios now lie in the range 0.5—0.7. In acid, Cr(VI) has been converted to Cr(III), probably as it oxidizes dissolved organic matter. This observation supports the suggestion of Nakayama et al. [3] that the high Cr(III) levels reported by some early workers may have been an artefact of sample acidification.

This work was supported by the Australian Research Grants Scheme. The x.r.f. equipment was made available by the Department of Geology and Geophysics at the University of Sydney; and we gratefully acknowledge the help provided by Dr. Michael Hough and Dr. Don Radford.

REFERENCES

1 T. M. Florence and G. E. Batley, CRC Crit. Rev. Anal. Chem., 9 (1980) 262.
2 G. E. Batley and J. P. Matousek, Anal. Chem., 52 (1980) 1570.
3 E. Nakayama, T. Kuwamoto, H. Tokoro and T. Fujinaga, Anal. Chim. Acta, 131 (1981) 247; Nature, 290 (1981) 768.
4 E. Nakayama, T. Kuwamoto, S. Tsurubo, H. Tokoro and T. Fujinaga, Anal. Chim. Acta, 130 (1981) 289.
5 S. Osaki, T. Osaki, N. Hirashima and Y. Takashima, Talanta, 30 (1983) 523.
6 A. J. Pik, J. M. Eckert and K. L. Williams, Anal. Chim. Acta, 124 (1981) 351.
7 K. Fujiwara, S. Toda and K. Fuwa, Bull. Chem. Soc. Jpn., 54 (1981) 3209.
8 G. E. Batley and Y. J. Farrar, Anal. Chim, Acta, 99 (1978) 283.

Analytica Chimica Acta, 175 (1985) 153—161
Elsevier Science Publishers B.V., Amsterdam — Printed in The Netherlands

EFFECTS OF WAVELENGTH RANGE ON THE SIMULTANEOUS QUANTITATION OF POLYNUCLEAR AROMATIC HYDROCARBONS WITH ABSORPTION SPECTRA

DAVID T. ROSSI[a] and HARRY L. PARDUE*
Department of Chemistry, Purdue University, West Lafayette, IN 47907 (U.S.A.)
(Received 4th March 1985)

SUMMARY

The study described was designed to evaluate the use of carefully selected wavelength ranges to improve the accuracy of results when multiwavelength absorption data are used to quantify components in mixtures. Mixtures of polynuclear aromatic hydrocarbons were used as test samples. It is shown that in some cases narrow wavelength ranges can yield substantially improved results relative to broad wavelength ranges. Such improvement is most likely when the component of interest is present in low concentration relative to other components with similar absorptivities and when the component of interest has fine structure in a limited region of the spectrum. Results for components with fine structure throughout broad regions of the spectrum are not likely to be improved by selection of a narrow range that emphasizes just one of the regions of fine structure. However, careful selection of such a region seldom degrades results.

Since the early work of Sternberg et al. [1], there have been many applications of matrix least-squares methods to resolve components in mixtures with multiwavelength absorption data. These applications have been enhanced by the availability of rapid-scanning spectrometers based on the use of imaging detectors [2]. To date, most applications of these methods have involved the use of the same range of wavelengths to resolve each component in a mixture. An earlier study in this laboratory indicated that it may be possible to achieve improved performance for some components by selection of sets of wavelengths that emphasize spectral characteristics of the component of interest and de-emphasize features of other potentially interfering components [3]. The purpose of this work was to study this possibility in more detail for normal, first-, and second-derivative absorption spectra.

Mixtures of polynuclear aromatic hydrocarbons (PAH's) for which chromatographic separations are difficult were chosen for this study. The ability to improve results by the use of different wavelength ranges for different components appears to depend upon the absorbance(s) of the components(s) of interest relative to the absorbances of potential interferents.

[a]Present address: Monsanto Company, St. Louis, MO (U.S.A.).

0003-2670/85/$03.30

If the absorbance of the component of interest is equal to or larger than absorbances of other components in a mixture, then little improvement is gained from a narrow wavelength range relative to a broad range. However, in "stressed" situations in which the absorbance of the component of interest is lower than absorbances of other components throughout most of the wavelength range, then selection of a narrow wavelength range that emphasizes the spectral features of the component of interest will usually yield improved results relative to broader ranges. In most instances in which there is a spectral range that emphasizes spectral features of the component of interest relative to other components, a narrow wavelength range will yield results similar to or better than results from broader, less-carefully selected ranges.

EXPERIMENTAL

Apparatus and reagents

All ultraviolet/visible absorption spectra were obtained with a HP8450A diode-array spectrophotometer (Hewlett-Packard), equipped with a floppy disk drive for bulk data storage (Hewlett-Packard model 82902M) and a digital plotter for graphical representation of data (Hewlett-Packard model 7225A). This instrument samples spectra at a data density of one point per nanometer between 200 and 400 nm, and one point per 2 nm between 400 and 800 nm. Derivative spectra and spectral-fitting processes were done by programs contained in the spectrophotometer.

The solvent for all PAH solutions was a 75:25 (v/v) mixture of spectroscopic-grade acetonitrile (Baker Resianalyzed) and distilled-deionized water. All solid reagents were analytical grade.

Procedure

Four multicomponent chemical systems were studied. The constituents in each system were selected because of difficulties in achieving chromatographic separations under one or more sets of conditions. These systems are, therefore, mixtures for which it is desirable to resolve the components without a separation step. Two two-component mixtures studied were fluorene with acenaphthene and benzo(e)pyrene with benzo(k)fluoranthene. A four-component mixture studied was 9-methylphenanthrene, fluoranthene, pyrene, and 9-methylanthracene. A three-component mixture studied was fluoranthene, pyrene, and 9-methylanthracene.

Five pure standards of each component were prepared over the concentration range of interest. This range was 0—20 $\mu g\ ml^{-1}$ overall, with a concentration range greater than one order of magnitude for each component. A spectrum of each standard solution was obtained by averaging 30 separate measurements over a period of 15 s. A normalized spectrum of unit concentration of each set of five pure standards was prepared by regressing absorbance vs. concentration of each wavelength of interest. This single

normalized spectrum is more easily used in the multicomponent calculations than are standard spectra for each of several concentrations.

For each multicomponent system, solutions were prepared at 4—15 compositions with three replicates per composition, for a total of 12—45 mixtures per chemical system. A spectrum of each solution was obtained by averaging 30 separate measurements over a period of 15 s. Special care was taken to ensure that the total concentrations for mixtures were such that the absorbance did not exceed the linear range of the instrument.

Programs supplied with the spectrophotometer were used to compute derivatives and concentrations for normal, first-, and second-derivative spectra over selected wavelength ranges.

RESULTS AND DISCUSSION

Results are given for two two-component mixtures, one four-component mixture, and one three-component mixture. Relative errors presented are averages for three replicates. Uncertainties reported for slopes and intercepts of regression data are given as one standard deviation (±s.d.).

Two-component mixtures

Figures 1A—C show absorbance, first-derivative, and second-derivative spectra, respectively, for fluorene and acenaphthene with selected wavelength ranges identified with letters e—k.

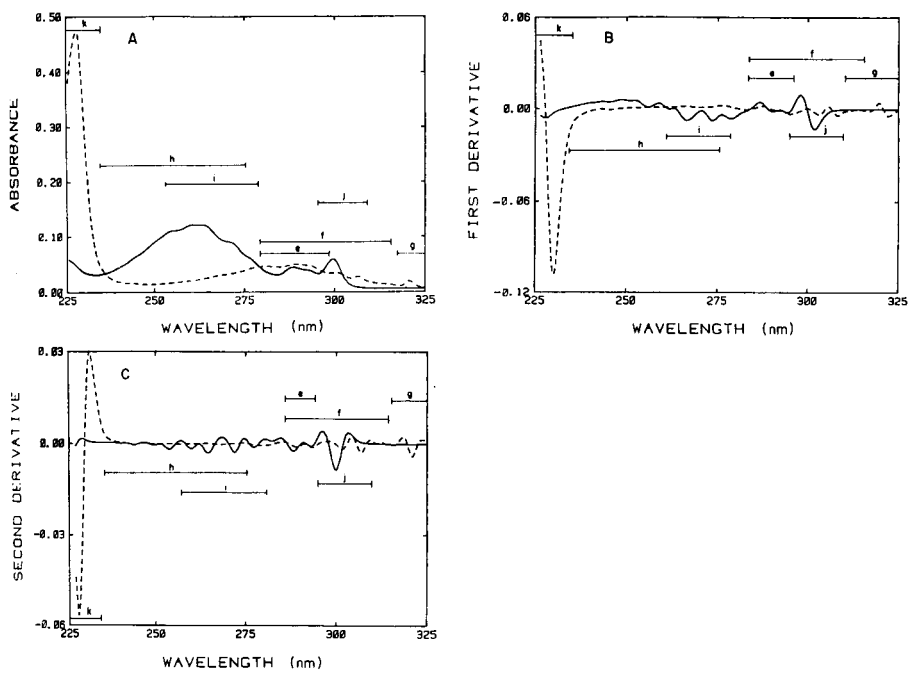

Fig. 1. Spectra for fluorene (—) and acenaphthene (---) (1.0 μg ml^{-1} each): (A) absorption spectra; (B) first-derivative spectra; (C) second-derivative spectra.

Broad concentration ranges. For solutions containing 0—10 $\mu g\ ml^{-1}$ fluorene and 0—19.7 $\mu g\ ml^{-1}$ acenaphthene, spectral data were processed over the full range shown in the figures (225—325 nm) as well as selected narrow ranges. For acenaphthene in the presence of fluorene, least-squares statistics for computed (y) vs. prepared (x) concentrations ($\mu g\ ml^{-1}$) were $y_0 = (1.012 \pm 0.004)\,x + 0.22 \pm 0.04$ with $S_{yx} = 0.14$, $y_1 = (1.009 \pm 0.002)\,x + 0.17 \pm 0.02$ with $S_{yx} = 0.009$, and $y_3 = (1.020 \pm 0.002)\,x + 0.14 \pm 0.02$ with $S_{yx} = 0.04$ for normal (y_0), first (y_1), and second (y_2) derivative spectra, respectively. In all cases, S_{yx} is the standard error of the estimate and correlation coefficients are greater than 0.99. For these wide concentration ranges, several other narrower wavelength ranges (e.g., 278—310 nm for normal spectra, 292—325 nm for first derivatives, and 303—325 nm for second derivatives) yielded similar results, but none yielded substantially better results than the wide wavelength ranges. Similar results were obtained for fluorene in these mixtures.

Low concentrations. The least-squares statistics presented in the previous subsection can be deceptive in the sense that they can mask large relative errors for concentrations near the low end of the range included in the study. It was reasoned that the principal advantage of more critically selected wavelength ranges could be for situations in which it is desirable to quantify a low concentration of a component in the presence of relatively high concentrations of one or more components. Data for acenaphthene and fluorene were evaluated with this point in mind.

Table 1 includes results for both components obtained from different spectral ranges. It is noted that although the imprecision is relatively independent of the spectral range, there are some situations in which the systematic errors are improved substantially by the use of a narrow wavelength range that emphasizes the component of interest. This is most apparent for acenaphthene with normal spectra and fluorene with second-derivative spectra. Although other differences are smaller, in every case, it is possible to select a narrow spectral range that yields as good or better results than the broader spectral range.

Similar experiments were done with mixtures of benzo(e)pyrene and benzo(k)fluoranthene for which normal absorbance spectra are presented in Fig. 2. Although the relative standard deviations for these components were somewhat larger (1.5—2.6%) than for fluorene and acenaphthene, systematic errors for the broader wavelength range (225—425 nm) were generally smaller, probably because these spectra have more structural characteristics than those for fluorene and acenaphthene. However, there still were situations in which carefully selected narrow wavelength ranges yielded improved results relative to the broader ranges. For example, for benzo(e)pyrene, average systematic errors for the full wavelength range for normal, first-, and second-derivative spectra were 3.4%, 1.3%, and 1.9% respectively, whereas the relative errors were 0.4% for each of the three data sets processed in the range labeled *g* in Fig. 2. For benzo(k)fluoranthene, absorbance data in range *i* (Fig. 2) yielded an improvement from 6.6% for the

TABLE 1

Relative errors for low concentrations of acenaphthene and fluorene in the presence of higher concentrations of the other

Acenaphthene			Fluorene		
Wavelength range(nm)	Rel. Error[a] (%)	RSD[b] (%)	Wavelength range (nm)	Rel. Error[c] (%)	RSD (%)
Normal spectra					
225—325	29.5	1.7	225—325	4.5	1.1
225—236 (*k*)	1.7	1.5	260—280 (*i*)	3.3	1.0
281—298 (*e*)	1.7	1.2	295—309 (*j*)	2.0	0.8
First derivative					
225—325	7.2	1.0	275—325	4.5	0.8
284—296 (*e*)	5.1	1.0	235—275 (*h*)	2.0	0.8
284—315 (*f*)	2.8	1.0	260—278 (*i*)	3.8	0.8
Second derivative					
225—325	2.4	1.1	225—325	19.6	1.3
227—236 (*k*)	2.7	1.5	235—275 (*h*)	2.6	0.7
287—315 (*f*)	1.8	1.2	260—280	2.8	0.8

[a]Average error for three runs at each of four concentrations (2—3 μg ml^{-1} with 6.3—10 μg ml^{-1} fluorene). [b]Pooled relative standard deviation for four sets of three runs each. [c]Average error for three runs at each of four concentrations (2.4—6.1 μg ml^{-1} with 4.6—19.7 μg ml^{-1} acenaphthene).

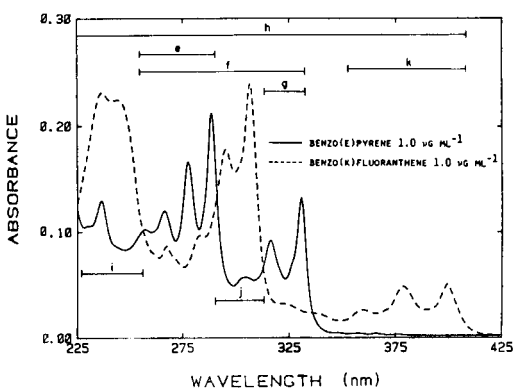

Fig. 2. Absorption spectra for benzo(e)pyrene (—) and benzo(k)fluoranthene (---) (1.0 μg ml^{-1} each).

full range (225—425 nm) to 0.5% (228—254 nm). Both the first- and second-derivative spectra yielded unusually large errors (17.7 and 5.1%, respectively) in this latter range. However, first- and second-derivative spectra in the 350—410 nm range provided modest apparent improvements relative to the full wavelength range (1.1 vs. 3.9% and 1.1 vs. 1.3%).

The most significant difference between these two sets of mixtures is that the former components (fluorene and acenaphthene) exhibit relatively broad, featureless spectra throughout much of the near ultraviolet region whereas the latter components (benzo(e)pyrene and benzo(k)fluoranthene) exhibit substantial fine structure throughout most of the region from 225 to 425 nm. In the former case, those narrow regions of the spectrum that do exhibit selective fine structure for the component of interest can be used to significant advantage. In the latter case, the distribution of fine structure throughout much of the spectrum enhances the quality of data obtained from the broad spectral range to the point that only modest if any really significant improvements are obtained from more narrow wavelength ranges. However, in these and all other combinations examined, narrow ranges can be selected that yield results as good or better than those obtained with broader wavelength ranges.

Three- and four-component mixtures

Spectra for 9-methylphenanthrene, 9-methylanthracene, fluoranthene, and pyrene shown in Fig. 3A—C were used to evaluate effects of wavelength ranges for three- and four-component mixtures. This combination is used to illustrate some important general points.

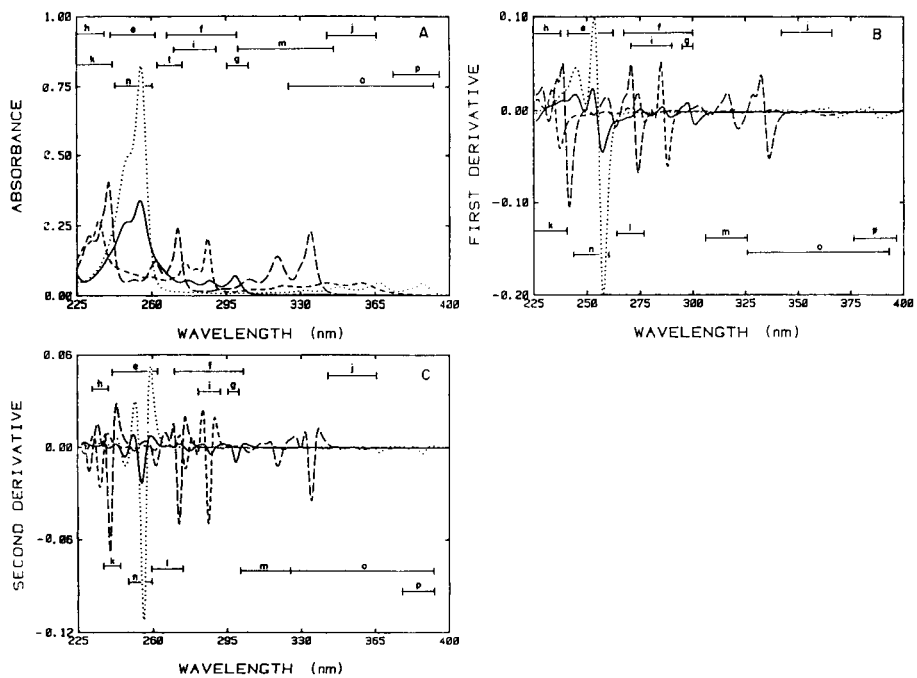

Fig. 3. Spectra for 9-methylphenanthrene (—), 9-methylanthracene (···), pyrene (---), and fluoranthene (———) (1.0 μg ml^{-1} each): (A) absorption spectra; (B) first-derivative spectra; (C) second-derivative spectra.

TABLE 2

Relative error for low concentrations of 9-methylanthracene (9-MA) in the presence of fluoranthene (Fl), pyrene (Py), and 9-methylphenanthrene (9-MP)

Wavelength range (nm)	Relative error (%)[a]					RSD[b]
	*C*1	*C*2	*C*3	*C*4	Ave.	(%)
Normal spectra						
225–400	−5.18	−8.86	−7.65	−10.18	7.97	1.37
243–259 (*n*)	−15.34	−21.44	−17.52	22.14	19.11	1.38
325–392 (*o*)	−2.78	−2.22	−5.32	−4.61	3.73	3.69
375–395 (*p*)	3.12	1.57	1.30	1.81	1.95	1.62
First derivative						
224–400	−8.10	−12.88	−9.81	−11.11	10.48	1.23
243–259 (*n*)	3.97	3.98	4.34	8.28	5.14	2.36
325–392 (*o*)	2.53	0.87	−0.39	0.47	1.07	1.65
375–395 (*p*)	3.49	1.83	1.55	2.23	2.28	1.66
Second derivative						
225–400	−5.80	−9.84	−6.94	−7.16	7.44	1.50
249–260 (*n*)	2.10	0.83	0.76	4.78	2.10	2.16
325–392 (*o*)	2.98	1.24	0.69	0.67	1.40	1.71
378–392 (*p*)	3.63	1.80	1.81	2.08	2.33	1.79
Concentrations (μg ml^{-1})						
	9-MA		9-MP	Fl		Py
*C*1	0.983		3.06	1.40		1.43
*C*2	0.787		3.57	1.60		1.14
*C*3	0.787		3.57	1.00		2.00
*C*4	0.590		4.08	0.802		2.29

[a] Average of three runs at each concentration. [b] Pooled relative standard deviation.

Table 2 contains a relatively complete data set for 9-methylanthracene in the presence of the other three components. It should be noted that the relative error for each concentration level (*C*1–*C*4) is the average of three runs on each sample; the "average error" is the average of the absolute values for all twelve runs for each wavelength range; and the relative standard deviation is the pooled value for the four sets of three samples each. Thus, conclusions implied by these and other results discussed below are based on a reasonably valid data base.

For each of the three spectral modes (normal, first, and second derivatives), at least one narrow wavelength range was found that yielded results superior to those obtained from the broader range. Although the spectral region labeled *n* involved so much overlap between 9-methylphenanthrene and 9-methylanthracene that it was impossible to resolve either accurately from the normal absorption spectra, both the first- and second-derivative spectra had sufficient differences to permit reasonably reliable resolution.

It would be expected that if either of these two components (9-methylanthracene or 9-methylphenanthrene) were absent, then the

243—259 nm range (range *n* in Fig. 3A) would be an excellent choice for the other component. To test this expectation, several three-component samples were prepared to contain between 0.6 and 0.9 $\mu g\ ml^{-1}$ 9-methylanthracene, 1.7—2.6 $\mu g\ ml^{-1}$ fluoranthene, and 2 $\mu g\ ml^{-1}$ pyrene. The average error for 9-methylanthracene for three runs on each of the four samples with absorbance data from the full wavelength range (225—400 nm) was 8.2% with a pooled RSD of 1.05%. The average error for the 243—259 nm range was 0.6% with an RSD of 1.00%. The average error for the full wavelength range dropped to 0.2% for first-derivative spectra and 3.9% for second-derivative spectra, with RSD values of 0.9% in each case. Some other narrow ranges (*n* and *o* for first derivative and *n* and *p* for second derivatives) yielded similar errors but none provided substantially better results.

Because pyrene exhibits significant fine structure throughout most of the spectral region examined here, it was expected that the broad spectral range will yield results similar to those for the narrower ranges. That this is true is illustrated by data in Table 3.

The spectrum for fluoranthene exhibits somewhat less fine structure than pyrene but perhaps more than the other two components, and perhaps more importantly, there is less overlap of major peaks with those of other components than is the case for 9-methylanthracene and 9-methylphenanthrene in the region marked *n* (Fig. 3A). For absorption data, regions *h* and *i* yielded significantly lower relative errors (0.5 and 1.0%, respectively) than the full range (4.7%). Both first- and second-derivative data processed over the full range (225—400 nm) yielded average relative errors (0.0% and 1.1%,

TABLE 3

Relative error for low concentrations of pyrene in the presence of 9-methylphenanthrene, fluoranthene, and 9-methylanthracene

Wavelength range (nm)	Average error[a] (%)	RSD[b] (%)
225—400	2.97	1.67
225—242 (*k*)	1.61	1.68
267—274 (*l*)	3.30	1.75
300—345 (*m*)	2.94	1.66
225—400	2.72	1.77
225—245 (*k*)	1.79	1.79
263—276 (*l*)	4.21	2.68
305—325 (*m*)	3.35	1.76
225—400	1.81	1.77
237—245 (*k*)	1.38	1.99
260—275 (*l*)	3.25	1.80
302—325 (*m*)	3.31	1.79

[a]Three replicates for each of four samples; concentrations as in Table 2. [b]Pooled relative standard deviation; three replicates for each of four samples.

respectively) well within the random uncertainty (pooled RSD values of 1.5 and 1.3%, respectively).

Conclusions

It is concluded that in most instances a carefully selected narrow wavelength range can be selected for each component to yield results with accuracy as good or better than the broader wavelength ranges that are more commonly used. If the component of interest has significant fine structure throughout the spectral range used, then it is less probable that a narrow wavelength range will yield improved results. However, if the fine structure for a component is limited to one region of the spectrum and if the absorbance of the component is small relative to that for potential interferences, then it is probable that proper selection of a narrow spectral range in which the spectral characteristics of the component of interest are emphasized will yield improved results.

To date, selection of best wavelength ranges is empirical and based on qualitative features of spectra as indicated above. Efforts to define a quantitative relationship that would permit an unambiguous prediction of the best wavelength range(s) to use for a particular component were unsuccessful.

This work was supported by Contract DE-ACOZ-79EV10240 from the U.S. Department of Energy.

REFERENCES

1 J. C. Sternberg, H. S. Stillo and R. H. Schwendeman, Anal. Chem., 32 (1960) 84.
2 Y. Talmi, Anal. Chem., 47 (1975) 658A.
3 D. T. Rossi, D. J. Desilets and H. L. Pardue, Anal. Chim. Acta, 161 (1984) 191.

Analytica Chimica Acta, 175 (1985) 163—169
Elsevier Science Publishers B.V., Amsterdam — Printed in The Netherlands

AN ULTRAMICRO ASSAY FOR HUMAN PLASMA PREKALLIKREIN ACTIVITY BY PHOSPHORIMETRY

NAOTAKA KURODA, HITOSHI NOHTA and YOSUKE OHKURA*

Faculty of Pharmaceutical Sciences, Kyushu University 62, Maidashi, Higashi-ku, Fukuoka 812 (Japan)

(Received 5th March 1985)

SUMMARY

A highly sensitive method for the phosphorimetric assay of prekallikrein in human blood plasma is described. Prekallikrein is converted to kallikrein (active form) by reaction at 0°C with actin. *p*-Nitroaniline, formed enzymatically from *H*-D-prolyl-L-phenylalanyl-L-arginyl-*p*-nitroanilide, is extracted with ether and determined phosphorimetrically in a mixture of ether and ethanol. The method is precise and highly sensitive, requiring as little as 0.25 μl of human blood plasma. The limit of detection for *p*-nitroaniline formed enzymatically is 5 pmol.

Prekallikrein (PK) is the precursor of kallikrein (KK; EC 3.4.21.8) which releases bradykinin from kininogen and participates in the intrinsic coagulation and fibrinolysis of plasma [1]. The PK activity in plasma is decreased in patients with liver cirrhosis [2, 3] and disseminated intravascular coagulation syndrome [3]. However, the relationship between PK activity in plasma and other diseases is not fully understood.

Prekallikrein has been assayed after conversion to its active form KK. Previously, KK in plasma was estimated by a bioassay technique based on measuring bradykinin formed enzymatically from plasma kininogen by using smooth muscle preparations [4]; the method was time-consuming and had poor reproducibility. Another assay was based on the hydrolytic activity of KK on an arginine ester, α-benzoyl-L-arginine ethyl ester or α-tosyl-L-arginine methyl ester [5]; these ester substrates are not very selective for KK. Recently, PK in plasma was assayed by spectrophotometric and fluorimetric methods. The former methods use *H*-D-prolyl-L-phenylalanyl-L-arginyl-*p*-nitroanilide dihydrochloride (S-2302) [6, 7] or *N*-benzoyl-L-prolyl-L-phenylalanyl-L-arginyl-*p*-nitroanilide hydrochloride (Chromozym PK) [8] as substrate and are insensitive. The fluorimetric method based on carbobenzoxy-L-phenylalanyl-L-arginine-4-methylcoumarinyl-7-amide [9] as substrate is more sensitive.

p-Nitroaniline phosphoresces intensely in a mixture of ether and ethanol at 77 K. This has been used for the ultramicroassay of γ-glutamyl transpeptidase and leucine aminopeptidase in biological materials, based on the

0003-2670/85/$03.30

phosphorimetric determination of the *p*-nitroaniline formed enzymatically [10, 11]. This paper describes an ultramicroassay for PK in human blood plasma. The PK is first converted to KK, the activity of which is determined by using S-2302 as substrate and measuring phosphorimetrically the *p*-nitroaniline formed.

EXPERIMENTAL

Reagents and apparatus

All chemicals and solvents were of analytical-reagent grade, unless otherwise stated. Double-distilled water was used throughout. *p*-Nitroaniline (Wako, Osaka) was purified by recrystallization from water. Other materials used were bovine serum albumin (BSA; Katayama Chemicals, Osaka) and actin, which contains ellagic acid and cephalin (Dade Diagnostica, Miami, FL); kaolin, chicken egg-white trypsin inhibitor (EWTI) and soybean trypsin inhibitor (SBTI) (all from Sigma); and *trans*-4-(aminomethyl)-cyclohexanecarboxylic acid (*t*-AMCHA; Nakarai Chemicals, Kyoto).

The substrate solution contained 1.8 mM S-2302 (AB Kabi, Stockholm, Sweden) in 0.05 M Tris-hydrochloric acid buffer (pH 7.8). The solution was stable for at least a month when stored at 4°C. All test tubes were siliconized in the usual manner by using Siliconize (Fuji System Co., Tokyo).

Uncorrected phosphorescence spectra and intensities of the sample solutions in ether/ethanol were measured in the form of the glassy solid at liquid nitrogen temperature (77 K), by using a Hitachi MPF-3 spectrofluorimeter equipped with a Hitachi phosphoroscope attachment and quartz sample tubes (4.0 mm i.d., 5.0 mm o.d., 200 mm long; sample volume ca. 150 μl). The spectral bandwidths of the excitation and emission monochromators were both 10 nm. The phosphorescence lifetimes were measured on a Hitachi V-550 synchroscope. The pH was measured with a Hitachi-Horiba M-7 pH meter at 25°C.

Diluted plasma solution. Blood samples were drawn from healthy volunteers in this laboratory. Citrated plasmas were obtained by mixing 1 volume of 0.12 M sodium citrate and 9 volumes of blood in plastic tubes and centrifuging briefly at 0°C. The plasmas were kept frozen at −20°C until used. The plasmas were diluted 200 times with 0.05 M Tris-hydrochloric acid buffer (pH 7.8) containing 0.5% (w/v) BSA before use.

Assay procedure

Diluted plasma solution (50 μl, corresponding to 0.25 μl of plasma) was transferred to a test tube, chilled in ice-water and allowed to stand at 0°C for ca. 30 min after addition of 50 μl of 2% (v/v) actin in 0.05 M Tris-hydrochloric acid buffer (pH 7.8) to convert PK to KK. When kaolin was required for the activation, 50 μl of its suspension (0.25 mg ml^{-1}) replaced the 50 μl of actin solution.

The activated sample was pre-incubated at 37°C for 30 s. The prewarmed

(37°C) substrate solution (100 μl) was added and incubated for exactly 5 min. The reaction was stopped by the addition of 20 μl of 8.3 M acetic acid. The *p*-nitroaniline produced was extracted into 2.0 ml of diethyl ether by shaking on a Iwaki KM shaker (amplitude, 5 cm; ca. 250 rpm) for ca. 3 min. After brief centrifugation, 1.4 ml of the ether layer was diluted with 0.35 ml of ethanol. For the reagent blank, the procedure was the same except that 50 μl of diluted plasma solution was replaced with 50 μl of the Tris buffer. The PK activity was calculated by subtracting the spontaneous activity, which was obtained according to the above procedure except that 50 μl of the Tris buffer was used in place of the actin solution. For calibration, 100 μl of the substrate solution was replaced by 100 μl of *p*-nitroaniline standards (0.5—500 nmol ml^{-1}) dissolved in the Tris buffer. Phosphorescence intensities were measured at 510 nm with excitation at 380 nm.

Procedure for testing the effect of inhibitors on PK activity

Diluted plasma solution (50 μl) was allowed to stand at 0°C for ca. 30 min after addition of 40 μl of 2.5% (v/v) actin in the Tris buffer. The activated sample was pre-incubated at 37°C for 30 s. The prewarmed (37°C) inhibitor solution (10 μl) and the substrate solution (100 μl) were added and again incubated for exactly 5 min. The incubated mixture was treated in the same way as in the assay procedure for the extraction of *p*-nitroaniline and the measurement of the phosphorescence intensity.

RESULTS AND DISCUSSION

The present method is highly sensitive and so allows a high plasma dilution (200 times) with Tris buffer, which serves to minimize the interference from KK inhibitors present in plasma (α_2-macroglobulin and Cl′-esterase inhibitor) [2].

Prekallikrein in plasma is activated with contact activators such as ellagic acid (a component of actin), kaolin or dextran sulfate [2]. The incubation time and temperature for activation with actin or kaolin had an effect on PK activity (Fig. 1). At 37°C, the activity reached a maximum within 5 min and then rapidly decreased for both actin and kaolin activation. The decrease may be due to the formation of a complex between the resulting KK and the KK inhibitors in plasma [12]. Activation at 0°C (cold activation) with actin or kaolin, however, gave maximum and constant values over a wide range of incubation times (20—60 or 30—60 min, respectively); the maximum activity obtained with actin was slightly higher than that with kaolin. Maximum, constant activity could be achieved by cold activation with actin for more than 20 min even when the plasma sample size was increased to at least 1 μl. Therefore, activation with actin at 0°C for 30 min is recommended for the assay procedure. The actin concentration also affected the activation of PK (Fig. 2). Actin gave almost maximum constant activity at concentrations of 0.5—1.5% (v/v) though the concentration

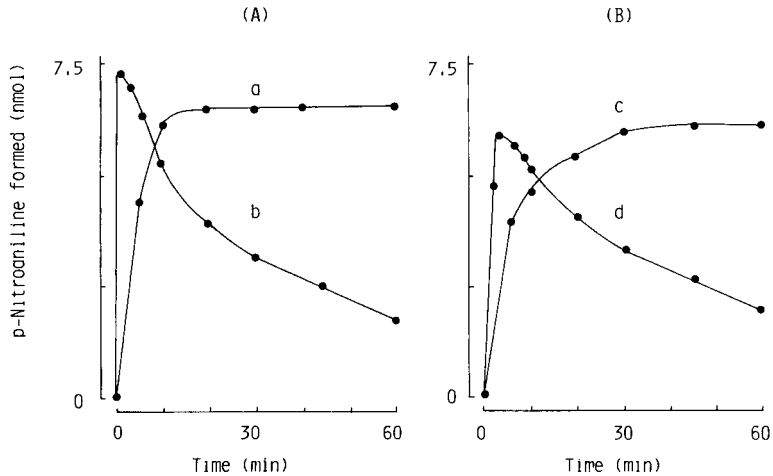

Fig. 1. Effect of incubation time on the amount of *p*-nitroaniline formed by activation with: (A) actin; (B) kaolin. 50-μl portions of 200-times diluted blood plasma were incubated at: (a, c) 0°C; (b, d) 37°C. (PK activity of the plasma, 5.30 μmol min^{-1} ml^{-1} when activated with actin).

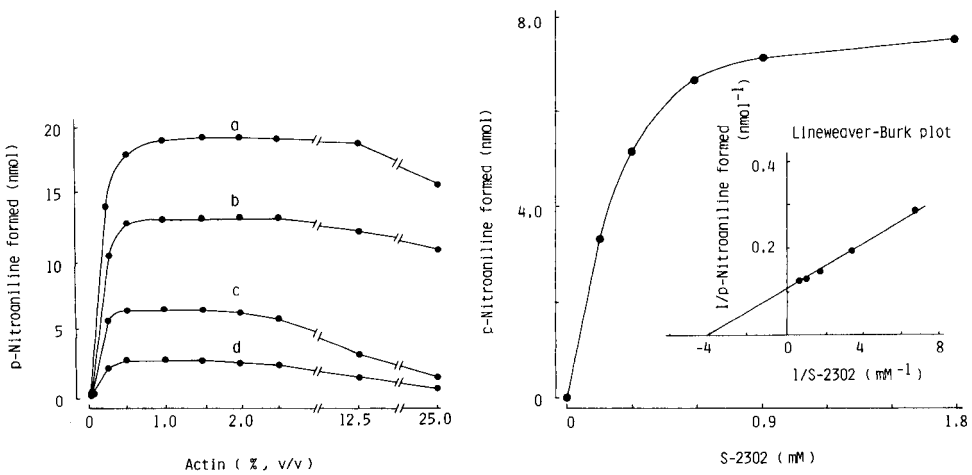

Fig. 2. Effect of actin concentration in the incubation mixture on the amount of *p*-nitroaniline formed by cold activation: 50-μl portions of diluted plasma (PK activity as in Fig. 1) were used as in the recommended procedure. Plasma sample size (μl): (a) 0.75; (b) 0.50; (c) 0.25; (d) 0.10.

Fig. 3. Effect of the concentration of S-2302 in the incubation mixture on the amount of *p*-nitroaniline formed: 50-μl portions of 200-times diluted plasma (PK activity of the plasma, 5.60 μmol min^{-1} ml^{-1}) were treated as in the recommended procedure.

required increased slightly with increasing plasma sample size; 1.0% is used in the recommended procedure.

The KK derived from PK was most active at pH 7.7—7.9 in 0.05 M Tris-hydrochloric acid buffer or 0.05 M phosphate buffer and the maximum activities obtained in both buffers were identical. Tris gave a maximum constant activity at concentrations of 0.04—0.06 M. Therefore 0.05 M Tris-hydrochloric acid buffer of pH 7.8 was selected in this procedure, as in the spectrophotometric and fluorimetric methods [6—8].

Almost maximum constant activity was obtained in the presence of 0.9—1.8 mM S-2302, with an observed Michaelis constant value of 0.24 mM (Fig. 3), which was almost identical with those obtained by other workers [13, 14]. Therefore, 0.9 mM was used for the enzyme reaction as a saturating concentration. This concentration is rather higher than those used in the spectrophotometric methods [6, 7].

The amount of *p*-nitroaniline formed for an incubation time of 5 min was not proportional to the plasma sample size when it was $\leqslant 0.45$ µl, even when the plasma was diluted with the Tris buffer in a siliconized test tube (Fig. 4a). The PK activity was greatly decreased in a non-siliconized tube. The loss of activity may be caused by nonspecific adsorption of PK or KK, or both, on the surface of the siliconized tube. Bovine serum albumin added in the buffer restored the activity probably because it prevented this adsorption (Fig. 4b). Maximum constant activities were attained at BSA concentrations greater than 0.25% in the Tris buffer for each plasma sample size (0.1, 0.25, 0.5 and 1.0 µl); buffer containing 0.5% (w/v) BSA was used for the dilution of plasma.

The enzyme activity was linear with time up to at least 10 min when incubated at 37°C; 5 min was used in the recommended procedure.

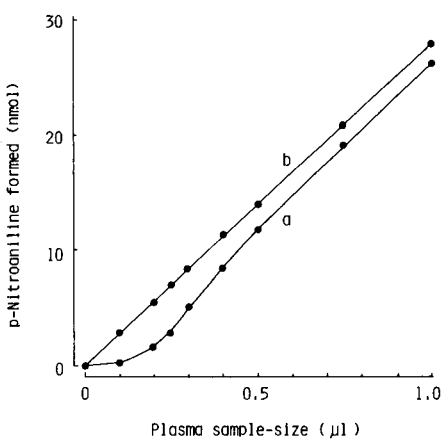

Fig. 4. Relationship between plasma sample size and the amount of *p*-nitroaniline formed: plasma (0.1—1.0 µl; PK activity 5.30 µmol min^{-1} ml^{-1}) was diluted to 50 µl with: (a) 0.05 M Tris-hydrochloric acid buffer (pH 7.8); (b) the Tris buffer containing 0.5% (w/v) BSA.

To check for prior activation of PK in the plasma sample, the spontaneous amidolytic activity of plasma for S-2302 was measured. The activity was less than 0.2% of the PK activity. The S-2302 substrate is fairly selective for KK but is hydrolyzed by other proteases such as plasmin and trypsin [15]. The effect of the proteases on PK activity was investigated by using their inhibitors, SBTI (inhibitor of KK and trypsin [16]), EWTI (inhibitor of trypsin [17]) and *t*-AMCHA (inhibitor of plasmin [18]). The SBTI and EWTI were added at 500 μg ml^{-1} and *t*-AMCHA at 3.2 mM in the reaction mixture. The enzyme activity toward S-2302 measured by the present method was strongly inhibited (95.5%) by SBTI but not by EWTI or *t*-AMCHA. This suggests that the present method can measure almost exclusively PK activity in plasma.

The *p*-nitroaniline was effectively extracted from the acidified incubation mixture with diethyl ether. The extract (1.4 ml) readily formed a clear solid at 77 K after mixing with 0.2—0.6 ml of ethanol; 0.35 ml of ethanol was used. The calibration graph was linear up to 50 nmol of *p*-nitroaniline. The phosphorescence excitation (maximum, 380 nm) and emission (maximum, 510 nm) spectra, and lifetimes (0.47 s) for the final solution were identical with those of *p*-nitroaniline dissolved in the same solvent (Fig. 5).

The limit of detection for *p*-nitroaniline was 5 pmol (phosphorescence intensity of twice the blank). This is much better than that of the fluorimetric

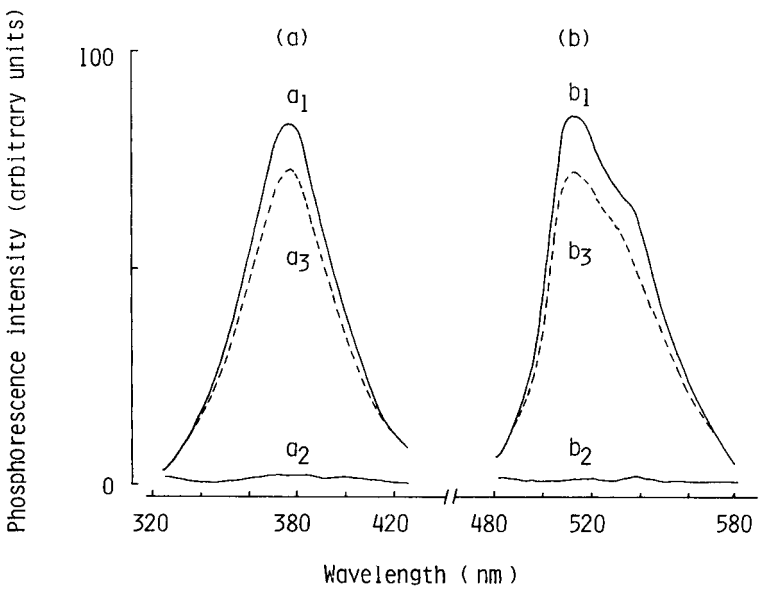

Fig. 5. Phosphorescence spectra of the final solution and of *p*-nitroaniline: (a) excitation (510 nm emission); (b) emission (380 nm absorption). (a_1, b_1) 50-μl portion of 200-times diluted plasma (PK activity of the plasma, 5.60 μmol min^{-1} ml^{-1}) treated according to the recommended procedure; (a_2, b_2) blank corresponding to a_1 and b_1; (a_3, b_3) *p*-nitroaniline (2.5 nmol ml^{-1}) dissolved in ether/ethanol (4:1, v/v).

method [9], and may permit the assay of PK in only 5 nl of normal plasma. The within-day precision of the present method was examined for a plasma with a mean PK activity of 5.23 μmol min^{-1} ml^{-1}. The relative standard deviation was 2.7% (n = 20).

The PK activity in plasma from normal subjects (22—53 years, n = 13) assayed by the present method was 5.42 ± 0.83 μmol min^{-1} ml^{-1} (mean ±SD). The values are in good agreement with data obtained by other workers [14].

The present method is not affected by bilirubin present in plasma though the spectrophotometric methods based on S-2302 [6, 7] and Chromozym PK [8] as substrate do suffer from bilirubin interference as a result of absorption of radiation at the same wavelength as p-nitroaniline.

This study provides the first phosphorimetric method for the assay of PK. The method is highly sensitive and precise and requires only a small amount of expensive substrate. It should be useful for biomedical investigation where only an extremely small amount of plasma is obtainable. Study on the assay of spontaneous activity toward S-2302 in plasma is in progress by taking advantage of the high sensitivity of this assay method.

REFERENCES

1 C. G. Cochrane and J. H. Griffin, Am. J. Med., 67 (1979) 657.
2 C. Kluft, J. Lab. Clin. Med., 91 (1978) 83.
3 N. U. Bang and L. E. Mattler, Thromb. Haemost., 38 (1977) 776.
4 K. Briseid, F. C. Arntzen and O. K. Dyrud, Acta Pharmacol. Toxicol., 26 (1968) 402.
5 R. W. Colman, J. W. Mason and S. Sherry, Ann. Intern. Med., 71 (1969) 71.
6 B. M. Alving, D. L. Tankersley and B. L. Mason, J. Lab. Clin. Med., 101 (1983) 226.
7 M. J. Gallimore and P. Friberger, Thromb. Res., 25 (1982) 293.
8 E. Amundsen, M. J. Gallimore, A. O. Aasen, M. Larsbnaaten and K. Lyngaas, Thromb. Res., 13 (1978) 625.
9 S. Ohishi and M. Katori, Thromb. Res., 14 (1979) 551.
10 M. Yamaguchi, N. Kuroda, K. Zaitsu and Y. Ohkura, Anal. Chim. Acta, 135 (1982) 313.
11 N. Kuroda, M. Yamaguchi, J. Ishida and Y. Ohkura, Chem. Pharm. Bull., 31 (1983) 2913.
12 M. Schapira, C. F. Scott and R. W. Colman, J. Clin. Invest., 69 (1982) 462.
13 G. Claeson, P. Friberger, M. Knos and E. Eriksson, Haemostasis, 7 (1978) 76.
14 R. Ito and B. E. Statland, Clin. Chem., 27 (1981) 586.
15 G. Claeson, L. Aurell, P. Friberger, S. Gustavsson and G. Karlsson, Haemostasis, 7 (1978) 62.
16 P. C. Harpel, J. Exp. Med., 132 (1970) 329.
17 S. Nakamura, N. Takizawa, K. Nakanishi and N. Igarashi, Rinsho Byori (Tokyo), 28 (1980) 670.
18 S. Okamoto, S. Oshiba, H. Mihara and U. Okamoto, Ann. N.Y. Acad. Sci., 146 (1968) 424.

Analytica Chimica Acta, 175 (1985) 171—179
Elsevier Science Publishers B.V., Amsterdam — Printed in The Netherlands

EVALUATION OF BATHOCUPROINE FOR THE SPECTROPHOTOMETRIC DETERMINATION OF COPPER(I) IN COPPER REDOX STUDIES WITH APPLICATIONS IN STUDIES OF NATURAL WATERS

JAMES W. MOFFETT, ROD G. ZIKA* and ROBERT G. PETASNE
University of Miami, 4600 Rickenbacker Causeway, Miami, FL 33149-1098 (U.S.A.)
(Received 25th March 1985)

SUMMARY

Copper(I) is determined at submicromolar levels in the presence of copper(II) in aqueous media by spectrophotometric measurement of the copper(I) complex of bathocuproine (2,9-dimethyl-4,7-diphenyl-1,10-phenanthroline). Copper(II) interference produced by reduction to copper(I) is described. Ethylenediamine can serve as a masking ligand to inhibit Cu(II) interference. The limit of detection is 1×10^{-8} mol l^{-1}. Although this is not sensitive enough for use at natural copper concentrations, the procedure can be used in laboratory studies of copper redox processes at elevated levels in natural waters such as sea water. The dependence of results on pH and ionic strength was studied to evaluate the usefulness of the method in other aqueous systems.

Redox reactions involving the Cu(I)/Cu(II) couple have received considerable attention in recent years, largely because copper can act as a catalyst in important biological and chemical systems involving oxygen. Recent evidence indicates that copper redox chemistry may also be important in copper speciation in natural waters [1]. This paper describes a procedure for the selective determination of copper(I) in the presence of copper(II) to examine copper redox processes in model systems of environmental interest. The procedure is based on the well known spectrophotometric determination of copper(I) with 2,9-dimethyl-4,7-diphenyl-1,10-phenanthroline disulfonic acid, disodium salt (bathocuproine disulfonic acid, disodium salt) [2—7]. However, problems associated with measuring Cu(I) in aqueous solution containing Cu(II) and reductants and oxidants have received insufficient attention. Preliminary experiments indicated that a significant interference in Cu(I) determination is the reduction of Cu(II) to Cu(I) initiated when the reagent is added to samples containing reducing agents. It was expected that these processes could be inhibited by the addition of a masking ligand which chelates Cu(II) and lowers its reactivity. However, many Cu(II) complexing agents also have a high affinity for Cu(I) and may prevent its chelation by bathocuproine. Consequently, a major goal of this study was the selection of a masking ligand which reacts rapidly with Cu(II) to form stable complexes

0003-2670/85/$03.30

which are inert to reduction, but does not compete with bathocuproine for Cu(I).

Hydrogen peroxide, which has been demonstrated to reduce Cu(II) [1] was used as a reductant to evaluate the proposed method. Hydroquinone and hydroxylamine, commonly used in the determination of Cu(II) with bathocuproine, were used as models for natural organic reductants; natural humic acid was also used. These experiments showed that formation and measurement of the Cu(I)/bathocuproine complex occurs rapidly compared with the interference created by Cu(II) reduction.

Other variables such as pH, ionic strength, oxidants (O_2) and other chelating agents were also studied.

EXPERIMENTAL

Reagents, solutions and equipment

Copper(I) stock solutions were prepared by dissolving copper(I) bromide (Fluka Garantie) in an acidified (0.1 mol l^{-1} hydrochloric acid) 1 mol l^{-1} sodium chloride solution which was purged with high-purity nitrogen to eliminate oxygen. Copper(I) was stable under these conditions. Heating to 50°C aided dissolution of the copper(I) salt. Stock solution concentrations ranged from 10^{-3} to 10^{-2} mol l^{-1} copper(I).

Stock solutions of bathocuproine disulfonic acid, disodium salt (Aldrich) at 10^{-2} mol l^{-1} were freshly prepared prior to each experiment.

Sea water was collected from a clean oceanic source in the Florida Current, 4 miles east of Key Biscayne, Florida, and was filtered (0.2-μm Nuclepore filter) before use. Deionized water was Milli-Q grade. All reagents used were analytical grade. Hydrogen peroxide solutions were prepared from a 30% (v/v) solution (Baker Analyzed Reagent) and were standardized iodimetrically. Solutions of hydroxylamine and hydroquinone were freshly prepared each day in distilled water, at pH 5. The solutions were purged continuously with nitrogen and kept in the dark. Humic acid (Aldrich) solutions were prepared by dissolving 10 mg dilute sodium hydroxide solution, diluting to 1 l with 0.7 mol l^{-1} sodium chloride and adjusting to pH 8.0.

Buffers used in this study were: acetate, pH 5—6; phosphate, pH 6—7.5; borate, pH $\geqslant$ 8. Buffer concentrations were kept as low as possible because all three form Cu(II) complexes. Generally, the buffer concentration was 10^{-3}—10^{-4} mol l^{-1}. For the stopped-flow kinetic studies, where precise pH control was important, 10^{-3} mol l^{-1} borate was used.

A Hewlett-Packard 8450 diode-array ultraviolet-visible spectrophotometer was used for all absorbance measurements. An Update Instruments stopped-flow spectrophotometer with a Tracor Northern (TN1710) u.v.-visible diode array detector was used for kinetic measurements of fast reactions. All lines and mixers in the system were teflon to avoid the problems of corrosion and contamination encountered with stainless steel.

Procedures

Absorbances were measured in 10-cm cylindrical cells. For experiments in deoxygenated systems, a 300-ml Erlenmeyer flask fitted with quartz windows with a 10-cm path length was used. The flask was continuously flushed with nitrogen during the experiments. To improve the signal-to-noise ratio, full u.v.-visible spectra (200—800 nm) were acquired 2 times per second for 10 s and then averaged. In addition to this signal averaging, routine individual sample runs were normalized by referencing to a background signal outside the absorption band for the complex. Under these operating conditions, the precision of the HP 8450 instrument was about ±0.0005 absorbance units.

The stopped-flow system was used to measure reduction rates of the bis(bathocuproine) copper(II) cation which under certain conditions were too rapid to be measured by other procedures. Reactions with half-lives greater than 10 ms could be studied. An advantage of this system was that more concentrated stock solutions of reducing agents could be used, which eliminated spurious results caused by contamination and oxidation observed in dilute solutions. A further advantage was that rapid mixing made it possible to distinguish reduction which occurred before or after addition of bathocuproine. For most experiments, three syringes were used in the system. Solutions from syringes 1 and 2 containing Cu(II) and reductant, respectively, were mixed in a teflon mixer and this solution was mixed with the assay reagents in syringe 3 in a second mixer. The reaction was then observed spectrophotometrically. Precision in these absorbance measurements was approximately 0.005 absorbance units.

RESULTS AND DISCUSSION

Spectral characteristics

Calibration graphs were made for the Cu(I)/bathocuproine complex in sea water, Milli-Q water and a 0.7 mol l^{-1} sodium chloride. The latter two were buffered at pH 8.1 with 10^{-4} mol l^{-1} borate. Aliquots of Cu(I) stock solution were added to the solutions, which contained 10^{-5} mol l^{-1} bathocuproine and were stirred rapidly. The molar absorptivities were calculated by linear regression of the calibration plots. The spectral characteristics for the Cu(I)/bathocuproine complex cation are λ_{max} = 484 nm, ϵ_{max} = 12,700 l mol^{-1} cm^{-1}, which are in reasonable agreement with earlier studies [3, 5]. The molar absorptivity exhibited no ionic medium dependence to a value of 0.7 mol l^{-1}. Solutions of 0.7 mol l^{-1} sodium chloride were maintained at a range of pH values between 5 and 8.1 with acetate, phosphate and borate buffers. Molar absorptivity was not a function of pH within this range.

The relative standard deviation for the molar absorptivity evaluations in sea water, Milli-Q water and 0.7 mol l^{-1} NaCl at pH 8.0 for 5 replicates was 2% in each solution. Absorbance was linear with concentration over the range 1×10^{-8} mol l^{-1} to 2×10^{-5} mol l^{-1}. The limit of detection for copper(I) in 0.7 mol l^{-1} NaCl solution based on a signal/noise ratio of 2:1, was 1×10^{-8} mol l^{-1}.

Complex stability

Calibration of standards was made in an identical manner to the above procedure at several pH values to determine the effect of pH on the absorptivity and stability of the Cu(I) complex. The absorbance was studied with time to indicate the stability of the complex as a function of pH in oxygenated solutions. In sea water, the complex was stable, as found by measuring absorbance for over an hour at pH values near 8. However, it exhibited some absorbance decay below pH 6 and rapid decay below pH 5. The pK_a of bathocuproine is approximately 5.6 (assuming that it is equivalent to that of 2,9-dimethyl-1,10-phenanthroline (neocuproine), pK_a = 5.6 [8]) and so exchange of a proton for Cu(I) in the complex followed by Cu(I) oxidation probably accounts for the decay observed. In oxygenated sea water, 100% yields of Cu(I) were obtained down to 3×10^{-6} mol l^{-1} bathocuproine. This indicates that the complex is very stable because chloride, which forms strong complexes with Cu(I) [9] is not able to compete. This is to be expected of bathocuproine because the stability constant for the Cu(I) complex of neocuproine is very high [8].

Interferences and masking ligands

The assay was evaluated for possible interference by common anions (i.e., nitrate, phosphate, bromide, perchlorate, sulfate, and borate) present at concentrations up to 10^{-3} mol l^{-1} at pH 7—8. No detectable interference could be measured at these concentrations which is in agreement with other work [5, 7]. Iron(II) is a major interference in copper(I) determinations with the parent compound 1,10-phenanthroline because it forms a strongly absorbing complex. However, bathocuproine does not form a colored complex with iron(II), because the methyl groups in the 2- and 9-positions of the 1,10-phenanthroline ring prevent Fe(II) complex formation [5].

To study the Cu(II) interference, standards were measured in 0.7 mol l^{-1} sodium chloride in the presence of 10^{-5} mol l^{-1} bathocuproine with 10^{-6} mol l^{-1} Cu(II) added. The result was identical to the previous measurements in solutions with no added Cu(II), indicating no interference in the absence of reducing agents. However, because preliminary studies indicated that Cu(II) interference occurs in the presence of reducing agents, a masking ligand for Cu(II) is necessary for unambiguous Cu(I) determination.

Initially, three masking ligands were studied: EDTA, histidine and ethylenediamine. However, only ethylenediamine was satisfactory. Histidine interacts strongly with Cu(I), lowering the assay yield unless it is present at levels too low to mask Cu(II) effectively, whereas EDTA interacts strongly with calcium and magnesium in sea water which limits its effectiveness as a masking ligand. Consequently, ethylenediamine was used in all subsequent experiments.

The assay yield as a function of ethylenediamine concentration was evaluated in the presence of oxidants such as oxygen. The variation of yield with ethylenediamine concentration in air-saturated saturated solutions at pH 8.0 is shown in Fig. 1; the yield decreases with increasing ethylenediamine

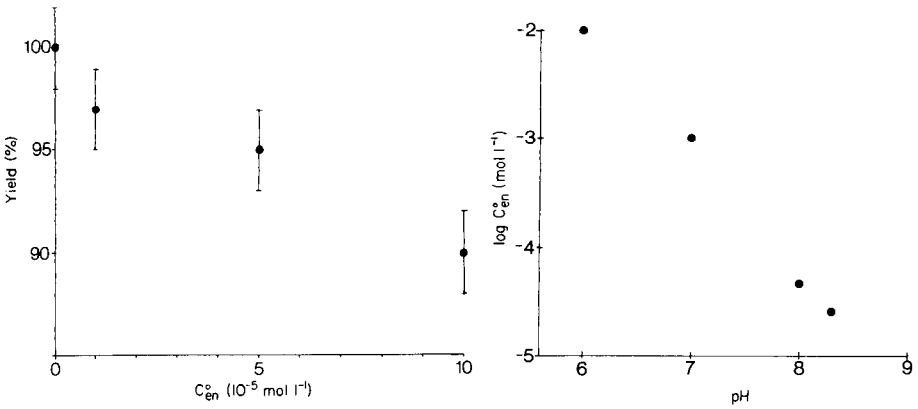

Fig. 1. The yield of Cu(I) as a function of ethylenediamine concentration in oxygenated 0.7 mol l^{-1} NaCl at pH 8.0 (10^{-5} mol l^{-1} bathocuproine present initially).

Fig. 2. Concentration of ethylenediamine to obtain a Cu(I) yield > 95% as a function of pH in 0.7 mol l^{-1} NaCl (10^{-5} mol l^{-1} bathocuproine present initially).

concentration. The effect of ethylenediamine concentration on yield is a function of the ratio of bathocuproine to ethylenediamine; the yield did not vary over the concentration range 10^{-5}—10^{-3} mol l^{-1} bathocuproine with a five-fold excess of ethylenediamine. In deoxygenated systems, however, much higher concentrations of ethylenediamine did not affect the yield. Other potentially important oxidizing species such as hydrogen peroxide and natural humic materials had a negligible effect on yield compared with oxygen.

The variation of yield with ethylenediamine concentration is highly pH-dependent. Figure 2 shows the maximum concentration of ethylenediamine which will give a Cu(I) yield $\geq$95% as a function of pH at an initial concentration of 1×10^{-5} mol l^{-1} bathocuproine. This pH-dependence probably indicates the importance of the unprotonated ethylenediamine species which represents a small, highly pH-dependent fraction of the total at the pH range studied here (pK_a ethylenediamine = 10 [8]).

Accuracy in Cu(I) oxidation studies

The oxidation of Cu(I) in air-saturated 0.7 mol l^{-1} chloride solution at pH 8 was followed by using the recommended assay. The results were compared with direct measurement of the u.v. spectra of Cu(I) in chloride media to evaluate the accuracy of the procedure. The oxidation is reversible and deviates from pseudo-first-order behavior almost immediately [1]. The experiment was therefore a test of the accuracy in the presence of oxygen, Cu(II) and reducing agents.

Copper(I) was added to the solution and its oxidation was followed by the bathocuproine assay by removing aliquots of solution and "quenching" with 10^{-5} mol l^{-1} bathocuproine and 10^{-5} mol l^{-1} ethylenediamine. Simultaneously, the u.v. spectrum of Cu(I) was observed directly and the decay of

a peak at 275 nm was followed. The peak corresponds to $CuCl_3^{2-}$ [10]; the molar absorptivity is 1730 l mol^{-1} cm^{-1}, based on total Cu(I). Copper(II) in chloride solution absorbs only weakly at this wavelength and so only a minor correction was necessary for the formation of Cu(II) during the course of the reaction.

The results obtained by using the two assays are shown in Fig. 3 and are identical within experimental error. Therefore, the bathocuproine assay provided an accurate measure of Cu(I) and there was no Cu(II) interference.

In most systems of interest, it is impossible to evaluate the assay by direct observation of the u.v. absorption of Cu(I) because other species interfere in this spectral region. Consequently, kinetic studies of Cu(II) interference reactions were made for a more general evaluation of the assay.

Stopped-flow experiments

The Cu(II) interference was studied with and without ethylenediamine in a series of stopped-flow experiments. All solutions were prepared in 0.7 mol l^{-1} sodium perchlorate buffered to pH 8.0 with borate. Rate constants for the reduction of the Cu(II)/bathocuproine complex were evaluated by mixing a solution containing the complex with the reductant and monitoring the absorbance. The results (Table 1) indicate that reduction of Cu(II) is indeed rapid once the complex forms.

Stopped-flow studies were then done to examine Cu(II) interference which might arise during an actual measurement when bathocuproine is added to a solution containing Cu(II) and a high concentration of reductant. These experiments were done under highly reducing conditions to maximize such interference. Deoxygenated solutions containing Cu(II) and reducing agents from syringes 1 and 2, respectively, were mixed and then combined with the assay reagents from syringe 3. The media were identical to those used in the previous experiments except that carbonate was also added to prevent precipitation of Cu(II) which was a problem at these concentrations in the absence of chelating ligands. The subsequent formation of the Cu(I)/bathocuproine complex was measured as a function of time from the

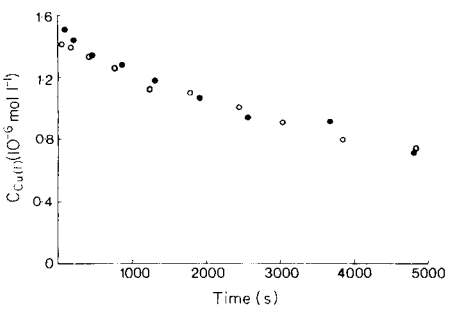

Fig. 3. Comparison of direct u.v. assay (○) and assay with 10^{-5} mol l^{-1} bathocuproine (●) during Cu(I) oxidation.

TABLE 1

Second-order rate constants for reduction of the Cu(II)/bathocuproine complex cation

Reductant	k_2 (mol^{-1} l s^{-1})
Hydroquinone	$4 \pm 1 \times 10^5$
Hydroxylamine	$7 \pm 1 \times 10^4$
Hydrogen peroxide	$2.2 \pm 0.5 \times 10^3$

bathocuproine addition. No Cu(I) was formed prior to addition of bathocuproine; all plots of absorbance vs. time went through the origin at $t = 0$.

The absorbance increase was measured as a function of time from the bathocuproine addition. Pseudo-first-order rate constants were calculated from the slopes of ln $(A_\infty - A_t)$ vs. time plots. These values were divided by reductant concentrations to give the second-order rate constants shown in Table 2. The standard error was about ±10%. These results indicate that Cu(II) reduction occurs more slowly than might be expected from rate data for the Cu(II)/bathocuproine complex reduction obtained above. This is evidently due to the masking of Cu(II) by ethylenediamine and the carbonate buffer (which was present at sea-water levels) which effectively slows down the formation of Cu(I) even at the reductant concentrations used in this experiment which were several orders of magnitude higher than those likely to be encountered in natural waters. In natural waters the concentration of reductants is a function of organic matter concentration, irradiation and other factors such as pO_2. Studies of the reducing properties of aquatic and soil humus indicate that this is unlikely to exceed 10^{-6} mol l^{-1} in natural waters with <10 mg l^{-1} humic material [11]. If this concentration of a reductant with similar kinetic properties to hydroquinone is assumed, then some calculations can be made based on these kinetic data. At pH 8 with $C^0_{BC} = 10^{-5}$ mol l^{-1}, $C^0_{en} = 10^{-4}$ mol l^{-1}, $C^0_{Cu(II)} = 10^{-6}$ mol l^{-1}, $C^0_{red} = 10^{-6}$ mol l^{-1} and $k_2 = 2.9 \times 10^2$ mol l^{-1} s^{-1} (Table 2), only 2% of the Cu(II) is reduced during 1 min, which is ample time to make a measurement. (Bathocuproine is abbreviated to BC and ethylenediamine to en.)

These conclusions were tested further by using natural reductants. Solutions containing 10 mg l^{-1} humic acid were irradiated for 2 h at 313 nm under a 1000-W HgXe lamp. Such treatment has been demonstrated to increase reducing properties [12]. Stopped-flow experiments similar to those described above were done with this material. In the absence of ethylenediamine, 40—50% of the Cu(II) was reduced within 10 s of addition of bathocuproine. In the presence of ethylenediamine no detectable Cu(II) reduction occurred up to 120 s after addition of bathocuproine.

Kinetic considerations

Ethylenediamine is an effective masking ligand because of its rapid rate of complexation with Cu(II). The second-order rate constant for this reaction is

TABLE 2

Reduction of Cu(II) initiated by the addition of bathocuproine to a Cu(II)/reductant mixture[a]

Reductant	C^0_{en}/C^0_{BC}	k_2 (mol^{-1} l s^{-1})	Reductant	C^0_{en}/C^0_{BC}	k_2 (mol^{-1} l s^{-1})
Hydroquinone	0	1.5×10^3	Hydroxylamine	10	4
	1	1.2×10^3	H_2O_2	0	3.2×10^1
	5	2.9×10^2		1	0
	10	2.0×10^2			

[a]Initial concentrations in syringes: $C^0_{Cu(II)} = 3 \times 10^{-5}$ mol l^{-1} Cu(II), 3×10^{-4} mol l^{-1} hydroquinone, 3×10^{-4} mol l^{-1} hydroxylamine, 3×10^{-3} mol l^{-1} bathocuproine, 3×10^{-3} mol l^{-1} H_2O_2.

2×10^9 mol^{-1} l s^{-1} [13]. The corresponding value for 1,10-phenanthroline is only 2×10^7 mol^{-1} l s^{-1} [14]. For bathocuproine, steric hindrance from methyl groups in the 2- and 9-positions probably leads to even slower complexation, particularly for coordination of the second bathocuproine molecule. Although at pH 8.0 only 1% of the ethylenediamine is present in the neutral form, it was used at a 5-fold excess over bathocuproine with only a slight effect on copper(I) yields in oxygenated systems. The rapid rate of Cu(II) complexation with ethylenediamine and high stability of the resulting mono and bis complexes inhibits Cu(II) reduction and accounts for these observations.

Optimum reagent concentrations

The results obtained in this study provide guidelines to select optimal reagent concentrations, which will vary with different experimental conditions. The concentrations of bathocuproine and ethylenediamine should be high enough to ensure complete chelation of Cu(I) and Cu(II), respectively. The concentration of ethylenediamine should be high enough to inhibit Cu(II) interference without significantly lowering Cu(I) yield. Results indicate that this is a function of pH, oxygen and bathocuproine concentration. For studies at pH 8.0, concentrations generally used were $C^0_{BC} = 10^{-5}$ mol l^{-1} and $C^0_{en} = 5 \times 10^{-5}$ mol l^{-1} for assay between 10^{-6} and 10^{-6} mol l^{-1} Cu(I). The yield at this pH was only 95 ± 2% but this was consistent over a wide concentration range. Furthermore, the five-fold excess of masking ligand inhibited Cu(II) interference more effectively than at lower concentrations; using less ethylenediamine resulted in only a minor increase in yield. However, in some studies such as Cu(I) oxidation, a 1:1 mole ratio of ethylenediamine to bathocuproine was sufficient to eliminate Cu(II) interference. In deoxygenated systems, higher concentrations of ethylenediamine can be used but this may render the yield sensitive to traces of oxygen or other oxidants. Therefore, in this work ethylenediamine was never used at higher than a ten-fold excess at pH 8.0 in deoxygenated systems.

Applications

Most of the experimental conditions in this study represent extreme situations in which conditions leading to Cu(II) interference were maximized. The inhibition of Cu(II) interference under these conditions indicates that the procedure is potentially useful in a variety of aqueous systems. While the emphasis has been on sea-water in this study, the procedure is also applicable to other natural waters and to other aqueous media in chemical and biochemical studies. The procedure is not suitable at natural concentrations of copper, which are at least an order of magnitude below the detection limit. However, it is suitable for laboratory studies modelling natural redox processes, for which purpose the convenience, selectivity and sensitivity make it useful. The technique is not suitable for use at low pH, or in media in which strong chelation of Cu(I) prevents complex formation with bathocuproine. It is probably not suitable in highly reducing environments such as anoxic pore waters without prior investigation of potential artefacts. Nevertheless, it is a valid procedure for copper redox studies because steps can be taken to minimize perturbations of the system resulting from addition of the chelating ligand, on the time scale of the measurement.

Technical assistance from Dave Odum and Mike Slifker in assembling and operating the stopped-flow system is gratefully acknowledged. This investigation was supported by a grant from the Office of Naval Research (N00014-80-C-0042).

REFERENCES

1 J. W. Moffett and R. G. Zika, Mar. Chem., 13 (1983) 239.
2 G. F. Smith and D. H. Wilkins, Anal. Chem., 25 (1953) 510.
3 B. Zak, Clin. Chim. Acta, 3 (1958) 328.
4 E. B. Sandell, Colorimetric Determination of Traces and Metals, 3rd edn., Interscience, New York, 1959.
5 A. A. Schilt, Analytical Applications of 1,10-Phenanthroline and Related Compounds, Pergamon Press, Oxford, 1969.
6 H. Mason and K. Ganapathy, J. Biol. Chem., 245 (1970) 230.
7 A. T. Pilipenko and E. R. Falendysh, Russ. Chem. Rev., 41(11) (1972) 991.
8 R. M. Smith and A. E. Martell, Critical Stability Constants, Vol. 2, Plenum, New York, 1975.
9 S. Ahrland and J. Rawthorne, Acta Chem. Scand., 24 (1970) 157.
10 K. Sugasaka and A. Fujii, Bull. Chem. Soc. Jpn., 49(1) (1976) 82.
11 S. A. Wilson and J. H. Weber, Chem. Geol., 26 (1979) 345.
12 T. D. Waite and F. M. M. Morel, Anal. Chim. Acta, 162 (1984) 263.
13 L. Kirschenbaum and K. Kustin, J. Chem. Soc. A, (1970) 648.
14 R. H. Hoyler, C. D. Hubbard, S. F. A. Kettle and R. G. Wilkins, Inorg. Chem., 4 (1965) 929.

Analytica Chimica Acta, 175 (1985) 181—188
Elsevier Science Publishers B.V., Amsterdam — Printed in The Netherlands

LUMINESCENCE DETERMINATION OF BENZOQUINOLINE ISOMERS IN COMPLEX SAMPLES

T. VO-DINH*, G. H. MILLER, D. W. ABBOTT[a], R. L. MOODY, C. Y. MA and C.-H. HO

Health and Safety Research Division, Analytical Chemistry Division, Oak Ridge National Laboratory, Oak Ridge, TN 37831 (U.S.A.)

(Received 3rd April 1985)

SUMMARY

The room-temperature phosphorescence (r.t.p.) and fluorescence spectra of benzoquinoline isomers are investigated. The isomers can be resolved into the linear or angular subgroups on the basis of their fluorescence and r.t.p. spectra by using conventional fixed excitation. Second-derivative and synchronous scanning techniques can be combined to improve the selectivity of the r.t.p. and fluorescence methods. These simple luminescence techniques were used to estimate three benzoquinoline isomers in a coal tar fraction. Direct analysis of this complex sample allowed acridine to be estimated and upper limits to be provided for benzo(h)quinoline and phenanthridine; the presence of three other isomers was not detected. Comparative studies with data obtained by high-performance liquid chromatography are reported.

The detection of aza-arenes is of great importance because these compounds, e.g., quinolines and benzoquinolines, are found in a wide variety of environmental samples including fossil fuels, automobile exhaust, lake sediments, and urban air [1—3]. The presence of these compounds in the environment has often been attributed to the use of fossil fuels [4]. Bioassay studies found three of the five isomers of benzoquinoline investigated, viz., benzo(f)quinoline, benzo(h)quinoline, and phenanthridine, to be mutagenic [4, 5]. Recent investigations have identified benz(g)isoquinoline-5,10-dione, as a primary contributor to insect teratogenicity in commercial acridine [6, 7]. Benz(c)acridine has been listed by the U.S. Environmental Protection Agency as a hazardous pollutant [8]. Various biological effects of acridine derivatives are reported to be closely linked with their ability to form complexes with nucleic acids [9]. In this study, further evaluation of two simple luminescence techniques, room-temperature phosphorimetry (r.t.p.) and synchronous luminescence spectrometry (s.l.s.) is reported for the identification and quantification of several isomeric benzoquinolines. These two spectrometric techniques have recently been reviewed [10, 11]. In this paper, the spectral characteristics of the compounds of interest are discussed in detail. An example of the determination of benzoquinoline isomers in a coal tar fraction

[a]Present address: Great Lake Chemicals Company, West Lafayette, IN 47906, U.S.A.

0003-2670/85/$03.30

illustrates the applicability of the spectrometric techniques. The results obtained by r.t.p. and s.l.s. are compared with data obtained by high-performance liquid chromatography (h.p.l.c.) and gas chromatography/mass spectrometry (g.c./m.s.) measurements.

EXPERIMENTAL

Instruments and techniques

Luminescence measurements. Fluorescence measurements were made with a Perkin-Elmer spectrofluorimeter (Model 650-40) equipped with a R928 photomultiplier tube. Standard quartz cells were used for the fluorescence measurements of liquid samples. A 150-W xenon lamp was used for excitation. The spectral bandwidth of the monochromator for fluorescence measurements was 1.5 nm. A wavelength interval, $\Delta\lambda$ = 3 nm, was used for synchronous fluorescence (s.f.) measurements.

Room-temperature phosphorescence measurements were conducted with a Perkin-Elmer spectrometer (Model 43A) equipped with a rotating phosphoroscope. Although several types of substrates may be used, the substrate preferred here was filter paper. Prior to sample delivery, the filter paper was spotted with a heavy-atom salt solution in order to increase the phosphorescence signal. A 2.5-μl sample solution was then spotted on the filter paper and, after a 5-min drying period, phosphorescence was measured. During the measurements, warm dry air was passed through the sample compartment to prevent r.t.p. quenching by moisture.

Analyses by h.p.l.c. and g.c./m.s. An h.p.l.c. system (Beckman, Model 345 Ternary Liquid Chromatograph) was used for the determination of benzoquinoline isomers in a fraction of a coal tar. The subfractions were also examined by g.c./m.s. (Hewlett-Packard, Model 5985A) set on both electron-impact and total-ion monitoring modes, to ensure the correct identification of the isomeric components. The identity of each benzoquinoline isomer was established by comparing g.c. and h.p.l.c. retention times with those of the reference standard. Each isomer was quantified by the internal standard method.

Materials and reagents

Reference standards. The structures of the eight benzoquinoline isomers studied are shown below. Acridine (I), benzo(f)quinoline (IV), benzo(h)-quinoline (VI) and phenanthridine (benzo(c)quinoline (VIII)) from Aldrich Chemical Company were purified by high-performance liquid chromatography. The remaining four isomers were prepared by unequivocal synthesis as follows. Benz(f)isoquinoline (V) and benz(h)isoquinoline (VII) were synthesized via photochemical cyclization of 3-stilbazole and 4-stilbazole, respectively [12]. Benzo(g)quinoline (II) and benz(g)isoquinoline (III) were synthesized by reduction of their dione derivatives [13, 14]. Correct structures were confirmed with mass spectrometry, infrared and ^{1}H-, ^{13}C-nuclear magnetic resonance spectra.

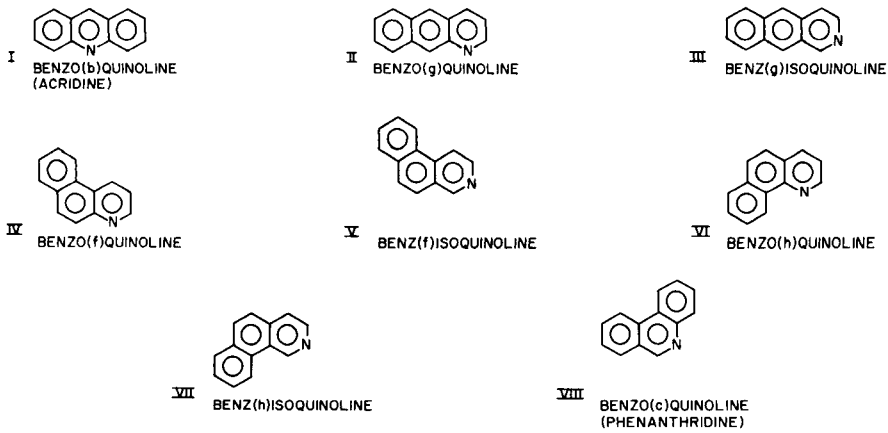

Coal tar fraction preparation. A gasifier tar sample (b.p. 300—413°C) collected from the electrostatic precipitator of the University of Minnesota-Duluth (UMD) low-BTU coal gasifier, was obtained from the U.S. Environmental Protection Agency/Department of Energy (EPA/DOE) Fossil Fuel Research Material Facility [15].

The basic fraction of the sample was generated by partitioning the sample between diethyl ether and 5 M hydrochloric acid [16]. An aliquot of the basic fraction (ca. 50 mg) was then injected into a preparative Zorbax-ODS column (250 mm × 21.2 mm i.d.), and then eluted with 80% (v/v) methanol in water at a flow rate of 6.2 ml min^{-1}. The benzoquinoline subfraction was collected in the retention time interval between 26.8 and 36.8 min. This retention time interval was predetermined with the eight reference standards.

RESULTS AND DISCUSSION

Luminescence spectra of benzoquinoline isomers

All the benzoquinoline isomers studied yield measurable fluorescence spectra at room temperature. The fluorescence and phosphorescence (r.t.p.) maxima of the benzoquinoline isomers are summarized in Table 1. The linear benzoquinoline isomers, benzo(b)quinoline (i.e., acridine), benzo(g)quinoline and benz(g)isoquinoline, exhibit maximum intensities at lower excitation and emission energies than do the five angular isomers.

All three of the linear isomers exhibit an excitation maximum in the 375—390 nm range, and an emission maximum in the 405—425 nm range. Acridine is only weakly fluorescent at room temperature, while benzo(g)quinoline and benz(g)isoquinoline yield relatively more intense fluorescence under the same conditions. The structure of the fluorescence spectra of benz(g)isoquinoline is better resolved than that of benz(g)quinoline. Synchronous fluorescence (s.f.) measurements with $\Delta\lambda = 3$ nm show a single peak for each linear benzoquinoline isomer in the 390—400 nm region.

The five angular isomers, benzo(f)quinoline, benz(f)isoquinoline, benzo-

TABLE 1

Location of maximum intensity in the fluorescence and phosphorescence spectra of benzoquinolines

Compound	Fluorescence			Phosphorescence		
	λ_{ex} (nm)	λ_{em} (nm)	$\Delta\lambda_{syn}$[a] (nm)	λ_{ex} (nm)	λ_{em}[b] (nm)	$\Delta\lambda_{syn}$[c] (nm)
Acridine	376	408	400	361	638	639 (254)
Benzo(g)quinoline	363	422	395	ND[d]	ND	—
Benz(g)isoquinoline	388	420	393	ND	ND	—
Benzo(f)quinoline	346	365	352	349	504	472 (122)
Benzo(h)quinoline	346	367	354	350	506	474 (124)
Benz(f)isoquinoline	346	368	352	354	506	475 (120)
Benz(h)isoquinoline	342	360	346	309	507	468 (120)
Phenanthridine	344	365	349	309	500	466 (118)

[a]Synchronous fluorescence at $\Delta\lambda$ of 3 nm. [b]Emission phosphorescence maximum with excitation at 354 nm. [c]Synchronous phosphorescence spectrum maximum with $\Delta\lambda$ value indicated in parentheses. [d]No phosphorescence activity was detected at the concentration levels available for testing.

(h)quinoline, benz(h)isoquinoline and benzo(c)quinoline (i.e., phenanthridine), exhibit similar fluorescence excitation and emission spectra under fixed excitation and emission conditions. All five angular isomers have their excitation maxima in the 342—346 nm range, while their emission maxima are in the 360—370 nm range. They are also similar in overall spectral structure and fluorescence intensity (Fig. 1). The s.f. spectra ($\Delta\lambda$ = 3 nm) of the angular isomers have one major peak in the 345—355 nm range.

Fluorescence measurements can thus be used to separate the linear benzoquinoline isomers from the angular isomers. Further differentiation within the structural subgroups by using conventional fixed-excitation or fixed-

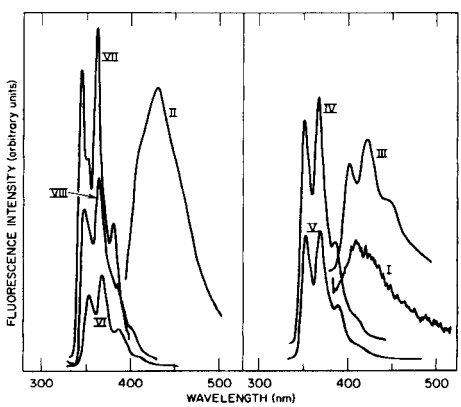

Fig. 1. Fluorescence spectra of benzoquinoline isomers.

emission luminescence techniques is a much more difficult task. Under certain conditions, s.f.s. may be used to resolve selected angular isomers in complex mixtures, as discussed below.

The benzoquinoline isomers can also be separated into the appropriate linear or angular subgroup on the basis of their r.t.p. excitation and emission spectra (Fig. 2). Acridine has its excitation maximum at 361 nm and its emission maximum at 638 nm. Synchronous r.t.p. measurements ($\Delta\lambda$ = 254 nm) revealed a peak at 639 nm. Interestingly, benzo(g)quinoline and benz(g)isoquinoline, the other two linear isomers, do not yield phosphorescence spectra under the conditions used in these studies.

The r.t.p. excitation spectrum of benz(h)isoquinoline is noticeably different from those of the other angular benzoquinoline isomers. While all five angular isomers yield excitation spectra containing peaks at similar wavelengths, the benz(h)isoquinoline maximum at 308 nm is greatly enhanced whereas the one at 345 nm is less intense than is observed for the other isomers. The excitation spectrum of phenanthridine appears to be intermediate between that of benz(h)isoquinoline and those of the remaining angular isomers. The fixed-excitation r.t.p. spectra of all five angular isomers are also similar, with maxima in the 465—475 nm region. The synchronous r.t.p. spectra of these isomers all exhibit large peaks in the 465—475 nm region (Table 1). From these results, acridine emissions may be readily identified even in the presence of the other acridine isomers.

Second-derivative spectra. The second-derivative (d^2) technique can be combined with synchronous excitation to enhance further the selectivity of

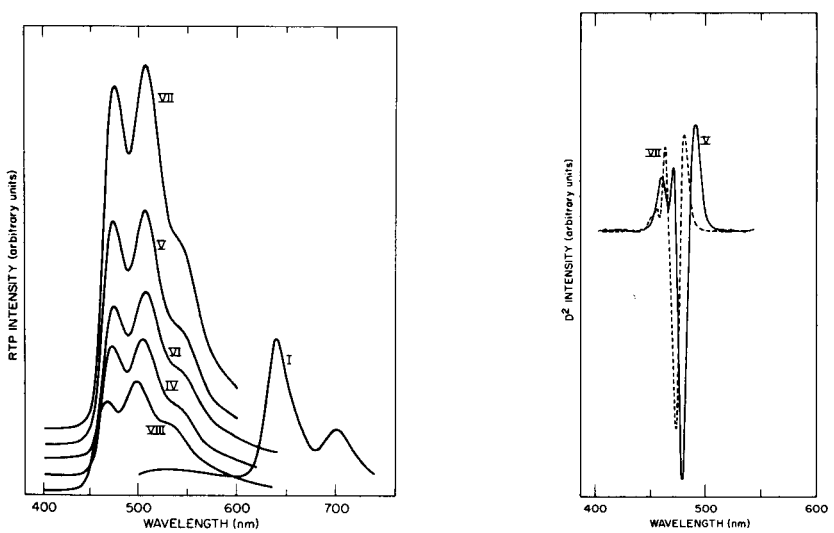

Fig. 2. Room-temperature phosphorescence spectra of benzoquinoline isomers.

Fig. 3. Differentiation between benz(h)isoquinoline (VII) and benz(f)isoquinoline (V) by second-derivative synchronous r.t.p. spectra.

r.t.p. spectrometry of benzoquinoline isomers. In the d^2 mode, a signal proportional to the second-derivative with respect to wavelength is recorded. Because one measures the rate of change in the curvature of a peak in the d^2 mode, not only the intensity but also the bandwidth of an emission peak are important factors. Broad peaks are reduced while narrow spectral bands are intensified. This feature is an important advantage in r.t.p. spectrometry because the broad structure of the paper background r.t.p. emission can be significantly reduced [17]. Figure 3 depicts the d^2 spectra of benz(f)isoquinoline and benz(h)isoquinoline for $\Delta\lambda$ = 120 nm. These two isomers, which have similar fixed-excitation r.t.p. spectra (Fig. 2) can be differentiated by their narrow d^2 peaks separated by 8 nm from each other.

Analysis of a coal tar fraction by luminescence methods

Analysis of the coal tar fraction sample was done with synchronous fluorescence, synchronous r.t.p., and the second-derivative method. The luminescence data were compared with results obtained independently by h.p.l.c. These results are summarized in Table 2.

The s.f. measurement ($\Delta\lambda$ = 3 nm) of the diluted sample yielded a very complex spectrum, to which the benzoquinoline isomers made only a small contribution. Several minor peaks were observed in the region expected to reflect the presence of the angular benzoquinoline isomers (345—355 nm); there was no evidence of the presence of linear isomers. The standard addition method of analysis was used to ensure that the correct peak was chosen for quantitation purposes. Good agreement was obtained between the s.l. and h.p.l.c. results for benz(h)isoquinoline and phenanthridine (Table 2). The results for these two isomers should be considered as the upper limit for each isomer, because of the close proximity of the s.f. peaks for the bent isomers and the likelihood of some degree of peak overlap. The benzo(f)quinoline, benzo(g)quinoline and benz(g)isoquinoline contents obtained by the h.p.l.c. method could not be substantiated by the s.l. measurements. These

TABLE 2

Estimation of benzoquinoline isomers in a coal-derived tar sample

Isomer	Isomer found ($\mu g\ g^{-1}$)	
	H.p.l.c.	S.f. and r.t.p.
Benzo(h)quinoline	20	$<47 \pm 15$[a]
Phenanthridine	32	$<133 \pm 45$[a]
Acridine	236	416 ± 140[b]
Benzo(g)quinoline	10.1	NQ[c]
Benz(g)isoquinoline	4.0	NQ
Benzo(f)quinoline	5.2	NQ

[a]Synchronous fluorescence ($\Delta\lambda$ = 3 nm). [b]Synchronous room-temperature phosphorescence ($\Delta\lambda$ = 280 nm, Hg(II) as heavy atom). [c]Not quantifiable because of spectral overlap.

compounds were very minor components of the overall complex sample, and could not be identified with certainty by luminescence spectrometry.

The synchronous r.t.p. ($\Delta\lambda$ = 254 nm) spectrum of the coal tar fraction was relatively broad and featureless when Pb^{2+}/Tl^{+} was used as the heavy-atom perturber. The use of mercury(II) to enhance the r.t.p. emissions of azaarenes while quenching those of polyaromatic hydrocarbons has recently been reported [18]. Therefore, the coal tar fraction was examined by synchronous r.t.p. in the presence of mercury(II), and the acridine peak was identified. A $\Delta\lambda$ value of 280 nm was also used to reduce interferences. The standard addition evaluation of this peak yielded a result of 416 ± 140 ppm, in semiquantitative agreement with the h.p.l.c. findings. No analysis for benzo(g)quinoline and benz(g)isoquinoline was made because these compounds do not give detectable r.t.p. emissions.

Conclusion

The eight benzoquinoline isomers studied here can be resolved into structural subgroups by the use of fluorescence and r.t.p. techniques. Differentiation among the five angular isomers by using conventional fixed-excitation luminescence is difficult, because of the similarity of their luminescence spectra. The linear isomers are somewhat easier to resolve because acridine has only weak solution fluorescence and benzo(g)quinoline and benz(g)isoquinoline do not phosphoresce at room temperature. The benzoquinoline isomers can be identified and semi-quantified in complex samples on the basis of their luminescence spectra. Acridine is by far the easiest isomer to differentiate, because of its lower phosphorescence emission energy. The use of synchronous luminescence, synchronous r.t.p. and its second-derivative modification, and an appropriate choice of heavy-atom perturbers combine to enhance the ability of luminescence methods to resolve similar isomers in a complex sample such as a coal tar fraction. However, substantial differences between the h.p.l.c. and luminescence results suggest that the luminescence measurements can be used as screening tools but need to be combined with suitable separation methods for good quantitative results with complex samples such as those examined here.

This research was sponsored by the Office of Health and Environmental Research, U.S. Department of Energy, under contract DE-AC05-840R21400 with Martin Marietta Energy Systems, Inc.

REFERENCES

1 E. Sawicki, J. E. Meeker and M. J. Morgan, Int. J. Air Water Pollut., 9 (1965) 291.
2 M. W. Dong, D. C. Locke and D. Hoffman, Environ. Sci. Technol., 11 (1977) 612.
3 M. Blumer and T. Dorsey, Science, 195 (1977) 282.
4 S. G. Wakeham, Environ. Sci. Technol., 13 (1979) 118.
5 E. A. Adams, E. J. Lavoie and D. Hoffman, in M. Cooke and A. J. Dennis (Eds.), Polynuclear Aromatic Hydrocarbons: Formation, Metabolism and Measurement, 1983, Batelle Press, Columbia, OH, pp. 73—87.

6 B. T. Walton, C. H. Ho, C. Y. Ma, E. G. O'Neill and G. H. Kao, Science, 222 (1983) 422.
7 C. Y. Ma, C. H. Ho, B. T. Walton, G. L. Kao and M. R. Guerin, Environ. Sci. Technol., 18 (1984) 362.
8 U. S. Environmental Protection Agency, Federal Register, 45 (98) (1979) 33119.
9 R. M. Acheson, Acridines, Wiley-Interscience, New York, 1973.
10 T. Vo-Dinh, Room Temperature Phosphorimetry for Chemical Analysis, Wiley-Interscience, New York, 1984.
11 T. Vo-Dinh, in E. L. Wehry (Ed.), Modern Fluorescence Spectroscopy, Vol. 4, Plenum Press, New York, 1981, pp. 167—192.
12 C. E. Loader, M. V. Sargent and C. J. Timmons, Chem. Commun., 7 (1965) 127.
13 A. Philips, Chem. Ber., 27 (1894) 1923; 28 (1895) 1658.
14 A. Etienne, Ann. Chim., 12 (1946) 16.
15 W. H. Griest, D. L. Coffin and M. R. Guerin, Fossil Fuels Research Matrix Program, ORNL-TM-7346, Oak Ridge National Laboratory, Oak Ridge, TN, June, 1980.
16 I. B. Rubin, M. R. Guerin, A. A. Hardigree and J. L. Epler, Environ. Res., 12 (1976) 358.
17 T. Vo-Dinh and R. B. Gammage, Anal. Chim. Acta, 107 (1979) 261.
18 D. W. Abbott and T. Vo-Dinh, Anal. Chem., 56 (1984) 1667.

Analytica Chimica Acta, 175 (1985) 189—201
Elsevier Science Publishers B.V., Amsterdam — Printed in The Netherlands

THERMODYNAMIC BINDING PARAMETERS EVALUATED BY USING PHASE-RESOLVED FLUORESCENCE SPECTROMETRY

FRANK V. BRIGHT[a], TERESA L. KEIMIG and LINDA B. McGOWN*
Department of Chemistry, Oklahoma State University, Stillwater, OK 74078 (U.S.A.)
(Received 25th March 1985)

SUMMARY

Equilibrium binding constants as a function of temperature were determined for the binding of 4-amino-*N*-methylphthalimide (4-AMP) to β-cyclodextrin and to human and bovine serum albumins, and for 6-propionyl-2-(dimethylamino)naphthalene (PRODAN) to β-cyclodextrin, by using phase-resolved fluorimetry to eliminate errors from the significant fluorescence contribution from the free 4-AMP or PRODAN. Enthalpy and entropy values were also calculated from these experimental data.

Phase-resolved fluorescence spectroscopy (p.r.f.s.) [1—3] provides a relatively simple, convenient means for implementing selectivity based on fluorescence lifetime (τ). The method is based on the phase-modulation approach for the determination of fluorescence lifetimes [4—6]. The phase-resolved fluorescence intensity (p.r.f.i.) is a time-independent signal proportional to the cosine difference between the detector phase angle (i.e., the relative position of the *k*-gate interval, ϕ_D, variable from 0 to 360°) and the phase angle of the fluorescing species (ϕ). For a sample containing *j* uncorrelated (non-interacting) fluorophores, the p.r.f.i. takes the form

$$\text{p.r.f.i.}(\phi_D) = \sum_{i=1}^{j} [A_{em_i} m_{ex} m_i \cos(\phi_D - \phi_i)] \quad (1)$$

where m_{ex} is the excitation beam modulation (ratio of a.c. to d.c. signals), and m_i is the demodulation factor ($\cos \phi_i = m_i$) and A_{em_i} is the d.c. emission component of the fluorescence signal of the *i*th fluorophore.

Several different p.r.f.s. approaches have been developed by which the individual components of a two-component system can be simultaneously determined. In the direct nulling approach [1, 2], the null phase angle for each component in a two-component system (A and B) is located using a standard solution of the component. The null phase angle of a component is the ϕ_D setting at which the p.r.f.i. of the component is zero, i.e., the angle at

---

[a]Present address: Department of Chemistry, University of Indiana, Bloomington, IN 47405, U.S.A.

0003-2670/85/$03.30

which the detector phase is exactly out of phase with that component [$\phi_D = (\phi_{comp} \pm 90°)$]. For example, if the ϕ_D setting were $\phi_A + 90°$, the p.r.f.i would take the form

$$\text{p.r.f.i.} = A_{em_B} m_{ex} m_B \sin(\phi_B - \phi_A) \quad (2)$$

and only the contribution from species B would be observed. The p.r.f.i. for the non-nulled component, B, is proportional to sin $(\phi_B - \phi_A)$, so that as ϕ_A approaches ϕ_B, the p.r.f.i. for component B will approach zero. Conversely, one could obtain the contribution from A alone at $\phi_D = (\phi_B - 90°)$, attenuated by sin $(\phi_B - \phi_A)$. Direct nulling is also useful for systems containing two or more components in which a standard can be prepared for only one of the components, if the goal of the experiment is to eliminate interference of that component to allow measurements of the remaining component(s).

A different approach can be taken to determine two or more components simultaneously; the p.r.f.i is measured at a series of detector phase angles for the mixtures and the standards of the individual components [7—9]. A curve can then be fitted for the p.r.f.i vs. ϕ_D function for each solution. Values of p.r.f.i. can be obtained from the curve at appropriate ϕ_D values to generate a series of simultaneous equations which can be solved for the concentrations of the individual components [8, 10].

The work described here demonstrates the use of both the direct nulling and simultaneous equation approaches for the evaluation of equilibrium constants (K), from which entropy (ΔS), and enthalpy (ΔH) values were then calculated, for the association of 4-amino-*N*-methylphthalimide (4-AMP) with β-cyclodextrin (β-CD), bovine and human serum albumin (BSA and HSA), and of 6-propionyl-2-(dimethylamino)naphthalene (PRODAN) with β-CD. The use of conventional steady-state fluorimetric measurements for the determination of these K values is subject to error caused by fluorescence contributions from the non-associated species, which can be overcome by using p.r.f.s. All three 4-AMP complexes were studied by the direct nulling approach, and the two albumin complexes were also studied by heterogeneity analysis of the fluorescence decay. The inclusion-complex between β-CD and PRODAN was studied by the simultaneous equation approach.

Evaluation of equilibrium binding constants

The equilibrium constant (K) for the association between fluorescent species (S) and "binder" (B), S + B ⇌ SB, takes the form $K = [SB]/([S][B])$. In this work, S is 4-AMP or PRODAN and B is β-CD, BSA or HSA. The classical method for the determination of K was developed by Benesi and Hildebrand [11]. The equilibrium expression can be rewritten as

$$K = [SB]/\{(C_S - [SB])(C_B - [SB])\} \quad (3)$$

where C_S and C_B are the analytical concentrations of S and B. If the concentration of ligand is very large with respect to complex ($C_B \gg [SB]$) then Eqn. 3 becomes

$$K = [SB]/\{(C_S - [SB])(C_B)\} \quad (4)$$

The general fluorescence quantum yield expression for SB takes the form

$$Q_{SB} = F_{SB}/\{k_{SB}[SB]\} \quad (5)$$

where Q_{SB} is the quantum yield for the complex, F_{SB} is the fluorescence signal from this complex, and k_{SB} is a constant characteristic of the fluorophore and instrumental parameters. Multiplication of Eqn. 4 by Eqn. 5, division by F_{SB} and rearrangement yields

$$C_S/F_{SB} = \{(Kk_{SB}Q_{SB})^{-1}(C_B)^{-1}\} + (k_{SB}Q_{SB})^{-1} \quad (6)$$

A plot of C_S/F_{SB} vs. $1/C_B$ yields K. Measurement of F_{SB} by conventional steady-state fluorimetry requires determination of the fluorescence signal, F_{S°, for a solution containing only S, which is subtracted from the total fluorescence signals (F_t) for solutions containing the same C_S at each binder concentration. To determine F_{SB}, F_{S° is subtracted from F_t. This method, however, can introduce a significant negative error in F_{SB} if Q_S is not very small relative to Q_{SB} (assuming that the molar absorptivities ϵ_S and ϵ_{SB} are equal), because the concentration of free S decreases as C_B increases. In these cases, the intensity, F_S, from the actual amount of S present at each C_B should be subtracted from F_t. However, if the spectra of S and SB are highly overlapping, it is not possible to measure the individual contributions of the two species to F_t. The addition of B (β-CD, BSA or HSA) causes the hypsochromic shifting of the emission spectrum of S (4-AMP) upon binding, along with an increase in the fluorescence signal. However, spectral overlap of S and SB fluorescence are extensive enough to preclude determination of either species in the presence of the other.

If S and SB have sufficiently different fluorescence lifetimes, p.r.f.s. can be used to study the equilibrium for the system. The p.r.f.i. can be expressed as

$$\text{p.r.f.i.}\ (\phi_D) = A_{em_S} m_{ex} m_S \cos(\phi_D - \phi_S) + A_{em_{SB}} m_{ex} m_{SB} \cos(\phi_D - \phi_{SB}) \quad (7)$$

The p.r.f.i. for SB can be measured by adjusting the phase angle of the detector to null the contribution from free S [$\phi_D = (\phi_S + 90°)$] regardless of its concentration. The measured p.r.f.i for the solution is then due only to emission from SB

$$\text{p.r.f.i.} = A_{em_{SB}} m_{ex} m_{SB} \sin(\phi_{SB} - \phi_S) \quad (8)$$

and is directly proportional to [SB]. A plot of $C_S/\{\text{p.r.f.i. [SB]}\}$ vs. $1/C_B$ will yield an equilibrium constant devoid of any error caused by the changing contribution of free S to the steady-state fluorescence intensity.

The simultaneous equation approach could also be used if a standard solution of SB can be prepared in which essentially all of the S is associated with B ([SB] = C_S). When a series of n detector phase angles is used, this approach is capable of evaluating the equilibrium concentrations of S and SB by solving the augmented matrix system [8, 10]

$$\begin{bmatrix} \bar{I}_{S,\phi_1} & \bar{I}_{SB,\phi_1} \\ \cdot & \cdot \\ \cdot & \cdot \\ \cdot & \cdot \\ \bar{I}_{S,\phi_n} & \bar{I}_{SB,\phi_n} \end{bmatrix} \begin{bmatrix} [S] \\ \\ \\ [SB] \end{bmatrix} = \begin{bmatrix} I_{\phi_1} \\ \cdot \\ \cdot \\ \cdot \\ I_{\phi_n} \end{bmatrix} \quad (9)$$

where the $\bar{I}$'s represent the p.r.f.i. per μM amount of S or SB in the standard solutions and the I's represent the p.r.f.i. for samples containing intermediate amounts of B. Then K is directly determined by substituting the values found for [S] and [SB] into Eqn. 3 or 4.

EXPERIMENTAL

Materials

1,4-Bis(4-methyl-5-phenyloxazol-2-yl)benzene (Me_2POPOP; Aldrich) in absolute ethanol (U.S. Industrial Chemical Co.) was used as the reference fluorophore for all fluorescence lifetime determinations [12]. 4-Amino-*N*-methylphthalimide (4-AMP; Aldrich) was prepared in distilled-deionized water by weighing 0.0176 g of 4-AMP, diluting to 100.0 ml and sonicating for 4 h. This solution was then filtered and diluted (1 + 1) with distilled-deionized water yielding a working solution of 0.500 mM 4-AMP. β-Cyclodextrin (β-CD, Sigma) was prepared by weighing 1.7172 g of β-CD and diluting to 100.0 ml with distilled-deionized water, sonicating for 2 h and filtering, yielding a 15.13 mM β-CD working solution. 6-Propionyl-2-(dimethylamino)-naphthalene (PRODAN) was a gift from Professor David M. Jameson and a standard solution was prepared by weighing 0.0794 g of PRODAN and diluting to 100.0 ml with distilled-deionized water and sonicating overnight, followed by filtration and 100-fold dilution, yielding a 3.50 μM PRODAN solution. Bovine serum albumin (BSA; Sigma, cat. no. A-6003) and human serum albumin (HSA; Sigma, cat. no. A-8763) solutions (2.00×10^{-4} M) were prepared by weighing 1.34 g of albumin and diluting to 100.0 ml with pH 7.00, 0.10 M phosphate buffer. Mixtures and blanks (solutions containing no fluorophore) were prepared by combining the appropriate volumes of the standards with distilled-deionized water in individual disposable polyethylene cuvets (Precision Cells).

Data collection

All u.v.-visible absorption measurements were made with a Hitachi 100-80A spectrophotometer (Lee Scientific, Houston, TX). All steady-state and phase-resolved fluorescence measurements were made with an SLM 4800S spectrofluorimeter (SLM/Aminco, Urbana, IL) with a 450-W xenon arc source and Hamamatsu R928 photomultiplier tube detection. An excitation polarizer at 35° was used to eliminate Brownian rotation effects [13]. The slits were set at 16, 0.5, 0.5, 16, and 16 nm for the excitation monochromator entrance and exit, modulation tank exit, emission monochromator entrance and exit,

respectively, for p.r.f.s. measurements, and at 16, 4, 4, 16, and 4 nm for the steady-state measurements. Unless otherwise noted, steady-state and p.r.f.s. measurements were obtained at excitation/emission wavelengths of 394/565 nm for all 4-AMP systems and 390/505 nm for all PRODAN systems.

Sample turret temperatures were set to values between 10.0 and 40.0 ± 0.1°C for all thermodynamic measurements by means of a Haake A81 temperature control unit (Fisher Scientific). All solutions were allowed to equilibrate thermally for 5 min before any measurements were made.

All measurements were made in triplicate for all 4-AMP samples and quadruplicate for all PRODAN samples, each measurement being the electronic average of 100 samplings obtained by integration over a 30-s interval. The average value of these triplicate and quadruplicate measurements were used for all subsequent work. All steady-state and p.r.f.s. measurements were blank-corrected, where appropriate, for the contributions from β-CD ($\leqslant$2%) and from albumin ($\leqslant$12%).

All data analyses were done on an Apple IIe microcomputer with an in-house BASIC linear least-squares routine for the direct nulling approach and a Gaussian-Newton iterative routine for the simultaneous equation approach. Heterogeneity analyses were done with SLM-supplied software based on Weber's algorithm [14].

RESULTS AND DISCUSSION

Binding of 4-AMP with β-CD

Results of u.v.-visible absorption studies (not shown) indicated a negligible (<1 nm) shift in the 4-AMP absorption wavelength on formation of the inclusion-complex, but there was no increase in the absorbance and hence molar absorptivity of the 4-AMP/β-CD inclusion-complex. The spectral shifts of 4-AMP depend on the solvent polarity [15, 16]. The effect of β-CD on 4-AMP fluorescence is to increase both the quantum efficiency and fluorescence lifetime because of inclusion-complexation. β-Cyclodextrins are believed to produce 1:1 inclusion complexes with many "guest" molecules [17].

The effect of added β-CD on the steady-state fluorescence intensity of 4-AMP is shown in Fig. 1. Steady-state emission spectra for 4-AMP in water and in β-CD are shown in Fig. 2. It is evident from these figures that inclusion-complex formation results in a more than 10-fold increase in the steady-state fluorescence signal relative to the free 4-AMP.

The fluorescence lifetimes of 4-AMP in water and in 15.13 mM β-CD were evaluated by both the phase-shift and demodulation methods [4, 5]. Table 1 shows the results at both 18 and 30 MHz. Heterogeneity analyses indicated essentially homogeneous fluorescence decays: fluorescence lifetimes for 4-AMP in water and in 15.13 mM β-CD were 0.97 (0.25) and 8.45 (1.11) ns, respectively, and the fractional intensities of the total fluorescence emission were 0.96 (0.04) and 0.91 (0.09), respectively (standard deviations are in parentheses).

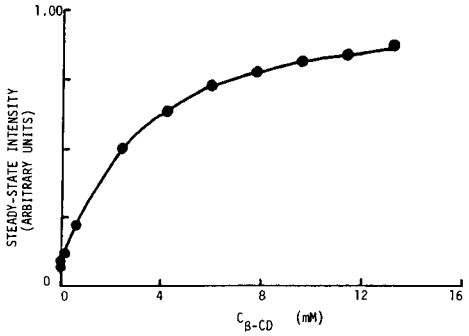

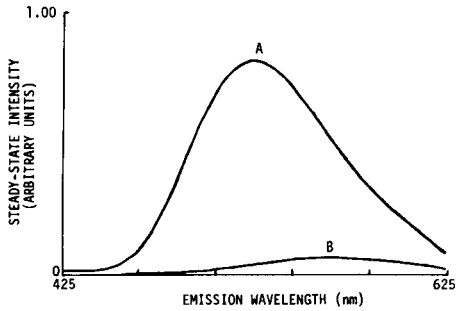

Fig. 1. Steady-state fluorescence intensity of 4-AMP as a function of added β-CD.

Fig. 2. Steady-state fluorescence emission spectra of 1.68 μM 4-AMP: (A) in water; (B) in 15.13 mM β-CD.

TABLE 1

Fluorescence lifetimes (τ) for free 4-AMP and its β-CD inclusion-complex

Sample	Modulation frequency			
	18 MHz		30 MHz	
	τ_p[a]	τ_m[b]	τ_p[a]	τ_p[b]
4-AMP[c]	1.03 (0.05)	1.27 (0.09)	1.07 (0.06)	1.32 (0.07)
4-AMP[d]	8.16 (0.06)	9.59 (0.10)	8.50 (0.03)	9.98 (0.05)

[a]Fluorescence lifetime (ns) by phase-shift method with absolute standard deviation (n = 100) in parentheses. [b]Fluorescence lifetime (ns) by demodulation method. [c]In distilled-deionized water only. [d]In 15.13 mM β-CD.

The shorter fluorescence lifetime component from free 4-AMP in solution was easily nulled (Fig. 3) by the p.r.f.s. method, by using a 1.68 μM 4-AMP solution in water to locate the null phase angle, at which the mixtures (described in Table 2) and their blanks were then measured. Equilibrium constants for the 4-AMP/β-CD inclusion-complex were determined at four temperatures (10.0, 20.0, 30.0, and 40.0°C) by using the direct nulling approach. The null phase angle was checked at each of the four temperatures used, and was found to be constant. Temperatures below 10.0°C and above 40.0°C were not used, because the solutions became slushy at lower temperatures and the polyethylene cuvets began to soften at higher temperatures. Figure 4 shows the effect of temperature on the equilibrium constant measurements for 4-AMP. Table 3 lists the equilibrium constants and correlation coefficients of the data contained in Fig. 4. Equilibrium constants for the inclusion-complex were also evaluated by using steady-state fluorescence measurements (Table 3). The values obtained by the steady-state method

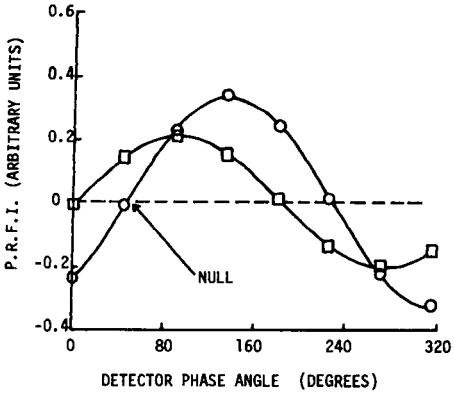

Fig. 3. Phase-resolved fluorescence intensity (p.r.f.i.) vs. detector phase angle of 1.68 μM 4-AMP: (○) in water; (□) in 15.13 mM β-CD. Arrow indicates the detector setting used to null the free 4-AMP contribution.

TABLE 2

Concentration ratios of binder to 4-AMP[a] for solutions used to determine thermodynamic constants

Mixture	β-CD/ 4-AMP	Albumin/ 4-AMP[b]	Mixture	β-CD/ 4-AMP	Albumin/ 4-AMP[b]	Mixture	Albumin/ 4-AMP[b]
1	0	0	4	3600	3.96	7	39.7
2	1200	0.398	5	7170	9.90	8	79.2
3	2400	1.97	6	8980	19.8	9	114

[a]1.68 μM in cuvet. [b]HSA or BSA.

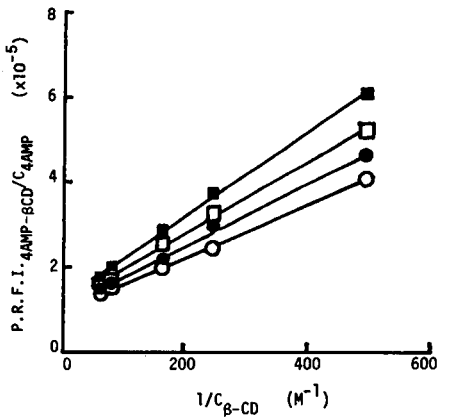

Fig. 4. Formation constant plots for the 4-AMP/β-CD inclusion-complex at various temperatures (°C): (○) 10.0; (●) 20.0; (□) 30.0; (■) 40.0.

TABLE 3

Effects of temperature on the equilibrium constants (K) evaluated by using the direct nulling approach for the 4-AMP/β-CD inclusion complex compared with the steady-state values

Equilibrium constants found (l mol^{-1})				
T[a]	K[b]	K[c]	K[d]	r[e]
283.2	146	122	147	0.9996
293.2	135	109	132	0.9992
303.2	122	94	117	0.9997
313.2	112	82	113	0.9995

[a]In Kelvin. [b]Direct nulling approach. [c]Steady-state method. [d]Corrected steady-state values. [e]Correlation coefficient for linear plots.

were all lower than those determined by the p.r.f.s. direct nulling approach because of the incorrect background subtraction (from free 4-AMP as discussed above). From the p.r.f.s. data, the equilibrium concentration, [4-AMP], was determined as a function of added β-CD (which was not possible by using steady-state methodology because of spectral overlap). It was then possible to calculate a new free 4-AMP background fluorescence value F(4-AMP) which was the true steady-state fluorescence signal of free 4-AMP as a function of β-CD. It takes the form

$$F(\text{4-AMP}) = [\text{4-AMP}]\ \{I_{S\text{-}S}(\text{4-AMP})/C(\text{4-AMP})\} \qquad (10)$$

where $I_{S\text{-}S}$(4-AMP) is the steady-state fluorescence intensity for 4-AMP completely free in solution (Table 2, cell 1) and C(4-AMP) is the analytical concentration of 4-AMP. The new F(4-AMP) values were then subtracted from F_t to obtain F_{SB}, and the equilibrium constants were recalculated using the steady-state data and found to increase as expected, and to be in excellent agreement with those acquired using the p.r.f.s. direct nulling approach (Table 3). The number of measurements required is the same for the steady-state method and p.r.f.s. direct nulling method; the measurements differ only in the instrumentation required to acquire them. The p.r.f.s. direct nulling method was suitable for evaluating equilibrium constants regardless of the free 4-AMP concentration because its contribution was nulled by the phase-sensitive detector.

The thermodynamic parameters ΔG, ΔH, and ΔS are related to K by the equation $\Delta G = -RT \ln K = \Delta H - T\Delta S$. A plot of $R \ln K$ vs. $1/T$ yields a slope of ΔH and a y-intercept of $-\Delta S$. The values of ΔH and ΔS from this method are -1.5 ± 0.2 kcal mol^{-1} and 4.4 ± 0.4 cal mol^{-1} K^{-1}, respectively, when the p.r.f.s. direct nulling approach is used.

Binding of 4-AMP to BSA and HSA

Steady-state emission spectra for free and HSA-bound 4-AMP are shown in Fig. 5 as a function of added HSA. The dip in the fluorescence intensity at

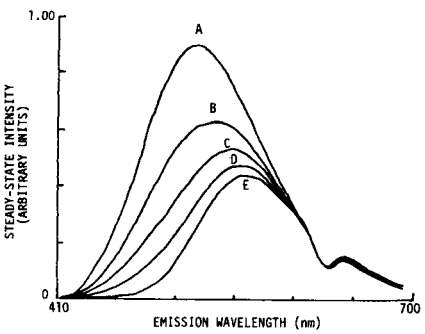

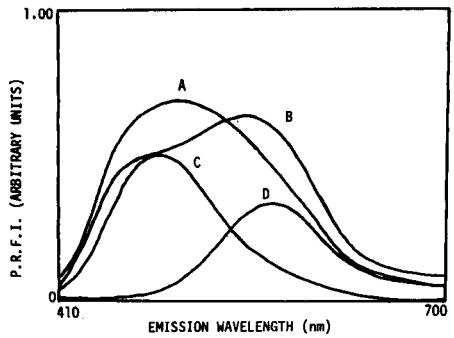

Fig. 5. Steady-state fluorescence emission spectra of 1.68 μM 4-AMP in different HSA solutions: (A) 1.70×10^{-5}; (B) 8.30×10^{-6}; (C) 3.30×10^{-6}; (D) 3.30×10^{-7}; (E) 0 M.

Fig. 6. Phase-resolved fluorescence emission spectra of 1.68 μM 4-AMP in 16.7 μM BSA at different phase angle settings: (A) 45.00°; (B) 90.00°; (C) 135.00°; (D) 180.00°.

ca. 610 nm is due to the Wood's polarization anomaly [18]. Results were similar for BSA. The concentrations of 4-AMP and albumin (BSA or HSA) used to determine the binding constants are shown in Table 2. "Binding" here means the association of 4-AMP to the albumin, which may be primarily an adsorption phenomenon. Equilibrium concentrations of free and albumin-bound 4-AMP were evaluated by monitoring the change in fluorescence lifetimes for a solution containing 16.7 μM BSA and 1.68 μM 4-AMP as a function of emission wavelength. Heterogeneity analysis at 6 and 30 MHz showed that the fluorescence emission is dominated by the longer-lived albumin-bound 4-AMP at shorter emission wavelengths and by the shorter-lived free 4-AMP at longer wavelengths (Table 4). The free 4-AMP showed

TABLE 4

Results from heterogeneity studies for a 4-AMP/β-CD solution (Table 2, mixture 5) as a function of emission wavelength[a]

Emission (nm)	Lifetime component 1		Lifetime component 2	
	τ_1[b]	F_1[c]	τ_2[b]	F_2[c]
450	0.98	0.12	16.73	0.88
470	1.47	0.17	16.91	0.83
490	0.93	0.18	17.03	0.82
510	1.10	0.21	16.72	0.79
530	1.31	0.31	16.93	0.69
550	0.99	0.43	17.11	0.57
570	0.97	0.58	16.77	0.42

[a]Using 6- and 30-MHz information. [b]Indicated fluorescence lifetime (ns). [c]Fractional intensity to the total fluorescence emission.

TABLE 5

Effects of added BSA on the fluorescence lifetime of 4-AMP at a constant emission wavelength (530 nm) at 30 MHz

BSA (μM)	τ_p[a]	τ_m[b]	S.d.[c]
0	1.03	1.07	0.02
0.67	1.11	3.07	0.04
3.33	1.39	3.99	0.02
6.67	1.54	4.80	0.03
16.7	2.15	6.29	0.07
33.3	2.82	8.32	0.04
66.7	3.66	10.90	0.02
133	4.76	12.56	0.01
193	5.55	13.47	0.06

[a]Fluorescence lifetime (ns) by the phase-shift method. [b]Fluorescence lifetime (ns) by the demodulation method. [c]Standard deviation for fluorescence lifetime determinations n = 100 (ns).

essentially homogeneous fluorescence decay, but upon association (complexation) with albumin the fluorescence decay became markedly heterogeneous (Table 5). Figure 6 shows the recorded phase-resolved emission spectra as a function of detector phase angle. The presence of at least two very distinct fluorescent components with fluorescence lifetimes of approximately 1 and 17 ns corresponding to the free and bound forms of 4-AMP, respectively, is evident from these spectra. The two components were easily resolved by using direct nulling and Fig. 7 shows the phase-resolved fluorescence emission spectra for the individual components for the same mixture described above. The steady-state emission spectrum for the albumin-bound 4-AMP could not be recorded directly because the albumins have a large background signal above 10^{-4} M. By using the direct nulling approach,

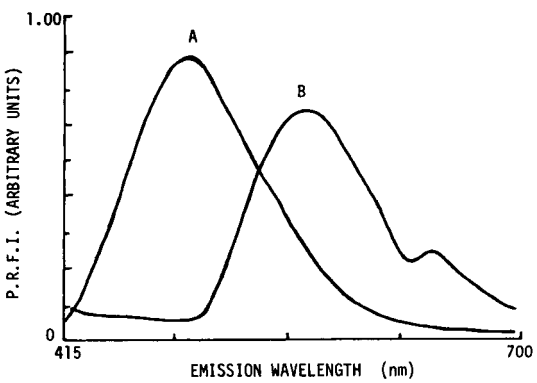

Fig. 7. Phase-resolved fluorescence emission spectra for the solution described in Fig. 6 at the detector phase angle setting required to null the free component (A), and to null the bound component (B).

TABLE 6

Effects of temperature on the overall equilibrium constants (K_o) determined by using the direct nulling approach for the 4-AMP/albumin system

T (K)	Overall equilibrium constant, K_o (l mol^{-1})		r^a
	4-AMP/BSA	4-AMP/HSA	
283.2	2.22×10^3	1.62×10^4	0.9992
288.2	9.40×10^2	9.00×10^3	0.9998
293.2	3.67×10^2	4.30×10^3	0.9976
298.2	2.04×10^2	2.92×10^3	0.9993
303.2	1.03×10^2	1.94×10^3	0.9995
308.2	4.51×10^1	8.40×10^2	0.9993
313.2	2.12×10^1	5.13×10^2	0.9995

[a]Average correlation coefficient for BSA and HSA plots used to determine K_o.

TABLE 7

Effects of temperature on the determined equilibrium constants for the PRODAN β-CD inclusion-complex using the p.r.f.i. vs. ϕ_D approach

T (K)	283.2	293.2	303.2	313.2
K (l mol^{-1})	2820	2250	1780	1460

overall equilibrium constants for the binding of 4-AMP to both BSA and HSA were determined as a function of eight temperatures (Table 7). Because the albumins potentially have more than one particular binding site, one can only discuss overall equilibrium constants. The information contained in Table 6 yields the thermodynamic binding parameters, ΔH and ΔS. For the HSA complex, ΔH and ΔS were found to be -26.8 ± 0.2 kcal mol^{-1} and 2.9 ± 0.1 cal mol^{-1} K^{-1}, respectively; for the BSA complex, the values were -20.0 ± 0.1 kcal mol^{-1} and 2.4 ± 0.1 cal mol^{-1} K^{-1}.

Binding of PRODAN and β-CD

The steady-state emission spectra for PRODAN as a function of added β-CD are shown in Fig. 8. PRODAN has been studied in poly-β-cyclodextrin systems as a function of pressure as a model for protein ligand interactions [19]. The steady-state fluorescence intensity is shown in Fig. 9 for PRODAN as a function of added β-CD, and appears to achieve a constant intensity level at high concentrations of β-CD. This indicates that standard solutions can be prepared in which PRODAN/β-CD is the sole species, so that the simultaneous equation p.r.f.s. approach can be used to determine K. Fluorescence lifetimes for free and β-CD inclusion-complexed PRODAN were 1.30 and 2.60 ns, respectively. It was possible easily to resolve these components by using the simultaneous equation approach at three detector phase angles (three simul-

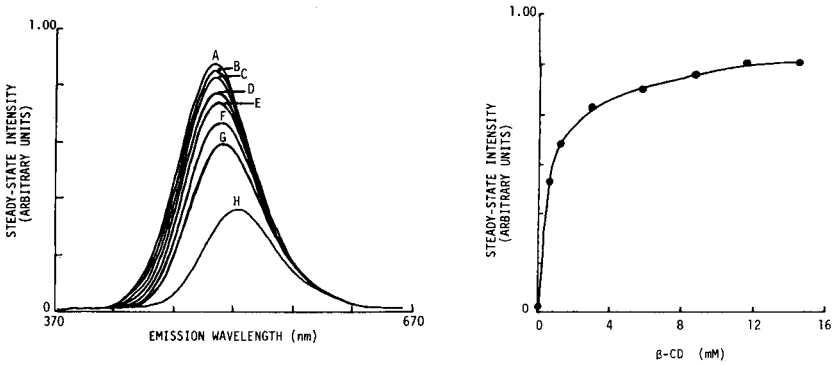

Fig. 8. Steady-state fluorescence emission spectra for PRODAN as a function of added β-CD: (A) 12.57; (B) 10.05; (C) 7.54; (D) 5.03; (E) 2.51; (F) 1.01; (G) 0.50; (H) 0 mM β-CD.

Fig. 9. Steady-state fluorescence intensity of 0.138 μM PRODAN as a function of added β-CD.

taneous equations in two unknowns). The equilibrium constants (Table 7) were evaluated at four temperatures. Values of ΔH and ΔS were subsequently found to be -3.9 ± 0.1 kcal mol^{-1} and 2.0 ± 0.2 cal mol^{-1} K^{-1}, respectively, for the PRODAN/β-CD inclusion-complex.

Conclusions

In all cases, enthalpies for binding of the fluorescent molecule were negative and entropies positive, indicating lower energy and higher entropy upon binding. The use of fluorescent lifetime selectivity to eliminate interference from the free fluorescent species in calculating thermodynamic binding constants is achieved effectively and conveniently by using the p.r.f.s. approaches described. Molecules such as 4-AMP and PRODAN that exhibit significant changes in fluorescence spectral and lifetime characteristics upon binding to cyclodextrins and proteins are useful probes for studying the binding interactions, and for analytical applications based on these interactions.

This work was supported by the National Science Foundation (Grant No. CHE-8403759).

REFERENCES

1 T. V. Veselova, A. S. Cherkasov and V. I. Shirokov, Opt. Spectrosc., 29 (1970) 617.
2 J. R. Lakowicz and H. Cherek, J. Biochem. Biophys. Methods, 5 (1981) 19.
3 L. B. McGown and F. V. Bright, Anal. Chem., 56 (1984), 1400A.
4 E. Gaviola, Z. Phys., 42 (1927) 853.
5 R. D. Spencer and G. Weber, Ann. N.Y. Acad. Sci., 158 (1969) 361.
6 J. B. Birks and D. J. Dyson, J. Sci. Instrum., 38 (1961) 282.
7 L. B. McGown, Anal. Chim. Acta, 157 (1984) 327.

8 F. V. Bright and L. B. McGown, Anal. Chim. Acta, 162 (1984) 275.
9 L. B. McGown and F. V. Bright, Anal. Chim. Acta, 169 (1985) 117.
10 F. V. Bright and L. B. McGown, Anal. Chem., 57 (1985) 55.
11 H. A. Benesi and J. H. Hildebrand, J. Am. Chem. Soc., 71 (1949) 2703.
12 J. R. Lakowicz, H. Cherek and A. Balter, J. Biochem. Biophys. Meth., 5 (1981) 131.
13 R. D. Spencer and G. Weber, J. Chem. Phys., 52 (1970) 1654.
14 G. Weber, J. Phys. Chem., 85 (1981) 949.
15 T. V. Veselova, L. A. Limareva, A. S. Cherkasov and V. I. Shirokov, Opt. Spectra, 19 (1965) 39.
16 T. V. Veselova and V. I. Shirokov, Izv. Akad. Nauk SSSR. Ser. Fiz., 36 (1972) 1024.
17 M. L. Bender and M. Komiyama, Cyclodextrin Chemistry, Springer-Verlag, Berlin, 1978.
18 D. M. Jameson, in E. Voos, Jr. (Ed.), Fluorescein Hapten: An Immunological Probe, CRC Press, Boca Raton, FL, Chapter 3, 1984.
19 P. M. Torgerson, H. G. Drickamer and G. Weber, Biochem., 18 (1979) 3079.

Analytica Chimica Acta, 175 (1985) 203—210
Elsevier Science Publishers B.V., Amsterdam — Printed in The Netherlands

REDUCTION DES INTERFERENCES SUR LA DETERMINATION DES METAUX LOURDS DANS LES SEDIMENTS DE COURS D'EAU ET LES BOUES DE STATIONS D'EPURATION PAR SPECTROMETRIE D'ABSORPTION ATOMIQUE EN FOUR GRAPHITE

M. LEGRET*, L. DIVET et D. DEMARE

Laboratoire Central des Ponts et Chaussées, B.P. 19, 44340 Bouguenais (France)

(Reçu le 11 janvier 1985)

SUMMARY

(Reduction of interferences in the determination of trace heavy metals in river sediments and sewage sludges by electrothermal atomic absorption spectrometry.)

The interferences of synthetic matrices of river sediments and sewage sludges in the determination of lead, copper, cadmium, chromium and nickel by electrothermal atomic absorption spectrometry were studied; Pb, Cd and Ni were the most sensitive to interferences. The effects of hydrochloric, nitric, perchloric and hydrofluoric acids were tested; perchloric acid was found to interfere most during the determinations. Hydrofluoric acid must be eliminated by evaporation. Techniques for reducing chemical interferences were evaluated. The best method was found to be matrix modification with ammonium dihydrogenphosphate and ascorbic acid for the determination of lead and nickel, and rapid heating (Max Power) for the determination of cadmium. Determinations of copper and chromium were less prone to interference.

RESUME

Les interférences de matrices synthétiques de sédiments de cours d'eau et de boues de stations d'épuration sur la détermination de Pb, Cu, Cd, Cr et Ni par spectrométrie d'absorption atomique sans flamme ont été étudiées: Pb, Cd et Ni sont les éléments les plus sensibles aux perturbations. Les effets des acides chlorhydrique, nitrique, perchlorique et fluorhydrique ont été étudiés: l'acide perchlorique provoque des interférences importantes. Différentes méthodes pour réduire les interférences ont été testées. La méthode de modification de matrice à l'aide de $NH_4H_2PO_4$ et acide ascorbique a été trouvée la meilleure pour le dosage de Pb et Ni, et la méthode de chauffage rapide (Max Power) pour celui de Cd.

La spectrométrie d'absorption atomique est la méthode d'analyse généralement employée pour la détermination des métaux lourds dans les milieux naturels, notamment dans les sédiments et les boues de stations d'épuration [1, 2]. Néanmoins, la détermination des métaux par atomisation électrothermique est souvent soumise à des interférences importantes. Dans une étude précédente [3], il a été montré que le dosage du plomb, du cadmium et du chrome dans les sédiments et les boues de stations d'épuration pouvait être perturbé par la présence des éléments majeurs de ces milieux. On a

0003-2670/85/$03.30

également constaté que les perturbations mesurées en présence de matrices complexes reconstituées ne correspondaient pas aux effets cumulés des interférents pris séparément.

Dans ce travail on a étudié les interférences causées par les acides utilisés pour la mise en solution des échantillons ainsi que celles dues à des matrices complexes sur différentes concentrations de plomb, cuivre, cadmium, chrome et nickel. La méthode des ajouts dosés est généralement utilisée pour corriger les effets de matrices, néanmoins elle augmente la durée et le coût des analyses ainsi que la variabilité des résultats [2]. On a donc cherché d'autres méthodes, rapides et simples, permettant de réduire ces interférences.

PARTIE EXPERIMENTALE

Les dosages ont été réalisés à l'aide d'un spectrophotomètre Perkin-Elmer modèle 5000 équipé d'un four graphite HGA-500 et d'un passeur d'échantillons automatique AS-40 effectuant des injections de 20 μl de solution. Les absorptions non spécifiques sont corrigées automatiquement par un arc au deutérium pour les longueurs d'onde inférieures à 350 nm et par une lampe tungstène au-delà de cette valeur. Le gaz de balayage est de l'argon et son débit est maintenu à 50 ml min^{-1} pendant l'atomisation. Chaque détermination est la moyenne de deux mesures.

L'eau utilisée pour les essais est purifiée sur une installation de déminéralisation Maxy comportant deux colonnes de résines échangeuses d'ions (Modèle Recherche). Les acides sont de qualité Merck Suprapur (HCl, HNO_3) ou Pro Analysi ($HClO_4$, HF). Les solutions de métaux traces ont été préparées à partir de Titrisol Merck (chlorures de Cu, Cr, Cd, Ni et nitrate de Pb). Celles contenant les éléments interférents ont été obtenues à l'aide des nitrates de Ca, K, Mg, Na (Suprapur) et des nitrates de Fe et Al (Pro Analysi, Merck). Toutes les solutions ont été préparées en double. Les résultats présentés sont la moyenne des deux essais après déduction du blanc.

RESULTATS ET DISCUSSION

Influence des acides sur le dosage des métaux lourds

Les acides les plus couramment utilisés pour la mise en solution des échantillons de sédiments et de boues sont les acides chlorhydrique, nitrique, perchlorique et fluorhydrique. Selon les procédures employées il subsiste des quantités variables de ces acides dans les solutions de dosage. Après évaporation, il peut subsister des quantités faibles d'acides (notamment $HClO_4$ et HF), et la reprise du résidu s'effectue en milieu acide 1—10%. Les solutions obtenues par l'utilisation de méthodes sous reflux peuvent contenir jusqu'à 10% d'acides. Enfin, les dilutions sont généralement effectuées en milieu chlorhydrique ou nitrique 0,2—1%.

Nous avons étudié systématiquement l'influence de la présence des acides

sur la détermination de Pb (80 $\mu g\ l^{-1}$), Cu (80 $\mu g\ l^{-1}$), Cd (5 $\mu g\ l^{-1}$), Cr (40 $\mu g\ l^{-1}$), et Ni (200 $\mu g\ l^{-1}$) pour des concentrations comprises entre 0,2 et 10% (v/v) d'acide concentré, l'acide fluorhydrique étant utilisé lors de minéralisation avec évaporation, sa concentration a été limitée à 3%. Les

TABLEAU 1

Conditions générales en atomisation électrothermique

Elément	Raie (nm)	Largeur de fente (nm)	Sensibilité (ng ml^{-1} pour 1% abs.)	Domaine analytique (ng ml^{-1})	Programme de température	
					Décomposition[a]	Atomisation[b]
Pb	283,3	0,7	8	10—100	550°C, 25 s	2200°C, 6 s
Cu	324,7	0,7	11	10—100	900°C, 25 s	2700°C, 6 s
Cd	228,8	0,7	0,35	0,4—5	270°C, 35 s	2150°C, 10 s
Cr	357,9	0,7	6,9	10—50	1050°C, 25 s	2700°C, 6 s
Ni	232,0	0,2	37	40—250	1000°C, 25 s	2700°C, 6 s

[a]Séchage 120°C, 30 s; temps de montée 1 s. Pour la décomposition, temps de montée 10 s.
[b]Temps de montée 1 s.

TABLEAU 2

Influence des acides sur le dosage de Pb (80 $\mu g\ l^{-1}$), Cu (80 $\mu g\ l^{-1}$), Cd (5 $\mu g\ l^{-1}$), Cr (40 $\mu g\ l^{-1}$) et Ni (200 $\mu g\ l^{-1}$)

Acide	Elément	Signal exprimé en absorbance					
		0,2[a]	0,5[a]	1[a]	3[a]	6[a]	10[a]
HCl	Pb	0,297	0,287	0,283	0,291	0,284	0,274
	Cu	0,307	0,297	0,316	0,291	0,298	0,294
	Cd	0,549	0,566	0,557	0,538	0,498	0,452
	Cr	0,257	0,247	0,269	0,259	0,254	0,239
	Ni	0,240	0,230	0,238	0,235	0,229	0,229
HNO_3	Pb	0,353	0,342	0,339	0,332	0,293	0,283
	Cu	0,308	0,309	0,318	0,314	0,307	0,302
	Cd	0,540	0,524	0,523	0,504	0,453	0,439
	Cr	0,280	0,268	0,270	0,265	0,247	0,252
	Ni	0,223	0,226	0,220	0,214	0,202	0,195
$HClO_4$	Pb	0,273	0,235	0,202	0,174	0,144	0,068
	Cu	0,344	0,332	0,322	0,320	0,342	0,340
	Cd	0,578	0,500	0,435	0,300	0,240	0,230
	Cr	0,255	0,254	0,256	0,218	0,179	0,137
	Ni	0,227	0,223	0,222	0,204	0,192	0,170
HF	Pb	0,248	0,263	0,301	0,345	—	—
	Cu	0,329	0,332	0,330	0,303	—	—
	Cd	0,492	0,505	0,496	0,505	—	—
	Cr	0,276	0,275	0,267	0,270	—	—
	Ni	0,205	0,205	0,206	0,185	—	—

[a]Concentration en acide en % (v/v).

programmes de température du four sont indiqués dans le Tableau 1. Les résultats des essais sont présentés dans le Tableau 2. L'acide chlorhydrique provoque peu d'interférence lorsque sa concentration est inférieure à 6%. L'absorption de Pb et Cr, mais surtout de Cd peut être fortement diminuée (—17% par rapport au signal mesuré avec 0,25% d'acide) à partir d'une concentration de 10% en acide. La présence de l'acide nitrique au-delà de 6% entraîne une diminution du signal de 15 à 20% pour Pb et Cd, et de l'ordre de 10% pour Cr et Ni. Par contre, l'acide perchlorique provoque des atténuations de l'absorption très importantes, supérieures à 10% à partir de 0,5% d'acide pour Pb et Cd, à partir de 3% pour Cr et Ni. Le dosage de Cu n'est pas perturbé par la présence de ces acides aux concentrations étudiées. L'acide fluorhydrique provoque une augmentation notable du signal de Pb à partir de 0,5%, ainsi qu'une diminution du signal de Cu et Ni pour une concentration de 3% en acide (—10% environ), alors que le dosage de Cd et Cr n'est pas perturbé.

Il apparaît donc que l'utilisation de l'acide perchlorique n'est pas à recommander pour la détermination des métaux lourds, notamment pour Pb et Cd; d'autre part les solutions obtenues à l'aide de méthodes de minéralisation sous reflux peuvent contenir des quantités d'acide, chlorhydrique ou nitrique, assez importantes pour gêner les dosages si on ne procède pas à des dilutions suffisantes. Enfin, il est nécessaire d'éliminer parfaitement l'acide fluorhydrique lors des évaporations.

Interférences dues aux matrices complexes

Afin d'étudier l'influence d'une matrice complexe sur le dosage des métaux lourds, on a préparé, en milieu nitrique 0,2% (v/v), une solution synthétique correspondant à la minéralisation de 1 g de sédiment sec dans 100 ml. La composition de ce sédiment est la suivante: Fe_2O_3 8%, Al_2O_3 20%, MgO 8%, CaO 7%, Na_2O 3%, K_2O 3%. Des quantités variables de métaux lourds ont été introduites dans cette solution qui correspondent aux teneurs généralement rencontrées dans les sédiments et les boues soit entre 10 et 1000 mg kg^{-1} pour Pb et Cu, entre 50 et 500 mg kg^{-1} pour Cu et Ni et entre 0,3 et 100 mg kg^{-1} pour Cd. Les concentrations en métaux ont été déterminées par rapport à une courbe d'étalonnage simple préparée en milieu nitrique, les programmes de température du four établis dans les mêmes conditions étaient ceux du Tableau 1. Les écarts entre les valeurs trouvées et les valeurs théoriques des teneurs en métaux introduites sont présentés dans le Tableau 3.

En présence de la matrice complexe le dosage de Cu et Cr n'est pas perturbé dans le domaine de concentration étudié. Les valeurs trouvées lors du dosage de Pb sont inférieures à la valeur théorique, et l'écart avec cette valeur dépasse 15% pour les teneurs en Pb inférieures à 300 mg kg^{-1}. Les valeurs trouvées pour Ni sont supérieures aux valeurs théoriques, les écarts dépassant 20% pour les concentrations inférieures à 100 mg kg^{-1}. Enfin, l'interférence de la matrice devient notable sur le dosage de Cd pour des

TABLEAU 3

Interférences dues à une matrice complexe sur la détermination des métaux lourds

Valeur théorique (mg kg^{-1})	0,3	1	5	10	50	100	300	500	1000
Ecarts (%)a									
Pb	—	—	—	−40	−28,6	−23	−15,3	−5,6	−1
Cu	—	—	—	+7	+7,2	+5	+1,3	+2	+1,4
Cd	−20	+10	+2	+3	−4,8	−7,5	—	—	—
Cr	—	—	—	—	−3,6	−11	−6,7	−6	—
Ni	—	—	—	—	+36,4	+22	+7,7	+3	—

[a]Par rapport à la valeur théorique.

teneurs inférieures à 1 mg kg^{-1}. Il apparaît donc que les interférences dues aux matrices complexes sont variables suivant les métaux et leurs concentrations. Les essais réalisés permettent d'évaluer les teneurs en métaux lourds à partir desquelles les perturbations sont à prévoir, la matrice choisie étant représentative d'un sédiment réel.

Réduction des interférences

Les causes de perturbations enregistrées lors des dosages en spectrométrie d'absorption atomique sont nombreuses. Il s'agit d'absorptions non spécifiques dues à la volatilisation de la matrice au cours de l'atomisation ou d'interférences inter-éléments susceptibles de modifier la vitesse d'atomisation de l'élément étudié ou d'entraîner la perte d'une partie de la vapeur atomique par formation de composés moléculaires parasites.

Différentes méthodes permettent de réduire les perturbations de l'atomisation [4]. La modification de la matrice par ajout d'un agent chimique, notamment $NH_4H_2PO_4$, permet d'augmenter la température de décomposition en rendant l'analyte moins volatil et facilite la volatilisation de la matrice [5]. L'addition de composés organiques comme l'acide ascorbique [6] produit lors de la décomposition un mélange intime entre l'échantillon et le carbone libéré ce qui peut contribuer à stabiliser l'analyte par carburation. Le signal peut être amélioré grâce à l'utilisation de tubes recouverts de graphite pyrolytique, qui supprime les pertes de certains métaux par diffusion à travers les parois du tube [4]. Les fortes absorptions non spécifiques causées par des milieux très chargés en sels peuvent être diminuées en utilisant le mode de chauffage rapide [7] lors de l'atomisation (Max Power). Le chauffage rapide permet en effet d'atomiser un élément volatil sans pratiquement covolatiliser sa matrice par suite du déplacement des températures optimales d'atomisation. Enfin, il est possible de réduire les interférences en phase vapeur et celles dues aux variations de la température d'atomisation en introduisant une plate-forme en graphite dans le tube sur laquelle on injecte l'échantillon [5, 8]. Dans ces conditions la

volatilisation est retardée jusqu'à ce que l'atmosphère dans le tube atteigne une température élevée et presque constante.

Nous avons testé ces différentes méthodes en étudiant plus particulièrement le cas de Pb, Cd et Ni qui sont les métaux les plus sensibles aux perturbations. Les méthodes retenues sont les suivantes: tube seul, tube avec modification de matrice, chauffage rapide (Max Power), plate-forme, et plate-forme + modification de matrice + Max Power. Pour les essais réalisés avec modification de matrice on a préparé une solution contenant 5% $NH_4H_2PO_4$ et 500 mg l^{-1} d'acide ascorbique (Pro Analysi, Merck) dont on a introduit 5 μl directement dans le four avec les 20 μl d'échantillon. Les essais avec plate-forme ont été effectués avec des plates-formes en graphite pyrolytique et des tubes recouverts de graphite pyrolytique. De même, on a effectué les dosages de Cr et Ni en mode Max Power à l'aide de fours recouverts de graphite pyrolytique ce qui permet de diminuer la température d'atomisation et donc de limiter la volatilisation de la matrice (2100°C en four pyrolytique au lieu de 2500 et 2700°C avec des fours normaux).

Les essais d'interférence ont été réalisés en présence de quatre matrices synthétiques dont les compositions sont présentées dans le Tableau 4. Les matrices étudiées sont représentatives de sédiments ou de roches (matrices A et D), et de boues de stations d'épuration, brutes ou traitées à la chaux (B et C). Les solutions synthétiques ont été préparées dans l'acide nitrique 0,2% (v/v) afin de représenter la minéralisation de 1 g d'échantillon sec dans 100 ml et les teneurs en métaux lourds choisies se situent dans le domaine de concentration sensible aux interférences. On a recherché les réglages optimaux du four graphite pour chaque mode de dosage à l'aide de la méthode de programmation variable [9] (Tableaux 1 et 5).

L'ajout de $NH_4H_2PO_4$ permet d'élever la température de décomposition d'environ 200°C et sans entraîner de pertes des éléments les plus volatils (Pb et Cd). En présence de plates-formes les températures de décomposition et d'atomisation sont plus élevées (environ 200°C, sauf pour Cd) afin que l'atmosphère dans le tube atteigne les températures optimales. En mode Max Power la température d'atomisation est diminuée; la montée en température étant très rapide, il est possible de réduire la durée d'atomisation (jusqu'à 2 s) sans influencer le résultat. La température optimale de décom-

TABLEAU 4

Composition des matrices complexes étudiées

Matrice	Composition (%)					
	Fe_2O_3	Al_2O_3	MgO	CaO	Na_2O	K_2O
A	8	20	8	7	3	3
B	3	2	1	3	1	0,5
C	3	2	1	33	1	0,5
D	5	13	3	6	2	3

TABLEAU 5

Programmes de températures du four graphite

Elément	Méthode	Séchage[a]	Décomposition[b]	Atomisation[c]
Pb	Tube + $(NH_4)H_2PO_4$	120°C, 30 s	750°C, 25 s	2400°C, 6 s
	Max Power	120°C, 30 s	600°C, 25 s	1400°C, 5 s
	Plate-forme	160°C, 30 s	750°C, 25 s	2300°C, 6 s
	Plate-forme + $(NH_4)H_2PO_4$ + Max Power	160°C, 30 s	500°C, 25 s	1900°C, 6 s
Cu	Tube + $(NH_4)H_2PO_4$	120°C, 30 s	1100°C, 25 s	2900°C, 6 s
	Max Power	120°C, 30 s	600°C, 25 s	2200°C, 5 s
Cd	Tube + $(NH_4)H_2PO_4$	120°C, 30 s	550°C, 25 s	2300°C, 8 s
	Max Power	120°C, 30 s	500°C, 25 s	1200°C, 5 s
	Plate-forme	160°C, 30 s	270°C, 25 s	2300°C, 8 s
	Plate-forme + $(NH_4)H_2PO_4$ + Max Power	160°C, 30 s	500°C, 25 s	1600°C, 5 s
Cr	Tube + $(NH_4)H_2PO_4$	120°C, 30 s	1300°C, 25 s	2900°C, 7 s
	Max Power	120°C, 30 s	1100°C, 25 s	2100°C, 5 s
Ni	Tube + $(NH_4)H_2PO_4$	120°C, 30 s	1200°C, 25 s	2700°C, 7 s
	Max Power	120°C, 30 s	1000°C, 25 s	2100°C, 6 s
	Plate-forme	160°C, 30 s	1200°C, 25 s	2900°C, 7 s
	Plate-forme + $(NH_4)H_2PO_4$ + Max Power	160°C, 30 s	1500°C, 25 s	2700°C, 6 s

[a]Temps de montée, 1 s. [b]Temps de montée, 10 s. [c]Temps de montée, 1 s; en Max Power, 0 s.

position peut également se trouver déplacée. Les résultats obtenus par ces différentes méthodes sont présentés dans le Tableau 6.

La détermination de Cu et Cr est relativement peu perturbée par la présence des matrices complexes. L'utilisation de plates-formes ne semble pas améliorer les dosages, seules les interférences constatées lors de la détermination de Pb sont réduites de façon notable. Le mode de chauffage rapide (Max Power) réduit sensiblement les interférences lors du dosage de Pb. La méthode de modification de matrice à l'aide de l'acide ascorbique et de $NH_4H_2PO_4$ permet d'obtenir des résultats satisfaisants pour le dosage de Pb et Ni. Enfin, c'est la méthode de chauffage rapide (Max Power) qui permet d'obtenir une détermination satisfaisante de Cd.

Conclusion

Les acides utilisés pour la mise en solution des échantillons de sédiments ou de boues sont susceptibles de perturber la détermination des métaux lourds par spectrométrie d'absorption atomique en four graphite. L'utilisation de l'acide perchlorique notamment n'est pas à recommander pour le dosage de Pb et Cd. Les acides chlorhydrique et nitrique peuvent également gêner les dosages s'ils sont en concentration importante et il est nécessaire

TABLEAU 6

Correction des interférences lors du dosage de Pb (20 mg kg^{-1}), Cu (10 mg kg^{-1}), Cd (0,3 mg kg^{-1}), Cr (50 mg kg^{-1}) et Ni (20 mg kg^{-1})

Elément	Matrice	Ecarts (%) par rapport à la valeur théorique				
		Tube seul	Tube + $NH_4H_2PO_4$[a]	Max Power	Plate-forme	Plate-forme + $NH_4H_2PO_4$[a] + Max Power
Pb	A	−49,5	−17	−30	−22	−27,5
	B	−44	−9,5	−21	−29	−29,5
	C	−35	−14	−16	−41	−23,5
	D	−47	−12	−30	−24	−39
Cu	A	+3	−13	−17	—	—
	B	+2	+1	−6	—	—
	C	−4	+10	−13	—	—
	D	+10	−2	−8	—	—
Cd	A	−20	−27	+7	+43	0
	B	−23	−17	0	+40	+60
	C	−23	−27	−10	−23	−33
	D	−27	−33	−7	−23	+10
Cr	A	−11	−9	−27	—	—
	B	−8	−4	−6	—	—
	C	−11	−10	−12	—	—
	D	−7	−5	−10	—	—
Ni	A	+35	0	−15	+57	+66
	B	+21	+5	−24	+25	+39
	C	+15	−11	−22	+2	+5
	D	+31	−5	−24	+51	+65

[a] 5 µl de 5% $NH_4H_2PO_4$/0,05% d'acide ascorbique.

d'éliminer complètement l'acide fluorhydrique par évaporation en particulier pour le dosage de Pb.

La présence de matrices complexes entraîne des perturbations lors du dosage de Pb, Cd et Ni. Les interférences peuvent être réduites en utilisant la méthode de modification de matrice à l'aide de l'acide ascorbique et de $NH_4H_2PO_4$ lors du dosage de Pb et Ni, et en utilisant la méthode de chauffage rapide (Max Power) pour le dosage de Cd.

BIBLIOGRAPHIE

1 S. Stoveland, M. Astruc, R. Perry et J. N. Lester, Sci. Total Environ., 13 (1979) 33.
2 P. Marchandise, J. L. Olié, D. Robbe et M. Legret, Environ. Technol. Lett., 3 (1982) 157.
3 M. Legret, D. Demare, P. Marchandise et D. Robbe, Anal. Chim. Acta, 149 (1983) 107.
4 S. R. Koirtyohann et M. L. Kaiser, Anal. Chem., 54 (1982) 1515.
5 T. W. May et W. G. Brumbaugh, Anal. Chem., 54 (1982) 1032.
6 M. Hoenig, R. Vanderstrappen et P. Van Hoeyweghen, Analusis, 7 (1979) 17.
7 C. Riandey, R. Gavinelli et M. Pinta, Spectrochim. Acta, 358 (1980) 765.
8 E. J. Hinderberger, M. L. Kaiser et S. R. Koirtyohann, At. Spectrosc., 2 (1981) 1.
9 M. Pinta et C. Riandey, Analusis, 2 (1975) 86.

Analytica Chimica Acta, 175 (1985) 211—217
Elsevier Science Publishers B.V., Amsterdam — Printed in The Netherlands

DETERMINATION OF MERCURY IN INDUSTRIAL MATERIALS BY ATOMIC ABSORPTION SPECTROMETRY AFTER THERMAL VOLATILISATION

B. RÓŻAŃSKA and E. LACHOWICZ*

Department of Analytical Chemistry, Technical University of Warsaw, 00-664 Warsaw (Poland)

(Received 9th August 1984)

SUMMARY

The pyrolysis of samples containing copper, lead, iron, sulphur compounds and organic carbon is applied to separate mercury prior to its determination by a.a.s. Amalgamation on gold collectors followed by thermal desorption, or trapping in an absorption solution followed by reduction/aeration were used depending on the mercury content in the materials. Appropriate additives to the samples and filters are used to ensure complete release of mercury and removal of interfering pyrolysis products.

The separation of mercury by pyrolysis of samples is fast; it excludes sample contamination by mercury contained in reagents and prevents mercury losses during dissolution. Depending on the mercury content of the sample, the released mercury vapours can be absorbed in an oxidizing solution (e.g., permanganate in sulphuric acid [1] or iodine in potassium iodide [2]) or trapped on a collector (e.g., Au, Pt, Cu, activated charcoal) and volatilized by heating. Many materials have been investigated in order to find the best collector of mercury; the most satisfactory were gold-coated sand [3, 4], gold-coated asbestos and gold or silver wires [5], gold-coated quartz wool [6] or gold coils [7]. One collector was often insufficient to eliminate interfering pyrolysis products. Two collectors [4], filters of alumina [8], silver [4, 7], alumina and silica [4], and heating the absorber to 100—170°C during amalgamation [7, 9] have been used to avoid interferences. Advantages have been observed for various additives ($MgO + Na_2CO_3 + Al_2O_3$ [10], $Mg(NO_3)_2 + MgO$ [11] and Florisil + CaO [12]). Pyrolysis and trapping on collectors have been applied to the determination of mercury in air [4, 6], environmental standard reference materials [4], sediments, rocks, coals, tissues and water [7], plants and blood [8] and solid fuels [10].

The purpose of the present work was to test the applicability of pyrolysis followed by trapping on gold (for ca. 10^{-5}% Hg) or by absorption in an oxidizing solution (for 10^{-4}—0.1% Hg), in the analysis of industrial samples containing considerable amounts of heavy metals (Cu, Pb, Fe), sulphur compounds, silica and organic carbon. Because of the different and complex composition

0003-2670/85/$03.30

of the samples, the influence of various filters and additives to the samples was studied. The mercury was finally determined by atomic absorption spectrometry (a.a.s.).

EXPERIMENTAL

Reagents and apparatus

All the chemicals used were of analytical-reagent grade. Mercury(II) stock standard solution (1 mg ml^{-1}) was prepared from 0.3384 g of mercury(II) chloride dissolved in 50 ml of (1 + 1) sulphuric acid and diluted to 250 ml with water. Working solutions (1—10 μg ml^{-1}) were freshly prepared by diluting the stock solution with 0.5 M sulphuric acid. The solution for absorbing mercury after pyrolysis was 0.5% potassium permanganate in 0.5 M sulphuric acid, prepared daily. A 10% (w/v) tin(II) chloride solution in 4 M hydrochloric acid was bubbled overnight with purified nitrogen (molecular sieves, silver gauze, gold wire coils) to remove traces of mercury. Magnesium oxide, calcium oxide and Florisil were heated for 1 h at 800°C before use.

The Pye-Unicam SP-90 series 2 atomic absorption spectrometer used was equipped with a quartz flow cell (10 mm i.d., 150 mm long) in place of a flame. The apparatus for pyrolytic decomposition of samples and amalgamation trapping followed by thermal desorption is shown in Fig. 1. It was made of quartz tubing (6-mm i.d.). Air was purified by passage through molecular sieves, silver gauze and gold wire coils. Silver gauze and gold coils were cleaned by heating at 800°C. Silicone rubber tubing was used to interconnect the tubes. The Kanthal wire windings of the furnaces, coated with insulating paint, were placed in silica tubes (12 mm i.d.). The scavengers in furnace II were tightly coiled silver gauze (20 mm long), silica (6 mm long), granular alumina (10 mm long) and quartz wool. Two gold collectors (each ca. 0.9 g of gold) consisting of coils (1.5 mm i.d., 6 mm long) of gold wire (0.038 mm diameter) were placed in furnaces III and IV.

The equipment for pyrolytic decomposition and mercury trapping in acidified permanganate solution consisted of furnaces I and II (as in Fig. 1) followed by a scrubber with a porous frit containing the absorbent solution. The arrangement for reduction/aeration consisted of a 250-ml Pyrex Erlenmeyer flask closed with the inserted bubbler (medium porosity frit) and a drying tube with anhydrous magnesium perchlorate placed between the

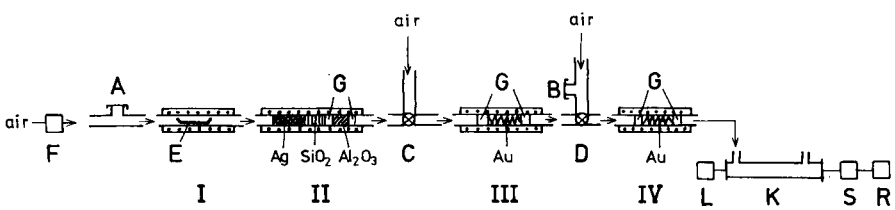

Fig. 1. Apparatus for determination of mercury: (A, B) septum; (C, D) 3-way cock; (E) quartz boat; (F) flow meter; (G) quartz wool; (K) flow cell; (L) mercury lamp; (S) spectrometer; (R) recorder.

reaction flask and the spectrometer flow cell. The air flow was controlled by a Chromatron gas regulator and a flow meter. There was no recirculation system.

Procedures

Method A (for 10^{-6}—10^{-4}% Hg). An accurately weighed sample (50—100 mg, <254 mesh) mixed with the appropriate additives if necessary (Table 1, Nos. 1, 2) was placed in a quartz boat in furnace I. The air flow (0.1 l min^{-1}) was switched on. Mercury liberated from the sample heated to 800°C for 15 min was passed through the scavengers in furnace II (725°C) and was trapped on gold at 170°C in furnace III. This furnace was in turn heated to 800°C for 3 min, so that mercury was transported to the second absorber(IV) at 170°C. Furnace IV was subsequently heated to 800°C with a flow of air at exactly 0.1 l min^{-1} passing through to the flow cell. The height of the absorbance peak was recorded. Calibration (0—60 ng Hg) was by injection of known volumes of mercury-saturated air through septum B (Fig. 1). The efficiency of mercury transport should be checked; peaks obtained for injection through septa B and A should agree.

Method B (for 10^{-4}—0.5% Hg). A weighed portion of sample (<254 mesh) mixed with magnesium oxide or Florisil and calcium oxide (see Table 1, Nos. 3—6) was placed in a quartz boat in furnace I. The air flow and heating of furnaces I and II were as in Method A. Mercury vapour was trapped in 100 ml of absorbing solution in a scrubber. An aliquot was transferred to the Pyrex bubbler flask and diluted with absorbent solution to 80 ml. A 10% (w/v) solution of hydroxylammonium chloride was added dropwise to reduce the permanganate, and 10 ml of tin(II) solution was added just before the measurement. The bubbler flask was closed immediately and the contents were mixed. An air flow of exactly 0.4 l min^{-1} was switched on and the mercury vapours were transferred to the flow cell. The absorbance was recorded. For calibration (0.1—1 μg Hg), aliquots of 1 μg ml^{-1} mercury solution were transferred into the Pyrex bubbler flasks containing 80 ml of absorbent solution. The reduction/aeration procedure was done as above.

TABLE 1

Experimental conditions for the analysis of various samples

Sample no.	Description	Weight taken (mg)	Additives (mg)	Method
1	Dust from fluidized bed furnace	50—100	—	A
2	Kaolin KK	100	Florisil/CaO (1:1) (50)	A
3	Dust from Doerschel furnace	25—50	MgO (25)	B
4	Sludge from sulphuric acid factory	5	MgO (20)	B
5	Copper concentrate (Lubin)	50	Florisil/CaO (2:1) (50)	B
6	Copper concentrate (Polkowice)	50	Florisil/CaO (2:1) (50)	B

Method C (for 10^{-4}—0.5% Hg). Weighed portions (100 mg) of samples 4—6 (Table 2; <254 mesh) were digested with a mixture of 5 ml of concentrated nitric acid, 5 ml of concentrated hydrochloric acid and 5 ml of concentrated sulphuric acid in a teflon-lined bomb for 2 h at 140°C. (For sample 3, which contained ca. 40% of lead, the sulphuric acid content was reduced to 1 ml.) The contents of the bomb were transferred to a 100-ml teflon beaker and heated for 1 h at 140°C on a silicone oil bath with 50 ml of saturated boric acid solution. The solution was transferred to a 100-ml volumetric flask. The lead sulphate precipitate remaining in the beaker (sample 3) was dissolved in 10 ml of saturated sodium chloride solution and added to the solution in the flask. The solution was diluted to volume with water.

Mercury was determined by reduction/aeration using a standard addition method. To three Pyrex bubbler flasks, 40-ml portions of 1 M sulphuric acid, a suitable volume of sample solution (diluted if necessary) and appropriate volumes of standard mercury solution (containing 0, 0.25 and 0.5 μg of mercury) were added. The solutions were diluted to 80 ml with water. A 10-ml portion of tin(II) solution was added to each flask just before measurement and aeration was done as in Method B.

RESULTS AND DISCUSSION

Method A

Before the experiments on the pyrolysis of these samples were started, the thermal characteristics of the furnace were established by measuring the change in temperature with time by means of a platinum/rhodium thermocouple at various flow rates. The constant temperatures given in the Procedures were attained after 3—4 min. The temperatures were only slightly

TABLE 2

Results of mercury determination

Sample no.[a]	Method	Mean Hg content (%)	*n*	R.s.d. (%)
1	A	1.48×10^{-5}	6	4.3
2[b]	A	8.63×10^{-6}	4	5.5
3	B	1.35×10^{-2}	8	4.4
	C	1.30×10^{-2}	3	3.1
4	B	5.10×10^{-1}	4	3.0
	C	5.17×10^{-1}	5	2.0
5	B	5.13×10^{-3}	8	2.1
	C	5.10×10^{-3}	6	3.0
6	B	7.15×10^{-3}	4	2.6
	C	7.14×10^{-3}	6	2.0

[a] As in Table 1. [b] Reported value 8.8×10^{-6}%.

dependent (ca. 6%) on the air flow rate in the range 0.1—0.4 l min^{-1}. The effects of air flow rate (in the above range) and current (4—6 A) on the process of mercury release from the gold absorber in furnace IV (and therefore on the height and shape of the peak) were also investigated and the values of 0.1 l min^{-1} and 4.5 A were found to be optimal.

Before the complex system of filters and absorbers was finally adopted, the possibility of using several simpler versions of the apparatus was investigated for sample 1. When silver gauze (at 725°C) alone was used in furnace II, and furnace III contained first an unheated or heated (100°C) gold absorber followed by a second gold absorber at 100°C, two peaks were observed (Fig. 2). The substance giving the first peak started to evolve at ca. 80°C, and the second at ca. 260°C. Measurements made with a palladium lamp at 247.6 nm showed the nonspecific character of the first peak; the mercury transported from the first to the second gold absorber was accompanied by a large amount of gaseous pyrolysis products absorbing at 247.6 nm, some of which was trapped on gold heated at 100°C. As a result of using the silver filter and heating both gold absorbers up to 170°C during amalgamation, only one peak, for mercury released at ca. 260°C, was obtained. In a series of experiments under these last conditions, consecutive peaks gradually decreased, and tarry organic substances appeared on the apparatus walls. The application of extra scavengers of silica and alumina removed these effects almost completely.

The apparatus had to be cleaned when the peak heights after the injection of known amounts of mercury vapour at points A and B were not equal, and when the sensitivity diminished. The silver gauze was washed with ammonia

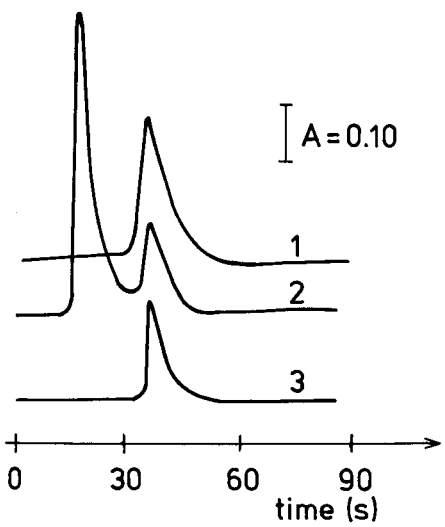

Fig. 2. Absorbance peaks obtained for: (1) 11.2 ng mercury (vapour); (2) sample 1, gold collectors during trapping at 100°C; (3) sample 1, gold collectors during trapping at 170°C.

and heated at 800°C. The silica and alumina packings were replaced by fresh portions purified by heating at 800°C. The gold absorber was washed with acetone. Before calibration, the whole apparatus must be carefully cleaned of mercury by successive heating of the furnaces. The mercury content of the saturated vapour was obtained from the data given by Joensuu [7]. The calibration graphs obtained by injection and by the addition of aqueous mercury(II) standard solutions to the boat were consistent. The calibration graphs were linear over the range 0—60 ng of mercury.

Additives (MgO, Florisil/CaO) had no effect on the results for sample 1. As an appropriate standard was unavailable, sample 2 (a kaolin standard in which the mercury content had been determined by 5 laboratories) was used to check method A. Addition of Florisil and calcium oxide to sample 2 was necessary to obtain results consistent with the standard value.

Method B

Sample 3 contained considerable amounts of lead compounds and silica. It had a melting point below 800°C, and could not be removed from the quartz boat after pyrolysis. Addition of magnesium oxide increased the melting point and made it easy to remove the pyrolysed sample from the boat. Results for mercury in sample 3 with and without magnesium oxide were the same. A substantial effect of magnesium oxide was observed during the thermal decomposition of sample 4. The oxide absorbed much of the gaseous pyrolysis products and prevented the formation of acidic droplets on the cold parts of the apparatus on which mercury was retained. A 4-fold amount of magnesium oxide was necessary to avoid losses of mercury. A 2:1 Florisil/calcium oxide mixture appeared to be the best additive for the pyrolysis of samples 5 and 6 (concentrates). The use of the set of scavengers was essential to obtain consistent results. The removal of any of the filters diminished the mercury recovery.

Method C

The accuracy of the procedure for mercury separation from samples 3—6 was checked by digestion of the samples and determination of mercury by reduction/aeration, using standard additions. Because of the high mercury content, much dilution of the samples solutions was required, which, in turn, made the interferences of the sample components on mercury determination negligible. Recovery of mercury added to samples 3—6 before digestion was complete. The results of mercury determination in samples 3—6 after pyrolytic liberation (method B) and after wet digestion were consistent (Table 2).

Conclusions

Pyrolysis is to be recommended as a method of separating mercury from industrial samples of complex composition. Two versions could be applied, depending on the mercury content: method A (10^{-6}—10^{-4}%) and method B (10^{-4}—0.5%). Method C, used in order to check the accuracy of method B, is

far more time-consuming, particularly for sparingly soluble materials (samples 5, 6) and needs standard additions for calibration. The precisions of methods B and C are similar.

The accuracy of the pyrolytic methods (A and B) depends not only on quantitative mercury release but also on reasonably complete oxidation of gaseous pyrolytic products evolved from samples containing considerable amounts of sulphur compounds and organic carbon. The oxidation on silver, alumina and silica filters assured mercury transport without any losses (on walls covered by pyrolytic products) only for furnace dusts (samples 1 and 3). The appropriate additives were essential in obtaining accurate results for the other materials. The role of the additives is difficult to explain because of the complex composition of the samples. They may facilitate mercury release as a result of solid-state reactions and may catalyse oxidation of pyrolytic products.

We thank Miss Mirosława Domańska for carrying out the a.a.s. measurements. This work was supported by the Scientific Programme M.R.I.32.

REFERENCES

1 Y. Kuwae, T. Hasegawa and T. Shono, Anal. Chim. Acta, 84 (1976) 185.
2 Yu. V. Zelyukova, R. A. Vitkun, T. O. Didorenko and N. S. Poluektov, Zh. Anal. Khim., 36 (1981) 454.
3 R. Dumarey, R. Heindryckx, R. Dams and J. Hoste, Anal. Chim. Acta, 107 (1979) 159.
4 R. Dumarey, R. Heindryckx and R. Dams, Anal. Chim. Acta, 116 (1980) 111; 118 (1980) 381.
5 I. Kunert, J. Komarek and L. Sommer, Anal. Chim. Acta, 106 (1979) 285.
6 Z. Yoshida and K. Motojima, Anal. Chim. Acta, 106 (1979) 405.
7 O. I. Joensuu, Appl. Spectrosc., 25 (1971) 526.
8 S. Dogan and W. Haerdi, Anal. Chim. Acta, 84 (1976) 89.
9 Zs. Wittmann, Talanta, 28 (1981) 271.
10 H. Uchikawa, R. Furuta and Y. Mihara, Bunseki Kagaku, 31 (1982) 367.
11 Yu. V. Zelyukova and T. O. Didorenko, Ukr. Khim. Zh., 49 (1983) 526.
12 T. Baba, S. Ohmiya, M. Hosokawa and T. Ishibashi, Seikatsu Eisei, 27 (1983) 258.

Analytica Chimica Acta, 175 (1985) 219—229
Elsevier Science Publishers B.V., Amsterdam — Printed in The Netherlands

TWO-DIMENSIONAL AND THREE-DIMENSIONAL FITTING OF ENZYME KINETIC DATA WITH THE KALMAN FILTER

SARAH C. RUTAN[a] and STEVEN D. BROWN*[b]

Department of Chemistry, Washington State University, Pullman, WA 99164-4630 (U.S.A.)

(Received 8th April 1985)

SUMMARY

The availability of instrumentation which is capable of collecting multidimensional data has put increased demands on the data-processing methods utilized to obtain information about reaction kinetics. An enzyme-catalyzed reaction, the hydrolysis of *p*-nitrophenyl phosphate to *p*-nitrophenol, is examined so that various data-processing methods and data-collection formats can be examined and compared. The extended Kalman filter is used to obtain rate constants and values for the initial substrate concentration for three-dimensional data, and for two-dimensional kinetically perturbed data. In addition, nonlinear least-squares regression with the simplex algorithm, and linear least-squares regression methods are used to analyze absorbance/time curves for this reaction. These results are compared to the results from a two-point kinetic method, and the accuracy and precision of each of the methods is evaluated. It is found that the methods based on the Kalman filter yielded results which were equivalent to or better than the results obtained from the other approaches.

Recently, instrumentation capable of obtaining u.v.-visible absorption spectra in a very short amount of time (<1 s) has become available commercially. In addition, techniques such as Fourier-transform infrared spectroscopy also permit a large amount of spectral information to be obtained in a relatively short time. The availability of such instrumentation has meant that studies of chemical kinetics and other dynamic processes can now rely on spectral data at several wavelengths, which can give information about a chemical reaction at a single instant in time, even for relatively fast reactions. While this increased information yield may be extremely valuable in obtaining concentrations or accurate kinetic parameters, much of this information may be wasted if effective data-processing methods are not used.

Several different approaches to data processing have been developed which allow complex data sets of this type to be evaluated. These approaches include nonlinear regression methods [1], computer graphic techniques [2], and digital filtering methods [3]. While all these methods, in principle,

[a]Present address: Department of Chemistry, Virginia Commonwealth University, Richmond, VA 23284-0001 (U.S.A.).
[b]Present address: Department of Chemistry, University of Delaware, Newark, DE 19716 (U.S.A.).

0003-2670/85/$03.30

permit data (in the form of absorbance vs. time and wavelength) to be analyzed from kinetic measurements obtained with rapid scanning spectrophotometers, relatively few studies comparing the efficacy of multiple- and single-wavelength experiments have appeared in the literature [1, 3].

The study described here examines the suitability of the extended Kalman filter, a digital filtering algorithm, for the analysis of a single, kinetically perturbed spectrum obtained during a chemical reaction. An alternative approach, also based on the Kalman filter, involves the analysis of an entire absorbance/time/wavelength data set. Results from these two approaches are compared with those obtained from the more conventional analysis of absorbance/time data at a single wavelength. The Kalman filter is suited for this type of comparative study, because it provides for time-dependent changes in models, and because it can include the spectral contributions of all reactants and products as part of the model, a feature which allows use of all of the data available from a multiwavelength kinetic experiment. It can be easily adapted to a wide variety of data formats, another feature which is convenient for such a study.

The chemical system chosen for this comparison involves the hydrolysis of *p*-nitrophenylphosphate, which is catalyzed by the enzyme alkaline phosphatase. This reaction has been studied extensively [6—8], and the kinetics are fairly well established [6]. Several of the commercially available methodologies for determining the activity of alkaline phosphatase in serum are based on kinetic methods. Most of these approaches are based on a two-point kinetic method, where the absorbance from a product species is measured at the start of the experiment and after a fixed time. The difference between these two absorbance values is related to the alkaline phosphatase activity in the sample.

In the study described here, several alternative data-collection schemes were applied, including two different absorbance/time (two-dimensional) formats, as well as a complete absorbance/time/wavelength (three-dimensional) format. All methods used for the collection of kinetic data in this study can be implemented with commercial instrumentation. Several different methods were used to calculate alkaline phosphatase activities from the data obtained, and the results for each of the different data collection and reduction approaches were compared.

THEORY

Data evaluation

The application of the Kalman filter to the study of first-order reaction kinetics has been described previously [3]. In that study, the extended Kalman filter was used to evaluate the first-order rate constant for a ligand exchange reaction, using the measurement model

$$Z(j) = [\epsilon_A(j) + \epsilon_B(j) - \epsilon_C(j) - \epsilon_D(j)][A]_0 \exp(-kt_j) + \epsilon_B(j)[B]_0 + [A]_0[\epsilon_C(j) + \epsilon_D(j) - \epsilon_B(j)] \quad (1)$$

In this case, wavelength was varied linearly with time, and a kinetically perturbed spectrum was obtained. Here, $Z(j)$ refers to the absorbance measurement at wavelength j (corresponding to time t_j), A and B, and C and D are reactant and product species, respectively, the ϵ values are the molar absorptivity values, $[A]_0$ and $[B]_0$ are the initial reactant concentrations, and k is the first-order rate constant. This model is particularly easy to apply when a conventional, scanning u.v.-visible spectrophotometer is used.

If a rapid scanning instrument is used, many absorbance measurements, $Z(j)$, can be obtained essentially at one time, t_k, during the experiment. When data can be obtained in this three-dimensional format, the model takes the form

$$Z(j, k) = [\epsilon_A(j) + \epsilon_B(j) - \epsilon_C(j) - \epsilon_D(j)]\,[A]_0 \exp(-kt_k) + \epsilon_B(j)[B]_0 + [A]_0[\epsilon_C(j) + \epsilon_D(j) - \epsilon_B(j)] \quad (2)$$

where $Z(j, k)$ represents an absorbance measurement obtained at wavelength j and at time t_k. Because of the recursive nature of the Kalman filter algorithm, the extension of the model to that given in Eqn. 2 is very easy to implement. On many small computers, the use of this model in conjunction with the Kalman filter allows the data to be processed in real time, between successive measurements of spectra.

Alkaline phosphatase kinetics

The activity of alkaline phosphatase can be measured by monitoring the rate of the reaction

$$C_6H_4NO_2PO_4^{2-} + OH^- \rightarrow C_6H_4NO_2OH + PO_4^{3-}$$

The substrate, *p*-nitrophenyl phosphate (NPP), is hydrolyzed to form *p*-nitrophenol; the rate of this reaction is accelerated in the presence of alkaline phosphatase. This reaction has been found to follow the rate law

$$(-d[NPP]/dt)_0 = k_p[E]_0[NPP]/(K_m + [NPP]) \quad (3)$$

when the initial rate of reaction is monitored at pH 10.1 [6]. Here, $[E]_0$ is the total enzyme concentration and K_m and k_p are constants derived from a Michaelis-Menten rate formulation, as given by Frazer et al. [2, 6]. For the case where $K_m \gg [NPP]$, this rate law reduces to

$$(-d[NPP]/dt)_0 = k[NPP] \quad (4)$$

where k is directly proportional to the enzyme activity. While this assumption is not strictly upheld for the above reaction catalyzed by alkaline phosphatase, under pseudo-zero-order conditions (when the substrate concentration is very large), the rate law expressed in Eqn. 4 is an adequate model. In this case, the exponential terms present in the first-order rate law are essentially equal to the linear terms present in a zero-order rate law, so both may be modelled by the same equation. Because the law described by

Eqn. 3 is, under limiting conditions, either zero order or first order, this approach should be valid, particularly when measurements are made at a single wavelength (typically 405 nm), where the nitrophenolate ion absorbs strongly compared to the substrate. The small changes in the absorbance caused by the reaction of the substrate cannot be observed at this wavelength. If measurements are made at wavelengths where the substrate absorbs strongly, small changes in the substrate concentration may be observed, and the rate law expressed in eqn. 3 may be more reliable. The use of the Kalman filter should facilitate the detection of this type of error [3]. In the studies described here, the model expressed by Eqn. 4 was chosen for the examination of the different data analysis methods, because it is a simpler model than Eqn. 3, and because the restrictions arising from the initial rate assumption will also limit the experimental conditions to pseudo-zero-order conditions. The parameters, $[NPP]_0$ and k, can then be estimated by using the Kalman filter models given by Eqns. 1 and 2.

EXPERIMENTAL

Spectra were obtained on a Hewlett-Packard model 5841A diode-array spectrometer with a 16K memory module. Data were collected from 390 nm to 450 nm, with a wavelength resolution of 2 nm. Ten spectra were averaged for each measurement, and a complete, averaged spectrum was acquired in 1 s. Spectral data were collected every 30 s, for a period of approximately 1000 s after the start of the reaction. The first spectral data were obtained within 60—200 s of mixing, and the time of data collection was carefully noted. This delay in beginning data collection was intended to allow complete mixing, which was done mechanically. In all cases, complete spectra were collected. All measurements were made using a fused silica cuvette with a 1-cm path length. Background spectra, taken just prior to collection of the kinetic data, were automatically subtracted from the spectra taken during the kinetic experiments by the diode-array spectrometer. Tests showed that the background spectra remained stable for periods exceeding the duration of these experiments. Background-corrected spectral data and the variance of the spectral measurements obtained from the diode array were stored in the spectrophotometer memory during data collection, then written to microfloppy disk, and subsequently transferred to an LSI-11/23, where the data-processing routines were available.

Programs used to analyze the data were written in FORTRAN and were run under the RT-11 operating system on the LSI-11/23 microcomputer. The Kalman filters used in these studies were modifications of programs previously reported [3, 9]. The Nelder-Mead simplex optimization algorithm was used to obtain non-linear least-squares fits, as described previously [3, 10]. The spectral data collected as a function of time and enzyme concentration were analyzed by five different methods. Two methods were based on the Kalman filter, one method utilized the simplex algorithm for non-linear

least-squares regression, another used linear least-squares regression, and the last was the standard two-point kinetic method.

Reagents were obtained in the form of an alkaline phosphatase enzyme analysis kit (Sigma, Method 246). Solutions and buffers were prepared according to the kit instructions. Freeze-dried serum enzyme control (Sigma S2005) was reconstituted as needed for the kinetic studies. All solutions were thermostatted at 25°C for at least 10 min prior to use. All measurements were made at pH 10.4. Nitrophenyl phosphate and nitrophenolate standards provided in the kit were found to have spectra in good agreement to those previously published [7]. Standard solutions with concentrations of 1.015×10^{-2} M and 5.00×10^{-5} M for nitrophenyl phosphate and nitrophenol, respectively, were used to obtain the molar absorptivity values required for the Kalman filter model. The hydrolysis of alkaline phosphatase was examined for several enzyme concentrations, ranging from 0.35 U l^{-1} to 3.2 U l^{-1}. These concentrations were obtained by the addition of microliter amounts of the enzyme control to solutions containing the substrate; the compositions of these solutions are summarized in Table 1.

RESULTS AND DISCUSSION

Three-dimensional Kalman filtering

The absorbance/time/wavelength data collected as described above were analyzed by the Kalman filter. The details of the Kalman algorithm have been reported previously [3, 9, 11]. For this study, the filter measurement model is given by Eqn. 2, which uses the separately measured spectra of the nitrophenolate product (species C in the model) and the nitrophenyl phosphate substrate (species A in the model). Species B (alkaline phosphatase) and D (phosphate) do not contribute to the absorbance and may be ignored. Estimates for the measurement variance were obtained from the standard deviation values generated by the diode-array spectrophotometer; these values were input to the filter as a separate disk file. Alternatively, a constant

TABLE 1

Characteristics of the kinetic data

File	Activity[a] (U l^{-1})	No. of spectra	Initial time[b] (s)	$[NPP]_0$[c] (10^{-3} M)
20	0.351	30	60.2	10.1
50	0.869	30	62.8	9.98
100	1.710	30	82.3	9.82
150	2.52	29	122.5	9.67
200	3.31	28	193.7	9.52

[a]Alkaline phosphatase activity. [b]Time when initial spectrum was acquired. [c]Substrate concentration at start of reaction.

estimate for the variance of the absorbance measurements of 1.0×10^{-7} could be used. Both of these approaches yielded similar parameter estimates. The initial guesses for the model for k and $[NPP]_0$ were set to zero. The variances in these guesses were given large values initially ($P = 1.0$) to ensure that unbiased estimates were obtained [11]. For each of the kinetic experiments, the filter was set to process the data sequentially, first in wavelength, then in time. The method is outlined in Fig. 1A. Results for fitting of the data by this "three-dimensional" filter are given in Table 2. The quality of the fits is quite good, as is evident from the small deterministic variances for fitting, and from the small values for the estimated variance (P) in the fitted parameters. After each absorbance measurement has been processed by the filter, the current estimates for k and $[NPP]_0$ are inspected. Examination of these estimates as the filter processes the data allows for the evaluation of the filter performance [12—14]. Plots of the parameter estimates as a function of the number of absorbance measurements processed by the filter are shown in Fig. 2. From these plots, it is apparent that the filter converges rapidly to stable estimates for substrate concentration, but to obtain stable estimates for the rate constant, several more absorbance measurements must be processed. For the largest value of k studied, the stability of the estimated k seems fairly poor; such behavior is typical of filters with incorrect models [12]. Possible reasons for the poor stability in this estimate for k may be temperature instabilities in the spectrophotometer, failure of the steady-state approximation (for the formation of the enzyme-substrate complex) as the enzyme concentration increases [6], or failure of the initial rate assumption.

Two-dimensional Kalman filtering

The data were also analyzed with the Kalman filter using Eqn. 1 as the model. The same species identities, measurement variances, and initial guesses were used in this analysis. This approach is outlined in Fig. 1B. Results for

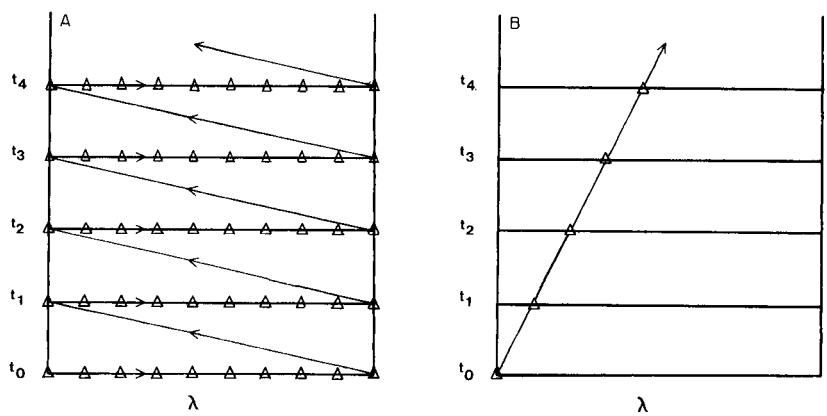

Fig. 1. Processing of three-dimensional kinetic data array by using the Kalman filter with different measurement models: (A) model given in Eqn. 2; (B) model given in Eqn. 1. (△) Points processed by the filter.

TABLE 2

Results for three-dimensional Kalman filter fits

File	$[NPP]_0$ (10^{-3} M)	$P(1,1)^a$ (10^{-16})	k (10^{-6} s^{-1})	$P(2,2)^b$ (10^{-20})	CD[c]	Var. Fit[d]
20	10.0	0.93	0.479	2.1	1.0000	6.3×10^{-6}
50	9.94	0.82	1.15	2.2	0.9999	7.0×10^{-5}
100	9.76	1.5	2.17	2.2	0.9997	3.0×10^{-3}
150	9.62	6.3	3.43	2.6	0.9996	3.8×10^{-4}
200	9.16	8.0	4.54	2.0	0.9991	1.3×10^{-3}

[a]Variance in the estimate for $[NPP]_0$. [b]Variance in the estimate for k. [c]Coefficient of determination. [d]Deterministic variance of the fit.

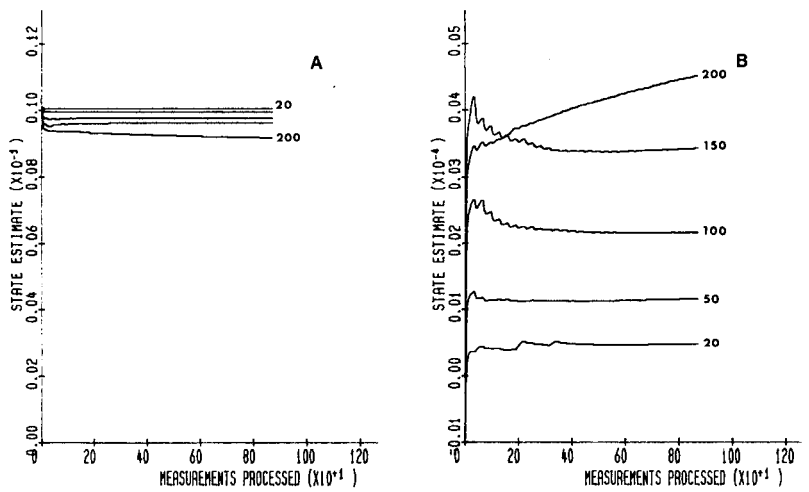

Fig. 2. (A) Evolution of the estimates for $[NPP]_0$ from the three-dimensional filter. (B) Evolution of the estimates for k from the three-dimensional filter.

the "two-dimensional" filtering of the single, kinetically perturbed spectrum obtained for each of the kinetic runs are presented in Table 3. The estimated values for $[NPP]_0$ and k agreed well with those found by using the three-dimensional filtering, even though substantially fewer data are used to obtain results, as is evident from a comparison of Fig. 1A and B. The effect of having fewer data points was noticeable only in the sizes of the estimated variances, P, which are slightly larger than the corresponding estimated variances in Table 2. The behavior of the current estimates for the parameters as a function of the number of data points processed by the filter is shown in Fig. 3; this behavior is similar to that for the three-dimensional filter, in that estimates for the substrate concentration settle quickly, but estimates for the rate constant require more data points to stabilize. Some instability in the

TABLE 3

Results for two dimensional Kalman filter fits on kinetically perturbed data

File	$[NPP]_0$ (10^{-3} M)	$P(1,1)^a$ (10^{-14})	k (10^{-6} s^{-1})	$P(2,2)^b$ (10^{-18})	CD[c]	Var. Fit[d] (10^{-4})
20	10.0	3.2	0.480	0.99	1.0000	0.18
50	9.95	3.5	1.15	1.1	1.0000	0.15
100	9.70	4.5	2.27	1.1	0.9999	0.88
150	9.58	4.8	3.51	1.0	0.9996	2.1
200	9.09	9.3	4.54	1.0	0.9988	9.1

[a–d]As for Table 2.

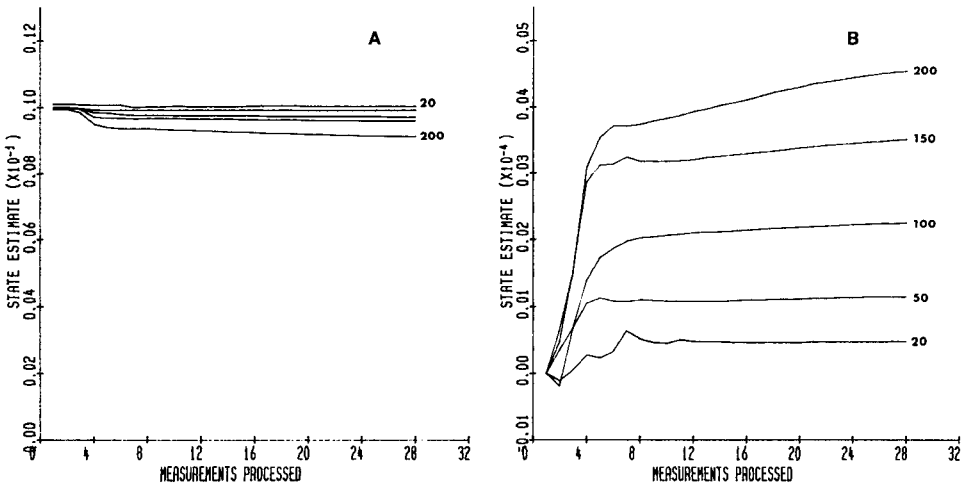

Fig. 3. (A) Evolution of the estimates for $[NPP]_0$ from the two-dimensional filter. (B) Evolution of the estimates for k from the two-dimensional filter.

estimates for the largest rate constant is also apparent; if model error of the types mentioned above were occurring, such instability would be expected.

Nonlinear least-squares fitting

To demonstrate the quality of the results obtained by use of the Kalman filter to fit kinetic data, "two-dimensional" fitting was also done with nonlinear least squares (assuming the first-order rate law given in Eqn. 4), and with linear least squares (assuming a zero-order rate law). Data used for these fits were generated by extraction of absorbance data at 404 and 406 nm as a function of time. The two absorbance values were averaged to produce an estimated value for the time-dependent absorbance of the solution at 405 nm, the wavelength often used in kinetic determination of alkaline phosphatase [8]. These data were fitted to the first-order model

$$Z(j) = \epsilon_{NPP}[NPP]_0\{\exp(-kt_j)\} + \epsilon_{NP}[NPP]_0\{1 - \exp(-kt_j)\} \quad (5)$$

where $Z(j)$ is the solution absorbance at time t_j, ϵ_{NPP} and ϵ_{NP} are the molar absorptivities of the substrate NPP and product NP species, respectively, and k is the first-order rate constant. The molar absorptivities for substrate and product species at 405 nm were estimated from spectra obtained for use in the filtering studies reported above. Results for the nonlinear least-squares fits are summarized in Table 4.

Linear least-squares fitting

Because the conditions under which the kinetic runs may be quite close to those for a zero-order reaction, the time-dependent absorbance data at 405 nm were also fitted to the zero-order model

$$Z(j) = Z(0) + k't_j \quad (6)$$

where $Z(0)$ is the initial solution absorbance, and k' is the zero-order rate constant. These results are also included in Table 4. Not surprisingly, the results for the nonlinear and linear least-squares are similar, no doubt because of the close similarity between the terms $[NPP]_0e^{-kt}$ and $-k't$. Estimation of $[NPP]_0$ made from the $Z(0)$ values obtained from the linear least-squares fitting produces results substantially different from those estimated by the nonlinear fitting, particularly for the two solutions with the highest enzyme activities. The fit results for the zero-order model are not as good as the fit results for the first-order model. This indicates that the choice of the first-order model for the Kalman filter studies was probably valid.

Comparison of the fitting methods

The precision and accuracy of the various fitting methods can be compared. Table 5 summarizes the enzyme activities and the values for the initial substrate concentrations obtained from each of the various fitting approaches. For comparison, results are also included for estimation of the enzyme

TABLE 4

Results for linear and nonlinear least-squares fits

File	Nonlinear fitting			Linear fitting		
	$[NPP]_0$ (10^{-3} M)	k (10^{-6} s^{-1})	CD[a]	$Z(0)$[b]	k' (10^{-8} M s^{-1})[c]	CD[a]
20	8.61	0.58	0.99989	0.376	0.47	0.9795
50	9.88	1.08	0.99996	0.433	1.10	0.9994
100	9.74	2.04	0.99996	0.426	1.95	0.9993
150	7.59	4.04	0.99994	0.333	3.07	0.9990
200	6.44	6.72	0.99990	0.283	4.32	0.9987

[a]Coefficient of determination. [b]Initial absorbance. [c]Zero-order rate constant.

TABLE 5

Comparison of accuracy[a]

File	True	3D-KF[b]	2D-KF[b]	Non-linear[b]	Linear[c]	Two-point[d]
20	1.01×10^{-2}	1.00×10^{-2}	1.00×10^{-2}	8.61×10^{-3}	8.58×10^{-3}	—
	53.0	55.3	55.3	57.0	54.1	45.7
50	9.98×10^{-3}	9.94×10^{-3}	9.95×10^{-3}	9.88×10^{-3}	9.88×10^{-3}	—
	53.0	53.3	53.3	49.6	51.1	51.6
100	9.82×10^{-3}	9.76×10^{-3}	9.70×10^{-3}	9.74×10^{-3}	9.74×10^{-3}	—
	53.0	50.0	52.0	46.7	46.0	42.2
150	9.67×10^{-3}	9.62×10^{-3}	9.58×10^{-3}	7.59×10^{-3}	7.60×10^{-3}	—
	53.0	52.8	53.8	48.9	49.2	45.0
200	9.52×10^{-3}	9.16×10^{-3}	9.09×10^{-3}	6.72×10^{-3}	6.46×10^{-3}	—
	53.0	50.7	50.3	52.6	52.6	46.7
Av. Activ. ($U\ l^{-1}$)		52.4	52.9	51.0	50.6	46.2
Std. Dev.		2.1	1.9	4.0	3.2	3.4

[a]Top value is initial substrate concentration, in M, bottom value is true value for the undiluted enzyme control. All results have been corrected for temperature. [b]Results are calculated from the first-order rate constant and the volume of enzyme control added. Substrate concentration is obtained directly. [c]Results are calculated from the zero-order rate constant and the volume of enzyme standard added. Substrate concentration is calculated from the initial absorbance obtained in the fitting. [d]Activity values calculated from the observed change in absorbance over a 180-s period.

activity using the two-point kinetic approach, as described in the Sigma analysis kit; with this approach, an estimation of substrate concentration was not possible. True values for each of these quantities are also included. The approaches based on filtering produced excellent estimates for both enzyme activity and for initial substrate concentration. While the precision demonstrated by the various fitting methods was similar, estimates for the enzyme activity from the nonlinear and linear least-squares estimation were somewhat less accurate than those produced from filtering (the t-test showed a difference between the filtering and single wavelength methods at confidence levels up to 80%), and considerably less accurate in estimating the substrate concentration. All methods were more accurate than the two-point method recommended by the kit manufacturer.

Conclusions

The successful estimation of both enzyme activities and substrate concentrations by the Kalman filter suggests that such fitting techniques may be especially valuable in substrate assays, enzyme assays, and in the analysis of other dynamic systems. The modest demands made on computers by the filter algorithm should allow its direct incorporation into real-time kinetic analyzers.

This work was supported by the U.S. Department of Energy through Grant DE-FG06-84ER13202. The authors are grateful for the loan of the diode-array spectrometer by Mr. Steve Sibley of the Hewlett-Packard Corporation.

REFERENCES

1 B. G. Willis, W. H. Woodruff, J. R. Frysinger, D. W. Margerum and H. L. Pardue, Anal. Chem., 42 (1970) 1350.
2 J. W. Frazer, L. P. Rigdon, H. R. Brand and C. L. Pomernacki, Anal. Chem., 51 (1979) 1739.
3 S. C. Rutan and S. D. Brown, Anal. Chim. Acta, 167 (1985) 23.
4 G. M. Ridder and D. W. Margerum, Anal. Chem., 49 (1977) 2090.
5 G. M. Ridder and D. W. Margerum, Anal. Chem., 49 (1977) 2098.
6 J. W. Frazer, L. P. Rigdon, H. R. Brand, C. L. Pomernacki and T. A. Brubaker, Anal. Chem., 51 (1979) 1747.
7 G. N. Bowers and R. B. McComb, Clin. Chem., 12 (1966) 70.
8 L. Berger and G. G. Rudolph, in S. Meites (Eds.), Standard Methods of Clinical Analysis, Vol. 5, Academic Press, New York, 1965, pp. 211—220.
9 T. F. Brown and S. D. Brown, Anal. Chem., 53 (1981) 1410.
10 J. J. Toman and S. D. Brown, Anal. Chem., 53 (1981) 1497.
11 S. C. Rutan and S. D. Brown, Anal. Chim. Acta, 160 (1984) 99.
12 A. Gelb (Ed.), Applied Optimal Estimation, M.I.T. Press, Cambridge, MA, 1974.
13 P. F. Seelig and H. N. Blount, Anal. Chem., 51 (1979) 327.
14 C. B. M. Didden and H. N. J. Poulisse, Anal. Lett., 13 (1980) 921.

Analytica Chimica Acta, 175 (1985) 231—237
Elsevier Science Publishers B.V., Amsterdam — Printed in The Netherlands

COMPARISON OF SIMPLEX ALGORITHMS[a]

L. R. PARKER, JR.[b], M. R. CAVE[c] and R. M. BARNES*

Department of Chemistry, GRC Towers, University of Massachusetts, Amherst, MA 01003-0035 (U.S.A.)

(Received 31st January 1985)

SUMMARY

A new modification of the super-modified simplex algorithm is described. The performance of this algorithm is compared with that of the super-modified simplex algorithm and the Nelder-Mead, or modified, simplex algorithm, using both mathematical functions and experimental optimization of an inductively coupled plasma spectrometer. The modification added to the super-modified simplex algorithm increases its speed and accuracy over the original super-modified algorithm.

Since its introduction in 1962 by Spendley et al. [1], the sequential simplex algorithm has been widely used for optimization in chemistry. A modification by Nelder and Mead in 1965 [2], which became known as the variable-size simplex, led to increased use, offering three primary advantages over the original (fixed-size) algorithm: the simplex could increase its size as it moved up a "hill", and thus cover the distance more quickly; it could contract and then reexpand in a different direction, and thus reorient itself to move more efficiently along a "ridge"; and it could contract repeatedly around the optimum, providing evidence that an optimum had been found and closely defining its location. The expansion in the Nelder-Mead simplex algorithm is fixed at twice the distance from $\bar{P}$ (the centroid of the hyperface defined by the vertices remaining after eliminating the worst) to W (the worst vertex); the contraction may be either plus or minus one-half this distance. A 1978 review [3] summarized the rules of both the fixed- and variable-size simplex algorithms, and gave examples of their application in analytical chemistry.

An additional modification of the simplex algorithm was introduced by Routh et al. [4], and became known as the super-modified simplex. Instead of limiting the new vertex to four possible locations [the original reflection,

[a]Presented in part at the 1982 Winter Conference on Plasma Spectrochemistry, Orlando, FL, 1982, U.S.A.

[b]On leave from: Department of Chemistry, Vassar College, Poughkeepsie, NY 12601, U.S.A.

[c]Present address: British Geological Survey, Nicker Hill, Keyworth, Nottingham, United Kingdom.

0003-2670/85/$03.30

R, given as $\bar{P} + (\bar{P} - W)$; an expansion, E, given as $\bar{P} + 2(\bar{P} - W)$; a contraction, C_r, given as $\bar{P} + 0.5(\bar{P} - W)$; and an alternative contraction, C_w, given as $\bar{P} - 0.5(\bar{P} - W)$], this new simplex algorithm allowed the new vertex to be anywhere on the line connecting W and $\bar{P}$, subject to minimum and maximum limits and boundary constraints. The algorithm basically involves running an experiment at the reflection vertex, R, and one at the hyperface centroid, $\bar{P}$. These values, along with the result at W, give three responses along the $W - \bar{P}$ vector, sufficient to fit a second-order model. The model expresses the change in response from $\bar{P}$ to W and from $\bar{P}$ to R as a function of the distance from $\bar{P}$ to W and from $\bar{P}$ to R. From the parameter values of this model, the distance from $\bar{P}$ which gives the highest response can be predicted. An experiment is done at this predicted location and the response is compared with that at R; the vertex giving the better response is the one retained to form the new simplex.

Certain constraints exist on the super-modified simplex algorithm. If the model shows a concave upward surface, no location can be found which would give the maximum response; in this case, the new vertex is placed a certain maximum distance from $\bar{P}$ (typically, three times the distance from $\bar{P}$ to W). If the predicted location is within the current simplex, a minimum value (the "safety interval factor" [4], typically 0.1 times the distance from $\bar{P}$ to W) prevents the new vertex from being placed too close to $\bar{P}$ (a situation which might remove some freedom of movement from the simplex). This minimum is removed when the simplex nears the optimum (using the "criterion for safety interval factor" [4]) to allow the simplex to contract about the optimum. In addition, if the predicted vertex is outside a boundary, the vertex is placed at the boundary.

The only obvious disadvantages of the super-modified simplex are the extra experiment required to evaluate the response at $\bar{P}$, and that model-fitting is required, normally involving matrix inversion and multiplication. This makes it more difficult to implement than the Nelder-Mead algorithm, but if the optimization is computerized, this presents no major limitation.

For this work, a further modification of the super-modified simplex algorithm was added. Instead of running an experiment to evaluate the response at $\bar{P}$, the response there was taken to be the average of the responses of the retained vertices (i.e., all the vertices in the current simplex with the exceptions of W and R). It was expected that this would decrease the number of experiments; studies were undertaken to evaluate how the performance of this modified super-modified simplex (SMS2) algorithm compared with both the super-modified simplex (SMS) and the Nelder-Mead modified simplex (MSM) algorithms.

EXPERIMENTAL

The comparison of simplex algorithms was undertaken in three separate phases. The generating factors for all simplexes were as follows: for MSM,

expansion factor = 2.0 and contraction factor = 0.5; and for SMS and SMS2, expansion factor = 3.0, criterion for safety interval factor = 0.5, and safety interval factor = 0.1.

The first phase compared the Nelder-Mead modified simplex method (MSM), the super-modified simplex method (SMS), and the proposed modification of the super-modified simplex method (SMS2) by using the following function:

$$Y = 250 - (X1 - 72)^2 - (X2 - 16)^2 - (X3 - 37.3)^2 - \mathrm{ABS}[1.1(X1 - 72)] - \mathrm{ABS}[0.8(X2 - 16)] - \mathrm{ABS}[0.9(X3 - 37.3)] \quad (1)$$

for which the optimum lies at $X1 = 72$, $X2 = 16$, and $X3 = 37.3$, with an optimum response of 250. Each factor has upper and lower boundaries of 0 and 100, respectively. The simplex was terminated when the range of responses, expressed as a percentage of the best response, fell within a certain value. Three different termination values used were 10%, 1%, and 0.1%. Three different sets of starting conditions used were each factor at 10 with a step size of 10, each factor at 80 with a step size of 10, and each factor at 10 with a step size of 70. In addition, the function was evaluated once with random noise added. Initial simplexes were constructed from these starting conditions according to the method of Spendley et al. [1] and Yarbro and Deming [5]. The basis for comparison was the number of evaluations (experiments) required by each simplex algorithm and the closeness of the best response to the true optimal value.

The second phase of the comparison used the following three mathematical functions. First,

$$Y = \sin(X1) + \sin(X2) \quad (2)$$

with a range of 0 to 270 degrees in each factor; the optimum is located at $X1 = X2 = 90$ degrees with a response of 2.0. Second,

$$Y = 100(X2 - X1)^2 + (1 - X1)^2 \quad (3)$$

(Rosenbrock's function [6]) with a range of −25 to +25 in each factor; the optimum (a minimum) is located at $X1 = X2 = 1.0$ with a response of 0.0. And third,

$$Y = \sin(X1) + \sin(X2) + \sin(X3) + \sin(X4) \quad (4)$$

with a range of 0 to 270 degrees for each factor; the optimum lies at $X1 = X2 = X3 = X4 = 90$ degrees with a response of 4.0. This phase of the study was designed in a similar manner to the method of Ryan et al. [7] with some modifications. Five initial starting sizes of the simplex for each function were chosen. For each starting size, ten randomly generated coordinates were produced within the boundaries of the regions defined for each function. Using these coordinates and the procedure described by Yarbro and Deming [5], the initial simplexes for each function and step size were constructed. The same set of initial simplexes for each step size was used for each simplex method (MSM, SMS, and SMS2).

Two criteria were used to compare the different simplex algorithms. One was the average number of evaluations; the other was the ratio of noncritical nonconvergences to critical nonconvergences. (A noncritical nonconvergence is defined as one for which the simplex converges to a false optimum more than 10 times the termination criterion distant from the true optimum; a critical nonconvergence is defined as one for which the simplex converges to a false optimum more than 1000 times distant.) In addition, these two criteria were combined to form a third criterion, the performance function (P), defined as

$$P = \log (A) \tag{5}$$

for which A is the average number of evaluations. If critical or noncritical nonconvergences occurred, then P is defined as

$$P = \log (A) + \log (10N) + \log(100C) \tag{6}$$

in which N is the number of noncritical nonconvergences and C is the number of critical nonconvergences. Thus, the P function combines a measure of speed and accuracy in one function, with the simplex method producing the lowest value of P being the most desirable.

Simplex optimization has been applied with success to the operation of an inductively-coupled plasma atomic emission spectrometer (i.c.p./a.e.s.) [8, 9]. The third phase of this comparison study used the MSM and SMS2 algorithms to optimize the signal-to-background ratio for the copper 324.75-nm and the manganese 257.61-nm emission lines in an i.c.p./a.e.s. Instrumental components used are summarized in Table 1. A six-parameter optimization was applied on the slit height, slit width, incident power, coolant gas flow, injector gas flow, and auxiliary gas flow. The initial values and step size used to construct the initial simplex are shown in Table 2 along with boundary conditions for each parameter. The simplex was terminated when the range of responses was within 10% of the best response.

RESULTS AND DISCUSSION

Some data for Eqn. 1 are given in Table 3. For a termination criterion of 0.1%, starting at 10 with a step of 70, the MSM, SMS, and SMS2 methods

TABLE 1

Instrumental components used in emission spectroscopic studies

Generator	Plasma-Therm Model HFS-5000D, 40.68 MHz, with 3-turn (1/8-in. copper) load coil
Nebulizer	Babington-style nebulizer pumped at 3 ml min^{-1}
Plasma torch	Conventional 18-mm i.d. quartz with 1.5-mm injector orifice
Detection	Minuteman monochromator Model 310-SMP, 1-m Czerny-Turner with 1200 grooves mm^{-1}; 1:1 image formed by quartz lens (Oriel A-11-661-37); RCA 1P28 photomultiplier tube (—700 V); Keithley 411 picoammeter connected via ADC to PDP-11/23 minicomputer

TABLE 2

Conditions for emission spectroscopic studies

Parameter	Initial value	Step size	Boundary condition	
			Low	High
Slit height (mm)	20.0	40.0	10	150
Slit width (μm)	3.0	15.0	1.0	20.0
Power (kW)	0.5	0.7	0.4	1.5
Injector gas flow[a]	0.4	0.8	0.4	1.2
Coolant gas flow[a]	11.0	7.0	10.5	20.0
Auxiliary gas flow[a]	0.7	1.1	0.0	2.0

[a]l min^{-1}.

TABLE 3

Results of first phase comparison of simplex algorithms (Eqn. 1) with termination criteria of 10% and 1%

Algorithm	10% criterion		1% criterion	
	No. of evaluations	Response	No. of evaluations	Response[a]
Starting at 10; step of 10				
MSM	30	217.4	44	247.5
SMS	64	239.2	76	248.5
SMS2	48	248.5	50	249.2
Starting at 80; step of 10				
MSM	38	234.0	49	246.7
SMS	82	238.5	88	244.7
SMS2	56	237.5	62	248.7
Starting at 10; step of 70				
MSM	27	225.8	41	247.8
SMS	22	210.1	34	227.1
SMS2	20	235.7	22	239.4

[a]Expected value, 250.

gave values of 249.5, 229.3, and 243.9 with 52, 76, and 60 evaluations, respectively. For a termination criterion of 10% with random noise, starting with a step of 10, results in the same order as above were 227.5, 230.7, and 231.2 with 32, 64, and 44 evaluations, respectively. In general, the SMS2 algorithm performed better than the SMS algorithm. In every trial, SMS2 required fewer evaluations to converge (25% fewer on the average) and, in 6 out of 7 trials, SMS2 found an optimum with response closer to the true value. Also, SMS2 displayed a significant advantage over SMS when a large

initial step size (70) was used. In the presence of random noise, the same trend is evident; SMS2 converged to a higher response in a smaller number of experiments than SMS.

Results for the different simplex algorithms on the mathematical functions used in the second phase are given in Table 4 with the average number of evaluations required for each step size and the number of noncritical and critical nonconvergences. For the two sine functions (Eqns. 2 and 4), the SMS2 algorithm showed a significantly lower number of evaluations than the MSM algorithm at initial step sizes over 10% of the range, based on a t-test. The SMS algorithm showed a tendency to require more evaluations than the MSM algorithm on the sine functions, although the level of significance was not very high. For Rosenbrock's function (Eqn. 3), the MSM and SMS2 algorithms performed essentially the same, and the SMS algorithm was significantly worse for all step sizes.

To show trends in speed and accuracy more clearly, the performance function, P (Eqns. 5 and 6), was calculated from the data for the functions given by Eqns. 2, 3, and 4, and is given in Table 4.

The best simplex algorithm should be the one which produces the minimum value of the performance function, P, over the widest range of initial step sizes. In general, for both the 2- and 4-factor sine functions (Eqns. 2 and 4), an improvement in performance occurs as the initial step size increases

TABLE 4

Results for comparisons in second phase of simplex optimization

Algorithm	Eqn. 2[a]			Eqn. 3[b]			Eqn. 4[c]		
	No. of eval.[d]	Nonconv. N/C[e]	P	No. of eval.[d]	Nonconv. N/C[e]	P	No. of eval.[d]	Nonconv. N/C[e]	P
MSM	34	2/1	4.8	170	0/0	2.2	130	9/0	11.1
SMS	51	0/0	1.7	282	3/0	6.9	140	8/4	18.2
SMS2	31	1/0	2.5	174	2/0	4.2	77	9/4	18.9
MSM	25	0/0	1.4	187	0/0	2.3	74	8/0	9.9
SMS	30	0/0	1.5	271	1/0	3.4	82	9/0	10.9
SMS2	21	1/0	2.3	187	1/0	3.3	70	8/0	9.9
MSM	22	0/0	1.3	174	0/0	2.2	49	0/0	1.7
SMS	24	1/0	2.4	317	2/0	4.5	57	7/0	8.8
SMS2	16	0/0	1.2	167	0/0	2.2	33	0/0	1.5
MSM	23	0/0	1.4	197	0/0	2.3	49	0/0	1.7
SMS	25	1/0	2.4	565	4/4	14.8	54	9/0	10.7
SMS2	15	0/0	1.2	303	2/2	8.5	31	0/0	1.5
MSM	35	1/0	2.5	225	1/1	5.4	53	0/0	1.7
SMS	28	0/0	1.5	334	1/0	3.5	56	6/0	7.8
SMS2	15	0/0	1.2	213	0/0	2.3	29	0/0	1.5

[a–c]Initial step sizes top to bottom (% of range): [a]1.85, 11.1, 33.3, 44.4, and 88.9; [b]2, 10, 20, 50, and 90; [c]1.85, 11.1, 33.3, 44.4, and 88.9. [d]Number of evaluations. [e]Nonconvergence, noncritical/critical.

up to 40%. The best algorithm for the two functions appears to be the SMS2, which consistently produced the lowest value of P over step sizes ranging from 30% to 90%. The MSM method was better than the SMS method.

For Rosenbrock's function (Eqn. 4), the general trend of improved performance for increased step size is no longer evident. The best performance over the widest step size range is found using the MSM method, with SMS2 again performing better than SMS.

The results for evaluations of the mathematical functions in the second phase suggested that SMS2 would be a superior algorithm to use on relatively simple response surfaces, while MSM might be better on more complex surfaces. Thus, for the instrumental optimization in the third phase, these two algorithms were compared. Each algorithm was used to optimize the i.c.p./a.e.s. parameters given in Table 2 for the copper and manganese lines. After the optimizations, univariate searches for each parameter were made in the manner of Ebdon et al. [10, 11] to confirm that the simplex algorithms had located a true optimum. For each parameter, an optimum range was calculated by using the centroid of the final simplex plus or minus one standard deviation of the final simplex. In all cases, this optimum range was in close agreement with the result of the univariate search.

For both methods, the optimum value for each parameter was well defined, with little overall difference in the two algorithms. The univariate search data also illustrated the steepness of the effect of each parameter on the optimum signal-to-background ratio, with the coolant and auxiliary gas flow rates showing the least effect on the optimum response. The two algorithms differed in the speed with which the optimum was located; SMS2 required an average of 12 evaluations while MSM required 24 evaluations.

In summary, a modification to the super-modified simplex algorithm that involves replacing an evaluation of the response at P with the average value of the retained vertices, produces improved performance, both in terms of reducing the number of evaluations required for convergence and the accuracy with which the optimum is located.

REFERENCES

1 W. Spendley, G. R. Hext and F. R. Himsworth, Technometrics, 4 (1962) 441.
2 J. A. Nelder and R. Mead, Comput. J., 7 (1965) 308.
3 S. N. Deming and L. R. Parker, Jr., CRC Crit. Rev. Anal. Chem., 7 (1978) 187.
4 M. W. Routh, P. A. Schwartz and M. B. Denton, Anal. Chem., 49 (1977) 1422.
5 L. A. Yarbro and S. N. Deming, Anal. Chim. Acta, 73 (1974) 391.
6 H. Rosenbrock, Comput. J., 3 (1960) 175.
7 P. B. Ryan, R. L. Barr and H. D. Todd, Anal. Chem., 52 (1980) 1460.
8 S. P. Terblanche, K. Visser and P. B. Zeeman, Spectrochim. Acta, Part B: 36 (1981) 293.
9 R. M. Barnes, H. S. Mahanti, M. R. Cave and L. Fernando, ICP Info. Newsl., 8 (1983) 562.
10 L. Ebdon, D. J. Mowthorpe and M. R. Cave, Anal. Chim. Acta, 115 (1980) 171.
11 L. Ebdon, M. R. Cave and D. J. Mowthorpe, Anal. Chim. Acta, 115 (1980) 179.

Analytica Chimica Acta, 175 (1985) 239—255
Elsevier Science Publishers B.V., Amsterdam — Printed in The Netherlands

ION-EXCHANGE RESINS CONTAINING S-BONDED DITHIZONE AND DEHYDRODITHIZONE AS FUNCTIONAL GROUPS
Part 2. Desorption Properties and development of Separation Procedures for Gold and Platinum Group Metals

M. GROTE and A. KETTRUP*

University of Paderborn, Dept. Chem., Applied Chemistry, P.O. Box 1621, D-4790 Paderborn (Federal Republic of Germany)

(Received 26th March 1985)

SUMMARY

The desorption of precious metals from the P-D and P-TD ion-exchange resins, containing S-bonded dithizone and dehydrodithizone as functional groups, is described. Each sorbent was loaded batchwise with individual or combined metals and then treated with excess of various extracting agents (6 M hydrochloric acid, 2 M perchloric acid, ammonium nitrate, sodium thiocyanate, thiourea). Strong retention of some adsorbed metals and instability during the loading and elution stages were found with the P-D resin, but a selective separation of palladium and gold from accompanying metals was possible. The P-TD resin had superior properties. Unusual effects were detected when elution rates were compared for individual metals and mixtures. While Pd and Pt, loaded individually, were desorbed quantitatively by thiourea, co-extracted Ir(IV) completely inhibited their elution. The regeneration of P-TD by special sequences of eluents was utilized for selective chromatographic separation of Pd, Pt, Os, Au and (with restrictions) Ir from each other and also from large amounts of base metals and salts.

In Part 1 of this series [1], the preparation of a novel anion-exchanger P-TD was described. The exchanger, based on polystyrene (P), contained S-bonded dehydrodithizone as functional groups and reduction of this product yielded the chelating resin P-D, characterized by S-bonded dithizone groups. Basic sorption properties established the high affinity and selectivity

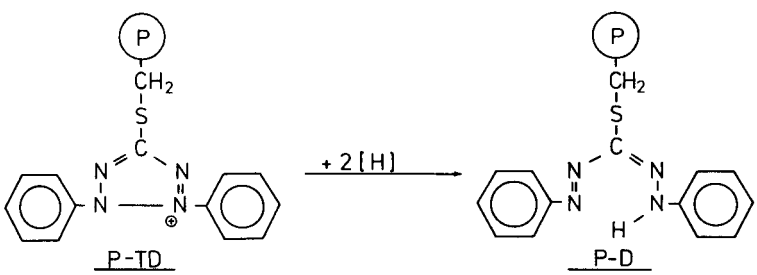

0003-2670/85/$03.30

of both resins for noble metals, but from its efficiency in column tests the anion-exchanger P-TD seemed to be more profitable.

The subject of this work was to test first the possibility of regenerating these sorbents, which is an important requirement for the development of cyclic separation procedures. However, as has been known for years, the chlorocomplex anions of platinum group metals can be eluted only inefficiently from conventional strong-base anion-exchange resins [2—4]. More satisfactory methods were developed with use of weakly basic sorbents, based on cellulose [5—8], polystyrene [9, 10] and other polymers [4, 11]. A variety of different sorption media and eluting reagents were tested, e.g., concentrated hydrochloric acid, perchloric acid [2, 3, 12], ammonium salts [13], thiocyanate [4, 11] and thiourea [10, 14]. However, because of their variability in forming complexes in aqueous solution, the sorption and elution behaviour of some platinum metals (Ru, Rh, Ir) remains troublesome. In many ion-exchange schemes, osmium is not taken into consideration, largely because its distillation as OsO_4 is a conventional part of platinum group separations.

In order to test the applicability of the P-TD and P-D resins synthesized, the recovery of precious metals was studied, as well as their separation from base metals in cyclic procedures, by use of those eluents mentioned above.

EXPERIMENTAL

The preparation of the sorbents P-D and P-TD and the evaluation of their sorption properties by use of sequential and simultaneous multi-element d.c. plasma emission spectrometry (d.c.p.) have been already described [1].

Methods

Determination of the rate of extraction of individual metals from the resins (Tables 1 and 3). Air-dried resin samples (200 mg) were loaded in 20 ml of 1 M hydrochloric acid, which was 10^{-2} M in the individual metal. After a shaking time of 4 h, the loaded resin was filtered off and washed with small portions of 1 M HCl, 0.1 M HCl and finally water. From the analysis of combined filtrate and wash solutions, the amount of metal taken was determined indirectly. Then the individual sorbents were suspended in 30 ml of each extracting solution. Within a total reaction time of 4 h, aliquots were taken for analysis after appropriate intervals.

Determination of simultaneous rates of extraction (Tables 2, 4 and 5). For this purpose, portions (400 mg) of resin were loaded in 20 ml of 1 M hydrochloric acid, which was 10^{-2} M in each precious metal. The determination of the initial amounts of metals on the resin and the amounts eluted in 50 ml of extracting solution as a function of time were done simultaneously, by using the d.c.p. emission spectrometer.

Elution-chromatographic procedures. Glass columns with an internal diameter (i.d.) of 0.5 cm were filled with 750 mg of resin, suspended and

pre-equilibrated in 1 M HCl. The height of the resin beds was about 4 cm. The outlet of the column was connected to a peristaltic pump either for coupling with the d.c.p. emission spectrometer (d.c.p./l.c. system [1]) or for collection of individual fractions ($\geqslant$2 ml).

Small sample volumes of 500 μl were fed onto the top of the column by a micropipette and large volumes (50 and 500 ml) by a second peristaltic pump. Further experimental details of the individual procedures are listed in the appropriate tables. The recoveries (%) of metals presented in Tables 6–10 are mean values of three separate procedures. All desorption studies under static and dynamic conditions were done at ambient temperature (20 ± 1°C).

DESORPTION PROPERTIES OF THE CHELATING RESIN P-D

First, batches of the sorbent P-D were loaded to the maximum with the appropriate metal and then treated with an excess of various extracting solutions. The concentrations of the extracted metals were subsequently determined as a function of time. The results obtained for a shaking time of 4 h are presented in Table 1. The data show that the individual metal ions are retained very strongly by the resin. Only the competing ligand, thiourea, and to a lesser extent thiocyanate, chelates the resin-bonded metals Au, Pd and Pt nearly quantitatively; the release of the other elements is very low. As expected by the high distribution coefficients in strong acid [1], desorption by hydrochloric or perchloric acid is usually poor.

These extraction studies were repeated with a simultaneously loaded sorbent, by applying a mixture containing the precious metals in their

TABLE 1

Extraction (%) of individual precious metals from P-D by various solutions (Loading conditions: 200 mg of resin, 20 ml of 1 M HCl, 10^{-2} M in the individual metal. Shaking time 4 h. Extraction with 30 ml of solution over 4 h.)

Metal	Initial amount on resin (mg)	Extraction (%) with different solutions				
		6 M HCl	2 M $HClO_4$	5% thiourea in 0.1 M HCl	0.5 M NaSCN	0.5 M NH_4NO_3 in 0.1 M NH_3
Au(III)	17.56	14.2	12.0[b]	95.0[a]	11.6	68.3
Pd(II)	8.65	21.2	0.01	97.7[a]	53.1	42.3[a]
Pt(IV)	7.19	32.1	7.0[b]	97.7	9.0[b]	5.3
Pt(II)	9.22	0.4	<0.01	81.6[a]	30.8	0.8
Ru(III)	1.73	12.4[a]	11.4[a]	30.7[a]	6.1	14.9[a]
Rh(III)	1.83	6.5[a]	1.2[a]	9.7[a]	6.7[a]	2.8[a]
Os(IV)	2.69	30.4[a]	31.5	5.9[b]	47.3	33.8[b]
Ir(IV)	3.37	10.2[a]	10.0[a]	5.3[a]	11.5[a]	7.9[a]
Ir(III)	0.81	9.3[a]	3.4[a]	10.9[a]	4.4[a]	20.9[a]

[a]Increasing extraction with extending shaking time. [b]Decreasing extraction with extending shaking time.

commonest oxidation states. The results in Table 2 exhibit in some cases marked differences compared to the desorption yields obtained with the individual elements (Table 1). Such effects were observed in the case of Pt(IV) with 2 M perchloric acid as extractant, and in ammoniacal medium for Au(III) or in 0.5 M thiocyanate for Pd, Pt and Os. Thus, the presence of accompanying metal ions on the resin seems to enhance or to retard the desorption of some elements. For illustration, two diagrams allow the rates of elution from P-D by sodium thiocyanate to be compared for an individually loaded resin (Fig. 1) and a simultaneously loaded resin (Fig. 2). Obviously the extraction of palladium(II) is almost prevented in presence of other co-extracted precious metals, whereas up to 50% of the individually loaded metal can be extracted (Fig. 1). Those effects were studied in detail in the case of P-TD (see below). In contrast, the desorption of osmium proceeds more completely from the simultaneously loaded sorbent. From this point of view, the behaviour of Pt(IV) is similar to that of Os(IV), but the progress of desorption during the shaking time is quite different.

Competing effects of desorption and re-extraction of platinum(IV) characterize the chelating resin P-D just like the anion-exchanger P-TD (see below). This similarity can be explained again [1] by redox reactions between the immobilized dithizone groups of P-D and the mixture of oxidizing metal ions during the loading stage, resulting in a partial conversion to tetrazolium groups. The rates of simultaneous desorption of Pd, Pt and Au (Fig. 3) by thiourea look like the individual rates. Because of the relatively rapid ligand exchange and formation of cationic complexes by thiourea [10], these precious metals are desorbed nearly quantitatively after a reaction time of 1 h, whereas osmium remains on the resin.

Considering the desorption properties of P-D discussed above and the previously presented sorption properties, separations of some precious metals

TABLE 2

Simultaneous extraction (%) of precious metals from P-D by various solutions (Loading conditions: 400 mg of resin in 20 ml of 1 M HCl, 10^{-2} M in each metal. Shaking time 1 h. Extraction with 50 ml of solution over 4 h.)

Metal	Initial amount on resin (mg)	Extraction (%) with different solutions				
		6 M HCl	2 M $HClO_4$	5% thiourea in 0.1 M HCl	0.5 M NaSCN	0.5 M NH_4NO_3 in 0.1 M NH_3
Au(III)	3.93	3.3[b]	0.02[b]	91.8	5.7	0.24[b]
Pd(II)	2.07	1.3[b]	~0	100.7	7.9	27.5[a]
Pt(IV)	0.64	73.0[b]	68.5[b]	90.5	43.1[b]	43.8[b]
Ru(III)	0.22	2.7	5.4[a]	5.9	~0	8.6[a]
Rh(III)	0.07	6.1[a]	5.4	10.6	39.0[a]	6.1[a]
Os(IV)	1.47	66.2[b]	82.4	1.3	96.8[a]	86.6
Ir(IV)	0.05	22.0	44.6[a]	~1.1	38.0	~1.7

[a,b] As in Table 1.

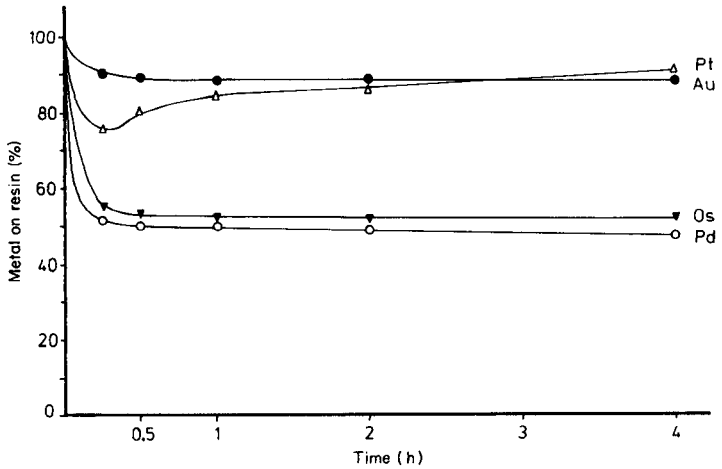

Fig. 1. Rate of extraction of individual precious metals from P-D by 0.5 M NaSCN. (Amount of individual metal on resin (mg/200 mg): Au(III) 17.56 mg, Pd(II) 8.65 mg, Pt(IV) 7.19 mg, Os(IV) 2.69 mg; extraction into 30 ml of solution.)

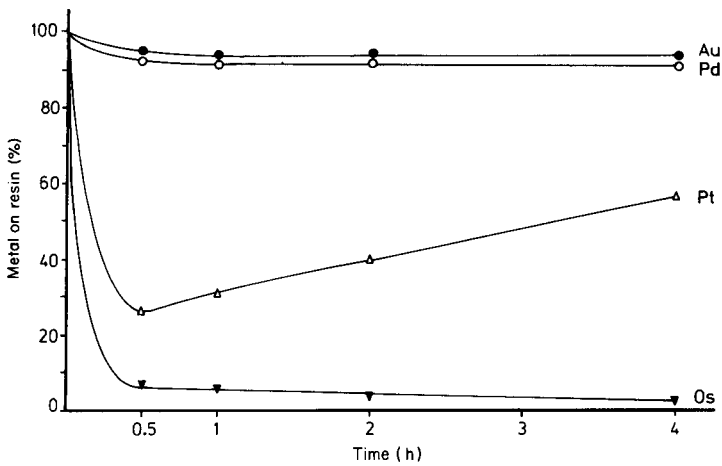

Fig. 2. Rates of simultaneous extraction of precious metals from P-D by 0.5 M NaSCN. (Amount of combined metals on resin (mg/400 mg): Au(III) 3.93 mg, Pd(II) 2.07 mg, Pt(IV) 0.64 mg, Os(IV) 1.47 mg; extraction into 50 ml of solution.)

from mixtures should be possible. Therefore, preliminary column tests were done with small samples (500 μl), containing 100 μg of each platinum group metal and gold in 1 M HCl. Subsequent washing with 20 ml of 4 M HCl at a flow rate of 2 ml min^{-1} immediately eluted Rh(III), Ru(III) and Ir(IV) and combined Pt(IV) and Os(IV) in a broad elution band. Then the sorbed species of gold and palladium were eluted satisfactorily with 10 ml of

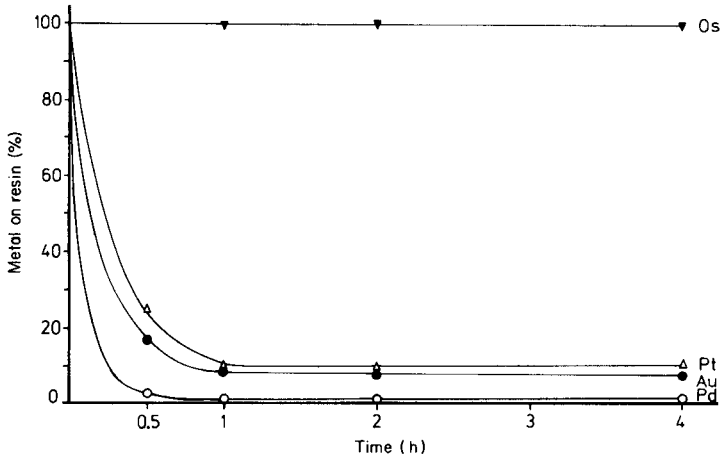

Fig. 3. Rates of simultaneous extraction of precious metals from P-D by 5% thiourea in 0.1 M HCl. (Amount of combined metals on resin (mg/400 mg): as for Fig. 2; extraction into 50 ml of solution.)

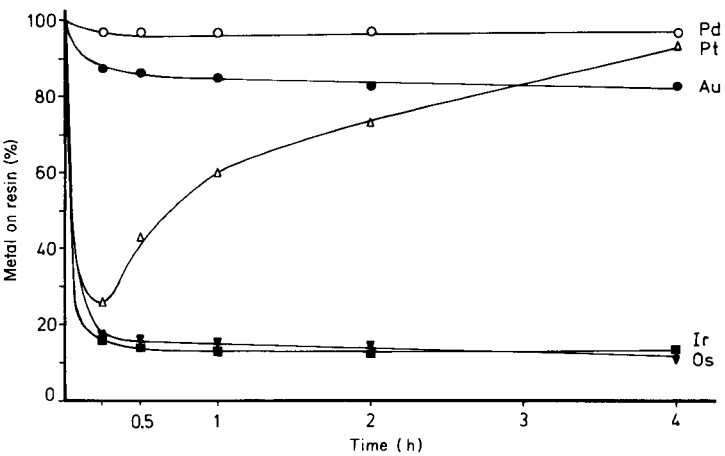

Fig. 4. Rate of extraction of individual precious metals from P-TD by 0.5 M NaSCN. (Amount of individual metal on resin (mg/200 mg): Au(III) 16.77 mg, Pd(II) 4.94 mg, Pt(IV) 8.37 mg, Os(IV) 9.15 mg, Ir(IV) 9.02 mg; extraction into 30 ml of solution.)

5% thiourea in 0.1 M HCl. From the results of the earlier sorption studies under dynamic conditions [1], one could expect that only these two elements would be strongly retained by the chelating resin and thus separated from accompanying elements. Because of the retarded sorption of platinum and osmium a batch procedure is recommended to achieve quantitative extraction. A similar process was feasible by using an arsonic acid/formazan-modified polystyrene for platinum(IV) extraction [15]. But it must be

emphasized that P-D cannot be utilized for cyclic separations as the capacity of the polymer is lowered drastically even after one sorption/desorption cycle; indeed, some decomposition of P-D during the elution step becomes visible by the formation of bubbles. Thus a complete loading of gold decreases the capacity to 70% of its starting value, whereas elution of osmium by thiocyanate produces less degradation (85%). The next section will confirm that the initial product P-TD is indeed more profitable than its conversion product P-D, as was suggested in Part 1 of this series.

DESORPTION PROPERTIES OF THE ANION-EXCHANGER P-TD

In the desorption studies with P-TD, the resin was also loaded to a maximum in acidic solutions with the appropriate metal. The results summarized in Table 3 show that the desorption of gold and the platinum group metals exceeds 80% in the first desorption cycle when a suitable agent is applied. Iridium(III), which is partly oxidized to Ir(IV) during the loading process, is the exception, as it can be eluted only incompletely. Generally the application of the ammoniacal mixtures cannot be recommended for extraction because of decomposition of the resin in such media.

Regarding the rates of elution, very contrary effects were observed; some metal ions exhibit in different eluents increasing or decreasing percentage desorption with extended shaking times. These effects are more striking for P-TD than for the chelating resin P-D. The course of the individual extraction of platinum(IV) by thiocyanate looks especially surprising (Fig. 4). Similarly to the simultaneous desorption from P-D (cf. Fig. 2), the 0.5 M thiocyanate extracts 75% of the initial amount of platinum on the resin within 15 min and

TABLE 3

Extraction (%) of individual precious metals from P-TD by various solutions (Loading conditions: 200 mg of resin, 20 ml of 1 M HCl, 10^{-2} M in the individual metal. Shaking time 4 h. Extraction with 30 ml of solution over 4 h.)

Metal	Initial amount on resin (mg)	Extraction (%) with different solutions				
		6 M HCl	2 M $HClO_4$	5% thiourea in 0.1 M HCl	0.5 M NaSCN	0.5 M NH_4NO_3 in 0.1 M NH_3
Au(III)	16.77	17.9	53.4	99.9	16.9[a]	6.4[a]
Pd(II)	4.94	70.7[a]	68.4	89.7	3.0	83.4[a]
Pt(IV)	8.37	60.2	89.5	103.7	6.5[b]	91.7[a]
Pt(II)	10.18	39.2[a]	19.6[a]	99.8	9.5[b]	68.9[a]
Ru(III)	1.86	92.6	84.8	81.4[a]	3.2[b]	16.2[a]
Rh(III)	1.23	82.0[a]	53.9[a]	76.3[a]	41.3[b]	38.8[a]
Os(IV)	9.15	38.8	93.6[a]	7.4[a]	87.1	81.5[a]
Ir(IV)	9.02	62.7[a]	89.9[a]	23.6[b]	85.7	101.3
Ir(III)	4.47	6.7[a]	5.2[a]	10.3[a]	20.6[a]	7.2[a]

[a,b] As in Table 1.

then the reverse reaction starts. Consequently, 4 h later, the metal is completely re-extracted onto the resin. Comparable kinetic effects have been observed in the case of liquid-liquid extraction systems [4, 16]. Thus, the photosensitive reaction between thiocyanate and platinum(IV) depends on either pH or thiocyanate concentration or both. In comparison, the formation of the tetrathiocyanatopalladium(II) anion is easier and less dependent on those factors than the conversion of $PtCl_6^{2-}$ to $Pt(SCN)_6^{2-}$. Analogously to the stripping of Pt(IV) from liquid tertiary amines with thiocyanate [16], it seems probable that the sorbed species of Pt(IV) are first displaced by thiocyanate in a fast reaction; subsequent slow formation of the thiocyanatoplatinum complex in the solution at pH 5.5 may lead to re-extraction of the metal by the anion-exchanger. It is important for the planning of separation procedures that, in 0.5 M thiocyanate, Pd(II) remains on the resin, probably as $Pd(SCN)_4^{2-}$, whereas Ir(IV) and Os(IV) are displaced. Both the individual and the simultaneous elutions of precious metals from P-TD by thiocyanate solution have similar patterns (Table 4).

In contrast, extreme differences were observed in the course of desorption of individual and combined metals by thiourea (Tables 3 and 4). While the desorption of gold remains relatively unaffected by accompanying platinum group metals, the release of palladium and platinum is drastically reduced. Comparison of Figs. 5 and 6 shows clearly that at the beginning of the elution step only gold is selectively separated from the adsorbed metal mixture. As mentioned above, analogous effects were observed with P-D. Because of the greater importance of the P-TD anion-exchanger, these unusual desorption behaviours were investigated in greater detail. For this purpose, batches of the resin were first loaded simultaneously with metal mixtures containing Au(III), Pd(II), Pt(IV), Os(IV) and Ir(IV). Because of their negligible sorption (Table 4), Ru(III) and Rh(III) were not included. Further, three

TABLE 4

Simultaneous extraction (%) of precious metals from P-TD by various solutions (Loading conditions: 400 mg of resin in 20 ml of 1 M HCl, 10^{-2} M in each metal. Shaking time 1 h. Extraction with 50 ml of solution over 4 h.)

Metal	Initial amount on resin (mg)	Extraction (%) with different solutions				
		6 M HCl	2 M $HClO_4$	5% thiourea in 0.1 M HCl	0.5 M NaSCN	0.5 M NH_4NO_3 in 0.1 M NH_3
Au(III)	3.98	0.5	35.6[b]	88.8	7.5	24.1[b]
Pd(II)	0.54	81.6	77.7	7.6[a]	1.6	81.3[a]
Pt(IV)	2.21	75.3	94.9	4.7[a]	51.9[b]	69.8[a]
Ru(III)	~0.06	25.0[a]	80.6	16.4	~0	16.1
Rh(III)	~0	—	—	—	—	—
Os(IV)	3.20	37.2[b]	85.3[a]	0.05	92.5	16.2[b]
Ir(IV)	2.54	89.9[a]	100.6	6.2[a]	93.6[b]	56.0

[a,b] As in Table 1.

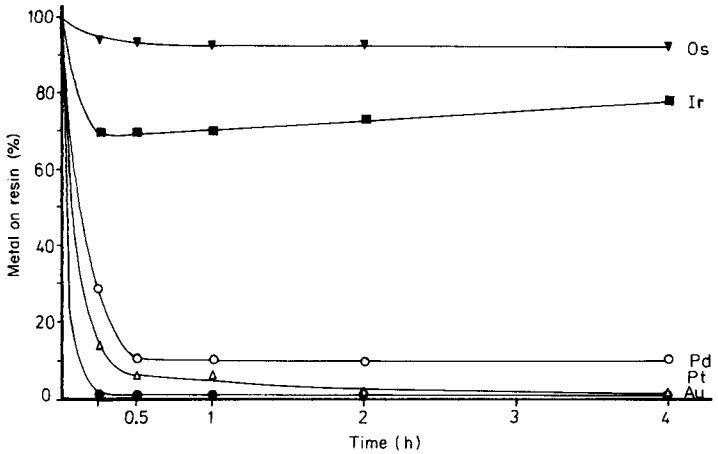

Fig. 5. Rate of extraction of individual precious metals from P-TD by 5% thiourea in 0.1 M HCl. (Amount of individual metal on resin (mg/200 mg): as for Fig. 4; extraction into 30 ml of solution.)

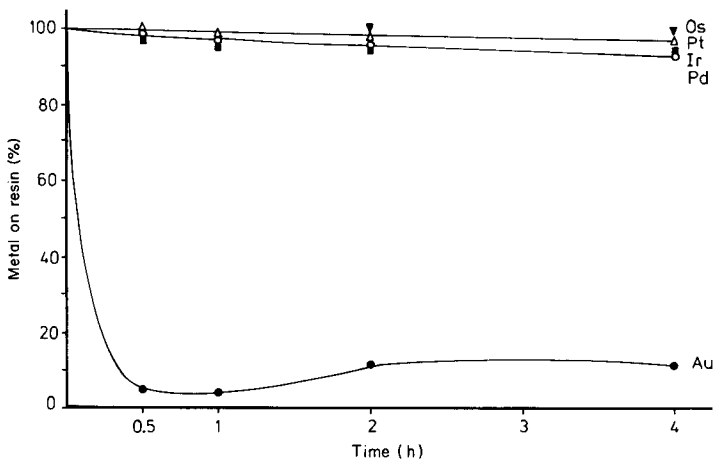

Fig. 6. Rates of simultaneous extraction of precious metals from P-TD by 5% thiourea in 0.1 M HCl. (Amount of combined metals on resin (mg/400 mg): Au(III) 3.98 mg, Pd(II) 0.54 mg, Pt(IV) 2.21 mg, Os(IV) 3.20 mg, Ir(IV) 2.54 mg; extraction into 50 ml of solution.)

different quaternary mixtures were composed with Pd(II), Pt(IV) and Ir(IV) or Os(IV) or Au(III) (Table 5). The four batches of ion-exchanger, loaded as described were then treated with 5% thiourea in 0.1 M HCl. The results for the individual eluates, summarized in Table 5, illustrate clearly the very high influence of co-extracted Ir(IV) on the desorbability of Pd(II) and Pt(IV); these two metals can be eluted satisfactorily by thiourea only in the absence of Ir(IV). But if the thiourea treatment of the completely loaded resin follows the

TABLE 5

The influence of the composition of the sorbed metal mixtures on the simultaneous extraction (%) of precious metals from P-TD by thiourea
(Loading conditions: 400 mg of resin, 20 ml of the individual metal mixture in 1 M HCl (10^{-2} M in each element). Shaking time 1 h. Extraction with 50 ml of 5% thiourea in 0.1 M HCl over 4 h.)

Composition of samples	Pd(II)		Pt(IV)		Os(IV)	
	Loaded (mg)	Extracted (%)	Loaded (mg)	Extracted (%)	Loaded (mg)	Extracted (%)
All metals combined	0.94	5.7	2.82	2.3	3.41	0.2
Samples without Ir	1.43	84.9[a]	3.43	97.5[a]	3.71	~0
Samples without Os	1.27	17.3[a]	3.35	7.5[b]	—	—
Samples without Au	1.26	3.0	2.31	5.1	3.17	2.9

Composition of samples	Ir(IV)		Au(III)	
	Loaded (mg)	Extracted (%)	Loaded (mg)	Extracted (%)
All metals combined	2.79	2.3	4.3	80.9[b]
Samples without Ir	—	—	4.12	94.8[a]
Samples without Os	3.16	2.1[a]	3.99	92.5
Samples without Au	3.17	2.9[a]	—	—

[a,b] As in Table 1.

action of 0.5 M thiocyanate, which extracts osmium and 50% of retained iridium, then palladium and platinum can be recovered nearly completely. It can be concluded that the inhibitory influence of Ir(IV) depends on its quantity ratio to the co-extracted elements. In addition, the desorption yields of the other precious metals (especially gold) were also slightly affected by the composition of the metal mixture on the resin.

Although it seems that iridium is mainly responsible for the observed differences, these effects require more clarification. According to published data [10, 17], some precious metals, normally present in their common higher oxidation states, are first reduced and then complexed by thiourea at varying rates; thus Ir(IV) → (III), Au(III) → (I), and Pt(IV) → (II). The formation of cationic thiourea complexes of Au(I), Pd(II) and Pt(II, IV) via anionic and neutral species is rapid. Therefore one can expect irreversible release of these metals from the positively charged tetrazolium groups of P-TD, as was

observed in the absence of Ir(IV). Indeed, Ir(IV) tends to form also cationic thiourea/chloride complexes, but after immediate reduction to Ir(III) negatively charged species may also be present. This reaction corresponds to the fact that at room temperature the initial product of Ir(IV) and thiourea cannot be sorbed onto a cation-exchange resin [17]. However, the presence of stable anionic complex compounds of Ir(III) could explain the inefficient removal of this metal from P-TD by thiourea. It is also possible that mixed ion-pairs composed of cationic and anionic thiourea species of Ir, Pd and Pt are retained strongly by the functional groups of the anion-exchanger. Full understanding of the inhibitory effect of iridium requires further investigation, however. The present comparative study on individual and simultaneous rates of desorption shows the strong interdependence of coextracted metals. Emphatically, prediction of separations based exclusively on individual elution data can lead to erroneous results.

The development of separation procedures by means of P-TD

To further these investigations, chromatographic procedures were tested for the separation of some platinum-group metals and gold. Rhodium and ruthenium were omitted from these tests because of their inefficient sorption. First, small samples (500 μl) of synthetic mixtures, containing about 100 μg of each relevant precious metal in 1 M hydrochloric acid were passed through an ion-exchange column (0.5 cm i.d., bed height 4 cm) filled with 750 mg of preconditioned resin. The application of a sequence of elution agents provided partial separation of some metals. Table 6 presents the results of two different procedures A and B.

In procedure A, the loaded resin was first washed with 1 M HCl, removing 25% of the initial amount of Ir(IV), then the column was eluted with 5% thiourea solution, causing the desorption of gold (97.3%) and palladium (82.2%) in a sharp elution peak. Some platinum was also detected. Subsequent washing with 1 M HCl removed the residue of iridium, and then perchloric acid eluted osmium nearly quantitatively as well as the residues of platinum and iridium. It is striking that Pd and Pt were recovered incompletely. This agrees with the results of simultaneous desorption studies under static conditions. The effect of iridium is obvious, though here, in contrast to the preceding tests, roughly equal amounts of metals were loaded. In procedure B, the inverse sequence of eluents was used (perchloric acid → thiourea); 2 M perchloric acid displaced a mixture of Pd(II), Pt(IV), Os(IV) and Ir(IV) but not gold. Gold was finally released from P-TD together with the residual palladium. But this alternative route is not advantageous because of an irreversible colour change of the sorbent during the last elution step.

An improved chromatographic separation of these precious metals even in presence of base metals was achieved by use of thiocyanate and thiourea (procedure C, Table 7). It is important that accompanying base metals can be washed from the column efficiently with diluted hydrochloric acid. Only negligible traces of copper and nickel were detected in the thiourea fractions.

TABLE 6

Results of chromatographic procedures A and B for precious metals
[Ion-exchange column (0.5 cm i.d.) with 0.75 g P-TD; 500 μl of 1 M HCl containing ≈100 μg of each element injected; flow rate during elution, 1 ml min^{-1}; eluates collected in fractions of 5 ml.]

Sequence of eluents	Total volume (ml)	Composition of combined fractions found (μg)[a]				
		Pd(II) (114.0)	Pt(IV) (96.6)	Os(IV) (91.3)	Ir(IV) (103.0)	Au(III) (108.0)
Procedure A (thiourea → perchloric acid)						
(1) 1 M HCl	5	—	—	—	26.3	—
(2) 5% thiourea/ 0.1 M HCl	15	97.2	63.8	—	1.3	105.1
(3) 1 M HCl	30	—	4.2	—	67.3	—
(4) 2 M $HClO_4$	15	—	22.8	89.3	6.8	—
Recovery (%)		82.2	93.9	97.8	98.7	97.3
Procedure B (perchloric acid → thiourea)						
(1) 1 M HCl	5	—	—	—	13.9	—
(2) 2 M $HClO_4$	15	33.8	90.6	90.3	84.1	—
(3) 0.1 M HCl	30	0.4	0.14	—	0.7	—
(4) 5% thiourea/ 0.1 M HCl	10	65.3	1.1	—	—	102.4
Recovery (%)		87.4	95.1	98.9	97.0	95.2

[a]The amounts of metal taken in the sample are given in parentheses.

TABLE 7

Results of chromatographic procedure C for the separation of precious metals and base metals
[Ion-exchange column (0.5 cm i.d.) with 0.75 g P-TD; 500 μl of 1 M HCl, containing ≈100 μg of each element; flow rates, 2 ml min^{-1} (wash), 1 ml min^{-1} (elution).]

Sequence of steps[a]	Volume (ml)	Composition of combined fractions found[b] (μg)							
		Pd(II) (106.0)	Pt(IV) (94.5)	Os(IV) (91.6)	Ir(IV) (104.0)	Au(III) (104.0)	Fe(III) (107.0)	Cu(II) (131.0)	Ni(II) (139.0)
(1) Loading	0.5	—	—	—	—	—	—	—	—
(2) 1 M HCl	10	—	—	—	4.9	—	105.7	133.3	136.5
(3) Water	10	—	—	—	—	—	1.03	—	—
(4) 0.5 M NaSCN	2	—	9.40	—	70.00	0.14	—	—	—
	2	—	73.60	6.36	12.64	0.07	—	—	—
	5	—	9.80	54.50	0.69	—	—	—	—
(5) 2 M NaSCN	9	—	1.27	28.34	0.09	—	—	—	—
(6) 0.1 M HCl	30	—	0.09	0.11	0.51	0.12	—	—	—
(7) 1% thiourea/	2	86.20	0.04	0.06	0.32	5.20	—	—	—
0.1 M HCl	2	18.92	0.17	0.08	0.18	80.40	—	0.13	0.05
	5	1.05	0.23	0.20	0.09	19.25	—	—	0.02
(8) 5% thiourea/ 0.1 M HCl	30	0.45	0.08	0.14	0.02	0.53	—	0.15	0.04
(9) 0.1 M HCl	30	—	0.97	0.40	0.37	0.33	—	0.01	—
(10) 2 M $HClO_4$	10	—	—	0.54	—	—	—	—	—
Recovery (%)		100.6	101.5	99.1	86.4	98.8	99.8	102.0	98.3

[a]Steps 2, 3, 6, 9 and 10 are washes; steps 4, 5, 7 and 8 are elution. [b]The amounts of metal taken in the sample are given in parentheses.

In the subsequent steps, two different concentrations of each eluting agent separate first Ir, Pt, Os (0.5 M and 2 M thiocyanate) and then Pd and Au (1% and 5% thiourea in 0.1 M HCl) from the bulk of each other. In the absence of Ir(IV), its desorption behaviour being erratic (see below), the elution profiles of the remaining precious metals exhibit reasonable chromatographic resolution, as shown by the combined d.c.p./l.c. technique (Fig. 7). It must be noted that small amounts of platinum were retained by the ion-exchange column during the thiocyanate elution; they were subsequently released, associated with palladium in the first fractions of the thiourea eluent. These residual quantities of platinum increased with increasing height of the resin bed and depended also on its original oxidation state (Table 8). Similar effects were reported on combined thiocyanate/thiourea strips of liquid-liquid extraction systems [16]. From some results of polyurethane extractions of Pt(IV)-thiocyanate complexes [11], it may be concluded that partial reduction of Pt(IV) to Pt(II) during elution causes incomplete release from the resin.

In comparison to the above procedures A and B, method C seems to be more profitable. However, the behaviour of Ir(IV) remains problematic. The sample solutions always contain some unadsorbable complex species of this metal, and irreversibly sorbed amounts of iridium remain on the resin, whereas all other metals can be recovered quantitatively. Attempts to elute the residual iridium by reducing agents (e.g., ascorbic acid, hydroxylamine) were a failure. Additional amounts could be recovered, by applying mixtures of potassium chlorate and hydrochloric acid (5% (w/w) in 4 M HCl) but then the resin decomposed. Somewhat similar results were reported for the recovery of iridium by use of commercially available isothiouronium resins (Srafion NMRR) [18, 19]. It was assumed that resin-bonded complex ions of Ir(IV) were reduced in part to the irreversibly sorbed metal. Special pretreatments such as evaporation of the sample in the presence of potassium chlorate were recommended to avoid hydrolysis and reduction of individual metal ions [8]. Such a procedure applied to an original Ir(IV) solution in the

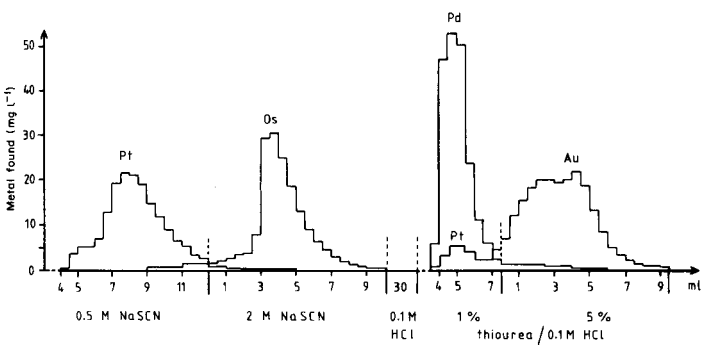

Fig. 7. Stepwise elution of precious metals from P-TD. (Bed height: 0.5 × 4 cm, flow rate 1 ml min^{-1}, 100 μg of each element, elution profiles obtained by the d.c.p./l.c. system.)

TABLE 8

The influence of oxidation states of metal ions on their elution behaviour
[Ion-exchange column (0.5 cm i.d.) with 0.75 g P-TD; 500 μl of 1 M HCl, containing ≈100 μg of the individual metal ion; elution with 2 × 10 ml of each eluent (1 ml min^{-1}).]

Sequence of eluents	Recovery (%)			
	Pt(II)		Pt(IV)	
(1) 0.5 M NaSCN	68.1		94.0	
(2) 1% thiourea in 0.1 M HCl	28.5		6.4	
Total	96.6		100.4	
	Ir(III)		Ir(IV)	
	Untreated	Treated[a]	Untreated	Treated[a]
(1) 1 M HCl	99.9	40.9	6.9	6.4
(2) 2 M $HClO_4$	—	51.9	84.6	76.1
Total	99.9	92.8	91.5	82.5
	Fe(II)[b]		Fe(III)	
(1) 1 M HCl	98.7		100.0	
(2) 5% thiourea/0.1 M HCl	—		—	
Total	98.7		100.0	
	Cu(I)[b]		Cu(II)	
(1) 1 M HCl	55.0		99.5	
(2) 5% thiourea/0.1 M HCl	40.0		—	
Total	95.0		95.0	

[a]Original samples containing $IrCl_3^{3-}$ or $IrCl_4^{2-}$ were first evaporated to dryness in presence of 5 mg $KClO_3$. [b]Reduced with ascorbic acid.

present work improved neither the retention nor the recovery of iridium in comparison with an untreated sample (Table 8). Alternatively the Ir(IV) may be reduced to Ir(III) by sulphite or hydroxylamine [2, 7] prior to the loading step. Because of its low distribution coefficient in 1 M HCl, Ir(III) passes quantitatively through the ion-exchange column but it cannot then be separated from accompanying base metals. Furthermore, admixed precious metals, e.g., Pt(IV), as well as Fe(III) and Cu(II) are also reduced. Thus, the selectivity of the elution of Pt(II) by thiocyanate and Cu(I) by hydrochloric acid in procedure C would deteriorate considerably whereas Fe(II) is essentially unaffected (Table 8). From these results, the adjustment of the higher common oxidation states of the metals appears to be profitable for procedure C.

The usefulness of this method was demonstrated by means of separations of some precious metals from synthetic mixtures of base metals and salts

such as would be required in the analysis of platinum-bearing geological materials. For this purpose, 500 ml of an acidic sample solution (1 M HCl) was prepared, containing ca. 0.2 μg ml^{-1} each of Pd(II), Pt(IV), Os(IV), Ir(IV) and Au(III) as well as Fe(III), Cu(II) and Ni(II) in the range 2100—2800 μg ml^{-1}, so that the mass ratio of combined precious metals to base metals was about 1:7700 (Table 9). From the beginning of the loading stage, the base metals break through and can be completely washed out by dilute hydrochloric acid and water (except for traces of Fe and Cu). Then the retained precious metals are released by the sequence of eluting agents summarized in Table 9. The recoveries for Pd, Pt, Os and Au are satisfactory, but significant losses of iridium were again obtained.

High concentrations of sodium chloride usually result from peroxide fusion for dissolution of ores and related materials. They may affect the retention of precious metals. To test the effectiveness of P-TD under such conditions three sorption/elution cycles were run. As shown in Table 10, the competing effect of chloride is demonstrated markedly in the case of Ir(IV), but the retention of Pd(II) is also decreased (to 70.2%) at a flow rate of 2 ml min^{-1}. Lowering the flow of the feed to 1 ml min^{-1} yields a slight improvement of the retention and recovery of palladium. Recovery of palladium would be more complete if a larger column were applied. However, throughout all these tests, the recoveries of Pt, Os and Au were excellent. After a series of ten cyclic tests irreversibly sorbed iridium had poisoned the resin; it was seen as

TABLE 9

Enrichment and separation of precious metals from large amounts of base metals by procedure C

[Ion-exchange column (0.5 cm i.d.) with 0.75 g P-TD; 500-ml sample with $\approx$0.2 μg ml^{-1} precious metal (each) and 2100—2800 μg ml^{-1} base metals in 1 M HCl; flow rates, 2 ml min^{-1} (loading, wash), 1 ml min^{-1} (elution); eluates collected in fractions of 5 ml.]

Sequence of steps[a]	Volume (ml)	Composition of combined fractions found[b] (μg)							
		Pd(II) (104.0)	Pt(IV) (92.5)	Os(IV) (87.2)	Ir(IV) (102.0)	Au(III) (109.0)	Fe(III) (1060 mg)	Cu(II) (1380 mg)	Ni(II) (1420 mg)
(1) Loading	500	—	—	—	—	—	—	—	—
(2) 1 M HCl	20	—	—	—	2.6	—	2.0 mg	1.24 mg	1.19 mg
0.1 M HCl	40	—	—	—	0.4	—	101.8 μg	2.73 μg	2.0 μg
water	10	—	—	—	—	—	1.18	0.10	—
(3) 0.5 M NaSCN	10	—	88.95	45.80	58.49	—	0.14	—	0.01
(4) 2 M NaSCN	10	0.28	2.14	39.07	0.26	0.42	—	—	—
(5) 0.1 M HCl	30	—	—	—	—	—	—	—	—
(6) 1% thiourea/ 0.1 M HCl	10	100.86	0.44	—	—	109.83	—	0.08	—
(7) 5% thiourea/ 0.1 M HCl	10	3.29	0.27	—	—	0.54	—	0.18	—
(8) 0.1 M HCl	30	0.16	0.11	0.34	—	—	—	—	—
(9) 2 M $HClO_4$	10	—	0.17	0.49	0.36	—	—	—	—
Recovery (%)		105.5	99.5	98.3	57.9	101.6			

[a]Steps 2, 5, 8 and 9 are washes; steps 3, 4, 6 and 7 are elution. [b]The amounts of metal taken in the sample are given in parentheses.

TABLE 10

The effects of high sodium chloride concentration on the retention and recovery of precious metals in presence of base metals in procedure C (as outlined in Table 9) [Ion-exchanger as in Table 9; 50-ml samples with ≈ 2 μg ml^{-1} precious metals (each) and ≈ 200 μg ml^{-1} Cu and Ni in 1 M HCl.]

NaCl added (g)	Flow rate of feed (ml min^{-1})	Percentage retention and recovery[a]									
		Pd(II)		Pt(IV)		Os(IV)		Ir(IV)		Au(III)	
		Ret.	Rec.	Ret.	Rec.	Ret.	Rec.	Ret.	Rec.	Ret.	Rec.
—	2	99.9	99.9	100	100.1	100	100.8	85.3	45.7	100	103
10	2	70.2	68.5	100	101.6	100	103.1	~5	~5	100	102
10	1	78.6	78.6	100	97.9	100	98.2	~3	~2	100	100.1

[a]Ret. indicates retention and rec. recovery.

a brown band at the middle of the ion-exchange column. However, comparison of the practical specific capacity for Pd(II) of this resin with a freshly prepared column showed no marked differences. The high stability of P-TD was further confirmed by capacity tests on a column which had previously been loaded to the breakthrough point with a mixture of precious metals and then eluted by procedure C. Even treatment for 24 h in an oxidizing solution (10% (w/v) sodium chlorate in 1 M HCl) caused a loss of only 4% of the initial capacity. It should be added that, in contrast to isothiouronium resins, which cannot be loaded from weak ($\leqslant 0.5$ M) hydrochloric acid because of irreversible formation of metal chelates [10], sorption of platinum group metals and gold onto P-TD from such solutions is quite viable.

Conclusions

Strong retention of precious metals but instability during the loading and elution stages characterize the behaviour of the P-D chelating resin. Selective separations of both palladium and gold are possible, but the resin is unsuitable for cyclic procedures. Considerably superior results were obtained with use of the P-TD anion-exchanger. The negligible retention of rhodium and ruthenium impairs the utility of the dehydrodithizone-functionalized polymer. But it can be regenerated (an important aim of these investigations) and can be utilized for selective separations of Pd, Pt, Os, Au and (with some restrictions) Ir from each other and from large excess of base metals and salts. The P-TD resin has useful applications in analytical chemistry and hydrometallurgy. Further work on such anion-exchangers is in progress.

Financial support from "Fonds der Chemischen Industrie" and "Deutsche Forschungsgemeinschaft" is gratefully acknowledged.

REFERENCES

1 M. Grote and A. Kettrup, Anal. Chim. Acta, 172 (1985) 223, (Part 1).
2 S. S. Berman and W. A. E. McBryde, Can. J. Chem., 36 (1958) 835.
3 M. Knothe, Z. Anorg. Allg. Chem., 463 (1980) 204.
4 S. J. Al-Bazi and A. Chow, Talanta, 31 (1984) 815.
5 R. Kuroda and N. Yoshikuni, Talanta, 18 (1971) 1123.
6 G. M. Varshal and I. V. Kubrakova, Zh. Anal. Khim., 36 (1981) 2373.
7 K. Brajter and K. Slonawska, Chem. Anal. (Warsaw), 24 (1979) 273.
8 C. Pohlandt, Rep.-Natl. Inst. Metall. (S. Afr.), 1964 (1978) 18 pp.
9 A. Warshawsky, M. Fieberg and Y. B. Ras, Rep.-Natl. Inst. Metall. (S. Afr.), 1364 (1979) 10 pp.
10 A. Warshawsky, M. Fieberg, P. Mihalik, T. G. Murphy and Y. B. Ras, Sep. Purif. Methods, 9 (1980) 209.
11 S. J. Al-Bazi and A. Chow, Anal. Chem., 55 (1983) 1094.
12 R. K. Petrie and J. W. Morgan, Radioanal. Chem., 74 (1982) 15.
13 F. V. S. Toerien and M. Levin, J. S. Afr. Chem. Inst., 27 (1974) 87.
14 G. Pfrepper and R. Liebmann, Kernenergie, 27 (1984) 34.
15 Zhang Bao Wen, M. Grote and A. Kettrup, Fresenius Z. Anal. Chem., (1985) in press.
16 A. Warshawsky, Sep. Purif. Methods, 11 (1982–83) 95.
17 C. H. S. W. Weinert and F. W. E. Strelow, Talanta, 30 (1983) 413.
18 K. Kritsotakis and H. J. Tobschall, Fresenius Z. Anal. Chem., 320 (1985) 15.
19 L. L. Sundberg, Anal. Chem., 47 (1975) 2037.

Analytica Chimica Acta, 175 (1985) 257—265
Elsevier Science Publishers B.V., Amsterdam — Printed in The Netherlands

RAPID-SCANNING CONSTANT-ENERGY SYNCHRONOUS FLUORESCENCE SPECTROMETER AS A LIQUID CHROMATOGRAPHIC DETECTOR

M. JONELL KERKHOFF[a] and J. D. WINEFORDNER*
Department of Chemistry, University of Florida, Gainesville, FL 32611 (U.S.A.)
(Received 8th April 1985)

SUMMARY

A rapid-scanning fluorimeter based on constant-energy synchronous scanning is described. It is used as a liquid chromatographic detector for polyaromatic hydrocarbons (PAHs). The computerized system scans at a rate of 200 nm s^{-1} and collects data in the forward and reverse directions. Data are processed in real time. The system is tested for 3-component and 9-component mixtures of PAHs. A synchronous fluorescence spectrum is obtained for each PAH being eluted in the chromatogram. The spectral peaks observed in the rapid scan correspond to the absorption/fluorescence transitions of the PAHs with an overall vibrational energy loss equal to the $\Delta\nu$ value chosen. Limits of determination for the PAHs are in the pg to low ng range. The system provides a reduced signal/noise ratio compared to the variable-wavelength fluorescence system for most PAHs examined.

There is a great need to monitor trace levels of polynuclear aromatic hydrocarbons (PAHs) in the environment [1]. Mixtures of PAHs can be analyzed by combining high-performance liquid chromatography (h.p.l.c.) with a fluorescence detection system. Fox and Staley [2] collected h.p.l.c. sample fractions and obtained conventional absorption-fluorescence spectra of each fraction as well as derivative and selective modulation fluorescence spectra for peak identification. Das and Thomas [3] used a variable-wavelength fluorescence detection system for h.p.l.c. of nine PAHs with three sets of excitation/emission wavelengths. Ogan et al. [4] successfully separated sixteen PAHs listed as EPA priority pollutants with three sets of excitation/emission wavelength pairs. Several environmental water samples were also analyzed for the sixteen PAHs. Nielsen [5] purified PAHs from automobile exhaust by thin-layer chromatography, separated them by h.p.l.c., and used a stop-flow fluorescence detection system to obtain fluorescence spectra for seven PAHs. Allen et al. [6] used corrected excitation fluorescence spectroscopy as a detection system for PAH components.

Fluorescence spectrometry has been shown to be a selective and sensitive technique with improvements in detection power over absorption spectro-

---

[a]Present address: Alcoa Technical Center, Building C, Alcoa Center, PA, U.S.A.

0003-2670/85/$03.30

photometry by at least one order of magnitude [7]. Problems with currently used fluorescence detection systems include the inability to resolve spectral overlap of the components by conventional fluorescence techniques and the inability to optimize the absorption and fluorescence wavelengths for each compound.

The most desirable fluorescence detection system would use major absorption/fluorescence wavelength pairs for monitoring eluting PAHs and would allow spectra to be obtained for identification. The potential utility and feasibility of a fluorescence detection system based on constant-energy synchronous scanning was evaluated at a 20 nm s^{-1} scan rate [8]. Constant-energy synchronous fluorescence spectrometry (c.e.s.f.s.) is a technique in which fluorescence measurements are obtained while the excitation and emission monochromators are synchronously scanned; a constant energy difference between the two monochromators is maintained during scanning. Spectral information is obtained for the absorption and fluorescence transitions so that the energy difference corresponds to a certain overall vibrational energy loss [8—10]. Polynuclear aromatic hydrocarbons exhibit predominant —C=C— vibrational bands at approximately 1400 cm^{-1}. The constant energy difference ($\Delta\bar{\nu}$) is chosen to equal one vibrational quantum, two or three vibrational quanta, or the Stokes shift energy of 200 cm^{-1}. The c.e.s.f.s. method has proven to be a selective and sensitive technique in which spectral bandwidth reduction, spectral profile simplification, and Rayleigh and Raman scatter minimization occur in comparison to conventional fluorescence scanning [9, 10].

In the present case, rapid-scanning constant-energy synchronous fluorescence spectroscopy encompasses synchronous fluorescence scanning with a constant energy difference at a scan rate of 200 nm s^{-1}. In this work, the capabilities of the rapid-scanning c.e.s.f.s. detection system in h.p.l.c. is evaluated with a three-component mixture. The proposed system and the u.v. absorbance system are compared for a nine-component PAH mixture. The figures of merit for 17 PAHs with the proposed system are compared to the u.v. absorbance system and to a variable-wavelength fluorescence system [4].

EXPERIMENTAL

Apparatus and chemicals

A schematic diagram of the rapid-scanning c.e.s.f.s. system at 200 nm s^{-1} is shown in Fig. 1. The components and manufacturers are listed in Table 1. An in-depth discussion of instrumentation and software development for the system will be given elsewhere. The motor resolution was 200 steps per turn resulting in 0.5 nm per pulse. The synchronous scanning and data collection were controlled by an Apple II+ microcomputer through an assembler program. The rapid scan at $\Delta\bar{\nu} = 4800\ cm^{-1}$ was attained by pulsing the excitation monochromator at a constant 400-Hz rate and the emission monochromator

TABLE 1

Experimental components for system scanning at 200 nm s^{-1}

Equipment	Model	Manufacturer
Xenon arc lamp, 150 W	VIX-150 UV	EIMAC, Division of Varian, San Carlos, CA 94070
Illuminator power supply at 12 A	P250S-2	EIMAC
Excitation monochromator[a]	H-10 UV	American ISA, Metuchen, NJ 08840
Emission monochromator[a]	H-10 V	American ISA
Monochromator motors	M063-FDD6E	Superior Electric Co., Bristol, CT 06010
Motor translation modules	STM103	Superior Electric Co.
Photomultiplier	1P928	Hamamatsu, Waltham, MA 02154
High voltage power supply at −1000V		Laboratory-constructed
Microcomputer	Apple II+	Apple Computer, Cupertino, CA 95014
Current/log voltage converter	755P	Analog Devices, Norwood, MA 02062
Analog/digital converter	AI13	Interactive Structures, Bala Cynwyd, PA 19004
Minicomputer	PDP 11/34	Digital Equipment Corp., Maynard, MA 02154
Analog/digital converter	LPSAD-12	Digital Equipment Corp.
H.p.l.c. system	332	Beckman Instruments, Altex Scientific, Berkeley, CA 94710
Recorder	OmniScribe	Houston Instruments, Austin, TX 78753

[a]f/3.5, holographic grating, 1200 grooves/nm.

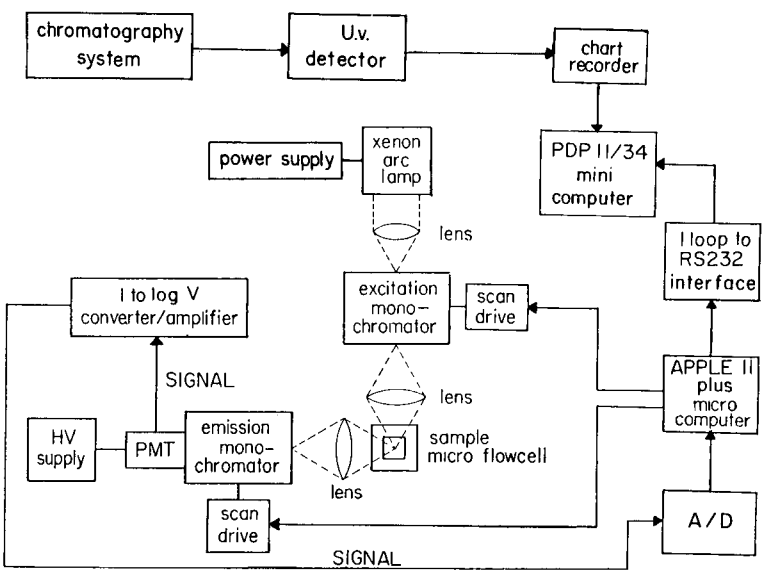

Fig. 1. Schematic diagram of rapid-scanning c.e.s.f.s. system for use as an h.p.l.c. detector.

at a faster rate varying up to approximately 700 Hz. A "look-up" table of emission pulse rates was generated by an initialization routine to provide the constant-energy synchronous scan. A versatile interface adapter (VIA, SY6522) was used for communication between the Apple microcomputer and the rapid-scanning c.e.s.f.s. system. The VIA timer was used for excitation and emission pulsing. The excitation and emission monochromator pulsing were interrupt-controlled. The data acquisition by the Apple II+ and transmission to the PDP 11/34 were synchronized with the excitation monochromator pulse rate. Data were acquired on alternate pulses to the excitation monochromator. Four analog-to-digital conversions were obtained and averaged during an excitation monochromator pulse. After the next excitation pulse, the averaged signal was sent to the PDP 11/34 through the Apple II+ serial interface port (California Computer Systems, Model 7710) at a rate of 19.2 kbaud. A current-to-log voltage converter was used, giving an output of 0—10 V corresponding to a current range of —0.1 nA to —10 μA.

A PDP 11/34 minicomputer received data from the Apple II+ for processing in real time. The main PDP program was written in Fortran with Fortran and assembler subroutines. Data were transmitted to the PDP through the Digital DZ11 serial port at a rate of 19.2 kbaud. The DZ11 serial port has a data buffer. Data were read in by an interrupt-controlled assembler subroutine only when the buffer was full. A total of 201 data points (200-nm spectral range) were transmitted to the PDP for each scan. After the 201 data points per rapid scan were received by the PDP 11/34, the area of the spectrum was integrated. The integrated fluorescence value was output to the recorder through the Digital Laboratory Peripheral System (LPS) digital-to-analog converter to reconstruct the chromatogram in real time. Each output value corresponded to the log fluorescence intensity per second.

Signal processing included noise, drift, and peak monitoring and the storage and output of spectra. Each integrated value was compared to a threshold value above the noise level and to the previous integrated value to distinguish a valid peak from drift over time or a noise spike. If a peak was present, monitoring continued as above until the slope was negative or zero (peak maximum). The spectrum was saved at that time. Times at the beginning and end of each chromatographic peak were also stored.

At the end of the run, the integrated values were printed out. The spectrum saved for each chromatographic peak was output to the recorder for PAH identification. The stored spectral values were also printed out.

A liquid chromatography system (Beckman Instruments, Altex Scientific, Berkeley, CA 94710, Model 332) was connected to the rapid-scanning system. The h.p.l.c. effluent first passed through the u.v. detector (Beckman Model 153) and then through the fluorescence flow cell. The u.v. detector measured absorbance at 254 nm. Absorbance measurements were taken from the chart recorder output. A Rainin "short one" Ultrasphere-ODS reverse-phase column was used.

Stock solutions (100 mg l^{-1}) of PAHs were prepared in acetonitrile.

Acetonitrile (Fisher Scientific) and water (80/20 by volume) comprised the mobile phase. Suppliers of the PAHs were Aldrich and Analabs.

Procedure

To insure reproducible filling of a 20-μl sample loop, 100-μl samples were used. Dilutions of the stock solutions, from 100 ng ml^{-1} to 10 $\mu g\ ml^{-1}$, were made for each PAH. Detection limits were obtained on the proposed rapid-scanning system and compared to those obtained on the u.v. absorbance system. Chromatographic separations were run on three- and nine-component mixtures. For both detection systems, the intensity measurements were evaluated from the chromatographic peak area. A solvent flow rate of 1 ml min^{-1} was used.

RESULTS AND DISCUSSION

Performance of the rapid-scanning system

Dilutions of a stock solution containing 5 $\mu g\ ml^{-1}$ anthracene, 30 $\mu g\ ml^{-1}$ chrysene, and 5 $\mu g\ ml^{-1}$ benzo(a)pyrene were made. The chromatogram of a 1:10 dilution of the three-component mixture with the rapid-scanning detection system is shown in Fig. 2. The fluorescence intensity scale corresponded to a current decade change for each 2-V change. The acetonitrile/water solvent system gave a signal of approximately 1 nA. The log integrated fluorescence intensity value for each scan was determined and output in real time, reconstructing the chromatogram. For each scan, the 201 data values (corresponding to a 200-nm excitation wavelength range) were summed and the total was divided by 201. A new log fluorescence value was obtained and output to the recorder every second.

An important feature of the rapid-scanning system is that fluorescence spectra are obtained. The integrated values sent out to the recorder were checked for drift and noise fluctuations versus real-time analyte signal levels. When analyte signals were present, monitoring of the integrated log fluores-

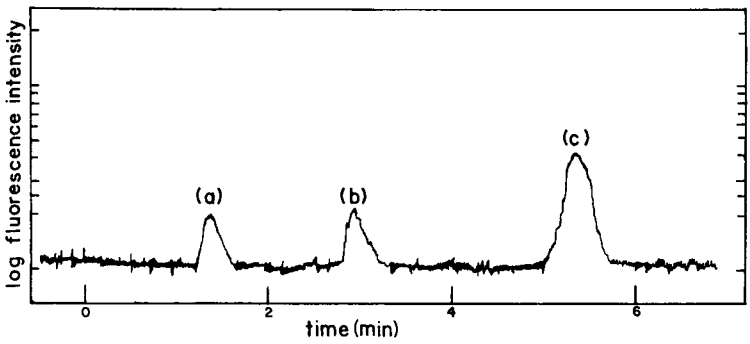

Fig. 2. Chromatogram of a three-component PAH mixture, with the signal processed and output in real time: (a) anthracene 0.5 $\mu g\ ml^{-1}$; (b) chrysene 3.0 $\mu g\ ml^{-1}$; (c) benzo(a)-pyrene 0.5 $\mu g\ ml^{-1}$.

cence values continued until the chromatographic peak maximum was established. At this point, the scan (201 data values) was stored in memory. When the analyte signal level returned to baseline, the time that the peak began and the time that the peak returned to baseline were also stored in memory. The spectra were sent out to the recorder at the end of the chromatographic run. In Fig. 3, the spectra obtained in this way for the three-component mixture are shown. The three spectra correspond to the peaks of anthracene (a), chrysene (b), and benzo(a)pyrene (c) as labelled in Fig. 2.

The rapid-scanning fluorescence system vs. u.v. absorbance

A nine-component mixture was separated in a 80:20 acetonitrile/water eluent. The stock solution consisted of 5 μg ml^{-1} each of fluorene, fluoranthene, benzo(k)fluoranthene, benzo(a)pyrene, and anthracene; and 30 μg ml^{-1} each of chrysene, pyrene, dibenz(a, h)anthracene, and benzo(g, h, i)perylene. The chromatograms obtained with the proposed rapid-scanning system at 200 nm s^{-1} and the u.v. absorbance detector at 254 nm are shown in Fig. 4. A 1:10 dilution of the stock solution was used. The PAHs are numbered according to the elution order as listed in Table 2. The limits of detection that were found for 17 PAHs by both the rapid-scanning c.e.s.f.s. and u.v. absorption detectors are listed in Table 2. With a programmable solvent-gradient system, all 17 PAHs could have been adequately separated. Ogan et al. [4] achieved a separation of seventeen PAHs in this manner. Because the feasibility of a separation of 17 PAHs had been demonstrated, it was felt to be unnecessary to repeat the episode in this work. The capabilities of the pro-

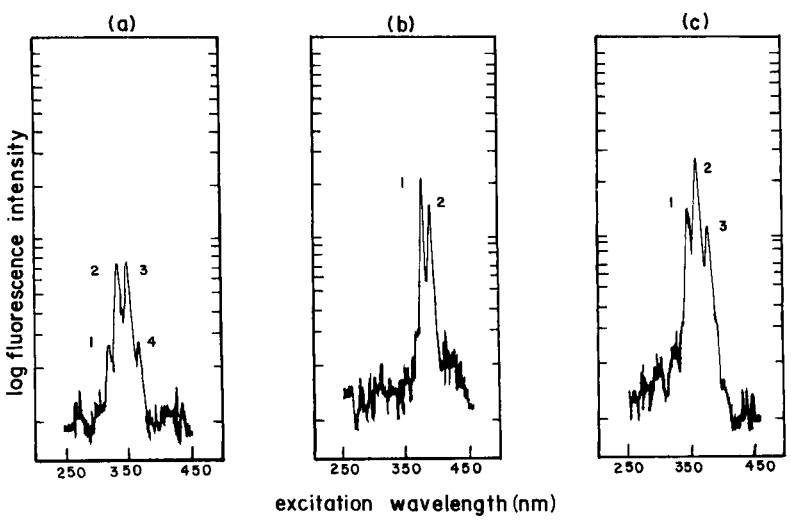

Fig. 3. Rapid-scan spectra output at the end of the chromatography: (a) anthracene; (b) chrysene; (c) benzo(a)pyrene. Excitation/emission wavelengths: for anthracene (1) 324/377 nm, (2) 338/399 nm, (3) 355/422 nm, (4) 375/466 nm; for chrysene (1) 306/362 nm, (2) 318/380 nm; for benzo(a)pyrene (1) 346/403 nm, (2) 362/427 nm, (3) 383/454 nm.

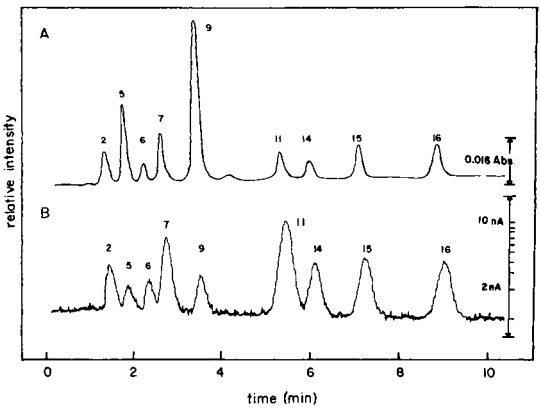

Fig. 4. Chromatograms of a nine-component PAH mixture (see Table 2 for identification of components) obtained with the u.v. detector (A) and the proposed rapid-scanning fluorescence detector (B).

TABLE 2

Comparison of three h.p.l.c. detection systems for 17 PAHs[a]

Compound	Rapid-scan c.e.s.f.s. ($\Delta\nu$ = 4800 cm^{-1}) S/N = 3		U.v. absorbance (254 nm) S/N = 3		Variable-wavelength fluorescence[b] S/N = 2
	LD (ng ml^{-1})	Absolute LD[c] (ng)	LD (ng ml^{-1})	Absolute LD[d] (ng)	Absolute LD (ng)
1. Naphthalene	550	10	415	2	0.03
2. Fluorene	15	0.27	30	0.15	0.01
3. Acenaphthene	45	0.81	950	5	0.0005
4. Phenanthrene	1000	20	5.5	0.03	0.13
5. Anthracene	40	0.72	30	0.15	0.12
6. Fluoranthene	30	0.54	15	0.075	0.04
7. Pyrene	20	0.36	40	0.20	0.075
8. Benz(a)anthracene	50	0.90	80	0.40	0.035
9. Chrysene	140	2.5	10	0.05	0.07
10. Benzo(b)fluoranthene	25	0.45	15	0.075	0.003
11. Benzo(k)fluoranthene	5	0.9	35	0.175	0.0003
12. Benzo(e)pyrene	85	1.5	25	0.125	0.045
13. Perylene	4.5	0.080	15	0.075	—
14. Benzo(a)pyrene	8.5	0.15	6.5	0.03	0.003
15. Dibenz(a, h)anthracene	40	0.72	420	2	0.004
16. Benzo(g, h, i)perylene	45	0.81	350	2	0.009
17. Indeno(1, 2, 3-c, d)pyrene	35	0.63	10	0.05	0.008

[a]The numbers listed before the compounds indicate the elution order for 80:20 acetonitrile/water with the chromatographic column used. The limit of detection specified (LD) is that concentration giving a signal at 3 or 2 times the standard deviation of the blank divided by the sensitivity (S/N = 3 or 2 as stated). [b]From Ogan et al. [4]. [c]The illuminated volume for the rapid-scanning c.e.s.f.s. system was 18 μl; the RSD for 20 blank measurements was 4—6%. [d]The illuminated volume for the u.v. absorbance system was 5 μl; the RSD for 20 blank measurements was 1.5—3.3%.

posed detection system were demonstrated adequately with a nine-component mixture.

For the rapid-scanning c.e.s.f.s. system, the limits of detection were in the ng ml^{-1} range with the exception of phenanthrene. The blank relative standard deviation (RSD) values ranged from 4 to 6% based on 20 blank measurements for the rapid-scanning system and from 1.5 to 2.5% for the u.v. absorbance system. The linear dynamic range was defined as the linear orders of magnitude from the detection limit to the concentration where the slope (sensitivity) fell by 5%. With the exception of phenanthrene, the linear orders of magnitude ranged from 2.3 to 3.7 for the proposed system. The limit of detection was lower with the u.v. absorbance system than with the rapid-scanning fluorescence system for phenanthrene (by a factor of 200) and chrysene (by 15). The limit of detection was lower with the rapid-scanning system than with the u.v. absorbance system for acenaphthene (by 20), dibenz(a, h)anthracene (by 100), and benzo(g, h, i)perylene (by 90). Most PAHs compared by a factor of 1.5—5 between the two systems.

The rapid-scanning system vs. variable wavelength fluorescence

The signal/noise reduction resulting from the faster scan speed of the rapid-scanning fluorescence system can be clearly seen in comparison to a variable-wavelength fluorescence detector. In the h.p.l.c. work by Ogan et al. [4], three pairs of excitation/emission wavelengths were used throughout the PAH analysis. The wavelength pair 280/340 nm was used for compounds 1, 2, 3, and 4 as numbered for the elution order in Table 2. The wavelength pair 305/430 nm was used for the measurement of compounds 5—16 (perylene was not measured). For indeno(1, 2, 3-c, d)-pyrene, the wavelength pair 305/500 nm was used. Ogan et al. [4] calculated limits of detection based on a signal/noise ratio of 2. A comparison was made with the absolute detection limits obtained from the proposed rapid-scanning system at 200 nm s^{-1} and the variable-wavelength fluorescence system [4]. The variable-wavelength system gave lower detection limits by a factor of 6 for anthracene to a range of 30—300 for the other PAHs over the proposed rapid-scanning system.

The equations of Foley and Dorsey [11] were used to normalize the chromatographic conditions for comparison of analytical figures of merit. No significant difference was determined when the normalized figures of merit for the work of Ogan et al. [4] and the unnormalized figures of merit given in Table 2 were compared.

There are two factors which greatly affect the detection limits obtained with the proposed rapid-scanning system: the scanning rate of 200 nm s^{-1} and the time constant of the current-to-log voltage converter. For the rapid-scanning c.e.s.f.s. system, measurements were taken each 1 nm over an excitation wavelength range of 250—450 nm. The wavelength range is scanned continuously in the forward and reverse directions at a scan rate of 200 nm s^{-1}. For the variable-wavelength fluorescence system, measurements are made continuously at the same excitation/emission wavelength pair. The S/N of

the rapid-scanning c.e.s.f.s. system will be reduced by a factor of 200 (1 s per spectral interval for variable-wavelength fluorescence system vs. 0.005 s per spectral interval for the rapid-scanning c.e.s.f.s. system). The time constant ranged from 400 μs to 4 μs over a current range of -0.1 nA to -10 nA for the current-to-log voltage converter. A time constant of 100 ms was assumed for the variable-wavelength fluorescence system. A further signal-to-noise reduction arising from the time constant was calculated to be a factor of $(100\ \text{ms}/400\ \mu\text{s})^{1/2}$ or 16. The loss in the detection limits observed in the rapid-scanning c.e.s.f.s. system compared to the variable wavelength fluorescence system would be up to a factor of ca. 3200 (16×200) but the rapid-scanning system obtained the result 200 times faster. The results obtained experimentally with the rapid-scanning system agreed with those predicted by the signal-to-noise comparison of the two systems.

This research was supported by NIH-5-R01-GM11373-22.

REFERENCES

1 M. L. Lee, M. V. Novotny and K. D. Bartle, Analytical Chemistry of Polycyclic Aromatic Compounds, Academic Press, New York, 1981.
2 M. A. Fox and S. W. Staley, Anal. Chem., 48 (1976) 992.
3 B. S. Das and G. H. Thomas, Anal. Chem., 50 (1978) 967.
4 K. Ogan, E. Katzk and W. Slavin, Anal. Chem., 51 (1979) 1315.
5 T. Nielsen, J. Chromatogr., 170 (1979) 147.
6 T. W. Allen, R. J. Hurtubise and H. F. Silver, Anal. Chim. Acta, 141 (1982) 411.
7 A. Jurgensen, E. L. Inman, Jr. and J. D. Winefordner, Anal. Chim. Acta, 131 (1981) 187.
8 M. Jonell Kerkhoff, E. L. Inman, Jr., E. Voigtman, L. P. Hart and J. D. Winefordner, Appl. Spectrosc., 38 (1984) 239.
9 E. L. Inman and J. D. Winefordner, Anal. Chem., 54 (1982) 2018.
10 E. L. Inman, Ph.D. Thesis, University of Florida, Gainesville, FL, 1982.
11 J. Foley and J. Dorsey, Chromatographia, 18 (1984) 503.

Analytica Chimica Acta, 175 (1985) 267—274
Elsevier Science Publishers B.V., Amsterdam — Printed in The Netherlands

EXCIPLEX LUMINESCENCE STUDIES OF THE SURFACE POLARITY OF END-CAPPED BONDED PHASES

C. H. LOCHMÜLLER*, M. T. KERSEY and M. L. HUNNICUTT
Paul M. Gross Chemical Laboratory, Duke University, Durham, NC 27706 (U.S.A.)
(Received 19th April 1985)

SUMMARY

The fluorescence intensities and emission maxima of surface-bound exciplexes were studied to determine the relative polarity of microparticulate silica before and after derivatization with trimethylchlorosilane (TMCS) and hexamethyldisilazane (HMDS). The results indicate that HMDS yields a bonded phase with greater average polarity relative to TMCS at equivalent surface coverages. This difference is attributed to the formation of basic sites on the surface by chemisorption of ammonia generated during derivatization with HMDS. The observation of exciplex emission on silica gel is novel and strongly supports clustering of surface-bound molecules into high-density regions.

Silanols on the surface of microparticulate silica act as derivatization sites in the synthesis of n-alkyl bonded phases commonly used in reversed-phase liquid chromatography. Preparation of these nonpolar bonded phases involves the reaction of surface silanols with a long-chain aliphatic silylating reagent (usually an n-octyl or n-octadecylsilane). Steric constraints imposed by the chain length and molar volume of these n-alkylsilanes do not permit complete derivatization of the silica surface. The remaining surface silanols act as strong adsorptive sites that are generally undesirable because they have been shown to account for large deviations in normal solute retention behavior. In an attempt to produce bonded phases with greater chemical homogeneity and hence better chromatographic behavior, n-alkyl-bonded phases are exhaustively "end-capped" or trimethylsilylated with either trimethylchlorosilane (TMCS) or hexamethyldisilazane (HMDS).

It seems important to determine how end-capping with TMCS or HMDS affects the properties of n-alkyl-bonded phases on a molecular level because the chromatographic properties of these materials have been shown to depend on the surface coverage and distribution of bonded alkyl chains as well as on the concentration and type of residual surface silanols present after derivatization [1—7]. End-capping with a mixture of TMCS and HMDS in pyridine has been shown to produce the greatest degree of surface deactivation; however, Bush et al. [8] recently reported enhanced surface deactivation, using sterically smaller alkylating reagents such as methylmagnesium chloride or methyllithium. Lochmüller and Marshall [1] evaluated the effect

0003-2670/85/$03.30

of end-capping on the chromatographic and spectroscopic properties of octadecylsilylated silicas that had been treated with TMCS and HMDS. Their results suggested that end-capping with HMDS yields a bonded phase with greater chemical heterogeneity, though lower average polarity than phases treated with TMCS. The spectroscopic and chromatographic data strongly suggested that the greater chemical heterogeneity of bonded phases end-capped with HMDS was due to the production of basic sites on the silica surface. These basic sites were believed to be formed via chemisorption of the reaction by-product (ammonia) generated during end-capping with HMDS.

The present study evaluates the surface polarity of microparticulate silica when treated with HMDS and TMCS by monitoring the luminescence of surface-bound "exciplexes". Exciplex formation involves the interaction of two hetero-molecules which form an excited-state complex that gives rise to a broad, structureless emission similar to that observed for excimer formation [9, 10]. The emission spectra of exciplexes are sensitive indicators of the polarity or polarizability of their environment and become red-shifted with increasing solvent dielectric constant. This behavior is paralleled by a large decrease in their fluorescence intensity and average lifetime [11, 12].

Weis et al. [13] attempted to study exciplex emission of a pyrene/dimethylaniline solution in contact with silica gel. They concluded that complete quenching of the solution exciplex emission was due to preferential hydrogen-bonding of dimethylaniline to the surface silanols. The results of recent studies of surface-bound excimers suggests that exciplex formation should be observed when molecules are covalently attached on the surface of silica [14, 15]. Steric effects imposed via the formation of siloxane linkages should inhibit molecular interaction with the underlying silica surface and enhance the probability of exciplex formation. Here, the observation of exciplex emission on silica gel is reported. This observation is novel and allows the relative polarity of the surface to be evaluated as a function of solvent polarity and subsequent secondary derivatization with TMCS or HMDS. The results indicate that, for equivalent surface concentrations of trimethylsilyl modification, TMCS produces a bonded phase of lower average polarity relative to HMDS because of the formation of basic sites on the silica surface during end-capping with HMDS.

EXPERIMENTAL

Materials

The silica gel used for the preparation of the exciplex-bonded phases was Whatman Partisil-10 with a surface area of 323 $m^2\ g^{-1}$, mean pore diameter of 9.3 nm, and a mean particle diameter of 10 μm. The aromatic monochlorosilanes, 3-(3-pyrenyl)propyldimethylchlorosilane (PPS), 3-(4-biphenyl)propyldimethylchlorosilane (BPS) and *N,N*-dimethylamino-*p*-(3-chlorodimethylpropyl)phenylsilane (DMA), were synthesized and their structures were

confirmed in this laboratory. The alkylsilanes, hexamethyldisilazane (HMDS) and trimethylchlorosilane (TMCS) (Aldrich), were used as received. *N,N*-Dimethylaniline and pyrene (Aldrich) were recrystallized prior to use; biphenyl (Eastman) was used without further purification. Reagent-grade chloroform was distilled from and stored over calcium hydride prior to its use in the derivatization reaction. Spectroscopic-grade hexane, tetrahydrofuran, dichloromethane, acetone, acetonitrile, and methanol were used as received. Special precautions were taken to ensure that the tetrahydrofuran did not form peroxides.

Preparation of exciplex bonded phase

The reaction was done under nitrogen in a three-neck 100-ml round-bottom flask equipped with an addition funnel and a teflon stir bar. All glassware was treated with trimethylchlorosilane and was then allowed to dry at 100°C prior to derivatization. Stock solutions of the aromatic silanes were prepared in dry chloroform to allow for quantitative preparation of either PPS/DMA or BPS/DMA exciplex mixtures. Approximately 0.5 g of hot, dried silica was quickly added into the reaction flask with 20 ml of dry chloroform. The appropriate volume of each aromatic silane was added to the addition funnel and the resulting mixture was diluted to a total volume of 10 ml. The diluted mixture was added dropwise at ambient temperature over 15 min while the silica was thoroughly dispersed by stirring. The contents of the flask were allowed to react for an additional 90 min after the silane mixture had been added. The chemically modified silica was then rinsed with two 100-ml portions each of chloroform, acetonitrile, methanol, and acetone. The silylated (exciplex) silica was dried in a vacuum desiccator for 24 h. Aliquots of the "exciplex silica" were then exhaustively treated with either HMDS or TMCS to produce the exciplex/HMDS or exciplex/TMCS silicas. All chemically modified silicas were stored under nitrogen in a dark and dry environment. The surface concentration of the bound silane (μmol m^{-2}) was evaluated from elemental carbon, nitrogen, and hydrogen determinations as described by Unger [16].

Fluorescence studies

All fluorescence spectra were obtained with a Perkin-Elmer model 650-10S scanning spectrophotometer. The silica samples were packed into a quartz column flow cell [15], and an infusion pump delivered argon-saturated solvents to the flow cell at a rate of 0.14 ml min^{-1}. The emission spectra were obtained after an equilibration time of 15—20 min. The excitation monochromator was set at 290 nm and 346 nm, respectively for the BPS/DMA and PPS/DMA silicas. The emission monochromator scanned from 320 to 490 nm at a scan rate of 60 nm min^{-1} for the BPS/DMA and from 360 to 540 nm for the PPS/DMA silicas. The excitation shutter was closed between measurements to avoid possible photodecomposition of the chemically modified silica. The molar absorptivity and surface concentration of PPS

necessitated dilution of the dry PPS/DMA silica with untreated Partisil-10 (1:20 by weight) to avoid inner-filter effects. No dilution of the BPS/DMA silica was found to be necessary. Biphenyl/*N,N*-dimethylaniline and pyrene/*N,N*-dimethylaniline solution spectra were obtained after the solution had been subjected to three cycles of freeze/pump/thaw to remove dissolved oxygen. The excitation and emission monochromator settings were identical to those used for the silica samples.

RESULTS AND DISCUSSION

Emission maxima for the free solution and surface bound pyrene/*N,N*-dimethylaniline and biphenyl/*N,N*-dimethylaniline exciplex systems are presented in Table 1. The emission maxima become red-shifted with increasing dielectric constant of the solvent and are indicative of the increased heteropolarity or charge-transfer nature of exciplexes in polar solvents [9]. The PPS/DMA and BPS/DMA emission maxima in hexane are red-shifted 36 and 34 nm, respectively, with respect to their free solution values. These differences reflect the enhanced charge-transfer character of surface-bound exciplexes resulting from the polarizability of residual surface silanols and surface water. The magnitude of the observed red-shifts in hexane are approximately equal and suggest that the surface perturbations affecting the charge-transfer nature of the PPS/DMA and BPS/DMA systems are nearly equivalent.

The free-solution emission maxima of the pyrene/*N,N*-dimethylaniline hetero-excimer are plotted (Fig. 1) as a function of solvent dielectric constant for the solvents used in this study as well as for solvents found in the literature [12, 17]. Although no correlation between emission maxima and solvent dielectric constant can be made when all solvents are considered, the emission maxima observed for solvents having a dielectric constant less than

TABLE 1

Emission maxima for free solution and surface-bound exciplex systems

Solvent	Dielectric constant	Emission maxima (nm)			
		Free solution		Bonded phase	
		B/DMA[a]	P/DMA[b]	BPS/DMA[c]	PPS/DMA[d]
Hexane	1.89	374	436	408	472
Tetrahydrofuran	7.59	—	490	431	496
Dichloromethane	9.08	—	489	426	500
Acetone	20.7	—	510	—	—
Acetonitrile	32.6	—	—	452	—
Methanol	37.5	—	516	450	521

[a] 1×10^{-3} M (biphenyl) + 1×10^{-1} M (*N,N*-dimethylaniline). [b] 1×10^{-5} M (pyrene) + 1×10^{-2} M (*N,N*-dimethylaniline). [c] 1.15 μmol m^{-2} (BPS) + 1.53 μmol m^{-2} (DMA). [d] 0.19 μmol m^{-2} (PPS) + 0.46 μmol m^{-2} (DMA).

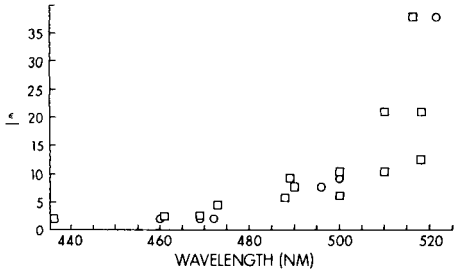

Fig. 1. Pyrene/*N*,*N*-dimethylaniline exciplex emission maxima as a function of solvent dielectric constant: (□) free solution; (○) PPS/DMA.

Solvent	Dielectric constant	λ_{max} (nm)	Ref.
In solution			
1. n-Hexane	1.890	436	11, this study
2. *p*-Xylene	2.270	461	11
3. Toluene	2.379	469	11, 17
4. Diethyl Ether	4.330	473	17
5. Chlorobenzene	5.621	488	17
6. Ethylacetate	6.020	500	17
7. Tetrahydrofuran	7.59	490	this study
8. Dichloromethane	9.08	489	this study
9. Dichloroethane	10.36	510	17
		500	11
10. Pyridine	12.30	518	11
11. Acetone	20.70	510	this study
		518	17
12. Methanol	37.5	516	this study
Bonded			
Hexane PPS/DMA/TMCS	1.89	460	
Hexane PPS/DMA/HMDS	1.89	469	
Hexane PPS/DMA	1.89	472	
Tetrahydrofuran PPS/DMA	7.59	496	
Dichloromethane PPS/DMA	9.08	500	
Methanol PPS/DMA	37.5	521	

ten show a consistent trend that could provide an estimate of the dielectric constant of the silica surface. The PPS/DMA emission maximum in hexane agrees well with the free solution value (473 nm) obtained for pyrene/*N*,*N*-dimethylaniline in diethyl ether [17]. Thus the apparent dielectric constant of the silica surface can be estimated to be 4.34 at 20°C, assuming that the energy difference between the ground and first excited-singlet state does not appreciably differ for the free solution and bonded-phase systems. This value agrees well with those obtained for glasses (ϵ = 3.75—6.75) at 20°C, and for chromatographic silica (ϵ = 2.20) [18, 19].

The emission maxima are expected to blue-shift because of a decrease in surface polarity following the reaction of residual surface silanols with either HMDS or TMCS. Results in Table 2 are consistent with this prediction; how-

TABLE 2

Exciplex emission maxima as a function of end-capping reagent

Solvent	Dielectric constant	Emission maxima (nm)			
		BPS/DMA[a] TMCS	BPS/DMA[b] HMDS	PPS/DMA[c] TMCS	PPS/DMA[d] HMDS
Hexane	1.89	396	404	460	469
Tetrahydrofuran	7.59	431	431	496	495
Dichloromethane	9.08	428	428	500	499
Acetone	20.7	—	—	516	514
Acetonitrile	32.6	452	452	520	521
Methanol	37.5	451	451	524	523

[a]1.15 μmol m^{-2} (BPS) + 1.53 μmol m^{-2} (DMA) + 0.3 μmol m^{-2} (TMCS). [b]1.15 μmol m^{-2} (BPS) + 1.53 μmol m^{-2} (DMA) + 0.4 μmol m^{-2} (HMDS). [c]1.19 μmol m^{-2} (PPS) + 0.46 μmol m^{-2} (DMA) + 2.4 μmol m^{-2} (TMCS). [d]1.19 μmol m^{-2} (BPS) + 0.46 μmol m^{-2} (DMA) + 2.6 μmol m^{-2} (HMDS).

ever, the emission maxima indicate that there is a substantial difference in interface polarity when end-capping is done with these reagents. The PPS/DMA and BPS/DMA silicas end-capped with TMCS are blue-shifted 12 nm in comparison to the 3—4 nm blue-shift observed with HMDS. Figure 2 shows the effect of end-capping reagent on the exciplex emission of the PPS/DMA

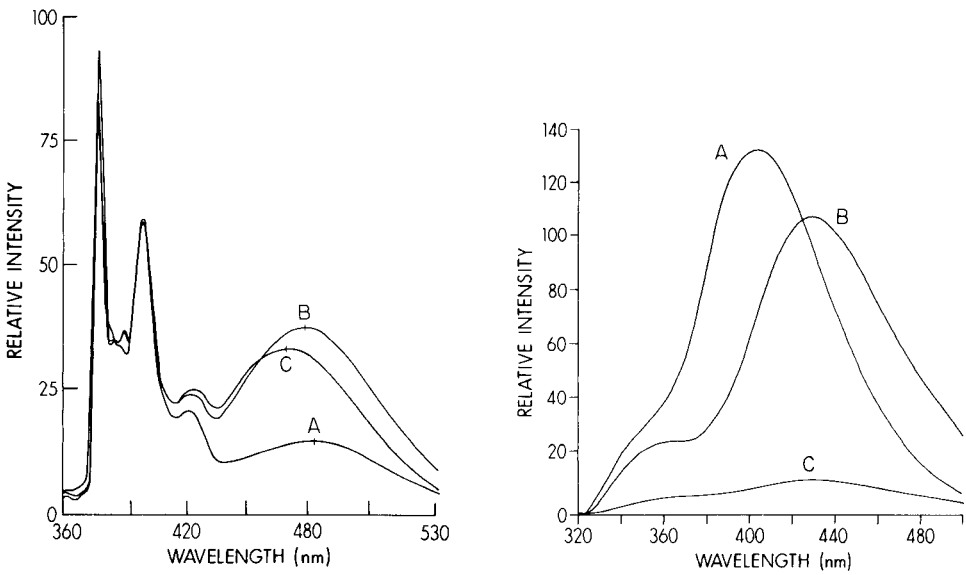

Fig. 2. Emission spectra for PPS/DMA as a function of end-capping reagent with hexane as solvent: (A) PPS/DMA; (B) PPS/DMA/HMDS; (C) PPS/DMA/TMCS.

Fig. 3. Solvent effect on the exciplex emission of BPS/DMA/HMDS silica. Solvent: (A) dichloromethane; (B) tetrahydrofuran; (C) hexane.

silica. The data in Table 2 indicate that a more nonpolar surface environment is achieved (for near equivalent trimethylsilylation) when TMCS is used instead of HMDS.

These results differ from those previously reported by Lochmüller and Marshall for octadecylsilylated silicas that were sparingly dansylated and then end-capped with either HMDS or TMCS [1]. There it was reported that end-capping with HMDS produced a bonded phase with greater chemical heterogeneity, though lower average polarity, than phases end-capped with TMCS. These differences were attributed to the production of basic sites on the silica surface formed during the reaction of HMDS with residual silanols, and the higher reactivity of HMDS relative to TMCS. Thus, the lower average polarity was attributed to the higher carbon content of the bonded phase end-capped with HMDS.

In contrast to the previous study, the PPS/DMA and BPS/DMA silicas here were exhaustively end-capped with either HMDS or TMCS to produce exciplex-bonded phases that had undergone equivalent trimethylsilylation to within ± 0.2 μmol m^{-2}. The luminescence spectra of the chemically modified silicas were also collected while in contact with solvent, rather than in the dry state as in the earlier study [1]. Under these conditions, the exciplex emission maxima indicate that TMCS rather than HMDS produces a bonded phase of lower average polarity. The observed difference in surface polarity is most likely due to the chemisorption of ammonia generated from the reaction of HMDS with surface silanols during the end-capping procedures as previously suggested [1]. Elemental analysis of the HMDS end-capped bonded phases showed a 0.2—0.3% by weight increase in nitrogen content relative to the untreated exciplex phase and is consistent with this hypothesis.

Apparently, the differences in surface polarity between exciplex-bonded phases becomes undetectable for solvents other than hexane because of the large increase in the exciplex dipole moment caused by the interaction of more polar solvent molecules. This change in electronic structure can be observed by the large decrease in exciplex emission intensity for solvents of increasing polarity and is illustrated in Fig. 3. It should also be mentioned that the exciplex emission observed in hexane increases approximately 50% following end-capping, which indicates that surface silanols effectively quench exciplex emission as was first suggested by Weis et al. [13].

Conclusions

The results indicate that for equivalent trimethylsilylation, TMCS produces a surface of lower average polarity than end-capping with HMDS. The higher polarity of the HMDS exciplex phases is attributed to the formation of basic surface sites generated during derivatization with HMDS. Changes in the exciplex emission maxima as a function of solvent dielectric constant provided an estimate of the apparent surface dielectric constant ($\epsilon = 4.34$) for microparticulate silica in contact with hexane.

This work was supported in part by the National Science Foundation under Grant CHE-8500658 (to C. H. L.). The silica was drawn from the Duke Standard Collection established by a grant from Whatman-Chemical Separations. Portions of these materials are available to serious investigators on request.

REFERENCES

1 C. H. Lochmüller and D. B. Marshall, Anal. Chim. Acta, 142 (1982) 63.
2 C. H. Lochmüller, K. A. Stutler and D. B. Marshall, J. Chromatogr. Sci., 22 (1984) 217.
3 A. Nahum and C. Horvath, J. Chromatogr., 203 (1981) 53.
4 K. E. Bij, C. Horvath, W. R. Melander and A. Nahum, J. Chromatogr., 203 (1981) 65.
5 K. Karch, L. Sebestian and H. Halasz, J. Chromatogr., 122 (1976) 3.
6 G. E. Berendsen and L. de Galan, J. Chromatogr., 196 (1980) 21.
7 J. M. McCall, J. Med. Chem., 18 (1975) 549.
8 S. G. Bush, J. W. Jorgensen, M. L. Miller and R. W. Linton, J. Chromatogr., 260 (1983) 1.
9 E. L. Wehry, Modern Fluorescence Spectroscopy, Vol. 2, Plenum Press, New York, 1976.
10 M. Gordon and W. R. Ware, The Exciplex, Academic Press, New York, 1975.
11 T. Okada, T. Saito, N. Mataga, Y. Sakata and S. Misumi, Bull. Chem. Soc. Jpn., 50 (1977) 331.
12 N. Mataga, T. Okada and N. Yamamoto, Chem. Phys. Lett., 1 (1967) 119.
13 L. D. Weis, T. R. Evans and P. A. Leermakers, J. Am. Chem. Soc., 90 (1968) 6109.
14 C. H. Lochmüller, A. S. Colborn, M. L. Hunnicutt and J. M. Harris, J. Am. Chem. Soc., 106 (1984) 4077.
15 C. H. Lochmüller, A. S. Colborn, M. L. Hunnicutt and J. M. Harris, Anal. Chem., 55 (1983) 1344.
16 K. K. Unger, Porous Silica, Elsevier, Amsterdam, 1979.
17 H. Beens, H. Knibbe and A. Weller, J. Chem. Phys., 47 (1967) 1183.
18 R. C. Weast (Ed.), CRC Handbook of Chemistry and Physics, 60th edn., CRC Press, FL, 1980.
19 J. M. Thorp and L. B. Nichols, Trans. Faraday Soc., 66 (1970) 1741.

Analytica Chimica Acta, 175 (1985) 275—280
Elsevier Science Publishers B.V., Amsterdam — Printed in The Netherlands

A NICKEL OXIDE AMPEROMETRIC DETECTOR IN THE CHROMATOGRAPHIC SEPARATION OF AMINO ACIDS

J. B. KAFIL and C. O. HUBER*

Department of Chemistry, University of Wisconsin-Milwaukee, Milwaukee, WI 53201 (U.S.A.)

(Received 8th April 1985)

SUMMARY

Reverse-phase ion-pair chromatography with a nickel oxide amperometric detector is evaluated for separation and detection of several amino acids. A simple T-junction allows post-column mixing of detector electrolyte. Mixer and detector dimensions are shown to contribute negligibly to band spreading. Picomole amounts of some amino acids can be detected. The system is evaluated for determination of amino acids in hydrolyzed bovine A-chain insulin and urine samples.

The ability to separate and quantify amino acids is of importance in studies of protein and peptide hydrolysates, biological fluids, pharmaceuticals, food and feed samples, etc. [1]. Several detection methods have been developed, including direct detection by ultraviolet absorbance in the 200-nm region or refractive index. More sensitive and selective detection is often achieved by derivatizing the amino acids. Recently, monitoring of derivatized and underivatized amino acids with electrochemical detectors has been reported [2]. Earlier work in this laboratory has introduced the anodic amperometric determination of amino acids at a nickel oxide electrode [3]. The electrode is conveniently maintained in an active state with a d.c. applied potential, with response to almost all amino acids, and can readily be incorporated into a small detector cell. Accordingly, in an earlier report [4], a system based on an amperometric nickel oxide detector was used to monitor classical ion-exchange chromatograms of several amino acids by an automatic intermittent sampling technique. For analytical scale high performance liquid chromatography (h.p.l.c.) however, continuous detection of the eluent is preferable.

Separation of underivatized amino acids has commonly been done in the past by low-pressure ion-exchange chromatography. The interaction of highly polar amino acids with reversed phases is not ordinarily sufficient for effective resolution. However, it has been shown that the separation of amino acids on reverse-phase columns in analytical h.p.l.c. can be done by using a mobile phase containing an anionic surfactant at subcritical micelle concentrations [5, 6].

0003-2670/85/$03.30

The mechanism of the interaction between the column eluent and the amino acid is not fully understood. The possibilities include dynamic ion exchange at the stationary phase interface and partition of neutral ion-pairs. The effectiveness of the anionic surfactant increases with alkyl chain length whereas the equilibration rate decreases with chain length. In the work reported here, heptane sulfonic acid as surfactant was examined. As reported earlier, the nickel oxide electrode yields maximum analytical response when the pH exceeds 12. Thus the typically lower pH column eluents require post-column mixing with alkaline solution. Post-column mixers have been widely used with derivatization in order to increase detector sensitivity.

In a properly designed post-column mixer, additional band broadening should be minimized. Band spreading includes column and mixer contributions: $\sigma_t^2 = \sigma_c^2 + \sigma_m^2$. A reasonable criterion is that the mixer should contribute less than 10% to total peak widths. From plate theory, $\sigma_c^2 = V_R^2/N$. A typical value for σ_c^2 is 6×10^{-3} ml^2. Scott and Kucera [7] have shown that for an open tubular mixer of radius r and length l with volume flow rate F:

$$\sigma_m^2 = \pi r^4 lF/24D$$

For typical mixer parameters of 0.1 mm × 125 cm at a flow rate of 1 ml min^{-1} and D of 1×10^{-5} cm^2 s^{-1}, σ_m^2 is equal to 3×10^{-4} ml^2, less than 10% of σ_c^2 as estimated above. Amperometric detectors are characteristically of such small dead volume that detector contributions to band broadening are insignificant [8].

EXPERIMENTAL

A high-performance liquid chromatograph with an electrochemical detector was assembled. Mobile-phase flow rates between 0.1 and 3.0 ml min^{-1} were delivered by a Waters Associates M-45 pump. Samples were injected with a Rheodyne 7010 valve with 25-μl loops. A chromatographic column (250 mm × 4.6 mm i.d.) prepacked with 5-μm silica particles bonded with octadecylsilane (Partisil PXS-1025 ODS3; Whatman) was used at ambient room temperature. The detector cell was a three-electrode system consisting of a nickel oxide working electrode, a platinum counter electrode, and a saturated calomel reference electrode. Two configurations of the working electrode were examined. The first, a tubular electrode, was constructed from nickel tubing (2 mm i.d., 5 mm long); the nominal surface area was 0.3 cm^2. The second was a 3-mm diameter planar nickel electrode in a thin-layer flow-through cell. The applied potential was 0.50 V vs. SCE. The detector circuitry consisted of op-amp (bi-FETT)-based potentiostat and current-to-voltage converter components with provision for offset current. A strip-chart potentiometric recorder was used for read-out.

A flow-injection system was used to simulate the chromatographic peaks. It consisted of a multichannel peristaltic pump (Cole-Palmer Masterflex 7545-12, variable speed pump drive), a four-way rotary injection valve

(Rheodyne, Model 50) with 25-μl injection loop, and an amperometric flow-through nickel oxide detector as described above.

Glycine and heptane sulfonic acid (Aldrich Chemical Co.) as well as other amino acids (Sigma) were used as purchased to prepare sample solutions. The sample solutions were filtered (Sep-Pak no. 51900; Waters Associates) before use. Bovine A-chain insulin was purified by semipreparative h.p.l.c. as described by Di Bussolo et al. [9]. The mobile phase was a mixture of acetonitrile and 0.05 M acetate buffer with heptane sulfonic acid (concentrations as stated below).

RESULTS AND DISCUSSION

The performance of the nickel oxide electrode was studied under simulated chromatographic conditions with the flow-injection apparatus. The mobile phase was mixed with an equal flow of 0.2 M sodium hydroxide. Three mixer designs were examined. Two designs were intended to optimize turbulent mixing while minimizing mixer volume. The third design, shown in Fig. 1, is simply a T-entry to a coiled 0.1-mm i.d. stainless steel tubing. Experimental examination of the tubing length indicated that about 125 cm yielded optimum measurable peak heights. The performance of the three mixer designs was similar, and subsequent work was done with the simple mixer (Fig. 1).

Individual amino acid peak widths when the u.v. detector was preceded by this mixer were not measurably greater than those without the mixer, showing an insignificant contribution to band spreading by the mixer. The internal volume of the mixer plus nickel oxide detector was about 30 μl. To examine the effect of mobile phase on the detector current, solutions consisting of buffer (pH 3.4) containing 10—30% (v/v) acetonitrile were used. Samples

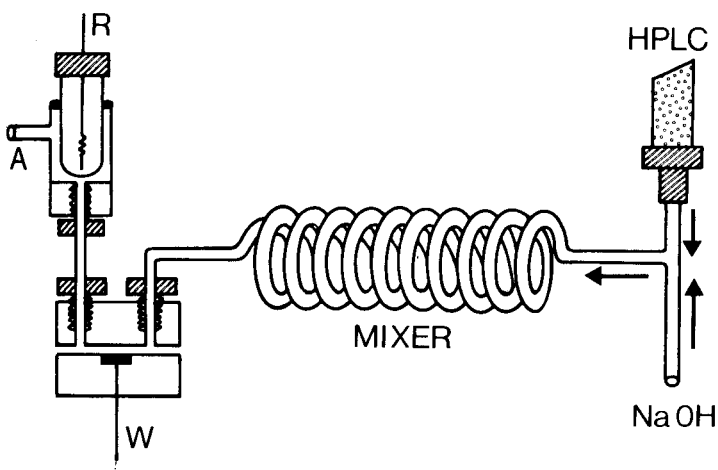

Fig. 1. T-tube mixer and detector. W, R and A are the working, reference and auxiliary electrodes, respectively.

(25 μl) of glycine were injected. Although the background current was changed slightly, the linear dynamic range of the detector was similar to that using only 0.1 M sodium hydroxide as the background electrolyte. The peak current varied linearly for samples from 2 pmol to 25 nmol. In this range, the slope was 0.2 nA l μmol^{-1} with a peak-to-peak noise of 2.0 pA. The presence of heptane sulfonic acid (HSA) in the background did not change the peak current or the baseline current.

The effects of the concentration of heptane sulfonic acid on the capacity ratio for several amino acids were observed. Results are shown in Table 1. The capacity factors were relatively insensitive to surfactant concentrations above about 20 mM, probably because of micelle formation. These findings are consistent with those reported by Kraak et al. [5] for other anionic surfactants. From the data of Table 1, a 0.01 M HSA concentration was selected to yield a favorable range of capacity factors.

The suitability of the nickel oxide detector for amino acids was examined for protein amino acids and for the determination of free amino acids. The former was done by hydrolyzing bovine A-chain insulin and the latter by using urine samples. The bovine insulin was first purified and then hydrolyzed to its amino acid constituents by using 6 M hydrochloric acid and established methodology [9, 10]. Dihydroxyphenylalanine was added to the hydrolysate as a marker. The u.v. detector (280 nm) and the nickel oxide amperometric detector were connected in series after the mixer to allow simultaneous detection of the chromatograms. The chromatogram obtained (Fig. 2) shows peaks for seven amino acids with the nickel oxide amperometric detector while the u.v. detector shows only the peak for tyrosine. The amperometric tyrosine peak is clearly broader than for the u.v. detector. This discrepancy does not appear for samples of tyrosine alone. This, together with the fact that both detectors follow the mixer, indicates that the peak broadening cannot be attributed to the mixer or the detector, but is probably due to electroactive components with retention times similar to tyrosine.

Urine samples were filtered and injected without pre-treatment. The chromatograms obtained with the nickel oxide detector for a mixture of

TABLE 1

Effects of surfactant (HSA) concentration on capacity ratios (k') at 25°C

Compound	k' values at various HSA concentrations (M)				
	0.001	0.005	0.02	0.2	0.5
Glycine	1.94	2.8	3.7	4.6	4.7
Serine	1.25	1.9	2.5	3.3	3.2
Aspartic acid	1.0	1.3	1.9	3.0	3.0
Tyrosine	5.7	6.0	6.5	7.5	7.2
Valine	6.3	6.9	7.7	9.0	9.1
Methionine	7.9	8.4	9.2	11.2	11.1

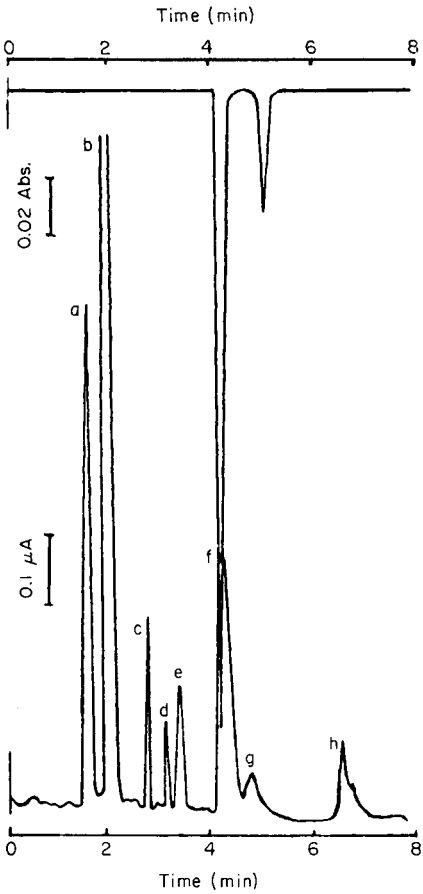

Fig. 2. Chromatogram of A-chain insulin hydrolysate. Mobile phase: 0.01 M sodium citrate, 0.01 M Na_2SO_4, pH 2.6, 10% (v/v) acetonitrile, 0.005 M HSA; flow rate 1.2 ml min^{-1}. Peaks: (a) serine; (b) glycine, glutamic acid; (c) alanine; (d) ammonia; (e) valine; (f) phenylalanine; (g) tyrosine; (h) leucine, isoleucine.

amino acids, diluted urine, and diluted urine with added amino acids are shown in Fig. 3. The chromatogram of the blank urine sample (Fig. 3A) is relatively featureless so that peaks from several amino acids are easily identified as shown in Fig. 3B, C. The limit of detection was 2—50 pmol, depending on the amino acid. These limits are comparable to those reported for u.v. absorbance [11, 12]. A linear quantitative response was found for glycine and serine from 2.5 pmol and 12.5 pmol, respectively, up to 25 nmol. The relative response of the nickel oxide electrode detector for various amino acids has been reported previously [3].

The chromatography of amino acids reported here demonstrates the applicability of the nickel oxide amperometric detector to h.p.l.c. The activity of the nickel oxide electrode to aliphatic as well as aromatic amines

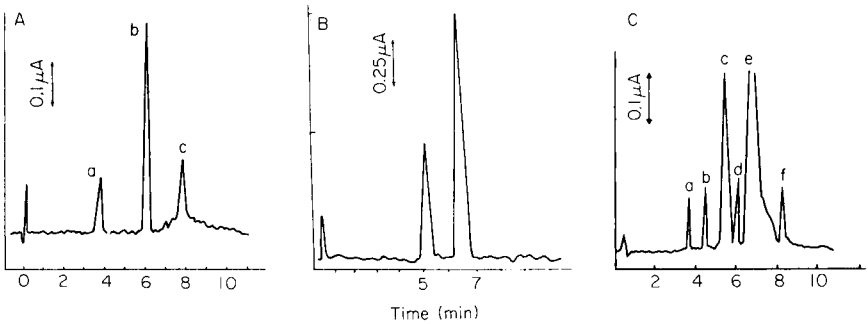

Fig. 3. Amino acid chromatograms. Mobile phase: acetate buffer (0.05 M), pH 3.4, 10% (v/v) acetonitrile, 0.010 M HSA; flow rate 1.4 ml min^{-1}. A. Aspartine (a), glycine (b), and lysine (c) in water (20 ng total). B. 10-fold diluted urine. C. 10-fold diluted urine plus aspartic acid, glycine and lysine.

and alcohols suggests its application to many other chromatographic separations. Reverse-phase ion-pair partition chromatography is especially well suited to this detector.

REFERENCES

1 G. J. Hughes, K. H. Winterhalter, E. Boller and K. J. Wilson, J. Chromatogr., 235 (1982) 417.
2 K. Bratin, C. L. Blank, I. S. Krull, C. E. Lunte and R. E. Shope, Am. Lab., (1984) 52.
3 B. S. Hui and C. O. Huber, Anal. Chim. Acta, 134 (1982) 211.
4 J. B. Kafil and C. O. Huber, Anal. Chim. Acta, 139 (1982) 347.
5 J. C. Kraak, K. M. Jonker and J. F. K. Huber, J. Chromatogr., 142 (1977) 671.
6 J. H. Knox and R. A. Hartwick, J. Chromatogr., 204 (1981) 3.
7 R. P. W. Scott and P. Kucera, J. Chromatogr. Sci., 9 (1971) 641.
8 J. M. Knox and M. T. Gilbert, J. Chromatogr., 185 (1979) 405.
9 J. M. DiBussolo, F. L. Vandemark and J. R. Grant, Am. Lab., (1983) 52.
10 A. Mondino and G. Bongioranni, J. Chromatogr., 52 (1970) 405.
11 R. Pfeifer and D. W. Hill, in J. C. Giddings and P. Brown (Eds.), Advances in Chromatography, Vol. 22, M. Dekker, New York, 1983, p. 37.
12 W. Th. Kok, U. A. Th. Brinkman and R. W. Frei, J. Chromatogr., 166 (1978) 403.

Analytica Chimica Acta, 175 (1985) 281—287
Elsevier Science Publishers B.V., Amsterdam — Printed in The Netherlands

FLOW-INJECTION EXTRACTION AND GAS-CHROMATOGRAPHIC DETERMINATION OF TERODILINE IN BLOOD SERUM

LAGE NORD*

Department of Analytical Chemistry, Royal Institute of Technology, S-100 44 Stockholm (Sweden)

STIG JOHANSSON and HARALD BRÖTELL

KabiVitrum AB, S-112 87 Stockholm (Sweden)

(Received 4th January 1985)

SUMMARY

Adsorption losses of terodiline (*N*-t-butyl-1-methyl-3,3-diphenylpropylamine) from aqueous and organic solutions in the different parts of a flow-injection extraction system are described. Terodiline base adsorbs strongly on PTFE and polypropylene tubing from aqueous solution; 60—80% is lost from low concentration samples during its passage through the tubing (2 m long, 0.7 mm i.d.). For nickel, stainless steel and glass, the adsorption losses were slight. Terodiline in organic solution did not adsorb on any of the tested materials. Based on these results, an extraction manifold was designed for mechanized work-up of human blood serum. The samples were injected from a valve with a steel loop (0.5 ml) at a rate of 30 h^{-1} into n-heptane + 2% n-pentanol, made alkaline, segmented with the organic phase and extracted. After phase separation, portions of the extract stream were collected in vials and analyzed for terodiline by using capillary gas chromatography with a nitrogen-selective detector.

Terodiline (*N*-t-butyl-1-methyl-3,3-diphenylpropylamine) (I) is a drug with anticholinergic and calcium antagonistic properties, for use in the treatment of urinary incontinence. Routine determination of terodiline at ng ml^{-1} concentrations in biological material is by batch extraction and capillary gas chromatography with a nitrogen-selective detector [1]. During recent years,

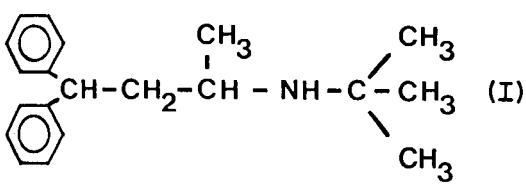

(I)

chromatographic instrumentation has become highly mechanized but the sample work-up that is frequently necessary before the chromatographic quantitation has not been mechanized to the same degree. This paper describes the mechanization of the extractive work-up step for terodiline assay.

Extraction based on flow injection analysis (f.i.a.) has proved to be a powerful tool for mechanizing sample work-up [2]. In flow-injection extrac-

0003-2670/85/$03.30

tion the sample is injected into a carrier stream, merged with a stream of reagent, segmented with an organic phase and extracted as the solutions flow through a coiled tube. The organic phase is separated and can be led to a flow-through detector or collected for off-line analysis. The first applications of such extractions utilized on-line spectrophotometric detection [2, 3]. The technique has been used for sample preconcentration prior to detection of the analyte by atomic absorption spectrometry, both as on-line [4] and off-line [5, 6] systems, reaching high concentration factors. Flow-injection extraction has also been used for sample work-up in combination with liquid chromatography [7, 8]. So far, little work has been done on the use of these extraction systems as a work-up procedure for gas-liquid chromatography (g.l.c.) of low levels of organic substances in matrices such as serum or plasma.

Losses of traces of organic analyte by adsorption on vessel walls are well known in batch methods [9] and must be carefully considered when flow-injection extraction is applied. In a batch extraction the sample is shaken with the organic phase in a single vessel until equilibrium is reached, so that the vessel surface area has no effect on the required extraction time. In contrast, a flow-injection extraction is achieved whilst the samples are transported through narrow bore tubing, the length of which governs the extraction time. This means that the ratio of surface area to sample volume in an extraction manifold is much greater than the ratio of vessel area to sample volume in a batch extraction. Furthermore, in a flow system, the sample will continuously meet tubing surface which has not been equilibrated with the analyte.

In the present work the effect of different tubing materials on the adsorption of terodiline in a flow-injection extraction manifold was studied. A manifold was then designed and evaluated for extractive sample work-up of blood serum samples containing terodiline prior to quantitation by g.l.c.

EXPERIMENTAL

Manifold design

Figure 1 shows the manifold employed to extract the serum samples. The equipment comprised a peristaltic pump (Ismatec mp-13 GJ-4, Switzerland), a FIA-05 analyzer (Bifok AB, Sollentuna, Sweden) with a single channel injector equipped with a 500-μl sample loop of stainless steel, a glass segmentor [2] and a membrane phase separator made of perspex [10]. The extraction coil was a 2-m stainless steel tube (0.7 mm i.d.) connected to a 2-m nickel tube (0.7 mm i.d.). A 3-way solenoid valve (Brunswick Corp.) was used to collect the part of the extract stream representing the sample. An electronic timer was used to control the cycle for sample injection and extract collection. Solvaflex and Tygon pump tubes (Technicon) were used.

Procedure

The serum sample was injected at point (1) (Fig. 1) into an organic carrier (1 ml min^{-1}) which transported the sample as an undivided plug. It was

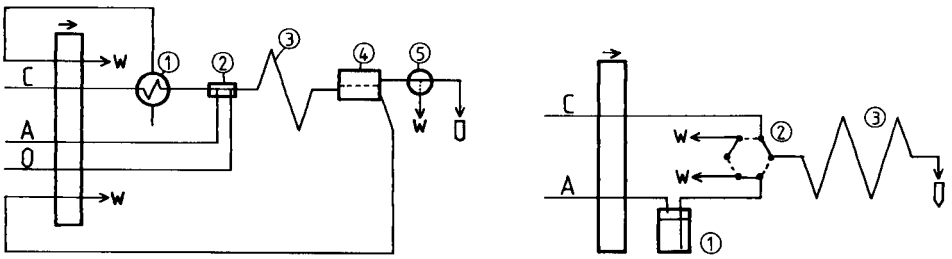

Fig. 1. Extraction manifold: (C, O) organic carrier and segmentation streams, 1.0 and 0.5 ml min^{-1}, respectively, of n-heptane/2% (v/v) pentanol containing 200 ng ml^{-1} PR-186; (A) aqueous alkali stream, 0.5 ml min^{-1}, 0.3 M NaOH; (1) sample injector, stainless steel loop, 0.5 ml; (2) T-connector for alkali stream and segmentor, all glass; (3) extraction coil, 2 m of nickel and 2 m of steel tubing, 0.7 mm i.d.; (4) membrane phase separator; (5) 3-way valve; (W) waste.

Fig. 2. Manifold for testing adsorption in different coils: (C) carrier, 1 ml min^{-1}, 0.1 M NaOH; (A) air, 1 ml min^{-1}; (1) sample reservoir; (2) injection valve; (3) coil tested. Sample: 100 ng ml^{-1} terodiline in 0.1 M NaOH.

mixed with an aqueous stream of 0.3 M sodium hydroxide (0.5 ml min^{-1}) and subsequently segmented with the organic phase (0.5 ml min^{-1}) at point (2). After extraction in coil (3), a fraction of the organic phase flow (0.4 ml min^{-1}) was separated at point (4) and directed by a 3-way valve (5), either to a sample vial for determination by g.c. or to waste. At a sampling rate of 30 h^{-1}, the sample injection/extract collection cycle was: injection, 0—40 s; wash 3-way valve, 50—60 s; collection of extract in vial, 105—120 s.

Investigation of adsorption losses

A manifold comprising a peristaltic pump with a Tygon pump tube, a segmentor, a PTFE extraction coil (2 m, 0.7 mm i.d.) and a membrane separator was used in an initial study of the adsorption losses. Only aqueous alkaline terodiline solution (pH 13, 1 μg ml^{-1}) was pumped into the manifold, with no organic phase present. Beginning with the pump tube, the manifold sections were successively added to the system. After connection of each section the test solution was pumped through for 5 min and a fraction was collected and analyzed for terodiline. Before each new section was added, the system was rinsed with dilute nitric acid.

To evaluate the adsorption losses for different tubing materials, the system shown in Fig. 2 was used. The valve (2) was switched over to injection position for 1 min, thus giving an injection volume of 1 ml from the displacement bottle (1). The aqueous stream coming out of tube (3) was collected in 88-μl fractions, 80 μl of organic phase was added to each, and the vials were capped and treated in an ultrasonic bath for 3 h. After cooling to room temperature, the aqueous phase was withdrawn with a syringe inserted through the cap membrane. The organic extract was analyzed by g.l.c.

Reagents

Terodiline hydrochloride (*N*-t-butyl-1-methyl-3,3-diphenylpropylamine hydrochloride) and the internal standard PR-186 hydrochloride (*N*-t-butyl-1-methyl-4,4-diphenylbutylamine hydrochloride) were synthesized at KabiVitrum (Stockholm). A stock solution of terodiline (1.3 mg ml^{-1} in ethanol) was used to prepare aqueous standards and to spike human serum in the concentration range 25—400 ng ml^{-1}. n-Heptane and n-pentanol were reagent grade. The organic phase was n-heptane containing 2% (v/v) pentanol and the internal standard (200 ng ml^{-1}).

Gas chromatography

A Hewlett-Packard 5730 gas chromatograph equipped with a 7671 Auto-Sampler and a nitrogen-selective detector was used. The 25-m fused silica capillary column, coated with OV-1701 (cross-linked), was operated isothermally at 180°C with a carrier gas flow of ca. 4 ml min^{-1} (8% hydrogen in helium). The same gas was introduced as scavenger into the detector, giving a total flow of ca. 40 ml min^{-1} through the detector jet. Detector air flow was 65 ml min^{-1}. Injector and detector temperatures were 250°C. The injection volumes were 2 or 7 μl.

RESULTS AND DISCUSSION

Influence of tubing material and pH on adsorption losses

Figure 3 shows the result from an initial test of the adsorption losses of terodiline in the different sections of the extraction manifold. As no organic phase was pumped into the system, the adsorption from aqueous alkaline solution (pH 13, 1 μg ml^{-1}) could be estimated. The total adsorption under these conditions was 89%. The pump tube and the PTFE extraction coil act as powerful adsorbents for terodiline in its unprotonated form and introduction of the sample through the peristaltic pump must be avoided. When, in another test, a terodiline solution of pH 7.7 was pumped through the pump tube connected to the extraction coil, adsorption was only 15%, because at this pH terodiline (pK_a = 9.85) is protonated and therefore more hydrophilic.

Figure 4 shows the effect of different tubing materials on the adsorption of terodiline from aqueous alkaline solution. Polytetrafluoroethane (PTFE), polypropylene, nickel, stainless steel and glass were tested in the manifold described in Fig. 2. The rectangles show the theoretical response of the injected samples when neither adsorption nor dispersion act on the sample zone. The experiments indicate a significant difference in adsorption properties between hydrophobic tubing materials (PTFE, polypropylene) and more hydrophilic materials (nickel, steel, glass). For PTFE and polypropylene, the peaks are low and the areas (33 and 20%, respectively) are only a fraction of what would be expected. For the hydrophilic materials, the peak area (Ni = 97%, glass = 97%, steel = 84%) corresponds to the amount of sample injected and the peak broadening is due to dispersion. No significant adsorption was

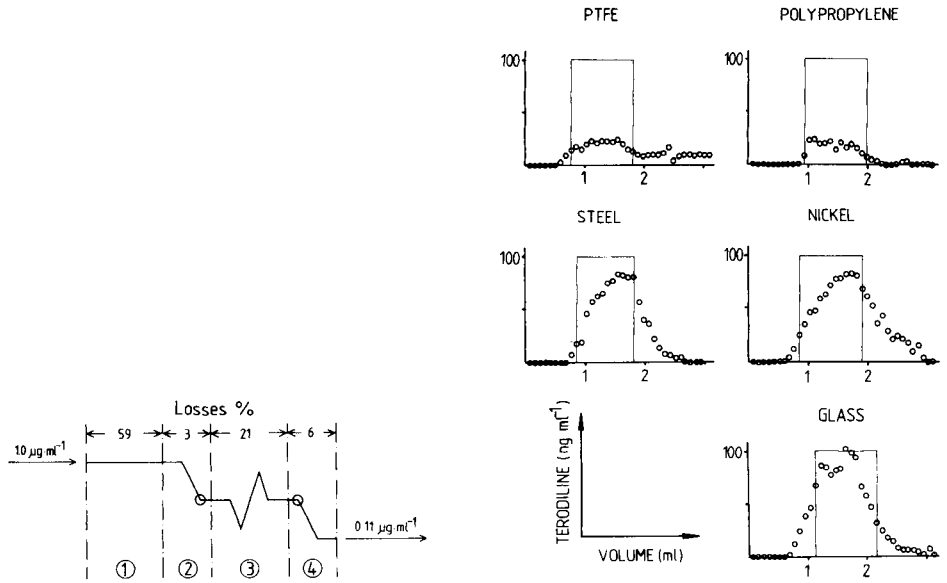

Fig. 3. Adsorption losses of terodiline (1 μg ml^{-1}, 0.1 M NaOH) from aqueous solution: (1) pump tube; (2) segmentor; (3) extraction coil, PTFE; (4) phase separator.

Fig. 4. Adsorption of terodiline from alkaline solution (100 ng ml^{-1}, 0.1 M NaOH) onto various tubing materials. Each point is the mean of 2 measurements; the manifold shown in Fig. 2 was used and 88-μl fractions were collected. Tubing: PTFE, 2 m long, 0.7 mm i.d.; polypropylene, 2 m, 0.8 mm i.d.; stainless steel, 2 m, 0.7 mm i.d.; glass, 1.8 m, 0.9 mm i.d.; nickel, 2 m, 0.7 mm i.d. Full lines show the theoretical response excluding adsorption and dispersion.

detected for any of the tested materials when an organic solution of terodiline was used. This observation is important because the PTFE membrane in the phase separator of the extraction system has a large surface area and it is wetted by the organic phase.

The results presented here indicate two ways to minimize adsorption losses of terodiline. First, the sample should be made alkaline as close as possible to the segmentation point in the manifold. Secondly, hydrophilic tubing material such as steel or glass should be used. The manifold in Fig. 1 is designed according to these observations. The serum sample has initially a pH of 7 and is aspirated into the steel sample loop so that contact with the pump tubing is avoided. The T-piece for the alkaline stream and the segmentor are made of glass and butt-connected to each other; the extraction coil is of steel and nickel tubing.

Sample injection technique

To retain sensitivity during the flow extraction, only that portion of the extract containing the peak concentration is cut out by the 3-way valve. As

at least a 50-μl extract is needed for g.l.c., rather large sample volumes must be injected. To avoid unnecessary band broadening caused by large sample volumes, two sample injection methods were studied. An extraction manifold, essentially the same as in Fig. 1, was used but fractions of the extract were continuously collected. Figure 5 shows the result of applying the different injection systems to this manifold. Peak A is the result of injecting the sample into an aqueous stream, the injection time being kept short enough for the tail of the peak to be cut off. Peak B is the result of injecting the same volume of sample into an organic stream (heptane/2% pentanol), the injection time being long enough to empty the whole loop. In the latter case, the sample is transported as an undispersed plug. The two-phase injection (B) results in an almost rectangular peak which facilitates the collection of the extract fraction, and consequently this injection method was used for the final extraction system (Fig. 1).

Determination of terodiline

Figure 6 shows the results obtained by extracting spiked serum samples in the recommended manifold (Fig. 1). The samples were injected in a sequence starting with blank serum going up to 400 ng ml^{-1} and down again to blank serum. The calibration points are well correlated. The fact that the results for decreasing concentrations are slightly higher than those for increasing concentrations suggests slight carry-over.

Solutions of terodiline in serum gave an extraction yield of ca. 60% when a 4-m extraction coil (0.7 mm i.d.) was used. The extraction of aqueous solutions of terodiline was quantitative in a 2-m coil. Results from batch

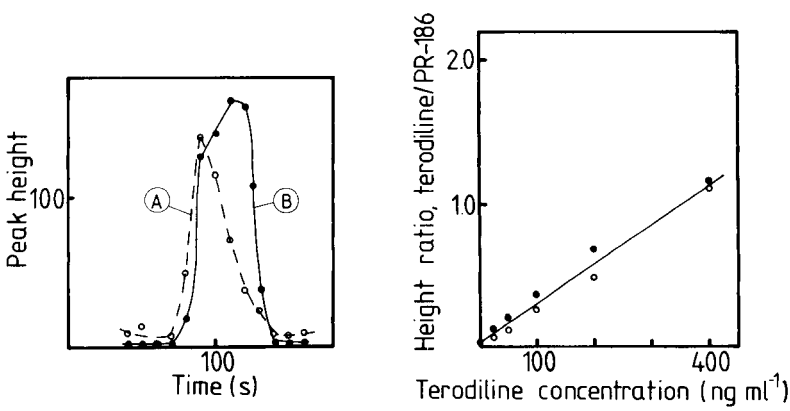

Fig. 5. Influence of sample injection system on the shape of the sample zone in an extraction system (500 μl sample 200 ng ml^{-1} terodiline). Curves: (A) aqueous carrier at 1 ml min^{-1}, injection time 22 s (without emptying the loop); (B) organic carrier at 1 ml min^{-1}, injection time 35 s (emptying the loop).

Fig. 6. Extraction of serum samples spiked with terodiline, in the manifold in Fig. 1. Sampling rate, 30 h^{-1}. Injection sequence: (○) from blank up to 400 ng ml^{-1}; (●) from 400 ng ml^{-1} down to blank.

experiments show that the extraction of terodiline from serum is slow and that the rate depends on the dilution of the serum [11]. For extraction into pure n-heptane, 30 min of shaking is needed to reach 100% recovery at 1:5 dilution while for 1:4 dilution only 60% is recovered after the same time [11]. It should be noted that in the flow-injection system the dilution of serum is only 1:1.5 and the residence time in the extraction coil is 50 s. Because of the highly repeatable timing in such systems, there is no need to establish equilibrium, but, by increasing the dilution of the serum, it may be possible to increase the recovery.

For the complete flow extraction/g.l.c. determination, the relative standard deviation was found to be 3% for spiked serum samples (7 determinations, 400 ng ml^{-1}) but 6% for aqueous standard solutions (10 determinations, 200 ng ml^{-1}, aqueous carrier as shown in Fig. 5A). The g.l.c. determination alone gave a relative standard deviation of 4% (10 injections of an organic extract).

Conclusions

The present work demonstrates the use of a flow-injection extraction system for sample work-up of low concentrations of an organic analyte in serum. It is clear that adsorption losses must be minimized and this is possible by a proper combination of materials and chemistry. Terodiline does not adsorb on hydrophilic materials such as steel and glass and in its protonated form adsorption on PTFE and polypropylene is small. The manifold presented is designed according to these observations and the results illustrate the usefulness of the system.

The proposed extraction system has its main advantage over the manual method in the high sample throughput (30 h^{-1}) and the possibility of miniaturization.

The authors are indebted to Prof. F. Ingman and Dr. B. Karlberg for valuable discussions. We also thank Sören Sandquist, KabiVitrum, for skillful technical assistance.

REFERENCES

1 H. Brötell and S. Sandquist, KabiVitrum AB. Technical report, 1983-03-14.
2 B. Karlberg and S. Thelander, Anal. Chim. Acta, 98 (1978) 1.
3 B. Karlberg and S. Thelander, Anal. Chim. Acta, 104 (1979) 21.
4 L. Nord and B. Karlberg, Anal. Chim. Acta, 145 (1983) 151.
5 K. Bäckström, L.-G. Danielsson and L. Nord, Analyst (London), 109 (1984) 323.
6 M. Bengtsson and G. Johansson, Anal. Chim. Acta, 158 (1984) 147.
7 D. Shelly, T. Rossi and I. Warner, Anal. Chem., 54 (1982) 87.
8 P. Neubert and K. Reif, Fresenius Z. Anal. Chem., 305 (1981) 277.
9 B. Brodie, S. Udenfriend and I. Baer, J. Biol. Chem., 168 (1947) 299.
10 L. Nord and B. Karlberg, Anal. Chim. Acta, 118 (1980) 285.
11 P. Hartvig, G. Freij and J. Vessman, Acta Pharm. Suec., 11 (1974) 97.

Analytica Chimica Acta, 175 (1985) 289—300
Elsevier Science Publishers B.V., Amsterdam — Printed in The Netherlands

DESCRIPTION OF THE SHAPE OF THERMOANALYTICAL CURVES Part 3. A Method for Estimating Kinetic Constants from Parameters Characterizing Peak Shape

GYÖRGY POKOL, SÁNDOR GÁL and ERNÖ PUNGOR*

Institute for General and Analytical Chemistry, Technical University of Budapest, Budapest 1521 (Hungary)

(Received 21st March 1985)

SUMMARY

The relationships between empirical parameters characterizing the shape of thermoanalytical curves and the constants of the kinetic equation, $d\alpha/dt = A \exp(-E/RT)(1-\alpha)^n$, are studied. A procedure is developed for the estimation of the three constants of this equation from the empirical parameters. The efficiency of this method is compared to that of model fitting. In evaluation of the confidence intervals of estimated constants and in the case of identification, least-squares (or similar) fitting is shown to be inferior because of its low sensitivity to properties other than the position of the peak along the temperature axis. This lack of sensitivity may be a major cause of the apparent kinetic compensation effect often encountered in the field of thermal analysis.

Many calculation methods have been worked out for the estimation of kinetic parameters from non-isothermal thermal analysis data (see, e.g., [1—3]). Most of these methods are based on model fitting, usually with the least-squares method: either a straight line is fitted to data calculated from the points of the experimental curve or curves (see, e.g., [4—8]), or the points of the measured curve are directly compared to those obtained from the theoretical model with different parameters [9]. The other way of estimation is based on calculation of the quantities characterizing the shape of the peak (of differential curves) or the step (of integral curves). Most papers dealing with the possibility of kinetic calculations describe the effect of kinetic parameters on the shape of thermoanalytical curves only qualitatively (see, e.g., [10—12]). Several methods have been suggested that involve the calculation of numerical quantities characterizing peak shape and the determination of the kinetic parameters from these quantities. Starting from the common equations

$$d\alpha/dt = A \exp(-E/RT)\, f(\alpha) \quad (1)$$

$$f(\alpha) = (1-\alpha)^n \quad (2)$$

(the meaning of symbols is summarized in Table 1), Kissinger [10] estimated the formal order of reaction from the asymmetry of the peak expressed as

0003-2670/85/$03.30

TABLE 1

Definition of symbols

p	An empirical parameter characterizing the shape of a peak
$\bar{P}$	The average of a parameter from replicate curves
t	Time
T	Temperature, K
δ	Temperature difference between two adjacent data points
α	Reacted fraction
$f(\alpha)$	A function of α in the rate equation
A	Pre-exponential factor, s^{-1}
E	Activation energy, kJ mol^{-1}
R	Gas constant
n	Formal reaction order
$t(\alpha)$, $T(\alpha)$	The time and temperature relevant to a reacted fraction
$\Delta t(\alpha_2, \alpha_1)$	$t(\alpha_2) - t(\alpha_1)$
$\Delta T(\alpha_2, \alpha_1)$	$T(\alpha_2) - T(\alpha_1)$
$T(\max)$, $\alpha(\max)$	The temperature and the reacted fraction at the maximum of the peak
M_{1R}	The first relative moment (i.e., the temperature of the centre of gravity of the peak)
W	The reciprocal of the maximum rate, i.e. $(d\alpha/dT)^{-1}_{max}$
U	$\Delta T(0.8, 0.2)/W$
$R(0.6)$	$\Delta T(0.6, 0.2)/\Delta T(0.8, 0.2)$
$R(\max)$	$[T(\max) - T(0.2)]/\Delta T(0.8, 0.2)$
D_1, D_2, D_3, D_4	Quantities describing the deviation of two curves (see Eqns. 3—6).

the ratio of the slopes at the inflexion points. Koch [2, 13] used the same shape index and "mechanistic" and "reaction-type" indices to evaluate non-isothermal kinetics. Balarin [14] divided the peak into two parts at the maximum and applied the ratio of the resulting partial areas. Good initial parameters for least-squares fitting were obtained by Várhegyi [9] from the properties of the peak shape; the position and the width of the peak were characterized by the time or temperature pertinent to a selected conversion, i.e., $t(\alpha)$ or $T(\alpha)$, and the difference between two of these values, i.e., $\Delta t(\alpha_2, \alpha_1)$ or $\Delta T(\alpha_2, \alpha_1)$, respectively. Later, Várhegyi and Székely [15] reached the conclusion that the position and the width of the peak (described as above) and the degree of asymmetry as given by Balarin's ratio [14] are suitable for the geometric characterization of a peak, and that the parameters of Eqns. 1 and 2 can be estimated from these data.

In Part 1 of this series [16], several empirical parameters characterizing peak shape were calculated for differential scanning calorimetric (d.s.c.) curves obtained for the decomposition of aluminium hydroxide. The parameters were evaluated on the basis of their reproducibility and sensitivity to choice of baseline. In Part 2 [17], the possibility of kinetic calculations was investigated by means of curves simulated by Eqns. 1 and 2 containing noise as well as baseline components. Comparison of the results from experimental

and simulated curves led to the conclusion that, given the experimental reproducibilities, the estimation of the parameters of Eqns. 1 and 2 is mathematically possible. In the present paper, the relationships between the empirical parameters and kinetic parameters are described by using simulated curves obtained at constant heating rate. A procedure for parameter estimation based on the empirical quantities is presented, and its effectiveness is compared to that of least-squares model fitting.

CALCULATIONS

The reproducibilities of the empirical parameters characterizing peak shape, and their sensitivity to noise and to the choice of baseline enabled some of the parameters most likely to be applicable in estimating the parameters of Eqns. 1 and 2 to be selected. The chosen parameters pertain to the four visible properties of the peak shape: (a) the temperature of the maximum, $T(\max)$, and the first relative moment, i.e., the temperature of the centre of gravity of the peak, M_{1R}, characteristic of the position of the peak along the temperature axis; (b) the reciprocal of the maximum rate, W, and the difference of the temperatures appropriate to the 80 and 20% reacted fractions, $\Delta T(0.8, 0.2)$, which is connected with peak width; (c) the ratio U characterizing the sharpness of the peak; and (d) the conversion at the maximum $\alpha(\max)$ and ratios $R(0.6)$ and $R(\max)$ related to the asymmetry.

The values of the parameters listed above were measured from simulated curves. The kinetic parameters were varied in wide ranges: 9×10^{-3}—25×10^3 K for E/R, 10^8—10^{14} s^{-1} for A, and 1/10 to 4/3 for n. Calculation procedures were reported in detail earlier [17, 18].

RESULTS

The effect of the pre-exponential factor, the activation energy and the formal reaction order on the empirical parameters

Figures 1 and 2 show that the parameters characterizing the location and width of the peak are linearly related to the activation energy provided that A and n are fixed. The same quantities give moderately curved plots if A is changed and the other two parameters are kept constant (Figs. 3 and 4). Changing the formal order of reaction leaves $T(\max)$ and M_{1R} almost unaffected, but it has a marked effect on W and $\Delta T(0.8, 0.2)$ as demonstrated by the lines relevant to $n = 1$ and $n = 2/3$ in Figs. 2 and 4. This effect is plotted in Fig. 5 for a wide range of n. Thus, the position of the peak is sensitive to the activation energy and the pre-exponential factor while the width depends on all three kinetic parameters.

The parameters related to the sharpness and asymmetry of the peak are plotted in Fig. 6 as functions of the formal order of reaction. Their values were found to be independent of E and A. Accordingly, the estimation of the formal reaction order may be the best first step of evaluation.

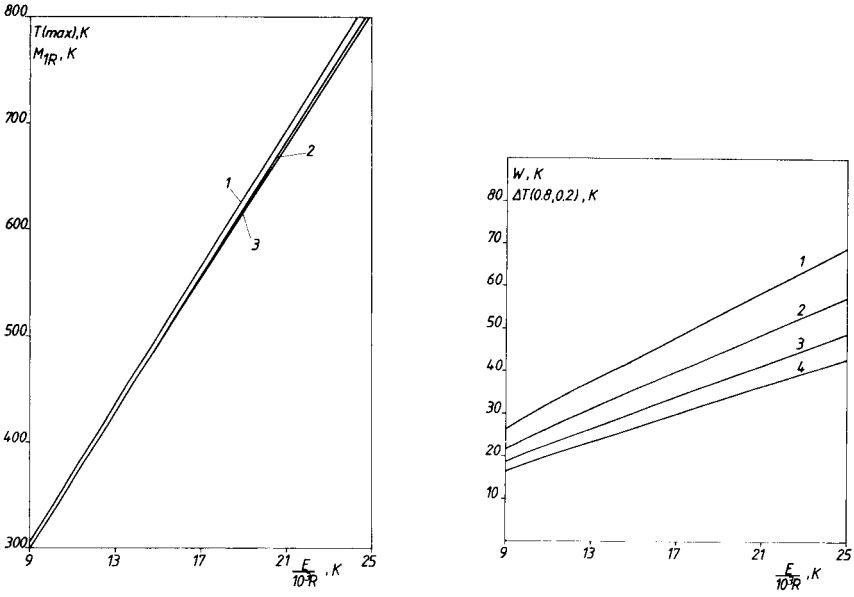

Fig. 1. The effect of the activation energy on parameters characterizing peak location, when $A = 10^{11}$ s^{-1} and $dT/dt = 10$ K min^{-1}. Curves: (1) T(max) for $n = 2/3$ and $n = 1$; (2) M_{1R} for $n = 1$; (3) M_{1R} for $n = 2/3$.

Fig. 2. The effect of the activation energy on parameters characterizing peak width, when $A = 10^{11}$ s^{-1} and $dT/dt = 10$ K min^{-1}. Curves: (1) W for $n = 1$; (2) W for $n = 2/3$; (3) $\Delta T(0.8, 0.2)$ for $n = 1$; (4) $\Delta T(0.8, 0.2)$ for $n = 2/3$.

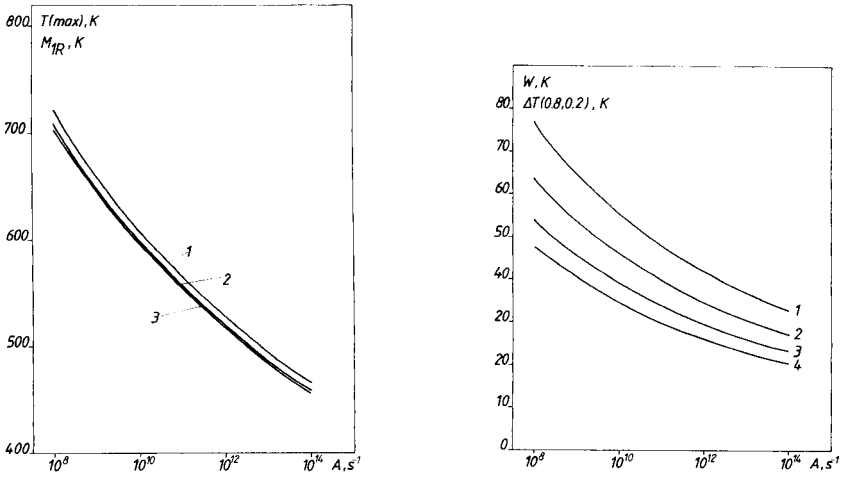

Fig. 3. The effect of the pre-exponential factor on parameters characterizing peak location, when $E/R = 1.7 \times 10^4$ K and $dT/dt = 10$ K min^{-1}. Curves 1—3 as for Fig. 1.

Fig. 4. The effect of the pre-exponential factor on parameters characterizing peak width, when $E/R = 1.7 \times 10^4$ K and $dT/dt = 10$ K min^{-1}. Curves 1—4 as for Fig. 2.

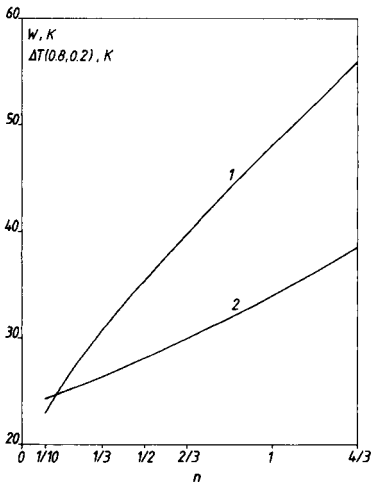

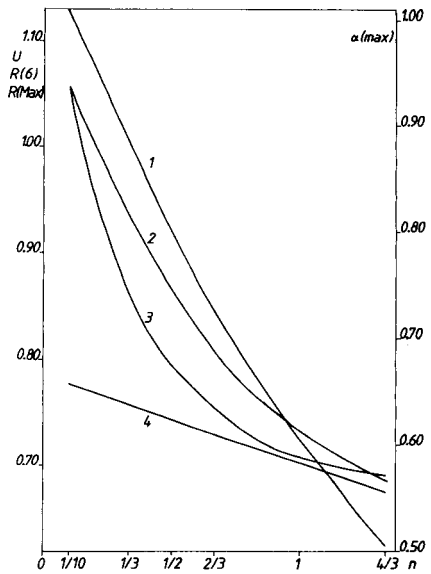

Fig. 5. The effect of the formal reaction order on parameters related to peak width (for $A = 10^{11}$ s^{-1}, $E/R = 1.7 \times 10^4$ K). Curves: (1) W; (2) $\Delta T(0.8, 0.2)$.

Fig. 6. The effect of the formal reaction order on properties related to the sharpness and asymmetry of the peak (for $A = 10^{11}$ s^{-1}, $E/R = 1.7 \times 10^4$ K). Curves: (1) R(max); (2) α(max); (3) U; (4) $R(0.6)$.

Table 2 contains the average values of the parameters in question and their standard deviations obtained from parallel d.s.c. curves of dehydration of the mineral gibbsite, $Al(OH)_3$; most of the values have already been included in Part 1 [17]. Using the curves presented in Fig. 6, the values of U, $R(0.6)$, R(max) and α(max) yield 0.69, 0.66, 0.75 and 0.71 for the formal reaction order, respectively. From the standard deviations, the uncertainty of n is

TABLE 2

Averages, standard and relative standard deviations of parameters of duplicate d.s.c. peaks from dehydration of gibbsite

Parameter	$\bar{P}$	S.d.	R.s.d. (%)
T(max) (K)	576	1	—
M_{1R} (K)	567.3	0.4	—
W (K)	34.9	0.6	2
$\Delta T(0.8, 0.2)$ (K)	26.2	0.4	1.5
U	0.75	0.01	1
α(max)	0.675	0.010	—
$R(0.6)$	0.729	0.003	0.4
R(max)	0.80	0.02	1.5

less than 0.1. Thus a formal order of 2/3 corresponding to a three-dimensional phase boundary process seems an acceptable solution.

Solution in two dimensions

As a first approximation, it may be assumed that the result of the first step of the evaluation is a single and accurate n. With this assumption, a two-parameter problem remains; the three-dimensional problem is discussed later.

In order to obtain the activation energy and the pre-exponential factor, a grid of A/E pairs can be constructed in the range of interest. Simulating curves belonging to each point (from the known formal reaction order) makes it possible to plot the levels of $T(\max)$, M_{1R}, W and $\Delta T(0.8, 0.2)$ in $\log A$ vs. E/R diagrams. Two such plots are shown in Fig. 7. Within the ranges tested, the levels are almost linear, but the slopes of the constant M_{1R} and constant W lines are different. Thus if the lines of M_{1R} and W obtained from the experimental curves are drawn in the same diagram, the intersection will yield the estimated pre-exponential factor and the activation energy. The average M_{1R} and W values of the d.s.c. curves for dehydration of gibbsite (Table 2) give $A = 6.1 \times 10^{13}$ s^{-1} and $E = 170$ kJ mol^{-1} if $n = 2/3$ is accepted. Of course, the values of the empirical parameters are not absolutely accurate; thus, instead of intersection of lines, it is more appropriate to refer to intersection (or overlapping) of zones, i.e., confidence intervals as a region of acceptable solutions [18]. As an example, zones $M_{1R} = 551 \pm 5$ K and $W = 40 \pm 2$ K are drawn in Fig. 8.

The half-width of the zones in Fig. 8 considerably exceeds the standard deviations shown in Table 1, because the replicate d.s.c. runs of gibbsite belonged to the same series of measurements; replicate measurements with different d.s.c. cells would result in greater standard deviations. Moreover, a special source of temperature error was taken into account, because such errors are systematic within one run. A change in the contact between the sample and the temperature sensor can result in a random displacement of the whole peak along the temperature axis. Because this effect occurs quite frequently, the confidence interval of the first relative moment

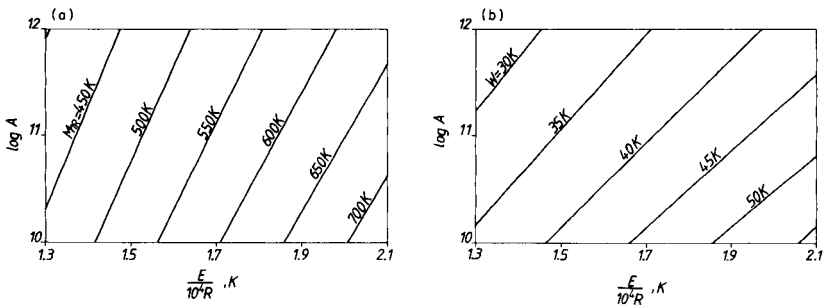

Fig. 7. Levels of (a) the first relative moment, M_{1R}, and (b) the reciprocal of the maximum rate, W, in the $\log A$ vs. E/R diagram for $n = 2/3$.

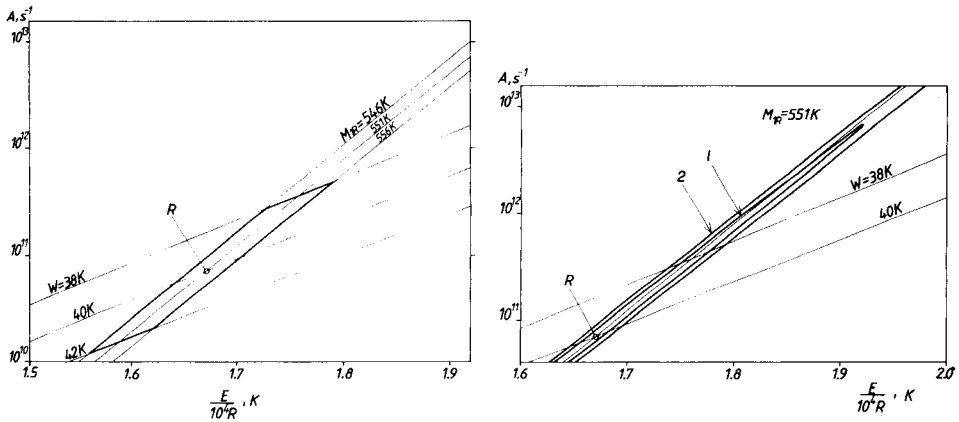

Fig. 8. Estimation of the pre-exponential factor and activation energy by means of intersecting zones.

Fig. 9. Comparison of least-squares model fitting with the method of intersecting zones; R represents the parameters of the reference curve. Curves: (1) the line of the $D_2 = 0.250$ level; (2) the line of the $D_2 = 0.500$ level (see Eqn. 4).

was selected to be as wide as 10 K. The points inside the region bordered by thick lines in Fig. 8 correspond to acceptable pre-exponential factor/activation energy pairs. The lowest and highest values of E/R occurring in the region of solutions are 1.57×10^4 K and 1.78×10^4 K; those of A are 1.4×10^{10} s^{-1} and 4.2×10^{11} s^{-1}, respectively. It should be noted, however, that not any pair selected from these two ranges will fulfil the conditions on M_{1R} and W. The region of solutions is an extended area, which means that the estimated activation energy and pre-exponential coefficient are not independent. The reason for this is purely mathematical because independent A and E values were used in the simulations and M_{1R} and W were obtained independently from the curves. The mathematical reason is the nature of Eqn. 1 which has been specified as a source of "kinetic compensation effect" by several authors [19—24].

Comparison with model fitting

The efficiency of the estimation procedure outlined above was compared to that of model fitting with the aid of simulated curves. The reference curve corresponded to the intersection of $M_{1R} = 551$ K and $W = 40$ K lines in Fig. 8, i.e., $n = 2/3$, $A = 7.8 \times 10^{10}$ s^{-1} and $E/R = 1.67 \times 10^4$ K. Several curves were simulated with A/E pairs inside and outside the intersection quadrangle of Fig. 8 and the deviations of these curves from the reference curve were obtained with the following equations

$$D_1 = \delta \sum \Delta |d\alpha/dT|; \quad D_2 = \delta [N \sum (\Delta |d\alpha/dt|)^2]^{1/2} \qquad (3,4)$$

$$D_3 = \delta \sum |\Delta\alpha|; \quad D_4 = \delta [N \sum (\Delta\alpha)^2]^{1/2}. \qquad (5,6)$$

Here summation covered the whole temperature range of the two curves to be compared, and N was the number of points in the same range.

The deviations D_1 to D_4 approximate the temperature integral of the differences, therefore their values can be practically independent of the temperature difference of subsequent data points. D_2 and D_4 correspond to the least squares applied to differential and integral data.

Figure 9 is a log A vs. E/R diagram (similar to Fig. 8) containing lines of two D_2 levels obtained from the calculations outlined above. According to the results of Arnold et al. [22] and Eisenreich [23], the oval regions bordered by the $D_2 = 0.250$ and $D_2 = 0.500$ lines are very prolate. The use of D_1, D_3 and D_4 as the criterion of fitting resulted in similar plots. The width of the two regions at the height of the reference point corresponds to about 5- and 8-K difference in the centre of gravity of the peak (M_{1R}). This means that, for example, the $D_2 = 0.250$ limit allows ±2.5 K displacement of the peak along the temperature axis. Conversely, if this range can be regarded as a realistic confidence interval of the peak position rather than a pessimistic assumption, the minimum acceptable deviation D_2 may not be less than 0.250. From the length of the region with $D_2 \leqslant 0.250$, the range of solutions for the activation energy would be about 40 kJ mol^{-1} (30% of the reference value). A ±4-K interval for the peak position (region $D_2 \leqslant 0.500$) would render the estimation of E practically impossible.

As in the preceding section, it may be assumed that the confidence interval for W, related to peak width, is 40 ± 2 K. Even the region $D_2 \leqslant 0.250$ corresponding to a ±2.5-K uncertainty in M_{1R} extends well beyond the line corresponding to $W = 38$ K. Thus the confidence interval calculated by means of the least-squares method will contain curves that have widths actually outside the range determined experimentally. In the case of identification, curves which have parameters lying in the confidence interval can be regarded as identical with the reference curve (marked by R in the figure). Consequently, least-squares fitting will accept significantly different curves as identical. Such a curve is shown in Fig. 10, together with the reference.

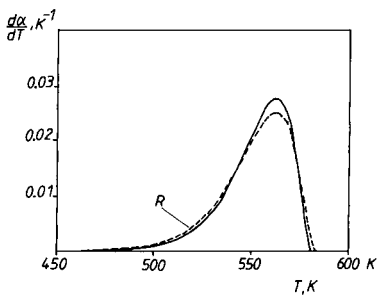

Fig. 10. The reference curve ($A = 7.08 \times 10^{10}$ s^{-1}, $E/R = 1.67 \times 10^4$ K and $n = 2/3$) and a curve of significantly different width ($A = 2.512 \times 10^{12}$ s^{-1}, $E/R = 1.865 \times 10^4$ K and $n = 2/3$) giving $D_2 = 0.206$.

It can also be seen from Fig. 9 that the longer axis of the regions with $D_2 \leqslant$ constant is nearly parallel to the line for M_{1R} = 551 K. Thus, in this case, least-squares fitting is not sensitive enough to changes of peak width. Experimental reproducibilities, of course, could lead to the opposite result also, if the confidence interval of W were several times wider.

Solution in three dimensions

As outlined above, the formal reaction order can be evaluated from the properties related to the sharpness and asymmetry of the peak, being practically independent of the pre-exponential factor and the activation energy. The parameter (or parameters) used in the estimation of the formal order also have deviation and confidence interval. Consequently, the resulting value of n is also more or less uncertain, and the estimation of the kinetic parameters is a three-dimensional problem. The method of intersecting zones demonstrated above is also applicable in this case. The acceptable solutions will be located in a three-dimensional region of the log $A - E/R - n$ space.

For the same example as that discussed above for the two-dimensional solution, Fig. 11 shows the region defined by the location and width (546 K $< M_{1R} <$ 556 K and 38 K $< W <$ 42 K). The longitudinal axis of the region (i.e., the points satisfying M_{1R} = 551 K and W = 40 K at different n values) is nearly linear, and is described by the following relations

$$\log A = 5.28 + 8.35\, n \tag{7}$$

$$E/10^4 R = 0.99 + 1.02\, n \tag{8}$$

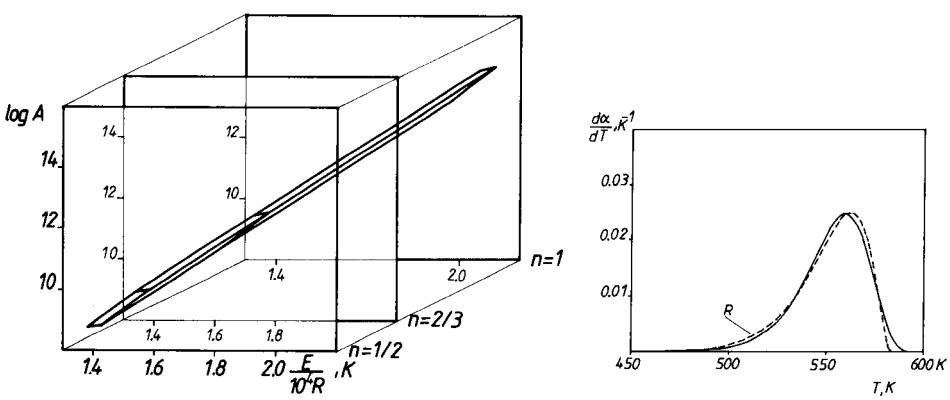

Fig. 11. The three-dimensional region defined by 546 K $\leqslant M_{1R} \leqslant$ 556 K and 38 K $\leqslant W \leqslant$ 42 K.

Fig. 12. The reference curve and a curve having similar M_{1R} and W but different formal reaction order (curve 1 of Table 3) giving D_2 = 0.194.

Now, any parameter characteristic of the formal reaction order and independent of A and E defines an upper and a lower acceptable n, i.e., two planes parallel with the log A and E/R axes. These planes will delineate the body of solutions of the region as demonstrated in Fig. 11. In this way, the uncertainty of the formal reaction order contributes to the potential error of A and E/R. A ± 0.1 error limit of the formal order, substituted into Eqns. 3 and 4, causes a contribution of ± 8 kJ mol^{-1} to the activation energy in the present example. (It should be noted that the uncertainty of n was found to be less than ± 0.1 in the case of gibbsite, as discussed above.) Expanding the region found in the two-dimensional solution (Fig. 9) by the contribution of the uncertainty in n produces an error limit of ± 16 kJ mol^{-1} for the activation energy.

The sensitivity of fitting to the sharpness and asymmetry of the peak was also found to be quite low. Apart from the data of the reference curve discussed in the preceding section, Table 3 contains some properties of two curves with different formal reaction orders, having similar M_{1R} and W. The peaks pertaining to the reference curve and curve 1 are drawn in Fig. 12. Properties related to the sharpness and asymmetry [n and $R(0.6)$] are significantly different in the columns of Table 3; however, the deviation D_2 is still considerably below the value corresponding to a ± 2.5-K displacement of the curves

DISCUSSION

If it is assumed that Eqn. 1 is valid, the pre-exponential factor, the activation energy and the formal order of the reaction can be estimated from the empirical parameters of thermoanalytical peaks such as those used in the present studies. At least three properties are required for the estimation: one connected with the position, one related to the width and one characterizing the sharpness or the asymmetry of the peak. This is in accordance with the

TABLE 3

The comparison of curves having similar M_{1R} and W values but different formal orders of reaction

Parameter	Reference curve	Curve 1	Curve 2
A (s^{-1})	7.08×10^{10}	4.27×10^{13}	2.09×10^{9}
$E/10^4R$ (K)	1.670	2.010	1.480
n	2/3	1	1/2
M_{1R} (K)	551.0	552.5	548.9
W (K)	40.0	40.2	39.9
U	0.753	0.711	0.791
$R(0.6)$	0.730	0.705	0.743
D_2	—	0.194	0.195

conclusions of Várhegyi and Székely [15] concerning the use of the position, width and degree of asymmetry in the calculations. There are several empirical parameters which are sensitive to the formal reaction order but practically independent of the other two kinetic constants. The estimated set of kinetic constants can be found in a $\log A - E/R - n$ space as the intersection of the surfaces defined by the calculated values of the empirical parameters. If the confidence intervals of the parameters are known (from experiment), the acceptable solutions will be situated in a region bordered by the surfaces belonging to the upper and lower limits of the intervals.

The use of more than three empirical parameters in the estimation may result in a more rounded region of solutions [18] and it can be useful in cases for which Eqns. 1 and 2 are only approximately valid or if there is a doubt about their validity. For example, a considerable distance between n values obtained from different properties characterizing sharpness and asymmetry would point to the invalidity of the kinetic equation used.

The examples used in this paper were based on the reproducibility of the d.s.c. peak for dehydration of the mineral gibbsite. In this case, the least-squares or any similar method of fitting has been shown to be very sensitive to the position of the peak and insensitive to other properties. The least-squares method can detect a good fit between curves which have positions (centers of gravity) close to each other while other properties are significantly different. Therefore, the use of the parameters characterizing various properties of peak shape are to be preferred in calculations related to the confidence intervals of estimated constants or identification. The unequal sensitivity of the least-squares method to different properties is a major mathematical source (beyond the nature of Eqn. 1) of the apparent kinetic compensation effect often encountered in studies based on model fitting.

Generally speaking, a comparison of two curves based on one criterion will not be equally sensitive to different properties. Therefore, procedures that seek a fit of several parameters should be superior for purposes such as identification and estimation of physicochemical constants.

The authors express their thanks to Dr. G. Várhegyi and Dr. G. E. Veress for helpful discussions and reading the manuscript.

REFERENCES

1 J. Šesták, V. Šatava and W. W. Wendlandt, Thermochim. Acta, 13 (1973) 333.
2 E. Koch, Non-isothermal Reaction Analysis, Academic Press, London, 1977.
3 J. Šesták, in G. Svehla (Ed.), Thermophysical Properties of Solids. Their Measurements and Theoretical Thermal Analysis, Wilson and Wilson's Comprehensive Analytical Chemistry, Vol. XII(D), Elsevier, Amsterdam, 1984.
4 E. S. Freeman and B. Carroll, J. Phys. Chem., 62 (1958) 394.
5 C. D. Doyle, J. Appl. Polym. Sci., 5 (1961) 285.
6 A. W. Coats and J. P. Redfern, Nature, 201 (1964) 68.
7 T. Ozawa, Bull. Chem. Soc. Jpn., 38 (1965) 1881; J. Therm. Anal., 2 (1970) 301.
8 J. Zsakó, J. Phys. Chem., 72 (1968) 2406.

9 G. Várhegyi, Thermochim. Acta, 28 (1979) 367.
10 H. E. Kissinger, Anal. Chem., 29 (1957) 1702.
11 J. Šesták, Talanta, 13 (1966) 567.
12 T. Székely, in B. Csákvári (Ed.), A Kémia Ujabb Eredményei; Application of Thermogravimetric Methods in Kinetic Description of Thermal Decomposition Reactions of Polymers, Vol. 12, Akadémiai K. Budapest, Hungary, 1973, p. 139.
13 E. Koch, Thermochim. Acta, 56 (1982) 1.
14 M. Balarin, Thermochim. Acta, 33 (1979) 341.
15 G. Várhegyi and T. Székely, Thermochim. Acta, 57 (1982) 13.
16 Gy. Pokol and S. Gál, Anal. Chim. Acta, 167 (1985) 183.
17 Gy. Pokol, S. Gál and E. Pungor, Anal. Chim. Acta, 167 (1985) 193.
18 L. Jánossy, Theory and Practice of the Evaluation of Measurements, Clarendon Press, Oxford, 1965.
19 A. V. Nikolaev and V. A. Logvinenko, J. Therm. Anal., 10 (1976) 363.
20 R. R. Krug, W. G. Hunter and R. A. Grieger, J. Phys. Chem., 80 (1976) 2335 and 2341.
21 J. Pysiak and B. Sabalski, J. Therm. Anal., 17 (1979) 287.
22 M. Arnold, G. E. Veress, J. Paulik and F. Paulik, J. Therm. Anal., 17 (1979) 507; Anal. Chim. Acta, 124 (1981) 341; Thermochim. Acta, 52 (1982) 67.
23 N. Eisenreich, J. Therm. Anal., 19 (1980) 289.
24 J. Šesták, in H. G. Wiedemann (Ed.), Thermal Analysis, Proc. 6th Int. Conf., Vol. 1, Birkhäuser V., Basel, 1980, p. 29.

Analytica Chimica Acta, 175 (1985) 301—304
Elsevier Science Publishers B.V., Amsterdam — Printed in The Netherlands

Short Communication

SIMULTANEOUS DETERMINATION OF L(+)- AND D(—)-LACTIC ACID BY USE OF IMMOBILIZED ENZYMES IN A FLOW-INJECTION SYSTEM

TOSHIO YAO* and TAMOTSU WASA

Department of Applied Chemistry, College of Engineering, University of Osaka Prefecture, Mozu-Umemachi, Sakai 591 (Japan)

(Received 16th April 1985)

Summary. The system comprises L(+)- and D(—)-lactate dehydrogenase reactors in parallel and a diaphorase electrode. Separate peaks are obtained for L(+)- and D(—)-lactic acid. The peak current is linearly related to the concentration of both isomers in the range 1×10^{-5}—2×10^{-3} M.

Several enzymatic methods have been reported for the determination of lactic acid in flow-injection systems [1—4]. Such methods are available to determine both the L(+) and D(—) forms of lactic acid by quantifying the NADH formed when the substrate is oxidized to pyruvate by L(+)- or D(—)-lactate dehydrogenase, respectively. Several reports [5—7] have indicated that NADH is oxidizable at a variety of solid electrodes, but the direct oxidation of NADH at such an electrode demands high potentials which causes high background currents [3].

In this communication, the NADH generated by lactate dehydrogenase produces hexacyanoferrate(II) at an immobilized diaphorase electrode. The hexacyanoferrate(II) is measured amperometrically at 0.4 V vs. Ag/Ag^+:

$$NADH + Fe(CN)_6^{3-} \xrightarrow{\text{diaphorase}} NAD^+ + Fe(CN)_6^{4-}$$

$$Fe(CN)_6^{4-} \rightarrow Fe(CN)_6^{3-} + e^-$$

A flow-injection system for the simultaneous determination of L(+)- and D(—)-lactic acid is described.

Experimental

Reagents. Diaphorase (EC 1.6.4.3, 100 IU mg^{-1}, from *Clostridium kluyveri*), L(+)-lactate dehydrogenase (EC 1.1.1.27, 400 IU mg^{-1} of protein, from pig heart), β-NAD^+ and β-NADH were commercial preparations (Oriental Yeast Co., Tokyo). D(—)-Lactate dehydrogenase (EC 1.1.1.28, 300 IU mg^{-1} of protein, from *Lactobacillus leichmannii*) and L(+)- and D(—)-lactic acids were obtained from the Sigma Chemical Co. Bovine serum albumin (BSA,

0003-2670/85/$03.30

96—99% albumin), glutaraldehyde and 3-aminopropyltriethoxysilane were as described previously [8]. Pyrophosphate buffers (0.1 M, pH 8.0—10.5) were prepared from sodium pyrophosphate (Wako Pure Chemicals) in distilled water and adjusted to the desired pH with 6 M hydrochloric acid. All other chemicals were of analytical-reagent grade.

Preparation of immobilized enzyme reactors. The alkylamino-bonded silica gel (200 mesh) prepared by the method described previously [9] was activated by reaction with a 5% (v/v) solution of glutaraldehyde in sodium hydrogencarbonate (0.1 M). The preparation was packed into glass tubing (10 mm × 4 mm i.d.), and L(+)- or D(—)-lactate dehydrogenase was loaded covalently by circulating a 10-ml solution of enzyme (ca. 500 IU) in phosphate buffer (0.1 M, pH 7.5) at 1.0 ml min^{-1} for 5 h at room temperature. Both reactors were washed for 12 h with a 0.1 M glycine solution at pH 8.5 and were stored at 5° C in the same solution when not in use.

Preparation of diaphorase electrode. Diaphorase (3 mg) and 30 μl of aqueous 10% (w/v) BSA were added to 50 μl of 0.02 M phosphate buffer (pH 7.5). An 8-μl portion of a 4% (v/v) solution of glutaraldehyde was added and mixed well. A 10-μl aliquot of this solution was spread on one side of a platinum sheet (2 × 2 cm) and silanized as described previously [10]. The membrane was allowed to form for 2 h at room temperature, open to the air. The resulting enzyme membrane was covalently bonded to some part of the platinum surface [10]. The amperometric flow cell was assembled as described before [9], with the diaphorase/BSA membrane attached to the platinum sheet over the anode of a Yanagimoto thin-layer electrochemical flow cell, which also had a silver/silver chloride reference electrode and a stainless steel tube as auxiliary electrode.

Flow system and procedures. The flow system used in this study is shown schematically in Fig. 1. The two immobilized enzyme reactors were inserted as shown. The configuration of the flow system was based on the splitting of the flow after the sample injection and subsequent confluence before reaching the enzyme electrode detector. The different dimensions of the two

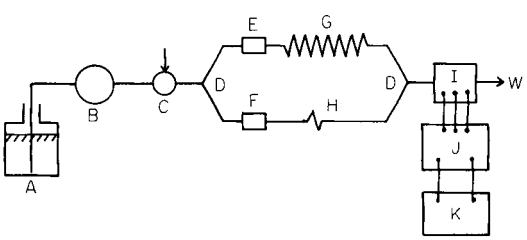

Fig. 1. Schematic diagram of the flow-injection manifold for simultaneous determination of L(+)- and D(—)-lactic acid: (A) carrier solution; (B) pump; (C) injector; (D) T-connector; (E) immobilized D(—)-lactate dehydrogenase reactor; (F) immobilized L(+)-lactate dehydrogenase reactor; (G) teflon coil (0.5 mm i.d. × 300 cm); (H) teflon coil (0.25 mm i.d. × 20 cm); (I) immobilized diaphorase electrode; (J) potentiostat; (K) recorder; (W) waste.

channels provided a different residence time for each channel, and so two peaks were obtained. A constant potential (0.4 V vs. Ag/Ag^+) was applied to the diaphorase electrode with a Yanagimoto potentiostat (VMD-101), and the current was recorded with a strip-chart recorder (Hitachi 056). A pyrophosphate buffer (0.1 M, pH 9.5) which was 0.5×10^{-3} M in NAD^+ and 10^{-3} M in potassium hexacyanoferrate(III) served as the carrier solution, and was pumped at 1.0 ml min^{-1} with an intermediate pressure pump (Yanagimoto RP-203).

Results and discussion

As shown in Fig. 2, the maximum response of the diaphorase electrode to NADH was at pH 8.5; the maximum activity of the immobilized lactate dehydrogenase was at a higher pH (pH > 10) [3]. Therefore, maximum response for L(+)- and D(−)-lactic acid was obtained at pH 9.5 in the flow system which comprised the L(+)- and D(−)-lactate dehydrogenase reactors and the diaphorase electrode; this pH was used throughout this work. The optimum reagent concentrations for the enzymatic reactions catalyzed by lactate dehydrogenases and diaphorase were 0.5×10^{-3} M in NAD^+ and 10^{-3} M in potassium hexacyanoferrate(III).

The flow system is based on splitting of the flow after the sample injection point, passing the two portions through two channels with different dimensions, and subsequent confluence of the streams before reaching the diaphorase electrode. The L(+)- and D(−)-lactate dehydrogenase reactors inserted into each channel catalyse specifically the oxidation of L(+)- and

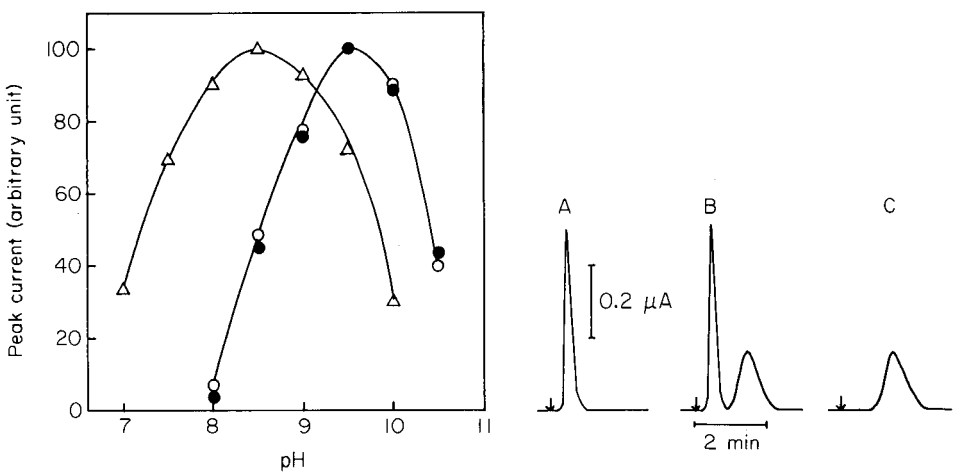

Fig. 2. Effect of pH on the peak current: (△) 1.0 mM NADH; (○) 1.0 mM L(+)-lactic acid; (●) 1.0 mM D(−)-lactic acid.

Fig. 3. Signals from solutions (10 μl) containing: (A) 1.0 mM L(+)-lactic acid; (B) 1.0 mM L(+)-lactic acid and 1.0 mM D(−)-lactic acid; (C) 1.0 mM D(−)-lactic acid.

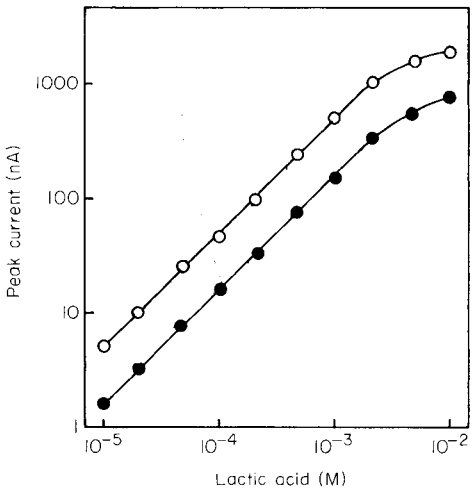

Fig. 4. Calibration graphs: (○) L(+)-lactic acid; (●) D(−)-lactic acid (10-μl sample).

D(−)-lactate, respectively. Because each channel has a different residence time, two peaks, for L(+)- and D(−)-lactic acid, are obtained (Fig. 3). The separation of these peaks depends on the relative lengths of the channels; a delay coil (G) of 0.5 mm i.d. and 3.0 m in length was needed to separate the two peaks completely.

Figure 4 shows typical calibration graphs for L(+)- and D(−)-lactic acid obtained by use of the present flow system. The graphs are linear up to 2×10^{-3} M, above which the sensitivity decreases. The relative standard deviations for 10 replicate injections were 2.3 and 2.0% for L(+)- and D(−)-lactic acid at the 1×10^{-4} M level, respectively. The lower limit of detection was 2×10^{-6} and 5×10^{-6} M for L(+)- and D(−)-lactic acid, respectively ($S:N = 2$).

The immobilized L(+)- and D(−)-lactate dehydrogenase reactors were used repeatedly to confirm their stabilities for a few months. Even after two months, both reactors retained more than 90% of their original activities. Also, the diaphorase electrode retained about 87% of its original activity after repeated use for one month.

REFERENCES

1 H. Durliat, M. Comtat and J. Mahenc, Anal. Chim. Acta, 106 (1979) 131.
2 A. S. Attiyat and G. D. Christian, Analyst, 105 (1980) 154.
3 T. Yao, Y. Kobayashi and S. Musha, Anal. Chim. Acta, 138 (1982) 81.
4 A. Schelter-Graf, H.-L. Schmidt and H. Huck, Anal. Chim. Acta, 163 (1984) 299.
5 W. J. Blaedel and R. A. Jenkins, Anal. Chem., 47 (1975) 1337.
6 J. Moiroux and P. J. Elving, Anal. Chem., 51 (1979) 346.
7 D. N. Grag, D. H. Keyes and B. Watson, Anal. Chem., 49 (1977) 1067A.
8 T. Yao, Anal. Chim. Acta, 153 (1983) 175.
9 T. Yao, M. Sato, Y. Kobayashi and T. Wasa, Anal. Chim. Acta, 165 (1984) 291.
10 T. Yao, Anal. Chim. Acta, 148 (1973) 27.

Analytica Chimica Acta, 175 (1985) 305—308
Elsevier Science Publishers B.V., Amsterdam — Printed in The Netherlands

Short Communication

THE APPLICATION OF STRONGLY REDUCING AGENTS IN FLOW INJECTION ANALYSIS
Part 5. Chromium(II) and Vanadium(II) in Acidic Medium

R. C. SCHOTHORST and G. DEN BOEF*

Laboratory for Analytical Chemistry, University of Amsterdam, Nieuwe Achtergracht 166, 1018 WV Amsterdam (The Netherlands)

(Received 24th May 1985)

Summary. Chromium(II) and vanadium(II) in acidic medium are applied as powerful reducing agents in flow injection analysis. Detection is done amperometrically. For the determination of nitrite with chromium(II), the limit of determination is 5×10^{-6} mol l^{-1} with a linear range up to 7.5×10^{-5} mol l^{-1}, similar to the case of uranium(III). Vanadium(II) is less suitable for the determination of nitrite. Nitrate, hydroxylamine and hydrazine could not be determined with these reagents.

The application of chromium(II) EDTA and vanadium(II) EDTA as powerful reducing agents in flow injection analysis (f.i.a.) in the pH range 5—10 has been described in previous parts of this series [1—3].

Both chromium(II) and vanadium(II) have been applied for titrimetric determinations in acidic medium [4]. Because of the low molar absorptivity of the ions involved, the application of these species in acidic medium in flow injection analysis with spectrophotometric detection is not feasible. In the present communication, the analytical applications of chromium(II) and vanadium(II) in acidic medium in f.i.a., with amperometric detection are presented.

Experimental

The instrumental set-up, including the flow system, was the same as for uranium(III) [5]. For the generation of both vanadium(II) and chromium(II), a Jones reductor was used (zinc, with a 5% degree of amalgamation). The reagent solutions were 1.1×10^{-3} mol l^{-1} green chromium(III) chloride in 2×10^{-2} mol l^{-1} hydrochloric acid and 10^{-3} mol l^{-1} vanadium(IV) sulphate in 10^{-2} mol l^{-1} hydrochloric acid. The loop volume of the injection valve was 38 μl. All solutions were carefully deaerated with nitrogen, because oxygen interferes with the determinations.

Results

Apart from the working potential of the amperometric flow-through detector, the experimental parameters were identical with those in the paper

0003-2670/85/$03.30

on chromium(II) EDTA [2]. For the selection of a suitable working potential, the same procedure as for vanadium(II) EDTA [3] was applied. Four polarograms in flow were recorded: (A) a polarogram of the reagent solution, chromium(II) or vanadium(II); (B) a polarogram of the background current by introducing a hydrochloric acid solution of the same acidity as the reagent solution into the Jones reductor; (C) a polarogram of the products of the reaction of the analyte under investigation with chromium(II) or vanadium(II) by replacing water in the carrier stream by a solution of the particular analyte in excess; and (D) a polarogram of the analyte itself by introducing a hydrochloric acid solution of the same acidity as the reagent solution into the Jones reductor and replacing water in the carrier stream by a solution of the particular analyte. Figures 1 and 2 present the four polarograms obtained for sodium nitrite as the analyte. In polarograms C and D the concentration of sodium nitrite in the carrier stream was 10^{-2} mol l^{-1}.

Chromium(II) (Fig. 1). In polarogram B, a minor wave starts at about —0.1 V; this wave can be ascribed to oxygen or hydrogen peroxide, the source of which is so far unknown. In polarogram A an oxidation wave starts at about —0.15 V. This wave corresponds to the reaction $Cr^{2+} \rightleftharpoons Cr^{3+} + e^-$. The small reduction wave starting at about —0.7 V can be ascribed to the reverse reaction, i.e., reduction of Cr^{3+}. Chromium(III) can be formed by reaction of chromium(II) with oxygen or hydrogen peroxide. Also the

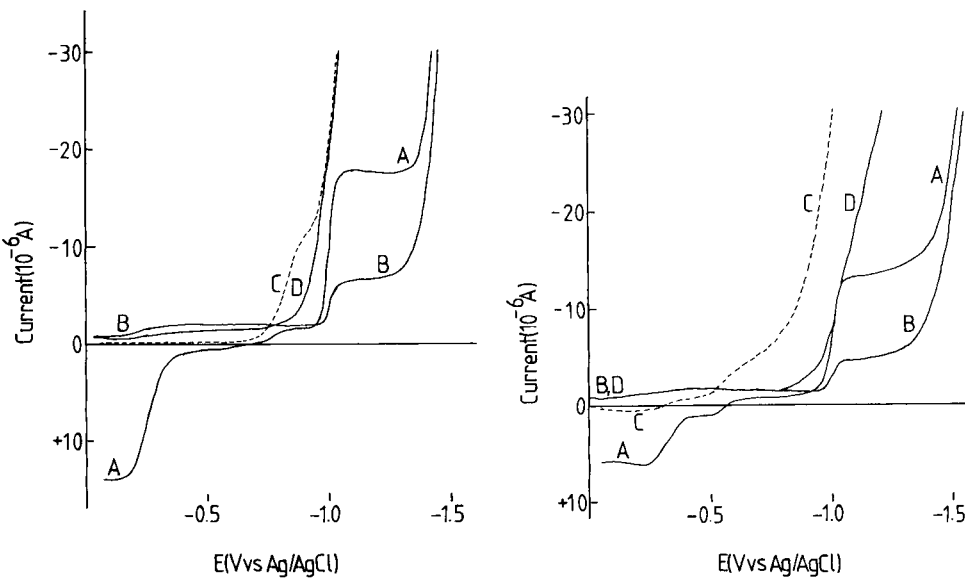

Fig. 1. Polarograms in flow for nitrite with chromium(II) as reagent. For explanation of A, B, C and D, see text.

Fig. 2. Polarograms in flow for nitrite with vanadium(II) as reagent. For explanation of A, B, C and D, see text.

reduction efficiency in the Jones reductor may be less than 100%. The reduction wave starting at about −1.0 V is the zinc wave; the hydrogen wave starts at about −1.3 V. Polarogram D shows that nitrite itself is electroactive under the experimental conditions used. The reduction wave starting at about −0.8 V can be ascribed to the reaction $HNO_2 + 4H^+ + 4e^- \rightleftharpoons NH_2OH + H_2O$. From polarogram C, it can be concluded that chromium(II) is completely oxidized by nitrite.

The conclusion from these experiments is that a working potential of the amperometric flow-through detector of −0.85 V is suitable for determinations of nitrite; at this potential the reduction of chromium(III) is very near its limiting current, the contribution of nitrite to the current is very small, and the noise in the baseline is also minimal. The same procedure was applied for nitrate, hydroxylamine and hydrazine, which show no reaction at all with chromium(II) and are not electroactive.

Vanadium(II) (Fig. 2). As with chromium(II), the oxygen or hydrogen peroxide wave is seen in polarogram B. Besides the reduction waves for zinc and hydrogen ions, two oxidation waves are seen in polarogram A, one starting at about −0.5 V, corresponding to the reaction $V^{2+} \rightleftharpoons V^{3+} + e^-$, and the other starting at about −0.25 V, which corresponds to the reaction $V^{3+} \rightleftharpoons V^{4+} + e^-$ [6]. As already stated for chromium(II), nitrite itself is electroactive under the conditions used (polarogram D). From polarogram C it can be concluded that vanadium(II) is not completely oxidized by the excess of nitrite. The two oxidation waves of vanadium have not totally disappeared, whereas a reduction wave appears, which can be ascribed to the reaction $V^{4+} + 2e^- \rightleftharpoons V^{2+}$. A working potential of the amperometric flow-through detector of −0.9 V seems suitable for the determinations of nitrite; at this potential the reduction of vanadium(IV) is near its limiting current, the contribution of nitrite to the current is small, and the noise in the baseline is minimal. As with chromium(II), nitrate, hydroxylamine and hydrazine show no reaction at all with vanadium(II).

Because the reaction between vanadium(II) and nitrite is rather slow, the dependence of the signal on the flow rate was evaluated. Peak heights resulting from the injection of a 7.5×10^{-4} mol l^{-1} sodium nitrite solution were

TABLE 1

Calibration lines for the flow-injection system with amperometric detection

Sample	Analyte concentration (mol l^{-1})	Regression line	Regression coefficient r	Limit of determination (mol l^{-1})
Chromium(II) as reagent				
$NaNO_2$	10^{-5}—7.5×10^{-5}	$I = (14.4 \pm 0.2) \times 10^{-3}\ C$	0.9998	5×10^{-6}
Vanadium(II) as reagent				
$NaNO_2$	5×10^{-4}—10^{-3}	$I = (1.72 \pm 0.05) \times 10^{-4}\ C$	0.9986	2×10^{-4}

recorded at different flow rates. Between 0.6 and 1.6 ml min^{-1}, the peak height is independent of the flow rate.

Results for the determination of nitrite by means of chromium(II) and vanadium(II) are summarized in Table 1. The limit of determination, which is defined here as the analyte concentration for which the current change equals ten times the peak-to-peak noise, is lower for the determinations with chromium(II) and about the same as for the determinations with uranium(III) [5]. For the determination of nitrite in acidic medium, vanadium(II) is less suitable.

REFERENCES

1 R. C. Schothorst, J. M. Reijn, H. Poppe and G. den Boef, Anal. Chim. Acta, 145 (1983) 197.
2 R. C. Schothorst and G. den Boef, Anal. Chim. Acta, 153 (1983) 133.
3 R. C. Schothorst, J. J. F. van Veen and G. den Boef, Anal. Chim. Acta, 161 (1984) 27.
4 A. Berka, J. Vulterin and J. Zyka, Massanalytische Oxidations- und Reduktionsmethoden, Akademische Verlagsgesellschaft, Geest u. Porlig K.-G., Leipzig, 1964.
5 R. C. Schothorst, M. van Son and G. den Boef, Anal. Chim. Acta, 162 (1984) 1.
6 A. J. Bard (Ed.), Encyclopedia of the Electrochemistry of the Elements, Vol. 7, M. Dekker, New York, 1976.

Analytica Chimica Acta, 175 (1985) 309—312
Elsevier Science Publishers B.V., Amsterdam — Printed in The Netherlands

Short Communication

ION-SELECTIVE ELECTRODES IN TITRATIONS INVOLVING AZO-COUPLING REACTIONS
Part 4. Determination of Secondary Amines

K. VYTŘAS*, J. KALOUS, P. PLUHAŘ[a] and T. ČAPOUN[b]

Department of Analytical Chemistry, College of Chemical Technology, 532 10 Pardubice (Czechoslovakia)

(Received 7th December 1984)

Summary. The determination of secondary amines (1—10 mg) is based on their reaction with arenediazonium ions to form triazenes. The sample is mixed with 4-bromo-1-naphthalenediazonium chloride and, when the coupling reaction is complete, the excess of diazonium salt is back-titrated with sodium tetraphenylborate. The end-point is easily evaluated from the sigmoidal potentiometric titration curves recorded with a PVC membrane indicating electrode plasticized with 2,4-dinitrophenyl n-octyl ether. Diethylamine, diethanolamine, piperidine, *N*-ethylaniline and 1-(*N*-methyl)amino-9,10-anthraquinone were used as test compounds.

Arenediazonium ions give a number of compounds by reaction with nucleophiles containing an HN= group [1]. The most important of these are the arenediazoamino compounds called triazenes, which are formed by reaction of diazonium ions with primary and secondary aliphatic and aromatic or heterocyclic amines of the HNRR′ type, where R is hydrogen or alkyl and R′ is alkyl or aryl:

$$Ar{-}N_2^+ + HN\!<^{R}_{R'} \rightleftharpoons Ar{-}N{=}N{-}NH\!<^{R}_{R'} \rightleftharpoons Ar{-}N{=}N{-}N\!<^{R}_{R'} + H^+$$

On the basis of this reaction, a method for determining secondary aliphatic amines was developed and used in analysis of dyestuffs and their intermediates [2]. The titration end-point was assessed externally by spot reaction on a filter paper. As such a subjective way of estimating end-points tends to be erroneous, a potentiometric titration with ion-selective electrodes [3, 4] was examined to monitor the reactions of secondary amines with arenediazonium ions. However, these reactions are so slow that the direct titrations with the arenediazonium salt solution become impractical. Indirect titrations [5] were therefore studied; the results obtained with five samples of different structures, explicitly, diethylamine, diethanolamine, piperidine, *N*-ethylaniline, and 1-(*N*-methyl)amino-9,10-anthraquinone, are given below.

[a]Present address: Regional Agricultural Laboratory, Agrochemical Corporation, 686 02 Uherské Hradiště — Staré Město, Czechoslovakia.
[b]Present address: Research Institute of Civil Defence, 113 84 Prague, Czechoslovakia.

0003-2670/85/$03.30

Experimental

Solutions and instrumentation. 4-Bromo-1-naphthalenediazonium chloride solution (0.01 M) was prepared and standardized as described previously [4]. Sodium tetraphenylborate solution (0.01 M) was standardized by potentiometric titration of thallium(I) nitrate [6].

Stock solutions of the secondary amines tested were prepared from accessible specimens of diethylamine (as a 33% solution), diethanolamine, *N*-ethylaniline (all "pure" grade, Lachema), 1-(*N*-methyl)amino-9,10-anthraquinone (VCHZ Synthesia), and piperidine (technical). Aqueous solutions (0.01 M) of diethylamine, diethanolamine and piperidine were prepared. *N*-Ethylaniline was dissolved in 10% (v/v) ethanol (0.01 M solution), and 1-(*N*-methyl)amino-9,10-anthraquinone in ethanol (0.0025 M solution).

A solution of sulphuric acid (0.01 M) was prepared, standardized, and used for control determinations. Concentrated Britton—Robinson buffers [3, 4] were used to adjust the pH value of the solutions titrated.

Instrumentation was the same as described previously [4]. The indicator electrode, with a membrane made from poly(vinyl chloride) plasticized with 2,4-dinitrophenyl n-octyl ether, was conditioned in a stirred aqueous suspension of 4-bromo-1-naphthalenediazonium tetraphenylborate.

General procedure. An appropriate volume of the sample solution (corresponding to about 30 μmol of the substance) and 70 ml of pH 10 buffer were measured into a 150-ml beaker and cooled externally with ice to 0°C, and 4-bromo-1-naphthalenediazonium chloride (10 ml of 0.01 M solution) was added (the pH of a mixture containing all the above components was about 6.5—7.0). The plastic membrane and reference electrodes were then placed in the mixture, which was stirred magnetically, and after the cell voltage had stabilized (the time necessary for the stabilization is given in Table 1), the solution was titrated with 0.01 M sodium tetraphenylborate.

TABLE 1

Characteristic values of the curves obtained in indirect potentiometric titration of secondary amines

Substance titrated	Titration curve		Time (min) necessary for	
	Overall potential change (mV)	Steepness near end-point (mV/0.1 ml)	full stabilization of potential after addition of diazonium salt	back-titration with $NaBPh_4$
Diethylamine	220—240	45—60	40	10
Diethanolamine	220—230	50—55	25	10
Piperidine	230—240	50—55	25	10
N-Ethylaniline	235—250	50—60	25	10
1-(*N*-methyl)amino-9,10-anthraquinone	200—210	40—50	10	15

Results and discussion

As listed in Table 1, back-titrations of the excess of 4-bromo-1-naphthalenediazonium salt with 0.01 M sodium tetraphenylborate ($NaBPh_4$) yield well developed sigmoidal titration curves; the potential breaks are about 200—250 mV and steepness of the curves is 40—60 mV per 0.1 ml of titrant near the inflexion point.

To confirm the reliability of the above method, control determinations were done by titration of the amine with 0.01 M sulphuric acid. Diethylamine (pK_b = 2.90), diethanolamine (pK_b = 5.05) and piperidine (pK_b = 2.80) (20 ml of 0.01 M solutions) were each titrated by using visual end-point indication (Tashiro indicator). As shown in Table 2, the results of the two methods agree with the given amounts of diethylamine or diethanolamine; the differences are statistically insignificant. The exception is piperidine: titration with sulphuric acid gave results in close agreement with the amount of the substance taken, whereas lower assays were calculated from the consumption of sodium tetraphenylborate in the back-titration of the excess diazonium salt. This difference can be ascribed to the purity of the technical-grade piperidine used; piperidine is produced by hydrogenation of pyridine, the molecular weight of which (79.10) is not very different from that of piperidine (85.15). Thus the titration with sulphuric acid can afford apparently accurate results provided that the concentration of pyridine is not too high, but only piperidine can react with the diazonium salt used in the indirect determinations. This explanation is not speculative; a control gas-chromatographic analysis of the technical-grade piperidine

TABLE 2

Statistical evaluation of titration results

Substance titrated	Titrant	Taken (mg)	Found (mg)	Assay[a] (%)
Diethylamine	$NaBPh_4$[b]	2.194	2.170	98.9 ± 1.0
	H_2SO_4[c]	14.63	14.60	99.8 ± 0.4
Diethanolamine	$NaBPh_4$	3.154	3.204	101.6 ± 1.5
	H_2SO_4	21.03	21.01	99.9 ± 0.7
Piperidine	$NaBPh_4$	2.556	2.344	91.7 ± 1.1
	H_2SO_4	17.04	16.97	99.6 ± 0.6
N-Ethylaniline	$NaBPh_4$	3.636	3.589	98.7 ± 2.2
1-(*N*-methyl)amino-9,10-anthraquinone	$NaBPh_4$	7.118	6.997	98.3 ± 1.1

[a]Assays are given for comparison of methods as a reliability interval expressed as a percentage, i.e., 100 $(\bar{x} \pm u_0 R)/X$ ($\bar{x}$ arithmetic mean, R the range, u_0 critical value for 5 replicates (n = 5 in all cases), and significance level α = 0.05). [b]Back-titration of excess of 4-bromo-1-naphthalenediazonium chloride with 0.01 M sodium tetraphenylborate. [c]Direct titration with 0.01 M sulphuric acid.

showed that the sample contained about 7% pyridine and a small amount of a third, undefined compound.

N-Ethylaniline and 1-(*N*-methyl)amino-9,10-anthraquinone are such weak bases that simple neutralization titrations could not be used for control. However, the assays given in Table 2 indicate that the method involving azo-coupling of these secondary amines and back-titration of the excess of 4-bromo-1-naphthalenediazonium chloride can be regarded as reliable.

REFERENCES

1 V. Štěrba, in S. Patai (Ed.), The Chemistry of Functional Groups. The Chemistry of Diazonium and Diazo Groups, Part 1, Wiley, Chichester, 1978, pp. 71—93.
2 A. P. Terentev and I. S. Tubina, Zh. Anal. Khim., 18 (1963) 114.
3 K. Vytřas, J. Kalous, Z. Kalábová and M. Remeš, Anal. Chim. Acta, 141 (1982) 163, (Part 1).
4 K. Vytřas, J. Kalous and T. Čapoun, Anal. Chim. Acta, 162 (1984) 141, (Part 2).
5 K. Vytřas, T. Čapoun and J. Kalous, Anal. Chim. Acta, 162 (1984) 373, (Part 3).
6 K. Vytřas, V. Říha and S. Kotrlý, Sb. Věd. Pr., Vys. Šk. Chemickotechnol., Pardubice, 35 (1976) 41.

Analytica Chimica Acta, 175 (1985) 313—317
Elsevier Science Publishers B.V., Amsterdam — Printed in The Netherlands

Short Communication

ION-SELECTIVE ELECTRODES IN TITRATIONS INVOLVING AZO-COUPLING REACTIONS
Part 5. Determination of Arenediazonium Salts of Ampholytic Character

K. VYTŘAS*, J. KALOUS and M. VOSMANSKÁ[a]

Department of Analytical Chemistry, College of Chemical Technology, 532 10 Pardubice (Czechoslovakia)

(Received 7th December 1984)

Summary. Determination of arenediazonium salts (0.3—0.7 g) of ampholytic character is based on their reaction with 1-phenyl-3-methyl-5-pyrazolone, the excess of which is titrated with a 4-bromo-1-naphthalenediazonium chloride solution. The titration is monitored potentiometrically with a PVC membrane electrode plasticized with 2,4-dinitrophenyl n-octyl ether. Eight arenediazonium salts containing hydrophilic groups (e.g., carboxylic and sulfonic acids) were determined without systematic errors.

Arenediazonium salts can be determined by titration with sodium tetraphenylborate, the titration being monitored with PVC membrane electrodes [1]. However, diazonium ions containing hydrophilic groups such as hydroxyl and carboxyl tend to form zwitterions, and the potentiometric titration curves then show only slight curvature, with ambiguous end-points. Salts containing a sulphonic acid group cannot be titrated directly with tetraphenylborate. These salts can be determined indirectly. The arenediazonium salt can be converted to an azo-dyestuff by rapid coupling with a passive compound, the excess of which is then titrated with a lipophilic diazonium salt titrant. Based on earlier experience [2], the reagents chosen were 1-phenyl-3-methyl-5-pyrazolone as the coupling component and 4-bromo-1-naphthalenediazonium chloride as the titrant.

Experimental

Solutions and instrumentation. 4-Bromo-1-naphthalenediazonium chloride (0.01 M) was prepared and standardized with sodium tetraphenylborate or purified 2,4-diaminotoluene as described previously [2]. Sodium tetraphenylborate (0.01 M) solution was standardized by potentiometric titration of thallium(I) nitrate [3].

1-Phenyl-3-methyl-5-pyrazolone (0.01 M) solution was prepared by dis-

[a]Present address: Department of Chemical Normalization, East-Bohemian Chemical Plants Synthesia, 532 17 Pardubice-Semtín (Czechoslovakia).

0003-2670/85/$03.30

solving a weighed amount of the substance in water/ethanol (9 + 1) mixture and filtering through a glass frit; the solution was standardized by potentiometric titration with 4-bromo-1-naphthalenediazonium chloride in pH 10 buffer at 0°C (cooled externally with ice). When the indicating electrode described below was used, the potentiometric titration curves showed sufficiently high (190—220 mV) and steep (30—35 mV/0.1 ml of 0.01 M titrant solution) potential breaks and the titration did not exceed 15 min.

Arenediazonium salts of ampholytic character were prepared from corresponding derivatives of aromatic amines by titration with sodium nitrite. The procedure was usually as follows: the substance (ca. 2.5 mmol) was weighed into a titration vessel (150 ml), distilled water (40 ml), concentrated hydrochloric acid (10 ml) and 10% (w/v) sodium bromide (10 ml) were added, and the mixture was titrated with sodium nitrite (0.25 M), the titration being monitored potentiometrically with platinum and saturated calomel electrodes. The titration was ended at the first permanent increase of potential. Then the solution titrated was quantitatively transferred to a volumetric flask (250 ml) and diluted with water to the mark, providing a ca. 0.01 M solution. It may be noted that the consumption of sodium nitrite served also as a check on the diazonium salt concentration. The bromide added catalyzes the diazotization reaction, so that titrations can be done at laboratory temperature [4]. Aminonaphthalenesulfonic acids (2.5 mmol) were dissolved in sodium carbonate (2 ml of 10% solution in 50 ml of water), and concentrated hydrochloric acid (2 ml) and 10% sodium bromide (10 ml) were added before they were titrated with sodium nitrite.

Concentrated Britton-Robinson pH 10 buffer was prepared by mixing 1000 ml of phosphoric, acetic and boric acids (all 0.4 M) with 780 ml of sodium hydroxide (2 M).

Potentials were measured with an OP-205 pH meter (Radelkis, Budapest). The diazotization was monitored as described above; for monitoring the azo-coupling titrations, a plastic membrane electrode and a saturated calomel electrode were used. The electrode membrane was made from poly(vinyl chloride) plasticized with 2,4-dinitrophenyl n-octyl ether; the internal electrolyte was sodium chloride/sodium tetraphenylborate (both 0.01 M), and a silver/silver chloride internal reference electrode was used. The electrode membrane was conditioned in a stirred aqueous suspension of the 4-bromo-1-naphthalenediazonium tetraphenylborate.

General procedure for indirect titrations. The arenediazonium salt to be determined (5 ml of ca. 0.01 M solution) was pipetted into a 150-ml beaker cooled in ice, and a mixture of 0.01 M 1-phenyl-3-methyl-5-pyrazolone (10 ml) and pH 10 buffer (70 ml) was added. The solution was stirred magnetically and, after the azo-coupling reaction had finished (i.e., the potential of the measuring cell had stabilized), the excess of pyrazolone was back-titrated with 4-bromo-1-naphthalenediazonium chloride (0.01 M) from a 10-ml burette.

Results and discussion

Although excess of the same coupling compound, 1-phenyl-3-methyl-5-pyrazolone, was back-titrated with 4-bromo-1-naphthalenediazonium salt in all cases, different shapes of potentiometric titration curves were recorded (see Fig. 1). This can be ascribed to the formation of the azo-dye and its extraction into the membrane plasticizer, influencing the electrode sensitivity. As is clear from Fig. 1, decreased potential breaks appear in determinations of the bulkier, more lipophilic arenediazonium salts; the corresponding azo-dyes are more readily extracted. Characteristic values of potentiometric titrations are given in Table 1. The curves were easily reproducible. Except for the diazonium salts derived from sulfanilamide and sulfacetamide, the time needed for one analysis was 15—30 min.

Quantitative data are given in Table 2, where the amounts found are compared with those calculated from the consumptions of sodium nitrite during the preparation of the respective diazonium salt. The results indicate that the back-titration method does not involve systematic errors in cases for which the titration time is short enough for the determination to be of practical importance.

Arenediazonium salts of hydrophilic character can be determined by the method suggested in monitoring of such processes, if for any reason reliable control of the original raw materials (i.e., aromatic amines substituted with hydrophilic groups) is impossible. It can also serve as a check on the assays of the diazotization reaction, which can be important in monitoring processes such as production of dyestuffs, pharmaceuticals, etc. The method,

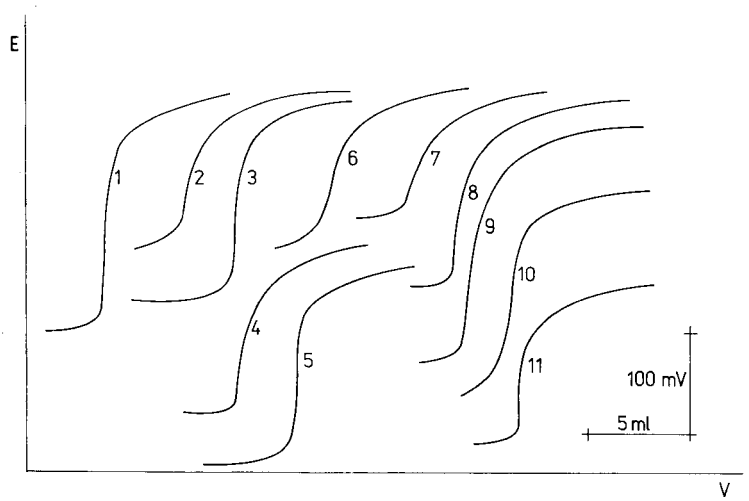

Fig. 1. Potentiometric titration with 0.01 M 4-bromo-1-naphthalenediazonium chloride titrant of 0.05 mmol of 1-phenyl-3-methyl-5-pyrazolone (1), and back-titrations of excess pyrazolone in determinations of arenediazonium salts derived from (2) 4-aminobenzoic acid; (3) 2-aminobenzoic acid; (4) 4-aminobenzenesulfonic acid; (5) 3-aminobenzenesulfonic acid; (6) 1-aminonaphthalene-6-sulfonic acid; (7) 1-aminonaphthalene-7-sulfonic acid; (8) benzocaine; (9) sulfanilamide; (10) sulfacetamide; (11) sulfamethoxydiazine.

TABLE 1

Characteristic values of potentiometric titration curves in indirect determinations of arenediazonium salts of ampholytic character

Substance determined	Titration curve		Time of analysis (min)
	Overall potential change (mV)	Steepness near end-point (mV/0.1 ml)	
4-Aminobenzoic acid	147—153	13—15	30
2-Aminobenzoic acid	200—210	25—30	25
4-Aminobenzenesulfonic acid	155—175	30—37	30
3-Aminobenzenesulfonic acid	190—200	30—35	20
1-Aminonaphthalene-6-sulphonic acid	151—158	10—12	15
1-Aminonaphthalene-7-sulphonic acid	110—123	8—11	20
Benzocaine	170—195	14—17	15
Sulfamethoxydiazine	150—158	14—20	20
Sulfanilamide	219—225	15—20	120
Sulfacetamide	200	15	300

TABLE 2

Statistical evaluation of titration results

Substance determined	Taken[a] (mg)	Found, mg (assay, %)[b]	
		Titration with $NaNO_2$	Back-titration of corresponding diazonium salt
4-Aminobenzoic acid	342.9	342.6 (99.9)	341.1 (99.5 ± 0.7)
2-Aminobenzoic acid	342.9	337.7 (98.5)	337.9 (98.5 ± 6.9)
4-Aminobenzenesulfonic acid			
p.a. grade	393.0	365.5 (93.0)	367.6 (93.2 ± 0.6)
pure grade	393.0	359.6 (91.5)	361.6 (92.0 ± 1.8)
3-Aminobenzenesulfonic acid	433.0	430.8 (99.5)	432.6 (99.9 ± 2.0)
1-Aminonaphthalene-6-sulfonic acid	424.7[c]	404.9 (95.3)	407.8 (96.0 ± 3.9)
1-Aminonaphthalene-7-sulfonic acid	384.5[c]	399.0 (103.8)	381.6 (99.2 ± 3.6)
Benzocaine	413.0	412.6 (99.9)	412.4 (99.9 ± 0.4)
Sulfamethoxydiazine	700.8	697.3 (99.5)	697.7 (99.5 ± 3.4)
Sulfanilamide	430.5	430.1 (99.9)	412.0 (95.7 ± 3.5)
Sulfacetamide	715.7[d]	700.7 (97.9)	608.0 (85.0 ± 4.6)

[a]The amounts of the amino acids taken. [b]For easier comparison of methods, assays are given as a reliability interval in percentage values, $100\ (\bar{x} \pm u_0 R)/X$, where $\bar{x}$ is the arithmetic mean, R the range, u_0 the critical value for 3 or 4 measurements at a significance level $\alpha = 0.05$. [c]558.1 mg of technical preparation was used; the content was 76.1% of the 6-isomer or 68.9% of the 7-isomer. [d]Weighed as the sodium salt dihydrate.

however, is not fully universal. Some arenediazonium salts are prone to auto-azo-coupling reactions; among the compounds tested, this was observed in the case of the diazonium salt derived from 1-hydroxy-6-aminonaphthalene-3-sulfonic acid. Others do not react with the coupling compound used; for example, diazonium salts prepared from 1-amino-4-bromo-9,10-anthraquinone-2-sulfonic acid or *p*-aminosalicylic acid did not react. The use of a coupling agent other than 1-phenyl-3-methyl-5-pyrazolone would probably help to extend the applications of the general method.

REFERENCES

1 K. Vytřas, M. Remeš and H. Kubešová-Svobodová, Anal. Chim. Acta, 124 (1981) 91.
2 K. Vytřas, J. Kalous and T. Čapoun, Anal. Chim. Acta, 162 (1984) 141.
3 K. Vytřas, V. Říha and S. Kotrlý, Sb. Ved. Pr., Vys. Sk. Chemickotechnol., Pardubice, 35 (1976) 41.
4 J. Šubert, Farm. Obz., 50 (1981) 273.

Analytica Chimica Acta, 175 (1985) 319—323
Elsevier Science Publishers B.V., Amsterdam — Printed in The Netherlands

Short Communication

USE OF A FURNACE ALIGNMENT JIG TO DECREASE ERRORS ASSOCIATED WITH BACKGROUND-CORRECTION IN GRAPHITE FURNACE ATOMIC ABSORPTION SPECTROMETRY

A. A. BROWN
Pye Unicam Ltd., York Street, Cambridge CB1 2PX (Great Britain)
(Received 11th January 1985)

Summary. The jig is used to align the beams from the analyte hollow-cathode lamp and the background-correction lamp. Gold or non-absorbing lead atomic lines are used for assessing background absorbance from sodium chloride. Correction accuracies approaching 100% are achieved.

Dabeka [1] recently reported the results of a collaborative study of a screening method based on graphite-furnace atomic absorption spectrometry (a.a.s.) for the determination of lead in infant food formulations. Of the nine participating laboratories only one produced consistent, accurate results for lead in all the eight samples supplied. When the results from the other eight laboratories were evaluated, a systematic error was found for the eight sample results which was different for each laboratory. After correction of the set of results from each laboratory for this bias (positive or negative), the overall accuracy of the inter-laboratory study showed a significant improvement.

It was suggested that the systematic errors were due to errors in the background-correction systems of the spectrometers used, even though the background absorbances were only 0.1—0.2. Dabeka [1] concluded that the errors were due to inadequate alignment of the hollow-cathode lamp and the deuterium lamp through the graphite furnace. It was also suggested that it is necessary to measure the background-correction errors associated with a particular sample assay; at the present time, there is no published method for doing this. Background-correction errors can result from misaligned analyte and deuterium lamp beams because the spatial and temporal distribution of the atom population and of the background-generating species are usually different. A misaligned deuterium lamp would measure a mean background absorbance at a position slightly different from that where the total background plus analyte atomic absorption signal is measured with the analyte hollow-cathode lamp. In the absence of analyte in a sample, a background-correction error would appear as a positive or negative signal which, in the former case, could be mistaken for an analyte signal. With analyte present, a background-correction error would produce either a positive or negative bias

0003-2670/85/$03.30

in the results. The same consideration applies to the choice of a deuterium arc or deuterium hollow-cathode lamp for background-correction. The hollow-cathode lamp is to be preferred because the radiation from the analyte and deuterium lamps have similar, if not identical, geometries and spatial intensity distributions whereas the deuterium arc has a completely different geometry and spatial intensity distribution. However, the high output intensity of the deuterium arc favours its use in most spectrometers with complex multicomponent optical systems with their associated high transmitted radiation intensity losses.

This communication addresses the problem of background-correction errors, suggests two methods of measuring these errors and presents a new simple method of graphite-furnace alignment which helps to reduce background-correction errors.

Optical and graphite furnace alignment

It has been normal to align the furnace to produce maximum transmission of energy from the deuterium lamp; the position of the analyte hollow-cathode lamp is then adjusted to give maximum transmission of energy through the furnace. This method is not particularly accurate or sensitive. A relatively large displacement of the furnace position is required to produce a small change in transmitted energy from the deuterium lamp. This may be the cause of the errors reported by Dabeka [1].

The method proposed for optical and furnace alignment is based on the use of a furnace alignment jig [2]. This jig is a plastic tube (4 cm long) with a 1-mm diameter hole drilled through the centre. The dimensions of the jig must be the same as those of the graphite tube used. Consequently, the design of the jig will be different for each of the commercially available graphite furnaces. However, the alignment procedure will always be the same. For furnace alignment, the jig is inserted in the furnace in place of the graphite tube. The furnace is then aligned to give maximum transmission from the deuterium lamp. The analyte hollow-cathode lamp is then adjusted to give maximum transmission through the jig. The jig produces more accurate alignment than other methods; because of the narrow hole and length of the jig, there is increased sensitivity of the transmitted radiation intensity to the source lamp or furnace position, so that a small change in furnace or hollow-cathode lamp position produces a large change in transmitted radiation intensity. Therefore, the alignment procedure is simple and takes only 5 min. Once alignment has been achieved, the jig is replaced by a graphite tube.

Tests of background-correction accuracy

Various methods have been used to test the accuracy of background-correction. In the old method, a static gauze was placed in the optical path of the spectrometer; however, this does not take into account the fast and transient nature of graphite furnace a.a.s. signals. Another method [3] is based on the lead/sodium chloride system; this involves atomising sodium

chloride in a graphite furnace, and measuring at a lead absorbing line (217.0 nm or 283.3 nm) with background-correction alternately on and off. The accuracy (%) of background-correction is expressed as [100 − (100 × mean background-corrected signal/mean total background signal)]. But, if the sodium chloride is contaminated with lead (a fairly common problem), then the result is meaningless. An improvement is to atomise sodium chloride and measure the background at lead non-absorbing atomic lines. For example, when lead is measured at the 217.0-nm resonance wavelength, the background could be measured at the lead non-absorbing line at 220.4 nm. This would eliminate contamination problems and the results obtained would be the "true" performance of the background-correction system. For the lead 283.3-nm absorbing line, the non-absorbing line at 280.1 nm is recommended. A table containing pairs of absorbing and non-absorbing atomic lines for many elements is available [3].

A more selective test is the gold/sodium chloride system. This has been used by the author for many years to test the background-correction accuracy of various spectrometers, but has not previously been published. It has two particular advantages: gold contamination is not a problem; and sodium chloride has a molecular band head at about 240 nm (gold atomic line 242.8 nm) and therefore increased background signals can be generated from a small amount of sodium chloride. For example, in the Pye Unicam PU9095 graphite furnace, 100 μg of sodium chloride produces a background absorbance of 2 at the lead atomic lines of 217.0 or 220.4 nm, whereas at the gold wavelength of 242.8 nm, only 15 μg of sodium chloride is required to produce a similar background absorbance. This decreases possible contamination of the furnace head during the test experiments.

Experimental

The instrument used was a Pye Unicam SP9 atomic absorption spectrometer with a PU-9095 graphite furnace. The furnace programme and other instrumental parameters are given in Table 1. The experiments were designed to test the ruggedness of the proposed furnace alignment method. The

TABLE 1

Graphite-furnace programme for background-correction tests[a]

	Temp. (°C)	Time (s)	Ramp
Dry	120	30	4
Ash	500	10	4
Atomise	2600	3	0[b]
Clean	2800	2	0

[a]Lamp current 10 mA, 242.8 nm, 10-μl sample, uncoated tube. [b]During atomisation, the functions of "temperature control", "recorder", "peak-timer" and "auto-zero" were selected.

graphite furnace was aligned with use of the furnace alignment jig, and the gold/sodium chloride background-correction test was applied. The graphite furnace was removed from the spectrometer, replaced, and realigned using the jig. The gold/sodium chloride background-correction test was done after each of ten realignments of the graphite furnace.

Results

The results of the study are shown in Table 2. In the peak-height mode, the mean accuracy was 98.8% with a background absorbance of 1.124. In the peak-area mode, the mean accuracy was 99.6%. The individual accuracies in the peak-height mode ranged from 98.2 to 99.4% with a relative standard deviation (r.s.d.) of 0.43%. In the peak-area mode, the accuracies ranged from 98.0 to 100.3% with a r.s.d. of 1.00%. To put these figures into perspective, a sample which did not contain any gold but produced an absorbance of 0.02 (because of a background-correction error) could be mistakenly quoted as containing 3—4 $\mu g\ l^{-1}$ gold. If a typical dissolution stage was taken into account (1 g of sample digested in acid and finally diluted to 100 ml), the concentration of gold in the sample would be quoted as 0.3—0.4 $\mu g\ g^{-1}$. In some geological applications, this might be mistakenly interpreted as indicative of a possible gold-containing material warranting further investigation. From the individual accuracy data, it is apparent that with care in the furnace alignment procedure, accuracies of 100 ± 1.0% can be achieved. Possibly more importantly, it is demonstrated that the proposed alignment method with the jig is reproducible on a between-run basis, so that less-skilled staff should be able accurately to align a graphite furnace system on a routine basis.

Discussion

It is important to measure the errors associated with the use of any background-correction system. The magnitude of these errors varies from

TABLE 2

Background-correction accuracy measured by atomisation of 5 μg of sodium chloride at the gold 242.8 nm atomic line

	Peak height (absorbance)	Peak area (abs. × s)
Background correction OFF	1.124	0.4456
Background correction ON		
Mean	0.0137	0.0016
No. of measurements	10[a]	10[a]
Accuracy of mean (%)	98.8	99.6
R.s.d. (%)	0.43	1.00

[a]Each of the 10 values was the mean of three furnace injections of 5 μg of sodium chloride.

instrument to instrument depending on differences in spectrometer design and electronics, modulation frequency and use of a deuterium arc or hollow-cathode lamp [3]. However, with any spectrometer, the background-correction error associated with a particular sample matrix should be measured. Furthermore, this procedure should become a routine laboratory operation prior to the analysis of samples. If the test produces unacceptably high errors then the furnace should be realigned.

Ultimately, background-correction errors must be related to analyte atomic absorption signals. The greatest errors in analytical results are for samples containing quantities of analyte at the detection limit. In extreme cases, background-correction errors may be larger than analyte signals. It is still important, therefore, to measure background-correction errors even if there is only a small background absorbance (0.2—0.4). Accurate graphite-furnace alignment is also important in order to minimise emission problems associated with elements with resonance wavelengths in the visible region of the spectrum (e.g., calcium or chromium). Emission breakthrough can occur when the intensity of the graphite wall radiation reaches such a level that the resulting d.c. signal from the photomultiplier tube overloads the demodulation electronics in the spectrometer. Therefore, the furnace alignment jig principle is still advantageous even when there is no matrix background present.

These simple yet effective procedures should be considered by most routine users of graphite furnace a.a.s. As the results reported by Debeka [1] show, there is certainly a need for such tests. Finally, background-correction errors are not just associated with deuterium background-correction. It will be in the interests of users of Zeeman or Smith/Hieftje background-correction systems, to measure the errors associated with these systems.

The furnace alignment jig was based on an idea suggested by A. J. Thompson, MCP Electronic Materials, Berks., U.K.

REFERENCES

1 R. W. Dabeka, Analyst, 109 (1984) 1259.
2 A. A. Brown and P. J. Whiteside, Int. Labmate, 9 (1984) 33.
3 R. A. Newstead, W. J. Price and P. J. Whiteside, Prog. Anal. At. Spectrosc., 1 (1978) 267.

Analytica Chimica Acta, 175 (1985) 325—328
Elsevier Science Publishers B.V., Amsterdam — Printed in The Netherlands

Short Communication

DETERMINATION OF ARSENIC IN STEEL AND CAST IRON BY HYDRIDE-GENERATION ATOMIC ABSORPTION SPECTROMETRY

B. VANLOO, R. DAMS and J. HOSTE*

Institute of Nuclear Sciences, Rijksuniversiteit Gent, Proeftuinstraat 86, B-9000 Gent (Belgium)

(Received 26th March 1985)

Summary. A procedure is described for the determination of arsenic in steel and cast iron by atomic absorption spectrometry after hydride generation with sodium tetrahydroborate. The samples are decomposed with a nitric/perchloric acid mixture. The data are evaluated directly against acidic standard solutions of arsenic(V). The limit of detection is about 1 $\mu g\ g^{-1}$ and the precision is better than 4% for concentrations exceeding 10 $\mu g\ g^{-1}$.

It is well known that trace or residual elements such as Pb, Sn, Bi, Sb, As, Te and Ag, have adverse effects on the mechanical properties of steel [1]. Arsenic, like phosphorus, reduces the ductility of steel while increasing its brittleness [2]. These influences on the quality of steel are observed even at very low concentrations (0.0002—0.02%), so that suitable methods for the fast, sensitive and accurate determination of arsenic in steel are essential. While electrothermal atomic absorption spectrometry (a.a.s.) may suffer from interferences by the accompanying elements present in steel, hydride-generation a.a.s. should provide more freedom from those interferences because the volatile metal hydride is separated from the interfering matrix. Non-specific light losses caused by molecular absorption or light scattering, and inter-element interferences in the gas phase, become unlikely, but in the reaction flask, transition metals, acids or anions like nitrate may interfere with the formation and volatilization of the metal hydride. There is little information on the determination of arsenic in metallurgical samples. Only Welz and Melcher [3] and Fleming and Ide [4] have reported critical studies on the application of hydride-generation a.a.s. in the analysis of steel.

In the present communication, arsenic in steel and cast iron is determined by evolution of arsine into an electrically heated quartz cell and a.a.s. The procedure is optimized and the method is validated by the analysis of reference steel and cast iron samples.

Experimental

Apparatus. A Perkin-Elmer model 3030 atomic absorption spectrometer equipped with a Perkin-Elmer arsenic electrodeless discharge lamp was used for all determinations. The lamp was operated at 8 W from an external power

0003-2670/85/$03.30

supply. A slit of 0.7 nm was selected to isolate the 193.7-nm arsenic line. The formation of the peak was observed on the video screen. The signals were printed on a Perkin-Elmer model PR-100 printer. Arsine was generated by an automatic mercury/hydride system (Perkin-Elmer model MHS-1). The electrically heated quartz cell atomizer was held at 900° C and program IV in the 1977 MHS-1 manual was used for the determination. This program includes a long purging time (65 s) with argon; with shorter purging times an absorption peak of air was observed.

Reagents and standards. Double-distilled water and analytical-grade reagents were used throughout. For the wet digestion of steels and cast irons, the acids were 70% nitric acid (J. T. Baker), 30% hydrochloric acid (J. T. Baker), 70% perchloric acid (Merck) and 50% hydrofluoric acid (Analyticals). For the hydride generation, the solutions were 96% sulfuric acid (J. T. Baker) and 5% (w/v) sodium tetrahydroborate (Aldrich) in 2% (w/v) sodium hydroxide (Carlo Erba). The sodium tetrahydroborate solution was filtered before use and stored in a refrigerator.

A standard arsenic(V) stock solution (500 mg l^{-1}) was prepared by dissolving 0.3835 g of arsenic pentoxide (UCB, pro analyse) in 25 ml of 10% (w/v) sodium hydroxide (Carlo Erba); after neutralization with sulfuric acid, this solution was diluted to 500 ml. Working standards (500 μg l^{-1}) were freshly prepared by dilution with 1% (w/v) sulfuric acid.

Sample decomposition. Fine drillings of the steel and cast iron samples are dissolved in a nitric/perchloric acid mixture in the same way as described for the determination of bismuth and lead [5]. The sample (0.1—1 g) is weighed into a 150-ml digestion flask and 25 ml of 6 M nitric acid is added. After the evolution of nitrogen oxides, 10 ml of perchloric acid is added and a Bethge digestion apparatus [6] is fixed on the flask. The solution is heated to 220° C. When dissolution is complete, the condensate is returned to the reaction flask by readjusting the stopcock of the Bethge apparatus. The contents of the flask are finally transferred to a 100-ml volumetric flask, together with 10 ml of 1 M hydrochloric acid. Generally a clear solution is obtained. If needed, 1 ml of hydrofluoric acid can be added to dissolve and subsequently evolve silica as silicon tetrafluoride. Blanks are prepared in a similar way by dissolving carbonyl iron, containing less than 0.002 μg g^{-1} arsenic.

Absorbance measurements. A 50—500-μl aliquot of the sample solution is injected into the reaction flask containing 10 ml of 5% (w/v) sulfuric acid solution. The total amount of iron in the cell is normally kept at 0.5 mg although measurements are possible with up to 2.5 mg of iron in the cell. When a dilution is used, an appropriate amount of the iron is added. The solution is purged with argon during 65 s to remove air from the system. On addition of 2.5 ml of 5% (w/v) sodium tetrahydroborate solution with simultaneous starting of the magnetic stirrer, the arsine is swept into the preheated quartz tube (program IV). In the same way a working curve is constructed by injecting 0—100 μl of a working stock arsenic(V) solution (500 μg l^{-1}), the same amount of iron being added as to the samples. Absorbances were measured as peak height, although peak-area integration can also be used.

Results and discussion

Influence of the valence state. The difference in sensitivity between As(III) and As(V) in the hydride a.a.s. technique is well known [7—10]. From 5% (w/v) sulfuric acid, the peak height for As(V) was found to be 20—30% less than that for As(III); also, the peak maximum occurred at ca. 10.6 s for As(III) but at ca. 14.1 s for As(V) from the time of addition of the tetrahydroborate. During the dissolution of the sample, arsenic is oxidized to arsenic(V) because the oxidation potential of boiling 70% perchloric acid is >1.5 V [6] whereas the oxidation potential of the As(V)/As(III) system is only 0.58 V [11]. Therefore all standardizations were done with acidic solutions of As(V).

Accuracy, precision and sensitivity. A known amount of As(III) was added to electrolytic iron. After digestion with the above-specified acids, these samples were measured by the standard addition technique and by comparison to a calibration line. For both methods, As(V) standards were used. The average arsenic recovery was 102 ± 5% (n = 9) after standard addition and 103 ± 4% (n = 6) from the calibration line. In further work, only the calibration line was used.

Four NBS standard reference materials with arsenic concentrations between 2 and 920 $\mu g\ g^{-1}$ were analyzed. The SRM's 7g and 6g are high-phosphorus cast irons while SRM 362 is a modified steel sample and SRM 365 is an electrolytic iron. The determinations were done with 0.5 mg and 2.5 mg of iron in the reaction vessel. As can be seen from the results (Table 1), the agreement with the certified values is good, indicating that iron contents of up to 2.5 mg do not interfere with the determination of arsenic. The precision was always better than 4% except for the electrolytic iron (SRM 365) where it was 8%.

The sensitivity was 0.5 ng for 0.0044 absorbance. This corresponds to a concentration of 1 $\mu g\ g^{-1}$ when 100 μl is injected from a solution of 0.5 g of steel in 100 ml. The blank obtained by injecting 100 μl of a solution of 0.5 g

TABLE 1

Determination of arsenic in NBS standard reference samples

Sample	Arsenic content ($\mu g\ g^{-1}$)		
	Certified[a]	Hydride generation[b]	
		0.5 mg Fe	2.5 mg Fe
SRM 365	(2)	—	3.9 ± 0.6 (3)
SRM 7g	140 ± 40	120 ± 5 (6)	118 ± 4 (3)
SRM 6g	420 ± 10	400 ± 19 (6)	402 ± 34 (3)
SRM 362	920 ± 50	991 ± 33 (6)	913 ± 58 (4)

[a]Value in parentheses is tentative. [b]Mean with 95% confidence limits; number of determinations in parentheses.

of carbonyl iron in 100 ml gave a signal equivalent to 2 ± 1 ng. The practical detection limit, defined as three times the standard deviation on the blank, can be estimated at 6 $\mu g\ g^{-1}$. This can be further reduced by using more concentrated sample solutions or injecting larger volumes. For an iron content of 2.5 mg in the reaction vessel, the limit of detection is calculated as 1.2 $\mu g\ g^{-1}$.

Conclusion

Arsenic can be determined accurately in steel and cast iron by a.a.s. after hydride generation. The technique offers high flexibility and sensitivity because of the wide variability in the volume of sample injected and the low probability of interferences by matrix components. The time-consuming method of standard addition is not required. Measurement and calibration with arsenic(V) solutions is advantageous.

The authors are indebted to Mrs. M. Coene for technical assistance. The investigation is part of a research program sponsored by the Instituut voor Wetenschappelijk Onderzoek in Nijverheid en Landbouw and the Center for Scientific and Technical Research of the Metalworking Industry in Belgium.

REFERENCES

1 G. Mayer and C. A. Clark, The Metallurgist and Materials Technologist, Nov. 1974, p. 491.
2 E. Hondremont, Handbuch der Sonderstahlkunde, Springer-Verlag, Berlin, Vol. 2, 1956.
3 B. Welz and M. Melcher, Spectrochim. Acta, Part B, 36 (1981) 439.
4 H. D. Fleming and R. G. Ide, Anal. Chim. Acta, 83 (1976) 67.
5 B. Vanloo, R. Dams and J. Hoste, Anal. Chim. Acta, 151 (1983) 391.
6 G. F. Smith, The Wet Chemical Oxidation of Organic Compositions Employing Perchloric Acid, G. F. Smith Chemical Co., Columbus, OH, 1965, p. 20.
7 I. Rubeska and V. Hlavinkova, At. Absorpt. Newsl., 18 (1979) 5.
8 A. Kuldvere, At. Spectrosc., 1 (1980) 138.
9 H. W. Sinemus, M. Melcher and B. Welz, At. Spectrosc., 2 (1981) 81.
10 P. N. Vijan, A. C. Rayner, D. Sturgis and G. R. Wood, Anal. Chim. Acta, 82 (1982) 329.
11 R. C. Weast and J. M. Astle (Eds.), Handbook of Chemistry and Physics, 60th edn., CRC Press, FL, 1979, p. D-155.

Analytica Chimica Acta, 175 (1985) 329—332
Elsevier Science Publishers B.V., Amsterdam — Printed in The Netherlands

Short Communication

NEBULIZATION EFFECTS IN ANALYTICAL ATOMIC SPECTROMETRY

E. D. PRUDNIKOV* and Y. S. SHAPKINA
Earth's Crust Institute, State University, Leningrad, 199164 (U.S.S.R.)
(Received 25th February 1985)

Summary. The effects of solvent vaporization and of element redistribution between the various fractions of an aerosol during sample nebulization in atomic spectrometry are examined. These effects govern the fluctuations of element concentration in the analytical zone of the flame. Sample composition modification can increase random errors to 5—10% in the absence of matrix matching.

Atomic spectrometry with nebulization of sample solution is widely used. It is well known that the composition and physical characteristics of the sample solution (temperature, viscosity, density, surface tension, etc.) influence the distribution of the aerosol droplet size and the value of the analytical signal [1]. The previously unrecognized effect of aerosol ionic redistribution in atomic spectrometry was recently examined [2]. It was shown that ionic redistribution on generation of aqueous aerosols by pneumatic nebulization depends on the mixture of ions in solution, the droplet size of the aerosol, and the ratio of the major to minor cations. It was concluded that this effect is relatively small in analytical flame atomic spectrometry but can cause significant errors in inductively-coupled plasma spectrometry. The aim of this communication is to investigate in more detail the analytical role of this effect.

Experimental

The apparatus used was as described previously [3]; the methods have also been reported [4]. A concentric nebulizer was used with a spray chamber of volume 1 l at an air pressure of 0.5 atm. The aspiration rate of the solutions was 3 ml min^{-1}, the nebulization efficiency was 5—10%, and the initial volume of the solutions used was 50 ml. Constant volumes of solutions containing various amounts of sodium, potassium, lithium, rubidium, caesium and calcium were nebulized repeatedly. The concentrations of the elements in the final solution passing to drain were measured for a range of inorganic and organic compounds in solution; the temperature change of the nebulizing air was also studied.

The procedure used was as follows. The spray chamber and nebulizing system was first washed by aspiration of distilled water for 1 h. The system was then washed out with the solution under test for 10 min. Finally, a measured volume of the given solution was aspirated and the portion of solution passing to drain was collected and aspirated again. This process was repeated 10—20 times. The amounts of element in the first and final solutions were compared by flame emission spectrometry as described previously [3—5]. The effect of nebulization, F, which quantifies the change in the element concentration in the analytical zone, was calculated from the equation $F = 1 - (I_{in}/I_f)^{1/n}$, where n is the number of aspirations, I_{in} is the emission signal of the element for the initial solution and I_f is the emission signal for the final solution. The concomitant element blank was always negligible.

Results and discussion

The suggested method permits quantification of a number of nebulization effects and gives an estimate of their analytical importance. The results obtained, shown in Tables 1—4, indicate the relative changes of the element concentration between the initial solution and aerosol. The effect of solvent vaporization during solution nebulization alone is shown in Table 1. However, the proposed method also allows characterization of the effects of element redistribution between the various fractions of aerosol. It is well known [1] that, in the analytical zone, only the fractions of aerosol with 3—5 μm diameter are found. Droplets of aerosol with diameters >5—10 μm do not reach the analytical zone, remaining in the unused portion of solution. This fact is well illustrated by Tables 2 and 3.

The physical interpretation of the effects of solvent vaporization is as follows. During the process of nebulization and the formation and transport of aerosol droplets, the solvent evaporates from the surface of droplets. The effect depends on the nature of the solvent, the droplet size and the nebulizing gas temperature. This process leads to the slight enrichment of the required element in the solution passing to drain. Further, it limits the useful transport efficiency available with highly volatile solvents or with air heating [4] (Table 1).

TABLE 1

Effect of solvent and temperature on pneumatic nebulization

Solvent[a]	Relative potassium atomic emission intensities with nebulizing air at 20 and 70° C	
	20° C	70° C
Water	1.0	2.5
Aqueous 20% (v/v) ethanol	2.0	2.8
Aqueous 20% (v/v) glycerine	0.7	1.5

[a]Containing 100 μg ml^{-1} sodium ion.

TABLE 2

Change in element concentration in the analytical zone

Measurement conditions			Nebulization effect, F				
Concentration ($\mu g\ ml^{-1}$)	Solvent	Air temp. (°C)	Na	K	Li	Rb	Cs
0.1	Water	20	−0.10	0.05	0.022	0.09	0.10
1.0	Water	20	−0.05	0.02	0.006	0.06	0.07
10.0	Water	20	−0.01	0.002	−0.006	0.02	0.04
10.0	Water	70	−0.04	−0.010	−0.010	0.03	0.05
80.0	Water	20	−0.002	−0.002	−0.002	−0.001	0.003
10.0	Ethanol/water (85:15)	20	−0.04	−0.05	−0.05	−0.03	−0.010
10.0	Ethanol/water (85:15)	70	−0.10	−0.12	−0.13	−0.09	−0.05
10.0	Glycerine/ water (20:80)	20	−0.002	0.03	−0.005	0.08	0.11

TABLE 3

Influence of solution composition

Solution composition[a]	Nebulization effect, F					
	Na	K	Li	Rb	Cs	Ca
H_2O only	−0.010	0.002	−0.006	0.020	0.04	−0.010
50 mg ml^{-1} NaCl	—	−0.010	−0.006	−0.006	−0.015	−0.007
50 mg ml^{-1} $NaNO_2$	—	−0.006	−0.007	0.003	0.002	−0.008
50 mg ml^{-1} KCl	−0.020	—	−0.009	−0.05	−0.07	−0.007
50 mg ml^{-1} KNO_3	−0.020	—	−0.007	−0.002	−0.017	−0.007
50 mg ml^{-1} NH_4CH_3COO	−0.012	−0.03	−0.012	−0.03	−0.05	−0.012
50 mg ml^{-1} $Mg(CH_3COO)_2$	−0.002	0.02	−0.006	0.03	0.05	−0.007
1 M HCl	−0.009	−0.04	−0.010	−0.05	−0.06	−0.020
1 M NH_3	−0.006	−0.01	−0.007	−0.008	0.020	−0.001
0.33 M H_3PO_4	−0.008	−0.02	−0.006	−0.020	−0.020	−0.009

[a]Element present at 10 $\mu g\ ml^{-1}$, air temperature 20° C.

Tables 2 and 3 also show the existence of processes of element redistribution between the various fractions of aerosol. The results obtained are in agreement with previous data [2]. The effect of element redistribution depends on the nature and concentration of the element, the solvent and solution composition, the temperature of the gas, the design of the nebulization system, and the conditions of nebulization.

It is important to realize that solution nebulization can cause errors in determinations by atomic spectrometry. The magnitude of these errors may reach 5—10% (see Tables 2 and 3). This is in accordance with literature data

TABLE 4

Effects of the nebulization and atomization processes on the emission intensity of 10 μg ml^{-1} thallium

Solution composition	Peak height (mV)
Water only	71.5
0.5 mg ml^{-1} $Al(NO_3)_3$	70.5
1.0 mg ml^{-1} $Al(NO_3)_3$	69.5
0.5 mg ml^{-1} $NaNO_3$	71.0
1.0 mg ml^{-1} $NaNO_3$	70.0
2.0 mg ml^{-1} $NaNO_3$	69.0

[6] on the magnitude of non-instrumental errors in flame emission spectrometry. The nebulization effects may also explain some of the changes in the analytical signal on introduction of small amounts of interfering matrix. The errors associated with effects of solution nebulization may be concurrent with errors produced during atomization [1]. It is difficult to separate these effects in real analytical conditions (Table 4). The results (Table 4) were obtained for thallium in order to eliminate ionization effects, and can be explained by the influence of nebulization processes.

The results obtained show the significance of nebulization effects with respect to precision in atomic spectrometry. For elimination of these effects, it is necessary to match as carefully as possible the chemical and physical identities of the standard and sample solutions. In practice, buffering compounds are widely used [1, 4, 7].

The manuscript was prepared for publication at Carleton University, Ottawa, Canada during a scientific mission of E.D.P. The authors thank Prof. C. L. Chakrabarti and Prof. D. R. Wiles for the opportunity to complete the manuscript.

REFERENCES

1 N. S. Poluektov, Methods of Analysis by Flame Photometry, Khimia, Moscow, 1967.
2 J. A. Borowiec, A. W. Boorn, J. H. Dillard, M. S. Cresser, R. F. Browner and M. T. Matteson, Anal. Chem., 52 (1980) 1054.
3 E. D. Prudnikov, Vestn. Leningrad Univ., No. 4 (1968) 137.
4 E. D. Prudnikov, Vestn. Leningrad Univ., No. 10 (1965) 125; Dissertation, Leningrad State University, 1968.
5 E. D. Prudnikov, Am. Lab., (1978) 17.
6 E. D. Prudnikov and Y. S. Shapkina, Vestn. Leningrad Univ., No. 24 (1978) 46.
7 W. Slavin, Atomic Absorption Spectroscopy, Khimia, Leningrad, 1971.

Analytica Chimica Acta, 175 (1985) 333—337
Elsevier Science Publishers B.V., Amsterdam — Printed in The Netherlands

Short Communication

DETERMINATION OF THE FLUORESCENCE PROPERTIES OF POLYNUCLEAR AROMATIC HYDROCARBONS IN THE VAPOR PHASE AND ADSORBED ON SOLID SUPPORTS BY LASER-INDUCED MOLECULAR FLUORESCENCE

LOUIS J. JANDRIS[a] and R. KEN FORCE*
Department of Chemistry, University of Rhode Island, Kingston, RI 02881 (U.S.A.)
(Received 2nd January 1985)

Summary. The fluorescence properties (lifetimes and spectra) of anthracene and fluoranthene were found to be independent of temperature in the ranges 80—110°C and 60—95°C, respectively, in vacuum and in helium, nitrogen, and air atmospheres. The fluorescence lifetimes and spectra were also measured for these two compounds individually adsorbed on silica, alumina, magnetite, or hematite. In all cases, the emission profiles for the adsorbed aromatic hydrocarbon were red-shifted with respect to the gas-phase spectra. The fluorescence lifetimes for both anthracene and fluoranthene increased for the different supports in the order alumina < silica < magnetite < hematite.

Polynuclear aromatic hydrocarbons (PAH) are formed at elevated temperatures by the incomplete combustion of organic matter. Reports on the concentration of atmospheric PAH have indicated that they are adsorbed onto the surfaces of particulate matter. However, it has been shown recently that many PAH evaporate at room temperature under a weak air flow, indicating that some PAH may exist in the vapor phase as well as on particles [1—4]. In addition, there is evidence that phenanthrene and pyrene exist in higher concentrations in the vapor phase than on particles [5]. Recently, it has been reported that the distribution of certain PAH between aerosol particles and the vapor phase is a function of the loading of PAH on the aerosol [6]. In this study, the vapor-phase fluorescence lifetimes and spectra of anthracene and fluoranthene were obtained in nitrogen, helium and air atmospheres, as well as in a vacuum of 3 torr. Similar measurements were conducted with either PAH adsorbed onto alumina, silica, hematite or magnetite, respectively. These oxides were chosen because they are some of the major inorganic components of fly ash [7].

Several reports are available on the fluorescence of different PAH in the gas phase [8—12]. Ehrlich and Wilson [11] reported a fluorescence lifetime of 22 ns for fluoranthene vapor in vacuum, using excitation at 28460 cm^{-1} (351.4 nm). In our work on fluoranthene, excitation was at 29665 cm^{-1}

[a]Present Address: Foss Manufacturing, Haverhill, MA 01830 (U.S.A.)

0003-2670/85/$03.30

(337.1 nm); thus, a different value may be expected. Aspects of this difference are discussed elsewhere [12]. Some work has been reported on the determination of certain PAH adsorbed on solids, such as titanium dioxide, silica, or alumina [13—16].

Experimental

The vapor-phase fluorescence spectra of both PAH at 95°C were obtained in nitrogen, helium, air, and in vacuum of 3 torr using the same system as previously described [4]. An opening at the top of the fluorescence cell cavity provided a connection to the appropriate compressed gas cylinder. Each gas was filtered through glass fiber to remove any suspended particles, and then passed through the system at a high flow rate (several hundred ml min^{-1}) for about 15 min to purge the cell of air. The flow was then adjusted to a rate of about 15 ml min^{-1} and the cell was heated throughout the experiment to 95°C by a laboratory-constructed tube furnace and was measured to ±1°C with an iron/constantan thermocouple. All fluorescence spectra were obtained using a 50-ns aperture on the boxcar averager.

The fluorescence lifetimes (τ) of both PAH were also measured in nitrogen, helium and air, each at one atmosphere pressure and in a vacuum of 3 torr, at temperatures of 60, 80 and 95°C for fluoranthene and at 80, 95 and 110°C for anthracene. A 5-ns window on the boxcar averager was used for all lifetime measurements. The decay curves were monitored at 390 and 459 nm for anthracene and fluoranthene, respectively.

In a second experiment, the fluorescence lifetimes of both PAH adsorbed onto solid supports in air were measured in the following manner. A 50-μl sample each of a 0.1 g ml^{-1} aqueous slurry of hematite (surface area, 31 m^2 g^{-1}), magnetite (surface area, 31 m^2 g^{-1}) or alumina (surface area, 29 m^2 g^{-1}) was spotted onto individual microscope slides; 50 μl of a 0.01 g ml^{-1} aqueous slurry of silica (surface area, 121 m^2 g^{-1}) was spotted onto a microscope slide. The surface area of each support was measured by a modified version of the BET equation [6]. Each slide was then placed in an oven at 120°C for 5 min to evaporate the solvent. After drying the slides, a 5-μl aliquot of a 1×10^{-3} M solution of anthracene or fluoranthene in hexane was spotted on each solid support. After the hexane had evaporated, a slide containing one of the supports spotted with the appropriate PAH was placed into the sample holder of the laser fluorimeter. The unfocused beam of the nitrogen laser (337.1 nm) was directed onto the solid support at an angle of about 30° and the fluorescence normal to the microscope slide was focused onto the entrance slit of the monochromator. The average power of the unfocused laser beam was 2 mW and was operated at 10 pulses per second. To minimize the possibility of PAH photodecomposition on the support, the laser beam (approximately 1 cm × 3 cm at the sample) was left unfocused so that the excitation light flux at the sample could be kept as low as possible. The sample occupied an area of approximately 0.2 cm^2 on the microscope slide. No evidence of photodecomposition was observed. Blanks were prepared for each support,

and no significant luminescence or laser scatter at the wavelengths of interest was observed. Because the laser pulse significantly overlapped both PAH fluorescence curves, deconvolution was used to obtain the fluorescence lifetimes. The deconvolution technique known as least-squares iterative reconvolution [17] was the method used.

Results and discussion

The vapor-phase fluorescence lifetimes of anthracene and fluoranthene are shown in Table 1. There does not appear to be a temperature-dependence (within experimental uncertainty) over the temperature ranges investigated. The fluorescence lifetime of anthracene in a vacuum of 3 torr correlated well with literature values [8, 10]. The shorter lifetimes for anthracene and fluoranthene in air can be attributed to quenching of the excited state by oxygen. The slightly shorter lifetimes for anthracene in nitrogen and helium and for fluoranthene in nitrogen are probably due to collisional deactivation of the excited state. The fluorescence lifetimes of fluoranthene vapor, both in a vacuum of 3 torr and in helium are equivalent within experimental error.

The fluorescence lifetimes of both anthracene and fluoranthene became progressively longer when sorbed in less than a monolayer coverage on silica, magnetite or hematite in comparison to their vapor-phase lifetimes in air (Table 2). The fluorescence lifetimes of anthracene or fluoranthene adsorbed on alumina were the same as their lifetimes in the vapor phase in air. Thus the alumina has no stabilization effects on the excited state of anthracene. Oelkrug and co-workers [13, 14] observed luminescence lifetimes of 34 ns for anthracene chemisorbed on alumina, which arises from a strong charge-transfer band with a luminescence maximum around 520 nm. This lifetime is not comparable to that obtained in the present work, because here the anthracene was physisorbed on the alumina. Also, the present emission

TABLE 1

Vapor-phase fluorescence lifetimes at different temperatures

Temp. (°C)	Lifetime (ns)[a]			
	Vacuum	Helium	Nitrogen	Air
Anthracene				
110	6.3 ± 0.4	5.1 ± 0.5	4.5 ± 0.8	3.3 ± 0.4
95	5.4 ± 0.5	5.2 ± 0.9	4.7 ± 0.6	3.2 ± 0.6
80	5.8 ± 0.4	5.0 ± 0.9	4.1 ± 0.3	3.4 ± 0.5
Fluoranthene				
95	38 ± 2	41 ± 5	36 ± 5	18 ± 2
80	39 ± 6	38 ± 4	33 ± 2	20 ± 2
60	37 ± 3	40 ± 6	33 ± 2	24 ± 4

[a]Uncertainties quoted are one standard deviation. Vacuum pressure 3 torr; gases all at one atmosphere pressure.

TABLE 2

Fluorescence lifetimes for anthracene and fluoranthene sorbed onto various solid support

Support	Fluorescence Lifetime (ns)[a]	
	Anthracene	Fluoranthene
Hematite	22.4 ± 0.9	56 ± 4
Magnetite	7.3 ± 0.2	45 ± 3
Silica	4.8 ± 0.3	32 ± 2
Alumina	3.1 ± 0.3	22 ± 1

[a]Uncertainties quoted are one standard deviation.

spectrum agrees well with the spectrum reported for physisorbed anthracene and no evidence of a charge-transfer spectrum at long wavelength was noted Bauer et al. [15] observed a fluorescence lifetime of 5—6 ns for anthracene physisorbed onto activated silica in an evacuated cell. These results are in fair agreement with the present value of 4.8 ± 0.3 ns for anthracene physisorbed on silica in air. Chandrasekaran and Thomas [16] observed a fluorescence lifetime of 7.1 ns for anthracene adsorbed onto titania particles suspended in water. A fluorescence lifetime of 7.3 ± 0.2 ns was observed here for anthracene adsorbed on magnetite. It is interesting to note the similarity in fluorescence lifetime for these two supports, particularly because both titania and magnetite have semiconductor properties.

Figure 1 illustrates the fluorescence spectra of anthracene and fluoranthene in air and physisorbed on silica, alumina, magnetite or hematite, respectively. Essentially identical results were obtained for anthracene in vacuum and in air. The fluorescence spectra of anthracene on alumina and silica were both red-shifted by about 10 nm, and on magnetite and hematite by about 30 nm with respect to the emission spectrum in air. There is also spectral evidence for a new band appearing at 380 nm for anthracene on hematite, which correlates well with the high-energy band at 380 nm for anthracene on silica and alumina. The fluorescence spectra for fluoranthene in vacuum and in air were essentially identical. The emission profiles for fluoranthene on silica and alumina were red-shifted by about 10 nm and on magnetite and hematite by about 5 nm relative to the vapor-phase spectrum in air. In addition, the fluorescence spectra of fluoranthene on both magnetite and hematite had a shoulder around 440 nm which was absent from the vapor-phase spectrum. For essentially equivalent loading of the different supports, the observed intensity was about tenfold less for both anthracene and fluoranthene on either magnetite or hematite compared to either alumina or silica.

The fluorescence properties of anthracene and fluoranthene appear to be highly sensitive to the nature of the solid support to which the PAH adsorbs Further work to understand more fully the mechanism of the adsorbent/

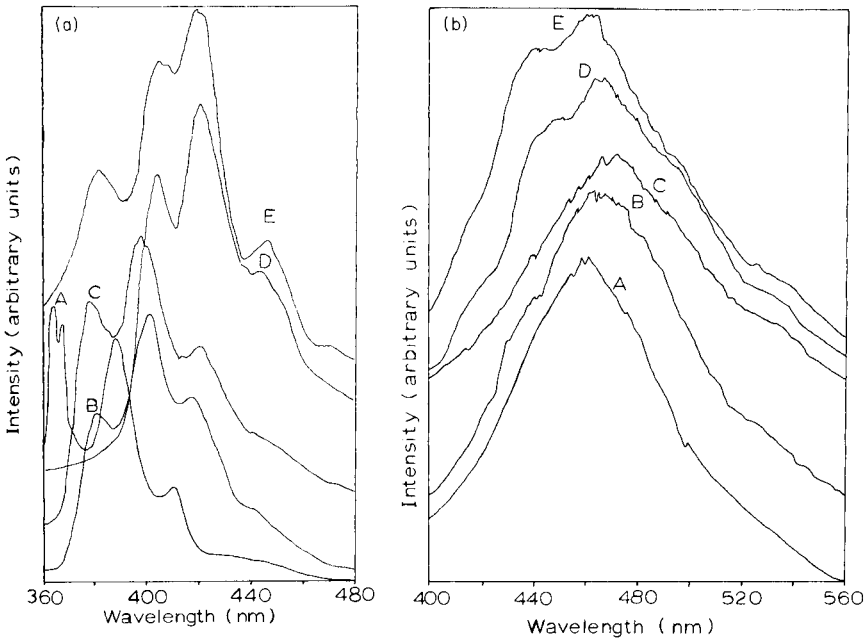

Fig. 1. Fluorescence spectra of (a) anthracene and (b) fluoranthene: (A) in 1 atmosphere of air at 95°C; and physisorbed on (B) silica; (C) alumina; (D) magnetite; and (E) hematite, respectively. The spectra have been offset along the ordinate for clarity. The observed intensities for magnetite and hematite are about tenfold less than for silica and alumina.

adsorbate interactions and the role that these interactions play in PAH gas/particle exchange reactions is presently under way.

REFERENCES

1 J. Konig, W. Funcke, E. Balfanze, B. Grosch and F. Pott, Atmos. Environ., 14 (1980) 609.
2 C. Pupp, R. Lao, J. J. Murray and R. F. Pottie, Atmos. Environ., 8 (1974) 915.
3 J. Peters and B. Seifert, Atmos. Environ., 14 (1980) 117.
4 L. J. Jandris and R. K. Force, Anal. Chim. Acta, 151 (1983) 19.
5 C. K. Dettmer and T. F. Bidleman, Pittsburgh Conference and Exposition on Analytical Chemistry and Applied Spectroscopy, Abstract, 701 (1982).
6 G. A. Eiceman and V. J. Vandiver, Atmos. Environ., 17 (1983) 461.
7 A. R. Ramsden and M. Shiboka, Atmos. Environ., 16 (1982) 2191.
8 J. E. Haebig, J. Phys. Chem., 71 (1967) 4203.
9 U. Laor, J. C. Hsieh and P. K. Ludwig, Chem. Phys. Lett., 22 (1973) 150.
10 W. R. Ware and P. T. Cunningham, J. Chem. Phys., 43 (1965) 3826.
11 D. J. Ehrlich and J. Wilson, J. Chem. Phys., 67 (1977) 5391.
12 L. J. Jandris, R. K. Force and S. C. Yang, Appl. Spectrosc., 39 (1985) 266.
13 D. Oelkrug, M. Plauschinat and R. W. Kessler, J. Lumin., 18/19 (1979) 434.
14 R. W. Kessler, S. Uhl, W. Honnen and D. Oelkrug, J. Lumin., 24/25 (1981) 551.
15 R. K. Bauer, R. Borenstein, P. deMayo, K. Okada, M. Rafalska, W. F. Ware and K. C. Wu, J. Am. Chem. Soc., 104 (1982) 4635.
16 K. Chandrasekaran and J. K. Thomas, J. Am. Chem. Soc., 105 (1983) 6383.
17 D. V. O'Conner, W. R. Ware and J. C. Andre, J. Phys. Chem., 83 (1979) 1333.

Analytica Chimica Acta, 175 (1985) 339—344
Elsevier Science Publishers B.V., Amsterdam — Printed in The Netherlands

Short Communication

FLOW-INJECTION SPECTROPHOTOMETRIC DETERMINATION OF ENALAPRIL IN PHARMACEUTICALS WITH BROMOTHYMOL BLUE

TOSHIHIRO KATO

Research Laboratories, Nippon Merck-Banyu Co., 810 Nishijo, Menuma-machi, Osato-gun, Saitama 360-02 (Japan)

(Received 4th January 1985)

Summary. Enalapril (1.5—60 $\mu g\ ml^{-1}$) in aqueous solution is extracted into dichloromethane as its ion-pair with bromothymol blue in an unsegmented flow system and quantified spectrophotometrically. Up to 80 samples h^{-1} can be processed, with r.s.d. of 1.0—3.4%. The degradation products of enalapril and excipients in the pharmaceutical dosage form do not interfere.

Enalapril (I) (1-[*N*-(*S*)-1-carboxy-3-phenylpropyl]-L-proline 1′-ethylester maleate) is an important compound to control hypertension based on its inhibition of the angiotensin-converting enzyme; its maleate derivative is used medicinally. Enalapril shows its inhibition activity by metabolizing to its diacid form (II) in vivo [1]. The diacid and diketopiperazine derivative (III) are the major potential degradation products resulting from the hydrolysis and intramolecular cyclization of enalapril. High-performance

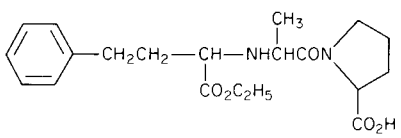
(I)

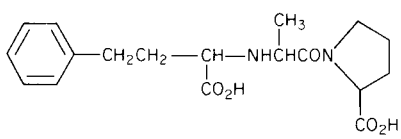
(II)

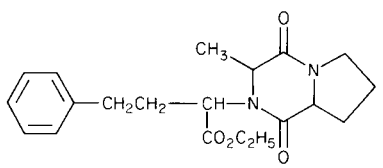
(III)

liquid chromatography (h.p.l.c.) has been the only practical technique for the determination of enalapril in pharmaceutical dosage forms without interference from degradation products. However, severe conditions that

0003-2670/85/$03.30

shorten column life, such as low pH of the solvent and high column temperature are required for acceptable peak shape, because enalapril exists as two rotational isomers owing to the alanyl-proline moiety in the structure [2].

Ion-pair extraction is used widely in the determination of a variety of pharmaceutical amines [3—9] and has been applied with AutoAnalyzers [6, 7] and with flow-injection analyzers [8, 9]. Enalapril is a secondary amine and forms ion-associates with sulphophthalein dyes. The yellow ion-pairs are extracted readily into organic solvents. Manual extraction of this ion-pair is time-consuming and troublesome, and results are variable owing to the rapid decrease of the absorbance of the ion-pair after its formation, and to ready contamination by impurities from glassware during the extraction.

The studies described here were aimed at establishing a rapid and selective assay for enalapril by using flow-injection analysis based on ion pair extraction, which overcomes these problems.

Experimental

Reagents. All chemicals and solvents were of analytical-reagent grade. Bromothymol blue (BTB) solution was prepared by dissolving 50 mg of BTB in 100 ml of dichloromethane. Hydrochloric acid/sodium acetate buffer, pH 3.2 [10] was used as the aqueous phase. Enalapril maleate (Merck, Sharpe & Doehme) was used as the standard and as the material for the optimization of the method.

Apparatus. A diagram of the flow-injection system is shown in Fig. 1. The aqueous and organic phases were pumped by a four-channel peristaltic pump (Gilson, HP-4) fitted with Tygon and Acidflex tubes (Technicon) for the aqueous and organic liquids, respectively. The sample was introduced into the aqueous stream by an autosampler (Kyowa Seimitsu, KSST-601), which is a rotary valve autoinjector for h.p.l.c. and can introduce variable volumes of samples smoothly into the system at rates up to 80 h^{-1}. The segmentor

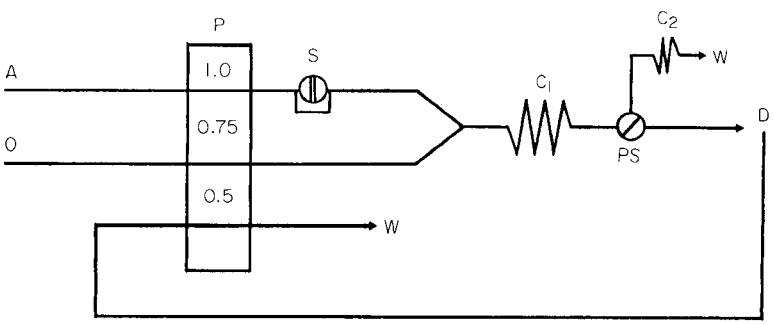

Fig. 1. Recommended manifold: A, aqueous stream; O, 0.05% BTB in dichloromethane; P, pump with flow rates (ml min^{-1}) indicated; S, injection from autosampler; C_1, 60-cm coil, 1.0 mm i.d.; PS, phase separator; C_2, 10-cm coil, 0.2 mm i.d.; D, spectrophotometric detector; W, waste. The tubing from S to C_1 is 10 cm long (0.5 mm i.d.); tubing from PS to D is 20 cm (0.5 mm i.d.).

and phase separator (Denki Kagaku Keiki) fitted with a teflon membrane (Sumitomo Denko, Fluoropore 1.2 μm) are shown in Fig. 2. The absorbance of the organic phase was monitored by a spectrophotometric detector (Waters Associates, Model-440) fitted with a 405-nm filter. A National VP-6521W pen recorder was used. All connecting tubing was of teflon; the lengths and inner diameters are given in Fig. 1.

Procedure. The aqueous and organic phases are pumped through the system before each run for at least 15 min in order to obtain a stable flow, and 20 μl of sample solution containing 1.5—60 μg ml^{-1} enalapril, is introduced into the aqueous stream. After phase separation, the absorbance of the organic phase is measured at 405 nm. Peak heights are measured manually.

Results and discussion

Reaction of enalapril with acid dyes. The formation of colored ion-pairs of enalapril with acid dyes was investigated. Enalapril formed associates with sulphophthalein dyes such as BTB, bromocresol green, bromocresol purple and bromophenol blue. The yellow ion-pairs were extracted quantitatively into dichloromethane and chloroform, but not into hexane. In this study, BTB and dichloromethane were adopted because of their solubility, sensitivity

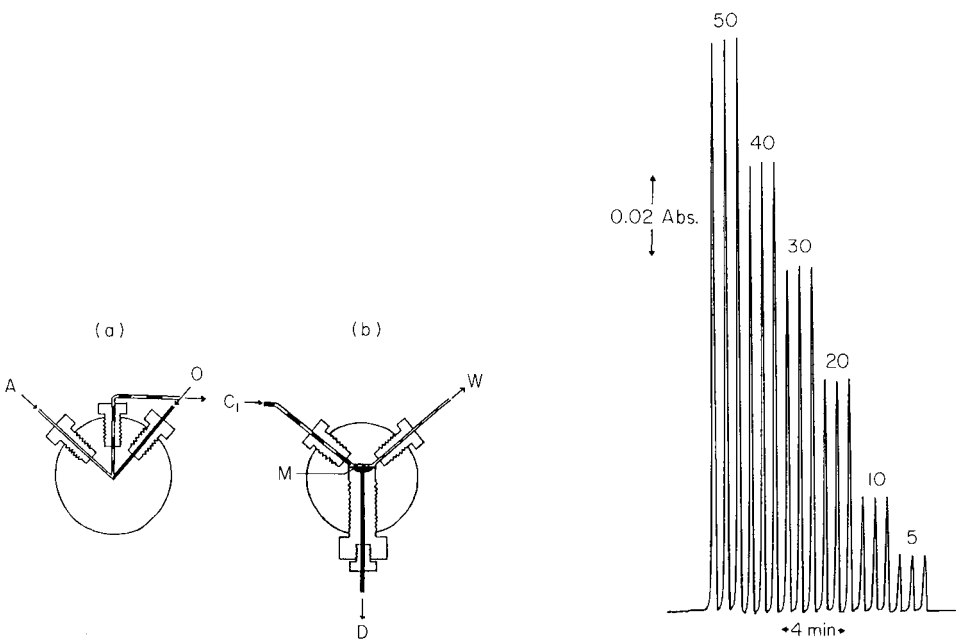

Fig. 2. Segmentor (a) and phase separator (b): M, teflon membrane, 1.2 μm pore, effective area 0.16 cm^2; other symbols as in Fig. 1.

Fig. 3. Recorder tracing for triplicate injections of standard enalapril solutions (5—50 μg ml^{-1}).

and low background. The ion-pair of enalapril with BTB has its absorption maximum at 410 nm in dichloromethane.

Optimization. The optimization of flow rates with due regard to sensitivity, peak resolution, phase-separation efficiency, and rapidity of the analysis resulted in the adoption of 1.0 and 0.75 ml min^{-1} for the aqueous and organic phases, respectively. Prevention of out-gassing from the solvent and stable flow after phase separation were achieved by pumping the dichloromethane flow stream leaving the detector at 0.5 ml min^{-1}. A suitable pore diameter for the teflon membrane for phase separation was 1.2 μm; this provided 70% recovery of the organic phase from the segmented stream. With an extraction coil (C_1) of 60 cm, the overall extraction efficiency for enalapril was 93%.

Hydrochloric acid/sodium acetate buffers, pH 2—5, were used to investigate the effect of the pH of the aqueous phase on the extraction of the ion-pair. The peak heights of the extracts were constant from pH 3 to 4. The dichloromethane phase formed an emulsion with the pH 5 buffer. A higher pH tended to give a higher background. The peak absorbance for 60 μg ml^{-1} enalapril increased with increase of BTB concentration in the range 0.01—0.04%, but further increase up to 0.07% did not improve the sensitivity.

Dyes dissolved in an aqueous phase were used in most of the extraction methods previously reported. In the present method, BTB is dissolved in dichloromethane in order to supply sufficient reagent in the aqueous phase even when a large sample volume is introduced. The organic solution of BTB is practically colorless or only very slightly yellow, and some of the excess of BTB passes into the aqueous phase in the extraction coil. Therefore, the background absorbance of the organic phase after phase separation is very low.

The peak widths at 60% of peak height for 1 μg of enalapril were 10 s, 11 s, and 12.5 s for 10-, 50-, and 100-μl injections, respectively. The proposed method gave a 35-s residence time and 32 s peak width at the baseline, thus the theoretical maximum sampling rate is 110 h^{-1}.

Interferences. The diacid (II) and the diketopiperazine derivative (III) are the major potential degradation products, and their interference in the assay of enalapril was examined. Enalapril maleate spiked with different levels of these compounds was assayed by the proposed method. As shown in Table 1, no significant error was observed. Compound **III** has no basic group that can associate with BTB. The diacid (II) associates with BTB, but the corresponding ion-pair is not extracted into dichloromethane because of the two carboxyl groups in the structure. Common excipients in tablets, such as sugars, cellulose and magnesium stearate, did not interfere.

Calibration and precision. Peak height was proportional to the enalapril concentration over the range 1.5—60 μg ml^{-1}. Figure 3 shows recorder tracings for a series of standard enalapril solutions run in triplicate at a rate of 80 h^{-1}. The relative standard deviations were 3.4, 1.1, and 0.98% (n = 10) for 1.5, 7.5 and 60 μg ml^{-1} enalapril, respectively.

TABLE 1

Effect of the diacid (II) and the diketopiperazine derivative (III) on the assay of enalapril (I)[a]

I:II[b]	Relative absorbance	I:III[b]	Relative absorbance
1:0	100	1:0	100
1:0.25	101	1:0.25	99
1:1	98	1:1	100
1:10	100	1:10	101

[a]60 μg ml^{-1}. [b]Mass ratio.

TABLE 2

Comparison of enalapril concentrations in tablets[a] measured by f.i.a. and h.p.l.c.

Method	F.i.a.	H.p.l.c.	F.i.a.[b]	H.p.l.c.[b]
Content found[c]	19.90	19.79	17.87	17.77
S.d.	0.28	0.05	0.20	0.05
R.s.d. (%)	1.40	0.25	1.12	0.28

[a]Nominal content, 20 mg/tablet. [b]After heating the tablets to 80°C. [c]Mean of 10 determinations.

Application. The method was applied to the analysis of enalapril tablets, and the results were compared with those obtained by the h.p.l.c. method; in the latter method, a Hewlett-Packard RP-8 (4 × 200 mm) column was used with pH 2 dilute phosphoric acid/methanol (1:1) as mobile phase; column temperature, 80°C; flow rate, 2 ml min^{-1}; injection volume, 20 μl; detection at 215 nm. The sample solutions were prepared by extracting enalapril from the tablets with dilute phosphoric acid (pH 3) and diluting to ca. 50 μg and 500 μg ml^{-1} for the f.i.a. and h.p.l.c. methods, respectively. Statistical evaluation showed good agreement between the means and no evidence of positive or negative bias in the assay values. The results for ten analyses of the same batch of tablets are shown in Table 2.

Conclusion

Enalapril can successfully be determined by extraction as an ion-pair with BTB in an unsegmented flow system. The method has the general advantages of f.i.a., namely, instrumental simplicity, high sampling rate, economy in use of reagents, and decreased exposure to organic solvent vapours. Additionally, the two potential major degradation products do not interfere. Therefore, the proposed method is useful for the evaluation of the stability profile of enalapril and for quality control of pharmaceutical dosage forms, and is superior in this respect to h.p.l.c.

REFERENCES

1 See, e.g., D. Tocco, F. DeLuna, A. Duncan, T. Vassil and E. Ulm, Drug metab. dispos., 10 (1982) 15.
2 W. Melander, J. Jacobson and C. Horvath, J. Chromatogr., 234 (1982) 269.
3 T. Sakai, Anal. Chim. Acta, 147 (1983) 331.
4 C. McMartin, P. Simpson and N. Thorpe, J. Chromatogr., 43 (1969) 72.
5 F. Matsui and W. French, J. Pharm. Sci., 60 (1971) 287.
6 J. Nyberg, J. Pharm. Pharmacol., 22 (1970) 500.
7 D. Robertson, F. Matsui and W. French, Can. J. Pharm. Sci., 7 (1972) 47.
8 B. Karlberg, P.-A. Johansson and S. Thelander, Anal. Chim. Acta, 104 (1979) 21.
9 P.-A. Johansson, B. Karlberg and S. Thelander, Anal. Chim. Acta, 114 (1980) 215.
10 G. Walpole, J. Chem. Soc., 105 (1914) 2501.

Analytica Chimica Acta, 175 (1985) 345—348
Elsevier Science Publishers B.V., Amsterdam — Printed in The Netherlands

Short Communication

SPECTROPHOTOMETRIC DETERMINATION OF ZIRCONIUM WITH ALIZARIN RED S IN THE PRESENCE OF POLYVINYLPYRROLIDONE

J. HERNÁNDEZ MÉNDEZ, B. MORENO CORDERO* and L. GUTIERREZ DÁVILA

Department of Analytical Chemistry, Faculty of Sciences, University of Salamanca, Salamanca (Spain)

(Received 11th February 1985)

Summary. The absorbance of the microcolloidal zirconium/alizarin red S/polyvinylpyrrolidone complex is measured at 525 nm in acetate buffered medium at pH 4.75. The molar absorptivity is 3.8×10^4 l mol^{-1} cm^{-1}, which is much greater than that of the classical method. Sulphate and fluoride do not interfere.

The spectrophotometric determination of zirconium is often based on the formation of the zirconium/alizarin S complex in acidic medium with measurements at 520—560 nm [1]. In recent years, micellar systems have become used routinely in both spectrophotometric [2—4] and fluorimetric [4—6] determinations in order to enhance sensitivity and, sometimes, selectivity. In the present communication, the effect of polyvinylpyrrolidone (PVP) on the zirconium/alizarin red S system is reported. Other surfactants tested were Brij 30, Tween 80, Triton X-100, sodium lauryl sulphate and benzyltrimethylammonium chloride; in these cases the colloidal suspensions formed prevented absorbance measurements. Polyvinylpyrrolidone has been used previously in titrimetric [7] and spectrophotometric [8, 9] determinations.

Experimental

Reagents. A stock zirconium solution was prepared from $ZrOCl_2 \cdot 8H_2O$ by dissolving 0.3223 g in 50 ml of 2 M hydrochloric acid and diluting to 100 ml with this acid. The concentration of the solution was checked by gravimetric determination of zirconium as ZrO_2 [10]. Aqueous solutions of alizarin red S (3.0×10^{-3} M), polyvinylpyrrolidone [PVP K-90; 5% (w/v)] and 1.0 M acetic acid/sodium acetate buffer were prepared.

Apparatus. The spectrophotometer with 1.0 cm cuvettes, recorder and pH meter were as described previously [8].

General procedure and calibration. To 15.0 ml of the buffer solution (optimal pH 4.75) was added 3.0 ml of alizarin red S solution; 2.0 ml of PVP K-90 was added followed by the zirconium sample containing <230 μg Zr. The mixture was heated for 15 min at 80°C and left to cool before dilution

0003-2670/85/$03.30

to 50 ml with water. The absorbance was measured at 525 nm against a reagent blank.

Results and discussion

Absorption spectra. The zirconium/alizarin red S system in 1.2×10^{-2} M hydrochloric acid has an absorption maximum at 520 nm with a molar absorptivity of 6.2×10^3 l mol^{-1} cm^{-1}. In the presence of PVP with 0.30 M acetate buffer at pH 4.75, maximum absorbance occurred at 525 nm while the absorptivity increased greatly (Fig. 1). Without PVP at pH 4.75, zirconium hydroxide (or basic salts) precipitated.

The zirconium/alizarin S/PVP reaction is slow, but can be made analytically acceptable by heating at 80° C for 15 min (Fig. 2). Without PVP, the reaction must be used at pH < 2, to avoid precipitation of zirconium hydroxide. In the presence of PVP, the optimal pH range is 4.50—4.80; outside this range, the absorbance was slightly lower. A working pH of 4.75 was chosen. The concentration of the buffer solution did not affect the absorbance within the range studied (0.10—0.50 M). The absorbance increased with PVP concentration reaching a maximum at 0.10%; above this concentration, absorbance was constant. Similar experiments with PVP of lower molecular weight (K-25 and K-10) showed that they behaved in the same way as K-90.

The mole-ratio method showed that the alizarin red S/zirconium ratio was 4 at a PVP concentration of 0.20%; 1:1, 2:1 and 3:1 complexes have been

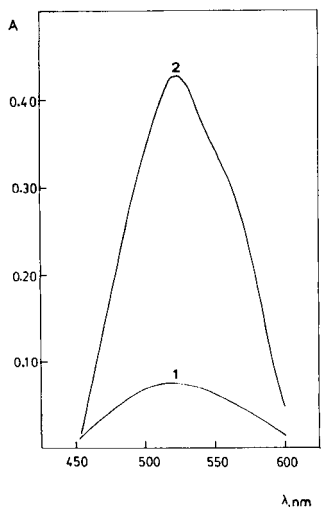

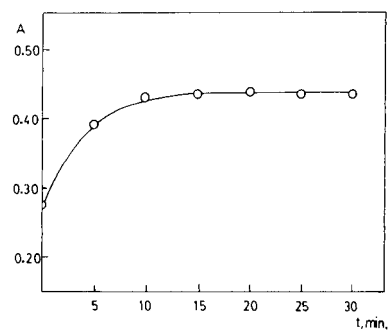

Fig. 1. Absorption spectra of the Zr/alizarin red S system: (1) without PVP in 1.2×10^{-2} M HCl; (2) with 0.20% PVP in acetate buffer, pH 4.75. In both cases, 1.8×10^{-4} M alizarin red S and 1.2×10^{-5} M Zr were present and absorbances were measured against the relevant reagent blank.

Fig. 2. Influence of heating time on the system containing 1.2×10^{-5} M Zr, 1.8×10^{-4} M alizarin red S, 0.30 M buffer (pH 4.75) and 0.20% PVP.

reported earlier depending on the pH [1]. Changes in stoichiometry obtained with micellar media have been reported previously [3].

Analytical characteristics of the method. Beer's law was obeyed at 525 nm for up to 4.6 μg ml^{-1} zirconium. The molar absorptivity was 3.80×10^4 l mol^{-1} cm^{-1}. Measurements of ten solutions containing 1.08 μg ml^{-1} zirconium gave a relative standard deviation of 0.57%.

Callahan and Cook [11] reported a systematic study of the effect of salts in sensitized spectrophotometric determinations. Neutral salts could alter the absorbances and the spectra, probably because of ionic exchange on the micelle surface. The behaviour of the present system with ten different salts was therefore examined; the results are shown in Table 1. The greatest effect is produced by the presence of ammonium ions.

TABLE 1

Effect of different salts on the molar absorptivity of the Zr/alizarin red S/PVP system[a]

Salt added (0.20 M)	λ_{max} (nm)	Molar absorptivity (10^4 l mol^{-1} cm^{-1})		Salt added (0.20 M)	λ_{max} (nm)	Molar absorptivity (10^4 l mol^{-1} cm^{-1})	
		At 525 nm	At λ_{max}			At 525 nm	At λ_{max}
None	525	3.80	3.80	Na_2SO_4	525	4.73	4.73
LiCl	525	4.02	4.02	$(NH_4)_2SO_4$	530	4.11	4.20
NaCl	525	4.06	4.06	$NaNO_3$	525	3.98	3.98
KCl	530	3.71	3.76	KNO_3	530	3.88	3.88
NH_4Cl	530	4.15	4.20	NH_4NO_3	530	3.88	3.93
				$NaClO_4$	525	3.93	3.93

[a]Conditions: 1.2×10^{-5} M Zr, 1.8×10^{-4} M alizarin red S, 0.20% PVP, pH 4.75.

TABLE 2

Effect of ions on the Zr/alizarin S/PVP system[a]

Ion added	Error (%)			Ion added	Error (%)		
	Mole ratio to Zr				Mole ratio to Zr		
	1	10	100		1	10	100
Ni	—	—	4.7	UO_2^{2+}	7.1	39.8	44.3
Sr	−16.5	−35.7	−39.3	Ca	−1.1	−9.1	−22.7
Pb	−21.2	−32.2	−1.1	La	−28.1	16.9	53.9
Ba	−24.7	−39.1	−37.9	F^-	—	—	5.6
Mn^{2+}	−2.2	−1.1	−1.1	Oxalate	—	−1.1	2.2
Hg^{2+}	−3.4	−3.4	−2.2	Tartrate	−4.5	−12.4	−22.5
Bi	27.1	58.8	[b]	Citrate	−2.2	−20.2	−46.1
Al	40.0	88.6	72.7				

[a]Conditions as outlined for Table 1. [b]Precipitate.

The effect of several metal ions on the determination of zirconium was studied for three different ratios (Table 2). There was no interference from lithium, cadmium, magnesium, zinc, cobalt, iodide, bromide, chloride, nitrate, perchlorate or sulphate even at 100:1 ratios. Of interest are the negative errors caused by the strontium, lead and barium, and the lack of sulphate and fluoride interference. These results are different from those described by earlier authors [12, 13] who found that lead did not interfere at low pH whereas sulphate and fluoride interfered seriously.

Zirconium, even in strongly acidic media, is usually hydrolyzed; in slightly acidic media, its hydroxide or basic salts precipitate. However, the zirconium/alizarin red S system is stable in the presence of PVP and no precipitate appears. This might be due to the formation of a transparent micellar system and to the inhibition of the growth of the precipitation nuclei of the hydroxide.

REFERENCES

1 See, e.g., Z. Marczenko, Spectrophotometric Determination of Elements, E. Horwood, Chichester, 1976.
2 W. L. Hinze, in K. L. Mittal (Ed.), Solution Chemistry of Surfactants, Vol. 1, Plenum Press, New York, 1979.
3 S. B. Savvin, R. K. Chernova and L. M. Kudryavtsera, J. Anal. Chem. USSR, 34 (1979) 51.
4 T. Taketatsu, Talanta, 29 (1983) 397.
5 M. R. de Moreno and R. Y. Smith, Anal. Lett., 16 (1983) 1633.
6 W. L. Hinze, H. N. Singh, Y. Baba and N. G. Harvey, Trends Anal. Chem., 3 (1984) 193.
7 J. Hernández Méndez and B. Moreno Cordero, Analyst, 107 (1982) 787; Afinidad, 40 (1983) 475.
8 J. Hernández Méndez, R. Carabias Martínez, B. Moreno Cordero and L. Gutierrez Dávila, Anal. Chim. Acta, 149 (1983) 379.
9 J. Hernández Méndez, B. Moreno Cordero, R. Carabias Martínez and L. Gutierrez Dávila, Microchem. J., in press.
10 G. Charlot, Chimie Analytique Quantitative, Vol. II, Masson, Paris, 1974.
11 J. H. Callahan and K. D. Cook, Anal. Chem., 54 (1982) 59.
12 C. Dragulescu, T. Simonesscu and S. Policec, Talanta, 11 (1964) 747.
13 L. Silverman and D. W. Hawley, Anal. Chem., 28 (1956) 806.

ANALYTICA CHIMICA ACTA, VOL. 175 (1985)

AUTHOR INDEX

ACA announcements

ANNOUNCEMENTS OF MEETINGS

4th INTERNATIONAL WORKSHOP ON TRACE ELEMENT ANALYTICAL CHEMISTRY IN MEDICINE AND BIOLOGY, NEUHERBERG, F.R.G., APRIL 21–23, 1986

The 4th Workshop will be the continuation of this well known series of meetings. A major aim of these meetings is to bring together experts highly experienced in the analytical and biomedical field. We believe that free and effective exchange of views between the analytical specialists on the one hand and biomedical specialists (users of analytical data) on the other is only guaranteed by joint discussion of definite problems. It is hoped that the 4th Workshop will lead again to a productive scientific dialogue between these two groups as far as biomedical applications of trace element analytical research is concerned. All relevant problems in medicine, biology and analysis relating to trace elements (essential and toxic elements) under special consideration of nutritional aspects will be the main scientific topics of the 4th Workshop. The most important aspects will be bioavailability, speciation, parenteral nutrition, recommended dietary allowances, interactions and analytical techniques. The invited papers will deal with modern developments and later scientific findings in these special fields. The Workshop will consist of invited papers on specific problem areas followed by an extended discussion period in which all participants will be invited to take part. Short contributed papers (oral or poster presentation) are also sollicited for the Workshop.

For further information, please contact: Dr. Peter Schramel, Gesellschaft für Strahlen- und Umweltforschung mbH, AG "Spurenelementanalytik", Ingolstädter Landstrasse 1, D-8042 Neuherberg, F.R.G.

2nd INTERNATIONAL SYMPOSIUM ON BIOLOGICAL REFERENCE MATERIALS, NEUHERBERG, F.R.G., APRIL 24–25, 1986

The aim of the symposium is to relate studies of certified and uncertified biological reference materials useful in the improvement of methods in the fields of clinical, environmental and nutrition analysis.

For further information, please contact: Dr. Markus Stoeppler, Institut für Angewandte Physikalische Chemie, Kernforschungsanlage Jülich GmbH, Postfach 1913, D-5170 Jülich 1, F.R.G.

2nd INTERNATIONAL SYMPOSIUM ON DRUG ANALYSIS, BRUSSELS, BELGIUM, MAY 27–30, 1986

The 2nd International Symposium on Drug Analysis will be held in the Catholic University of Louvain-en-Woluwe (U.C.L.) avenue E. Mounier 50, 1200 Brussels, from Tuesday 27 till Friday 30 May, 1986. The purpose of the symposium is to bring together people from industry, universities, control laboratories and hospitals to discuss the current status of analytical techniques including instrumental applications and theoretical developments.

The scientific programme of the symposium will be focused on the presentation and discussion of contributed papers on all aspects of drug analysis. It will include the following topics: Fundamental Aspects of Drug Analysis, Quality Control of Natural and Synthetic Raw Materials, Analysis of Pharmaceutical Preparations, Determination of Drugs in Biological Media, and Automation in Drug Analysis.

For further information, please contact: Mrs C. van Kerchove, Société Belge des Sciences Pharmaceutiques – Belgisch Genootschap voor Farmaceutische Wetenschappen, Rue Stévinstraat 137, B - 1040 Brussels, Belgium. Tel.: 32-2-230 26 85, ext. 333.

10th CONFERENCE OF THE AUSTRALIAN AND NEW ZEALAND SOCIETY FOR MASS SPECTROMETRY, DUNEDIN, NEW ZEALAND, AUGUST 26–29, 1986

The 10th Conference of the ANZSMS has been planned to integrate with other important scientific meetings in New Zealand, including a specialist meeting on Genetic Manipulation: Its application and potential, at the Hanmer Springs (South Island), and the Annual Conferences of the New Zealand Institute of Chemistry and New Zealand Biochemical Society at the University of Otago, Dunedin.

For further information, please contact: Dr. John Cutfield, Department of Biochemistry, University of Otago, P.O. Box 56, Dunedin, New Zealand.

SCIENTIFIC SOFTWARE

SOFTWARE AVAILABLE FROM AUTHORS

A new section of this journal has started, which will give authors of computer programs the opportunity to announce software that they are willing to share with their colleagues. The aims of the section have been outlined in an Editorial (*Anal. Chim. Acta*, 173 (1985) 1). The programs offered will be listed in this section of the journal, as information becomes available.

Further details and forms for entry are available from Professor J.T. Clerc, Universität Bern, Pharmazeutisches Institut, Baltzerstrasse 5, CH-3012 Bern, Switzerland.

CALENDAR OF FORTHCOMING MEETINGS

Jan. 2–8, 1986 Maui, HI, U.S.A.	**1986 Winter Conference on Plasma Spectrochemistry** Contact: 1986 Winter Conference, c/o ICP Information Newsletter, Department of Chemistry, GRC Towers, University of Massachusetts, Amherst, MA 01003-0035, U.S.A. Tel.: (413) 545-2294.
March 10–14, 1986 Atlantic City, NJ, U.S.A.	**37th Pittsburgh Conference and Exposition on Analytical Chemistry and Applied Spectroscopy** Contact: Mrs. Alma Johnson, Program Secretary, 12 Federal Drive, Suite 322, Pittsburgh, PA 15235, U.S.A.
April 21–23, 1986 Neuherberg, F.R.G.	**4th International Workshop on Trace Element Analytical Chemistry in Medicine and Biology** Contact: Dr. P. Schramel, Gesellschaft für Strahlen- und Umweltforschung mbH, Institut für Angewandte Physik, Physikalisch- Technische Abteilung, Ingolstädter Landstrasse 1, D-8042 Neuherberg, F.R.G.
April 22–24, 1986 Noordwijkerhout, The Netherlands	**Anatech '86 – An International Symposium on Applications of Analytical Chemical Techniques to Industrial Process Control** Contact: Prof. W.E. van der Linden, Laboratory for Chemical Analysis, Department of Chemical Technology, Twente University of Technology, P.O. Box 217, 7500 AE Enschede, The Netherlands. (Further details published in Vol. 169.)
April 24–25, 1986 Neuherberg, F.R.G.	**2nd International Symposium on Biological Reference Materials** Contact: Dr. M. Stoeppler, Institut für Angewandte Physikalische Chemie, Kernforschungsanlage GmbH, Postfach 1913, D-5170 Jülich, F.R.G.

May 18–23, 1986 San Francisco, CA, U.S.A.	**HPLC '86. New Frontiers in HPLC. 10th International Symposium on Column Liquid Chromatography** Contact: Ms. Shirley Schlessinger, 400 E. Randolph Drive, Chicago, IL 60601, U.S.A. (Further details published in Vol. 169.)
May 26–29, 1986 Lerici, Italy	**III CAC – Meeting of the Chemometrics Society** Contact: Prof. M. Forina, Istituto di Analisi e Tecnologie Farmaceutiche ed Alimentari, Via Brigata Salerno (ponte), I-16147 Genova, Italy. Tel.: (010) 3993656. (Further details published in Vol. 172.)
May 27–30, 1986 Brussels, Belgium	**2nd International Symposium on Drug Analysis** Contact: Mrs. C. van Kerchove, c/o Société Belge des Sciences Pharmaceutiques, Rue Stévinstraat 137, B-1040 Brussels, Belgium. Tel: 32-2-230 26 85, ext. 333.
June 3–6, 1986 Munich, F.R.G.	**Analytica 86, 10th International Trade Exhibition and 10th International Conference 'Biochemical Analytics'** Contact: Dr. Rosemarie Vogel, Nymphenburgerstrasse 70, D-8000 München 2, F.R.G.
June 10–12, 1986 Dublin, Ireland	**Electroanalysis na h'Eireann** Contact: Dr. Malcolm R. Smith, School of Chemical Sciences, National Institute for Higher Education, Glasnevin, Dublin 9, Ireland.
June 23–27, 1986 Copenhagen, Denmark	**Modern Trends in Activation Analysis, 7th International Conference** Contact: Dr. K. Heydorn, General Chairman MTAA-7, Risø National Laboratory, Post Box 49, DK-4000 Roskilde, Denmark. (Further details published in Vol. 169.)
July 7–10, 1986 Bordeaux, France	**2nd International Meeting on Chemical Sensors** Contact: Dr. Claude Lucat, 2nd International Meeting on Chemical Sensors, Université de Bordeaux I, 351, cours de la Libération, 33405 Talence, Cedex, France.
July 14–17, 1986 Ottawa, Canada	**10th International CODATA Conference** Contact: Mrs. Lois Baignée, Executive Secretary CODATA '86, Conference Services, National Research Council of Canada, Montreal Road, Ottawa, K1A OR6 Canada. (Further details published in Vol. 172.)
July 20–26, 1986 Bristol, U.K.	**SAC 86 – International Conference and Exhibition on Analytical Chemistry** Contact: Miss PE. Hutchinson, Royal Society of Chemistry, Analytical Division, Burlington House, London W1V 0BN, U.K. Tel.: (01) 734-9971, (Further details published in Vol. 169.)
Aug. 10–17, 1986 Ottawa, Canada	**6th International Congress of Pesticide Chemistry** Contact: T.H.G. Micheal, Chemical Institute of Canada, 151 Slater Street, Suite 906, Ottawa, Ontario, Canada K1P 5H3. Tel.: (613) 233-5623. Telex: 053-4306 AIC.
Aug. 25–29, 1986 Antwerp, Belgium	**10th International Symposium on Microchemical Techniques** Contact: Dr. R. Dewolfs, University of Antwerp, Department of Chemistry, Universiteitsplein 1, B-2610 Wilrijk, Belgium. Tel.: 03/828.25.28 (ext. 204). Telex: 33646. (Further details published in Vol. 169.)
Aug. 26–29, 1986 Dunedin, New Zealand	**10th Conference of the Australian and New Zealand Society for Mass Spectrometry** Contact: Dr. J. Cutfield, Department of Biochemistry, University of Otago, P.O. Box 56, Dunedin, New Zealand.

Sept., 1986 Graz, Austria	**4th Conference on Computer Based Analytical Chemistry** Contact: Dr. Wolfhard Wegschneider, Institut für Analytische Chemie, Mikro- und Radiochemie, Technische Universität, Technikerstrasse 4, A-8010 Graz, Austria. Tel: (0316) 7061-8300/8301. (Further details published in Vol. 172.)
Sept. 8–10, 1986 Freiburg, F.R.G.	**4th International Symposium on Bioluminescence and Chemiluminescence** Contact: Dr. J. Schölmerich, Medizinschi Universitätsklinik, D-7800 Freiburg, F.R.G.
Sept. 9–12, 1986 London, U.K.	**5th Meeting of the International Electrophoresis Society, "Electrophoresis '86"** Contact: Dr. M.J. Dunn, Muscle Research Unit, Royal Postgraduate Medical School, DuCane Road, London W12 0HS, U.K., Tel.: 01-743-2030 ext. 338.
June 21–26, 1987 Toronto, Canada	**XXV Colloquium Spectroscopium Internationale** Contact: Mr. L. Forget, Executive Secretary XXV CSI, National Research Council of Canada, Ottawa, K1A 0R6 Canada. Tel.: (613) 993-9009, telex: 053-3145. (Further details published in Vol. 172.)

A NEW title in Elsevier's Analytical Chemistry Symposia Series

Volume 18:
MODERN TRENDS IN ANALYTICAL CHEMISTRY

Proceedings of Two Scientific Symposia held in Matrafüred, Hungary, October 17-20 and October 20-22, 1982

edited by E. PUNGOR, I. BUZAS *and* G.E. VERESS, *Institute for General and Analytical Chemistry, Technical University, Budapest, Hungary*

Two symposia were held in Matrafüred, Hungary, in October 1982 and the proceedings of both are contained in this book.

The first was the Symposium on Electrochemical Detection in Flow Analysis, the aim of which was to define the physical parameters of electrochemical detectors that are most important in flow applications, and to study how and under what conditions these detectors can be used in other fields in addition to direct flow analysis, e.g. in chromatography or clinical analysis.

The other meeting was the first international symposium to be held on Pattern Recognition in Analytical Chemistry. This was a particularly successful meeting and both lectures and discussions are presented in the second part of the book. The volume will provide much information and food for thought for many workers in various fields of analytical chemistry.

(Due to limitations of space, only the plenary and keynote lectures from the first conference and the topics of the second conference are listed below.)

CONTENTS

1984 xxii + 628 pages
US $ 129.75 / Dfl. 350.00
ISBN 0-444-99631-1

ELSEVIER

P.O. Box 211
1000 AE Amsterdam
The Netherlands

P.O. Box 1663
Grand Central Station
New York, NY 10163

low also available in a student edition

Contemporary Practice of Chromatography

y **COLIN F. POOLE** *and* **SHEILA A. SCHUETTE**, *Department of Chemistry, Vayne State University, Detroit, MI, USA*

ere is a book written for scientists a wide variety of disciplines who se chromatography as an analytical ool.

satisfies the need for:

- a graduate-level student textbook in chromatography / separation science
- a text for professional institutes offering short courses in chromatography
- a text for chromatographers who graduated some time ago and who wish to keep up to date with the field
- a comprehensive review of modern separation techniques.

ll areas of gas, liquid, and thin-ayer chromatography are covered; **o other book available offers the ame scope**.

mphasis is on the practice of chro-natographic methods, including how to" sections and numerous xamples of calculation methods. xtensively illustrated, it contains a reat many tables of all useful con-tants, materials and formulas fre-uently used by chromatographers. aluable features are the chapters n sample preparation for chroma-ographic analysis, and on instru-nental methods for sample identifi-ation, plus the comprehensive up-o-date literature review.

he authors have considerable xperience teaching graduate-level ourses and the material presented here has been tried and tested, having formed the basis for short courses taught to groups of industrial chemists. A must for chemists, clinical chemists, biologists, pharmacists, environmental scientists, instrument manufacturers and many others.

CONTENTS: 1. Fundamental Relationships of Chromatography. 2. The Column in Gas Chromatography. 3. Instrumental Requirements for Gas Chromatography. 4. The Column in Liquid Chromatography. 5. Instrumental Requirements for HPLC. 6. Preparative-Scale Chromatography. 7. Sample Preparation for Chromatography Analysis. 8. Hyphenated Methods for Identification after Chromatographic Separation. 9. HPTLC. Subject Index.

1984 x + 708 pages
Hardbound Edition:
US $ 59.00 (USA & Canada)
Dutch guilders 159.00 (Elsewhere)
ISBN 0-444-42410-5
Student Edition:
US $ 37.50 (USA & Canada)
Dutch guilders 110.00 (Elsewhere)
ISBN 0-444-42506-3

P.O. Box 211
1000 AE Amsterdam
The Netherlands

P.O. Box 1663
Grand Central Station
New York, NY 10103, USA

ELSEVIER

7313A

Completely Revised

Instrumental Liquid Chromatograph

A Practical Manual on High-Performance Liquid Chromatography Methods

Second, completely revised edition

by **N.A. PARRIS,** E.I. du Pont de Nemours & Company, Biomedical Products Department, Research and Development Division, Experimental Station Laboratory Wilmington, DE, USA

Journal of Chromatography Library 27

This extensively revised and up-to-date book is an essential tool for the HPLC user in the laboratory. It first appeared in 1976, was twice reprinted and was described in Laboratory Practice as "one of the more useful and successful texts on HPLC . . . a most readable book packed with valuable information and advice . . . strongly recommended."

Practically orientated, it is an easy-to-follow guide containing the minimum essential theoretical background. The majority of the material is based on practical experience and highlights details which may have important operational value for laboratory workers. It helps the HPLC user to select the most appropriate instrumentation, injectors, columns etc.

Applications of liquid chromatography are described with reference to the potential of the technique for qualitative, quantitative and trace analysis as well as for the preparative application. Numerous applications from the literature are tabulated and cross-referenced to sections concerned with the optimization procedures of the particular methods. The format of the original edition proved so successful that it has remained unchanged, but some 45% of the material is either new or completely revised in order to bring the column technology and applications data up-to-date.

"The style . . . is clear. The subject i placed in perspective by comparisons wit other separation techniques and shoul provide a good reference book for a involved in practical LC," (Laborator Practice).

"Overall the book is well written, anc because of its practical emphasis, it is high ly recommended for both the aspiring an experienced chromatographer," (J. Am Chem. Soc.).

CONTENTS: Fundamentals and Instrumenta tion. 1. Introduction and historical backgroun 2. Basic principles and terminology. 3. Th chromatographic support and column. 4. Liqui chromatographic instrumentation. 5. Liqui chromatographic detection systems. 6. Moder electronic technology and its impact on L automation. **Factors Influencing Chromat graphic Selectivity.** 7. Nature of the mobi phase. 8. Liquid-solid (adsorption) chromat graphy. 9. Liquid-liquid (Partition) chromat graphy. 10. Bonded-phase chromatography. 1 Ion-exchange and ion-pair chromatograph 12. Steric exclusion chromatography. **Uses Liquid Chromatographic Procedures.** 13. Qua itative analysis. 14. Quantitative analysis. 1 Practical aspects of trace analysis. 16. Practic aspects of preparative liquid chromatograph **Applications of Liquid Chromatography.** 1 Published LC applications. Appendices. List abbreviations and symbols. Subject index.

1984 xiv + 432 pages. Price: US $ 83.25 / Df 225.00 (including postage).
ISBN 0-444-42061-4

ELSEVIER SCIENCE PUBLISHERS

P.O. Box 211, 1000 AE Amsterdam, The Netherlands
P.O. Box 1663, Grand Central Station, New York, NY 10163, USA

tinued from outside back cover)

CONTENTS

(Abstracted, Index in: Anal. Abstr.; Biol. Abstr.; Chem. Abstr.; Curr. Contents Phys. Chem. Earth Sci.; Life Sci.; Index Med.; Mass Spectrom. Bull.; Sci. Citation Index; Excerpta Med.)

(continued on inside back co